The dynamics of reactivated landslides: Utiku and Taihape, North Island, New Zealand

MASSEY, CHRISTOPHER,IAN

The dynamics of reactivated landslides: Utiku and Taihape, North Island, New Zealand

Christopher Ian Massey

Department of Geography

Thesis submitted for the degree of Doctor of Philosophy

2010

Declaration

I confirm that no part of the material presented in this thesis has previously been submitted for a degree at this or any other university. In all cases the work of others, where relevant, has been fully acknowledged.

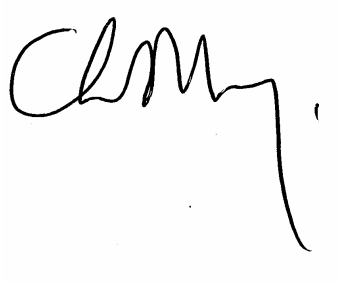

Christopher Ian Massey

Date: 18 December 2010

Abstract

The primary aim of this research was to study the relationship between landslide motion and its causes, with reference to large, slow moving, reactivated translational rock slides. The movement of such slides has often been assumed to be uniform over time because poor temporal and spatial monitoring resolutions have not allowed the processes and mechanisms governing the velocity to be identified. The increased spatial and temporal resolution of the monitoring carried out for this research allows these processes to be better understood.

Two deep-seated, reactivated translational slides were selected to represent over 7,000 mapped landslides of this type in Tertiary-age sedimentary rocks of New Zealand. Each was closely monitored with an automated network of instruments to detect and measure the effects of rainfall, pore pressure, earthquakes and river stage on changing surface and subsurface movement patterns, with sufficient resolution to link periods of movement to their triggering factors. The dynamics and controls upon these landslides have been investigated by combining multiple interdisciplinary approaches including geology, geomorphology, geotechnics and geomatics. Without such an approach the mechanisms governing their motion could not have been adequately resolved.

The deformation behaviour at the two slides during the period of observation would best be described as episodic post-failure creep. The creep patterns observed typically comprised periods of accelerated-, slow- and vertical-creep, punctuated by intervals of rest, which recurred both seasonally and independent of season. Three systems were identified within the recorded unsteady, non-uniform motion: 1) basal sliding; 2) internal plastic deformation and basal sliding; and 3) seasonal surficial shrinkage and swelling unrelated to landsliding. Basal sliding by frictional slip along thin clay seams led to the largest horizontal displacements recorded at both landslides. However, once triggered by pore-pressure increase, accelerated-creep motion by basal sliding did not tend to arrest when basal pore pressure decreased. At both landslides slow horizontal- and vertical-creep occurred together over much of the monitoring period and was related to plastic deformation of the slide mass and basal sliding. This motion occurred at a constant velocity and did not vary with fluctuating pore pressure. Accelerated- and slow-creep motion was regulated by the geometrical complexity of the landslide mass rather than basal pore-pressure-induced increases in shear resistance, or rate-induced increases in material shear resistance.

A slow moving translational landslide at Taihape, New Zealand

Acknowledgements

I would like to express my gratitude to the Institute of Geological and Nuclear Science (GNS Science), New Zealand, which has supported me throughout this research. This research was funded by the New Zealand Foundation for Research Science and Technology and by New Zealand's Earthquake Commission through their funding of the GeoNet project.

I am very grateful to my two main supervisors, Professor David Petley and Dr Mauri McSaveney. This research really has been a journey starting in the King of Bhutan's guesthouse at Dagana, Bhutan. This project has travelled through Nepal, Austria, Taiwan, Hong Kong, New Zealand and Durham, UK. Throughout this journey Dave has always been positive and enthusiastic about my work and has been insightful and a constant source of support. Dave, you're a good friend, thank you. Mauri has kept me on the straight and narrow, albeit via a few side roads and roundabouts. Mauri has been a strong source of support and wisdom throughout this research. I feel very lucky to have worked with both Dave and Mauri.

This research could not have been realised without the technical abilities of many GNS Science research and technical staff, which is testament to the breadth of professional skills found at GNS Science. I would like to particularly acknowledge: Ken Gledhill, Director of the GeoNet project, for realising early on the potential of this research and for continuing to support it over the years; Geoff Clitheroe and Richard Guest for designing, implementing and maintaining the monitoring networks at both landslides; Neville Palmer, John Beavan and Garth Archibald for giving me some understanding of survey principals, but more importantly for helping to setup and process the data from the surface movement monitoring networks; the GeoNet technical team Colin Dyer, Jonathan Adie, Todd Chandler and Sam Tyler for helping to install and maintain the monitoring equipment; Stuart Read, Simon Nelis, Sam McColl, Peter Barker and Zane Bruce for helping with planning and supervising the Utiku drillholes, logging their materials, laboratory testing and unearthing the 50-year old monitoring stations; Bilijana Lukovic for her GIS expertise and Serbian melancholy; David Rhoades for carrying out the rainfall and pore pressure regression analysis; Agnes Reyes for carrying out the SEM and XRD analyses and for her in depth knowledge of clays; Dougal Townsend for his considerable geological knowledge of the Central North Island of New Zealand; Philip Carthew, Carolyn Hume and Penny Murray for their drafting and editing expertise and more importantly, patience; and Graham Hancox and Laurie Richards for providing peer review services

I would also like to acknowledge others outside GNS Science that have contributed to the success of this research: Hugh Cowan, Lance Dixon and Keith Long (Earthquake Commission) for their support of this research; Kate Williams (Tonkin and Taylor) for time spent on the ground at Taihape discussing the engineering geology of the landslide; Nick Rogers (also Tonkin and Taylor) for his support during the rather heated Taihape community meetings; Walter Rushbrook and Richard Justice (KIWI Rail formerly Ontrack) for funding the Utiku ground investigation and for being supportive of this research; Graham Ohara (Rangitikei District Council) for his invaluable local knowledge of the Taihape region and for all his support during the project, including the manual dipping of the Taihape piezometers five days a week, for over three years; Ray Copeland (Global Survey Ltd) for his advice setting up the Leica total survey station and GeoMos software at Taihape; and the residents of the landslide for allowing monitoring equipment to be sited on and around their properties.

My friends and Colleagues within the Geography department at Durham, Nick Rosser and Stuart Dunning, have helped me through various stages of this research, but more importantly I would like to thank them for their ability to survive sleeping on the concrete floor of an infant school in Bhutan at over 3000 m above sea level, with nothing but whiskey and beer for solace. Unfortunately the data collected during that particular fieldtrip has not been used for this research, sorry. Finally, I would like to acknowledge the examiners of this thesis, Dr Nick Rosser (Durham University) and Prof. Neil Dixon (University of Loughborough). Their constructive comments were greatly appreciated.

This thesis is dedicated to Charlotte Fowler (spouse), for editing and for putting up with my long hours at work while looking after our two small, but very cute kids, Joe and Theo.

TABLE OF CONTENTS

List of tables

Chapter 2 Literature review

Chapter 3 Site description

Chapter 4 Methodology

Chapter 5 Results

Chapter 6 Discussion

List of figures

Chapter 2 Literature review

Chapter 3 Site description

Chapter 4 Methodology

Chapter 5 Results

Chapter 6 Discussion

List of equations

Chapter 2 Literature review

List of Notations

The following symbols (BSI, 1990a; Head, 1998) and notations have been used in the thesis, with the term and the International System (SI) of Units defined where appropriate. An asterisk indicates no unit, multiple units or dimensionless.

Symbol	Description	Unit
AMSL	Above mean sea level	m
α	Angle of the slide surface	degrees
η_0	Apparent viscosity at zero shear	GPa s
CF	Clay faction	%
UTK1 to UTK4	Continuous GPS monitoring sites on the Utiku landslide	*
η	Dynamic viscosity	GPa s
c'	Effective cohesion	kPa
σ_f'	Effective stress at failure	kPa
ϕ'	Effective friction angle	degrees
ϕ_r'	Effective residual friction angle	degrees
σ'	Effective stress	kPa
σ_v'	Effective vertical stress	kPa
F	Factor of Safety	*
FE	Finite element method of slope stability analysis	*
G_s	Gaussian smoothing window	mm
BH1 to BH5 TPE3 to TPE5	Inclinometers installed in drill holes on the Taihape landslide	*
BH1A and BH3A	Inclinometers installed in drill holes on the Utiku landslide	*
Λ	Inversed velocity	s/m
LE	Limit equilibrium method of slope stability analysis	*
LL	Liquid limit	*
ML	Local earthquake Richter magnitude	*
MM	Modified Mercalli ground shaking intensity	MMI
σ, σ_n	Normal stress	kPa
N-C	Normally consolidated	*
O-C	Over consolidated	*
PGA	Peak ground acceleration (as a fraction of gravity)	g
BH1A to BH5A	Piezometers installed in drill holes on the Taihape landslide	

BH1 to BH4 and PZA	Piezometers installed in drill holes on the Utiku landslide	*
PL	Plastic limit	*
U	Pore water pressure	kPa
τ_r	Residual shear strength	kPa
RQD	Rock quality designation	%
τ_f	Shear resistance/stress at failure	kPa
τ	Shear resistance; shear stress	kPa or MPa
SSR	Shear strength reduction	*
SRF	Strength reduction factor	*
h_m	Thickness of the slide surface	m
τ_0	Threshold shear stress	kPa
σ_1, σ_2, σ_3	Total principal effective stresses	kPa
UCS	Unconfined compressive strength	kPa/MPa
γ	Unit weight	kN/m3
V	Velocity	m/s
VBW	Vibrating wire pore-pressure transducer	*

Glossary of key terms

Accelerated creep: Short-duration relatively rapid motion represented by steep positive gradients or steps in the cumulative horizontal displacement plots, which typically occur over days and weeks.

Angle of translation: Represents in two-dimensions the movement angle of the measurement points (CGPS or prism) from the horizontal plane. This should represent the angle of the surface along which the landslide mass is translating.

Basal sliding: Where down slope movement is occurring on a surface of rupture (slide surface), but where the surface of rupture is at the base of the sliding mass and forms the boundary between the intact and displaced masses.

Creep (creeping): Creep in the context of this study refers to the post-failure velocity of the landslide mass with no reference to the mechanism of deformation. In this context it relates to extremely slow to very slow landslide motion (16 mm/yr < X < 1.67 m/yr), (Cruden and Varnes, 1996).

Critical state: The critical state concept in soil mechanics relates the effective stresses and the corresponding specific volume of a material during shearing under drained or undrained conditions. There are three commonly identified shear strengths for a soil undergoing shear: 1) Peak strength; 2) Critical state or constant volume strength; and 3) Residual strength.

Finite element (method of stability analysis): The modelling carried out for this research utilises the software Phase2, developed by Rocscience. Phase2 is a 2-dimensional elasto-plastic finite element program for calculating stresses and displacements for geotechnical and civil engineering problems. All modelling uses the plane strain analysis type, adopting the Gaussian elimination solver. The meshes were generated using uniform, 3-noded triangles with about 2,000 to 3,000 elements and 1,000 to 1500 nodes per model. Stress analysis was carried out using 500 iterations, with a tolerance of 0.001 using the “absolute energy” convergence type. The groundwater method adopted for all models was that of piezometric lines. The factor of safety for each model was calculated using the shear strength reduction technique.

Infinite slope: A method of calculating the factor of safety of a slope (ratio between shear resistance and shear stress), which incorporates the Mohr-Coulomb failure criterion with the simplified two-dimensional geometry of the landslide.

Limit equilibrium (method of slope stability analysis): Conventional limit equilibrium methods allow the equilibrium of a soil mass to sliding down slope under the influence of gravity to be assessed. Translational or rotational movements can be considered, where displacement occures along a known or unknown failure surface. All methods allow the factor of safety to be claculated, which is the ratio between the shear resistance and the shear stress. Two-dimensional sections are typically analysed assuming plain strain conditions. These methods assume that the shear strength of the materials along the potential failure surface are governed by the *Mohr-Coulomb* failure criteria, which is a linear relationship between shear strength and the normal stress at failure. The most common limit equilibrium techniques are methods of slices where the soil mass is discretized into vertical slices where each individual slice is treated as a unique sliding block. The calculated factor of safety derived from the different methods can vary, as many of the methods do not satisfy all of the equations of equilibrium (Morgenstern and Price, 1965).

Peak ground acceleration (PGA): Measure of the amplitude of a particular ground motion. For the context of this research the PGA relates to the largest (absolute) value of acceleration in the horizontal access obtained from an accelerogram.

Peak strength may occur before or at critical state, depending on the initial state of the soil particles being sheared. A loose soil will contract in volume on shearing, and may not develop any peak strength above critical state. In this case 'peak' strength will coincide with the critical state shear strength, once the soil has ceased contracting in volume. It may be stated that such soils do not exhibit a distinct 'peak strength'. A dense soil may contract slightly before granular interlock prevents further contraction (granular interlocking is dependent on the shape of the grains and their initial packing arrangement). In order to continue shearing once granular interlocking has occurred, the soil must dilate (expand in volume). As additional shear force is required to dilate the soil, 'peak' strength occurs. Once this peak strength caused by dilation has been overcome through continued shearing, the resistance provided by the soil to the applied shear stress reduces (termed "strain softening"). Strain softening will continue until no further changes in volume of the soil occur on continued shearing.

Plastic deformation: Plastic deformation in the context of this study refers to the deformation of slope materials under constant shear stress prior to failure. In material science this process is usually referred to as creep, and occurs prior to the development of an unstable mechanism e.g. formation of a surface along which sliding could occur.

Reactivated landslide: A landslide that is again active after being inactive (Cruden and Varnes, 1996).

Residual strength: the post-peak drop in drained shear strength. The residual strength occurs for some soils where the shape of the particles that make up the soil become aligned during shearing (forming a slickenside), resulting in reduced resistance to continued shearing (further strain softening). This is particularly true for most clays that comprise plate-like minerals, but is also observed in some granular soils with more elongate shaped grains.

Rock Quality Designation (RQD): The RQD is based on a modified core recovery procedure which, in turn, is based indirectly on the number of fractures and the amount of softening or alteration in the rock mass as observed in rock cores from a drill hole. Instead of counting the fractures, an indirect measurement is obtained by summing up the total length of core recovered but counting only those pieces of core which are 10 cm in length or longer, and which are hard and sound.

Seasonal creep: Patterns of motion that appear similar to the periods of accelerated creep, however, seasonal creep occurs in multiple directions, giving the cumulative horizontal displacement plots a “saw-tooth” pattern. These patterns are cyclic and the periods of up- and down-slope motion follow each other and repeat on about a yearly basis indicating seasonality. At some locations no net-gain in down-slope displacement is apparent.

Shear strength (peak shear strength): The resistance of a soil or rock to failure in shear. The shear resistance of soil is a result of friction and interlocking of particles, and possibly cementation or bonding at particle contacts. Due to interlocking, particulate material may expand or contract in volume as it is subject to shear strains (refer to “peak strength”).

Shear strength reduction: For this research the shear strength reduction (SSR) option in the *Phase2* software has been used to perform a finite element slope stability analysis, and compute a critical strength reduction factor for the models. The critical strength reduction factor is equivalent to the "factor of safety" of the slope (Dawson et al., 1999). The basic concept of the SSR method is:

1. The strength parameters of a slope are reduced by a certain factor (SRF), and the finite element stress analysis is computed.

2. This process is repeated for different values of strength reduction factor (SRF), until the model becomes unstable (the analysis results do not converge).
3. This determines the critical strength reduction factor (critical SRF), or factor of safety, of the slope.

Slide: A slide is a down slope movement of soil or rock mass occurring dominantly on surfaces of rupture or on relatively thin zones of intense shear strain (Cruden and Varnes, 1996).

Slow creep: Long-duration slower motion typically lasting many months and often years. Represented by low gradients in the cumulative horizontal displacement plots. The term “creep” relates to the velocity of the landslide and not the mechanism of movement.

Vertical creep: Long-duration slower motion typically lasting many months and often years. Represented by low gradients in the cumulative vertical displacement plots. The term “creep” relates to the velocity of the landslide and not the mechanism of movement.

CHAPTER 1 INTRODUCTION

1.1 Context and justification for this thesis

1.1.1 What is a landslide?

Landslides are defined as mass movements that involve perceptible downslope movement of slope materials along discrete shear surfaces under the influence of gravity (Cruden and Varnes, 1996). Landslides with long displacements (runout) such as rapid debris flows, debris avalanches (volcanic and non-volcanic), earth flows, rock avalanches, and failures of loose fill and mining waste are among the most dangerous and damaging of all landslide phenomena (Hungr, 1995). While the losses resulting from rapid landslides are the highest and most severe, extremely slow to slow landslides (movement rates of <16 mm/yr to 150 m/yr (Cruden and Varnes, 1996)) have adverse effects on the facilities and infrastructure on and around them. The accumulated slow movement can disrupt the serviceability of facilities and, in some cases, movement can accelerate to cause significant damage (Schuster and Highland, 2007) and loss of life (Mansour, et al., 2010). Many form subtle features, which together with their size and complexity can make them difficult to identify, avoid and mitigate.

1.1.2 Mechanisms of extremely slow to slow landslide motion

In large (typically >1M m^3), slow, translational slides, the sliding mass displaces along a planar or undulating surface of rupture, with a shear zone located at the base of the landslide body (Schuster and Krizek, 1978; Cruden and Varnes, 1996; Picarelli, 2007), which is generally assumed to correspond to a pre-existing discontinuity in the soil/rock mass (Cruden and Varnes, 1996). Movement of reactivated slides occurs along fully developed slip surfaces (Leroueil et al., 1996), which are at residual strength (Skempton, 1985). The reactivation behaviour of translational slides is governed by the Mohr-Coulomb failure criterion, in particular by the ratio of shear force to normal force on the sliding surface, with slip occurring when the Mohr-Coulomb failure criterion is met at the appropriate coefficient of static friction (Terzaghi and Peck, 1948). Under quasi-static conditions, the shear force, and therefore landslide acceleration, depends on variations in the resisting force caused by changes of effective stress (Picarelli 2007) and material properties (Terzaghi and Peck, 1948).

The motion patterns of slowly-moving landslides is often referred to as post-failure creep (Hutchinson, 1988), which is assumed to be uniform over time, mainly because monitoring frequency has failed to resolve variations (Picarelli, 2007). However, as quasi-continuous monitoring data become available, many landslides of this type show

time-variable motion, with distinct movement patterns (Petley et al., 2005) believed to be driven largely by pore-pressure changes occurring over short periods of time (Van Genuchten, 1988; Petley et al., 2005; Picarelli, 2007). Despite the empirical evidence, there is very little research describing the dynamics of such relations (both pore-pressure and earthquake-induced reactivations) and their patterns of surface/subsurface movement (e.g. Allison and Brunsden, 1990).

Velocity changes (accelerations) in slow landslides are thought to be controlled primarily by changes in water levels (Bertini et al., 1984; Nakamura, 1984; Picarelli, 2004; Corominas, 2005; van Asch, 2007; Gonzalez et al., 2008). Corominas et al., (2005); Gonzalez et al., (2008); Matsuura et al., (2008), found that speed increased non-linearly as pore pressure increased. In addition, Bertini et al., (1984) and Gonzalez et al., (2008) showed that, for the same value of pore pressure, the speed when groundwater was rising was higher than during lowering (Picarelli, 2007). The relationship between pore pressure (groundwater) and landslide movement is complicated by the complex landslide hydrogeology, in particular by the contrasting permeability of intact, fissured and sheared materials forming the slide mass, and the presence of large-scale heterogeneities providing direct conduits for surface water into the landslide (e.g. Corominas et al., 1999; Van Asch, et al., 2007). Consequently, large and slow slides often show an erratic and complex response to water input (Corominas, 2000; Malet; et al., 2005; van Asch et al., 2007). Although pore pressure response to water input can be complex, pore pressures are routinely monitored in many landslides and the equipment and techniques used have been developed and refined over many years. Therefore, the distribution of pore pressures within the landslide mass can in most cases be resolved, enabling the influence of other controlling factors to be differentiated.

1.2 Research aim and objectives

The primary aim of this research was to study the relationship between landslide motion and its causes, with reference to large (>1M m^3), deep-seated (slip plane typically > 10 m below ground level), reactivated translational slides, that typically move at rates varying from extremely slow to very slow. The major objectives of this research are:

Objective 1

Design and compare systems capable of high temporal- and spatial-resolution monitoring of the variables that influence landslide motion (typically rainfall-triggered groundwater rises, earthquakes and loss of toe support) of two large, deep-seated and slow-moving, reactivated translational slides;

Objective 2

Parameterise the relationship between landslide motion and its causes, focusing primarily on rainfall-induced changes in groundwater and its effect on landslide velocity;

Objective 3

Evaluate the mechanisms thought to govern landslide motion (using field data and analytical techniques).

1.3 Scope of the study

The two monitored landslides are complex, reactivated, translational rock slides-earth flows (Cruden and Varnes, 1996), or block slides (Panet, 1969), with movement occurring along fully developed slip surfaces at residual strength in weakly indurated Tertiary-age marine sedimentary rocks. They are two of over 7,000 mapped New Zealand landslides of this type (Dellow et al., 2005) and their movement rates are typically extremely slow to very slow (16 mm/yr < x < 1.6 m/yr, Cruden and Varnes, 1996).

Monitoring systems were designed and installed on the two landslides (Objective 1), to monitor:

- surface and subsurface movement
- pore-water pressure
- rainfall
- transient ground accelerations (earthquakes)
- river stage

The research focused in particular on examining relationships between changes in pore-water pressure and deformation behaviour of the two monitored landslides (Objective 2). Similarities and differences between the landslides were identified and discussed and mechanisms thought to govern their motion evaluated (Objective 3).

Equipment to monitor earthquake ground accelerations and river stage were installed. However, their relationships with landslide motion were not the primary aim of this research, because there was little likelihood of recording significant earthquakes or floods during the study period. Pre-failure landslide mechanisms also were not within the scope of this study.

1.4 Structure of the thesis

The thesis is presented in seven chapters, of which Chapter 1 is an introduction.

Chapter 2 reviews previous research on movement patterns and mechanisms governing the motion of slow reactivated landslides.

Chapter 3 describes the geological and geomorphological setting of the two selected landslides. Engineering geological models for the landslides are presented, detailing their geometry and materials. These models were developed from historical and recent ground investigations.

Chapter 4 describes the monitoring equipment installed on the landslides and explains why the particular choices were made and how the raw data was collected and processed.

Chapter 5 summarises the monitoring data. The objective of this chapter is to present the collated data, quantify its errors and measurement from the various instruments and to discuss statistically significant trends and relationships and compare them with longer-term historical monitoring results. The results from both landslides are then discussed further and key themes highlighted for subsequent analysis and discussion.

Chapter 6 discusses the significance of slow, reactivated landslides and compares the monitoring systems installed at the Utiku and Taihape landslides with other comparable systems detailed in the scientific literature. This is followed by discussion of the motion patterns of such slow landslides, focusing on the relationship between rainfall and groundwater, and then the relationship between groundwater and landslide motion. Using the field data and analytical techniques, some mechanisms thought to govern their motion are then evaluated.

Chapter 7 summarises the principal findings of the thesis and makes recommendations on further research.

CHAPTER 2 LITERATURE REVIEW

2.1 Types of landslide

A range of classification schemes are used to define the various types of landslide (e.g. Sharpe, 1938; Skempton and Hutchinson, 1969; Zaruba and Mencl, 1969 Carson and Kirkby, 1972; Varnes, 1978; Hutchinson, 1988; Cruden and Varnes, 1996). Most of these schemes are based on the three key elements: the type of movement; the kind of material; and the rate of movement (Varnes, 1978). The classification proposed by Varnes (1978) is the most widely accepted and utilised (Figure 2.01). The main landslide types include falls, topples, slides, spreads and flows, which can occur in rock, debris and earth materials. The rate of movement ranges from “extremely slow” (< 16 mm/yr) to “extremely rapid” (> 5 m/sec) (Varnes, 1978; Cruden and Varnes, 1996). A recent comprehensive review on the terminology used in the classifications is provided by Shroder et al. (2005).

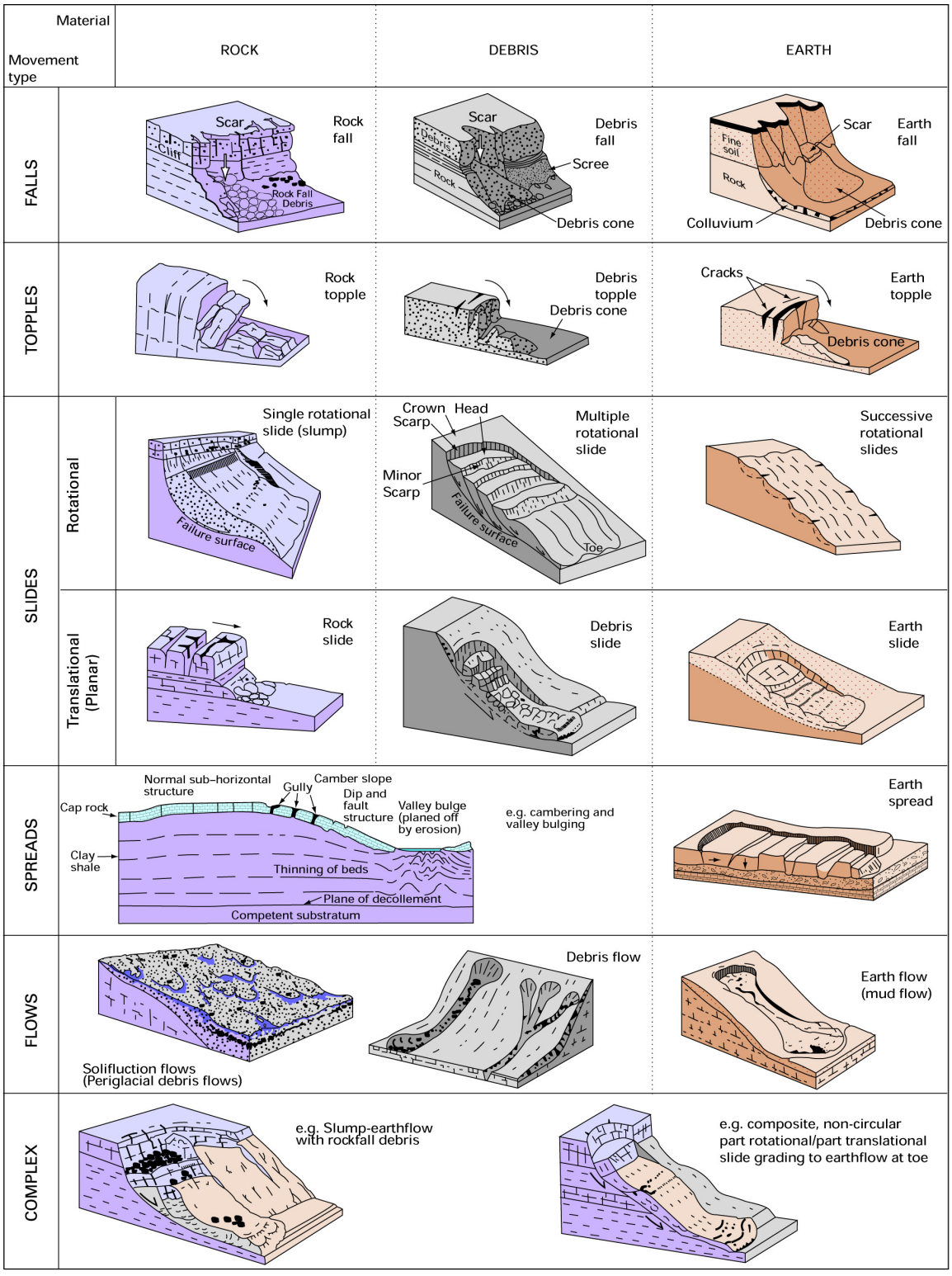

Falls mass detached from steep slope/cliff along surface with little or no shear displacement, descends mostly through the air by free fall, bouncing or rolling.
Topples forward rotation about a pivot point.
Rotational slides sliding outwards and downwards on one or more concave-upward failure surfaces.
Translational (planar) slides sliding on a planar failure surface running more-or less parallel to the slope.
Spreads fracturing and lateral extension of coherent rock or soil materials due to liquefaction or plastic flow of subjacent material.
Flows slow to rapid mass movements in saturated materials which advance by viscous flow, usually following initial sliding movement. Some flows may be bounded by basal and marginal shear surfaces but the dominan movement of the displaced mass is by flowage.
Complex slides slides involving two or more of the main movement types in combination.

Figure 2.01 Classification of type of landslide (modified after Varnes, 1978 and DoE, 1990).

Using the classification scheme proposed by Varnes (1978) and modified by Cruden and Varnes (1996), this research is concerned with the movement patterns of complex, reactivated, translational rock slides-earth flows, or block slides (Panet, 1969). A conceptual diagram for these types of landslide found in the Tertiary-age sedimentary rocks of New Zealand, is shown in Figure 2.02.

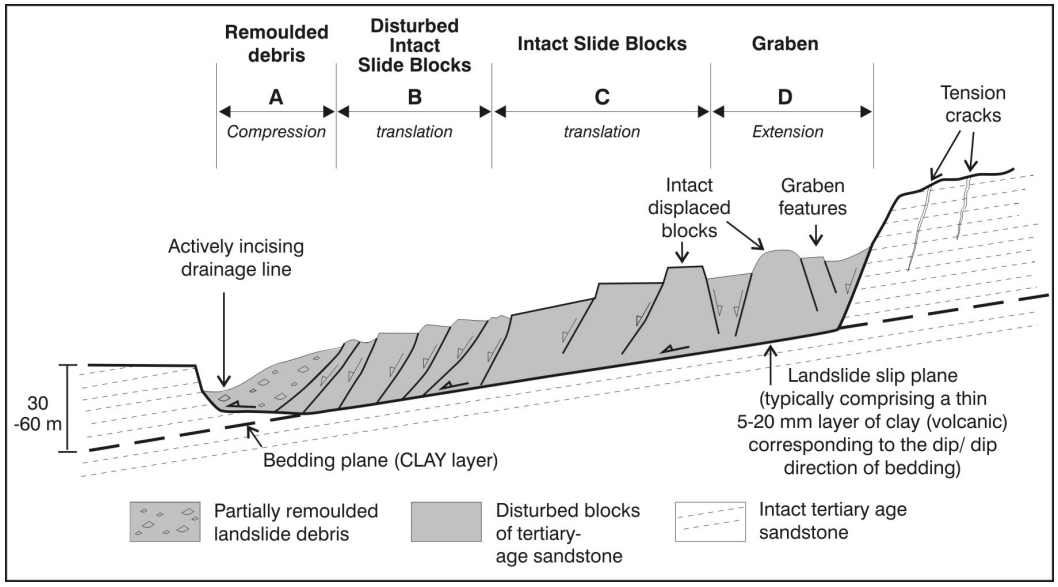

Figure 2.02 Schematic cross section through a typical translational slide in Tertiary-age sedimentary rocks of New Zealand.

2.2 The behaviour of reactivated landslides

2.2.1 Landslide movement mechanisms

Analyses of movement patterns permit a better understanding of deformation processes in landslides (Terzaghi, 1950). Generally, slope movements can be classified into four stages: pre-failure; post-failure; occasional reactivation; and active landslide (Leroueil et al., 1996), (Figure 2.03). Stages three and four (occasional reactivation and active landslide) refer to those bodies which have experienced failure and are still moving (Urciouli et al., 2007) and where the body slides along one or several pre-existing shear surfaces (Fell et al., 2000). Stages three and four, however, are essentially the same, and can be termed 'the reactivation stage' (Fell et al., 2000), as the shear/slide surface has fully developed and the material through which sliding is occurring is assumed to be at residual strength (Skempton 1985) (Figures 2.04, 2.05 and 2.06). The point of failure, however, is somewhat relative; in a geotechnical sense, failure is assumed once the material exceeds its peak shear strength, which is usually followed by a post peak drop in shear strength to residual values. The relationship between peak and residual shear strengths depends upon the type of material. For clays, the post peak drop in shear strength is typically a result of the reorientation of platy clay minerals (Skempton 1985). However, the term 'failure' could be used in reference to describe for example, the specified minimum yield strength of a pipeline or other piece of infrastructure. It is

possible that the yield strength of a pipeline could be reached or exceeded even though the material in which it resides has not yet failed. Geotechnically pre-failure deformation mechanisms are usually referred to as creep, which is continuing deformation under sustained load (Varnes, 1983).

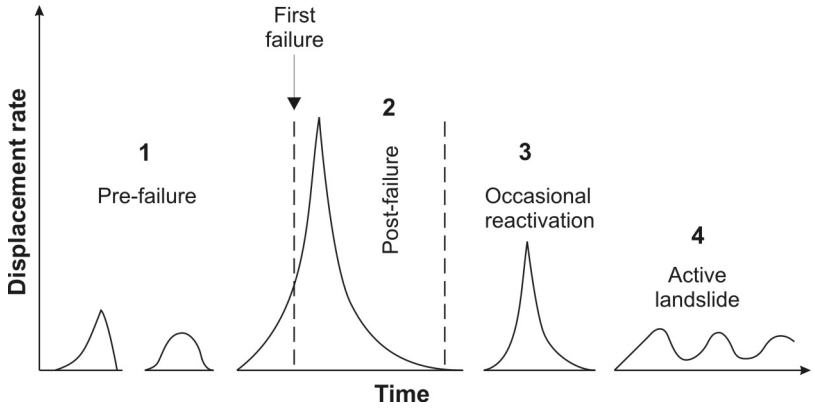

Figure 2.03 The different stages of slope movements (source: Leroueil, 1996).

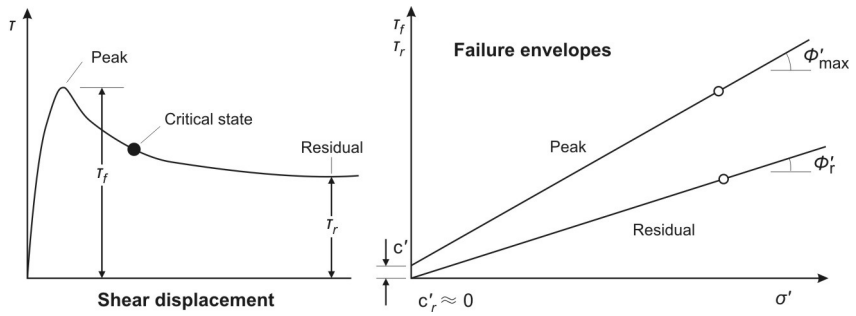

Figure 2.04 Diagrammatic shear strength envelopes (source: Craig, 1997).

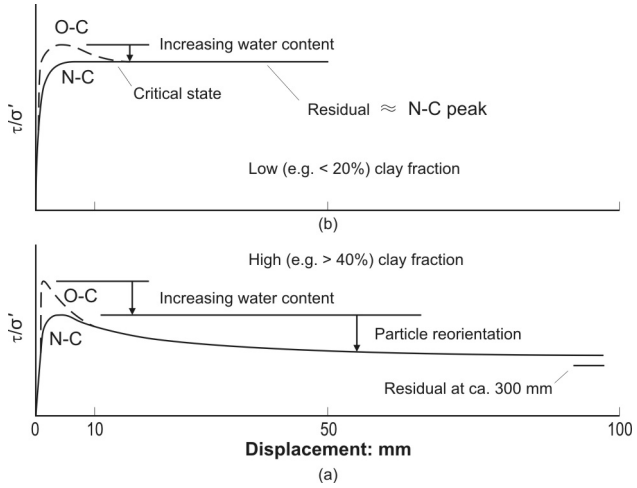

Figure 2.05 Diagrammatic stress-displacement curves at constant normal effective stress (source: Skempton, 1985).

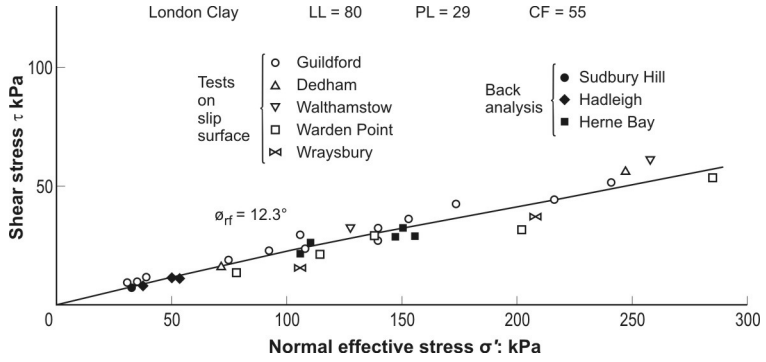

Figure 2.06 Residual strength for London Clay (source: Skempton, 1985).

The term creep usually refers to the tendency of a solid material to slowly deform permanently under the influence of an applied stress, which occurs prior to the development of an unstable mechanism e.g. formation of a surface along which sliding could occur (Craig, 1997). The creep phenomenon has been studied under different disciplines including geomorphology (e.g. Selby, 1993), engineering (e.g. Varnes, 1983), materials science (e.g. De la Cruz-Reyna and Reyes-Dávila, 2001), and rheology (e.g. Ranalli, 1995). A comprehensive classification of creep in landslides has been given by Hutchinson (1988) namely: (1) "superficial, predominantly seasonal creep or mantle creep", (2) "deep-seated, continuous creep or mass creep", (3) "pre-failure creep or progressive creep", and (4) "post-failure creep". The main characteristics of each creep type are shown in Table 2.01.

Table 2.01 Definitions of creep (modified after Hutchinson, 1988 and Ng, 2007).

Type	Key approach	Type of creep described	Key characteristics	References
1	Geomorphology	Superficial, predominantly seasonal creep; mantle creep	Confined to surface layer (less than 1 m deep); involves changes of volume due to changes in water content and temperature	Terzaghi (1953); Carson and Kirkby (1972); Selby (1993)
2	Engineering	Deep-seated, continuous creep; mass creep	Occurs at constant stress below the maximum strength of the material	Terzaghi (1953); Varnes (1978, 1983); Selby (1993); Fell *et al.* (2000)
3	Materials science	Pre-failure creep; progressive creep	Accelerating displacements towards shear failure; involves progressive development of shear structures from discrete shear zones to continuous displacement shears	Terzaghi (1950); Bjerrum (1967); Ter-Stipanian (1980); De la Cruz-Reyna and Reyes-Dávila (2001)
4	Rheology	Post-failure creep	Involves small renewals of failure on a pre-existing slip surface	Van-Asch (1984); Ranalli (1995)

Engineering (Type 2) and material science (Type 3) definitions consider deformation below maximum shear stress/strength prior to failure. The key distinction between these two creep types is that the former emphasises the time-dependent dimension of the deformation, while the latter involves the dynamic nature of pre-failure movement, highlighting the changing stress distribution within materials (Ng, 2007). Rheological (Type 4) creep is a post failure mechanism as it involves reactivation by sliding along an existing shear surface. This definition therefore, relates to the velocity of motion (i.e. creeping) and not to the mechanism, which should not be confused with type 2 and 3 definitions. For the purpose of this research the term “creep” is used to describe the post-failure patterns of landslide velocity (Type 4) with no reference to the mechanism of displacement, the term “plastic deformation” is used to describe pre-failure Type 2 and 3 creep.

Allison and Brunsden (1990), based on work carried out on mud slides (Hutchinson and Bhandari, 1971), identified four components of post-failure creep, which they termed: A) small, multiple, stick-slip movements, which are grouped temporally; B) gradual or ‘graded slip’ within defined temporal limits; C) rapid ‘surge’ events, which occur over a short time interval and involve large displacements; and D) ‘random’ movements. The post failure movement types A, B and C are shown in Figure 2.07.

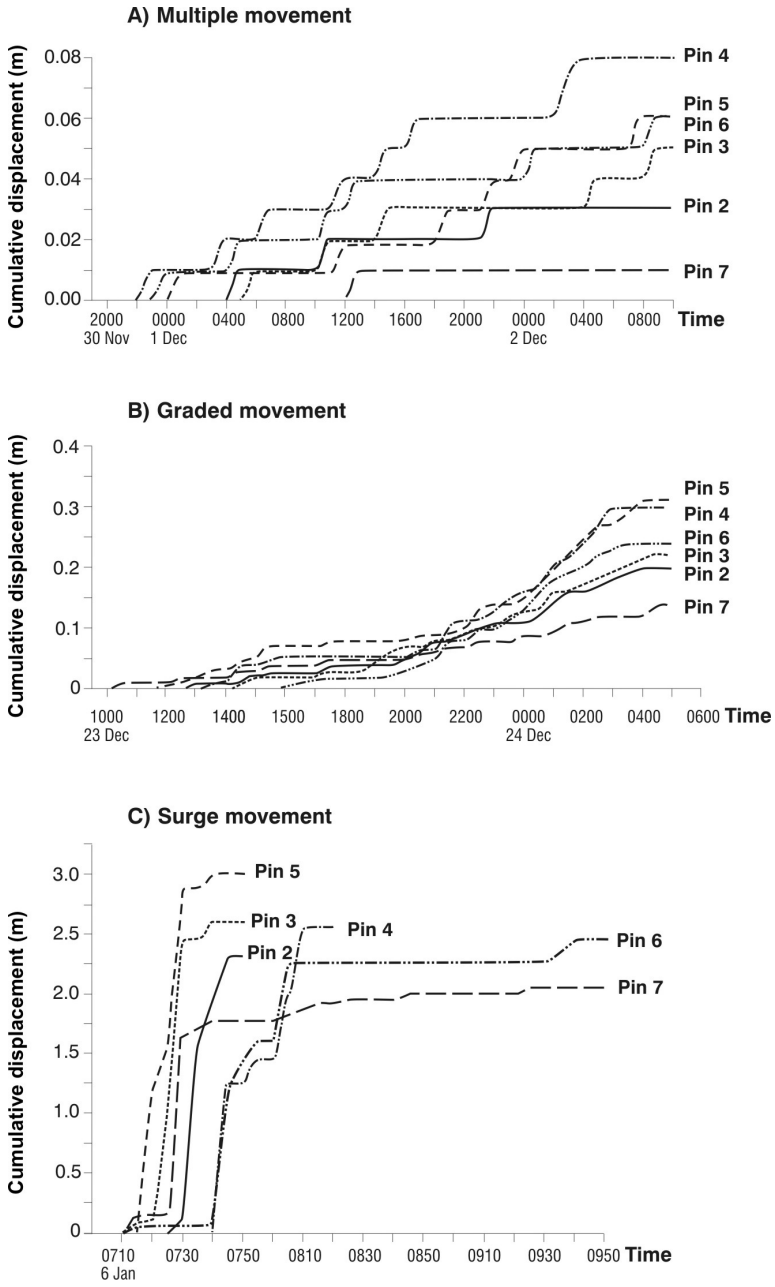

Figure 2.07 Landslide displacement patterns (source: Allison and Brunsden,1990).

Petley et al., (2005), found similar patterns to those identified by Allison and Brunsden (1990), but went on to suggest that these patterns are dependent upon their morpho-dynamic position within the landslide, and that motion characteristics change as a theoretical point moves through the landslide system. Petley et al., (2005) proposed four stages of motion for the Tessina landslide in Italy: Type I motion occurs within the 'detaching zone' located above the landslide crown; Type II motion also occurs within the detaching zone, but here they are associated with material that has become fully detached and incorporated into the landslide; Type III motion is associated with blocks that are disintegrating; and Type IV motion is when the material moves as a remobilised mudflow. These four stages are shown conceptually in Figure 2.08. Motion Types I and II relate to pre-failure motion as the shear surface is developing, and probably relates to

displacement by plastic deformation (Types 2 and 3 plastic deformation, Table 2.01), where a slip surface has not fully developed and the slope materials have not reached failure. Types III and IV relate to post-failure motion when the shear surface is fully developed and the materials are at residual strength, as in stages 3 and 4 (Figure 2.03), (Leroueil et al., 1996). The boundary between Type II and III is probably graded and relates to the post peak drop in shear strength, prior to full reorientation of the particles in the shear zone and achievement of true residual strength.

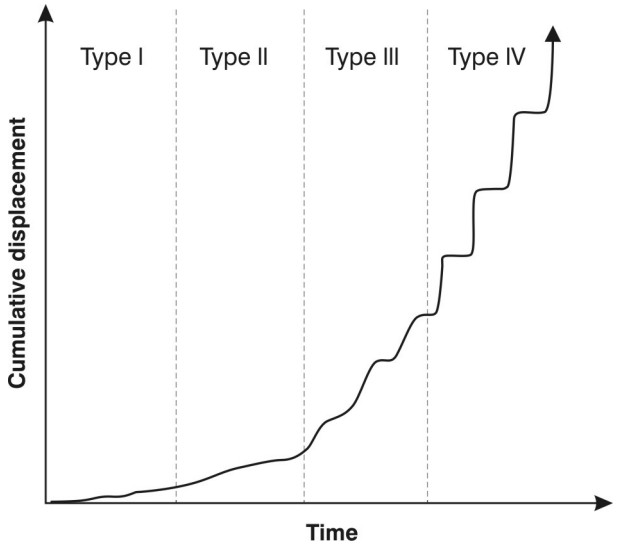

Figure 2.08 Schematic displacement patterns of the Tessina landslide, Italy (source: Petley et al., 2005).

The Type III and IV motions shown by Petley et al., (2005) are somewhat similar to those post-failure patterns discussed by Allison and Brunsden (1990), where the Type III motions relate to gradual or graded slip and the Type IV to rapid surge events. However, it is unclear what happens to the landslide movement rate following Type IV motions (Petley et al, 2005) or rapid surge events (Allison and Brunsden 1990). If the movement has radically reduced the resistance properties of the sliding mass causing a change in the movement mechanism, i.e. a translational block-slide transforms into a debris or earth flow (Cruden and Varnes, 1996 and Panet 1950), acceleration could continue until the landslide fails catastrophically (Terzaghi, 1950). However, periods of rapid acceleration e.g. Type IV movements, or rapid surge events could be followed by periods of equally rapid deceleration and rest (Allison and Brunsden, 1990; Angeli et al., 1996). Several authors suggest that in large deep-seated translational slides, different types of post-failure creep motion (reactivations) can occur with varying frequency and at different times within the seasonal record (Allison and Brunsden, 1990; Crosta and Agliardi, 2003; Corominas et al., 2005, and van Asch et al 2007). This repetition of landslide displacement patterns through time is well represented in the literature, e.g. Iverson, (1985); Allison and Brunsden (1990); Bracegirdle et al., (1991): Angeli et al., (1996); Petley et al., (2005); Matsuura et al., (2008); Ranalli et al., (2009); Schultz et al.,

(2009a, 2009b). The frequency and magnitude of these post-failure motion events will depend upon the frequency and magnitude of the destabilising events, such as pore pressure increases, earthquake-induced ground accelerations, changing material properties e.g. strain softening of the shear-surface clay and changes in load e.g. loss of toe support.

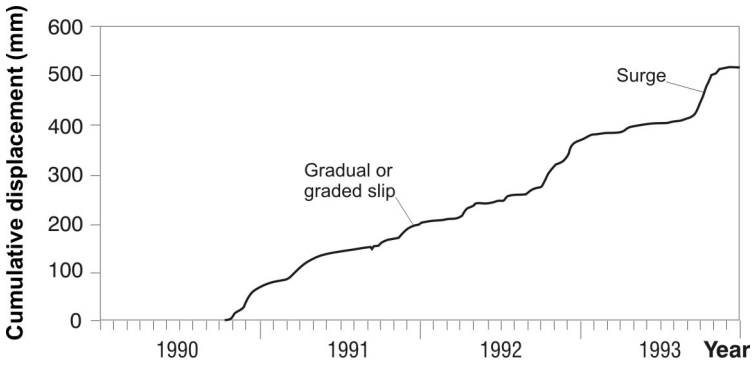

Figure 2.09 Recorded displacement of the Alvera mudslide, Spain (source: Angeli et al., 1996), which shows all three of the motion patterns identified by Allison and Brunsden (1990).

Saito (1965 and 1969) first examined the movement patterns on landslides in Λ-t space, where Λ = 1/velocity and t = time. Petley et al., (2002, 2005), identified a relationship between landslide movement patterns at failure and basal-deformation processes by analysing movement in Λ-t space, from landslides in various materials and in a range of environments (Ng, 2007). Petley et al. (2002) present a hypothesis whereby the two main identified trends: 1) linearity, indicates rupture-surface development (crack propagation) dominated by brittle-failure mechanisms (Kilburn and Petley, 2003; Petley et al., 2005); and 2) asymptotic trend, suggesting sliding on pre-existing slip surfaces (crack nucleation) or ductile deformation (Petley et al., 2005), Figure 2.10. However, if rupture surface development is by brittle failure it must be sudden and dramatic – 0.6 times the seismic wave speed (Atkinson and Meredith, 1987; Olsen, 2001). It is more likely that progressive development of a shear zone might occur by intermittent brittle failure, but only over very short distances.

Landslide Movement styles/patterns	Type I	Type II
Landslide acceleration behaviour (1/velocity against time)	• Linear trend 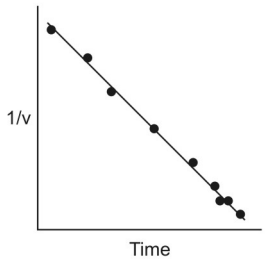 • Bulk Movement accelerates *linearly* with time	• Asymptotic trend 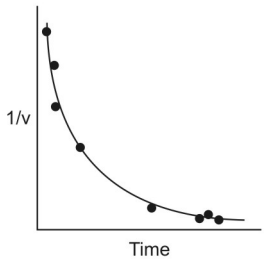 • Bulk Movement accelerates *exponentially* with time
Dominant basal (at depth) deformation process	• Crack propagation/growth • New cracks join together (micro-cracking process) • Development of discrete shear/rupture surface • Shear surface generation • Brittle failure mechanisms	• Crack nucleation • New cracks remain isolated • Sliding on existing planes of weaknes • Reactivation of existing landslide systems • Ductile deformation processes
Material behaviour Stress-strain relationship	• Brittle • Commonly occurs in bonded or cemented materials at relatively low confining pressures	• Ductile/plastic/non-brittle • Shown by materials with little or no interparticle bonding at high confining pressures
Failure	• First-time failure • Catastropic • Sudden and rapid dispalcement	• Landslide reactivation • Non catastropic/not intrinsically dangerous • Continual, slow, creep-like movement

Figure 2.10 Summary of the Λ-*t* analyses and their implications on landslide behaviour (source: Ng, 2007).

The brittle- and ductile-deformation mechanisms can be illustrated by the stress-strain curve, where linearity in Λ-t space is thought to represent brittle failure (Type I. movement patterns, Figure 2.10), characterised by a peak in strength on the stress-strain curve corresponding to development of a shear surface. The asymptotic trend (Type II. movement patterns, Figure 2.10) is thought to represent the post-peak drop to residual strength values, when the shear surface is fully developed (Petley and Allison, 1997; Cooper et al., 1998; Kilburn and Petley, 2003; Ng, 2007). Examples of reactivated slides from the literature where motion is characterised by an asymptotic trend in Λ-t space are shown in Figure 2.11.

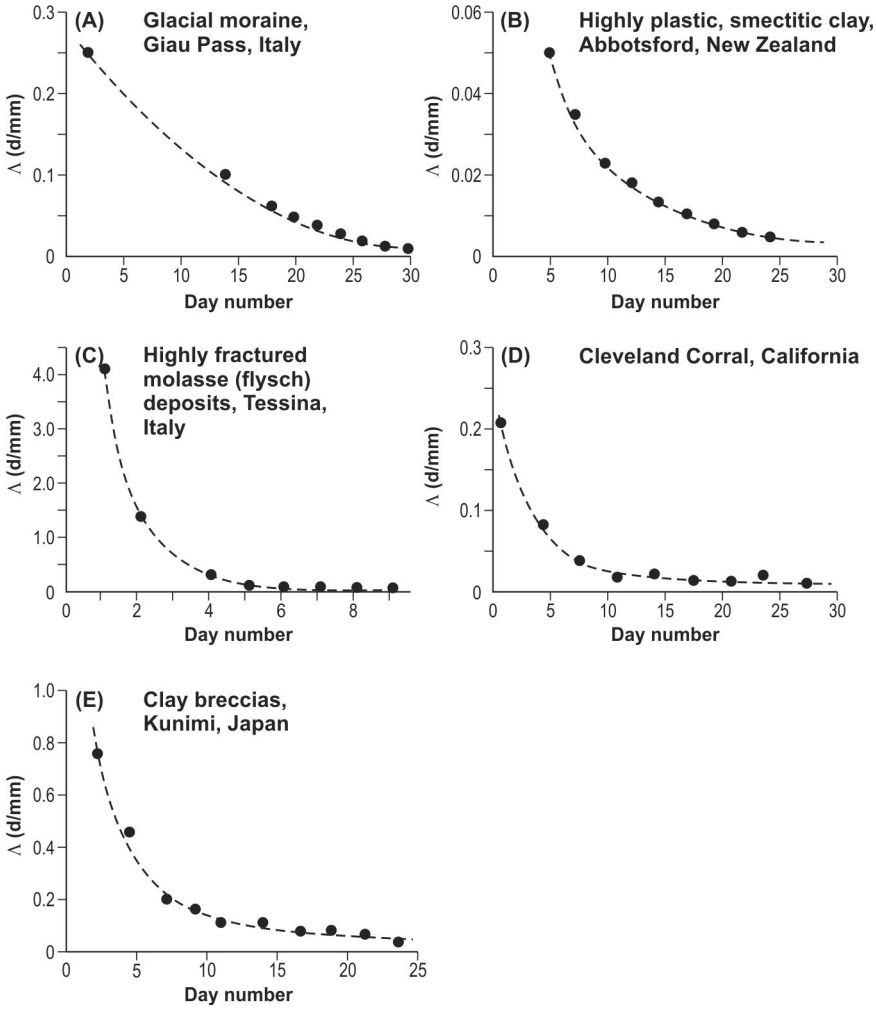

Figure 2.11 Asymptotic trends are shown in Λ-*t* space plots derived from landslide data in (A) Italy (Angeli et al., 1989), (B) New Zealand (Salt, 1985), (C) Italy (Consiglio Nazionale delle Richerche, 2001), (D) California (U.S. Geological Survey) and (E) Japan (Shuzui, 2001). (source: Petley et al., 2002).

These time-dependent failure relationships relate to post-failure reactivations, where the asymptotic trend of the displacement curve in Λ-t space represent individual periods of landslide reactivation in response to destabilising events. These processes may continue for years with repeating periods of acceleration punctuated by periods of inactivity, which become the *status quo*. In rare cases, movement rates can increase rapidly leading to failure. Two examples of such landslides are Abbotsford (Hancox et al., 1980) and Vajont (Vaiont), (Kilburn and Petley, 2003). However, some authors have suggested that Vajont was a first-time failure (Skempton, 1966; Petley, 1966) rather than a reactivation (Hendron and Patten, 1985; Pasuto and Soldati, 1991), whilst the Abbottsford landslide may have slid along a pre-existing failure surface (Hancox et al., 1980) and its head scarp appeared along the up-slope edge of a pre-existing, but subdued graben. In the case of Abbotsford, it could be argued that the peak and residual strengths of the smectite clay forming the slide surface are similar, based on the recorded liquid limits (> 120) (Hancox et al., 1980; Phoon and Kulhawy, 1999).

2.2.2 The shear strength of the slip surface

The behaviour of reactivated translational slides is governed by the Mohr-Coulomb failure criterion, in particular by the ratio of shear force to normal force on the sliding surface, with slip occurring when the Mohr-Coulomb failure criterion is met (Terzaghi and Peck, 1948). The shear strength (τ_f) of a soil at a point on a particular plane was originally expressed by Coulomb as a linear function of the normal effective stress (σ') on the plane at the same point (Craig, 1997) where *c'* (apparent cohesion) and ϕ' (friction angle) are the shear-strength parameters in terms of effective stress, (Figure 2.12 and Equation 2.1).

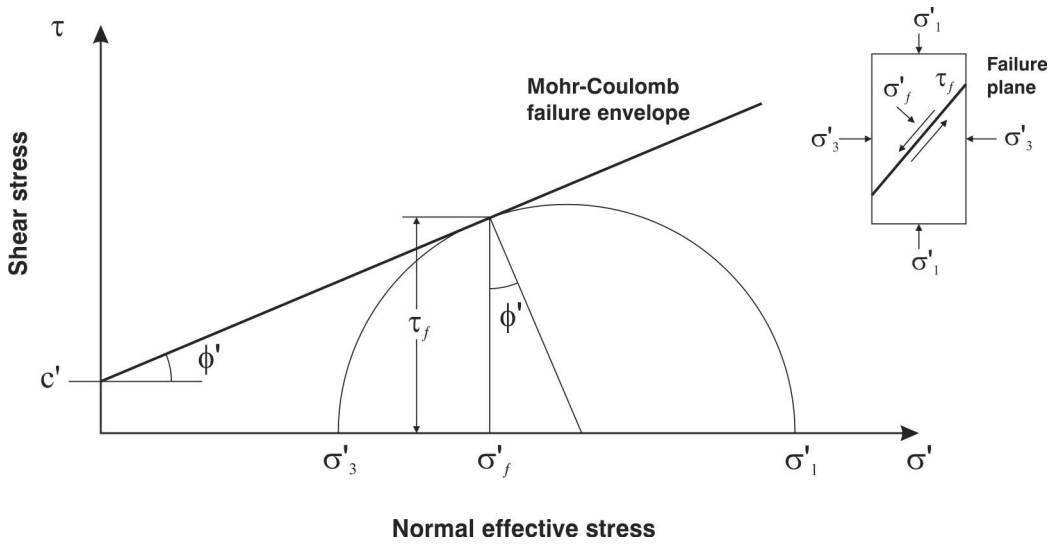

Figure 2.12 The Mohr-Coulomb failure envelope (source: Craig. 1997).

$$\tau_f = c' + \sigma' . \tan \phi' \qquad \text{Equation 2.1}$$

Failure will occur at any point where a critical combination of shear stress and effective normal stress develops or is exceeded (Craig, 1997). Under pseudo-static conditions, the shear stress operating along the slip surface, and therefore landslide acceleration, depends on variations in the resisting force caused by pore-pressure induced changes (including changes in seepage forces) of effective stress (Picarelli 2007), and changes in material properties (Terzaghi and Peck, 1948; Lupini et al., 1981; Skempton, 1985).

As these landslides displace along a pre-existing shear surface, it is assumed in most cases that the materials on the slip surface are remoulded and at post-peak or residual values. Skempton (1985) found that for both normally-consolidated and over-consolidated clays, the post-peak drop in drained shear strength to residual values is due entirely to destruction of the original soil structure and particle reorientation. A Keynote paper prepared by Morgenstern (1995) suggests that the movement of slow landslides is regulated by a combination of factors. He states: “In addition to rate-

dependence of residual strength of clay, it was noted that the velocity of sliding would also be influenced by the geometrical complexity of the landslide mass. Thickness, water pressure distribution, slope of slip surface, lateral restraint due to channelisation and other factors vary from place to place in all but the simplest landslides. Hence not all locations within a landslide would be mobilized simultaneously and the velocity would be moderated".

2.2.3 Rainfall and pore pressure as movement triggers

Individual landslides can have many causes, including geological, morphological, physical and human causes (Cruden and Varnes 1996), but typically only one trigger (Varnes, 1978). The four main triggers for inducing movement of reactivated landslides, like first-time failures, are thought to be: 1) rainfall-induced groundwater rises; 2) earthquake ground shaking; 3) drainage-line incision; and 4) anthropogenic activities, (Schuster and Highland, 2007; Mansour et al., 2010). By definition, a trigger is an external stimulus such as intense rainfall, earthquake shaking, volcanic eruption, storm waves or stream erosion that causes a near immediate response in the slope by rapidly changing the stresses or by reducing the strength of slope materials (Wieczorek, 1996). In some cases landslides may occur without any obvious trigger. This may be due to a variety of causes, but principally "static fatigue" (Petley and Allison, 1997), that gradually bring the slope to failure, a process termed "slope ripening".

Landslides therefore, initiate when the shear stress (the driving force that causes downslope movement of slope materials or the "external" force) is greater than the shear resistance of the material (the resistance of movement or the "internal" force) (Terzaghi, 1950). Their relative relationship is expressed as the factor of safety (*F*), which is a ratio between the shear resistance and the shear stress (τ) (in the case of reactivated landslides, the residual shear strength τ_{fr}). Using this ratio the slope is assumed to be in a stable condition when $F \geq 1$ but unstable when $F \leq 1$. The infinite slope method for non-circular failure surfaces, such as those methods proposed by Morgenstern and Price (1965) or Sarma (1973), incorporates the Mohr – Coloumb failure criterion (Equation 2.1) with the two-dimensional landslide geometry to simply estimate the factor of safety:

$$F = \frac{c' + (\sigma_n - u).\tan\phi}{\sigma_n.\sin\alpha, \cos\alpha} \qquad \text{Equation 2.2a}$$

$$\tau = \sigma_n.\sin\alpha.\cos\alpha \qquad \text{Equation 2.2b}$$

where σ_n is the total normal stress, u is the pore-water pressure and $\sigma_n - u$ is the

effective stress, as originally defined by Terzaghi, (1936), α is the angle of the slide surface and τ is the shear stress. *F* can be calculated for any point on the shear surface where the depth of movement and pore pressure conditions are known. This method assumes that the slope extends for a relatively long distance, has a consistent subsoil profile, the failure plane is parallel to the surface of the slope and is planar in nature and therefore not appropriate for use on circular slip surfaces..

Based on this equation, the triggering mechanism of rainfall-induced landslides can be attributed to the increase of pore water pressure. This has been termed “hydrological triggering” by Terlien (1998). On a natural slope receiving rainfall, the shear stress is approximately constant due to gravity. However, the increase of pore pressure as a result of rainfall infiltration progressively reduces the normal effective stress of the slope materials acting on a shear surface. The shear resistance decreases as the inter-particle friction is reduced by the buoyancy force and eventually reaches a critical value equal to the shear stress (i.e. F = 1), with slip occurring when the Mohr-Coulomb failure criterion is met.

The infinite slope method (Equation 2.2a), is one of many limit equilibrium analyses techniques that are routinely applied in geotechnical practice. Limit equilibrium analyses, however, can only determine the triggering conditions. As such, the factor of safety has been criticised as an “all-or-nothing” approach that simply defines slopes as either stable or unstable (Helmstetter *et al.*, 2004; Sornette *et al.*, 2004; Ng, 2007), and cannot explain the movement style and displacement rates recorded in the field (Leroueil et al., 1996).

Field measurements of landslide motion show that the cumulative displacement patterns of several reactivated landslides can be linked to changing pore pressures. For example, the different movements patterns proposed by Allison and Brunsden (1990) and Petley et al., (2005) can be related to seasonal fluctuations of pore water pressure (e.g. Bhandari, 1988; Allison and Brunsden, 1990; Petley et al., 2005), (Tables 2.02 and 2.03) and geomorphic position on the landslide. However, these relationships depend upon all other destabilising factors, such as changes in the shear strength of the materials and load, to remain constant. The relationship between pore pressure and landslide movement is also complicated by the complex landslide hydrogeology, in particular by the contrasting permeability of intact, fissured and sheared materials forming the slide mass, and the presence of large-scale heterogeneities providing direct conduits for surface water into the landslide (e.g. Corominas et al., 1999; van Asch, et al., 2007)

Table 2.02 Patterns of mudslide movement in relation to pore water pressures, in the Wealden Beds of the Isle of Purbeck, Dorset (redrawn from Allison and Brunsden, 1990 and modified by Ng, 2007).

Movement type	Displacement characteristics	Related pore water pressures (PWP)
A) Stick slip	Small individual spatial movements < 1 cm Total displacement up to 0.08 m Separated by varying time intervals with zero displacement	Slowly rising PWP Slowly declining PWP
B) Graded slip	Larger gradual spatial movements over proportionally shorter time periods (maximum displacement record: 35 cm in 17 hrs)	Gradual rise in PWP Rapid rise followed by declining PWP
C) Surge	Large spatial displacement over short time periods (3 m in 20 mins)	Highest rate of increase in PWP
D) Random	Small, irregular slips through space and time	Related to other factors, such as internal deformation, effects of plasticity, seasonal cycles and gravitational forces

Table 2.03 Patterns of landslide movement in relation to pore water pressures for the Tessina landslide, Italy (redrawn from Petley et al., 2005 and Ng, 2007).

Movement type	Displacement characteristics	Related pore water pressures
Type I	Very slow movements at less than 1 mm/day; consist of slow creep	Increase in velocity associated with wetter winter months
Type II	Low velocity movements 2-3 mm/day Typical block movements; highly variable movement rate	Gradual rise in PWP Faster movements occur during months with high groundwater levels
Type III	Movement rates at 10 mm/day; creep occurs at similar, continuous rates	Relatively small seasonal fluctuations
Type IV	Episodic, very rapid movements. Movements initiated rapidly and terminate abruptly, but static in between movement events Peak rates more than 1-2 m/day	Periods of reactivation associated with wetter winter months when PWP are seasonally high

2.3 Problems in assessing the mobility of slow-moving landslides

It has been found by several researchers that the relationship between pore pressure and landslide acceleration is non-linear (e.g. Skempton, 1985; Corominas et al., 2005; Gonzalez et al., 2008; Matsuura et al., 2008), implying that the relationship between shear stress and normal stress, as assumed by the Mohr-Coulomb failure criterion is non-linear. In addition, Bertini et al. (1984) and Gonzalez et al. (2008) showed that different values of landslide acceleration were recorded for the same value of pore pressure (Figure 2.13). It has been hypothesised that landslide velocity, although clearly linked to pore-pressure-induced changes in effective stress, is also governed by rate-induced changes in shear strength of the materials, caused by behaviour of the clay

particles during shearing (Lupini et al., 1981; Skempton, 1985; Angeli et al., 1996; Picarelli, 2007); and/or consolidation and strength regain during periods of rest (Nieuwenhuis, 1991; Angeli et al., 2004). It has also been proposed that shear-strength parameters, represented as c' and ϕ' in the Mohr-Coulomb failure criterion, can be modified by inclusion of a viscous resistance component (Bertini et al., 1984; Leroueil et al., 1996; Corominas et al., 2005; van Asch, 2007; Picarelli, 2007; Gonzalez et al., 2008). Many authors have used viscosity functions to better describe and in some cases predict the motion patterns of these types of landslide assuming that once motion is triggered the landslides move by visco-plastic flow, rather than by rigid-plastic frictional slip, e.g. Iverson (1985), Angeli, et al., (1996); Corominas et al., (2005); van Asch et al., (2008); Ranalli et al., (2009).

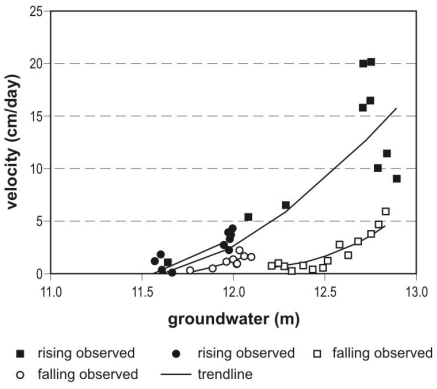

(A): Relationships between velocity and groundwater height in the La Valette landslide, for respectively two periods of rising and falling groundwater level (Van Asch et al., 2007).

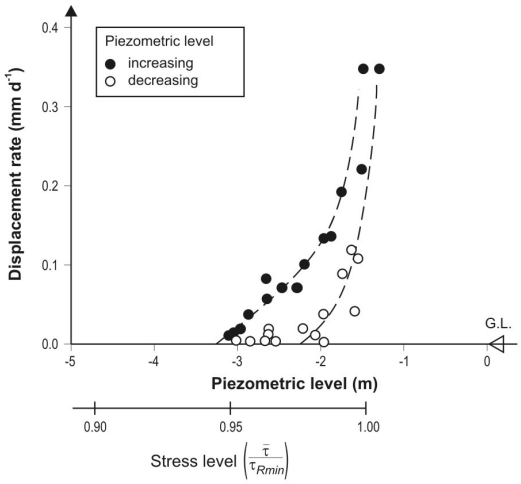

(B): Relationship between displacement rate and water level for the Fasio San Martino landslide (central Italy) (from Bertini et al., 1986).

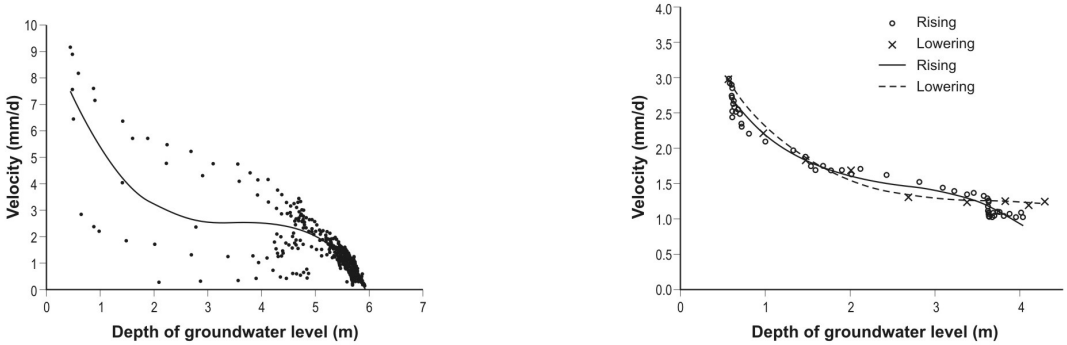

(C): Landslide velocities versus water table depths for the Vallcebre landslide in the Eastern Pyrenees, Spain. Data correspond to mean daily values, for the periods: November 1996 to August 1998; and december 1996.

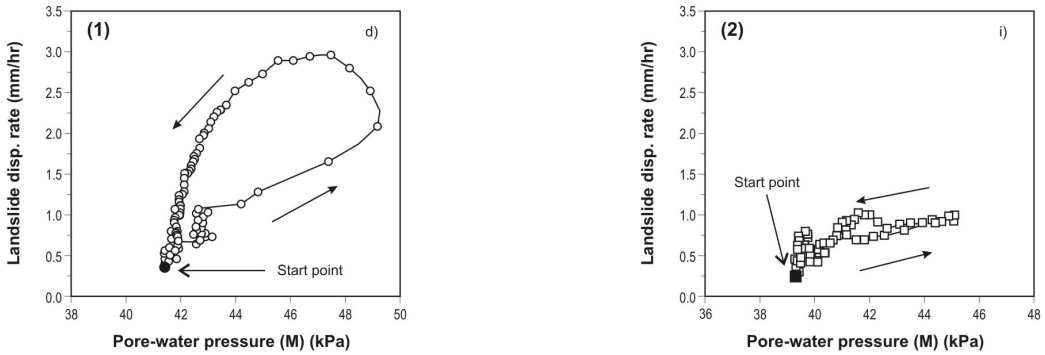

(D): Hysteresis relationship between pore water pressure and landslide displacement for a landslide in the Tertiary materials of Japan (Matsuura et al., 2008).

Figure 2.13 Groundwater and velocity graphs for landslides where different values of landslide velocity were recorded for the same value of pore pressure.

2.3.1 Rate effects

Rates of landslide displacement on pre-existing shear surfaces can vary by many orders of magnitude from extremely slow movement to extremely rapid (< 16 mm/year to > 5 m/second, Cruden and Varnes 1996). For several large reactivated rock slides in Tertiary-age sedimentary materials of New Zealand, the recorded average landslide

speeds vary between 0.3 to 0.5 mm/day for the Taihape landslide, 1 to 27 mm/day for the Utiku landslide, 10 to > 400 mm/day for the Abbotsford landslide (Hancox et al., 1980) and up to 430 mm/day for the Deans landslide (McSaveney and Griffiths 1987). Changes in the residual shear strength of the slide surface materials could be caused by changes in movement (shear) rate. Rate induced changes in shear strength could therefore be an important control on landslide movement.

Skempton (1985) using the results from ring-shear tests on clays carried out by Petley (1966) and Lupini (1981), found that when sheared at slow rates the average change in strength is less than 2.5% per order of magnitude variation in shear rate, and that variations in strength within the usual range of slow laboratory tests (0.0001 to 0.01 mm/minute or 0.1 to 14.1 mm/day) are negligible (Figure 2.14). From ring-shear tests on clays sheared at higher rates, an increase in strength becomes pronounced at rates exceeding 100 mm/minute, when a qualitative change in behaviour occurs (Figure 2.15). Lupini et al. (1981) and Skempton (1985) suggested that this behaviour was probably associated with the disturbance of the originally ordered structure, and termed it 'turbulent shear'. Some disturbance appears plausible, as when sheared at rates ~ 300 mm/minute followed by reimposed lower rates of shear a peak in strength is observed, with resistance falling to the residual only after considerable further displacement (Skempton, 1985). However, this process cannot involve turbulence. Nieuwenhuis, (1991) and Angeli et al., (2004), suggest that once residual strength has been achieved and shearing has stopped, consolidation of the shear band may lead to strength regain, attenuating the likelihood of reactivation (van Asch et al., 2007), i.e. consolidation theory.

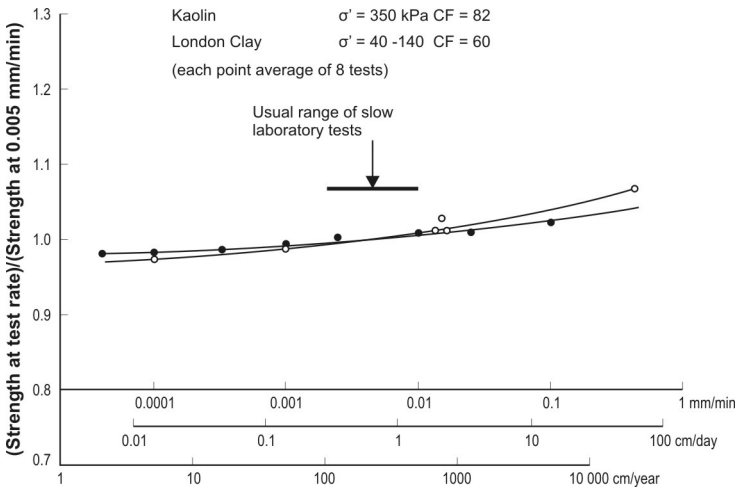

Figure 2.14 Variation in residual strength of clays at slow rates of displacement (source: Skempton, 1985).

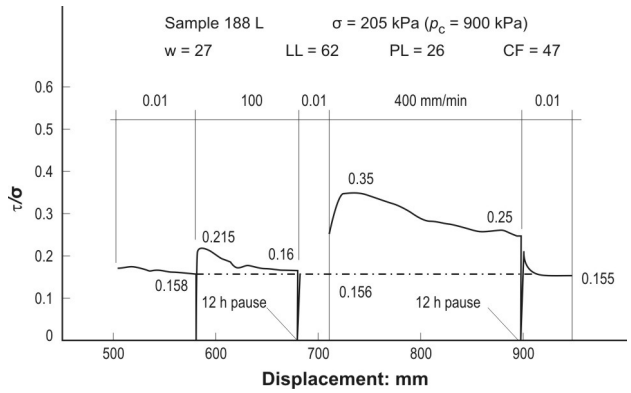

Figure 2.15 Kalabagh Dam ring-shear test, August 1983. (source: Skempton, 1985).

2.3.2 Dynamic viscosity

To investigate these differences, several authors have modified the Mohr-Coulomb failure criterion to include a viscosity component, assuming that the material along the slip "surface" is a layer with a finite thickness and behaves as a visco-plastic material (fluid) during periods of landslide acceleration (e.g. Bertini et al., 1984; van Asch, 2007; Picarelli, 2007; Gonzalez et al., 2008). However, in reality, displacement occurs by slip along a large number of shear surfaces within the material forming the slide "surface", and the material between these shear surfaces is also likely to deform plastically. Therefore not all of the material forming the zone of deformation has to deform during a period of displacement; instead, the width of the shear band mobilised during a particular displacement period can change and may do so as a function of the applied stress. Unlike Coulomb friction which ignores the thickness of the shear zone, viscosity takes the shear-zone thickness into account.

Viscosity is defined as the resistance of a liquid to shear forces (Newton). In any flow, there is generally a gradient in shear across the flow and the fluid's viscosity (which determines the shear gradient) arises from the shear resistance across the flow. Several flow models have been proposed to describe the mobility of slow-moving landslides. Flow models based on Bingham's law are frequently used (e.g. Yen, 1969; Van Genuchten, 1988; van Asch, 1990; Angeli et al., 1996; Corominas, 2005), (Equation 2.3):

$$\frac{dV}{dZ} = \frac{1}{\eta}.(\tau - \tau_0) \qquad \text{Equation 2.3a}$$

$$\tau_0 = (\sigma - u).\tan\phi'_r \qquad \text{Equation 2.3b}$$

$$\tau = \sigma.\sin\alpha.\cos\alpha \qquad \text{Equation 2.3c}$$

Note equation 2.3b is the Mohr Coulomb failure criterion. V is the relative velocity (m/s), Z is the depth, η is the dynamic viscosity (GPa s), τ is the shear stress (kPa), τ_0 is the threshold shear stress (kPa) (or residual shear strength) calculated using the Mohr-Coulomb failure criterion, σ is the normal stress (kPa), u is the pore pressure (kPa), ϕ'_r the residual friction angle (c' = 0 when relative motion is occurring), and α is the angle of the slip surface (Corominas et al., 2005; van Asch et al., 2007). For narrow shear bands < 5 cm, van Asch et al., (2007), found that one could assume a straight velocity profile (Newtonian viscosity) and thus a linear relationship between the velocity and depth, giving:

$$V = \frac{h_m}{\eta}.(\tau - \tau_0) \qquad \text{Equation 2.4}$$

where h_m is the thickness of the slip surface (m). For large ranges of excess stress (τ - τ_0) it has been found that the relationship is non-linear (Bertini et al., 1984; Salt, 1988; Bracegirdle et al., 1991; Cornforth and Vessely, 1991):

$$V = \frac{h_m}{\eta_0}.(\tau - \tau_0)^b \qquad \text{Equation 2.5}$$

The exponent b can be interpreted as a non-Newtonian viscosity and can be derived from back analyses, while η_0 (the apparent viscosity at zero shear) can be considered as the "intrinsic viscosity" of the material (van Asch et al., 2007).

These concepts have been applied to several flow-type landslides to predict their movement patterns (e.g. van Asch et al., 2007), using both laboratory ring-shear tests and back-analyses. Some authors have applied them to translational slides but with limited success (Picarelli, 2004; Corominas et al., 2005). Van Asch et al. (2007) found that there were significant discrepancies between laboratory-scale and field-scale viscosity parameters. These variations were thought to have been due to one or a combination of:

(1) Errors in calculating the excess shear stress and that the excess shear stress may not be constant over the landslide, and that the infinite-slope model used to calculate these values was too simplistic;
(2) Apparent viscosity can be generated by negative as well as positive pore pressures and confound the truly intrinsic viscous behaviour of the material;
(3) The intrinsic viscosity changes with effective stress and is therefore a function of

pore pressure and seepage forces;

(4) Identifying and measuring the thickness of the shear band, and testing techniques used to determine its parameters.

Other models, such as Voight's semi-empirical time-dependent failure criterion (Voight, 1989), have been used as a tool to forecast the failure of large rock slides using monitoring data, however, it can only be applied to data characterised by continuous acceleration and constant external conditions (Crosta and Agliardi, 2002), severely limiting its application to reactivated landslides.

2.3.3 Temporal and spatial monitoring data resolution

The movement of extremely slow to slow reactivated slides has often been assumed to be uniform with time (governed by creep), mainly because monitoring frequency has failed to resolve variations (Picarelli, 2007). However, many such landslides show time-variable motion with distinct movement patterns (Petley et al., 2005).

In many studies, a thorough analysis of movement patterns and mechanisms is inhibited by poor temporal and spatial resolution monitoring data. As a result many landslide monitoring projects are unable to link movement to its cause and in some cases doubts can be raised as to whether the data adequately represents the conditions and processes controlling the landslide. Schulz et al. (2009b) base their analyses of the Slumgullion landslide in Colorado, USA, on data collected at two locations. Although a very novel study, the data represents only two points on a landslide that is several kilometres long, where the depth of landslide movement is not well constrained and where measured pore pressures may not represent pore-pressure conditions along the slide surface.

2.4 Types of monitoring equipment

A review of the different field sensors currently available for landslide monitoring has been undertaken to determine which sensors would be most applicable to monitoring these types of slow moving landslide, considering the extremely slow to slow rates of movement and apparent susceptibility to small changes in pore pressure.

2.4.1 Field sensors

2.4.1.1 Movement monitoring

The landslide type, velocity (bearing in mind slow slides can become rapid earthflows), and site constraints dictate the type and nature of the equipment deployed to monitor displacements. The wide range of landslide type and movement styles mean that some

equipment may be appropriate for one landslide type but not for another. In most reactivated landslides in Tertiary-age, sediments of New Zealand the recorded landslide displacements vary between 0.3 and >400 mm/day (Williams and Sinclair, 2010).

In some circumstances, where direct surface measurements are either not required or too difficult to monitor, ground deformation surveys can be carried out using remote sensing techniques such as airborne light detection and ranging equipment (LIDAR), interferometric synthetic aperture radar (InSAR) and terrestrial laser scanning (TLS). Both airborne LiDAR and terrestrial laser scanning have been particularly effective for quantifying change (e.g. Massey et al., 2010). InSAR and airborne LiDAR are costly and take time to implement and repeat. While TLS surveys can be implemented more rapidly, the reduction of the data can take considerable time. The temporal resolutions of such remote-sensing approaches, however, are limited, making it difficult to link movement to the cause. Table 2.04 summarises the advantages and disadvantages of the different direct measurement sensors currently available to monitor movement.

For direct surface movement measurements GPS and Robotic total stations offer the most advantages, as they are precise, typically mm to cm in horizontal and cm in the vertical and can be operated at high temporal resolutions. Both systems can be managed remotely but the robotic total station has potentially the highest spatial resolution, as prisms can be included into the monitoring network at relatively little cost.

Monitoring sub-surface displacements can be costly considering that the depth of the slide surfaces in these types of landslide are typically >20 m below ground level. To monitor displacement at these depths requires boreholes, into which monitoring equipment can be placed. The boreholes and inclinometer tubes tend to be sacrificial; however, they are a tried-and-tested method, where the equipment and techniques have been developed over many years.

Table 2.04 Monitoring equipment for the direct measurement of landslide movement

Description of monitoring equipment	Locations typically used	Advantages/disadvantages
Direct surface measurement		
Global positioning system (GPS and GNSS) In-situ single/dual-band receivers with antennae located on the object being monitored	• Slow slides • Landslide dams • Areas of ground settlement e.g. mining subsidence • Engineered structures (bridges, dams etc)	• Highly accurate and precise (mm to cm). The resolution depends upon measurement epoch • High temporal resolution (e.g. ability to record one second epoch) • Poor spatial coverage as one receiver will monitor one point, creating a significant cost component when more than one is required. • Can be operated remotely or manually • Requires complex post-processing for maximum precision, but can be run in near-real time, if a communications network is established • Software is expensive • Takes time to install and set up
Robotic total station A robotic total survey station used to find and measure targets (prisms) located on the monitoring object at set time intervals	• Slow slides • Landslide dams • Areas of ground settlement e.g. mining subsidence • Engineered structures (bridges, dams etc)	• Highly accurate and precise (mm to cm) • High temporal resolution (user defined) • Good spatial coverage/ resolution (depends upon number of survey prisms installed) • No post processing of data (software automatically calculates and displays the movement data) • Takes time to install and set up
Tilt meters Tilt meters are used to monitor changes in the tilt of a structure. Tilt changes may be caused by construction activities, such as excavation, tunnelling, and dewatering, that affect the ground that supports the structure. Changes in tilt may also result from loading of a structure, such as the loading of a dam during impoundment, the loading of a diaphragm wall during excavation, or the loading of a bridge deck due to wind and traffic	• Stabilisation measures, such as pressure grouting and underpinning • Structures for the effects of tunnelling and excavating. • Stability of structures in landslide areas • Deflection and deformation of retaining walls • Convergence and other movements in tunnels	• Highly accurate and precise (mm to cm) • Typically used to measure deformations of structures in response to ground deformation • Not typically used to measure direct ground deformation • If fixed tilt meters are used, then they can be measured remotely at high temporal resolutions • Data requires post processing • Translational movements not detected

Description of monitoring equipment	Locations typically used	Advantages/disadvantages
Extensometers Extensometers are used to measure movements of soil and rock along a single axis. Numerous types of extensometer are available *The Rod Extensometer* consists of anchors set at specified depths/distances, rods inside protective tubing, and a reference head. Measurements are taken at the reference head by micrometer or by an electric sensor *The Magnet Extensometer:* consists of a series of magnets that are installed with an access pipe. The magnets are anchored at specified depths. Measurements are taken by lowering a probe through the access pipe to detect the depth of the magnets.	• Settlement in excavations, foundations, and embankments • Subsidence above mines and tunnels. • Movements in rock slides, walls, and abutments • Consolidation of soil under embankments and surcharges • Compression of piles and soil under piles • Monitoring spread in embankments • Convergence in underground openings, such as tunnels	• Highly accurate and precise (mm to cm) • Rod extensometers: can be automated, and read remotely, works in any orientation and can measure multiple points. Limited measurement range (50 to 100 mm) • Magnet extensometers: can monitor large settlements; works with inclinometer casing and can supplement inclinometer data, relatively easy to operate, indicates incremental settlements. Cannot be automated, practical limit of 15 or 20 magnets, vertical installation only
Accelerometers (accelerograph) Records ground shaking (accelerations) in response to earthquakes (as a movement trigger), or in response to landslide movement	• Rapidly moving landslides • Ground accelerations from earthquakes etc	• To identify landslide movement multiple sensors are needed around the landslide • Requires post processing of data • Require accurate seismic-velocity structure in geological model • Difficult to differentiate periods of movement from 'back-ground noise' • Topographic effects need to be taken into account • May not be able to record low-strain rate displacements (i.e. creep-style movements)
Direct sub-surface measurement		
Time-domain reflectometry A coaxial cable is installed in a borehole and grouted in place. A test unit is used to generate a voltage pulse along the cable as well as to record the reflections. Reflections are generated by cable deformations, abrasions and severing. Crimps along the cable at set intervals are used to provide a depth datum. As movement occurs, the reflections along the cable change, as the cable deforms	• Rock and soil movement e.g. landslide displacements • Subsidence e.g. above abandoned mine workings • Structural deformations e.g. retaining walls	• Highly accurate and precise (mm to cm), but becomes less accurate with depth/length of cable used • High temporal resolution • Requires borehole installation, therefore spatial resolution depends on borehole coverage • Requires backfill material to have similar properties to the soil/rock • Post processing of data required through custom software

Description of monitoring equipment	Locations typically used	Advantages/disadvantages
Inclinometers An inclinometer casing is permanently installed in a borehole that passes through a suspected zone(s) of movement. Inclinometer casing can also be embedded in fill, buried in a trench, cast into concrete, or attached to a structure. When installed in boreholes the casing is grouted in-situ typically using a bentonite/grout mix. Important features include the diameter of the casing, the coupling mechanism, groove dimensions and straightness, and the strength of the casing. A probe is then used to measure defections/shears in the casing. Two measurement options exist: 1) a portable traversing probe; and 2) an in-situ system *Portable system:* The traversing probe obtains a complete profile because it is drawn from the bottom to the top of the casing. The first survey establishes the initial profile of the casing. Subsequent surveys reveal changes in the profile of the casing if movement has occurred *In-situ system:* In-place inclinometer sensors are placed at specific depths to span a zone of suspected movement. They are left in-place (unlike the traversing probe) and usually monitored continuously to ensure safety. The costs for an in-place system are greater because the sensors are dedicated to a particular installation	• Slopes and landslides • Engineered structures to check that deflections are within design limits • Effects of tunnelling operations to ensure that adjacent structures are not damaged by ground movements • Applications for horizontal inclinometers include: providing settlement profiles of embankments, foundations, and other structures	• Used to identify movement zones, and can be used to monitor velocity and changes in velocity. However, these systems have a limited life due as movement can lead to shearing of the casing • Require borehole installation, therefore spatial resolution depends on borehole coverage • Precision ±6 mm per 50 readings • Temporal resolution depends on system type, e.g. portable or in-situ. In-situ systems have high temporal resolution, but are costly and require advance knowledge of the movement zone. Portable systems are read as/when required and therefore the temporal resolution will vary, but daily and weekly reading frequencies are unlikely due to logistical issues

2.4.1.2 Movement triggers

An important aspect of this research is to be able to closely link specific changes in movement to the time-varying factors that influence them. Typical factors that influence landslide movement rates are: rainfall; changing pore pressures at locations within the landslide; loss of toe support (or gain of head load) and earthquake induced ground accelerations. In some circumstances, the factors are internal and time and (or) displacement dependent (e.g. slope maturation, and strain or strain-rate hardening).

Table 2.05 outlines the types of monitoring equipment available and currently in use by landslide researchers, the situations (landslide types) where the equipment is best utilised, and some discussion on the advantages and disadvantages relating to particular types of equipment.

Table 2.05 Monitoring equipment for recording landslide triggers

Monitoring Equipment	Locations used	Advantages/disadvantages
Water level (Vibrating wire and bubbler systems) To record groundwater levels in landslides, or immersed in lake to measure filling rate, static levels or draw down in the event of breaching	• Landslide dammed lakes • River levels along the flow paths of break out floods/debris flows • Groundwater levels within slow moving landslides	• High temporal resolution (e.g. ability to record 30 second epochs) • Does not require post processing of data • Requires data logger • Requires calibration
Rain gauge (0.2 mm tipping bucket) To provide information on rainfall in the catchment/landslide area, with relevance to filling rate (landslide dams), or as a trigger for landslide movement	• All landslides including landslide dams	• High precision, but not always accurate (records rainfall as and when it occurs using a 0.2 mm bucket) • Requires data logger • Not useful for snow, and may record dew and hoar frost
Strong motion accelerograph To record ground shaking in response to earthquakes (as a movement trigger)	• All landslides • Debris flow (including lahar) travel paths • Landslide dam breach floods	• Good for assessing ground shaking intensities in response to nearby earthquakes (very little data exists for movement triggering MMI values), or landslide movement • Also used to assess whether strong ground shaking triggered landslide movement • Requires post processing of data
Visual monitoring Time-lapse still cameras used to capture sequential photographs of landslide/dam failure sequence	• Debris flow (including Lahar) travel paths • Down stream of dam-break floods • Landslide dams • Loss of toe support	• Good for capturing failure sequences and processes, and toe erosion • Generates large volumes of data, which may be difficult to transfer via a communication network

2.5 Summary

This chapter has reviewed the literature on the movement patterns and mechanisms of large, deep seated, reactivated translational rock slides-earth flows and discussed some of the advantages and disadvantages of the equipment and methods that can be used to monitor them.

Current gaps in the research of these types of landslide include:

- **Temporal resolution of landslide monitoring data** – Their movement has often been assumed to be uniform with time (governed by creep), mainly because monitoring frequency has failed to resolve variations (Picarelli, 2007). However, as quasi-continuous monitoring data become available, many landslides show time-variable motion with distinct movement patterns believed to be driven largely by pore-pressure changes occurring over short periods of time (Van Genuchten, 1988; Petley et al., 2005; Picarelli, 2007). Despite the empirical evidence, there is little research describing the detailed dynamics of such relations (both pore-pressure and earthquake-induced reactivations). This is in part due to the fact that in the past it has proven difficult to monitor landslide movement and pore-pressure changes within the landslide mass with sufficient temporal resolution (Gonzalez et al., 2008). As a result, many monitoring programmes fail to link specific periods of landslide movement to the appropriate triggering factor (e.g. Massey and Nelis, 2008).

- **Relationship between pore-pressure and landslide movement** – Velocity changes (accelerations) in these landslides are thought to be controlled by changes in water levels (e.g. Bertini et al., 1984; Nakamura, 1984; Picarelli, 2004; Corominas, 2005; van Asch, 2007; Gonzalez et al., 2008). Corominas et al., 2005, Gonzalez et al. (2008), and Matsuura et al. (2008), found that velocity increased non-linearly as pore pressure increased. In addition, Bertini et al., (1984) and Gonzalez et al., (2008) showed that for the same value of pore pressure, the velocity when groundwater was rising was higher than during lowering (Picarelli, 2007). The relationship between pore pressure (groundwater) and landslide movement is complicated by the complex landslide hydrogeology, in particular by the contrasting permeability of intact, fissured and sheared materials forming the slide mass, and the presence of large-scale heterogeneities providing direct conduits for surface water into the landslide (e.g. Corominas et al., 1999; van Asch, et al., 2007). Consequently, large, slow slides often show an erratic and complex response to water input (Corominas, 2000; Malet; et al., 2005; van Asch et al., 2007).

- **Constraints on movement –** It has been hypothesised that landslide velocity, although linked to pore-pressure-induced changes in effective stress, is also governed by rate-induced changes in shear resistance (Petley, 1966; Lupini et al., 1981; Skempton, 1985; Lemos, 1986; Angeli et al., 1996; Picarelli, 2007). The relationship between landslide velocity and the apparent viscosity of soil along the slip surface has been investigated by several authors, with deceleration linked to increasing viscosity (e.g. Bertini et al., 1984; Corominas et al., 2005; Picarelli, 2007; van Asch, 2007; Gonzalez et al., 2008). These changes in viscosity may be a function of the changing material properties of the clay in response to strain and/or changes in strain rates. Other factors such as landslide geometry e.g. buttressing of slide blocks and shear resistance developed along the landslide flanks and between the slide blocks may also control the movement arresting processes (Morgenstern, 1995).

CHAPTER 3 SITE DESCRIPTION

3.1 Introduction

This research focuses on two large (> 1M m^3), complex, reactivated translational rockslide-earth flows (Cruden and Varnes, 1996), or block slides (Panet, 1969), in Tertiary-age sedimentary rocks of North Island New Zealand: the West Taihape (39°40'S, 175°47'E); and the Utiku Landslides (39°45'S, 175°50'E) (Figure 3.01). These active landslides have long histories of monitoring (1930 to present) and they continue to damage infrastructure and property.

The selection of the two landslides was based on the following criteria:

(i) Representativeness – the selected landslides should represent the typical characteristics of large, deep-seated, reactivated translational slides, which are typically moving at rates varying from extremely slow to very slow (Cruden and Varnes, 1996).
(ii) Activity – only landslides that are currently active should be selected, bearing in mind the short-duration of the monitoring with regards to the extremely slow to very slow movement rates of the landslides.
(iii) Accessibility – the selected landslides should be accessible in consideration of safety of the field workers during equipment installation. In addition, the sites should render equipment maintenance and ongoing investigative works feasible.
(iv) Historical data – historical monitoring and ground investigation data should be available for the landslides, allowing the proposed monitoring to be put into a longer historical framework.
(v) Utility – the monitoring should benefit any stakeholders with assets located on the landslides. The latter provides commercial incentive to invest the substantial capital and resources required for their detailed investigation that are not commonly available for academic research.

Tertiary-age sedimentary rocks cover approximately 17% of the New Zealand surface area and are host to many large landslides. The West Taihape (hereinafter shortened to Taihape) and Utiku landslides are two of over 7,000 mapped large landslides (> 10,000 m^2 in plan area) in these materials (Dellow et al., 2005), the majority of which comprise deep-seated (i.e. depth of movement typically > 10 m), translational landslides. This chapter details the geological and geomorphological setting of the two landslides and the historical geotechnical investigations and monitoring that have been carried out to assess them. These data are then synthesized and engineering-geological conceptual models for each are presented.

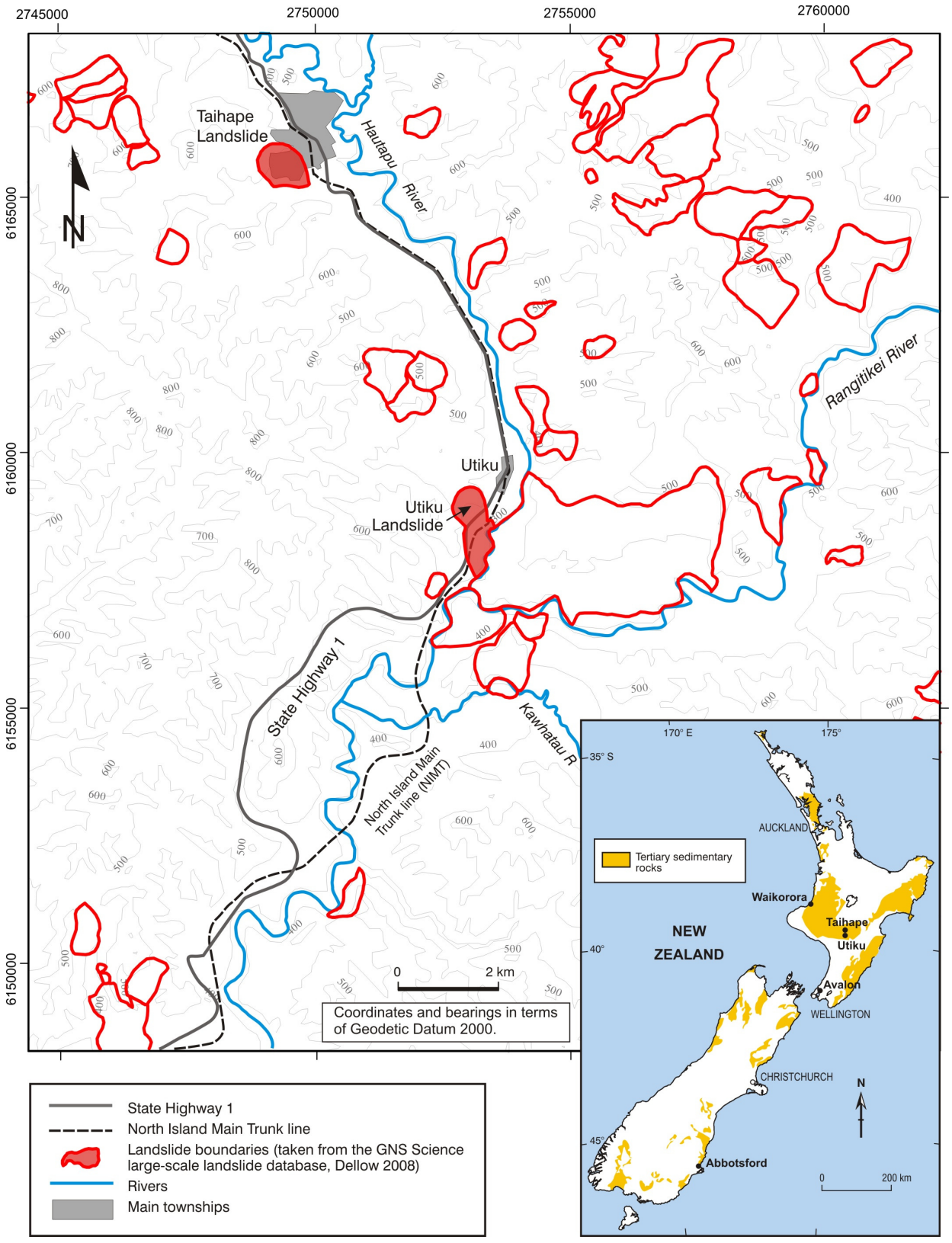

Figure 3.01 Map showing the location of the Utiku and Taihape landslides in New Zealand, along with the extent of Tertiary-age sedimentary rocks found at surface. Contours derived from Land Information New Zealand, 1:50,000 scale topographic map sheet 260, T22 and T21.

3.2 Geological setting

3.2.1 Geology

Regional geological mapping (QMap Series, Sheet 8, Lee et al., in prep) shows that both landslides have developed in Tertiary (2 to 65 million years old) sediments of the Wanganui Basin. The Utiku landslide is located south of, down dip from, and stratigraphically above the Taihape landslide (Figure 3.02).

The Utiku landslide developed at the boundary between Tarare Sandstone, part of the Utiku Group (Journeaux, et al., 1996), and underlying Taihape Mudstone (Thompson 1982), which is now referred to as the Tangahoe Mudstone (Naish and Kamp, 1995; Journeaux, et al., 1996; Lee et al., in prep). The Taihape landslide is within a sandy member of the Taihape Mudstone, which was referred to by Thompson (1982) as the Taihape Sandstone, and underlies the Tarare sandstone. Both the Tarare sandstone and Taihape mudstone are early Pliocene (3.6 to 5.3 million years) marine sediments.

In the field both the Tarare sandstone and Taihape mudstone are described as extremely weak to weak (NZGS, 2005), UCS <1 to 20 MPa, blue-grey (when fresh) or yellowish-brown (when highly weathered), very silty sandstones, with flattened (ovoid to irregular in shape) calcareous concretions (average diameter 0.2 m). Although classified as Taihape mudstone, the unit comprises an upper sandstone and a lower siltstone unit, with the Taihape landslide being within the upper sandstone unit. Concretions in both materials occur in distinct layers that are thought to represent bedding (Stout, 1977; Thompson, 1982). Bedding is also represented by about eight thin (2 to 20 mm thick) clay seams (Stout, 1977; Thompson, 1982).

The regional setting of the Taihape-Utiku area is tectonically dominated by gentle folds from east-west compression. This has lead to geologically relatively rapid uplift (Lee et al., in prep). The regional dip of bedding is approximately 3° – 7° towards the south-southeast (Thompson, 1982). The area is traversed by a series of NNE – SSW striking faults. The Taihape fault, strikes NNE – SSW through the western flank of the Taihape landslide, and is listed as an ‘active fault’ (Litchfield et al., 2007). An ‘active fault’ is defined as a fault that has moved in the last c.125,000 years, and is likely to move again in the foreseeable future causing a large earthquake (≥ M7) and possibly ground-surface rupture (Kerr et al., 2003). However, the activity status of the fault has yet to be confirmed in the field. The apparent fault trace is very short, about 500 – 700 m in length and there is some doubt as to whether it should be considered a potential earthquake-generating source. The closest faults to the Utiku landslide are the

Rangitikei and Rauoterangi fault zones, respectively 5 km west and 4 km east of Utiku, and striking NNE – SSW. A section of the Rangitikei fault 5km NW of Utiku is listed as active (Litchfield et al., 2007).

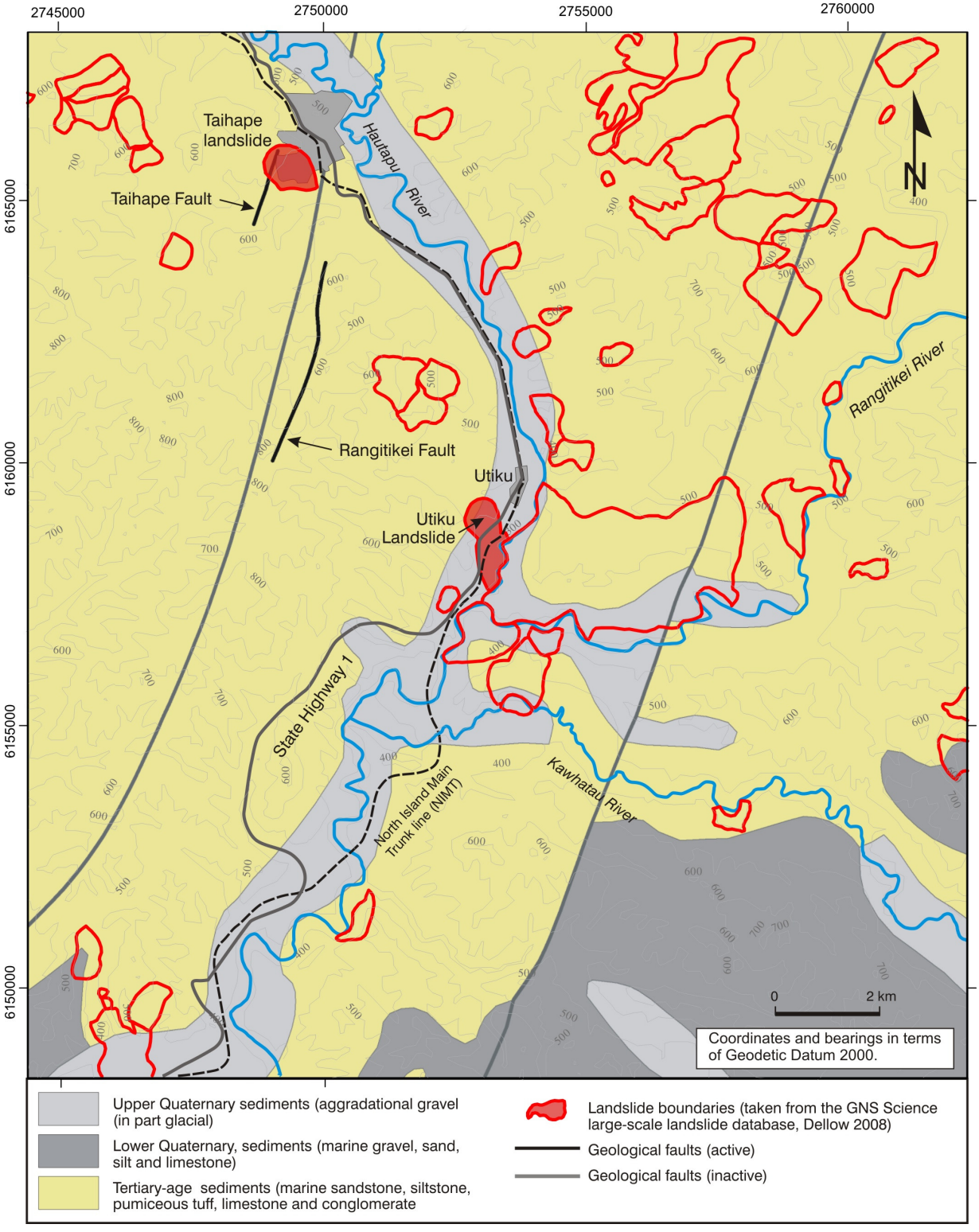

Figure 3.02 Map showing the regional geology of the Utiku and Taihape area (source: QMap Series, Sheet 8, Lee et al., (in prep).

3.2.2 Geomorphology

The Tarare sandstone and Taihape mudstone within the Taihape-Utiku area are deeply

incised by streams and rivers, with several different levels and ages of river terraces. These terraces are detailed and dated by Milne (1973a; 1973b) based on the different cover-beds of dated loess and volcanic-ash deposits. Subsequent work by Litchfield (2003) placed the terraces identified by Milne (1973a; 1973b) in a regional context, relating to the nine main rivers of the North Island, New Zealand, using radiocarbon and optically stimulated luminescence (OSL) dating techniques. The dating of the different terraces, loess and volcanic-ash deposits formed the basis from which Thompson (1982) derived an approximate time for initiation of these landslides. Thompson (1982) estimated that both landslides initiated between 1,800 and 11,000 BP, as they are mantled with tephra of the Tongariro Subgroup (dated 1,800 to 11,000 BP), (Thompson 1982; Litchfield 2003). However, the possible age range may be even broader because landslide initiation could easily pre- or post-date the deposition of tephra and tephra can be preserved during movement episodes. The relative disturbance of tephra is difficult to assess on the landslide as a result of ongoing movement and substantial anthropogenic changes.

3.3 Climate

The climate is temperate oceanic in the Köppen-Geiger classification, and characterised by warm summers (December through to February) where the average daily temperature is 22°C, and cooler winters (June to August), where the average daily temperature is 11°C. Rainfall does not vary much between winter (mean monthly rainfall 70 mm), and summer (mean monthly rainfall 81 mm), with total annual rainfalls of about 960 mm (Figure 3.03). These data for Taihape cover the 50-yr period 1951 to 2009 and are provided by New Zealand's National Institute of Water and Atmospheric Research (NIWA).

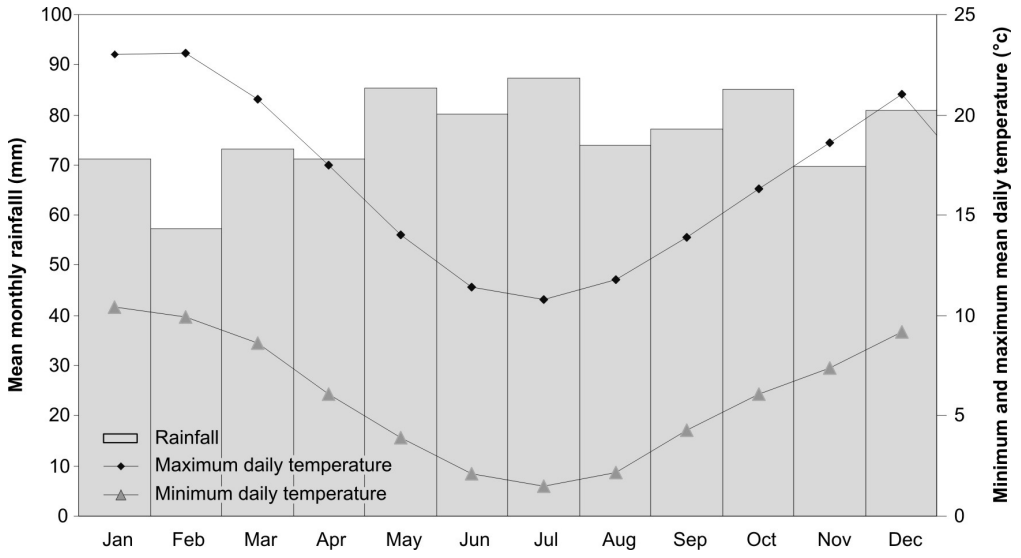

Figure 3.03 Taihape rainfall and temperature trends for the 50-yr period 1951 to 2009, provided by New Zealand's National Institute of Water and Atmospheric research.

3.4 Utiku landslide

3.4.1 Location

The Utiku landslide is crossed by State Highway 1 (SH1) and the North Island Main Trunk Railway Line (NIMT) 1 km south of the central North Island township of Utiku, about 7km south of Taihape in Rangitikei District. The landslide has two main parts; a historically active, and a historically inactive area (Figures 3.04, 3.05 and 3.06). Its total area (including the inactive and active slide areas) is about 800,000 m^2, with the active area being about 260,000 m^2. The landslide has been the subject of several studies, in particular following a major reactivation in 1964 (Belz, 1967; Ker, 1972; Stout, 1977). The active landslide is 1,100 m long, extending from SH1 in the north (the head scarp of the landslide), south to the Hautapu River (the landslide toe); it is 400 m wide.

3.4.2 Site history

Utiku landslide is thought to have initiated prehistorically at a similar time to that of the Taihape landslide (Thompson, 1982), however, no quantifiable data are available to support this assertion. Following reactivation of landslide movement in 1964, Toe Toe Road was realigned away from the landslide, and extensive engineering works to the NIMT alignment were undertaken. The landslide has been intermittently active, but less so since 1973.

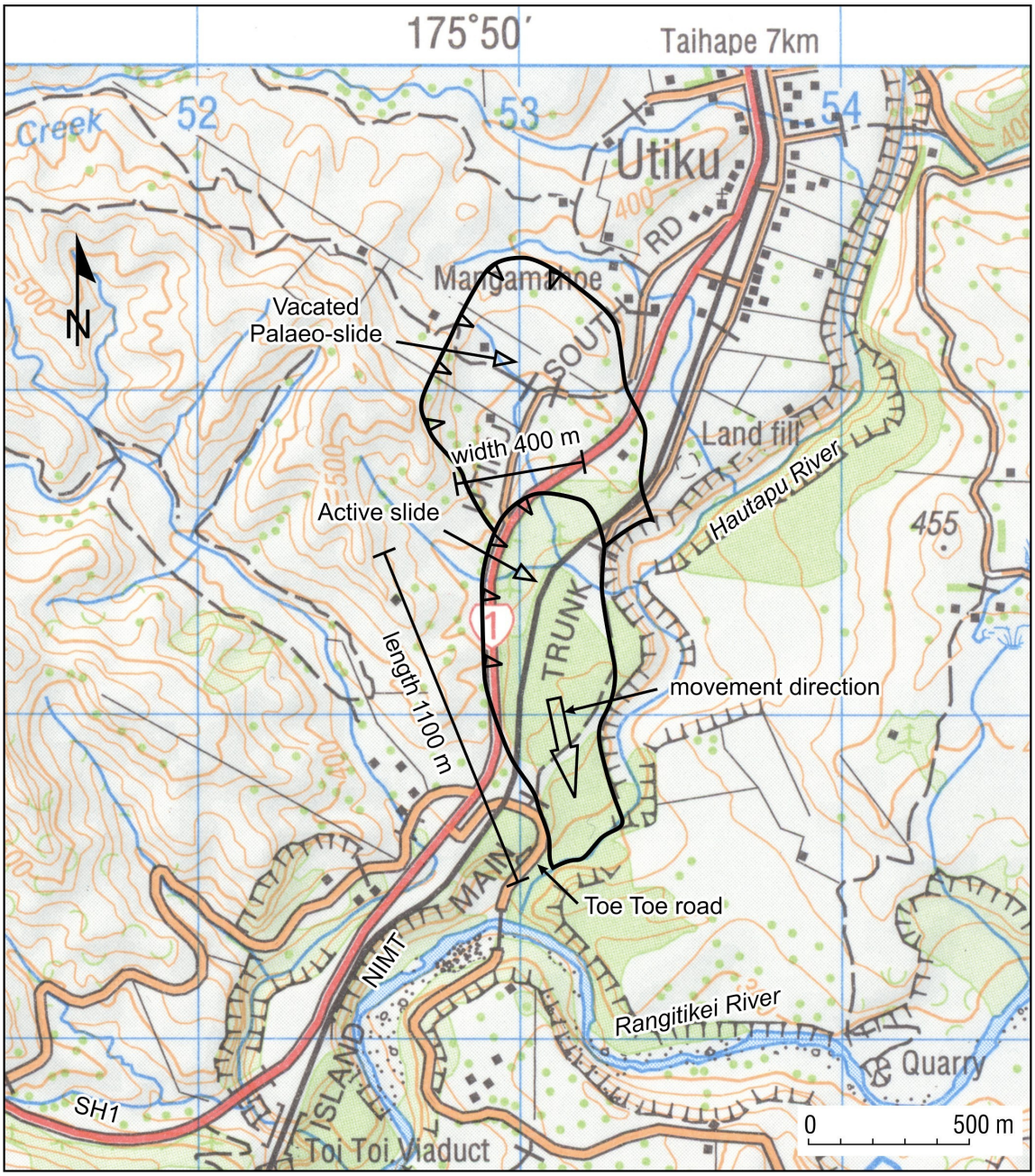

Figure 3.04 Utiku landslide location map. Extract from the Land Information New Zealand, 1:50,000 scale topographic map sheet 260. T22.

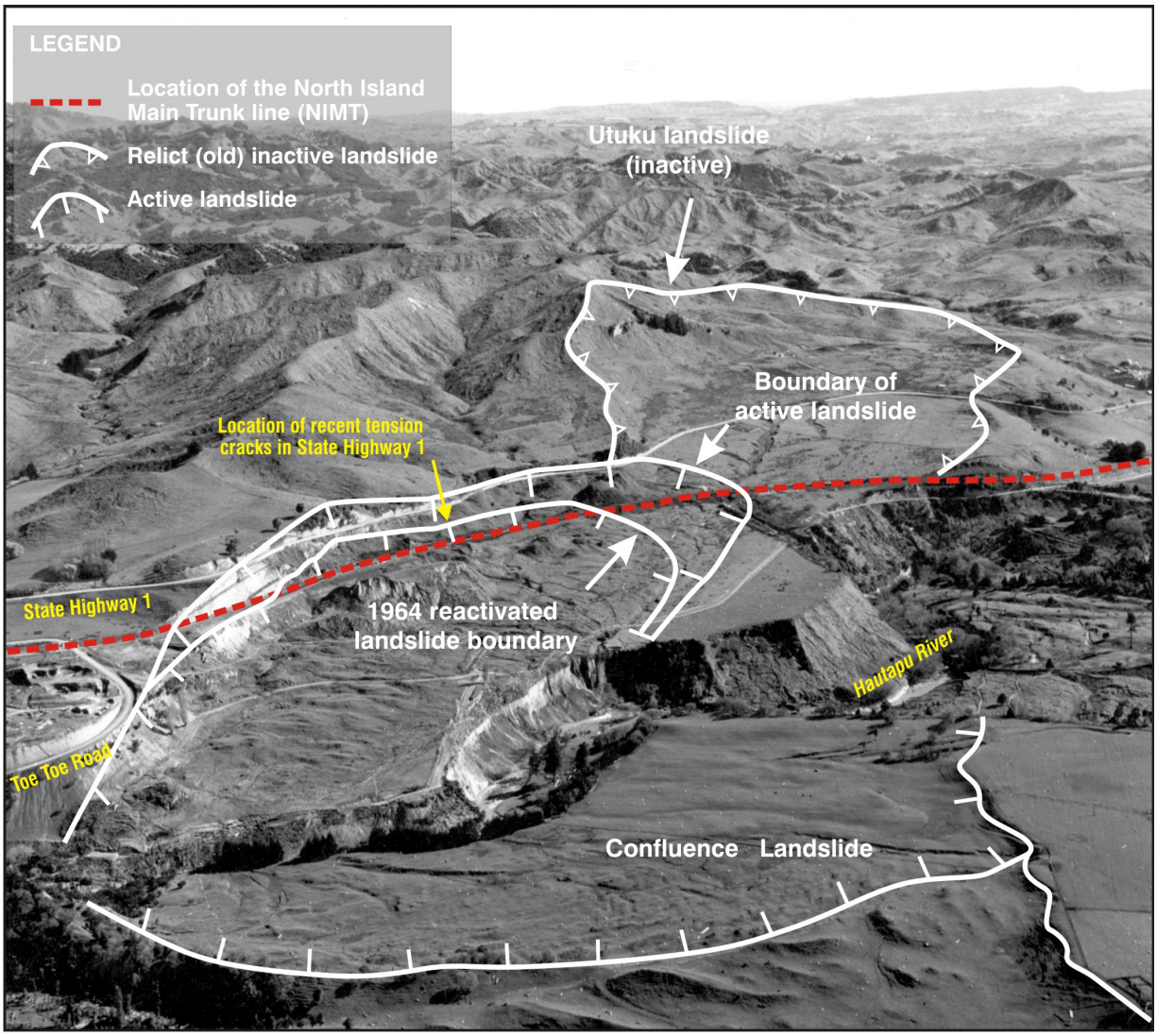

Figure 3.05 Aerial oblique view of the Utiku landslide taken in 1965 (source: L. Homer)

Figure 3.06 Aerial oblique view of the Utiku landslide taken in 2010 (source: G. Hancox)

3.4.3 Geotechnical investigations

Numerous ground investigations of the landslide were carried out between 1965 and 2008 (Table 3.01 and Figure 3.07).

Table 3.01 Historical ground investigation details (Utiku)

Date	Consultant	Ground investigation details	Typical depths (m bgl[1])	Instrumentation/testing
Aug to Sept 1965	NZ Railways	28 No. boreholes (diamond drill with core barrel and split barrel sampler). Carried out in the 1964 reactivated landslide area. (NZ Railway Boreholes 1 to 28).	20 to 30	None
		9 No. Proline auger holes carried out along the new SH1 alignment. (PR 1 to 9)	5	None
Jan to Aug 1969	Ministry of Works	De-watering Shaft 1 (Jan 1969) and Shaft 2 (Aug 1969), both excavated using mechanical auger, 1-m diameter and steel lined. (Shafts 1 and 2)	Shaft 1: 27.4 Shaft 2: 30.5	None/Atterberg limits. Particle size distribution (PSD)
		12 No. Piezometer boreholes (PB1 to 12)	20 to 30	Piezometers
Nov 1973	Ministry of Works (assumed)	10 No. boreholes carried out in the inactive area of the landslide towards the northwest of the new SH1. (TS1 to 10)	10	None
1995 to 1998	Opus	• 3 No. Piezometer boreholes installed in the 1964 reactivated landslide area. (PZA, B and C)	20	None
2008	GNS Science	• 4 No. Piezometer boreholes • 2 No. Inclinometer boreholes	50 to 70	Piezometers and inclinometer/Atterberg limits, PSD, ring- and direct-shear

[1]Depths are meters below ground level

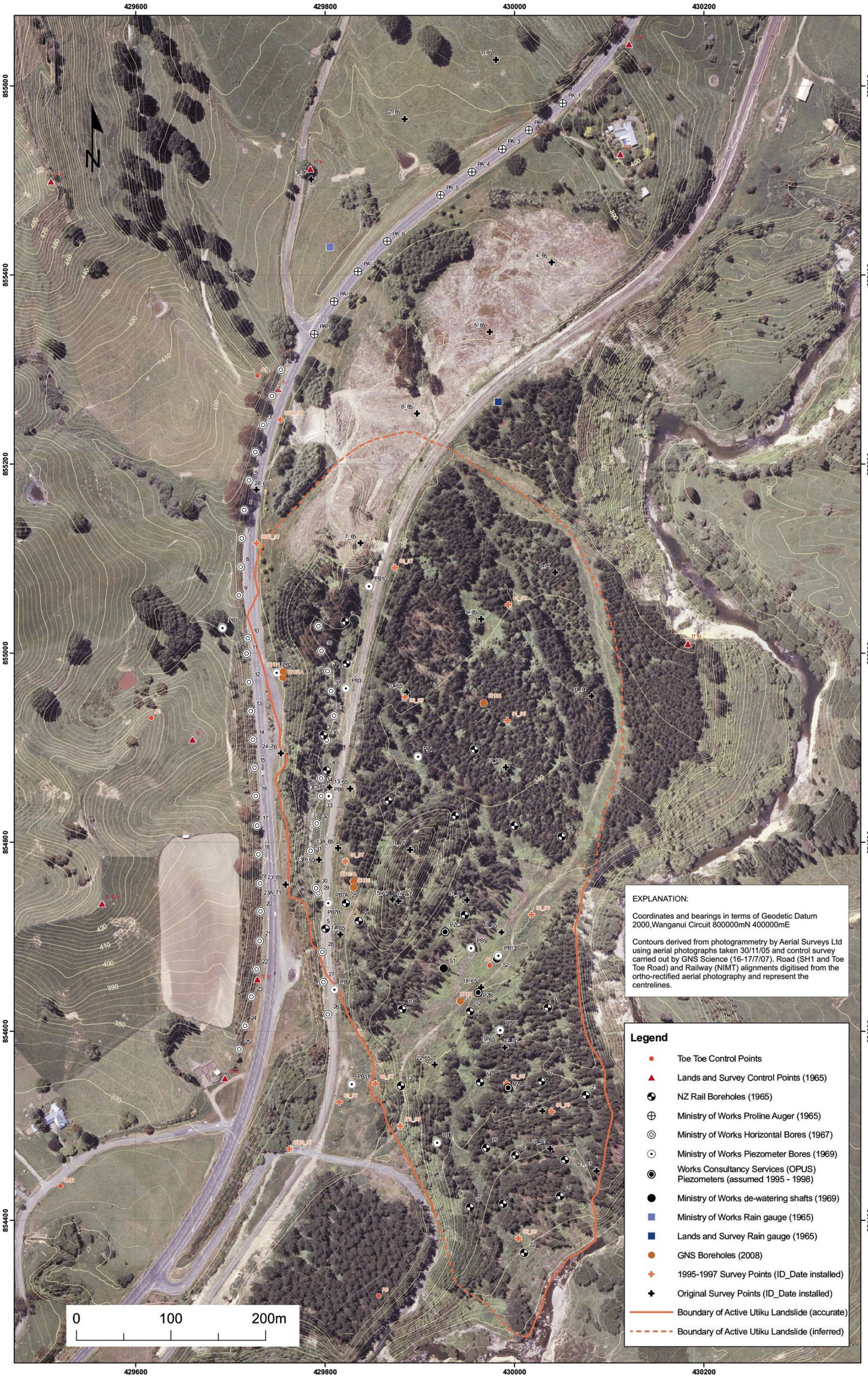

Figure 3.07 Map showing the locations of recent and historical ground investigations and monitoring equipment on the Utiku landslide.

3.4.4 Engineering geology of the landslide

The active part of the Utiku landslide is a composite landslide, formed by a series of slide blocks. These can be grouped into two broad zones: a lower zone comprising predominantly remoulded materials, with numerous closely spaced tension cracks and landslide scarps; and an upper zone comprising displaced, relatively intact blocks (rafts) of Tarare sandstone. On this basis, it may be classified as a complex, reactivated, translational rock slide-earth flow (Cruden and Varnes, 1996) or block slide (Panet, 1969) (Figure 3.08).

The western flank of the landslide is a steep (typically 45° to 60°), linear lateral scarp, that is linearly stepped and ranges in height from about 20 m in the north to 60 m in the south. This feature is more distinct towards the southern end of the landslide, where Toe Toe road is cut into its upper part. The eastern flank is not so well defined, but is marked by the near exposure of the slide surface, where landslide debris is missing or very thin. In the lower landslide, the flanks are thin zones of closely-spaced sub-parallel scarps.

The toe of the landslide, adjacent to the Hautapu River, is a highly-active zone which can be classified as an earth flow (Cruden and Varnes, 1996). In this area, the landslide materials are remoulded with occasional small rafts of sandstone. Surface ponding of water is apparent and slopes are typically about 10°. Upslope (north), the ground is characterised by closely-spaced (typically < 1 m) tension cracks, with vertical offsets ranging from 0.5 m to 2.0 m. Cracks often appear fresh (no vegetation and minor surface discolouration on exposed surfaces).

The upper part of the landslide has a different morphology characterised by several large hillocks (locally referred to as knobs). The largest is 30 to 40 m high, with side slopes of 35° to 45°. A tension crack approximately 3 m deep, 2 m wide and 100 m long extends up the flank and along the crest of the hillock. Minor landslide scarps are apparent on its flanks particularly the down slope (eastern face), indicating that the block is breaking up during movement. Between the hillocks are several small valleys interpreted as grabens between slide-blocks. Natural drainage lines (visible in 1950's aerial photographs, but now modified by various mitigation works) follow these grabens. The NIMT traverses one of these grabens on a fill embankment, approximately 5 to 8 m in height across the upper (western) side of the landslide.

Figure 3.08 Engineering geology map of the Utiku landslide

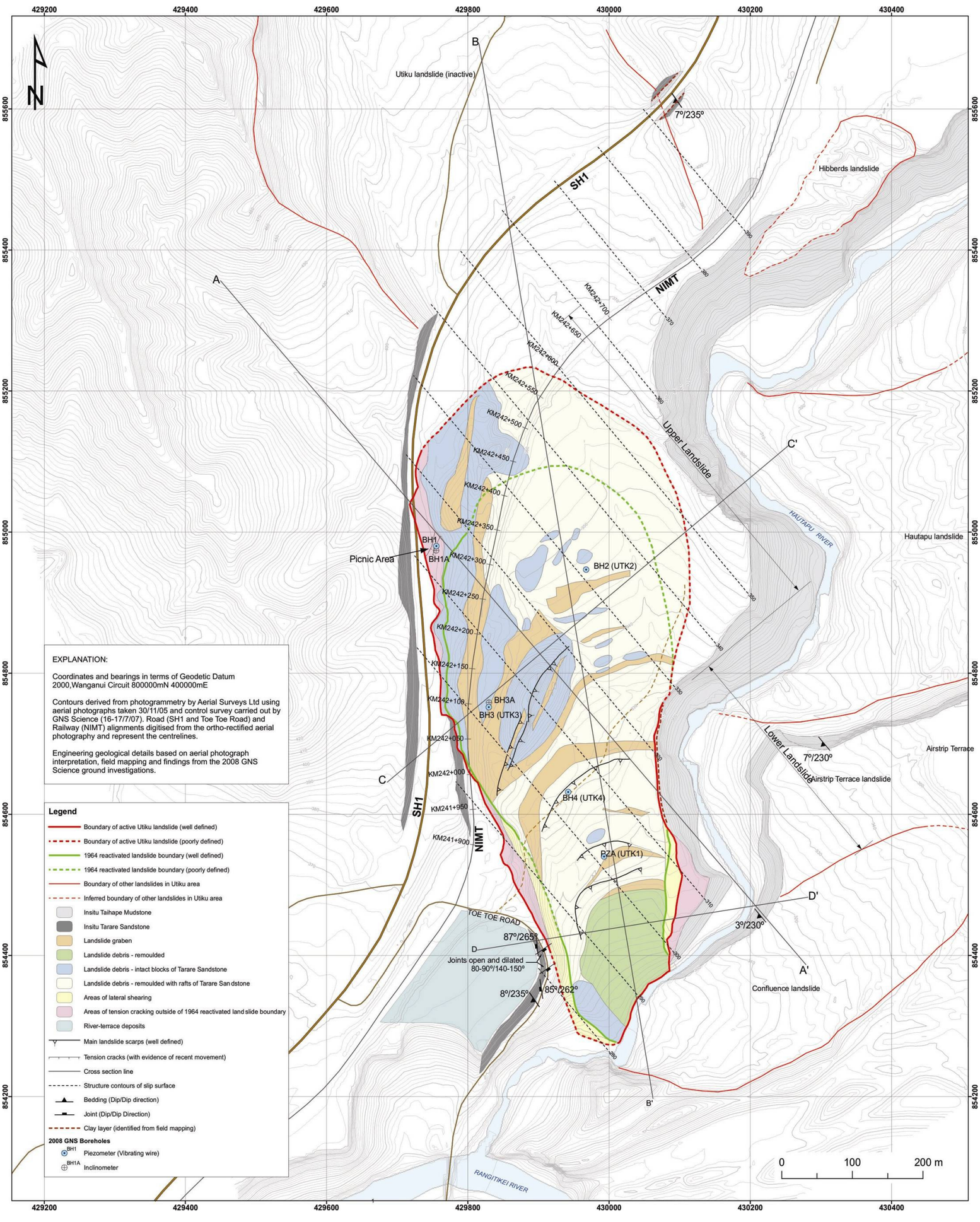

Upslope of the NIMT, are several blocks of sandstone which have undergone only limited horizontal and vertical displacement. The upper limit of the 1964 reactivation is a scarp up to 6 m high and locally near vertical and is located immediately below (east) of a SH1 picnic area. No movement was identified in the area traversed by SH1 between 1964 and 1991. Since then, however, subsidence of the SH1 carriageway and picnic area has occurred indicating further retrogression.

The morphology of the debris in the active eastern area is more subdued and hummocky when compared with the relatively intact-displaced blocks along the western flank. This may indicate that the debris is older than the intact blocks peeling off the western flank. The eastern debris has translated from the vacated source area further upslope, which is now assessed as inactive as most of the debris overlying the slide surface has been removed. It may be possible to estimate the age of the vacated landslide source area using the mean historical motion rates, which are about 0.07 m/year. Assuming a distance of 1,200 m (the length of the vacated source area, from head scarp to the Hautapu River), it would take about 17,000 years for the debris to vacate the source area, which would suggest that the 11,000 year age, estimated by Thompson (1982), is more accurate than the 1,800 year age. At current motion rates it would take about 12,000 years for the debris to vacate the currently active part of the landslide, suggesting the landslide is geologically ephemeral.

The main geological materials found in the landslide area are, in reverse chronological order (youngest first): landslide debris, further subdivided into three sub-units, representing increasing remoulding with displacement from the head scarp; landslide slide surface; river terrace gravels; in-situ Tarare sandstone; and Taihape mudstone (Table 3.02).

Table 3.02 Geological units (Utiku)

Geological Unit[1]		Description
Landslide debris	Remoulded	Dark, brownish grey, silty sand with occasional cobble and boulder sized clasts of sandstone (possible concretions). Remoulded Tarare Sandstone.
	Remoulded with rafts	Similar to remoulded landslide debris but with rafts of intact Tarare Sandstone.
	Intact displaced blocks	Intact blocks of Tarare Sandstone.
Landslide slip surface		Dark grey, plastic clay.
River Terrace		Rounded to sub-rounded gravel, cobble and boulder sized clasts of andesite, greywacke and limestone with a sandy matrix.
Bedrock	Tarare Sandstone	Grey, very fine grained, sandstone with very rare cobble and boulder sized concretions. The sandstone has high silt content.
	Taihape Mudstone	Dark bluish grey, sandy siltstone with occasional cobble and boulder sized concretions. The Taihape Mudstone has higher silt content than the Tarare Sandstone and contains several dark grey clay interbeds, varying in thickness from 2 mm to 200 mm. The largest of these interbeds forms the landslide slip surface and is thought to represent the boundary with the overlying Tarare Sandstone.

[1]The names of the bedrock geological units are taken from Lee et al., (In prep)

3.4.4.1 Landslide debris

The landslide debris comprises three main materials representing different proportions of remoulding during movement, which increases with distance/displacement from the landslide crest.

1. Remoulded – medium dense, silty sand, derived from remoulding of the Tarare Sandstone with voids and occasional cobble to boulder-sized clasts of intact Tarare Sandstone (possible concretions). Found predominantly in the active toe area of the lower landslide.
2. Rafts of intact sandstone – similar to the remoulded landslide debris but with rafts (> 10 m in width) of intact Tarare Sandstone. The sandstone rafts may have multiple fractures and show a loss of strength with increasing movement. Forms the transitional zone between the active lower landslide and the less active upper landslide.
3. Intact, displaced blocks – blocks of weak, intact, Tarare Sandstone. Typically > 50 m in size with some movement-induced fractures apparent (from core samples and in outcrop). Found only in the upper landslide.

3.4.4.2 Landslide slide surface

All six of the recent (2008) boreholes identified a clay layer that typically comprised: a dark grey, soft, silty clay (highly plastic) of the smectite group, with minor angular fine gravel (of fine-grained sandstone) and with a well-developed shear fabric (slickensides), which is interpreted as the primary shear surface at the base of the landslide. The fine

to coarse gravel-sized clasts are typically found at the upper part of the clay and are interpreted as comminuted Tarare Sandstone (Table 3.03 and Figure 3.09).

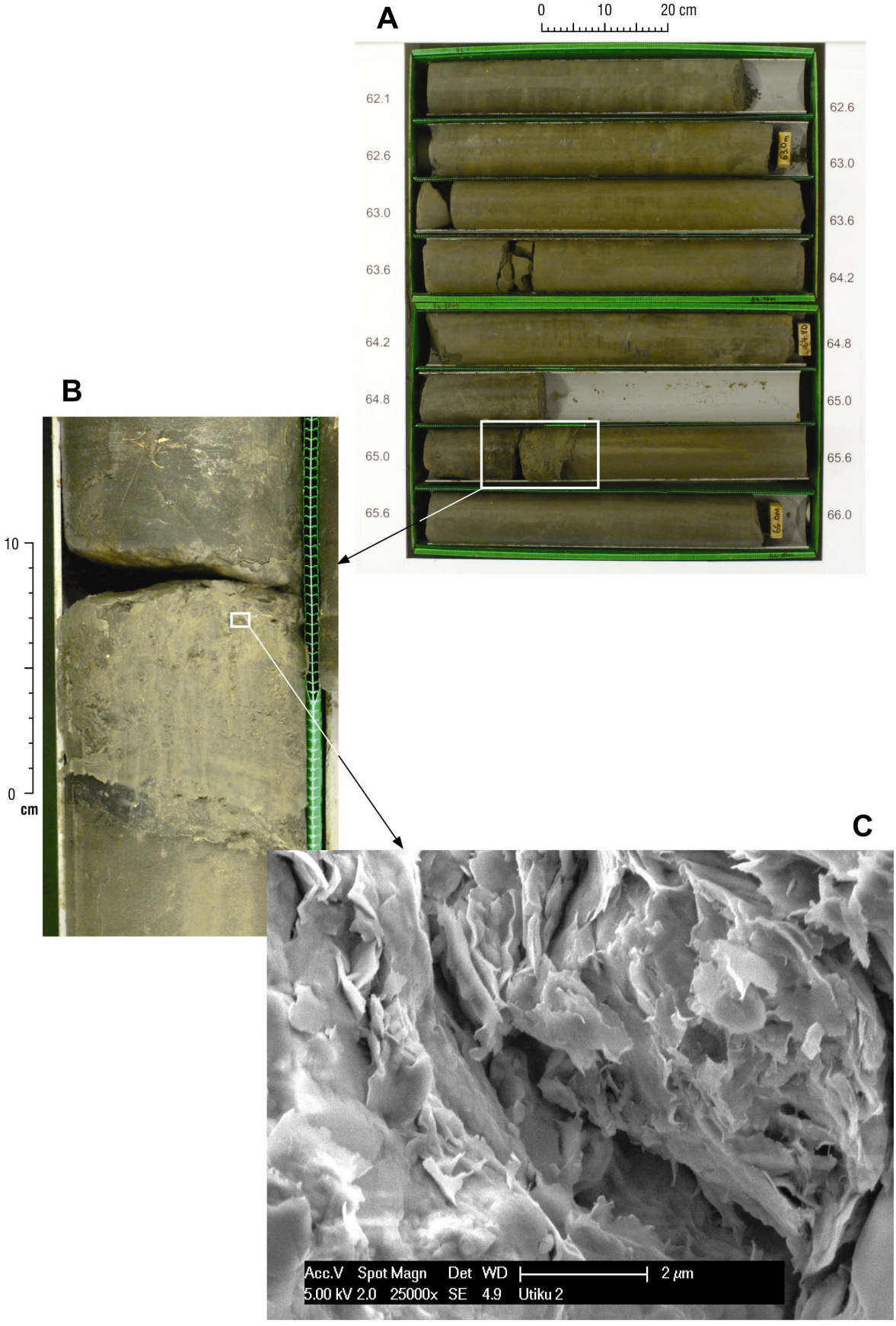

Figure 3.09 Utiku landside slide surface, taken from drill hole BH1. A: The Utiku slide surface in BH1. B: A close-up view of the Utiku slide surface in BH1. C: Scanning electron microscope view of the Utiku slide surface in BH1.

Table 3.03 Landslide slide surface details derived from drill holes (Utiku)

Borehole	Depth below ground level	Slip plane elevation (m AMSL[1])	Slip surface thickness (m)	Description[2]
BH1	65.15	313.96	0.05	Silty CLAY, minor angular fine gravel of fine grained sandstone; dark grey, soft. With shear fabric.
BH1A	65.82	313.38	0.10	
BH2	15.42	331.48	0.08	Silty CLAY, some angular fine gravel of fine grained sandstone; dark grey to black, soft. Brecciated with shear fabric.
BH3	49.05	302.72	0.05	CLAY, minor angular fine to coarse gravel of fine grained sandstone; dark grey, soft tending firm to stiff with depth. With shear fabric.
BH3A	48.90	303.40	0.10	
BH4	28.05	302.55	0.20	CLAY; dark grey speckled light grey, firm. With shear fabric.

[1]Elevation meters above mean sea level using the Moturiki vertical datum 1953
[2]Material descriptions as per NZGS (2005)

The slide surface corresponds to the upper and thickest of the clay layers within the Taihape Mudstone. Three-point solutions between BH1, BH2 and BH3, and between BH2, BH3 and BH4, indicate that the slide surface is planar, with a dip/dip direction of 7°/230° and very little variation across the landslide (Figures 3.10 and 3.11). The full extent of the slide surface was not identified until 2008. Historically, multiple slide surfaces had been interpolated from drillhole records (e.g. Ker, 1972), however, these ground investigations were limited as no clay layers were identified in the drillhole records. Stout (1977) inferred that the slide surface was likely to coincide with a clay layer, concordant with bedding, identified in the SH1 road cutting at the eastern flank of the landslide and along the top of the western cliffs of the Hautapu River, east of the active landslide area. However, no drillholes were carried out at the time to corroborate this.

Field mapping carried out in 2008 as part of this research identified a clay layer in the SH1 slope cutting, and at the toe of the landslide, close to the Hautapu River level, and in the western cliff of the Hautapu River. During mapping, bedding and joint orientations were recorded where possible in stable ground, around the edge of the landslide. The dip/dip direction of bedding was typically 3° to 7°/230° to 240°, which is coincident with the dip/dip direction of the landslide slip surface derived from three-point solutions using the depths of the slip surfaces identified in the 2008 boreholes. Structural contours of the slip surface are shown on Figure 3.08.

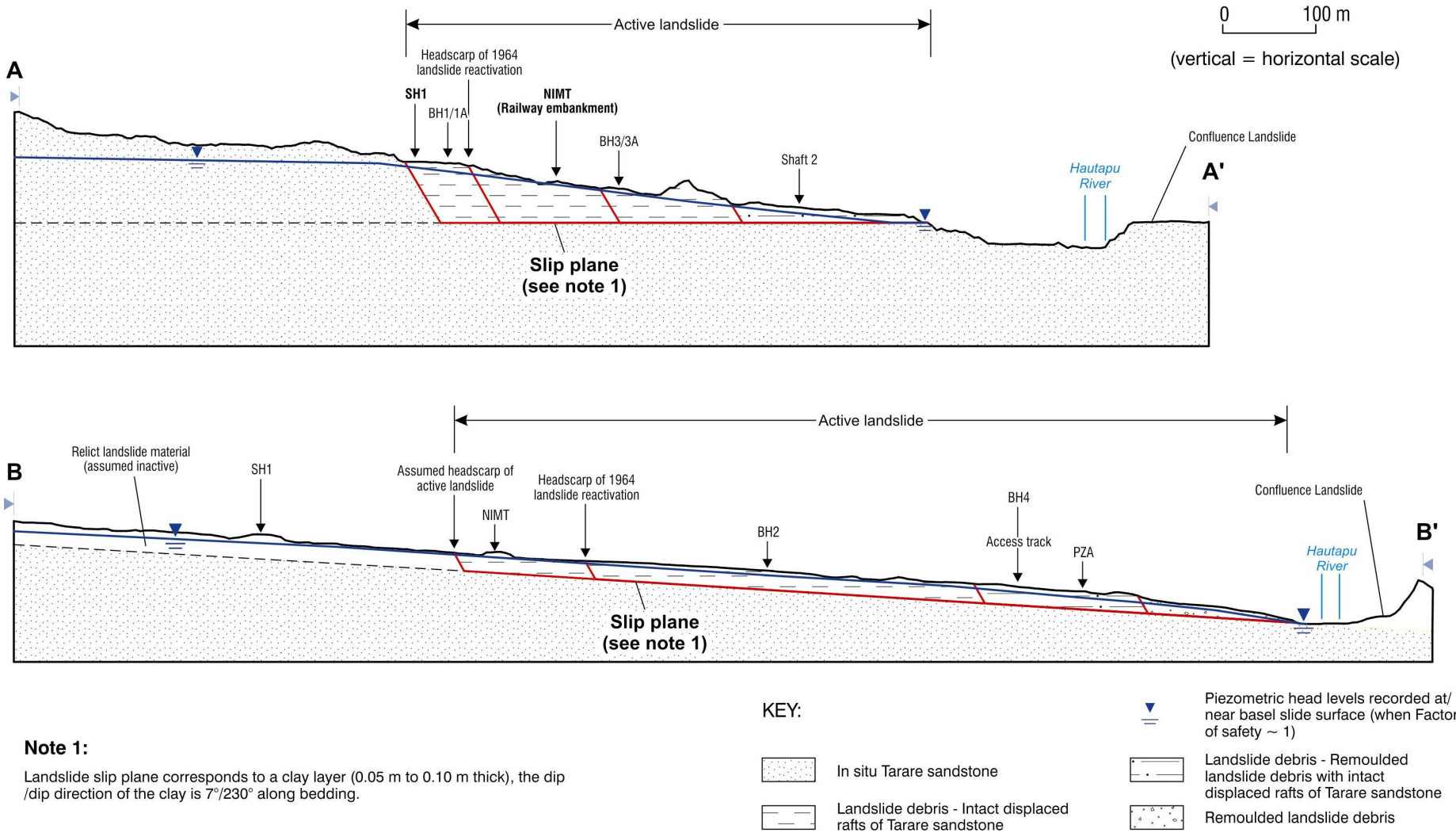

Note 1:

Landslide slip plane corresponds to a clay layer (0.05 m to 0.10 m thick), the dip /dip direction of the clay is 7°/230° along bedding.

Figure 3.10 Long section A-A' and B-B' (Figure 3.08) through the Utiku landslide.

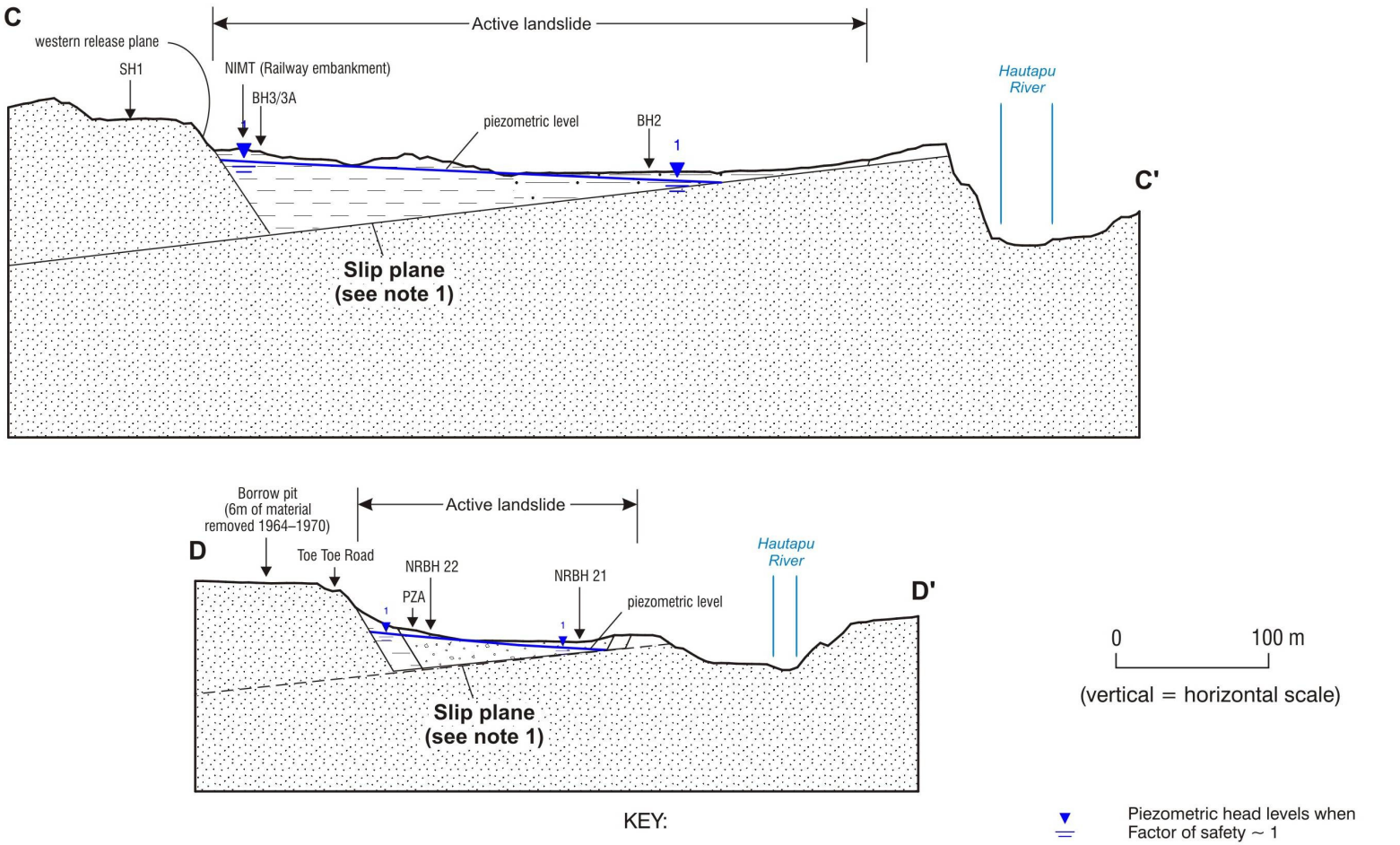

Figure 3.11 Cross section C-C' and D-D' (Figure 3.08) through the Utiku landslide.

Note 1:

Landslide slip plane corresponds to a clay layer (0.05 m to 0.10 m thick), the dip /dip direction of the clay is 7°/230° along bedding.

3.4.4.3 River-terrace deposits

River-terrace deposits are found south of Toe Toe Road and were used during re-construction of the NIMT after damage caused by movement in 1964 and during realignment of SH1 in the 1970's. The deposits are rounded to sub rounded, gravel, cobbles and boulders of andesite, greywacke and limestone with minor sand. The strength of clasts ranges from weak to strong, but due to the lack of clay and silt, the material is loose. There are no in-situ terrace deposits on the landslide, however, disturbed terrace deposits (rounded to sub rounded andesite cobbles and boulders) are found in the lower central and toe areas of the landslide.

Cover-beds of tephra and loess are also found in isolated pockets on the landslide. These deposits typically appear disturbed by landslide movement, and in many areas appear to be reworked.

3.4.4.4 Tarare sandstone

The majority of the active Utiku landslide is within the Tarare Sandstone that outcrops at various locations around the margins of the landslide. In outcrop, and where undisturbed, the material is slightly greenish grey, very weak, very fine grained, silty sandstone, with rare ovoid cobble and boulder-sized concretions. In general, the sandstone appears massive with very few structures and visible defects. Defects that are apparent tend to be within material located on or immediately adjacent to the landslide and are assumed to have been induced by landslide movement.

3.4.4.5 Taihape mudstone

The Taihape Mudstone underlies the Tarare Sandstone and only outcrops in the SH1 road cutting at the eastern flank of the stable relict landslide. The Taihape Mudstone is similar to the overlying Tarare Sandstone, but is finer grained, with more silt than sand (Thompson, 1982). The material when freshly exposed is dark bluish grey, moderately weak, sandy siltstone. The upper part of the mudstone towards the boundary with the overlying Tarare sandstone, contains several soft clay layers (ranging in thickness from 2 to 5 mm), with the thickest layer (typically 50 mm) possibly forming the boundary between the Tarare Sandstone and the Taihape Mudstone, and the surface along which the landslide mass is sliding on. These clay layers are thought to have derived from volcanic ash deposited in a marine environment (Thompson, 1982; Reyes, 2007).

3.4.4.6 Material parameters

Geotechnical parameters for the landslide materials were derived from laboratory testing on core samples from the Utiku 2008 drill holes, as well as undisturbed field

samples from the adjacent Confluence landslide, which is sliding along the same bedding surface as the Utiku landslide. Geotechnical parameters for the bedrock materials were taken from Read and Miller (1990), who tested a number of intact samples of the Tarare sandstone and Taihape mudstone in the area. Laboratory testing of the Utiku slide-surface clay and remoulded landslide debris comprised consolidated drained ring-shear tests carried out by GNS Science. Ring-shear tests were also carried out on samples of the slide-surface clay from the Confluence landslide by the University of Portsmouth, UK (Kilsby, 2007). Results from the Utiku slide-surface clay show no post-peak drop in shear strength indicating that the clay forming the landslide slide surface is at residual value. The parameters derived from laboratory testing are summarised in Table 3.04.

Table 3.04 Geotechnical parameters from testing (Utiku)

Material	Description[1]	Unit weight kN/m^3	Strength parameters	Young's Modulus (MPa)	Poisson's ratio	Test method
Landslide debris – remoulded	Silty, fine SAND, medium dense	20	c' = 0 kPa ϕ' = 28° ±(5)	20	0.3	2 Ring shear tests
Landslide slip surface Utiku[2]	Silty CLAY, very soft	19	c' = 4 ±(6) kPa ϕ'_r = 8.3° ±(1).	-	-	5 ring- and direct-shear tests
Landslide slip surface Confluence[2]	Silty CLAY, very soft	20	c' = 0 ±(3) kPa ϕ'_r = 8.2° ±(1).	-	-	3 ring-shear tests (Kilsby, 2007)
Bedrock – Tarare Sandstone	Silty fine SANDSTONE, very weak	21	c' = 300 ± (50) kPa ϕ' = 45° ±(10)	1,000 ±(500)	0.35	Triaxial tests (Read and Miller, 1990)
Bedrock – Taihape Mudstone	Sandy SILTSTONE, very weak	21	c' = 300 ±(50) kPa ϕ' = 50° ±(10)	1,000 ±(500)	0.35	

[1]Material descriptions as per NZGS (2005)
[2]Landslide slip surface assumed to be at/near residual strength values

3.4.4.7 Landslide model

Displacement of the landslide blocks that form the active landslide occurs as slip along a thin planar horizon of clay parallel to bedding. The active landslide was subdivided into two parts, based on geomorphology and movement characteristics: 1) a larger volume, upper translational block-slide, moving parallel to the strike of the bedding plane (bearing 140°), where the apparent dip of the slip surface parallel to the main movement direction is ~ 1° (Section line A-A', Figure 3.10); and 2) a smaller volume, lower translational block-slide/earth-flow, moving towards bearing 155°, where the apparent dip of the slip surface parallel to the main movement direction is ~ 3° (Section B-B', Figure 3.10).

The boundary between the two coincides with a scarp and a gradational change in material properties of the landslide debris, which represents the effects of increasing amounts of deformation from the head scarp towards the toe. The upper landslide predominantly consists of intact displaced blocks of Tarare sandstone, which become more remoulded and disaggregated towards the landslide toe, where they have become completely remoulded to form an earth flow.

The head scarp of the active landslide is formed by a 30° to 35° slope, which dips towards bearing 110°. The western flank is well defined by a persistent and stepped scarp slope dipping about 35° to 40°, but in contrast the eastern flank is poorly defined where the slip surface is thought to be at or near to ground level. The landslide toe is defined by the Hautapu River. The bedding plane forming the landslide slide surface is at or near ground level along the eastern edge of the landslide, increasing in depth westward at the base of the landslide. At the toe, the slip surface daylights at the Hautapu River on the eastern edge, but dips below it in the west.

Section lines C-C' and D-D' (Figure 3.11) are perpendicular to the main directions of landslide movement. These illustrate that the landslide is a wedge that thickens towards the west. The base of the wedge is formed by the slip surface corresponding to the clay layer (dip/dip direction 7°/230°), the lateral (western) release plane is formed by the persistent and stepped western scarp (approximate dip/dip direction 60°/065°), which does not appear to relate to any regional structural trend. The top of the wedge corresponds to the landslide head scarp (approximate dip/dip direction 60°/110°), which is also sub-parallel to the main graben features. The plunge and trend of the wedge intersection is approximately 2°/154° and is inside the landslide movement envelope (Figure 3.12).

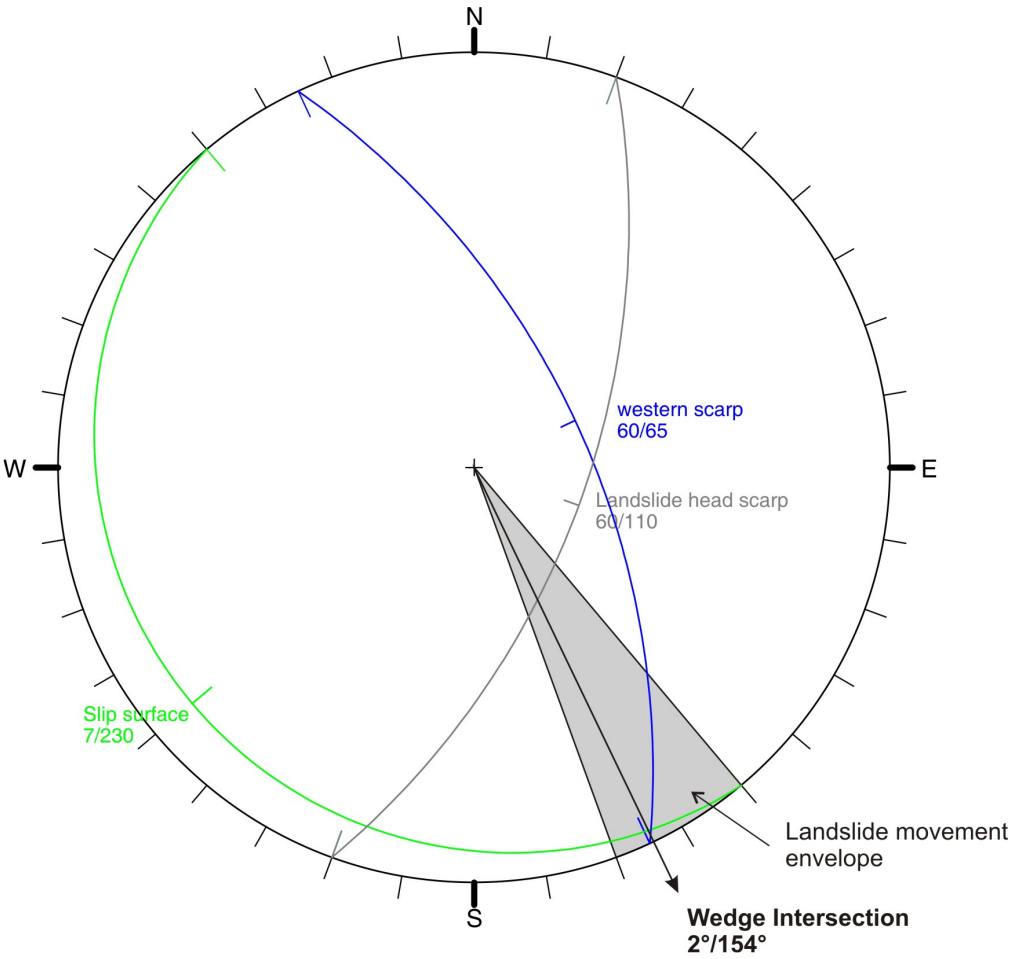

Figure 3.12 Stereonet showing the geometry of the Utiku landslide

3.5 Taihape landslide

3.5.1 Location

The Taihape landslide is west of SH1 in the township of Taihape, Rangitikei District, central North Island, New Zealand. The landslide was first noted by the District Council in 1971 following movement in the toe of what is now recognised to be a larger landslide complex (Figures 3.13 and 3.14).

The area of the landslide based on Thompson (1982), is estimated to be 67 hectares, and contains over 200 households along with the former St Josephs Primary School. The school site was abandoned in April 2007 following deterioration of the grounds and buildings during landslide movement. The landslide is about 1,300 m long, extending from Otaihape Stream in the south (the toe of the landslide) to beyond Kiwi Road in the north (the head scarp of the landslide), and is over 900 m wide.

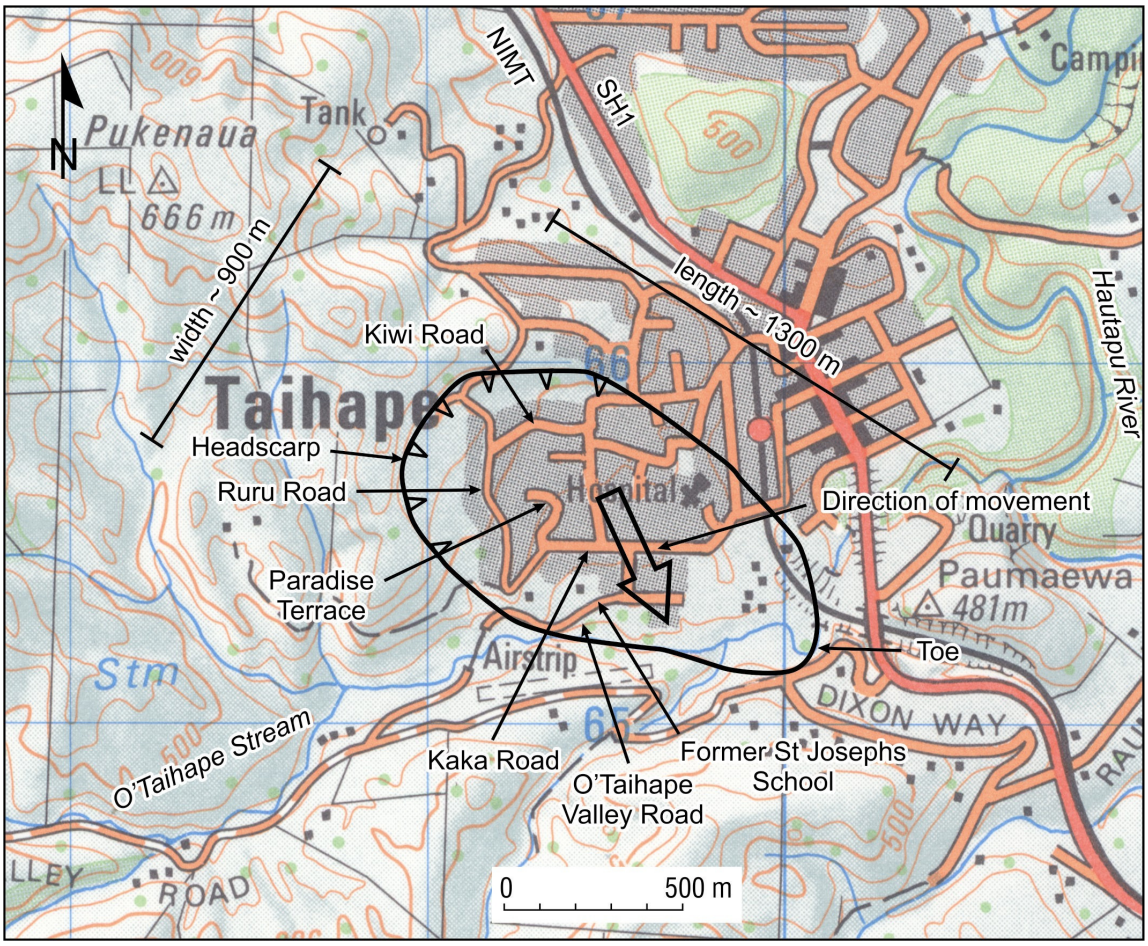

Figure 3.13 Taihape landslide location map. Extract from the Land Information New Zealand, 1:50,000 scale topographic map sheet 260. T21.

Figure 3.14 Aerial oblique view of the Taihape landslide taken in 2007 (source: G. Hancox)

3.5.2 Site history

The Taihape landslide is reasoned to have initiated sometime between 11,000 and 1,800 years ago (Thompson 1982), however, no quantifiable data are available to support this assertion. The full extent of the landslide was not recognised until 1982, when Thompson (1982) found that the 1971 area of movement was part of a much older and larger landslide. There were several episodes of investigation and analysis of the landslide between 1983 and 2006. During this period, ground investigations were undertaken and a movement-survey network established on the surface of the landslide in 1985. Surveys of the network were made at two- to five-year intervals, with no major changes in movement rate identified until May 2005.

3.5.3 Geotechnical investigations

Geotechnical work carried out to investigate the landslide comprised interpretation of aerial photographs, field mapping of the geology and geomorphology, drillhole investigations, and laboratory testing of selected landslide materials.

Four phases of ground investigation using drillholes were carried out; in 1984, in November 2004, August/September 2005 and May 2006 (these are detailed in Table 3.05 and shown on Figure 3.15).

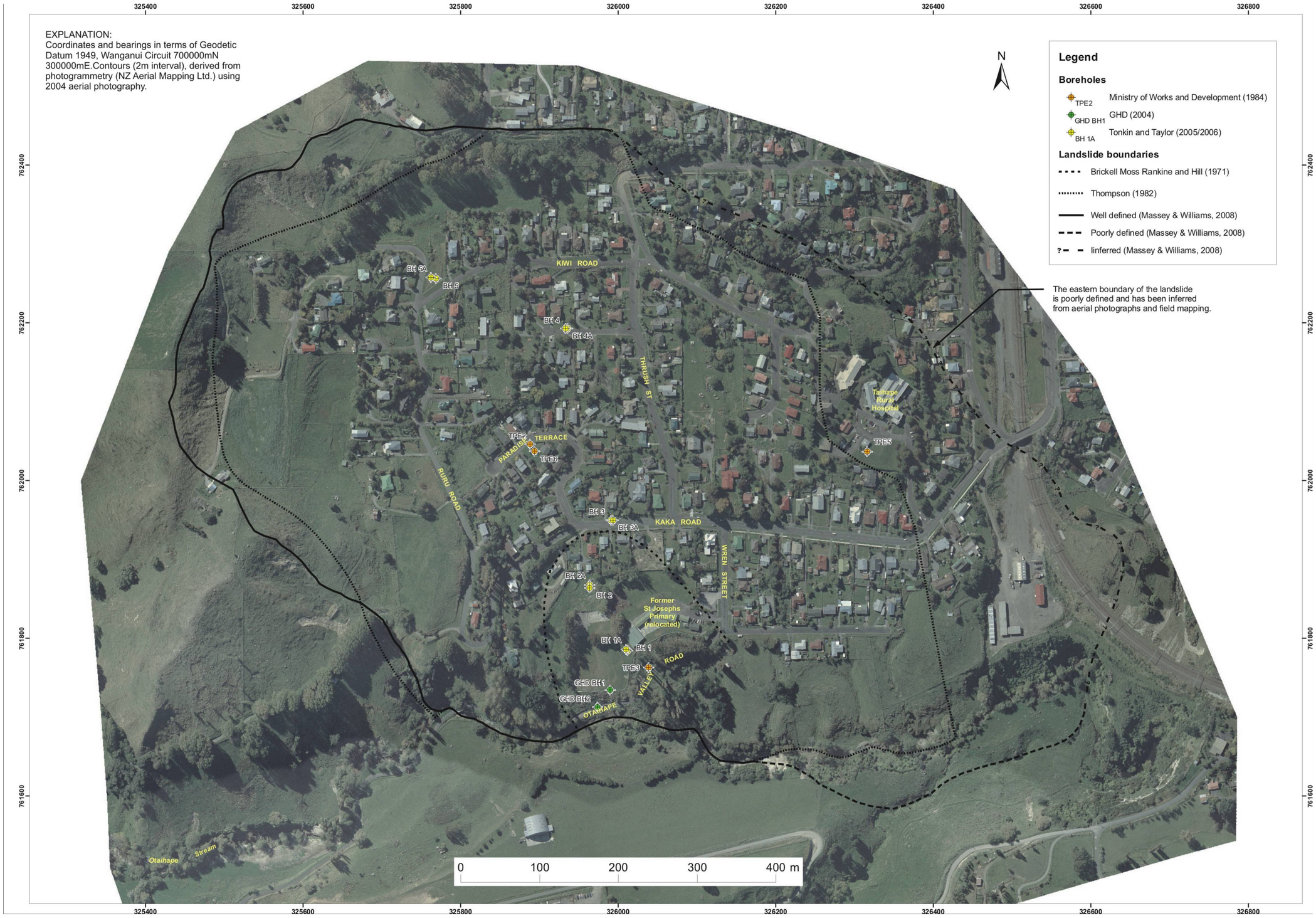

Figure 3.15 Map showing the locations of recent and historic ground investigations and monitoring equipment on the Taihape landslide

Table 3.05 Historical ground investigation details (Taihape)

Drill hole	Year	Easting (m)[1]	Northing (m)[1]	Elevation[2] (m AMSL)	Depth (m bgl[3])	Instrumentation/ testing
TPE2	1984	325888.62	762046.68	481.89	34.50	Inclinometer
TPE3	1984	326039.01	761763.52	444.40	18.00	Inclinometer
TPE5	1984	326316.68	762037.11	468.82	13.50	Inclinometer
TPE6[4]	1984	325893.00	762038.00	481.70	34.50	Piezometers
GHDBH1	2004	325989.78	761734.72	450.00	29.50	Piezometer/SPT
GHDBH2	2004	325974.38	761713.46	440.82	15.00	SPT
BH1	2005	326012.47	761784.89	450.80	30.00	Inclinometer
BH1A	2005	326010.34	761786.60	451.20	30.00	Piezometers
BH2	2005	325963.95	761864.48	459.10	33.00	Inclinometer
BH2A	2005	325963.77	761868.32	459.20	33.00	Piezometers
BH3	2005	325991.00	761950.16	465.40	34.50	Inclinometer
BH3A	2005	325993.98	761950.32	465.30	34.50	Piezometers
BH4	2005	325933.32	762193.26	485.50	45.00	Inclinometer
BH4A	2006	325935.75	762193.27	485.40	45.00	Piezometers
BH5	2006	325768.85	762257.25	508.40	63.00	Inclinometer
BH5A	2006	325762.80	762258.39	509.00	63.00	Piezometers

[1] Coordinates are in terms of Geodetic Datum 1949, Wanganui Circuit 700000mN, 300000mE
[2] Elevation meters above mean sea level using the Moturiki vertical datum 1953
[3] Depths are meters below ground level
[4] No drillhole logs are available, assumed to be a wash-drilled piezometer hole, adjacent to TPE2

3.5.4 Engineering geology of the landslide

The Taihape landslide has a prominent grass-covered head scarp, and consists of a series of slide blocks. Most of these slide-blocks are bounded by drainage lines that have been modified during urban development. Distinct breaks in slope form scarps between slide-blocks and depressions within the slide mass are generally extensional features (grabens) in which water ponds. The landslide is bounded at the toe by Otaihape Stream and at its head by two linear scarp slopes (slope angles 30° to 35° and dip directions of 100° and 170° respectively), one of which has been classified as an active fault (Litchfield et al., 2007). The eastern boundary of the landslide is not as well defined as the western one, and may have been modified by both human activity and other landslides unrelated to the main slide.

Geomorphic appearance splits the landslide broadly into two zones; a more active central zone, which extends to the toe and forms a general depression, within a less active, more blocky zone surrounding it. The two zones can be further subdivided on the basis of geomorphological features, which reflect the different surface-movement rates of the slide-blocks (Figure 3.16).

The toe zone between Kaka Road and Otaihape Stream, is the most active with extensive areas of hummocky ground (below Otaihape Valley Road), high groundwater levels (surface ponding of water), and back-tilted mature trees. The surface morphology is of multiple scarps with vertical ground offsets of 2 – 6 m, and possible pressure ridges. A prominent scarp and graben (immediately south of Kaka Road), form the main boundary between the more active toe zone and the less active central zone. This boundary was the mapped limit of the 1971 landslide reactivation. Many engineered structures in this zone such as houses, roads and walls show signs of deformation.

The landslide morphology changes upslope (north) from Kaka Road. This area has been termed the central zone, and extends from Kaka Road to Kiwi Road. Several distinct scarps and possible pressure ridges within larger slide-blocks are present in this zone. Vertical ground offsets across scarps range between 0.5 and 4.0 m. Evidence of surface deformation reduces towards the north from Kaka Road, with damage to structures (houses, roads and walls) around Paradise Terrace. Of particular note are springs (around BH4 and BH4A, Figure 3.16), and perennial seeps in Paradise Terrace, indicating high and artesian groundwater levels. The mapped eastern boundary of this zone is an open drain trending north – south from Kiwi Road to Wren Street.

The central and toe zones are surrounded to the east and west by several large, and apparently intact, slide-blocks (head and flank zones), with grabens (forming natural drainage lines) between the blocks. The density of different geomorphic features is much reduced in these zones. No obvious landslide-related damage to structures is apparent in these areas. Signs of recent and localised instability are found along graben flanks, some of which affect residential properties, but are not thought to relate to deep-seated landslide movement.

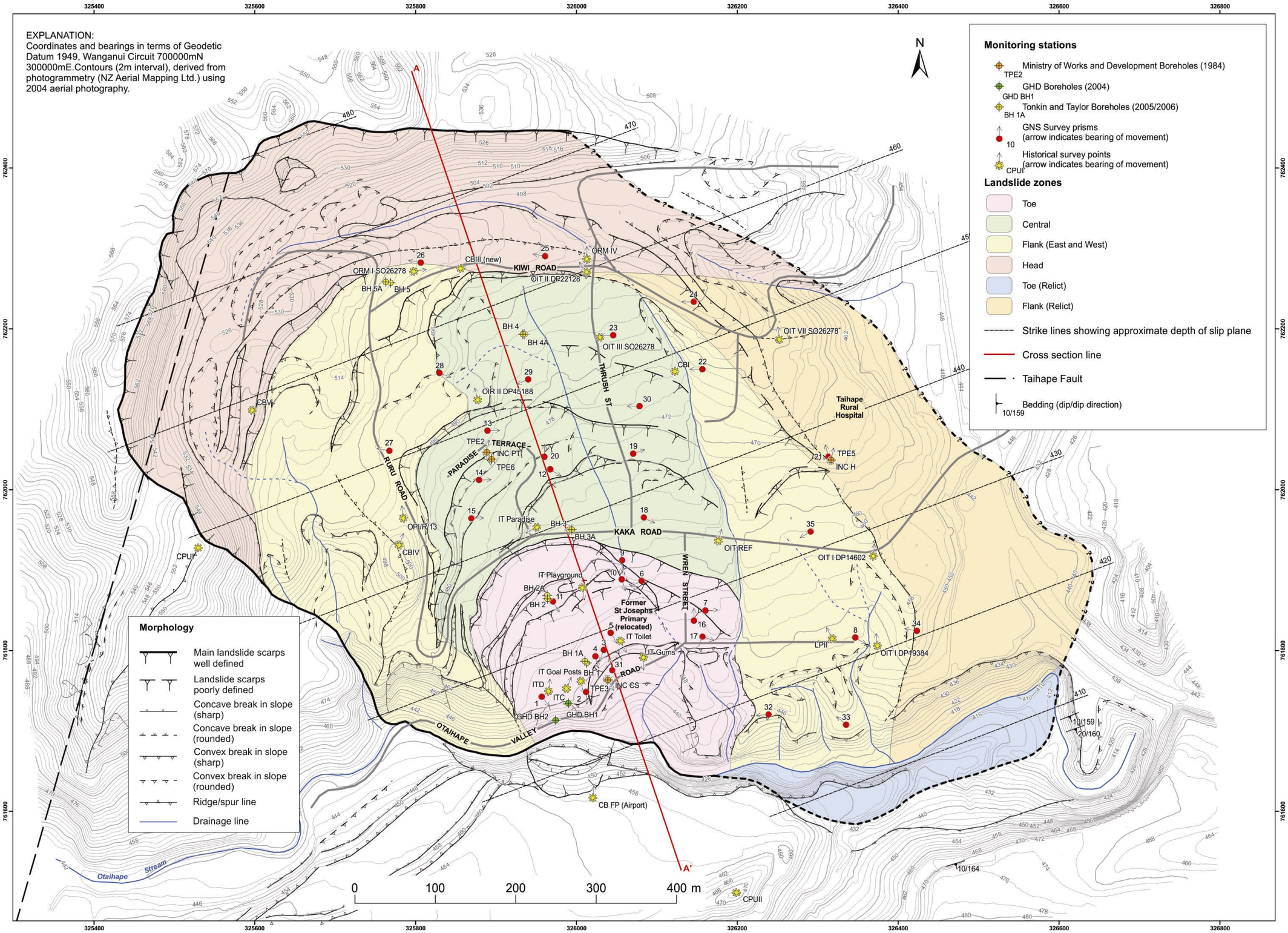

Figure 3.16 Engineering geology map of the Taihape landslide

Between the eastern landslide boundary defined by Thompson (1982), and the revised boundary, there is an area of what is now interpreted as relict intact slide-blocks (relict flank and toe zones). No evidence of recent instability has been identified in this area and no cracking of properties or infrastructure consistent with deep-seated landslide movement has been reported. Similarly, east of the active toe zone, near the North Island Main Trunk Line is an area of hummocky ground thought to have originally been part of the main landslide (relict toe zone). This has been incised by Otaihape Stream and apparently is inactive.

The main difference between the Utiku and Taihape landslides is that Taihape is not actively retrogressing along the head scarp or flanks. At historically recorded motion rates of about 0.01 m/year, it would take about 130,000 years for the debris to vacate the source area, indicating the landslide is likely to stay on the landscape longer than the Utiku landslide. Although there is no quantifiable data relating to the age when the landslide first initiated, it is likely to be old given the subdued rounded topography of the more intact blocks. The age of the landslide is estimated to be about 80,000 years based on historical motion rates and estimates of the amount of material that has been removed to date. The relative estimates of the ages of both the Utiku and Taihape landslides suggest that these features are relatively ephemeral that come and go from the landscape quite quickly (geologically).

The main geological materials found in the landslide area are, in reverse chronological order (youngest first): Landslide debris, further subdivided into three sub-units, representing increasing remoulding with displacement from the head scarp; landslide slide surface; and Taihape mudstone.

3.5.4.1 Landslide debris

The landslide mass comprises four main material types within different zones on the landslide that represent the effects of increasing disaggregation with displacement from the head scarp:

1. Landslide head and flank zones: Blocks of intact, but displaced sandstone – silty sandstone, very weak to weak, with strong concretions (where present). Some fractures apparent (in core samples and in outcrop).
2. Landslide central zone: Blocks of disturbed intact but displaced sandstone – silty sandstone, very weak, with a disturbed (relaxed) texture indicative of breakage. Many fractures apparent (in core samples).
3. Landslide toe zone: Disturbed landslide debris – silty, fine sand, medium dense to dense. Typically, little original rock structure is observable and the material

appears remoulded with occasional cobble- to boulder-sized clasts of intact sandstone (possible concretions), typically weak and weathered.

4. Relict flank and toe zones: Blocks of intact, but displaced sandstone, with some remoulded material in the toe zone.

Upper Quaternary debris flow/lahar deposits from Mount Ruapehu, an active volcano about 100 km north of Taihape, mantles the landslide. This material is referred to as the Hautapu Valley Agglomerate (Cotton, 1944; Te Punga, 1952; Thompson, 1982). The agglomerate comprises up-to-large-boulder-sized andesite clasts in a loose to medium dense, sandy silt matrix. The boulders generally form a lag, however, relatively thick (9 m) sequences of boulders and gravel were identified in the majority of drillholes.

3.5.4.2 Landslide slide surface

A slide surface is identified in the majority of drill holes carried out on the landslide (Table 3.06). Slide-surface materials typically comprised: silty clay, with angular fine gravel (of fine-grained sandstone); dark grey, soft, with a shear (slickensided) fabric in parts. The fine to coarse gravel is found in the upper part of the slip-surface material and is interpreted as comminuted Taihape sandstone (Figure 3.17). The slide-surface material is similar to that found in boreholes at the Utiku landslide. X-ray diffractometry (XRD), scanning electron microscopy with an energy dispersive x-ray attachment (SEM-EDX) and chemical composition analytical testing was carried out on the slide surface clay by Reyes (2007). These results showed that the slip-surface material comprised silty sandy clay with 30 – 35 % smectite matrix.

Least-squares analysis of three-point solutions from various combinations of drillholes indicates the slide surface is essentially planar, with an average dip/dip direction of 4° - 5°/160° - 165°). The dip/dip direction of bedding noted in the area is typically 5° - 10°/150–190°, which is similar to the dip/dip direction of the clay layer forming the landslide slip plane. Geological strike lines (Figure 3.16) represent the depth of the slip plane along strike perpendicular to the dip direction of the layer.

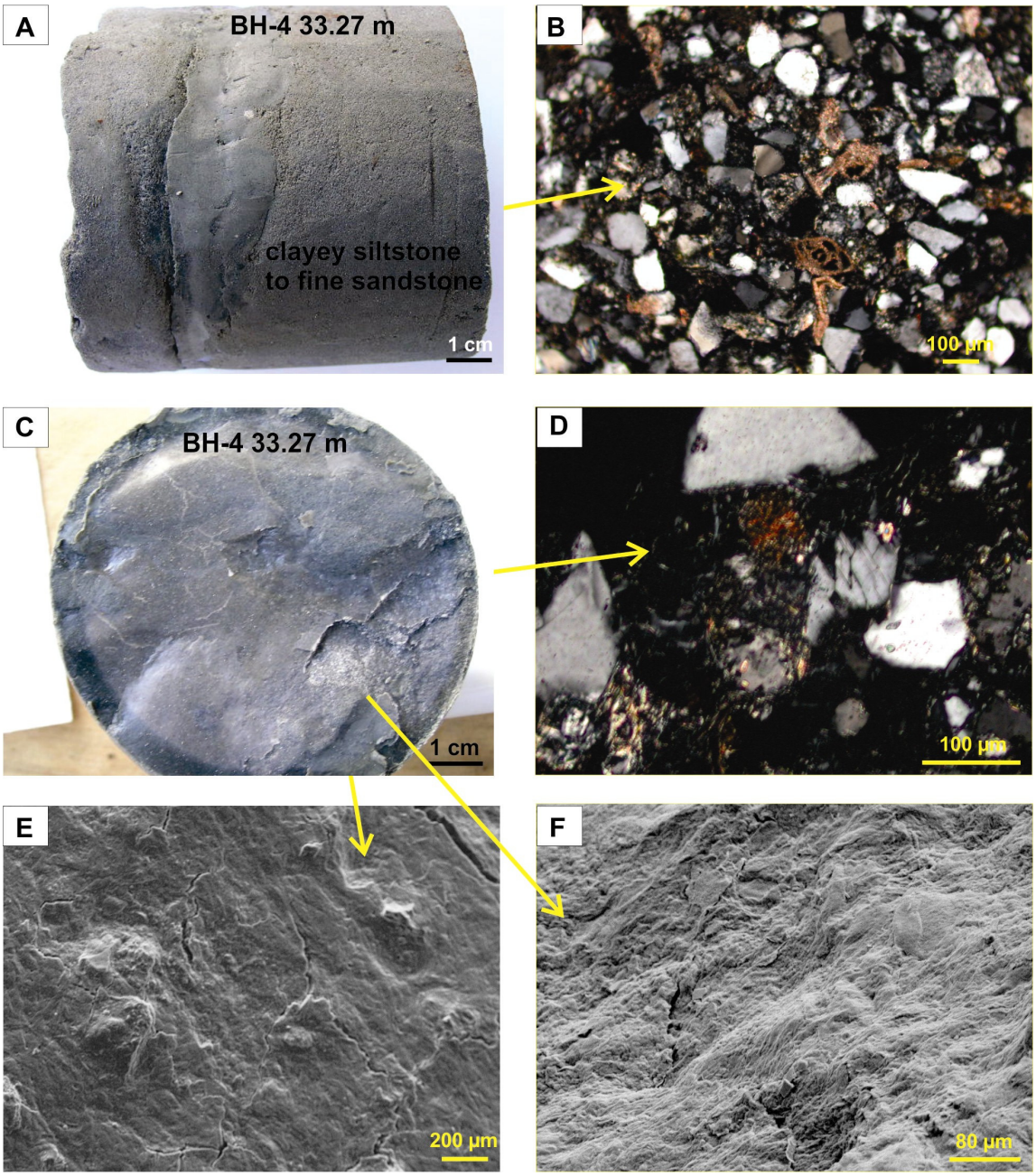

Figure 3.17 Taihape landside slide surface taken from drill hole BH4. A: BH4 (33.27 m bgl) core sample showing (B) Clayey sandstone under crossed nicols. C: Close-up of the slip surface. D: View under crossed nicols showing a few broken plagioclases. E and F: Show slickensides in the landslide slip surface under the SEM using secondary electrons. (Reyes, 2007.)

Table 3.06 Landslide slide surface details derived from drill holes (Taihape)

Drill hole	Depth below ground level (m bgl[1])	Slide surface elevation (m AMSL[2])	Slide surface thickness (m)	Description[3]
TPE3	16.50	411.40	0.03	1-cm thick soft fracture zone; hard, brittle fractures. Contains fragments up to 2 cm of blue grey sandstone.
GHD BH1	24.30 to 24.60	396.20	0.30	Wet, loose, silty sand with gravel base (thin shear zone).
BH1	22.85	427.9	0.15	Highly fractured zone of sheared material (crush zone) with some clay gouge directly overlying assumed bedrock.
BH2	24.50	433.6	0.10	Highly disturbed sheared zone of silty sand/sandstone with a 10 mm thick layer of clay bands (2 to 3 mm thick), at 24.5 m bgl.
BH3	24.15	441.5	0.03	Sharp sheared contact between disturbed landslip debris and assumed bedrock. Shear surface consists of a clay band (2 to 3 mm thick), within a crushed zone with polished slickenside surfaces.
BH4	33.25	452.3	0.02	Sharp sheared contact between disturbed landslide debris and assumed bedrock. Shear surface consists of a clay gouge (up to 20 mm thick).
BH5	44.15	464.3	0.01	Sandy clay layer up to 7 mm thick, with dark brown staining below, dry, darker grey slightly wavy base. (Not an obvious feature, slip surface could be lower)

[1]Below ground level (bgl)
[2]Elevation meters above mean sea level using the Moturiki vertical datum 1953
[3]Descriptions taken directly from drill hole logs and reports using NZGS (2005)

3.5.4.3 Taihape Mudstone

The majority of the Taihape landslide mass is derived from Taihape mudstone, displaced blocks of which occur at various locations within the landslide. In outcrop and in situ, the material comprises silty sandstone, very fine grained, slightly greenish grey, very weak to weak, with some ovoid cobble- and boulder-sized concretions. It is generally massive with very few discontinuities. The discontinuities tend to be either within blocks that have been displaced or within outcrops adjacent to the landslide, and are possibly movement-induced. Multiple thin (1 – 20 mm) clay seams were recognised by Thompson (1982) within the underlying Taihape mudstone formation. Although not found outcropping in the Taihape sandstone, these clay layers are thought to be marine-altered air-fall tephra (Thompson, 1982; Reyes 2007). Other bedding inferred from concretionary layers exposed outside the landslide boundary have mapped dip/dip directions of between 5° – 10°/150° – 190°, similar to regional trends, although bedding becomes locally steeper (10° – 20°) close to the Taihape fault.

3.5.4.4 Material parameters

Geotechnical parameters for materials within the landslide have been derived from laboratory tests on core samples from the 2005 drill holes. These laboratory tests comprised consolidated undrained (with pore-pressure measurement) triaxial tests on samples from drill holes BH2 and BH3 carried out by Geotechnics Ltd. Geotechnical parameters for the Taihape mudstone (bedrock) were taken from Read and Miller (1990) and are from geologically and stratigraphically similar materials. These are summarised in Table 3.07. The material forming the landslide slide surface has yet to be tested in the laboratory, but ring-shear and direct-shear test are currently underway.

Table 3.07 Geotechnical parameters from testing (Taihape)

Material	Description[1]	Unit weight kN/m^3	Strength parameters	Young's Modulus (MPa)	Poisson's ratio	Test method
Landslide debris – intact displaced blocks	Very fine grained SANDSTONE, extremely weak	21	c' = 35 ±(5) kPa ϕ' = 37° ±(8)	800 ±(100)	0.3	3 Triaxial tests (Geotechnics Ltd.)
Bedrock – Taihape Mudstone	Sandy SILTSTONE, very weak	21	c' = 300 ±(50) kPa ϕ' = 50° ±(10)	1,000 ±(500)	0.35	Triaxial (Read and Miller, 1990)

1Material descriptions as per NZGS (2005)

3.5.4.5 Landslide model

The complex, reactivated, translational rock slide (Cruden and Varnes, 1996) known as the West Taihape landslide was thought to have initiated prehistorically, most likely due to a combination of factors, but primarily by the incision of Otaihape Stream making slip along the identified planar slide surface kinematically feasible (Figure 3.18). Strong ground motions from displacement along the Taihape fault or along some other active fault in the area may have also been a contributory factor.

The current landslide complex can be divided into two broad zones representing the effects of increasing amounts of material disaggregation with distance from the head scarp:

1. A central zone of disturbed intact displaced Taihape mudstone that extends to the toe and forms a general depression containing abundant geomorphic signs of historic and recent instability, with materials that are partially remoulded;
2. A surrounding zone of relatively intact slide blocks of displaced Taihape mudstone, which form a series of horsts and grabens, and where there is little sign of historic or recent landslide activity.

Displacement of the landslide occurs by slip along a thin planar horizon of clay parallel to bedding with displacements typically diminishing upslope (north) from the toe. The dip and dip direction of the clay layer forming the slip surface is 4° - 5°/160° - 165°), and does not daylight at the landslide toe. The slide surface is about 6 m below the current base level of Otaihape Stream, indicating that the landslide toe is confined. The landslide head scarp may be coincident with other geological discontinuities; the western scarp appears to have formed along the Taihape fault; and the northern scarp may be along an older geological fault or some other dominant discontinuity. The trend of the northern scarp slope is aligned to other faults in the region, however, no obvious evidence of a fault has been found on site.

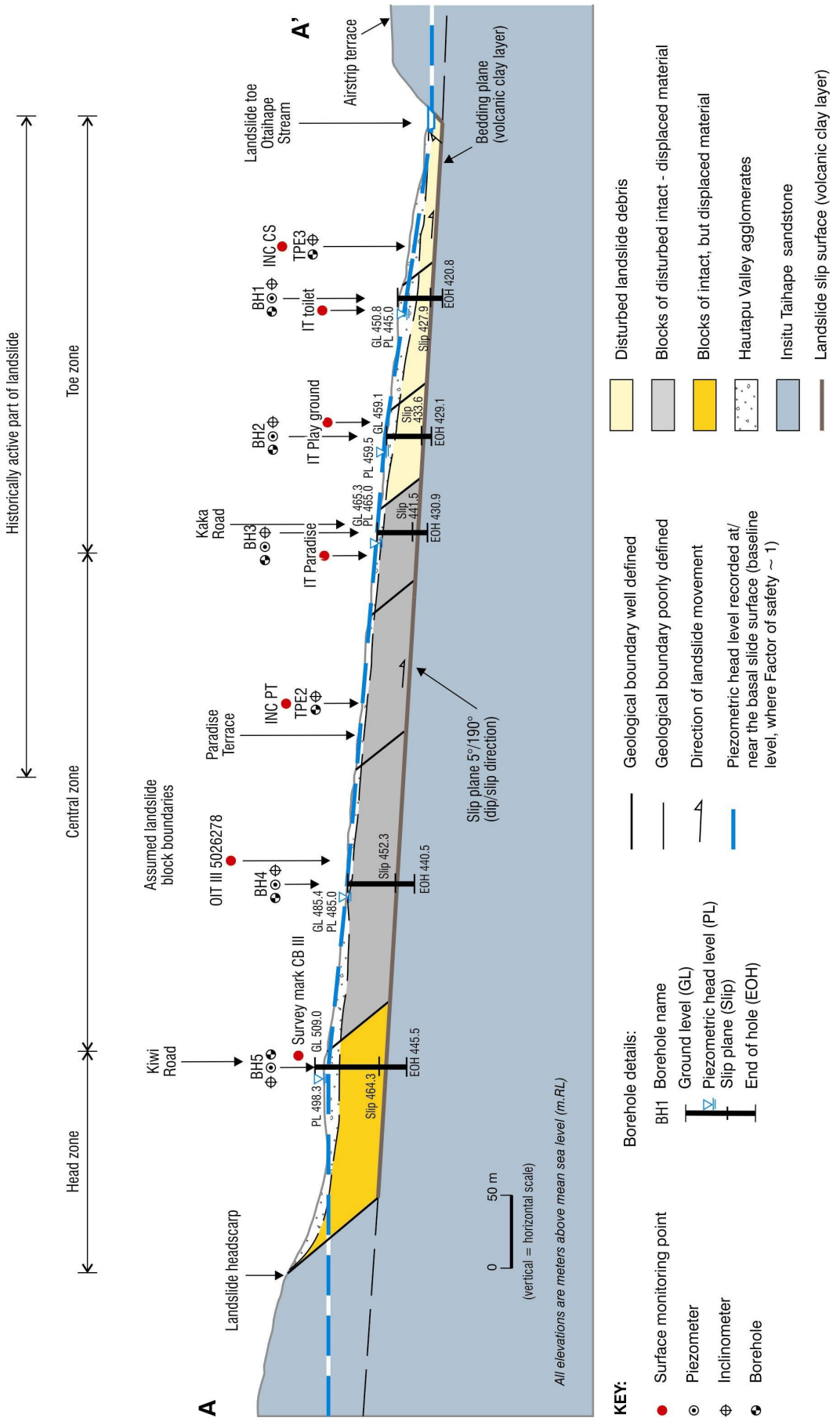

Figure 3.18 Long section A-A' (Figure 3.16) through the Taihape landslide.

3.6 Summary

The Utiku and Taihape landside were chosen for this study because they are well studied and are representative of the 7,000 mapped, large translational slides in Tertiary-age sediments of New Zealand (Dellow et al., 2005).

This chapter described their characteristics and the area in which they occur. In overview:

1. The Utiku and Taihape landslides are complex, reactivated, translational rock slides, although the toe of the Utiku slide forms an earth flow (Cruden and Varnes, 1996).
2. Both landslides occur in similar materials with similar geotechnical properties.
3. The landslides comprise a series of slide blocks formed of relatively intact materials that are sliding along thin planar horizons of clay parallel to bedding.
4. Slide-surface materials typically comprise silty clays of the smectite group that are thought to be volcanic in origin. Results from SEM and XRD testing show that the clays at Utiku and Taihape are similar in composition.
5. The geometries of the two landslides are different, however, with Utiku sliding on two perpendicular planes as a wedge, while Taihape is essentially planar.
6. At both landslides the debris generally represents different proportions of remoulding caused by landslide movement, which becomes more remoulded with distance/displacement from the landslide crest.
7. Both landslides terminate at drainage lines, with the slide surface of the Utiku landslide day lighting in the Hautapu River, however, the slide surface of the Taihape landslide is several meters below the base of Otaihape Stream.

CHAPTER 4 METHODOLOGY

4.1 The monitoring networks

This chapter describes the monitoring equipment installed on the landslides and explains how the raw data have been derived and processed. Two networks capable of high temporal and spatial resolution monitoring of landslide movement and the variables that influence movement (Objective 1 of this research) have been installed on the Taihape and Utiku landslides. Monitoring equipment was selected primarily on the temporal resolution that could be achieved; so that periods of landslide movement could be linked to the triggering factor(s), (Objective 2 of this research).

Each installed monitoring network comprises equipment to monitor surface and subsurface landslide movement, rainfall, earthquake ground accelerations, pore pressures, river stage, barometric pressure and air temperature on and immediately adjacent to the landslide. The equipment used to monitor surface movement varies between the landslides, while the other equipment installed is near identical. The surface-movement monitoring systems were designed specifically for each landslide, taking into account such constraints as: the site logistics (e.g. remoteness, power, cell-phone coverage); historic movement rates; morphology (relating to restrictions on survey line-of-sight and GPS sky view); vegetation (again relating to restriction of line-of-sight or sky view); and land use. Figures 4.01 and 4.02 show the locations of the monitoring equipment installed on the landslides.

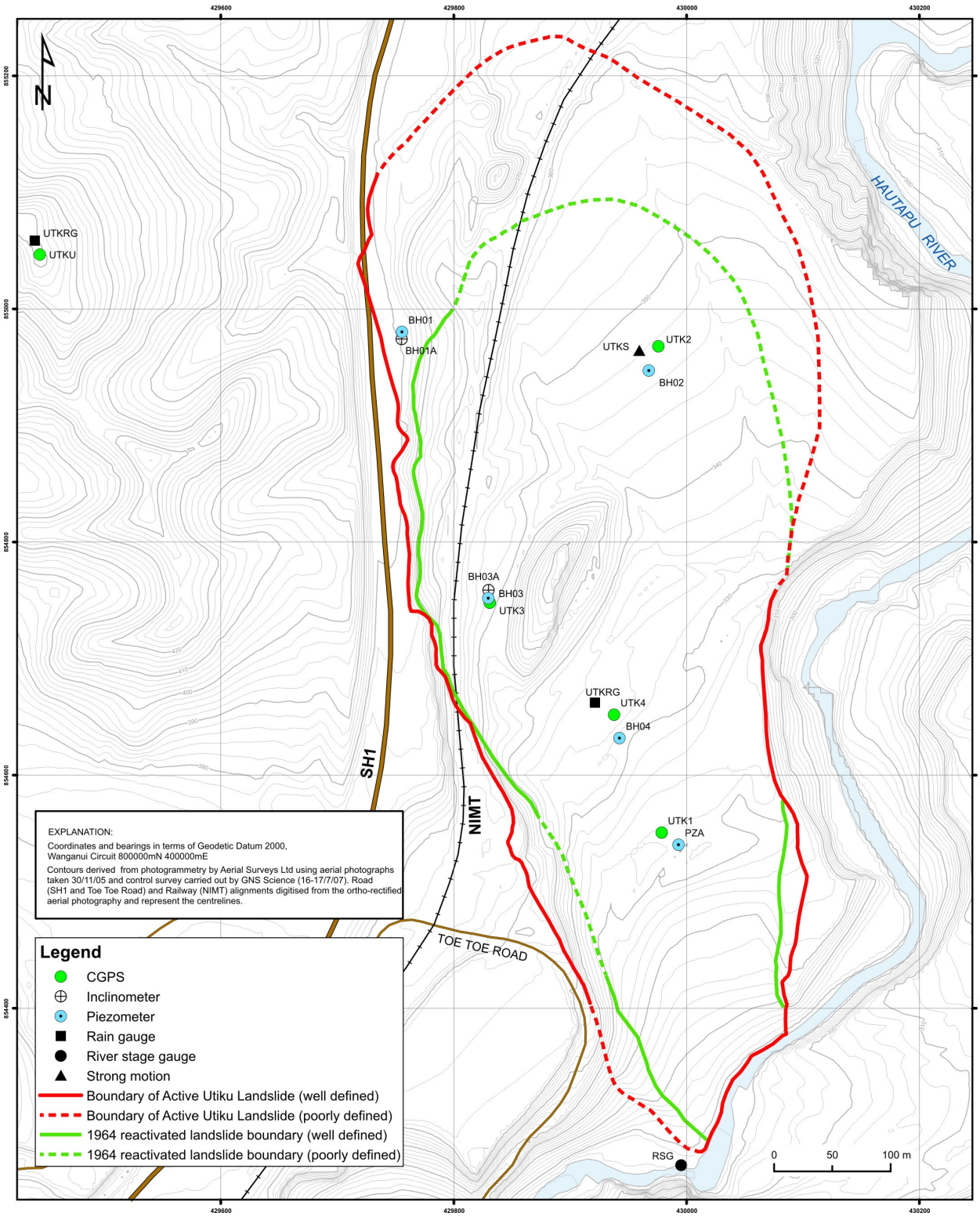

Figure 4.01 Map of the Utiku monitoring network

Figure 4.02 Map of the Taihape monitoring network

4.1.1 Surface movement

4.1.1.1 Utiku

In June 2008, four continuous GPS (CGPS) receivers were installed on the landslide to monitor surface movement. The instruments are Trimble Net RS dual-band (L1 and L2) receivers, recording at 30-second epochs (Figure 4.03). The nominal listed precision of the Trimble NET RS is ± 5 mm + 0.5 ppm horizontal RMS and ± 5 mm + 1 ppm vertical RMS (Trimble, 2010). Data recorded by the four CGPS receivers on the landslide are referenced to a CGPS receiver installed on stable ground, allowing the system to be operated as a localised deformation network, removing effects such as tectonic and tidal movements and limiting atmospheric refraction issues. CGPS antennae are mounted on I-beam galvanised-steel beams, 6 m in length, inserted 4 to 4.5 m in holes drilled in the landslide, and backfilled with concrete.

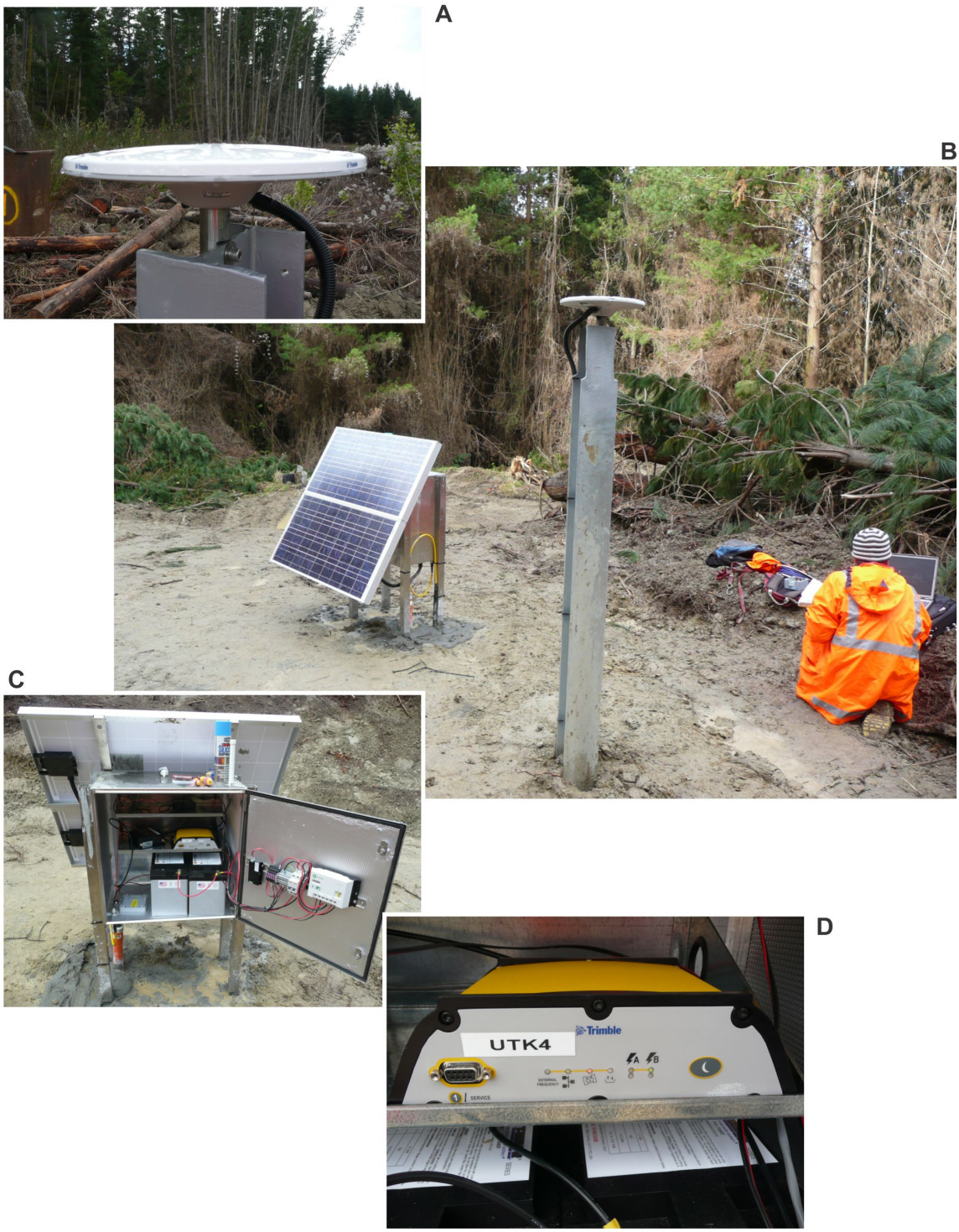

Figure 4.03 Photograph of a typical continuous GPS site at Utiku. A: GPS antenna. B: Solar panel, cabinet and galvanised-steel I-beam on which the GPS antenna is mounted. C: cabinet containing the CGPS receiver, batteries, regulator and pore pressure data logger. D: Installed Trimbe NetRS GPS receiver.

4.1.1.2 Taihape

A semi-permanent, semi-continuous, surface-movement monitoring system was installed on the Taihape landslide in June 2006. The system uses a Leica robotic total-survey station (TCA2003) that sequentially seeks and measures the locations of survey reflectors (prisms) at hourly intervals. The data are managed and displayed through custom software, and the system is run remotely. The total-survey station is installed on

a hillside south of the landslide toe (Figure 4.04). The precision of the total survey station is: angular ±0.5" (horizontal and vertical angle measurement); and distance ±1 mm ± 1 ppm; and the range is specified as 2,500 m (Leica, 2010).

Figure 4.04 Photograph of the robotic total station at Taihape

The total survey station is protected in a custom-built housing and is installed on a reinforced-concrete survey pillar anchored in bedrock (Taihape mudstone). There is a gap between the pillar and the concrete base slab of the building, which isolates the pillar from any movement of the building. The total survey station looks through a window that is angled at 20 degrees from the vertical to minimise reflection through the glass. Power for the equipment is generated from solar panels on the roof of the housing (Figure 4.05).

Figure 4.05 Photograph of the monitoring hut at Taihape

The total station is operated by the proprietry software Leica GeoMos. Three back-sight prisms on stable ground on the western and eastern flanks of the landslide (prisms 1001 and 1002 respectively), and above the landslide head scarp (prism 1003), provide survey control. The prisms on each landslide flank are on reinforced-concrete survey pillars anchored in Taihape mudstone, and were originally part of the Land information New Zealand (LiNZ) national survey network. The head scarp back-sight (prism 1003) is anchored to a house, with the house founded on a reinforced concrete base slab. Slope distances to the prisms are 697.3 m (prism 1001), 488.7 m (prism 1002) and 1179.7 m (prism 1003). Back-sight prism locations for prisms 1001 and 1002 were taken from the LiNZ survey network and checked by a standard geodetic GPS survey. The position of prism 1003 was determined from a weekly average of measurements made by the total survey station. The positions of the back sights are assumed to be fixed. The position of the total survey station is also assumed fixed and was derived from averaging two-weeks of observations made of back-sight prisms 1001 and 1002.

Thirty-five prisms are currently installed on the landslide (Figure 4.06). The prism sites were selected based on the engineering geological mapping and historical ground deformation surveys. Where possible, sites were selected to measure relative displacements across significant geomorphological features and some prisms were placed on houses with varying foundation types, ranging from piles to concrete slabs. Where prisms were pole mounted, the poles are galvanised steel pipes (70 mm external diameter, 60 mm internal diameter, installed about 1.5 m into a 200 mm diameter augured hole backfilled with concrete. Each pole is about 1 m in height, above ground level, however, heights vary at each site to avoid local line-of-sight obstructions.

Figure 4.06 Photographs of the monitoring prisms at Taihape. A: Prism 24. B) Prism 23. C) Prism 8. Locations of prisms are shown on Figure 4.02.

4.1.2 Subsurface movement

Borehole inclinometer tubes are used at both landslides to monitor displacements at depth, assess whether movement is occurring along single or multiple slide-surfaces, and to independently verify the results of surface monitoring. Monitoring is undertaken manually by commercial contract using a portable system at approximately three-monthly (Utiku) and bi-monthly (Taihape) intervals, or when requested if significant movement has been noted. Four inclinometer tubes are currently functional at Taihape and two at Utiku.

The slope inclinometer installation and interpretation processes involve several important considerations so that the resulting measurements and differences from the zero (the average of two initial surveys following installation) in subsequent readings are meaningful. (1) The inclinometer base must be below the landslide slide surface; (2) The same probe and electrical cable used for the zero readings should be used for subsequent readings so all readings are comparable (Stark and Choi, 2008). At both landslides, all inclinometer tubes extend past the inferred slide surfaces from the logging of boreholes and the same instrument and cable used for the zero reading is used for each round of measurements. Inclinometer casings were installed as per the recommendations made by Stark and Choi (2008) using bentonite grout backfill material.

4.1.2.1 Utiku

Inclinometer tubes were installed in two boreholes on the landslide in May 2008 (BH1A and BH3A). Displacements of the Slope Indicator® 85 mm diameter, plastic inclinometer casings (installed to the base of drillholes), are monitored based on test method ASTM D6230:05, using Probe-type Inclinometers with readings at 0.5 m intervals. Inclinometer accuracy is quoted as ± 6 mm over 25 m of tubing (Slope Indicator, 2005). Zero readings were conducted on 9th July, 2008, when each inclinometer was read twice (Table 4.01).

Table 4.01 Summary of inclinometer details (Utiku))

Inclinometer	Tube top (m AMSL)	Inclinometer depth		First-reading date	Subsequent reading dates
		m bgl	m (AMSL)		
BH1A	379.7	71.0	308.2	9/07/2008	14/08/08, 11/09/08, 10/11/08, 21/12/08, 16/04/09 and 20/06/09
BH3A	351.8	51.9	300.4	9/07/2008	

4.1.2.2 Taihape

Inclinometer tubes were installed on the landslide in August 1984 (TPE2, TPE3 and TPE5), however, they did not intercept the landslide slide surface and are of limited use. Displacements were measured using Soil and Rock Instruments Limited® 58mm diameter aluminium inclinometer casings installed to the base of the drillholes. Monitoring was undertaken using probe-type inclinometers at 0.5 m intervals. Zero readings were conducted on 8th August, 1984.

Three inclinometers were installed in July 2005 (BH1, BH2 and BH3) and a further two (BH4 and BH5) in June 2006. All of these inclinometer tubes were anchored below the identified slide surface. Displacements of the Slope Indicator® 70 mm diameter plastic inclinometer casings (installed to the base of drillholes), are monitored based on test method ASTM D6230:05 using Probe-type Inclinometers with readings at 0.5 m intervals. Inclinometer accuracy is quoted as ± 6 mm over 25 m of tubing (Slope Indicator, 2005). Zero readings were conducted on 15th September, 2005, for BH1 to BH3, with BH4 and BH5 installed the following year and base readings conducted on 15th June, 2006 (Table 4.02).

Table 4.02 Summary of inclinometer details (Taihape)

Inclinometer	Tube top (m AMSL)	Inclinometer depth		First reading date	Subsequent reading dates
		m bgl	m AMSL		
TPE2	481.89	34.0	447.9	8/08/1984	8/08/1984, 3/11/1988, 19/04/2000, 15/06/2004, 3/05/2005
TPE3	444.40	18.0	426.4	8/08/1984	8/08/1984, 13/09/1984, 25/10/1984, 11/06/1985, 18/09/1985, 28/11/1985, 20/05/1986, 23/05/1991, 3/06/1993, 3/11/1988, 23/05/1993, 19/04/2000, 15/06/2004, 3/05/2005
TPE5	468.82	13.0	455.8	8/08/1984	8/08/1984, 18/09/1985, 3/06/1993, 19/04/2000, 15/06/2004, 3/05/2005
BH1	450.80	30.0	420.8	15/09/2005	From 15/09/2005 to present, readings are made at intervals of two to three weeks.
BH2	459.10	33.0	426.1	15/09/2005	
BH3	465.40	34.5	430.9	16/09/2005	
BH4	485.50	43.0	442.5	27/06/2006	
BH5	508.40	63.0	445.4	27/06/2006	

4.1.3 Groundwater measurement

Pore pressures within the landslides are measured using Casagrande piezometers (standpipes) in boreholes. Each piezometer tube measures piezometric pressure within a screened response zone with two tubes per hole, with the depth and length of each response zone selected on the basis of logging of materials from the boreholes (Figure 4.07). Each response zone was sealed using bentonite clay. Typically these response

zones correspond to the assumed landslide slip surface, and zones where materials appeared to be particularly disturbed within the landslide mass. Vibrating-wire (VBW) pressure transducers are installed in those standpipes with response zones corresponding to the assumed landslide slip surface. The VBW transducers measure the pressure head of water within the Casagrande (standpipe) piezometer. Measurements are taken at 5-minute intervals and stored in data loggers before being sent via remote communications to the GNS Science servers. Power is generated by solar panels (Figure 4.08). Other standpipes are manually monitored with a dip meter.

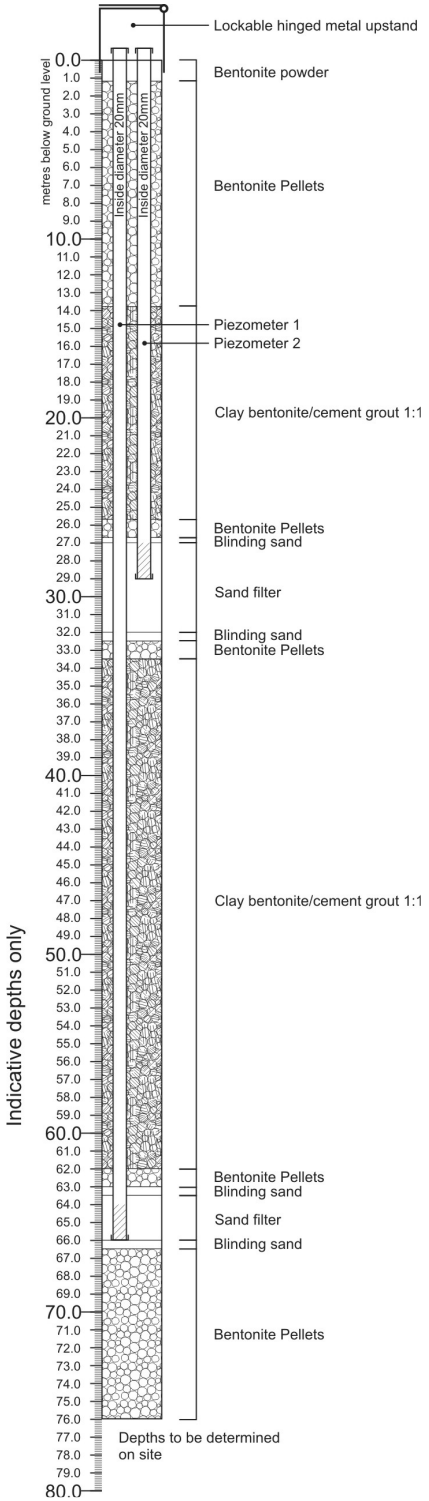

Figure 4.07 Schematic diagram of a typical piezometer borehole

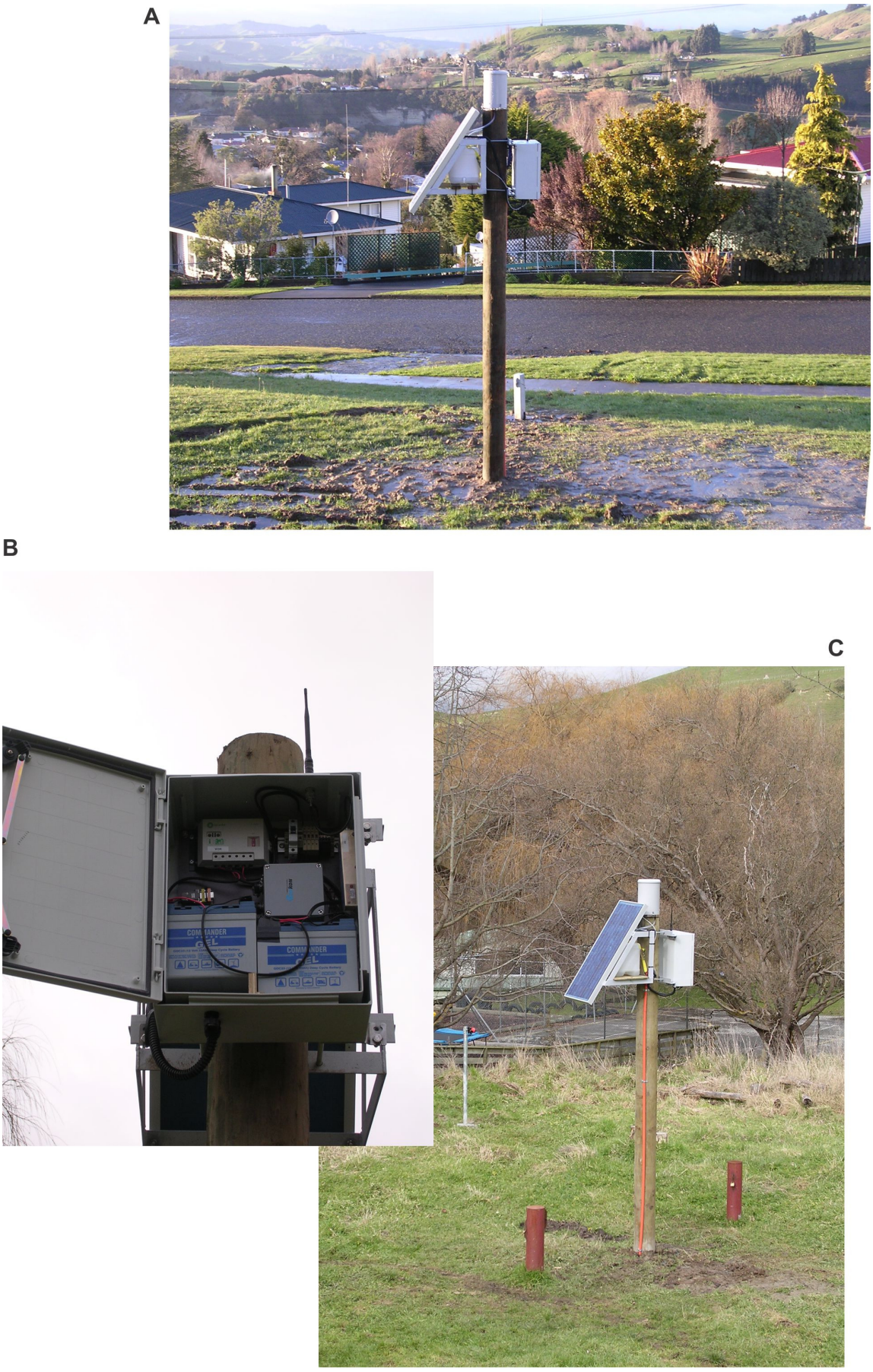

Figure 4.08 Photographs of a typical piezometer setup at Taihape. A: Rain gauge and piezometer cabinet at BH5. B: Piezometer cabinet at BH1. C: Rain gauge and piezometer cabinet at BH2.

4.1.3.1 Utiku

Four vibrating-wire (VBW) piezometers were installed in Casagrande standpipe piezometer installations in boreholes BH1, BH2, BH3 and BH4. The four installed in 2008 (BH1 to BH4) comprise two casagrande piezometer standpipes, a lower and upper installation. An additional VBW piezometer was installed in piezometer PZA, drilled sometime between 1994 and 1995. The VBW piezometers in BH1, BH2, BH3 and BH4 are placed in the Casagrande standpipes with response zones closest to the logged landslide slide surface (Table 4.03). Although the tip of the Casagrande standpipe in PZA is above the inferred depth of the slip surface, no records were available at the time of writing.

Table 4.03 Piezometer installation details (Utiku)

Location	Ground elevation (m AMSL[1])	Slide surface elevation (top) (m AMSL)	Depth of VBW Piezometer tip (m bgl[2])	Casagrande standpipe response zone		Data collection
				From (m AMSL)	To (m AMSL)	
BH1	379.1	314.0	64.5	316.1	313.1	Manual
BH2	346.9	331.5	15.0	334.2	331.6	Automated
BH3	351.8	302.7	45.0	309.8	305.3	Automated
BH4	330.6	302.6	21.5	310.4	304.6	Automated
PZA	321.4	Unknown	19.0	Unknown		Automated

[1]Elevation meters above mean sea level using the Moturiki vertical datum 1953
[2]Depth below ground level

4.1.3.2 Taihape

Four vibrating wire (VBW) piezometers were installed in Casagrande standpipe piezometer installations in boreholes BH1A, BH2A, BH3A and BH5A. Each of the 2005/2006 drillholes (BH1A to BH5A) comprise two Casagrande piezometer standpipes, a lower and upper installation. The VBW piezometers in BH1A, BH2A, BH3A and BH5A were placed in the Casagrande standpipes with response zones closest to the logged landslide slide surface. All other Casagrande piezometers are manually measured by local council staff on a daily to weekly basis (Table 4.04).

Table 4.04 Piezometer installation details (Taihape)

Location	Ground elevation (m AMSL)	Slide surface elevation (top) (m AMSL)	Depth of VBW Piezometer tip (m bgl)	Casagrande standpipe response zone		Data collection
				From (m AMSL)	To (m AMSL)	
TPE6 (upper)						
TPE6 (middle)	481.7	Unknown	N/A	Unknown		Manual
TPE6 (lower)						
BH1A (upper)	451.2	427.9	N/A	440.2	437.2	Manual
BH1A (lower)			21.0	430.4	428.4	VBW, Automated
BH2A (upper)	459.2	433.6	N/A	446.7	443.7	Manual
BH2A (lower)			18.5	439.7	436.7	VBW, Automated
BH3A (upper)	465.3	441.5	N/A	443.3	441.3	Manual
BH3A (lower)			26.5	438.8	437.8	VBW, Automated
BH4A (upper)	485.4	452.3	N/A	469.9	467.8	Manual
BH4A[1] (lower)			N/A	454.9	452.9	Manual
BH5A (upper)	509.0	464.3	N/A	499.5	496.5	Manual
BH5A (lower)			36.5	477.0	471	VBW, Automated

[1]No VBW piezometer was installed in BH4 as piezometric head levels in the deeper standpipe are almost always at the top of the standpipe tube, which is 0.4m above ground surface.

4.1.4 Rainfall

Rainfall on each landslide is monitored using two 0.2 mm tipping-bucket rain gauges. At Utiku, one is located above the head scarp and the second is in a large clearing at the centre of the landslide. At Taihape one is located at the head scarp and the second is near the toe. There is historical daily rainfall data for both landslides. The Taihape data dates back to 1912 and the Utiku data dates back to 1964.

4.1.5 Earthquakes

Earthquake ground accelerations at each landslide are monitored using strong-motion accelerographs (Etna) in vaults on each landslide. The triggering threshold for these instruments is 0.2 % of gravity (0.002 g) and the frequency response is DC to 80 Hz.

4.1.6 River stage

The toe of the Taihape landslide is coincident with O'Taihape Stream, while at Utiku the toe coincides with the Hautapu River. Water levels are monitored using Solinst Level loggers (Divers®). Loggers record water level and temperature and are corrected for barometric effects using barometric divers located on each landslide. Measurements are taken at hourly intervals.

4.2 Temporal resolution of the measurements

The temporal resolution of the monitoring data are summarised in Table 4.05.

Table 4.05 Temporal resolution of the measurements

Description	Equipment	Resolution
Utiku surface movement	CGPS	30-second epochs averaged over successive 24-hourly (daily) periods (midnight to midnight UTC)
Taihape surface movement	Total station and prisms	Hourly measurements averaged over successive 24-hourly (daily) periods (midnight to midnight UTC)
Utiku subsurface movement	Inclinometers	As/when required but typically every three months
Taihape subsurface movement		As/when required but typically every two/three weeks
Groundwater (pore pressure)	Vibrating wire piezometers	Hourly intervals averaged over successive 24-hourly (daily) periods (midnight to midnight UTC)
Rainfall	Tipping bucket rain gauges	As and when rainfall occurs, but accumulated over successive 24-hourly (daily) periods (midnight to midnight UTC)
Earthquake ground accelerations	Strong motion accelerometer	As and when strong motions ≥0.2g occur
River stage	Pressure transducer	Hourly measurements

4.3 Data transfer, processing and display

An integral part of these monitoring networks has been the automated data transfer, processing and display systems, which were set up to minimise the loss of data from malfunctioning equipment. Both monitoring networks operate in near-real time, which can be defined as the delay between the occurrence of an event and the availability for use of the processed data (introduced by automated data processing and network transmission). There is a variable end-to-end (site to office) data transfer delay of approximately one hour.

At Utiku, wireless transfer of data from the GPS receivers, piezometers, rain gauges and strong-motion sensors is achieved via a commercial mobile phone network. At Taihape, wireless transfer of data from the robotic total station and other equipment is achieved via free-wave radios to the Taihape Town Hall and via commercial internet land line to GNS Science buildings in Wellington (250 km south of Taihape) (Figure 4.09). The data is automatically processed, formatted, checked and placed on the internet as both graphical images and data files. The results for both landslides are presented in charts on the GeoNet website: http://www.geonet.org.nz/resources/landslide/, and are updated at hourly intervals. This allows the data to be easily used and interpreted (Figure 4.10 and 4.11). Equipment and network faults are also remotely monitored.

Figure 4.09 Schematic map of the monitoring and communication network at Taihape

Figure 4.10 The on-line Utiku landslide monitoring applet

Figure 4.11 The on-line Taihape landslide monitoring applet

4.4 Analysis methods of landslide-movement mechanisms

4.4.1 Landslide surface movement

Data from the high-resolution monitoring have been used to assess: when landslide movement initiates; its duration and rate; bearing; location within the landslide; and relationships between slide-blocks. Motion at each landslide is recorded using different equipment, which each require different processing methodologies.

4.4.1.1 Utiku

The GPS processing is done using Bernese v5.0 software developed by the Astronomical Institute of the University of Bern (AIUB), using current models which are routinely used and available to GNS Science. Details of the processing are contained in Beavan, http://www.geonet.org.nz/resources/gps/gps-processing-notes.html, (2010). For each GPS receiver the processed data comprise the coordinates and their formal uncertainties, which are converted to (east, north, up) displacement in millimetres from an initial point. For Utiku stations, the initial point is the first point in the time series using New Zealand Geodetic Datum (NZGD) 2000.

The GPS time series from Utiku are regionally filtered following the procedure described by Beavan (2005), treating the east, north and up components at each site separately. A reference station that is as free as possible from non-linear signals, i.e. located off the landslide and on stable ground, is used to estimate the common-mode signal, which is done by simple averaging. The reference station is located at Taihape (identifier THAP) about 6 km north of the landslide.

The following procedures are undertaken to prepare the reference station for averaging:

- Removing any offsets in the time series due to known equipment changes at the station or to known coseismic offsets;
- The time-series are de-trended to remove any long-term cumulative displacements caused by e.g. plate tectonic motion. This is done by best-fitting a linear trend to the time series, which is then subtracted from each time series;
- the daily mean value is taken point-by-point through the time series, including all reference station solutions that exist on each day;
- a best-fitting linear trend is subtracted from the mean time series.

This results in the common-mode time series. Then, for each CGPS on the landslide the raw time series is processed by:

- removing offsets in the time series due to known equipment changes at the station (coseismic offsets are not removed as these represent real ground deformation);
- the common-mode time series is subtracted;
- a best-fitting linear trend and annual sinusoid are subtracted;
- outliers from the results are trimmed;
- the linear trend and the annual sinusoid (but not the offsets due to equipment changes) are added back.

Identified outliers are then ignored in the raw time series, and the five operations are repeated. This ensures that all identifiable outliers are removed. The result is a regionally-filtered time series for each station (station identifiers UTK1, UTK2, UTK3 and UTK4).

Users can see the effect of outlier removal and regional filtering by comparing “raw” and “regionally-filtered” time series available at the GeoNet website, http://www.geonet.org.nz/resources/gps/timeseries/index.html (Beavan, 2005) (Figure 4.12).

Figure 4.12 The on-line New Zealand GPS monitoring applet which includes the Utiku landslide GPS data

4.4.1.2 Taihape

The robotic survey station records bearing and distance to each prism at hourly intervals. The three backsight prisms are measured first using both faces of the total station. This occurs prior to measuring the prisms on the landslide and is done to ensure that the orientation and position of the total station are within pre-determined error limits. It is also used to estimate the survey precision, which varies with atmospheric refraction caused mainly by air-temperature gradients, air-pressure gradients, lunar and seasonal cycles. The effects of atmospheric refraction are estimated by comparing the measured positions to the original 'fixed' positions to derive the bearing and distance errors. The positions of the prisms on the landslide are then measured sequentially, using two faces of the survey station. These positions are then corrected by subtracting the errors derived from the backsights, which are scaled based on the slope distance from the total station to the prism (along line-of-sight).

The survey station is equipped with automatic target recognition (ATR), to locate each prism. During each hourly measurement cycle, the survey station looks for each prism at its last known location (i.e. the last measured position of the prism). The ATR searches for the strongest return signal, in most cases the prism, within a specified

radius of the last known position and once identified, the prism location is measured. The hourly measurements are converted from polar to rectangular coordinates and averaged over successive 24-hour periods from midnight to midnight UTC. This process is fully automated, and displacements of each prism are calculated and plotted as cumulative displacement along the main historical movement bearing of the landslide, and are then displayed on the GeoNet website.

4.4.1.3 Surface movement – estimating the uncertainty

At Utiku, an estimate of the uncertainties associated with the daily position of each CGPS receiver was made by taking three random samples of about 100 measurements (days) through the easting, northing and vertical time-series data from each station. The data were checked to ensure the sample contained no large changes in velocity. A linear trend was fitted to the sample and the difference between the measured and the linear values calculated. The distribution of the residuals was checked to ensure they were normally distributed and the standard deviation of the mean calculated, which is used as an estimate of the precision. Using the standard deviation to calculate errors assumes independence of variables from one day to the next and so is appropriate for time-series data derived from surveying.

At Taihape, an estimate of the uncertainties associated with the daily position of each prism was made by calculating the mean of the 24-hourly measurements (midnight to midnight UTC), treating the angle and horizontal and vertical distance measurements separately. The distribution of the residuals was checked to ensure they were normally distributed and the standard deviation of the mean calculated. The standard deviation of the mean of each daily position was then averaged over the time series, which is used as an estimate of the precision.

4.4.1.4 Filtering techniques

In most cases the daily positional data is used to determine relationships between GPS/prism movement and the destabilising factors such as pore pressure and rainfall. However, when trying to establish longer-term trends in motion it is advantageous to filter or smooth the displacement time series. The purpose of the smoothing is to estimate the actual motion from the measured apparent motion to help identify the trends. This can be done using various techniques, ranging from moving averages to more complex Gaussian and Savitzky–Golay (1964) smoothing functions.

A Gaussian smoothing kernel was used as this smoothing function tends to preserve features of the distribution such as relative maxima, minima and width, which may be 'flattened' or shifted by other smoothing techniques such as moving averages. In its

averaging, it assigns higher weights to points closer to the middle of the “Smoothing Window” compared with those on the far edge of the smoothing window. Conversely, in a moving average, all points in a window size are equally weighted. The distribution of the weighted values in the smoothing window follows a Gaussian distribution shape. Theoretically, a Gaussian smoothing filter is best to remove normally distributed noise, where the variables are assumed to be independent of one another.

The severity of the smoothing depends upon the window size (G_s) of the Gaussian smooth, which can be varied using an assumed standard deviation, where the window size is 6 times G_s. Where used, the precision of the Gaussian smoothing kernel is estimated by calculating the difference between the measured and the smoothed cumulative displacement time-series. The distributions of the residuals are checked to ensure they are normally distributed and the standard deviation of the mean is calculated, which provides the estimate of the precision of the smoothing kernel. The effects of varying the G_s of the smoothing kernel are shown in Figure 4.13.

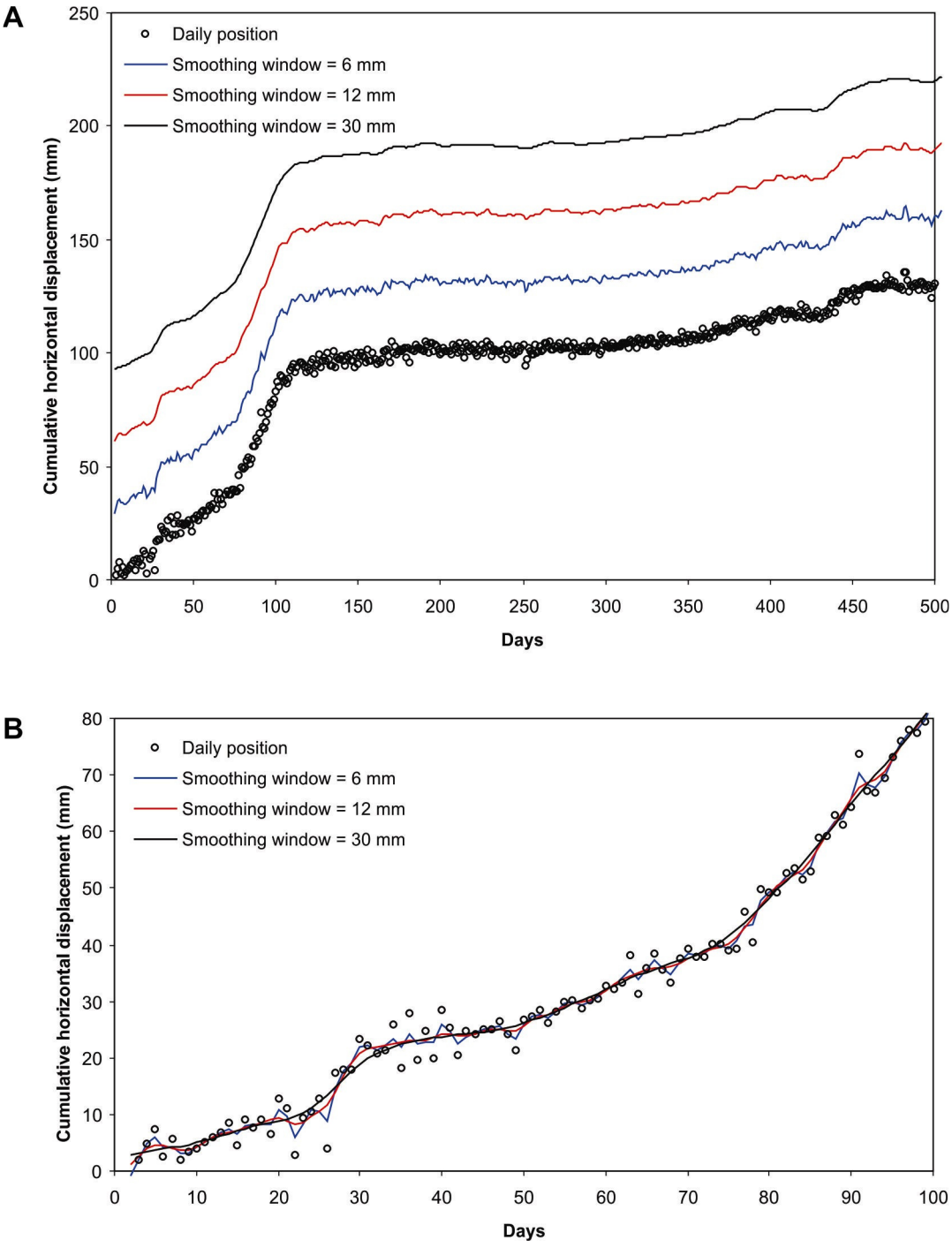

Figure 4.13 Diagram showing the effects of the Gaussian smoothing kernel for different smoothing windows (G_s). A: Daily and smoothed cumulative horizontal displacements for station UTK1. B: Extract of the time series from A, showing daily and smoothed cumulative horizontal displacements.

4.4.2 Subsurface movement

Subsurface displacements have been compared to surface displacements to determine the proportion of surface displacements corresponding to displacements along the slide surface.

Results from each period of inclinometer monitoring are referenced to the zero reading. Each period of inclinometer monitoring records the incremental displacement and

cumulative deflection over the length of the inclinometer tube, relative to the bottom of the hole. The cumulative deflection profiles provide a representation of the actual deformation pattern of the inclinometer tube, however, for deep installations errors can be accumulated. To minimise these systematic errors the magnitude and direction of motion at the slide surface is calculated for each survey using the incremental displacements and the pre-set A- and B-axes of the inclinometer tube. The cumulative displacements along the main movement direction are plotted to show changes in surface position relative to the landslide base.

4.4.3 Rainfall and groundwater

The purpose of this analysis was to determine the relationship between rainfall and changes in piezometric head levels, as changes in piezometric levels can cause landslide movement. Reactivation of the Utiku slide in 1964 was attributed to high pore pressure (Belz, 1967) and the 2004 reactivation of the Taihape landslide occurred following the largest recorded daily rainfall in the area. The largest inflows into the landslides are from precipitation, mainly rainfall and minor snow melt. Other inflows include: leakage from sewage, storm water and potable water reticulation (Taihape only), however, these are not measured.

Instantaneous hourly gauge readings (in Hertz) from the vibrating-wire piezometers are converted to pressure using the method of Geokon (2008). These pressures are then averaged over each UTC day (from midnight to midnight) to obtain a daily average pore pressure for each instrument. Readings are then corrected for barometric effects by subtracting the daily mean change in barometric pressure, using data from a barometric-pressure sensor installed at Taihape, from the daily averaged pore-pressure readings.

To quantify relationships between rainfall and piezometric levels a correlation analysis was undertaken where the pore pressure at each piezometer and the antecedent rainfall (as recorded on the landslide) were assessed to establish the time frame over which rainfall influences piezometer response. The pore pressure at a given time and the accumulated antecedent rainfall was assessed incrementally, e.g. $P_t \rightarrow R_{t\text{-}1\text{-}2}$; $P_t \rightarrow R_{t\text{-}1\text{-}2\text{-}3}$; $P_t \rightarrow R_{t\text{-}1\text{-}2\text{-}3\text{-}4....}$ where P_t is the pore pressure at a given time and R_t is the antecedent rainfall. The correlation analysis assumes a linear relationship between pore pressure and rainfall. The correlation is obtained by dividing the covariance of the two variables by the product of their standard deviations. This procedure establishes what duration of rainfall is needed to cause a statistically significant change in daily pore pressure, i.e. estimating the lag time between rainfall and piezometer response. The influences of evapotranspiration and soil moisture, and leakage from services on the

Taihape landslide are not taken into account in the correlation analysis as these variables are not monitored.

4.4.4 Groundwater pressure and movement

Velocity changes (accelerations) in this type of landslide are thought to be controlled primarily by changes in basal pore-water pressure (Bertini et al., 1984; Nakamura, 1984; Picarelli, 2004; Corominas, 2005; van Asch, 2007; Gonzalez et al., 2008). Piezometric levels (daily averages of the hourly records) have been correlated with daily landslide displacements to quantify the relationship between rainfall-triggered groundwater rises and landslide velocity (Objective 2 of this research).

Pore pressures from both landslides were analysed: 1) for each discrete period of detected significant displacement; and 2) for the entire monitoring period. Relationships between pore pressure and landslide velocity were assessed by applying both the Mohr-Coulomb failure criterion and a Bingham viscosity model to determine the relative importance of pore-pressure induced changes in effective stress on the initiation, rate and arrest of landslide movement (Objective 3 of this research).

4.4.5 Stability analysis

The aim of the quantitative stability modelling was to verify that residual shear-strengths of the clays forming the slip surfaces of the Utiku and Taihape landslides derived both from laboratory testing of slip-surface material and from the literature, were correct and appropriate, and that the monitored pore pressures and calculated stresses were representative and capable of causing the observed motions. Landslide stability was assessed using limit-equilibrium software SLIDE™ and finite element software PHASE2™.

Sensitivity of the landslide models to the estimated material strength of the slip surface was assessed using both the factor-of-safety (Morgenstern and Price, 1965) and the shear-strength-reduction (Dawson et al., 1999) approaches. Both types of modelling software analyse two-dimensional (2-D) problems, however, the landslides in reality are three-dimensional (3-D) problems. Therefore, the 2-D analysis cannot take the full landslide geometry into account and therefore any strength developed on the sides of the actual 3-D landslide or between the different slide blocks, is neglected.

4.4.5.1 Limit equilibrium method

Conventional limit equilibrium methods allow the equilibrium of a soil mass to sliding down slope under the influence of gravity to be assessed. Translational or rotational movements can be considered, where displacement occures along a known or

unknown failure surface. All methods allow the factor of safety to be calculated (Equation 2.2), which is the ratio between the shear resistance and the shear stress. Two-dimensional sections have been analysed assuming plain strain conditions. These methods assume that the shear strength of the materials along the potential failure surface are governed by the Mohr-Coulomb failure criteria (Equation 2.1), which is a linear relationship between shear strength and the normal stress at failure. The most common limit equilibrium techniques are methods of slices where the soil mass is discretized into vertical slices where each individual slice is treated as a unique sliding block. The calculated factor of safety derived from the different methods can vary, as many of the methods do not satisfy all of the equations of equilibrium (Morgenstern and Price, 1965).

The method of Morgenstern and Price (1965) on which the general limit equilibrium (GLE) method is based, is one of the few limit equilibrium methods where the solution of the governing equations ensures that all equilibrium and boundary conditions are satisfied, including the distribution of the interslice force angles. The GLE method relies on the selection of an appropriate function that describes the variation of the interslice force angles. This method allows the user to ensure that the failure criterion i.e. tensional failure, of the soil mass above the slide surface is not violated. To investigate whether tension is implied, the position of the line of thrust can be calculated for each slice and if it falls outside of the potential sliding mass tension must exist within (Morgenstern and Price, 1965). To do this an interslice force angle function must be chosen which relates the internal forces between the slices. This function can be estimated from the elasticity solutions contained in Morgenstern and Price (1965) or specified on the intuitive assumptions that: for most cross-sections the higher rate of curvature of the slide surface, the greater the ratio between shear and horizontal forces at the slice interface; or if the slice interface is within a zone of high pore pressure, the amount of shear that could be mobilised would be reduced and the function should take a lower value in these regions.

Four main functions are typically used to describe the variation of the interslice force angles, these are: 1) constant (equivalent to the Spencer LE method); 2) Half-sine; 3) clipped-sine; and 4) user specified (Abramson et al., 1997). The distribution is usually implemented with a function that is normalised with respect to the lateral (horizontal) extent of the failure surface.

The GLE method of Morgenstern and Price has been adopted to analyse the Utiku and Taihape landslides. In the case of Utiku and Taihape, constant, half-sine and clipped-sine functions were used and the resultant thrust lines and factors of safety compared.

In all cases the thrust lines were located entirely within the sliding mass, indicting tensional failure is not occurring. The calculated factors of safety using the different functions were almost identical indicating the selected interslice force angle function does not significantly affect the magnitude of the factor of safety, however, the half-sine function gave the lowest factor of safety and given the lateral extent of the failure surface this function was thought to be reasonable, and has therefore been adopted for all LE analyses presented in this research.

4.4.5.2 Finite element method

Back-analysis of the main landslide movement periods using the monitored piezometer levels and associated ground displacements for these periods was undertaken using the finite-element software PHASE2™. PHASE2 is a 2-dimensional elasto-plastic finite element program for calculating stresses and displacements for geotechnical and civil engineering problems. All modelling uses the plane strain analysis type, adopting the Gaussian elimination solver. The meshes for the models were generated using uniform, 3-noded triangles with about 2,000 to 3,000 elements and 1,000 to 1500 nodes per model. Stress analysis was carried out using 500 iterations, with a tolerance of 0.001 using the “absolute energy” convergence type. The groundwater method adopted for all models was that of piezometric lines. The factor of safety for each model was calculated using the shear strength reduction technique.

The shear strength reduction (SSR) technique allows a critical strength reduction factor to be calculated for the models. The critical strength reduction factor is equivalent to the "factor of safety" of the slope (Dawson et al., 1999). The basic concept of the SSR method is: 1) The strength parameters of a slope are reduced by a certain factor, termed “strength reduction factor” (SRF), and the finite element stress analysis is computed; 2) This process is repeated for different values of SRF, until the model becomes unstable (the analysis results do not converge); and 3) This determines the critical strength reduction factor (critical SRF), or factor of safety, of the slope.

4.5 Summary

This chapter presented an approach to quantitatively monitor the behaviour of two large, translational slides that are representative of many similar landslides in the region. It addresses the three main research objectives:

(1) Systems capable of high temporal- and spatial-resolution monitoring of landslide velocity and the variables that influence it have been installed on both landslides;

(2) The temporal- and spatial-resolution of the monitoring networks have allowed the relationship between rainfall-triggered groundwater rises and landslide

speed to be quantified.

(3) The analysis techniques used to process the monitoring data have allowed the mechanisms thought to govern landslide motion to be evaluated.

The first objective was addressed by designing and installing two different systems to record landslide surface movement at temporal- and spatial-resolutions that are appropriate for these types of landslide. Data from the surface monitoring was used to assess landslide movement rates, their timing, duration and bearing and variation in space. Data from instruments monitoring the variables believed to influence landslide velocity, mainly rainfall, groundwater, earthquake ground accelerations and river stage, have similar temporal resolution to the surface-movement monitoring data.

Periods of movement were assessed against the potential triggering factors and their relationships quantified to address the second objective.

The third objective was to evaluate the mechanisms thought to govern landslide motion. The temporal-and spatial-resolution and precision of the readings from the monitoring equipment as well as the techniques used to process the data collected have allowed the movement patterns of both landslides to be assessed and the factors thought to be controlling their movement identified.

CHAPTER 5 RESULTS

5.1 Introduction

This chapter presents data recorded by the monitoring equipment installed on the Taihape and Utiku landslides. The objective of this chapter is to present the collated data, quantify its errors and measurement from the various instruments and to discuss statistically significant trends and relationships and compare them with longer-term historical monitoring results. The results from both landslides are then discussed further and key themes highlighted for subsequent analysis and discussion.

5.2 The Utiku Landslide – monitoring results

Monitoring of the Utiku landside commenced in July 2008 and is ongoing. The 31st October 2009 has been used as a cut-off date for the monitoring data presented here, providing 15 months of data for analyses. The landslide monitoring data focuses primarily on recorded surface/subsurface motion, rainfall and pore-pressures. Earthquake ground motions and changes in the level of the Hautapu River are also included but to a lesser extent as they were not a primary concern of this research.

5.2.1 GPS error analyses

Surface movement is monitored by four continuous Global Positioning System (CGPS) receivers (referred to as stations), utilising a further two CGPS stations located off the landslide for control. Only minor periods of data-loss have occurred, caused by equipment malfunction, primarily related to power loss as a result of prolonged cloudy weather. These are summarised in Table 5.01.

Table 5.01 CGPS summary of data

Site	Date installed	No. days installed (to 31/10/09)	No. 24 hour (daily) readings	No. days with no data	Data coverage
PZA UTK1	4/08/2008	455	449	6	98.7%
BH2 UTK2	22/07/2008	456	455	1	99.8%
BH3 UTK3	18/07/2008	460	460	0	100%
BH4 UTK4	17/07/2008	461	456	5	98.9%

5.2.1.1 Horizontal displacements

Scatter plots showing the "raw" deviations from the mean horizontal East- and North-coordinate values (observations), calculated for each 24-hour epoch, for stations on the landslide (UTK1 to UTK4), are shown in Figure 5.01. These plots show the spread and sequence of observations and are unadjusted, so may, for example, contain offsets due to earthquakes, and seasonal signals due to various causes. They may also contain a "common-mode" noise signal that is reasonably constant across a wide region. This may arise from the use of slightly erroneous satellite orbits, regional-scale or global-scale mass redistributions (in the ocean, atmosphere or groundwater), the use of non-optimal models in the daily processing, and perhaps other causes (Beavan 2005). Although the data presented in Figure 5.01 is unadjusted, stations UTK1 and UTK4, located on the landslide, show discernable trends where the localised movement of these stations exceed the likely sum of the factors discussed.

For those stations on the landslide, the "raw" data were adjusted to remove: offsets; common-mode noise; and plate-tectonic displacements, by referencing their motions to a locally stable station located away from the landslide. CGPS station THAP was chosen as an appropriate reference station as it is located only 6 km north of the landslide. This adjustment was done by subtracting the "raw" daily readings (observations) from reference station THAP, from the "raw" daily readings recorded at those stations on the landslide, to give a "filtered" time series. The localised stability of THAP was verified by installing a 2nd reference station at Utiku, about 0.5 km east of the landslide, scatter plots showing the raw data from both THAP and UTKU are shown on Figure 5.02.

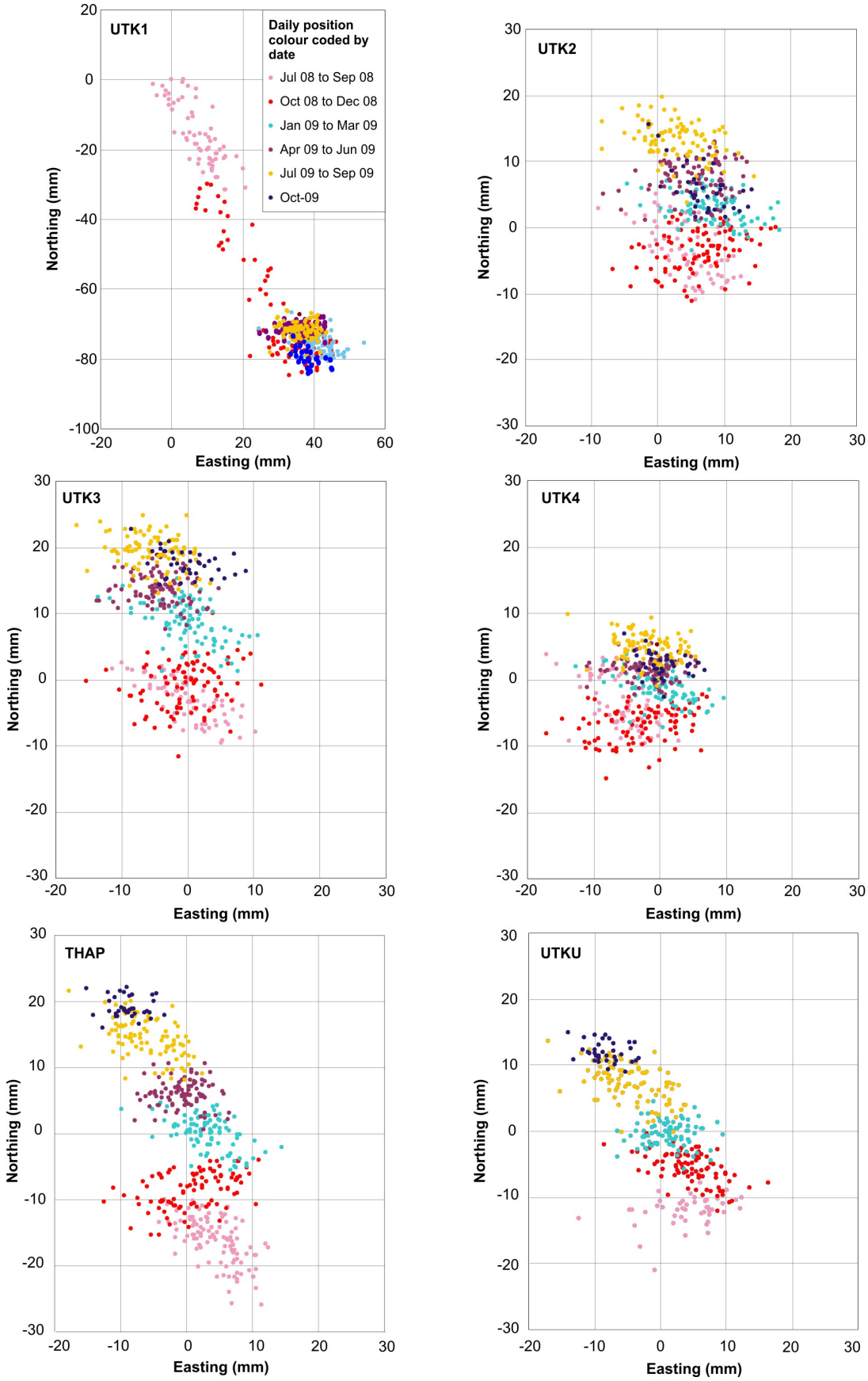

Figure 5.01 Scatter plots showing the "raw" deviations from the mean horizontal East- and North-coordinate values (observations), calculated for each 24-hour epoch, for stations on the Utiku landslide (UTK1 to UTK4) and the control stations (THAP and UTKU).

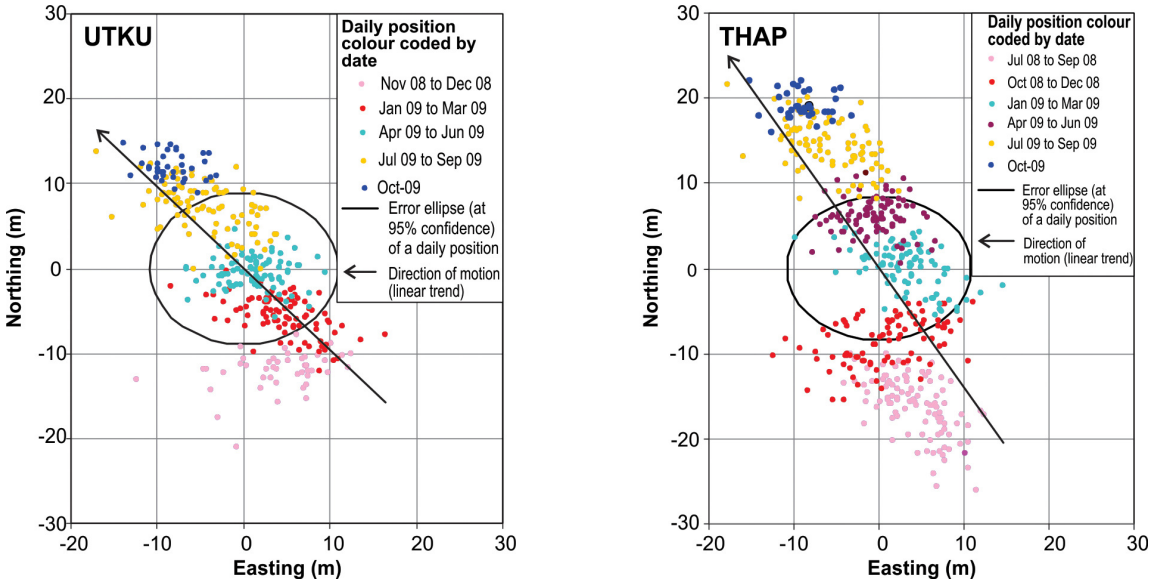

Figure 5.02 Scatter plots showing the "raw" deviations from the mean horizontal East- and North-coordinate values, calculated for each 24-hour epoch, for stations THAP and UTKU.

To verify that the reference station THAP is stable and that any motions of this station are not related to local effects such as landslides and/or settlement, the "raw" time series for THAP has been correlated with the "raw" time series from UTKU. Motion bearings of THAP and UTKU have been derived by fitting a simple linear relationship to the raw daily east and north records; these are shown in Figure 5.02 along with their associated error ellipses at 95% confidence. The errors were calculated as per the procedure described in Section 4.4.1.3, treating the northing and easting components separately. The residuals were normally distributed and the standard deviations of the means of each random sample were averaged. These errors are shown graphically as error ellipses at 95% confidence (two times the standard deviation) on Figure 5.02. These plots show that both stations have records outside their associated 95% error ellipses, indicating statistically significant motions have occurred at both stations, with motions towards bearing 325° (THAP), and 314° (UTKU). The time series plots for both stations show that their motions follow a consistent trend through time, and are near identical in form (Figure 5.03). This consistency indicates station motions are regional and not the result of localised factors. Although these are "raw" time series, and therefore not corrected, the motion bearings between the two stations do differ, considering they are only located about 6 km apart. To assess whether these are consistent with regional-scale tectonic deformations of New Zealand, the motions from THAP and UTKU have been compared to the regional North Island GPS velocity field described in Wallace et al., (2004). Motions of THAP and UTKU, relative to the Australian plate, are consistent with the regional GPS velocity field in the North Island of New Zealand, which is dominated by the long-term tectonic rotation of the eastern North Island (Wallace et al., 2004). Station THAP is therefore assumed to be locally stable.

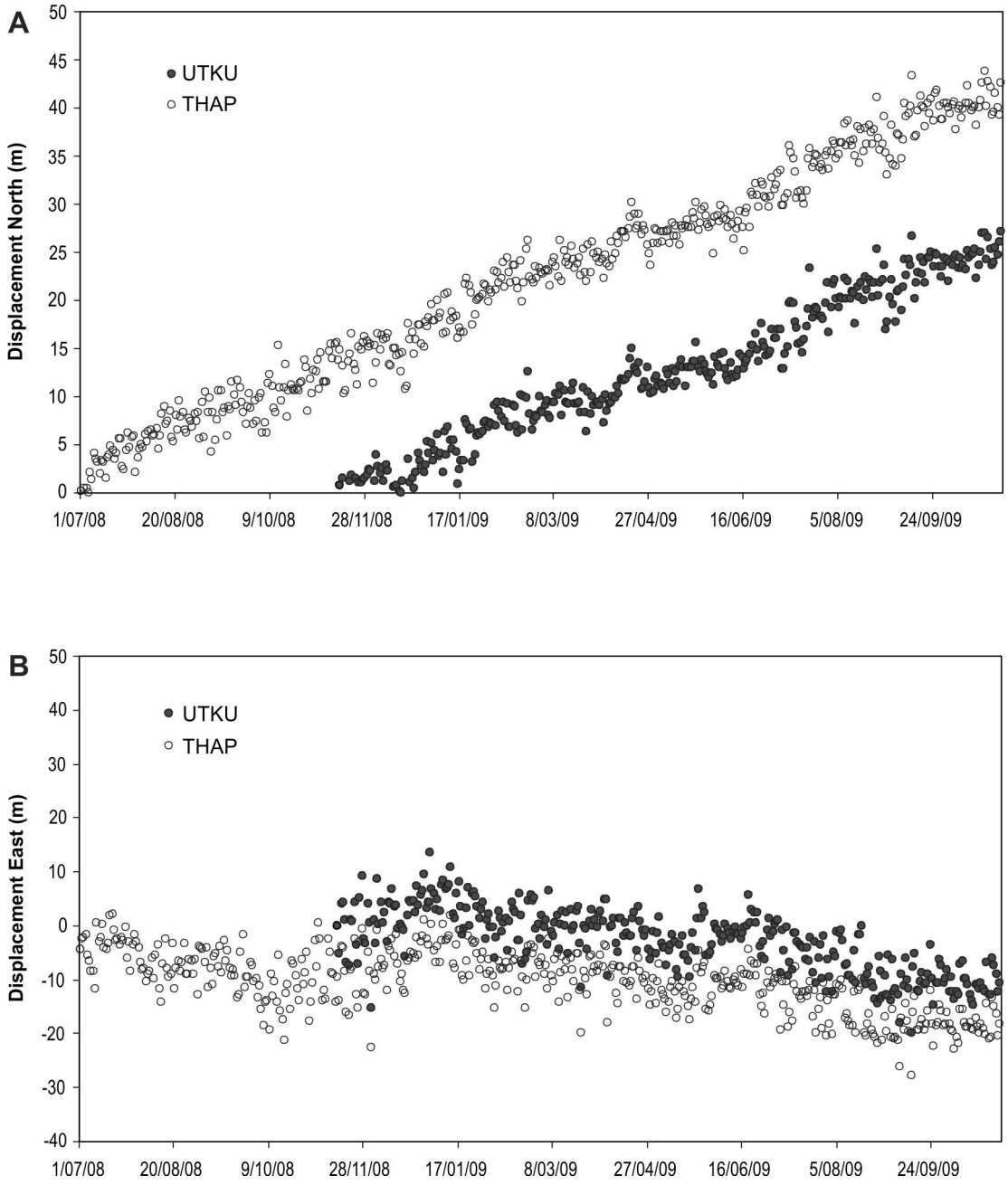

Figure 5.03 Cumulative horizontal displacement against time for stations THAP and UTKU. A: Represents the displacement in the Northing direction. B: Represents the displacement in the Easting direction. Station UTKU was installed in October 2008.

The precision of the daily filtered readings from those stations on the landslide have been estimated by following the same methodology used to asses the precision of the daily readings from stations THAP and UTKU (procedure described in Section 4.4.1.3), these are shown in Table 5.02. The residuals are all normally distributed and the uncertainties are shown graphically on the filtered time-series for those stations on the landslide as error ellipses at the 95% confidence limit (Figure 5.04). These error ellipses give a visual indication of whether movement beyond expected survey error has occurred. That is, if all observations lie inside the error ellipse then no movement can be inferred. These data indicate that for those stations on the landslide the standard deviations on the east and north readings are between 5.5 mm and 6.6 mm, with UTK4

showing the lowest associated error and UTK2 the largest. In comparison, stations THAP and UTKU have standard deviations of between 3.4 mm to 4.5 mm, which are lower than those from the landslide stations. These differences are related to the sky view at each station. Stations THAP and UTKU are located on stable hill tops, with unrestricted sky view while, for those stations on the landslide, sky view is limited by trees and topography. For those stations on the landslide, UTK4 is the most open site while UTK2 is the most restricted.

These data show that for all stations on the landslide there are observations outside the associated 95% error ellipses, indicating that displacements outside of error have been recorded, with a consistent direction to the south east, which is consistent with the historical motion bearing of the landslide.

Table 5.02 Measurement precision of the regionally filtered time-series data.

Station	Errors on the daily readings		Errors on the daily readings at 95% confidence (mm)	
	σE	σN	σE	σN
UTK1	±6.0	±5.6	±11.8	±11.0
UTK2	±6.6	±6.1	±12.9	±12.0
UTK3	±6.3	±5.5	±12.3	±10.8
UTK4	±5.1	±4.5	±10.0	±8.8
THAP	±4.4	±3.4	±8.6	±6.7
UTKU	±4.5	±3.6	±8.8	±7.1

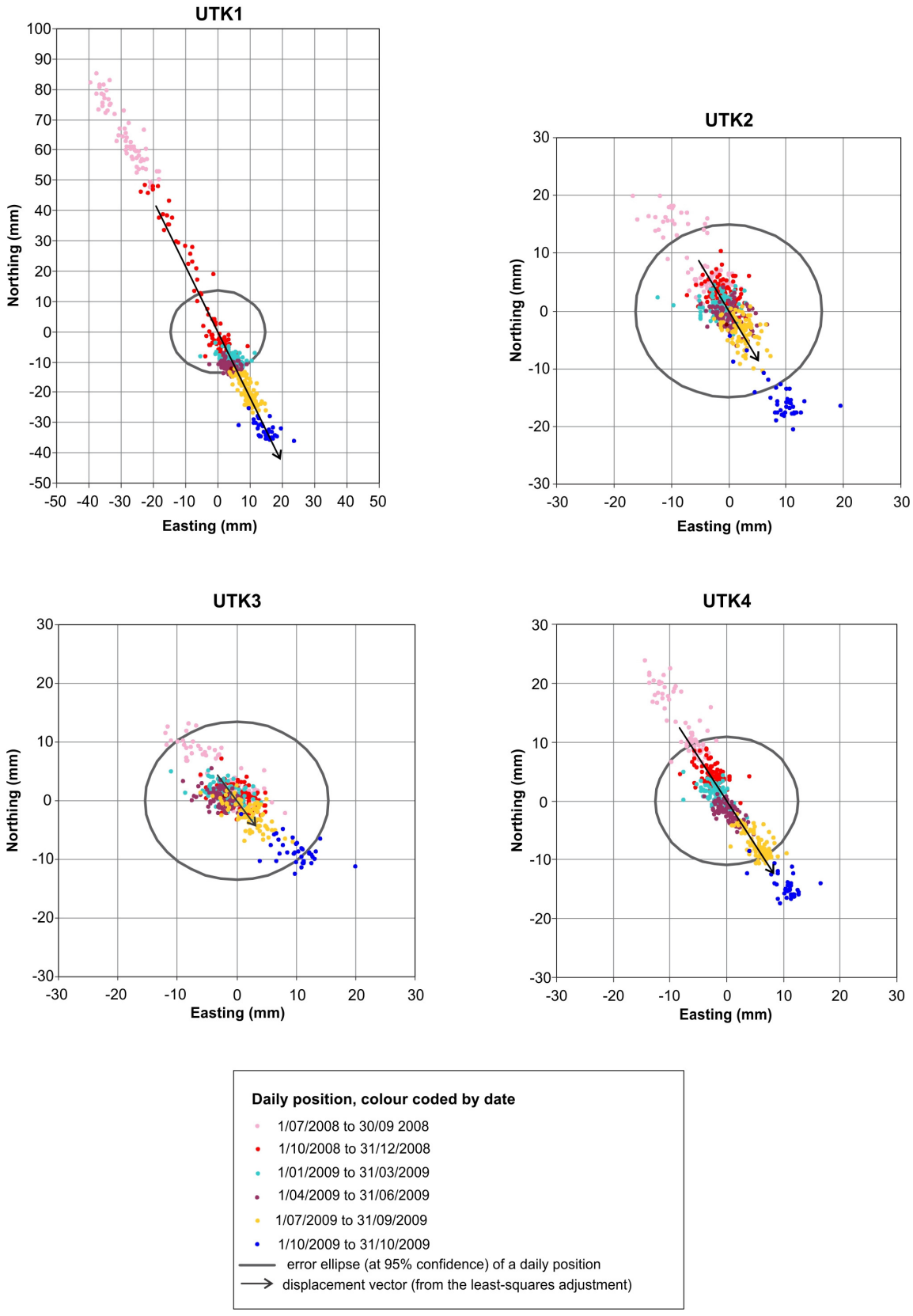

Figure 5.04 Scatter plots showing the "filtered" deviations from the mean horizontal East- and North-coordinate values calculated for each 24-hour epoch, their associated errors and motion vectors, for stations on the landslide.

A least-squares adjustment of the CGPS daily east and north readings was undertaken to determine motion vectors, and associated errors, for each station. Least-squares adjustment is a standard statistical technique for calculating the best-fitting estimate of the rate and direction of movement, based on an assumed linear model path. The best-fitting estimate is defined as the estimate that deviates least (has lowest variance) from all the observations, while considering their relative reliability (Anderson and Mikhail, 1998).

The results from the least-squares adjustment are shown in Table 5.03 and graphically as motion vectors on Figure 5.04. The time-series plots have been colour-coded to reflect the timing of the records, with each colour code representing a three-month period of records. The coloured time series for all stations show that rates of horizontal motion have varied over the monitoring period. The greatest changes can be seen in the time series plot from UTK1, for the period October to December 2008. These data show that motion gradients are not linear with time, as assumed for the least-squares adjustment. Therefore, although the least-squares adjustment method is useful to determine the bearing of displacement, it is not a useful method to assess changes in displacement rate.

Table 5.03 Station velocity and motion bearings from the least squares analysis

Station	Least-squares adjustment	
	Bearing (errors on the bearing at 95% confidence)	Velocity (mm/year)
UTK1	155° ±(3°)	71.7 ±(4)
UTK2	149° ±(4°)	15.9 ±(3)
UTK3	142° ±(7°)	8.4 ±(1)
UTK4	146° ±(2°)	23.2 ±(1)

5.2.1.2 Vertical displacements

The “raw” vertical measurements for the Landslide CGPS were filtered using the corresponding vertical time series from reference station THAP (Figure 5.05). The errors associated with vertical measurements when using GPS are greater than those for the horizontal measurements (Tables 5.02 and 5.04). The stated equipment vertical errors for the NetRS are ± 5 mm + 1 ppm vertical RMS (Trimble, 2008). An estimate of the precision of the vertical readings was calculated using the procedure described in Section 4.4.1.3. The residuals were normally distributed and the standard deviations of the means of each random sample were averaged. The results show that the estimated

errors are an order of magnitude larger than those estimated for the horizontal readings. Station UTK2 displays the largest error and UTK4 the lowest, and are consistent with those errors estimated from the horizontal readings.

To assess whether the vertical displacements are statistically significant, analyses using the least-squares method has been carried out on the daily vertical time series from each CGPS station, which assumes a linear relationship. Vertical motion is deemed to be statistically significant if the vertical-displacement gradient is larger than the standard error of the gradient, at the 95% confidence limit. Results indicate that vertical motions are statistically significant for stations UTK1, UTK2 and UTK4, with UTK 1 showing the largest vertical displacements over the period. Vertical motions at UTK3 are marginal, and do not indicate any statistically significant vertical motion. The magnitudes of vertical displacement (and errors) are shown in Table 5.04.

Although the analyses have shown that vertical motions are statistically significant for UTK1, UTK2 and UTK4, they have been analysed assuming that the motion gradient is constant (linear) with time. The vertical time series plot for UTK1 (Figure 5.05), show that this is not the case, as the vertical motion occurred over a six-month period and was followed by a period during which no vertical motions were recorded.

Table 5.04 Vertical measurement precision and displacement magnitudes (July 2008 to October 2009)

Station	GPS vertical error[1] (mm)	Vertical motion gradient (mm/day)	Error on the vertical gradient at 95% (mm/day)	Difference between the gradient and 95% error (mm/day)	Total vertical displacement over period with the error at 95%[2] (mm)
UTK1	22	-0.094	0.011	0.083	-42 ±(5)
UTK2	28	-0.042	0.010	0.032	-20 ±(5)
UTK3	22	-0.014	0.008	0.006	-7 ±(4)
UTK4	15	-0.025	0.006	0.020	-12 ±(3)

[1]Estimate of the vertical precision of the of the daily GPS readings
[2]Errors calculated from the statistics of the least-squares analyses assuming a simple linear relationship

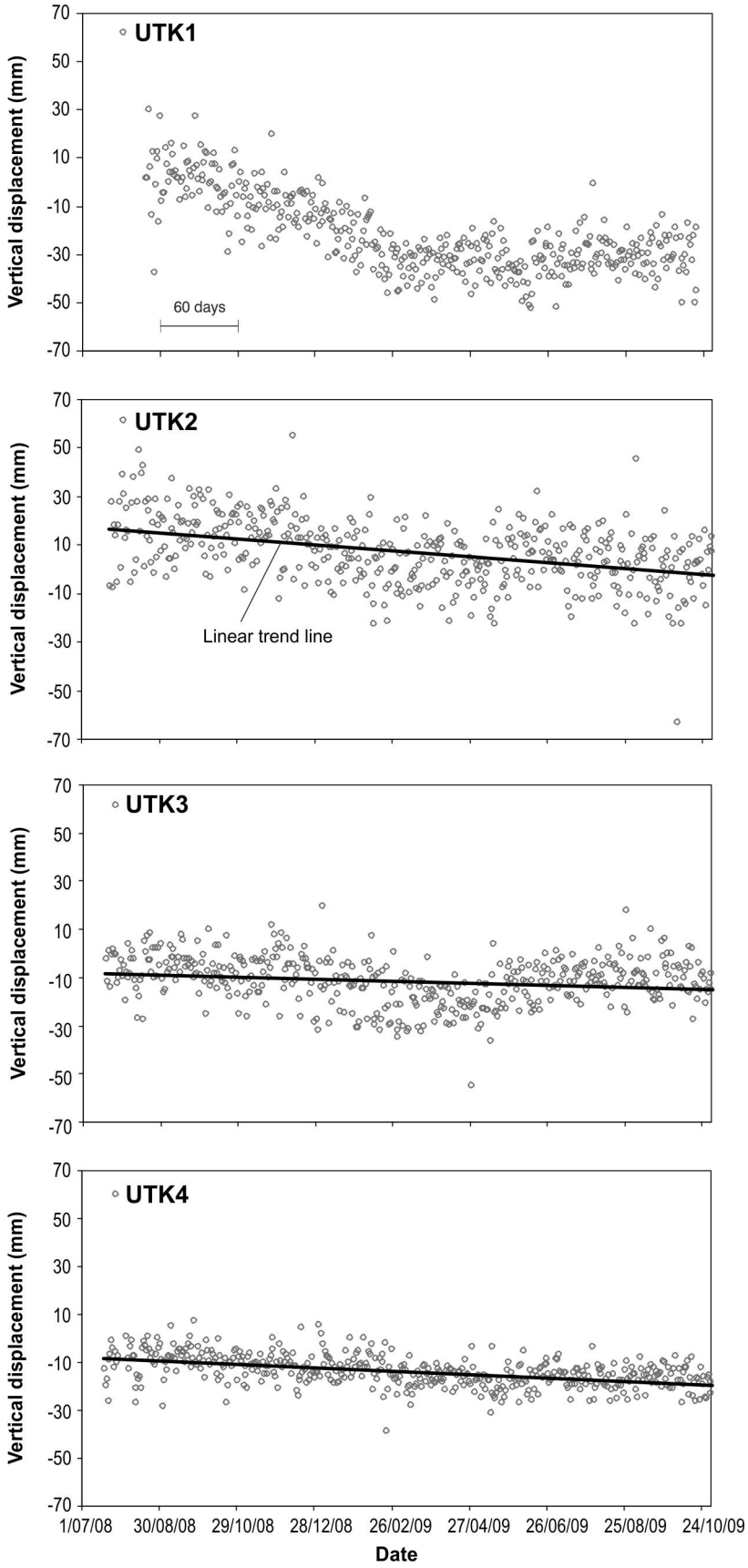

Figure 5.05 Cumulative vertical displacements against time for stations UTK1, UTK2, UTK3 and UTK4 on the landslide.

5.2.2 Landslide movement patterns

5.2.2.1 Cumulative displacements

The horizontal motion bearings for each station were derived from a least-squares adjustment, which assumes motion gradients are consistent (linear) over time (Table 5.03). The scatter plots in Figure 5.04 show that motion gradients are not necessarily linear, but can change, with these changes representing periods of acceleration and rest. To identify patterns in station velocity the filtered daily time series from the landslide CGPS stations were plotted as cumulative horizontal displacements along their main movement bearings. Each time series was smoothed using a Gaussian smoothing kernel through the daily cumulative horizontal displacements, as per the procedure described in Section 4.4.1.4 (Figure 5.06). A smoothing window of G_s = 2 mm was adopted for all stations. The residuals are all normally distributed and the uncertainties are shown in Table 5.05.

Table 5.05 Precision of the daily and smoothed daily cumulative horizontal displacement measurements.

Station	Horizontal motion Bearing (°)	Smoothing errors (mm)	Smoothing errors at the 95% confidence limit (mm)
UTK1	155	1.6	3.2
UTK2	149	1.9	3.6
UTK3	142	2.0	3.9
UTK4	146	1.3	2.6

A summary of the motions for each station, calculated over the monitoring period from the smoothed cumulative horizontal displacements are shown in Table 5.06, along with the vertical displacements.

Table 5.06 Summary of measured CGPS surface motion for the monitoring period.

Station	Total cumulative horizontal motion and errors at 95%[1] (mm)	Mean horizontal motion rate[2] (mm/day)	Horizontal motion bearing[3] (°)	Total vertical motion and errors at 95%[4] (mm)
UTK1	128 (± 3)	0.30	155	-42 (± 5)
UTK2	40 (± 4)	0.09	149	-20 (± 5)
UTK3	30 (± 4)	0.07	142	-7 (± 4)
UTK4	41 (± 3)	0.09	146	-12 (± 3)

[1]Calculated over the monitoring period from the smoothed cumulative horizontal displacements with errors calculated from the precision of the smoothing function at the 95% confidence limit.
[2]Calculated over the monitoring period from the smoothed cumulative horizontal displacement.
[3]Horizontal motion bearings calculated from the least-squares method
[4]Vertical motions and errors are calculated from the least squares method assuming a linear relationship.

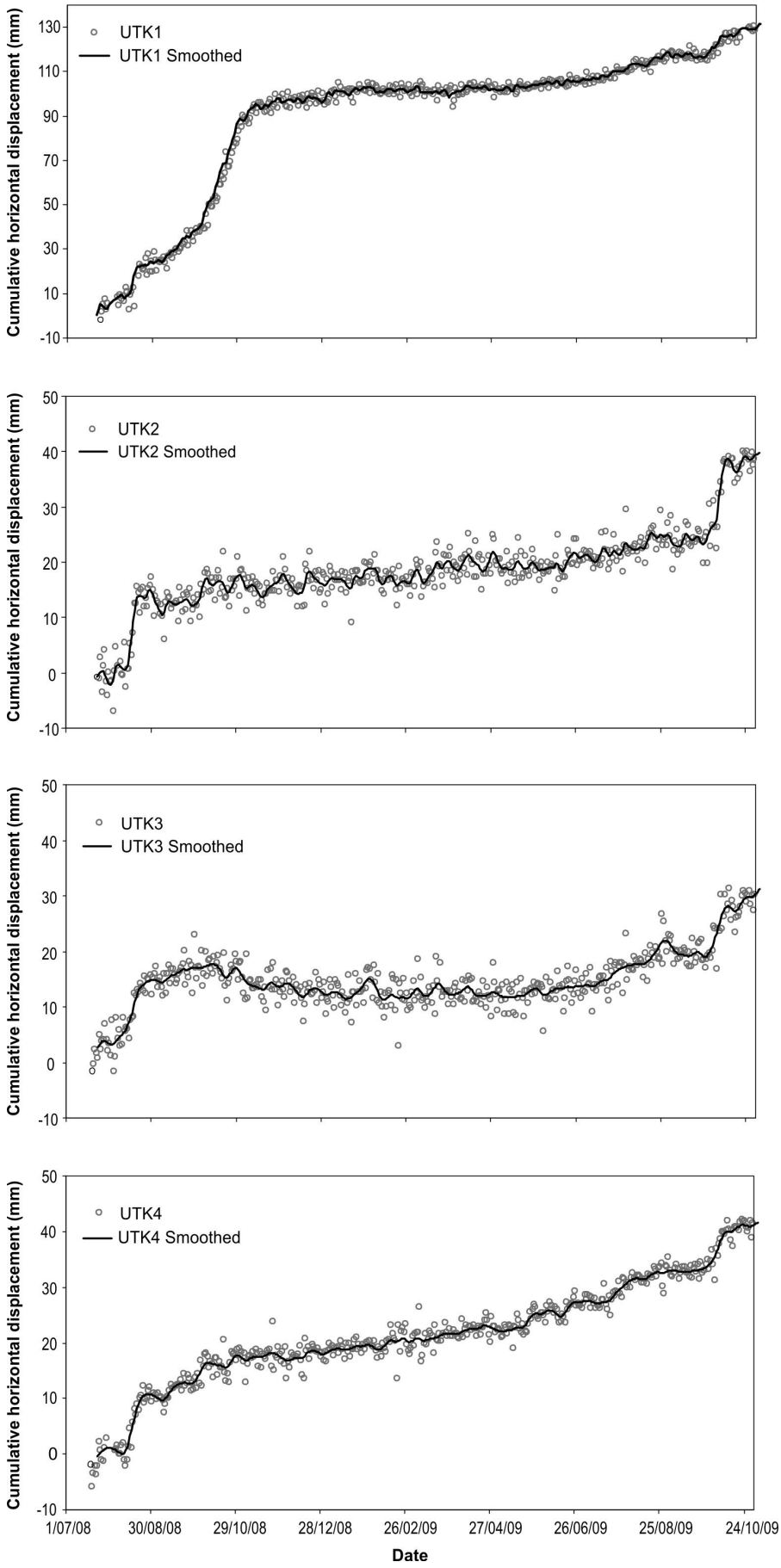

Figure 5.06 Cumulative horizontal displacements over time calculated along their main movement bearings. Daily and smoothed values are shown. Smoothed values are derived using a Gaussian smoothing kernel where G_s = 2 mm.

The magnitude and bearing of horizontal motions for each station on the landside, over the monitoring period, are shown graphically on Figure 5.07, along with their associated errors at 95% confidence (from Table 5.02). Figure 5.07 shows that the largest recorded displacements were in the toe of the landslide at UTK1. Generally, displacement magnitudes decrease towards the landslide head scarp (northwest), with the lowest displacement recorded for UTK3. There is a significant change in displacement magnitude between UTK1, on the lower landslide, and UTK4 on the upper landslide, with the motion magnitudes of those stations on the upper landslide being of a similar order. Motion bearings of those stations on the upper landslide are about 145°, while the motion of UTK1 on the lower landslide is 155°.

The recorded surface motion allows the landslide to be classified as extremely slow to very slow (16 mm/yr < x < 1.67 m /yr, Cruden and Varnes, 1996), with all GPS stations on the active landslide showing similar creep-type rates of motion. Interpretation of the cumulative horizontal displacement plots (Figure 5.06), indicate two main types of motion: 1) short-duration, relatively rapid motions, represented by steep positive gradients, or steps, in the cumulative displacement plots, which typically occur over days and weeks; and 2) longer-duration slower motions typically lasting many months to years, which are only discernable from the long-term trends in the cumulative displacement plots. The short-duration relatively rapid motions have been termed “accelerated creep” while the longer-duration slower motions have been termed “slow creep”.

Station UTK1, is located on the lower landslide and has recorded the largest displacements over the monitoring period (128 mm). Displacement magnitudes decrease upslope from UTK1 (west) towards the landslide head scarp, with station UTK3 recording the smallest displacements (30 mm). At least three distinct periods of accelerated creep are discernable from the cumulative displacement plots. Two of these periods correspond to similar motions recorded at other stations on the landslide, indicating movement of the larger landslide as a whole, while the other period represents the largest magnitude of displacement, and was recorded at UTK1 only, located on the lower landslide.

The cumulative displacement plots for all GPS stations show that slow creep has been recorded at all stations, with these motions being most obvious at UTK2 and UTK4. Slow creep at UTK3 indicates both a negative and positive gradient to the displacement, which would indicate upslope and down-slope movement of the landslide over about a year.

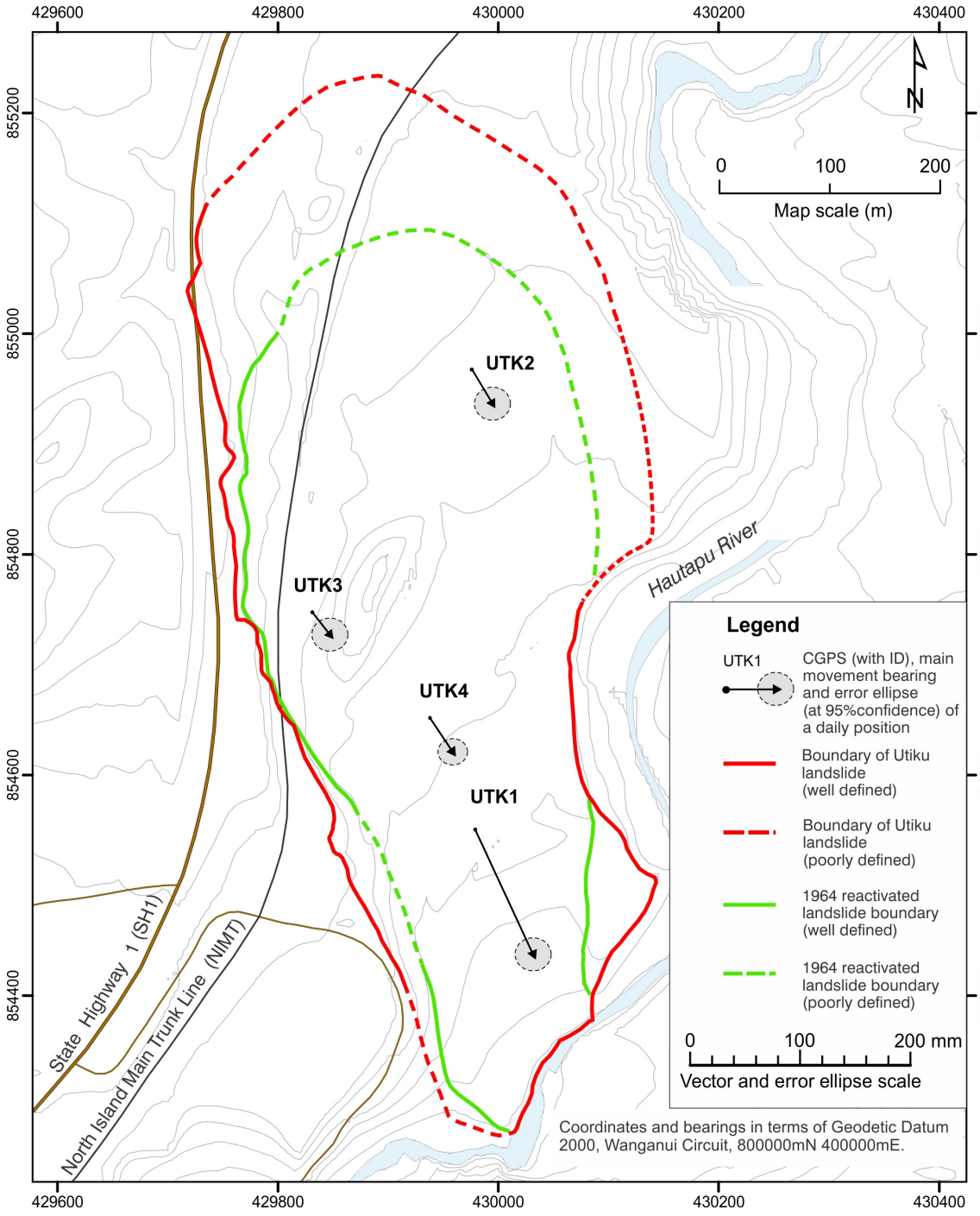

Figure 5.07 Map showing the magnitude and bearing of horizontal motions for each station on the landside, calculated over the monitoring period.

5.2.2.2. Accelerated creep

The rationale used to help identify statistically significant accelerated creep from periods of rest or slow creep, assumes that the motion is statistically significant if the cumulative horizontal displacements are larger than the error (at the 95% confidence limit), for any two daily cumulative displacements (Table 5.07). Errors are calculated from the difference between the daily mean and the smoothed daily mean cumulative horizontal displacements for each station over the monitoring period.

To identify periods of accelerated creep which are outside survey error, the velocity of each station (mm/day along the main movement bearing), was calculated over a moving 14-day period. A 14-day period was used as this represents the approximate duration of each accelerated creep period. Statistically significant periods of accelerated creep are those where station velocities are greater than the standard deviation on the velocity at the 95% confidence limit, calculated from any two daily cumulative displacements over a 14-day period (Table 5.07). These periods are shown Figure 5.08.

Three periods of statistically significant accelerated creep were identified over the monitoring period. Periods 1 and 3 (15/08/2008 to 22/08/2008 and 30/09/2009 to 10/10/2009, respectively), were recorded by all landslide GPS stations, while period 2 (6/09/2008 to 6/11/2008) was only recorded at UTK1 on the lower landslide (Table 5.8). A few additional minor periods of accelerated creep are present in the time series from UTK1, however, these are only marginally significant.

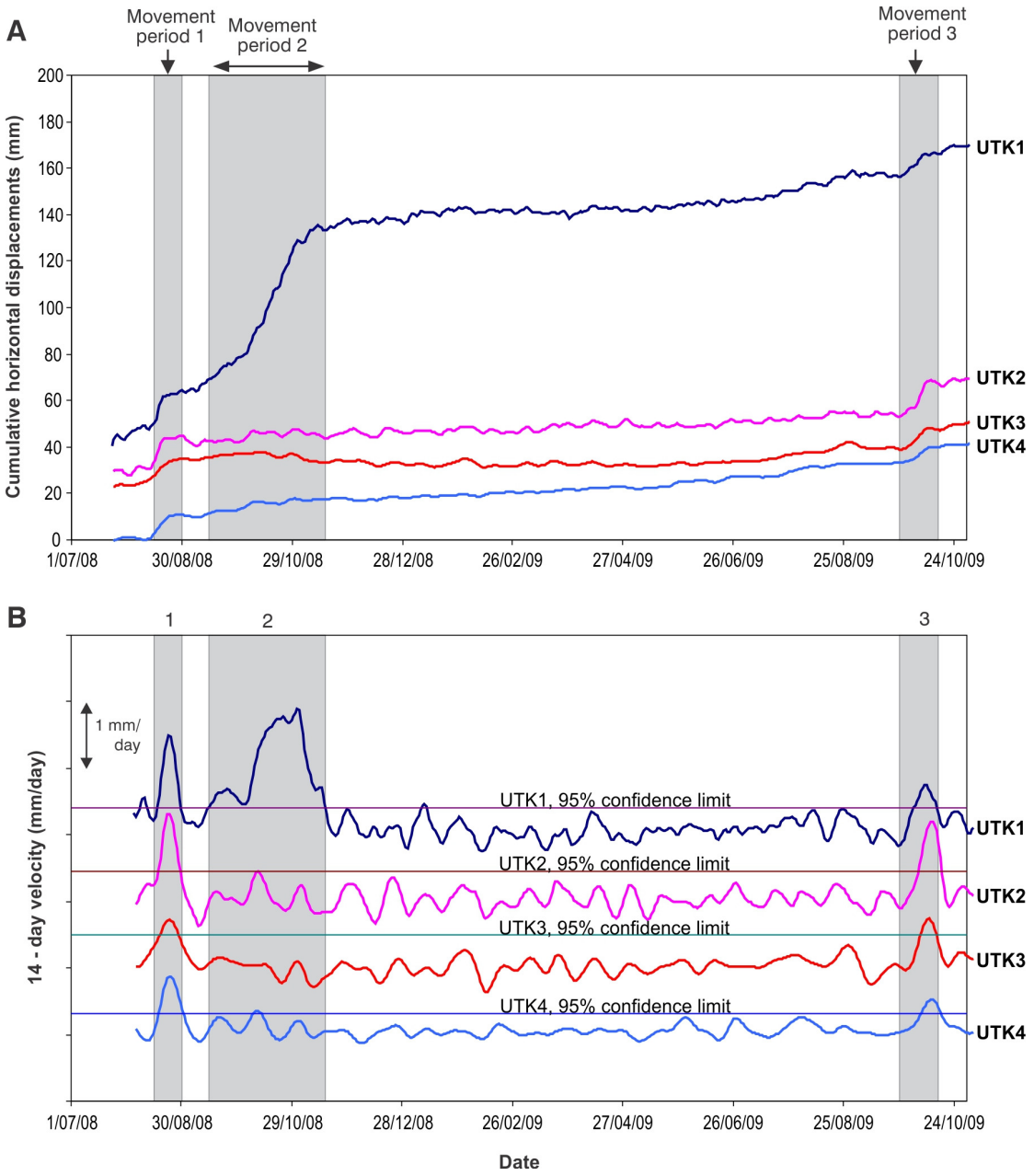

Figure 5.08 Accelerated creep displacements (Utiku)

Table 5.07 Cumulative horizontal displacement errors

Station	Error of any two daily cumulative displacements[1]				Velocity[2] (mm/day) at 95% confidence limit
	Standard deviation (mm)	90% confidence (mm)	95% confidence (mm)	99% confidence (mm)	
UTK1	2.28	4.90	5.59	6.92	0.40
UTK2	2.61	5.61	6.39	7.93	0.46
UTK3	2.85	6.11	6.97	8.64	0.50
UTK4	1.85	3.96	4.52	5.60	0.32

[1] Calculated as the square root of two, times the standard deviation.
[2] Velocity (mm/day) is calculated at 95% confidence over a moving 14-day period.

Table 5.08 Recognised accelerated creep.

Movement period	Date from/to	Cumulative horizontal displacements along main movement bearings[1] (mm)			
		UTK1	UTK2	UTK3	UTK4
1	15/08/2008 to 22/08/2008	12	9	6	7
2	6/09/2008 to 6/11/2008	43	N/A	N/A	N/A
3	30/09/2009 to 10/10/2009	7	11	7	6

[1]Main movement bearings and measurement precision are shown in Table 5.05

The three periods of statistically significant accelerated creep are plotted in Figures 5.09, 5.10 and 5.11, representing movement periods 1, 2 and 3 respectively and show the daily and smoothed displacements. Figure 5.12, shows the smoothed CGPS motions for all three periods plotted together. Movement periods 1 and 3 are similar in both magnitude (7 to 15 mm) and duration (about 7 to 15 days), with UTK1 and UTK2 showing the largest magnitudes of displacement (Table 5.09). Movement period 2 (UTK1 only) is longer in duration, and represents the largest magnitude event recorded by the CGPS stations to date (about 70 mm over 62 days).

The timing of the onset of accelerated-creep periods 1 and 3 are synchronous, i.e. they all started moving on about 15/08/2008 for movement period 1 and 25/09/2009 for period 3 (taking into account the daily temporal resolution of the data), and the durations of motion for all stations are similar. Each period is consistent in form, whereby motions tend to increase relatively rapidly, then become steady, followed by a period of rapidly slowing motion. This gives the cumulative displacement plots an open “S-shape” form.

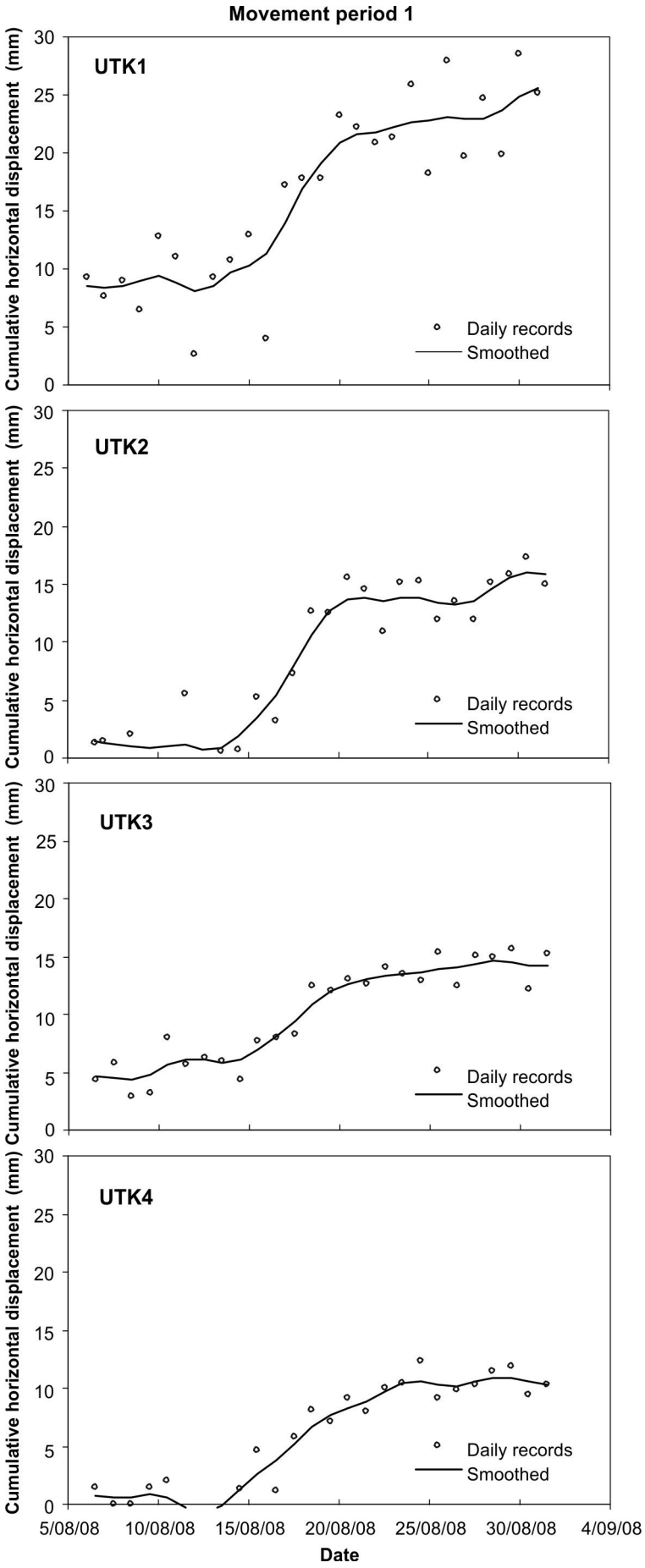

Figure 5.09 Cumulative horizontal displacements for accelerated creep period 1. Daily and smoothed displacements are shown. Smoothed values are derived using a Gaussian smoothing kernel where G_s = 2 mm.

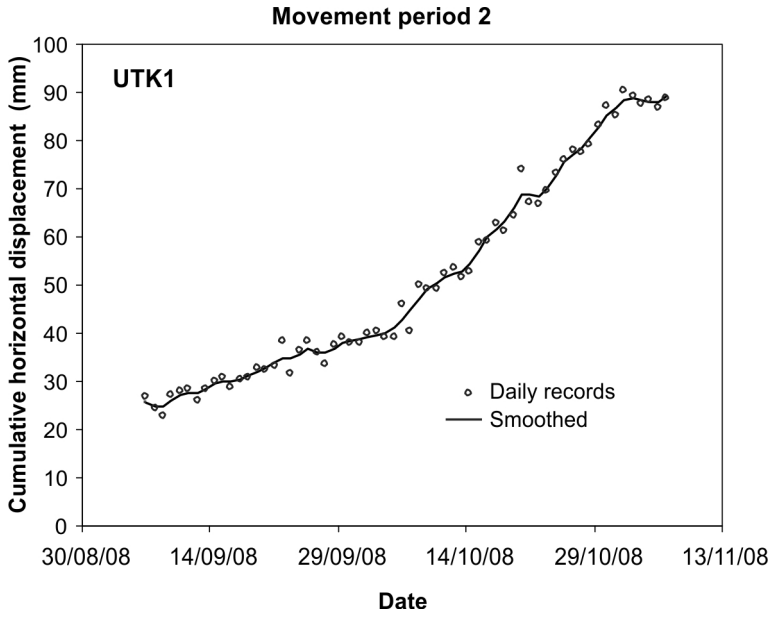

Figure 5.10 Cumulative horizontal displacements for accelerated creep period 2. Daily and smoothed displacements are shown. Smoothed values are derived using a Gaussian smoothing kernel where G_s = 2 mm.

Table 5.09 Summary of accelerated creep events

Station	Movement event 1			Movement event 2			Movement event 3		
	Disp. (mm)	Duration (days)	Mean rate (mm/day)	Disp. (mm)	Duration (days)	Mean rate (mm/day)	Disp. (mm)	Duration (days)	Mean rate (mm/day)
UTK1	12	7	1.7	70	62	1.1	10	15	0.7
UTK2	10	7	1.4		N/A		15	15	1.0
UTK3	7	11	0.6		N/A		10	15	0.7
UTK4	8	11	0.7		N/A		7	15	0.5

Displacement rate (Figure 5.13) and acceleration (Figure 5.14) of the stations through each movement period were calculated. The data for movement periods 1 and 3 have a similar form for all CGPS stations, with peak displacement rates being about 2.5–3.5 mm/day. The displacement-rate plot for movement period 3, suggests that it may comprise two events, an initial lower-rate followed by a higher-rate event. Movement period 2 (UTK1 only) also appears to comprise multiple (3), shorter duration (9 days), relatively rapid events, which are each comparable in rate and duration to movement events 1 and 3. For each accelerated-creep event, including those periods with multiple events, peak rates (speeds) are typically attained 1 to 3 days after initiation; with post-peak rates either decreasing rapidly until stopping, or being sustained for 1 to 3 days at near peak rates followed by a rapid decrease. These patterns show more clearly in plots of station acceleration (Figure 5.14), where the stations accelerate rapidly from rest, and achieving peak accelerations within 1 to 2 days of initiation. These rapid accelerations are followed, in most cases by equally rapid decelerations, the exception being movement period 1, where the stations decelerate more gradually.

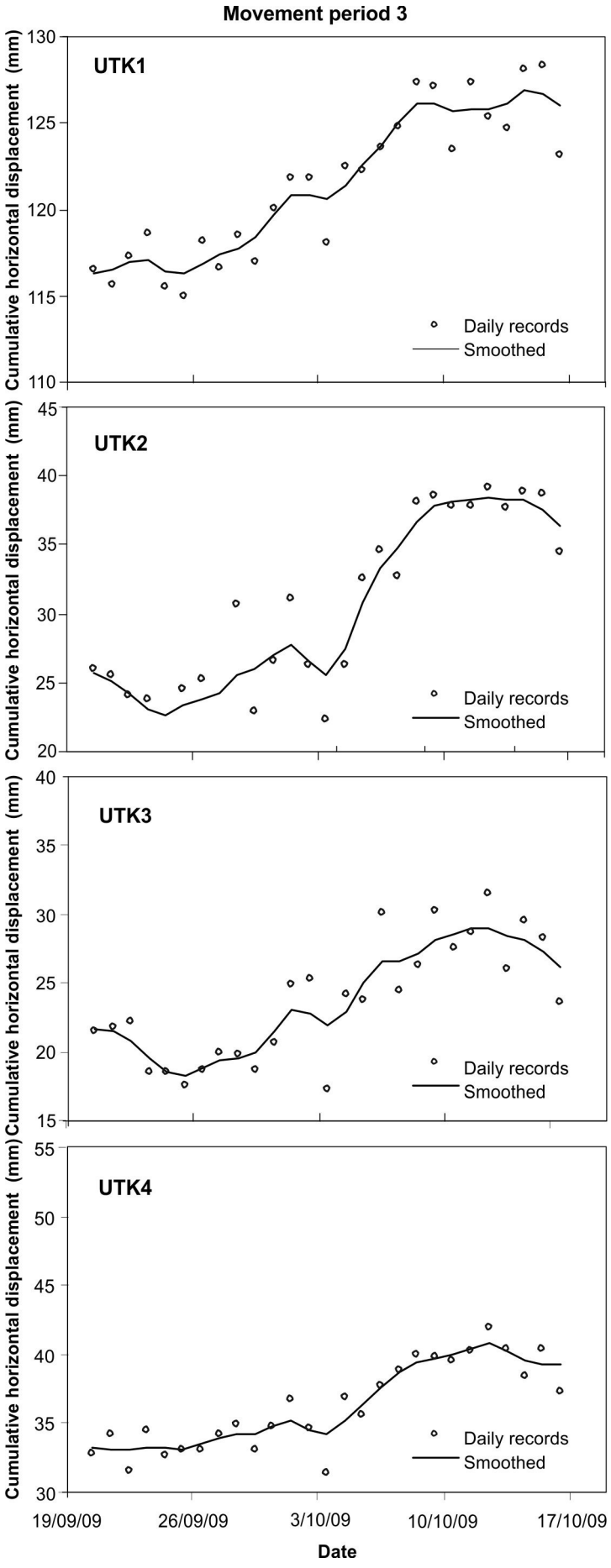

Figure 5.11 Cumulative horizontal displacements for accelerated creep period 3. Daily and smoothed displacements are shown. Smoothed values are derived using a Gaussian smoothing kernel where G_s = 2 mm.

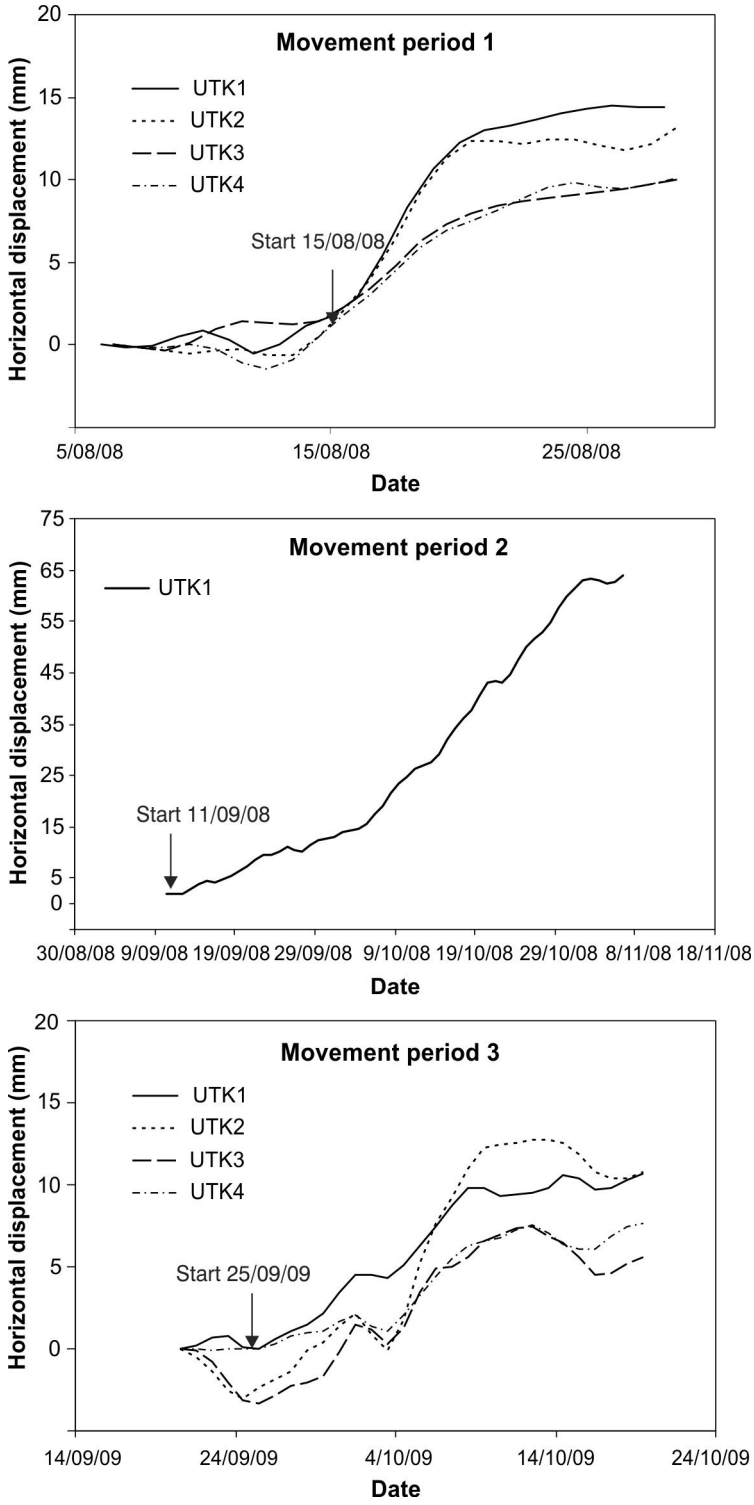

Figure 5.12 Smoothed cumulative horizontal displacements for all three periods of accelerated creep. Smoothed values are derived using a Gaussian smoothing kernel where G_s = 2 mm. N.B. the time-scales for each movement period vary.

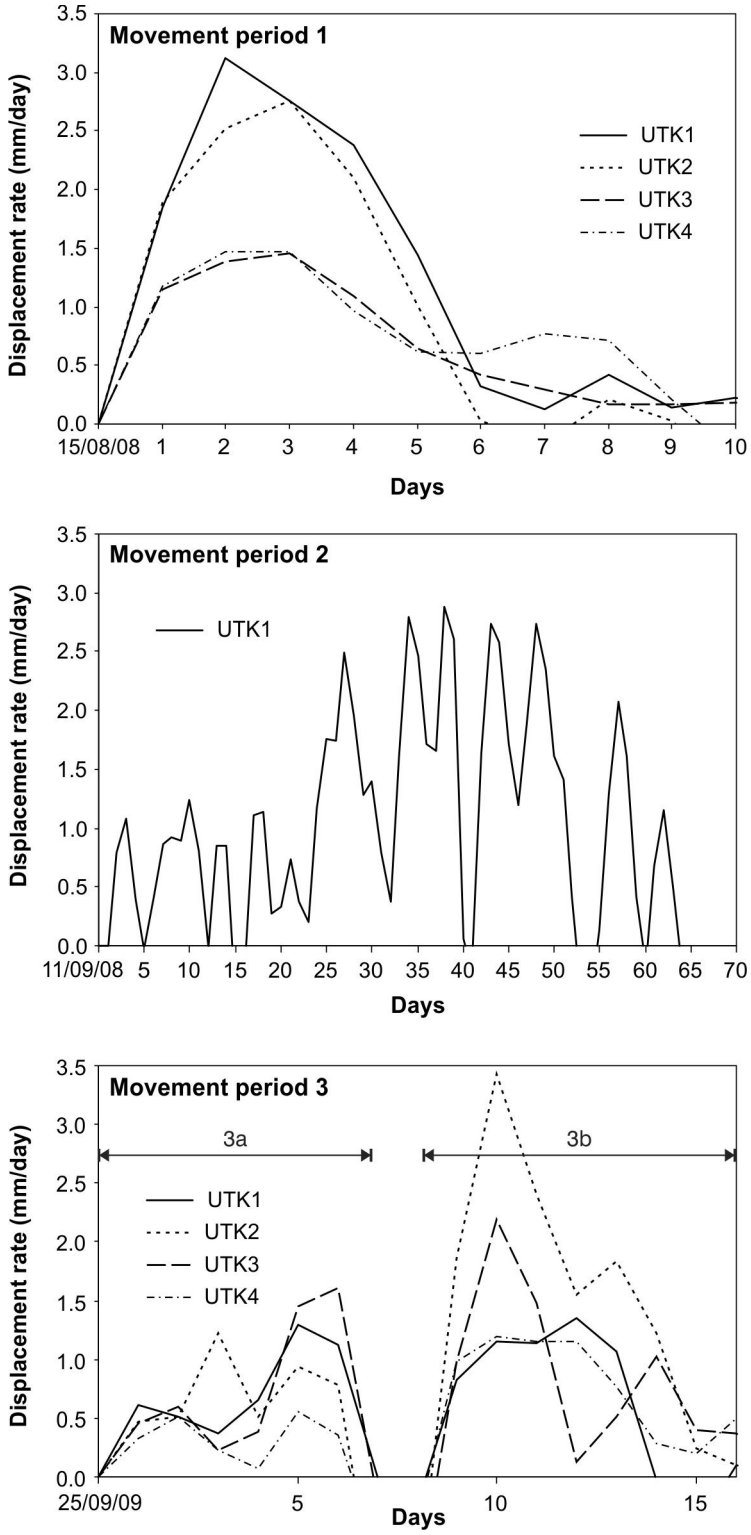

Figure 5.13 Displacement rates calculated for the three periods of accelerated creep using the smoothed cumulative horizontal displacement data. Smoothed values are derived using a Gaussian smoothing kernel where G_s = 2 mm. N.B. the time-scales for each movement period vary.

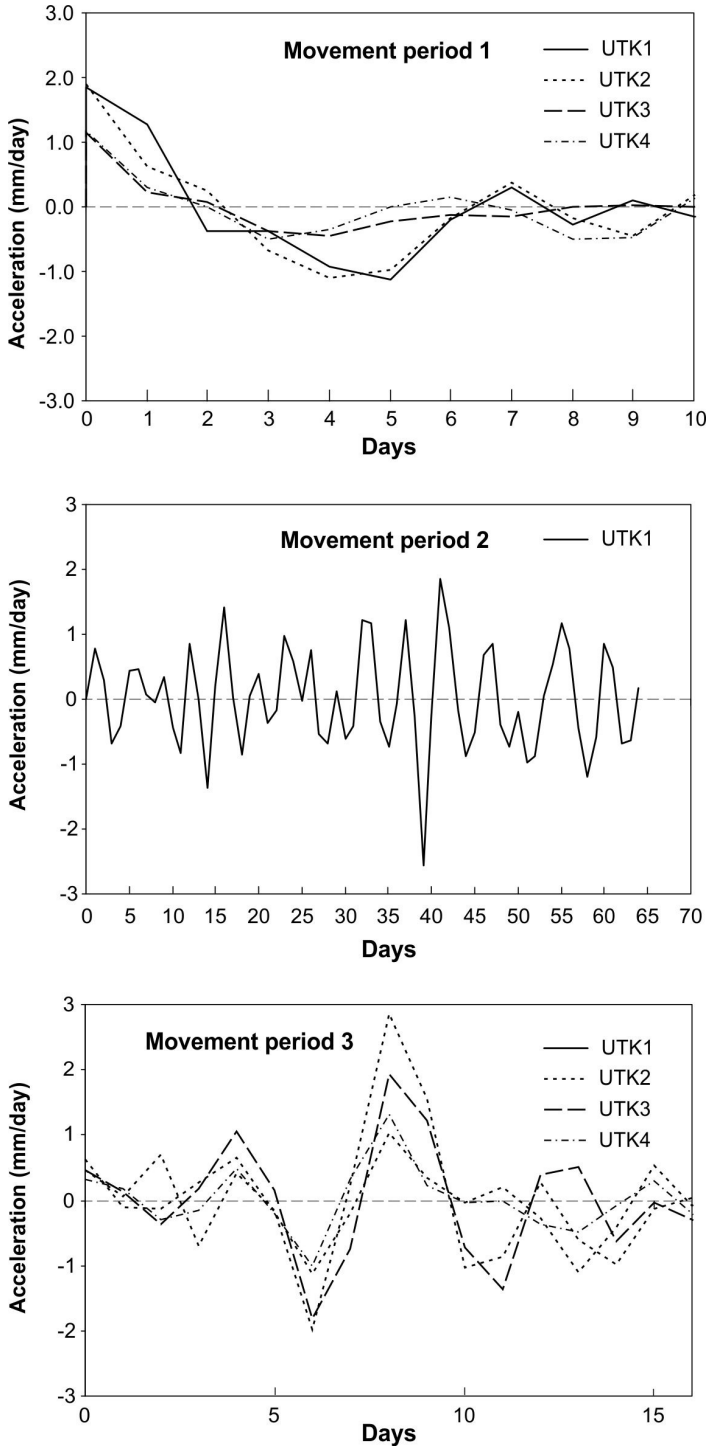

Figure 5.14 Accelerations calculated for the three periods of accelerated creep from the smoothed cumulative horizontal displacement data (Utiku landslide). Smoothed values are derived using a Gaussian smoothing kernel where G_s = 2 mm. N.B. The time-scales for each movement period vary.

The acceleration of station UTK1 during movement period 2 shows a “saw tooth” pattern, with periods of rapid acceleration followed by equally rapid periods of deceleration, typically lasting 8 to 10 days, which recur throughout the movement period. This would suggest that this movement period comprises multiple short-duration and small-magnitude events, which are typical of those shown during movement periods 1 and 3.

5.2.2.3 Slow creep

Other types of creep motion have been detected; these appear to represent longer duration, slower motion (termed "slow creep"). To assess whether these apparently longer periods of low magnitude displacement were statistically significant, analyses using the least-squares method was carried out on the daily cumulative horizontal displacements between the periods of recognised accelerated creep (Table 5.08). The rationale used is the same as that adopted for analysing the vertical motions, whereby the motion is deemed to be statistically significant if the horizontal displacement gradient (assuming a simple linear relationship), is larger than the standard error of the gradient at 95% confidence limit. Results indicate that these motions are statistically significant, and were recorded at all GPS stations on the landslide (Figure 5.15 and Table 5.10). Due to the low rates of displacement associated with these movement periods, it is difficult to identify their precise start and end dates. Estimates of when these motions occurred are shown in Table 5.10.

Table 5.10 Summary of slow creep motion

Station	Motion date Start/stop	No. days	Slow creep motion gradient (mm/day)	Error on the creep gradient at 95% (mm/day)	Difference between the gradient and the error	Total slow creep displacement over period (mm)[1]
UTK1	7/11/08 to	326	0.063	±0.004	0.059	41
UTK2	23/08/08 to	402	0.027	±0.002	0.025	11
UTK3	30/09/09		0.007	±0.004	0.003	3
UTK4			0.052	±0.002	0.050	21

[1]Calculated from the motion gradient

Slow creep motion relates to steady displacements, which continue at similar rates (between 0.03 to 0.06 mm/day), over much of the monitoring period and are in similar directions to the accelerated creep motion, i.e. down slope. The slow creep motion at station UTK3 is different as it occurs both in the up slope and down slope directions, which result in no net change in horizontal motion.

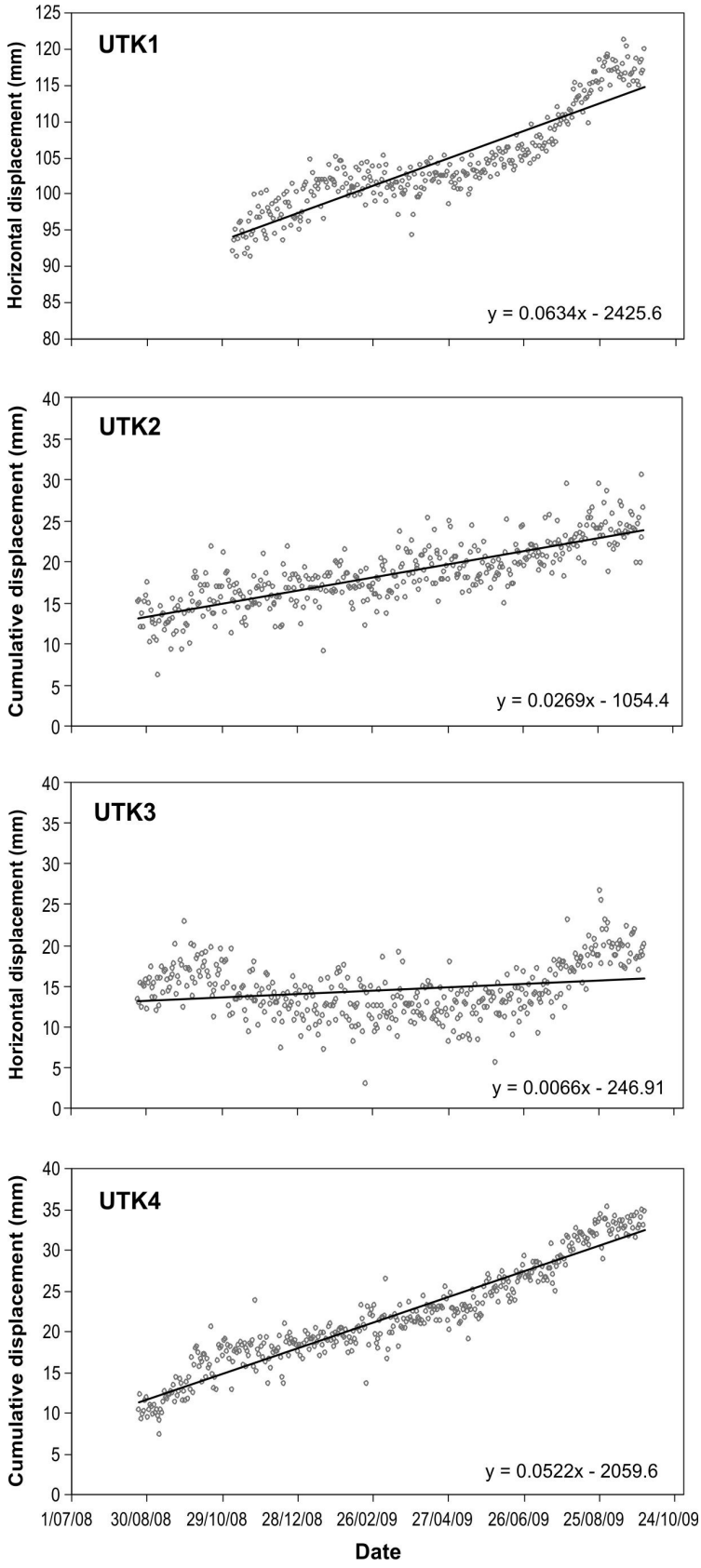

Figure 5.15 Cumulative horizontal "slow creep" displacements calculated along the main motion bearing (Utiku landslide). Displacements shown are the filtered daily time series with modelled linear trend lines.

5.2.2.4 Vertical creep

A longitudinal section through the landslide is shown in Figure 5.16, which is annotated

with the vertical and horizontal CGPS motions, recorded during the monitoring period. The long-sectional angle of displacement is also shown, which represents in two-dimensions, the movement angle of each GPS station from the horizontal. This should represent the angle of the surface along which the landslide mass is translating; these angles are shown in Table 5.11.

Table 5.11 Summary of horizontal and vertical motion over the monitoring period

Station	Total cumulative horizontal motion and errors at 95%[1] (mm)	Total vertical motion and errors at 95%[2] (mm)	Long-sectional angle of translation (°)
UTK1	128 (± 3)	-42 (± 5)	19
UTK2	40 (± 4)	-20 (± 5)	25
UTK3	30 (± 4)	-7 (± 4)	11
UTK4	41 (± 3)	-12 (± 3)	16

[1]Calculated over the monitoring period from the smoothed cumulative horizontal displacements with errors calculated from the precision of the smoothing function at the 95% confidence limit.
[2]Vertical motions and errors are calculated from the least squares method assuming a linear relationship.

The calculated angles of translation differ significantly from the angle of the basal slide surface formed by the clay layer, which in the upper landslide is assumed to be about 0° to 1°, increasing to about 3° to 4° in the lower landslide as the motion bearing changes. However, the way in which the angle of translation has been calculated assumes that vertical and horizontal motions are synchronous. For CGPS stations UTK1, UTK2 and UTK4, where motions are statistically significant, the vertical time series have been plotted against the horizontal time series (Figure 5.17). Vertical creep motions trends for UTK1 are the most obvious, which show motions are steady, about 0.22 mm/day, and occur over an approximate six month period. The trends from UTK2 and UTK4 are comparable, although the rates are lower, about 0.11 mm/day for UTK2 and 0.04 mm/day for UTK4 over similar six-month periods. The timing of vertical creep motions is interesting as these data show each period of accelerated- and vertical-creep are mostly discrete, but that vertical creep does coincide with periods of slow creep.

The significance of the relationship has been tested using linear least-squares regression. The horizontal and vertical time-series have each been separated into three discrete periods, using the start and end of the accelerated-creep movement periods as the section breaks (for UTK1 periods 1 and 2 have been grouped together as they follow each other) (Figure 5.18). The analyses indicate that for UTK1 and UTK2 motion vectors during each accelerated-creep period do not significantly differ from the angle of the slide surface. Vertical motion outside of the accelerated-creep periods is statistically significant, and coincides with some horizontal slow-creep motion, although the translational angle is 60–70° indicating vertical motion predominates, and is significantly steeper than the angle of the slide surface, suggesting the slide mass is thinning.

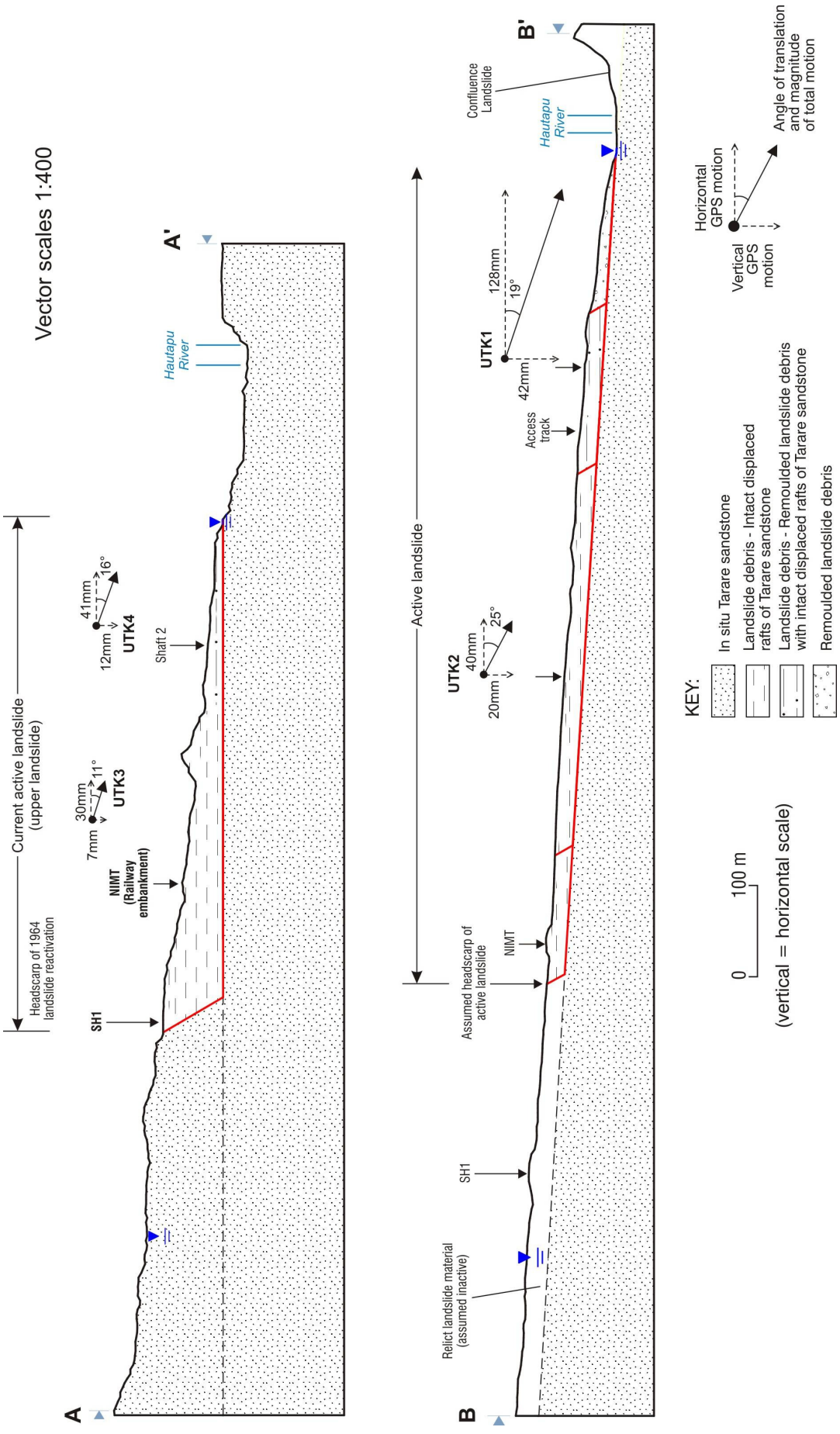

Figure 5.16 Longitudinal sections through the Utiku landslide, which is annotated with the total vertical and horizontal displacements, recorded at each prism along the section line, during the monitoring period. Sections A-A' and B-B' are shown on Figure 3.08.

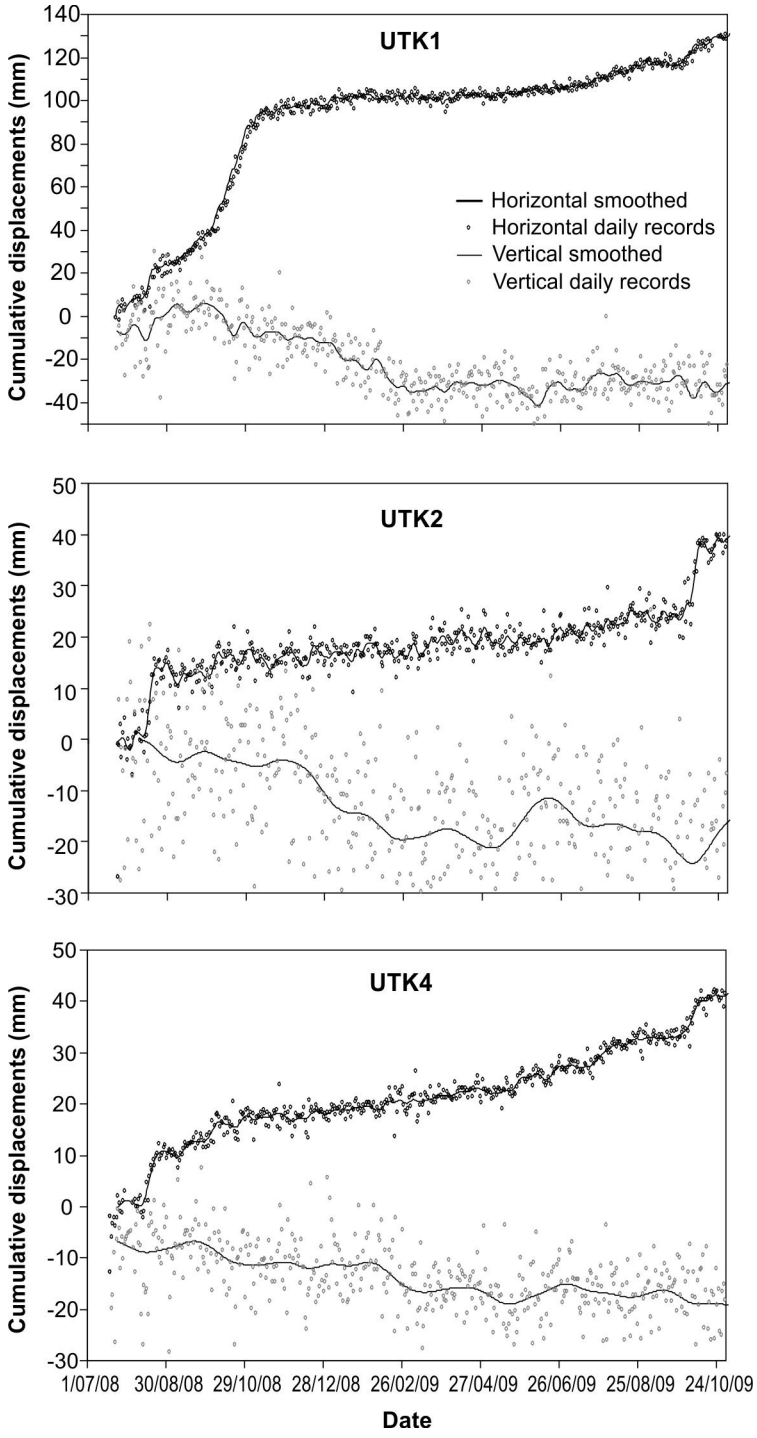

Figure 5.17 Cumulative horizontal and vertical displacements for stations UTK1, UTK2 and UTK4. Smoothed values are derived using a Gaussian smoothing kernel with a smoothing window of G_s = 2 mm for the horizontal time series and G_s = 5 mm for the vertical time series.

The data are consistent with a varying vertical deformation rate in which a change in vertical-deformation rate occurred around the beginning of March 2009 (UTK1 Figure 5.17) and is not coincident with the timing of changes in horizontal-displacement rate. This information is more clearly resolved by reference to the periods of accelerated horizontal creep, because the precision on the vertical displacement is insufficient to pick up vertical displacements over short periods of time such as are represented by the intervals of accelerated creep, and hence cannot resolve the timing of periods of

accelerated vertical deformation, if they occur. Changes in vertical deformation rate at UTK4 are not statistically significant, but may follow a similar trend to that of UTK1 and UTK2.

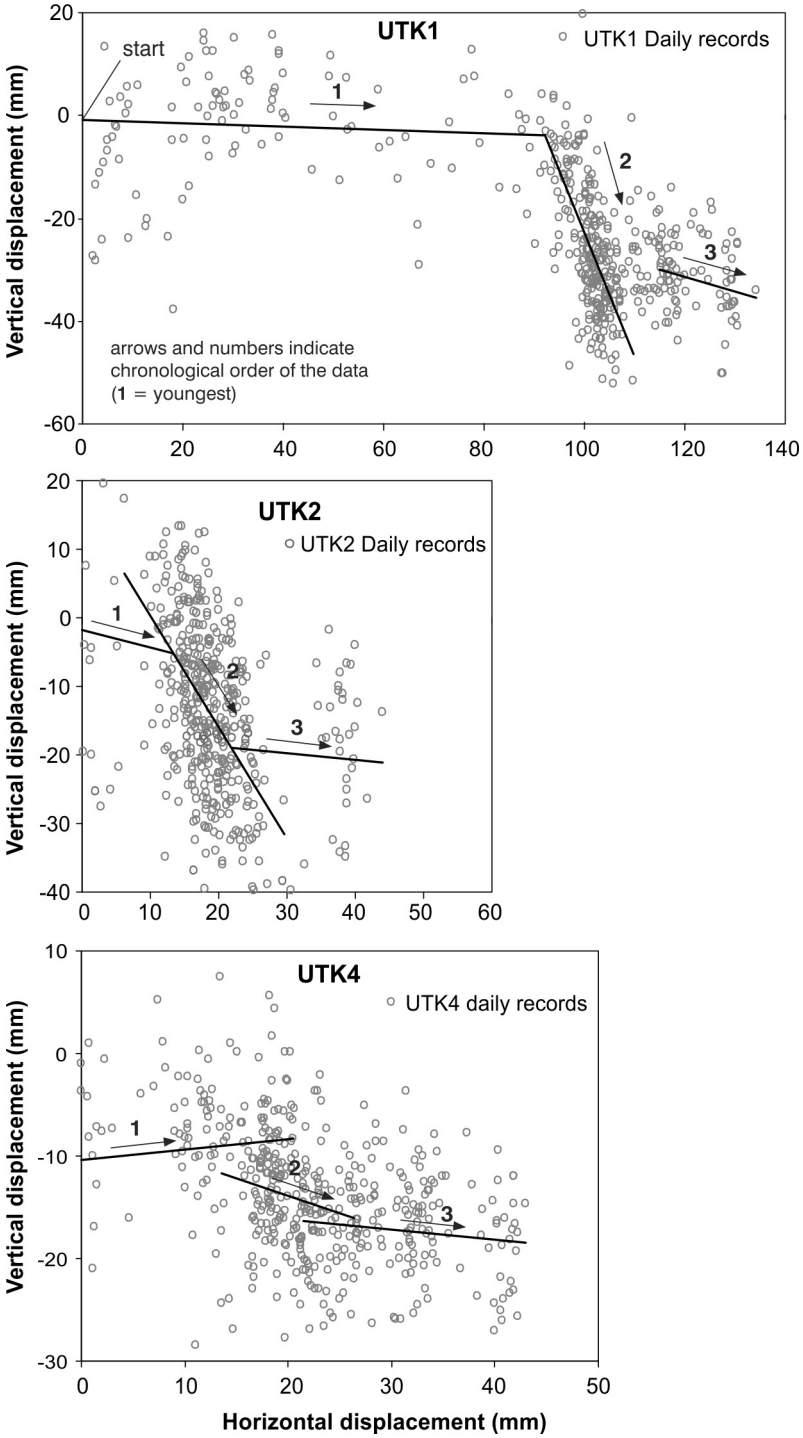

Figure 5.18 Horizontal and vertical time-series data separated into three discrete periods, using the start and end of the accelerated-creep movement periods as the section breaks. Trend lines are based on linear models.

5.2.3 Subsurface motion

Subsurface motion and depth relative to the ground surface has been derived from the inclinometer monitoring. The cumulative displacements calculated from the

inclinometers installed at BH1 and BH3, from the bottom of the inclinometer tube, indicate the presence of one slip surface, at depths corresponding to those surfaces identified in the drillhole logs. The displacement data for BH1 also shows sinusoidal-shaped deformation between 12 m and 26 m depth below ground level. This is thought to be due to the existence of voids between the inclinometer casing and the in-situ ground, which allows the casing to deform into the voids (Stark and Choi, 2008). Borehole logs for these depths corroborate the presence of voids, although these are thought to be related to the deformation of the area in response to landslide movement. Results from the inclinometer testing are summarised in Table 5.12 and Figure 5.19.

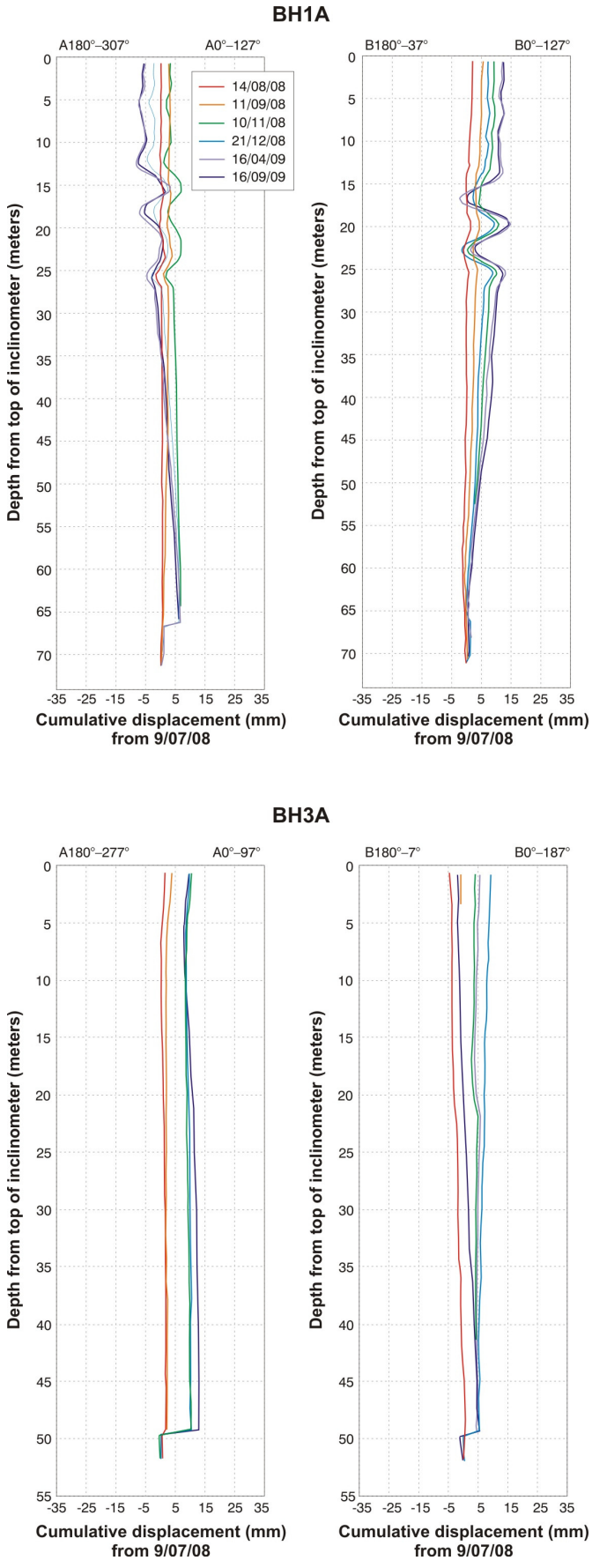

Figure 5.19 Cumulative inclinometer displacements (Utiku landslide). The cumulative displacements are calculated for the A- and B-axes.

Table 5.12 Summary of inclinometer results (July 2008 to September 2009)

Inclinometer	Top of Inclo-Tube	Approx. Movement depth		Depth of logged slide surface[1]	Total displacement in period and errors at 95%[2] (mm)	Movement bearing and errors at 95%[2] (°)
	m AMSL	m bgl	m AMSL	m AMSL		
BH1A	379.7	66.3	313.4	313.38	5 (±2)	115 (±2)
BH3A	351.8	49.5	302.3	303.40	14 (±2)	124 (±1)

[1]Depth of slide surface identified from logging of the drill holes
[2]Equipment precision calculated from the equipment specifications (Slope Indicator, 2005), and are based on measurements between two surveys, the reference survey 9/07/08 and the most recent survey 16/09/09. All errors calculated at 95% confidence limit from the bottom of the inclinometer tubing.

The cumulative displacements of the inclinometers at the depth of the slide surface have been calculated from the incremental displacement data, which shows displacements that occur at each single depth interval, thereby limiting any systematic errors associated with cumulative displacement plots (Figure 5.20).

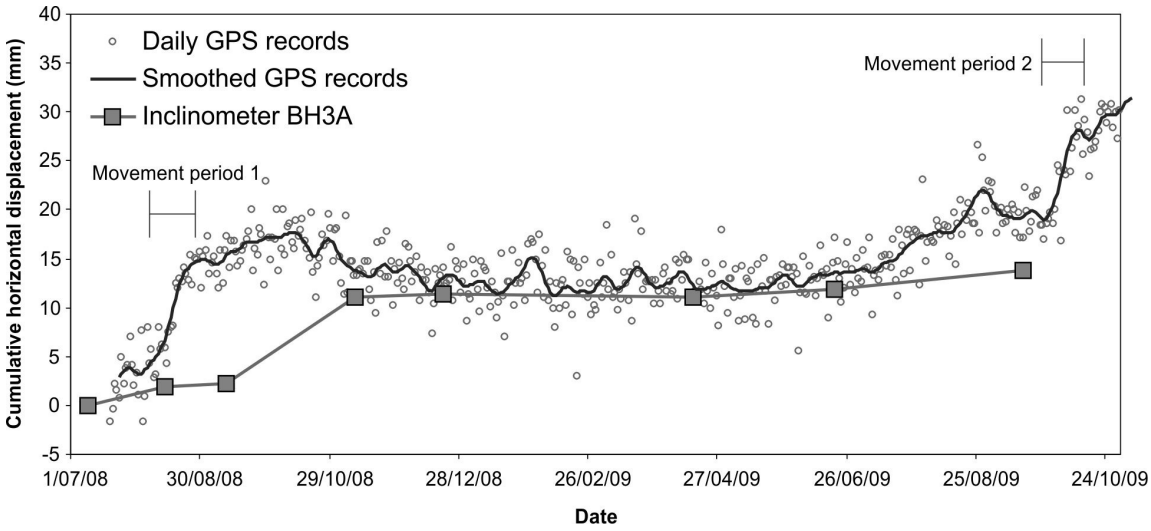

Figure 5.20 Cumulative displacements along the slide surface plotted with cumulative displacements at the surface. Daily and smoothed GPS records from station UTK3 are shown. Smoothed values are derived using a Gaussian smoothing kernel where G_s = 2 mm.

Subsurface motion derived from the inclinometers has poor temporal resolution, but can be used to compare the timing of accelerated creep period 1, between the ground- and slide-surface. The magnitude and timing of horizontal displacement between the slide- and ground-surface can be assessed using inclinometer BH3A and CGPS station UTK3, about 5 m to the south of BH3A, for a similar time period corresponding to the first and last inclinometer measurements (9/07/2008 to 16/09/2009). Table 5.13 summarises these data.

Table 5.13. Comparison between the cumulative horizontal displacements calculated at the surface from CGPS station UTK3 and those at depth along the slide surface from inclinometer BH3A. For the period 9/07/2008 to 16/09/2009.

Location	Equipment type	Total displacement and errors at 95% (mm)	Rate of displacement (mm/year)	Bearing and errors at 95% (°)
UTK3	CGPS	18 (±5)	15	142 (±7)
BH3A	Inclinometer	14 (±2)	12	124 (±1)

These data show that the total horizontal displacements and rates, for the same period, are nearly consistent between the slide surface and the ground surface, although surface motions are consistently greater than those along the slide surface. Figure 5.20 shows that the motion along the slide surface lagged the motion at the surface for accelerated creep period 1, although this lag is represented by only one data point in the inclinometer time series and may be attributed to error.

Motion bearings, however, are slightly inconsistent, which may be the result of equipment errors. Although the statistical analyses of the inclinometer data using the least-squares method suggests a relatively small random error on the readings, systematic errors can also occur, especially if the inclinometer casing twists during installation or as a result of movement (Green and Mikkelsen, 1988; Richardson, 2002). Therefore, displacement measurements may be correct and but may not represent the true bearing of landslide motion. However, the directions of motion from both the CGPS and the inclinometer are close, although the CGPS motions are more similar to those of the historical surface motions, which, may indicate the inclinometer tube has indeed twisted.

5.2.4 Factors affecting movement

5.2.4.1 Rainfall

Rainfall recoded at Taihape (BH2, Figure 4.02), located about 6 km north of the Utiku landslide has been used for analyses purposes because the records from Utiku do not cover the entire monitoring period. Records from the Taihape rain gauge have been checked against those recorded on the landslide at Utiku. Summary rainfall statistics for Taihape and Utiku are shown in Table 5.14.

Table 5.14 Rainfall statistics for Utiku and Taihape gauges for the same period (5/09/2008 – 31/10/2009).

	Taihape	Utiku
Total rainfall (over monitoring period)	986.8	1123.4
Mean daily rainfall (mm)	2.5	2.7
Max. daily rainfall (mm)	33.4	32.2

Daily rainfall at Taihape and Utiku gauges have been plotted against each other for the same period of time (1/09/2008 to 31/10/2009), (Figure 5.21). Differences between Taihape and Utiku rainfalls have a standard deviation of ±1.7 mm, and r^2 correlation coefficient, assuming a simple linear relationship, of 0.9. Statistics relating to the linear relationship indicate a gradient of 1.15 with a standard error of ±0.02. The residuals are normally distributed and positively skewed and there are 420 degrees of freedom. The relationship indicates that the rainfall between the two sites does vary in a statistically significant manner, and that the daily rainfalls at Utiku are slightly larger than those at Taihape (the gauges are about 6 km apart).

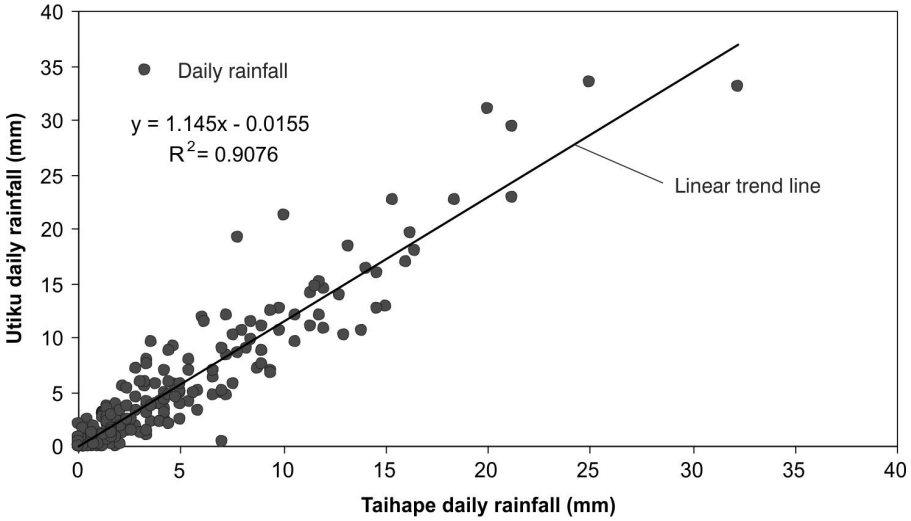

Figure 5.21 Daily rainfalls at Taihape and Utiku gauges plotted against each other for the same period of time (1/09/2008 to 31/10/2009).

Daily and cumulative daily rainfalls for both Taihape and Utiku are shown in Figure 5.22. Cumulative rainfalls for both gauges show alternating summer and winter trends, whereby summers (December to May), tend to be dryer (mean rainfalls ~2 mm/day) and winters (June to November) wetter (mean rainfalls ~3 mm/day). The daily rainfall has been plotted as the cumulative deviation from mean daily rainfall to show these seasonal trends more clearly (Figure 5.23). The wetter winter months show positive gradients, where daily rainfalls are typically greater than mean, and the drier summer months show negative gradients, where daily rainfalls are typically less than mean.

The rainwater input to the Utiku landslide during the monitoring period, using the rainfalls recorded at Taihape, was: 11 litres/sec for the landslide area (assumed to be 26 hectares); and 42 litres/sec for the entire catchment area (assumed to be 100 hectares), including the landslide, which accounts for 26% of the entire catchment area. Surface runoff and evapotranspiration from the catchment are not being measured and so it's not possible to estimate the amount of surface water that would likely enter the groundwater system.

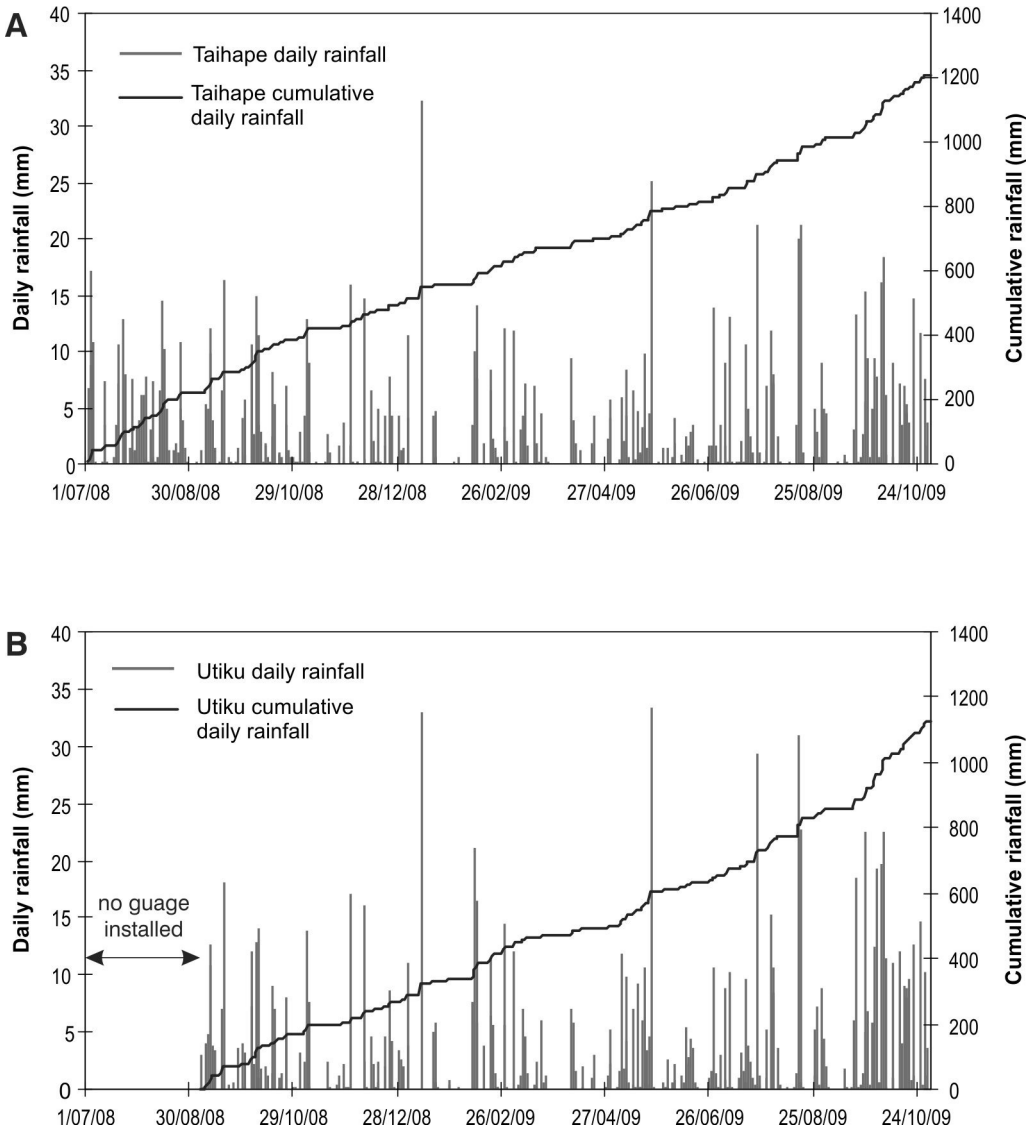

Figure 5.22 Daily and cumulative daily rainfall at Taihape (A) and Utiku (B) gauges.

Daily rainfalls recorded during the monitoring period have been compared against the magnitude/frequency of daily rainfalls recorded during a longer record from the Taihape gauge operated by Rangitikei District Council, in this case between 1912 to present day. To date, the maximum daily rainfall recorded during the monitoring period was 32.3 mm, which occurred 10/01/2009, and has an annual exceedence probability of 280 % (2.8 times per year), indicating that the rainfalls during the monitoring period were not exceptional (Figure 5.24).

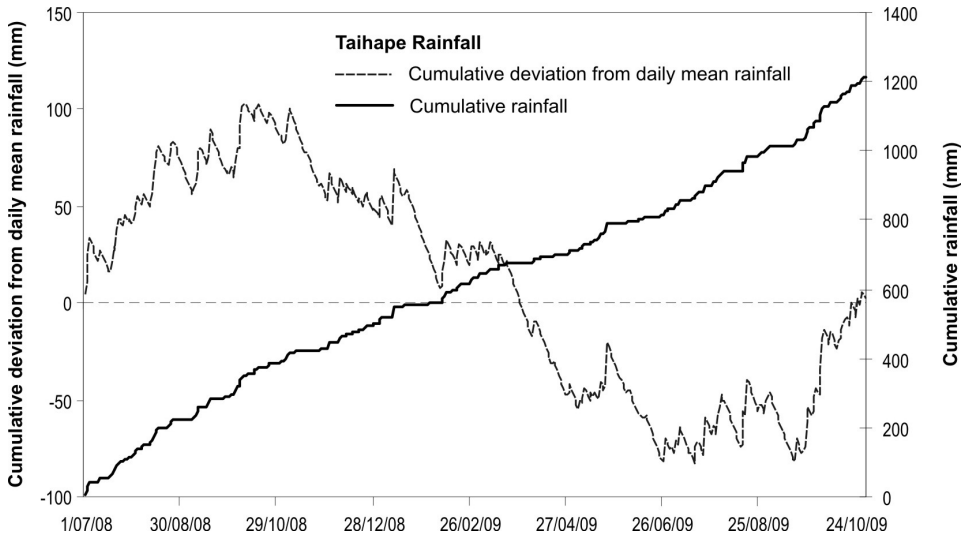

Figure 5.23 Cumulative deviations from daily mean rainfall and cumulative rainfall calculated using data from the Taihape rain gauge at BH2.

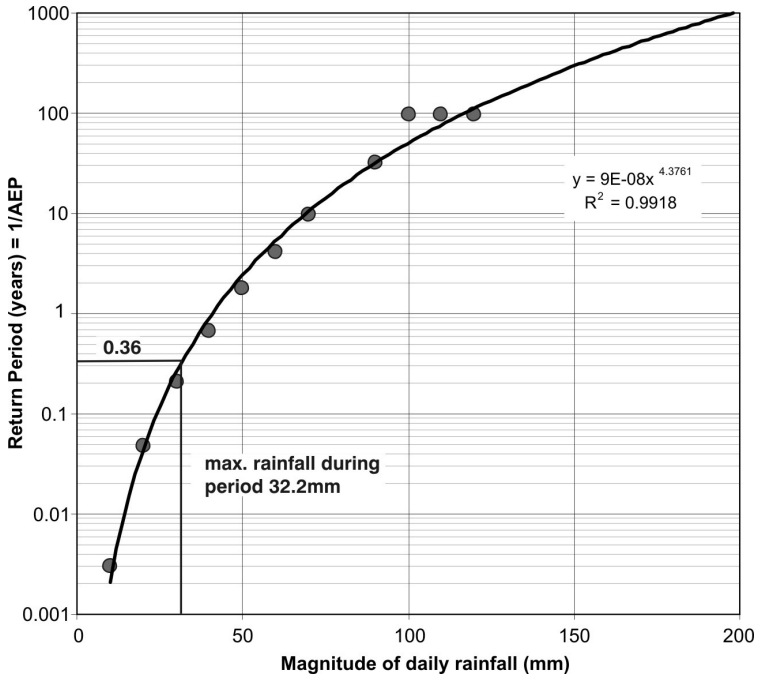

Figure 5.24 Rainfall magnitude and return period for the period 2/01/1912 to 31/10/2009. Data is from the Rangitikei District Council operated rain gauge at Taihape. The maximum daily rainfall recorded at the Utiku landslide rain gauge installed at BH4 during the period 1/09/2008 to 31/10/2009 is shown for comparison purposes.

5.2.4.2 Groundwater pressures

The installed vibrating-wire instruments (VBW) record pore pressures in Casagrande standpipe piezometer tubes which have sealed response zones above (but near to) the identified landslide slide surface (Chapter 4). All pore-pressure measurements used in these analyses are recorded at the sensor tip. No adjustments have been made to take into account the width of the Casagrande standpipe response zone, or the depth of slip surface.

The hourly readings (in Hertz) from VBW piezometers BH1, BH2, BH3, BH4 and PZA have been converted to pressures following the method discussed in Chapter 4. Hourly pressure measurements have then been averaged over each 24-hour period (UTC), to obtain a daily averaged pore pressure for each instrument. Readings were then corrected for barometric effects (following the method detailed in Chapter 4), using data from the barometric-pressure sensor installed at Taihape. Statistics relating to this sensor are summarised in Table 5.15.

Table 5.15 Summary of barometric changes recorded at Taihape

Location	Elevation (m AMSL)	Max ΔP (kPa)	Min ΔP (kPa)	Standard deviation of the mean
Taihape (BH4)	485.4	2.6	-2.7	0.6 kPa 0.07 m H^2O

Piezometers BH3 and BH1 have periods of data loss due to power failures and faulty equipment. The longest period of data loss (July 2008 and November 2008), was due to a faulty VBW instrument, which was subsequently replaced. Since replacement no data have been lost. The VBW piezometer in BH1 requires manual download and is powered from batteries; periods of missing data represent either lack of power or when the data logger was full. The stated precision of the VBW piezometers is ±0.1% of the operating pressure (Geokon, 2005), which for the Utiku piezometers is 700 kPa, giving an error of ± 0.7 kPa. This equates to about ±0.07 m of piezometric head.

The piezometer installation (not the instrument) at BH2 is thought to have initially been faulty, as records show a continuing rise in piezometric head level, with no lowering during dry periods, which is inconsistent with the data from BH3, located closest to BH2. The BH2 VBW instrument was working correctly based on manual water-level checks and it was therefore assumed that the Casagrande standpipe piezometer installation was faulty e.g. blocked. However, following the period of accelerated creep (30/09/2009 to 10/10/2009), pore-pressure trends recorded at this piezometer became consistent with those from BH3 (Figure 5.25). One explanation for this change is that the piezometer tube was sheared off as a result of landslide displacement along the slip surface and that groundwater can now enter the standpipe piezometer. Another explanation is that this piezometer took longer than the others to equilibrate, following installation. Although this piezometer now appears to be working correctly, due to the initial uncertainty, no records from this installation (BH2) have been further analysed or interpreted.

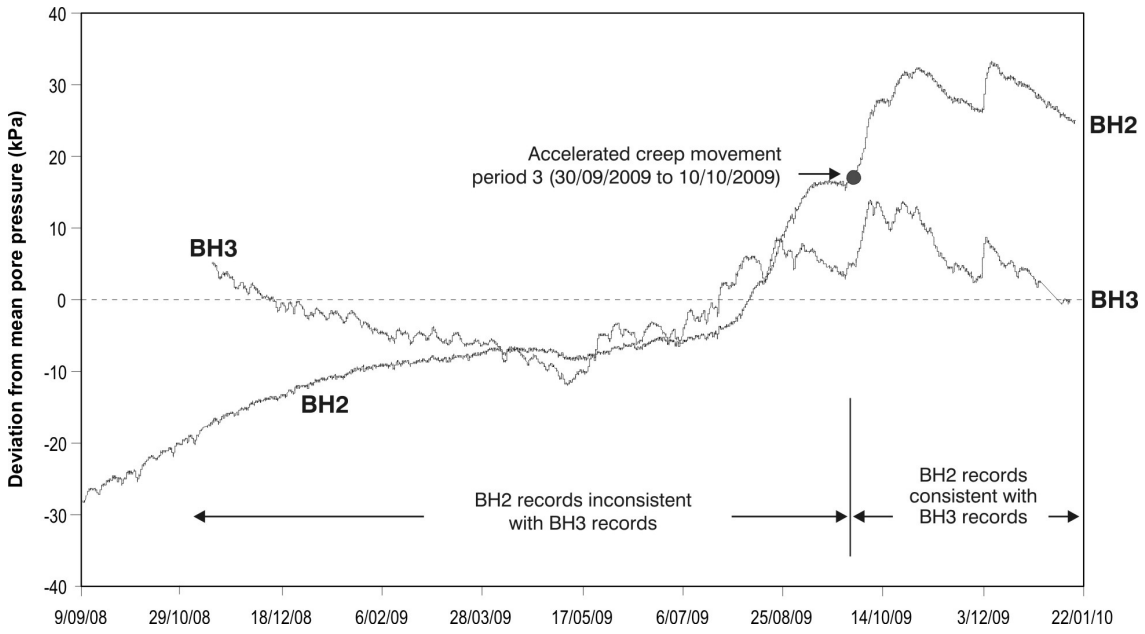

Figure 5.25 Pore pressures recorded at piezometers BH2 and BH3 over the monitoring period.

A Gaussian smoothing kernel was used to smooth the daily averaged pore pressure time-series for each piezometer to give an indication of the probable measurement precision (Table 5.16). Smoothing windows (G_s) = 1, 2, 3 and 5 kPa were assessed and the precision estimated as per the procedure in Section 4.4.1.4. The precision of the smoothing kernel for VBW piezometers BH1, BH3, BH4 and PZA, using G_s = 2 kPa, is about ±0.6 kPa (0.06 m H^2O), based on the standard deviation of the residual mean. The smoothing window G_s = 2 kPa, gave the best fit by preserving the relative maxima, minima and width of the distribution while minimising the standard deviation.

Table 5.16 Precision of the smoothing kernel (G_s = 2 kPa) with respect to corrected daily mean pore pressure values.

Piezometer	Standard deviation from mean (kPa)	95% confidence limit (kPa)
PZA_UTK1	±0.6	±1.2
BH1	±0.7	±1.4
BH3_UTK3	±0.6	±1.2
BH4_UTK4	±0.6	±1.2

The corrected daily pore pressure time series for each VBW piezometers (BH1, BH3, BH4 and PZA), along with the smoothed data are shown in Figure 5.26. In general all piezometers follow a consistent summer/winter cycle, whereby pore pressures decrease during the drier summer months and increase during the wetter winter months. Pore-pressure magnitudes decrease from the upper landslide to the lower landslide, which correspond to the decreasing depth, below ground level, of the

landslide slide surface towards the toe. Superimposed on the longer-term trends are many small magnitude, short-duration pore-pressure changes, which give the time-series plots a “saw-tooth” shape. Piezometric head levels calculated from the pore-pressure data indicate that levels are at, or close to ground level in the upper part of the landslide between piezometers BH4 and BH3, during the winter periods.

To aid comparison the daily records from the piezometers have been plotted as deviations from mean pore pressures (Figure 5.27). Of the four piezometers BH1, which is located in the area that has recently shown movement, above the historical landslide head scarp, displays the largest rates and magnitude of pore-pressure change over the period. The pore-pressure patterns of BH3 and BH4 are nearly identical and follow consistent trends and rates of change. These piezometers are located on the upper landslide within the historically active area. The time-series plot from PZA, located on the lower landslide, is similar to that of BH3 and BH4, but peak pore pressures in the wetter winter months lag behind the peaks at BH3 and BH4, which may indicate a decrease in the permeability of the landslide debris in the toe. Typical pore-pressure gradients for both the rising and recessional limbs recorded at BH3, BH4 and PZA, are about 0.1 kPa/day, and for BH1 about 0.2 kPa/day, assuming a linear relationship.

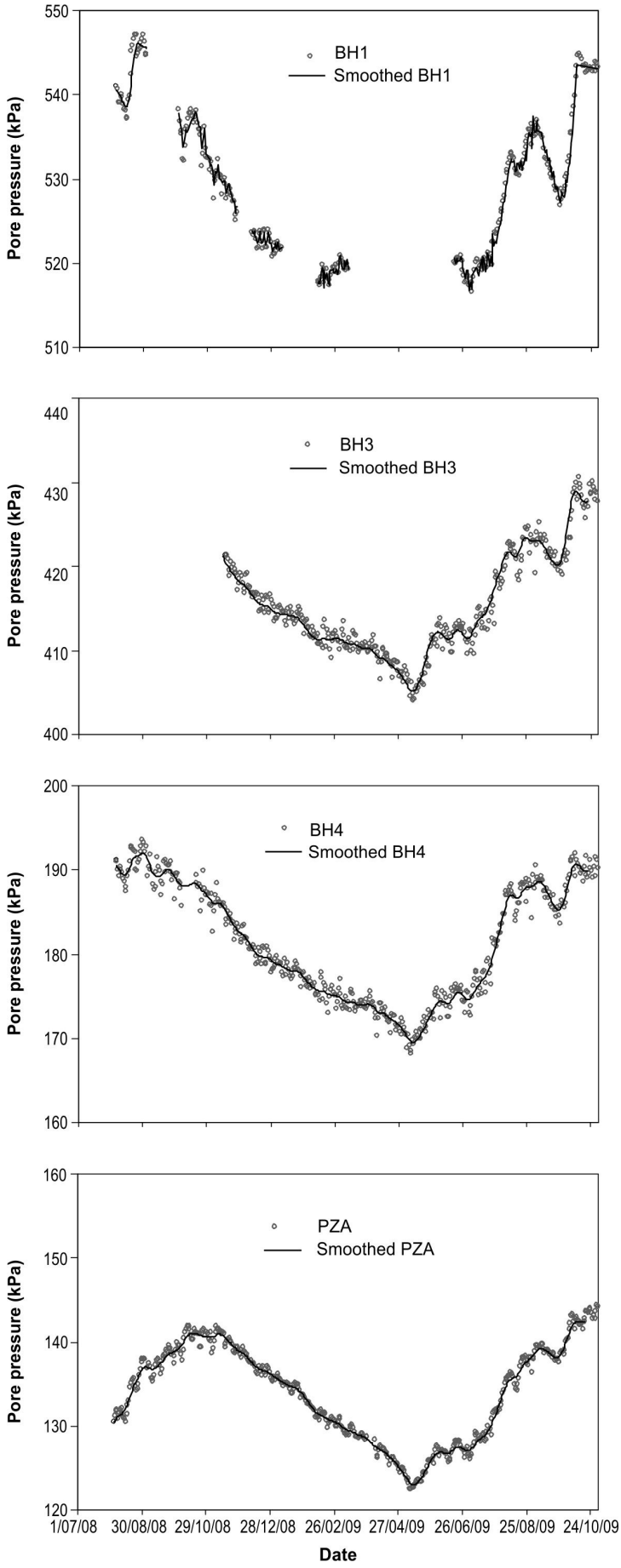

Figure 5.26 Pore pressures recorded at piezometers BH1, BH3, BH4 and PZA over the monitoring period. Daily pore pressures and smoothed daily pore pressures are shown, with the smoothed values calculated from a Gaussian smoothing kernel where G_s = 2 kPa.

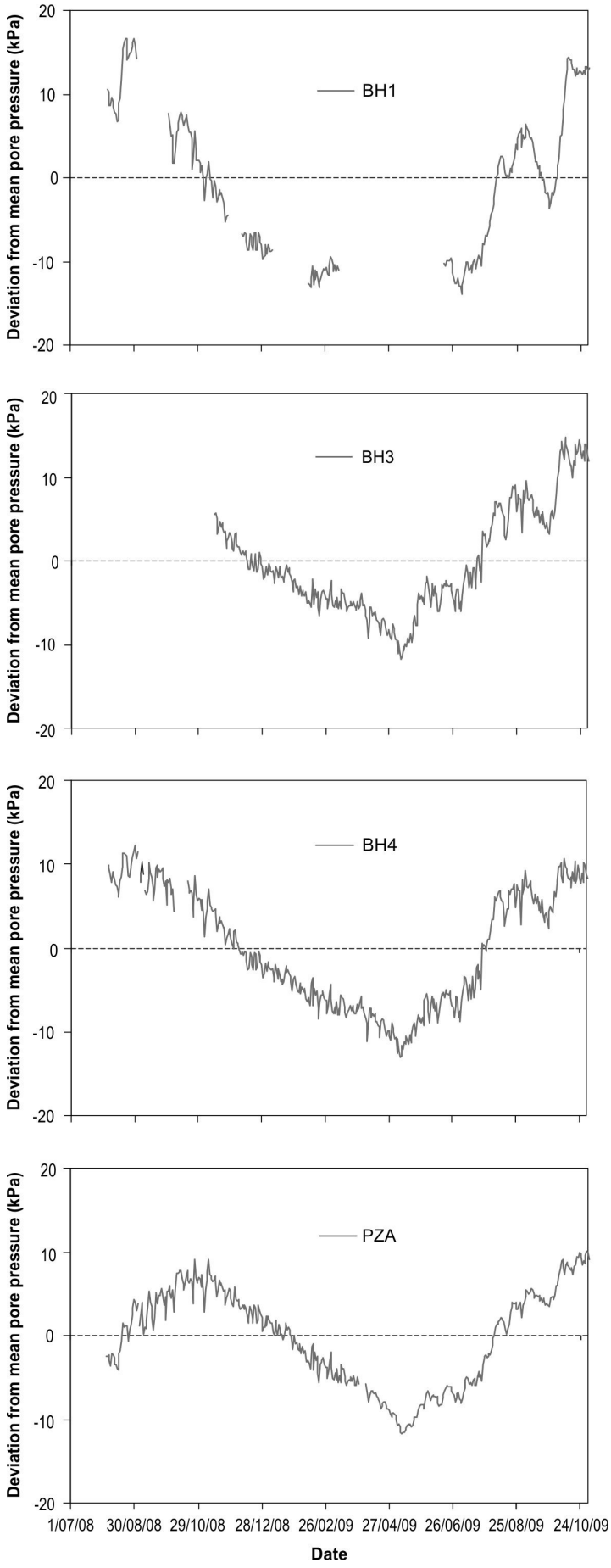

Figure 5.27 Deviation from daily mean pore pressures for piezometers BH1, BH3, BH4 and PZA, showing daily pore pressure readings.

Histograms of deviations from mean pore-pressure, for all piezometers are bimodal (Figure 5.28), and reflect the seasonal (winter / summer) variations shown by the time-series plots. Deviation from mean pore pressures for all VBW piezometers, show that maximum fluctuations in piezometric head levels are about 18.7 kPa (1.9 m) above and 12.8 kPa (1.3 m) below mean values, representing seasonal fluctuations of between 3% and 6% from mean values (Table 5.17). Piezometer BH1 shows the largest variation from mean and PZA the lowest, although readings from PZA, BH3 and BH4, located on the historic landslide, are all very similar, the exception being BH1, which is located above the historic landslide head scarp. Histograms of the daily change in pore pressure for all piezometers are unimodal, and approximately normally distributed with means of zero and ranges of typically ±3 kPa, and standard deviations of about ±1 kPa (Figure 5.29). These data suggest that the rate of pore-pressure change, for all piezometers, is slow, with large changes in pore pressure taking many days to occur.

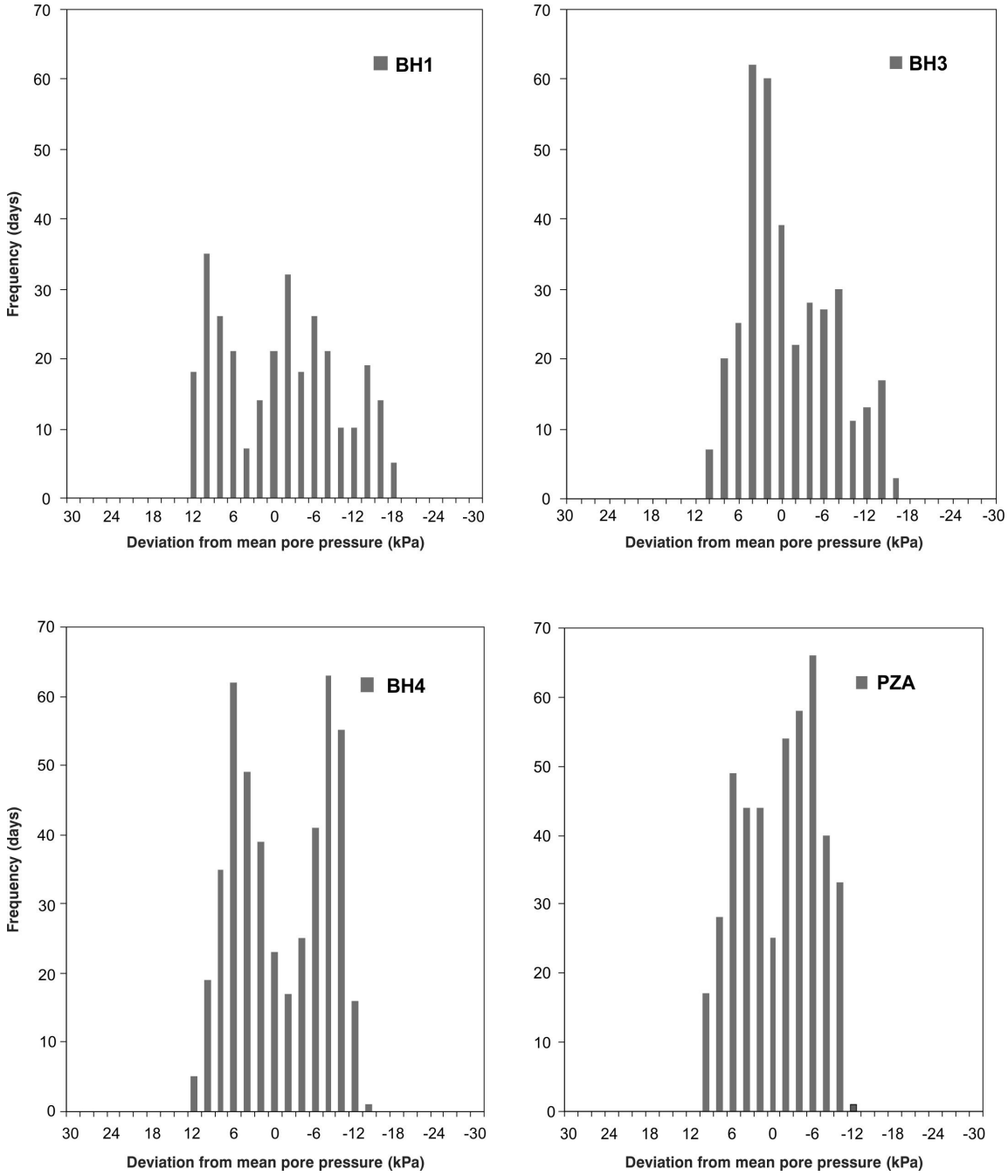

Figure 5.28 Histograms of deviations from daily mean pore-pressure, for piezometers BH1, BH3, BH4 and PZA (daily pore pressure readings).

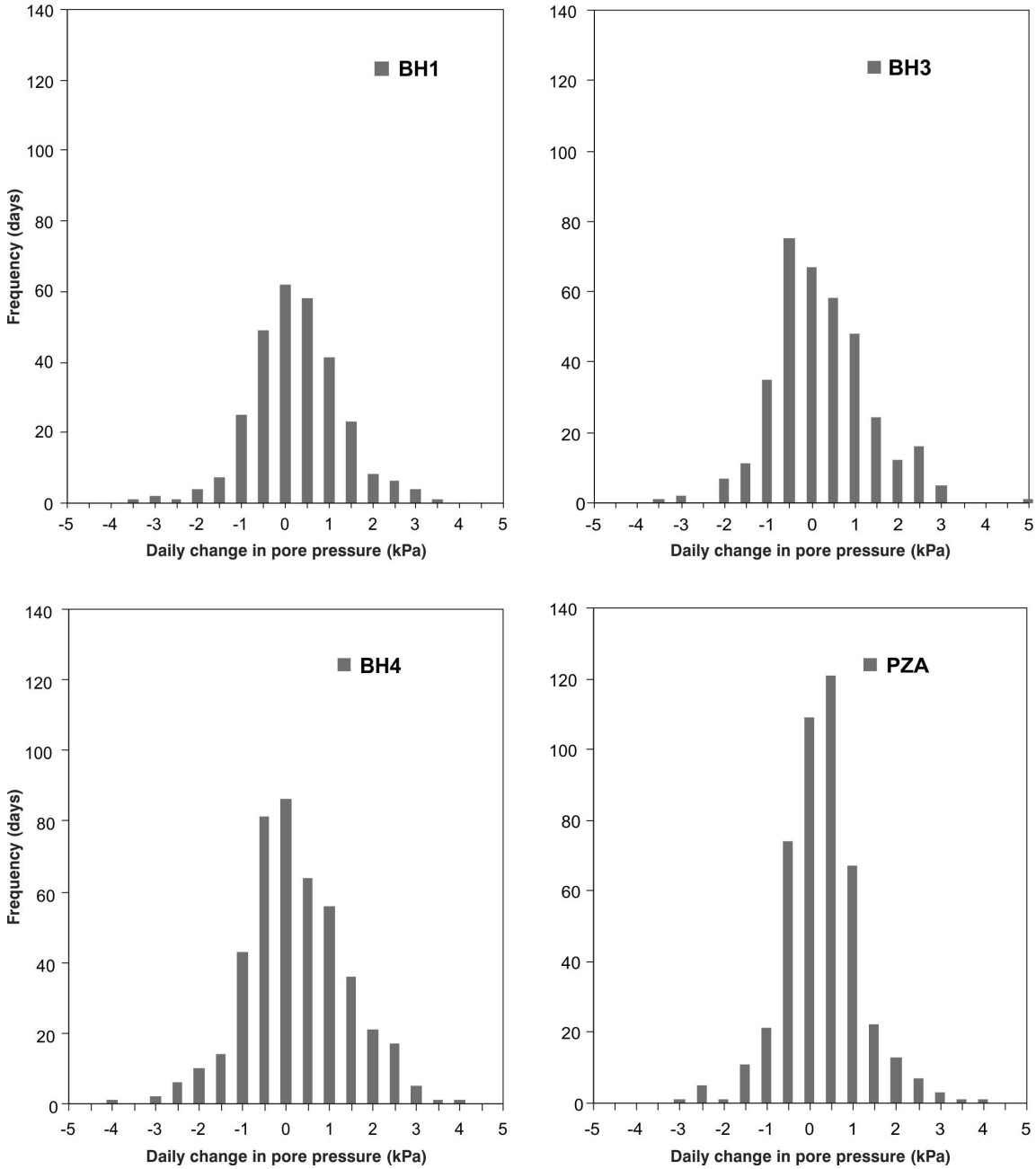

Figure 5.29 Histograms of the daily (day-to-day) change in pore pressure for piezometers BH1, BH3, BH4 and PZA (daily pore pressure readings).

Table 5.17 Statistics relating to the daily mean pore-water pressures recorded at each installation.

Piezometer	No. of daily records[1]	Mean value (kPa)	Deviations from mean (kPa)		Deviations from mean (m H^2O)		Standard deviation of the mean (kPa)
			Max.	Min.	Max.	Min.	
PZA	460	169.6	10.2	-11.7	1.0	-1.2	±5.8
BH1	255	539.1	18.7	-12.5	1.9	-1.3	±8.6
BH3	364	459.8	14.8	-11.4	1.5	-1.2	±6.3
BH4	450	248.6	12.5	-12.8	1.3	-1.3	±6.9

[1]Maximum number of daily records is 460 (degrees of freedom)

5.2.4.3 Rainfall and groundwater pressures

Although pore-pressure changes appear to be linked to rainfall, the histograms of pore-pressure change suggest pore pressures respond slowly to rainfall. A correlation analysis was undertaken to determine relationships between pore pressure at each piezometer, and antecedent rainfall (as recorded on the landslide), in order to establish the time frame over which rainfall influences piezometer response. Thereby establishing what period of antecedent rainfall is needed to cause a statistically significant change in daily pore pressure, i.e. estimating the lag time between rainfall and piezometer response.

The pore pressure at a given time and the accumulated antecedent rainfall has been assessed incrementally, e.g. $P_t \rightarrow R_{t\text{-}1\text{-}2}$; $Pt \rightarrow R_{t\text{-}1\text{-}2\text{-}3}$; $Pt \rightarrow R_{t\text{-}1\text{-}2\text{-}3\text{-}4....}$ where P_t is the pore pressure at a given time and R_t is the antecedent rainfall, using daily mean pore pressures and daily rainfall totals. The correlation analysis assumes a linear relationship between pore pressure and rainfall. The correlation is obtained by dividing the covariance of the two variables by the product of their standard deviations. The results (Figure 5.30) show that the correlation is highest for antecedent rainfalls accumulated over 10 to 15 weeks, indicating that pore pressures respond to long periods of antecedent rainfall. The exception is piezometer BH1 which peaks at antecedent rainfalls accumulated over about 5 weeks, however, this piezometer is located in the recently active area of the landslide outside the 1964 boundary of movement and has a small catchment area. These results imply that pore-pressure responses, triggering the accelerated creep motion (at Utiku), are a result of long periods of wet weather rather than large magnitude, short-duration rainfalls.

Table 5.18 Results from the pore pressure rainfall correlation analysis.

Piezometer	Rainfall accumulation period (antecedent rainfall) (weeks)	Peak correlation
BH1	17	0.92
BH3	12	0.82
BH4	12	0.79
PZA	20	0.85

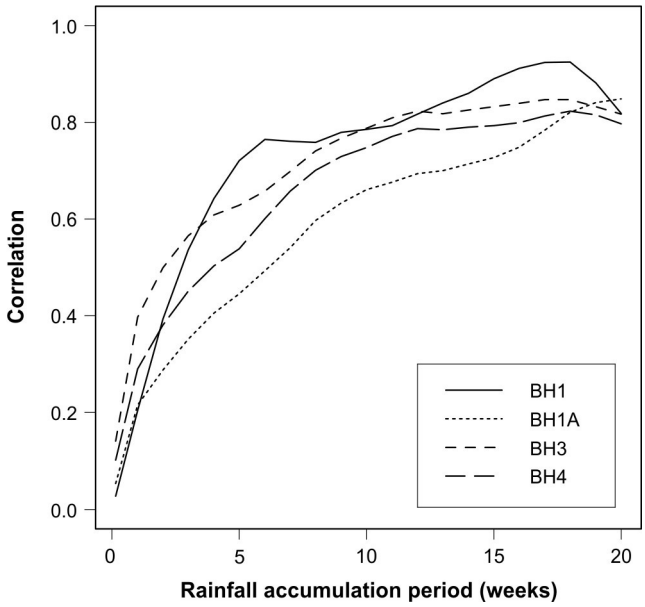

Figure 5.30 Results from the pore pressure and rainfall analysis (Utiku). The pore pressure at a given time and the accumulated antecedent rainfall were assessed incrementally, using the daily rainfall and pore pressure values recorded on the landslide. The correlation analysis assumes a linear relationship between pore pressure and rainfall.

5.2.4.4 Landslide hydrogeology

The landside is only 26% of the total catchment area contributing runoff to groundwater, with the upper catchment being formed by an older and now vacated landslide scar. It is possible that the four-day pore-pressure response is due to a combination of: the time it takes for surface water to enter the groundwater system; and to a lesser extent, the time it takes for surface water from elsewhere in the catchment to enter the groundwater system. The hydrogeology of the landslide is complex, due to the disturbed nature (and therefore contrasting permeability) of the materials forming the landslide mass, and the presence of preferential flow paths such as grabens, sinkholes and tension cracks, which are the result of historic and recent landslide motions. Drilling Logs from the boreholes indicate that the landslide debris (material overlying the slide surface) comprises a mixture of soil (remoulded Tarare Sandstone) and intact displaced rafts of Tarare Sandstone, which are highly fractured as a result of landslide motion, with typical rock quality designations (RQD) of < 50%. Below the slide surface, which marks the boundary between the Tarare Sandstone and Utiku Sandstone, the RQD of the intact sandstone is typically 100%. This abrupt change in material properties, as well as the presence of a clay layer (forming the slide surface), would form a distinct hydrogeological boundary. It is therefore probable groundwater within the landslide mass is perched above this boundary.

Piezometric head levels, calculated from the corrected daily mean pore-pressure measurements at BH3 and BH4 indicate that the piezometric surface is more or less

coincident with the ground surface, while at BH1 and PZA the piezometric surface is respectively about 10 and 5 m below ground level. Surface springs in and around BH3 and BH4 have been observed, with water bubbling out of the ground under pressure, however, the majority of the area is dry, even though the graben between the two boreholes, is several meters below the projected, piezometric level (from measurements in BH3 and BH4). The mean maximum piezometric head levels recorded prior to accelerated-creep-movement periods 1 and 3 have been used to generate groundwater contours. These suggest that piezometric levels have a typically constant gradient through the landslide, with contours striking north-south, parallel to the main slope aspect and strike of the Hautapu River (Figures 5.31 and 5.32).

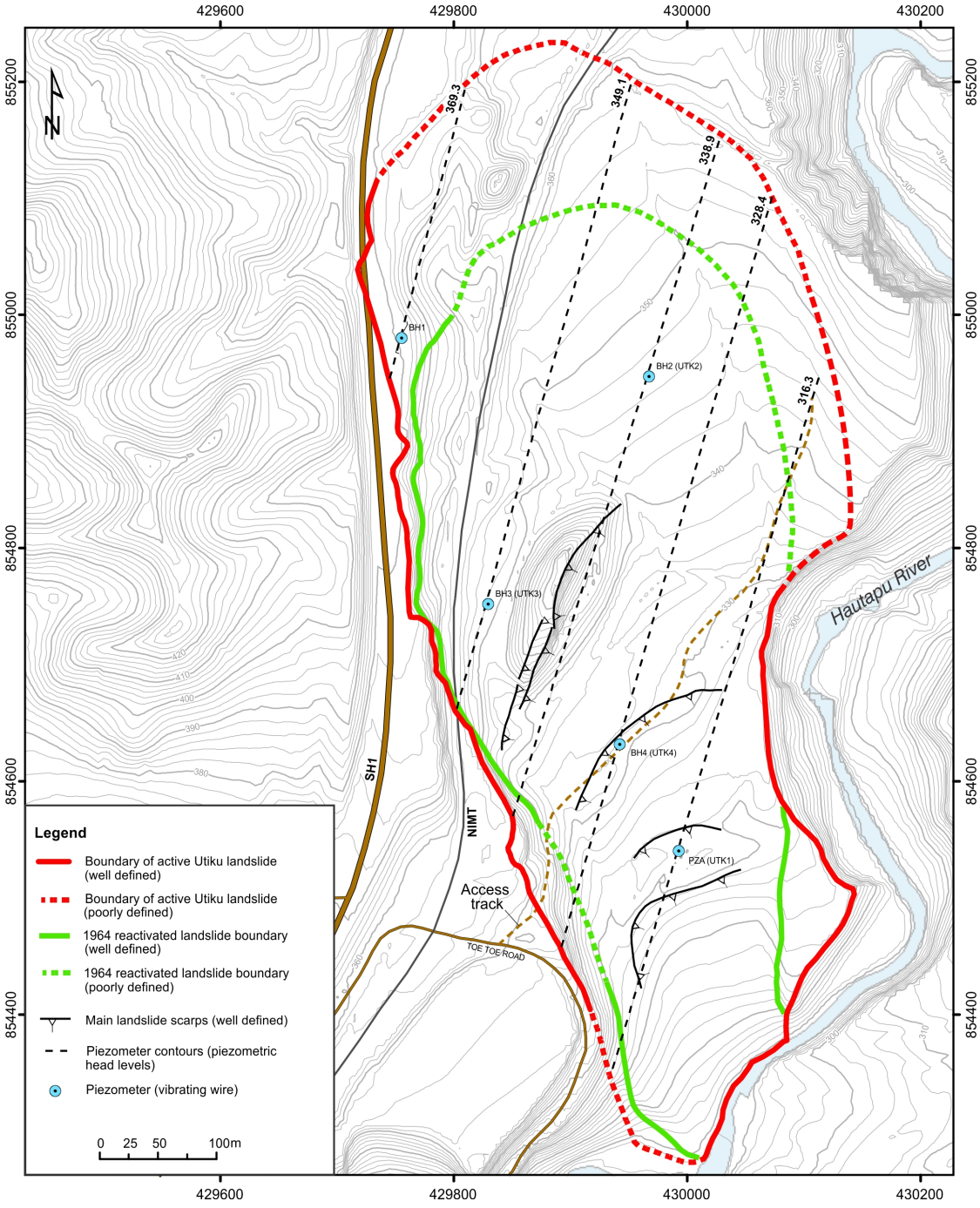

Figure 5.31 Piezometric contours of the mean maximum piezometric head levels recorded prior to accelerated-creep-movement periods one and three.

These observations combined with the pore-pressure monitoring data suggest that pore pressures within the landslide are partially confined. The partially confined aquifer is thought to be bound by the slide surface, at its base, and by intact rafts of sandstone, and disturbed clay/silt colluvial material at its upper margin, and due to the wedge-shape of the landslide, its southern flank is bound by intact Tarare sandstone. The aquifer is thought to be partially confined as borehole logs show significant losses of water circulation occurred during drilling in the upper part of the landslide, with these zones located below the projected piezometric head levels from the piezometers. The loss of circulation also suggests preferential groundwater flow paths (soil pipes), exist within the landslide mass, which form direct conduits for surface water into the landslide mass.

The timing of pore-pressure responses between the piezometers on the landslide has been investigated by plotting simultaneous pore pressures for different piezometers together, starting at the landslide crest and moving toward the toe, these are shown in Figure 5.33. The hysteresis between UTK3 and BH1 suggests pore pressures follow alternate paths between cyclic rising and falling periods. The shapes of the hysteresis loops also indicate that the rates of pore-pressure change between the piezometers differ. Pore-pressure changes at BH1 are generally larger in magnitude than those at UTK3 and occur more rapidly at BH1, both on the rising and falling limbs of the loop. However, it should be noted that there are significant gaps in the pore-pressure time-series from both of these piezometers.

The relationship between UTK3 and UTK4 is linear, and shows no hysteresis, indicating the rising and falling limbs follow similar trends. The gradient of this trend, does not significantly differ from 1, and so the magnitudes, rates and timing of the pore-pressure changes between the piezometers are statistically similar and would imply that pore pressures within the upper landslide are consistent.

However, this relationship does not hold true for the lower landslide, where the relationships between PZA and UTK3, and PZA and UTK4 show hysteresis. Although the gradient of pore-pressure change between these piezometers, using a simple linear relationship shows that that they do not differ significantly from 1, the hysteresis loops show differences between the piezometers. For both plots (Charts C and D) the falling pore-pressure limbs are curved; pore pressures on the upper landslide (UTK3 and UTK4) start to decrease more rapidly than those on the lower landslide, and similarly for the rising limb, pore pressures on the upper landslide start to rise more quickly than those on the lower landslide, indicating a lag between peak pore pressure on the upper landslide and those on the lower, with the pore pressure on the lower landslide taking

longer to rise and fall than those on the upper (Figure 5.34). This lag may be caused by contrasting permeability's of the landslide debris, with the more disturbed debris in the toe having a lower permeability than the debris in the central and upper parts of the landslide.

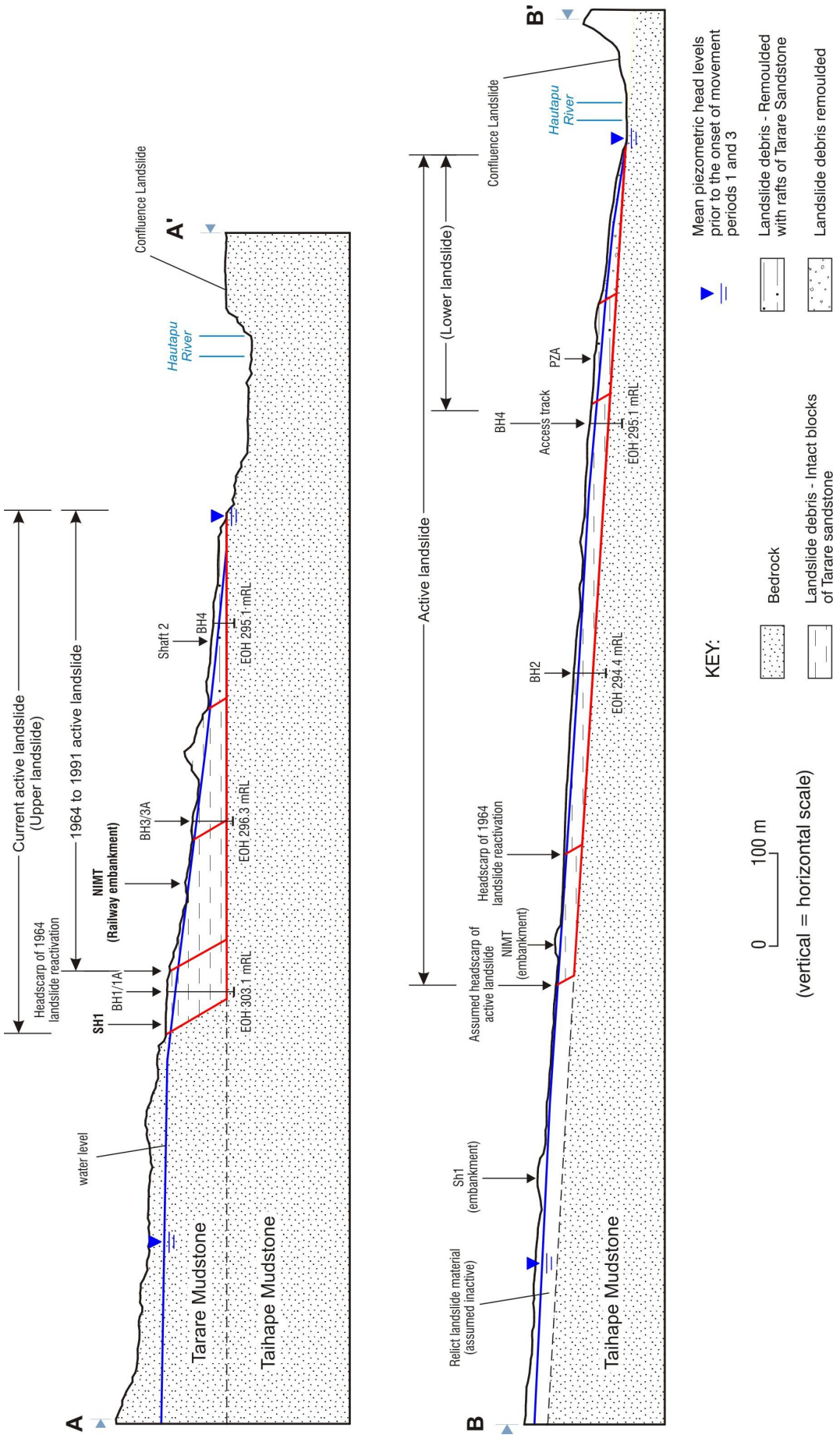

Figure 5.32 longitudinal sections A-A' and B-B' (Figure 3.08) through the landslide showing the mean maximum piezometric head levels recorded prior to accelerated-creep-movement periods one and three.

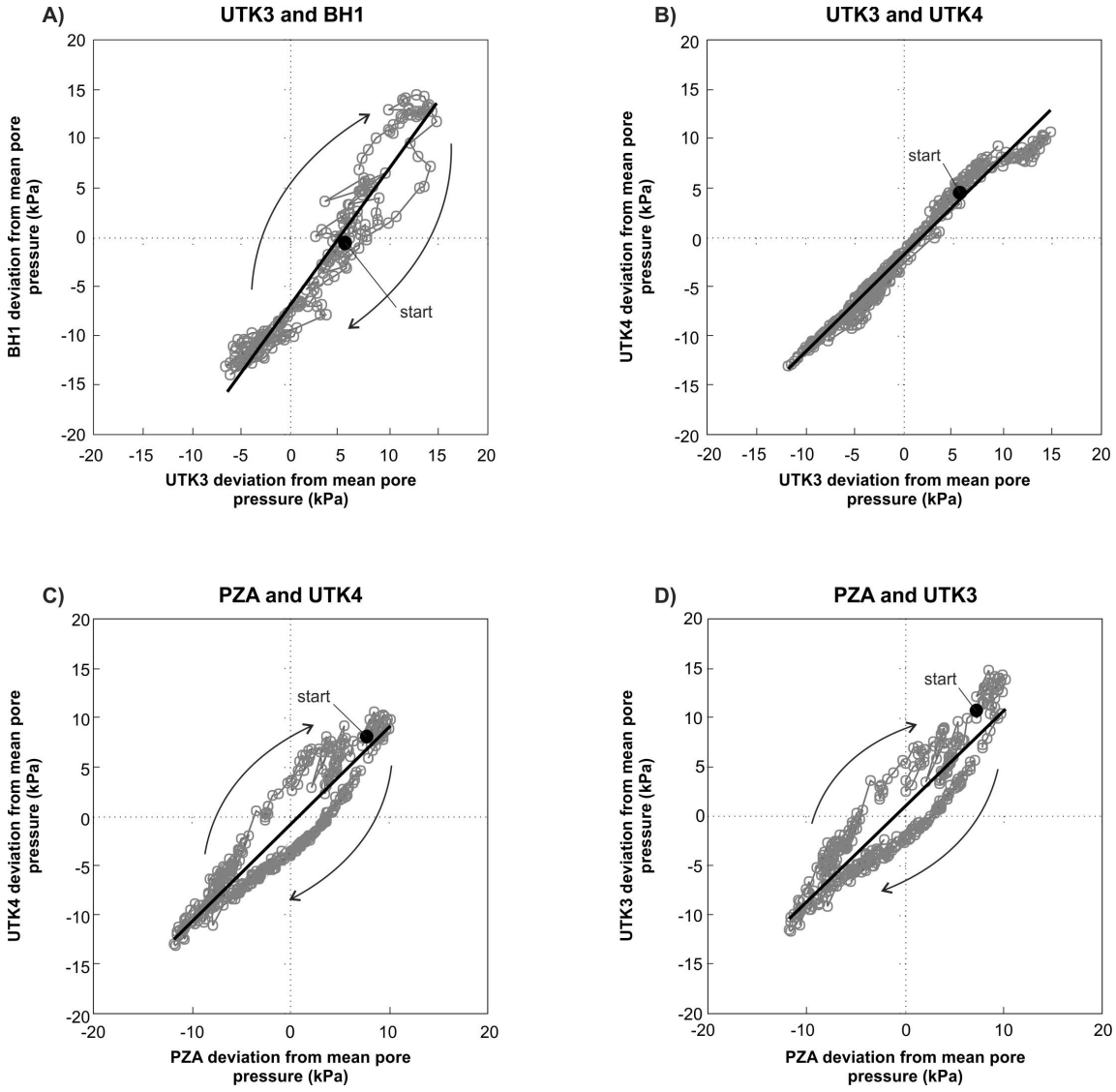

Figure 5.33 Simultaneous daily pore pressures for different piezometers plotted together (Utiku). A: The landslide crest (piezometers UTK3 and BH1). B: The centre of the landslide (piezometers UTK3 and UTK4). C and D: The lower central landslide (piezometers PZA, UTK3 and UTK4).

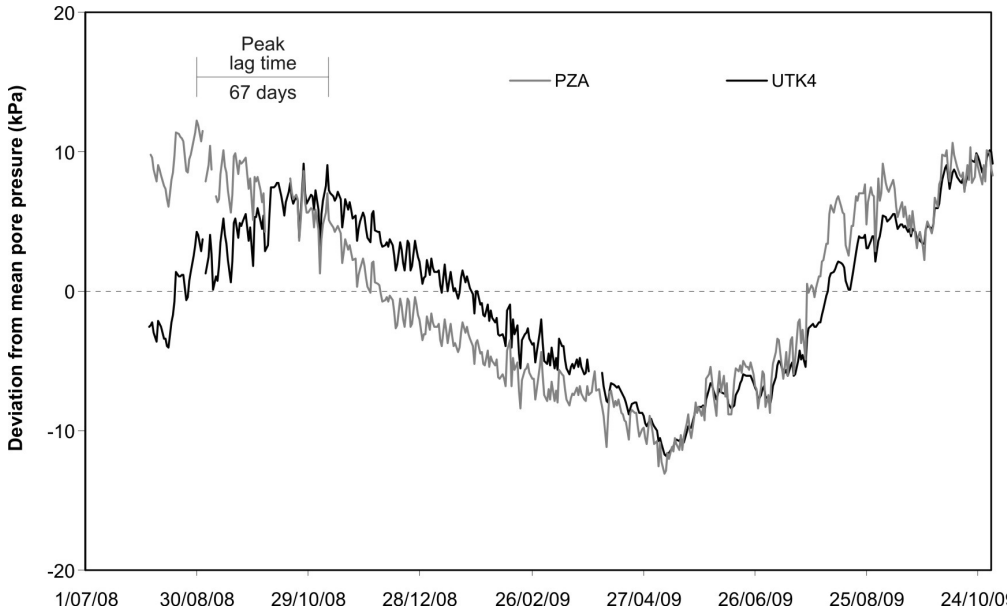

Figure 5.34 Relationship at Utiku between pore pressures on the upper landslide (piezometer UTK4) and the lower landslide (piezometer PZA).

5.2.4.5 Earthquakes

During the monitoring period, none of the periods of GPS motion (e.g. movement periods 1 to 3) can be attributed to earthquake-induced ground motions. Several earthquakes occurred during the monitoring period, and their associated strong motions (ground accelerations), measured by the sensor on the landslide located at BH2, are listed in Table 5.19.

The largest ground acceleration (PGA ~0.01 g) recorded on the landslide was in response to a M_L4.7 earthquake, which occurred on 16/10/2009 at 01:27:11 hours UTC (equivalent to a 1 in 3-year PGA, Stirling et al., 2000). This earthquake occurred about 6 days after the end of accelerated-creep period 3, when piezometric levels were greater than mean values. No GPS motions outside survey error were identified, indicating that the landslide is not particularly sensitive to earthquake-induced ground accelerations

Table 5.19 Earthquake ground accelerations recorded by the landslide instrumentation (Utiku).

Date UTC	Time (UTC)	Latitude	Longitude	Depth (km)	Magnitude (M_L)[1]	Ground acceleration (Gals)
14/09/08	09:52:12	-40.28	174.53	93.09	5.13	0.37
24/10/08	17:47:48	-39.67	176.82	35.50	4.43	0.25
19/12/08	00:21:05	-38.24	176.13	186.88	5.82	0.52
18/01/09	22:29:57	-40.31	176.15	38.68	4.10	0.49
21/03/09	20:28:18	-37.78	176.76	158.34	6.14	0.28
26/06/09	13:01:57	-38.97	175.76	5.00	4.45	0.27
1/09/09	00:18:05	-36.93	176.98	280.16	6.06	0.25
15/10/09	08:59:48	-39.72	176.82	30.96	4.61	0.37
16/10/09	01:27:11	-39.62	176.00	47.82	4.73	1.09
18/11/09	18:04:01	-40.41	175.59	40.11	5.11	0.50

[1] M_L Local earthquake magnitude

5.2.4.6 River stage

Changes in the level of Hautapu River could have an impact on landslide stability, through ongoing erosion leading to removal of toe support. The level of the Hautapu River is monitored, however, no periods of landslide motion correlate with increased river flows since river monitoring began in June 2008, although ongoing river-erosion is removing material from the toe of the landslide.

5.2.5 Summary of results – Utiku landslide

For the monitoring period 1/07/2008 to 31/10/2009, the GPS equipment on the landside has successfully recorded landslide motion outside survey error. These can be classified as extremely slow to very slow (16 mm/year < x < 1.67 m /year, Cruden and Varnes 1996), with two main motion patterns predominating: 1) “accelerated” creep; and 2) “slow” creep, with periods of vertical creep occurring at similar times. The periods of slow creep and in some cases accelerated creep, could comprise multiple rapid, short-duration, small-magnitude displacements which would not be resolvable at the precision and frequency of the surveying.

The lower Utiku slide is the most active part, recording the largest displacements to date. The magnitude of movement decreases upslope to the landslide head scarp. Motion of the upper landslide is approximately consistent in timing, magnitude and direction. The greatest magnitude event (movement period 2), was recorded on the lower landslide only, and did not retrogress into the upper landslide. Motion bearings recorded at all CGPS stations are consistent with a down-slope translational mechanism. The displacements calculated from the inclinometers installed at BH1 and BH3 indicate the presence of one slip surface, at depths corresponding to clay layers identified in the drill hole logs.

Landslide motion shows no correlation with earthquake-induced ground accelerations or river stage levels. Daily rainfalls and pore pressures have been compared to GPS motions and are shown together on Figure 5.35. The comparisons indicate that the three periods of accelerated creep motion (movement periods 1 to 3) correspond to periods of high pore pressure. Periods of slow- and vertical-creep appear to be unrelated to pore-pressures or any other measured factor(s).

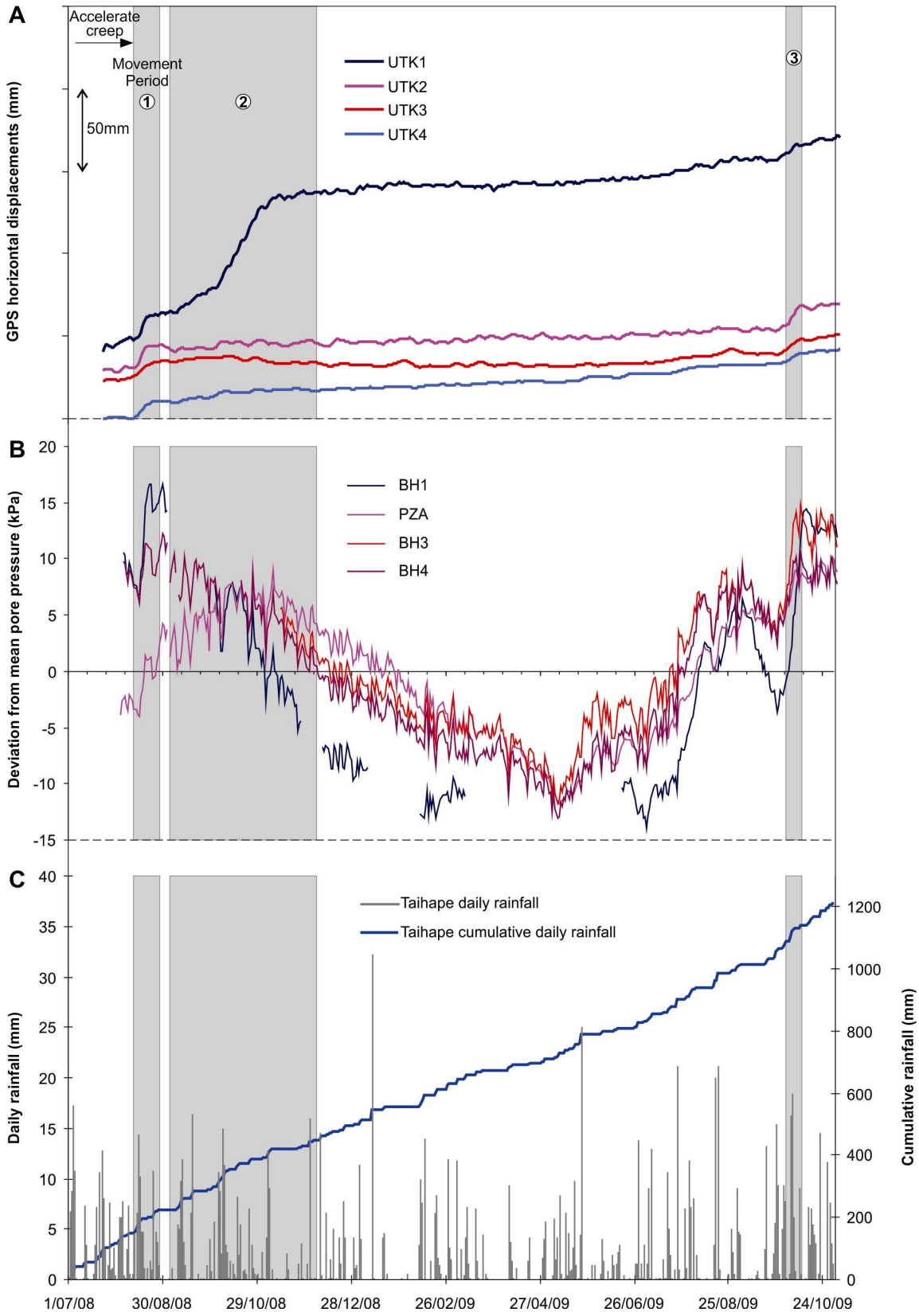

Figure 5.35 Relationship between cumulative horizontal displacements, pore pressures and rainfall for the Utiku landslide over the monitoring period. A: Cumulative displacements of stations UTK1, 2, 3 and 4 along their main movement bearings (smoothed displacements calculated using G_s = 2 mm). B: Daily pore pressures from piezometers BH1, BH3, BH4 and PZA. C: Daily and cumulative daily rainfall recorded by the Taihape landslide gauge at BH2.

Pore-pressure magnitudes decrease from the upper landslide to the lower landslide, and correspond to the decreasing depth, below ground level, of the landslide slide

surface towards the toe. Of the four piezometers installed on the landslide, BH1 has recorded the largest rates and magnitude of pore-pressure change over the period. However, BH1 is located off the historical landslide, in an area that has only recently (post-1991) shown signs of movement. Pore-pressure patterns recorded by the piezometers installed on the upper part of the historical landslide (BH3 and BH4), are near identical and follow consistent trends and rates (gradients) of change. The piezometer installed in the lower part of the historical landslide (PZA), shows similar pore-pressure patterns to BH3 and BH4. However, peak pore pressures are achieved later than those at BH3 and BH4, indicating a pore-pressure lag-time between the upper and lower landslide. It is this delayed response, recorded by BH1, which appears to have initiated the largest accelerated-creep movement event recorded to date (movement period 2, recorded on the lower landslide only), when piezometer levels on the upper landslide were decreasing over the same time period. Deviations from mean pore pressure, for all piezometers, show that the maximum variation in piezometric head levels are about 3% and 6% above mean, which represents a variation of about 29 kPa (or 3 m of head). These anomalies and similarities warrant further analyses and discussion.

The pore pressure at a given time and the accumulated antecedent rainfall has been assessed incrementally by performing a correlation analysis assuming a linear relationship between pore pressure and rainfall. The results show that the correlation is highest for antecedent rainfalls accumulated over 10 to 15 weeks, indicating that pore pressures respond to long periods of antecedent rainfall. For all piezometers, however, the daily change in pore pressure is small with standard deviations of about $\pm$1 kPa/day. The long-term pore-pressure trends show that the rising limbs of the pore-pressure graphs have typical gradients of about 0.1 kPa/day for PZA, BH3 and BH4, indicating that pore pressures respond slowly to rainfall. This can be seen in the combined plot of rainfall, pore pressure and landslide movement (Figure 5.35), which shows that the main periods of accelerated creep appear to correlate with steeper gradients in the cumulative rainfall trend. These results imply that pore pressures respond to long-periods of wet weather rather than large magnitude, short-duration rainfalls, and that rainfall takes time to enter the landslide groundwater system.

5.3 The Taihape Landslide – monitoring results

Monitoring of the Taihape landslide commenced at the beginning of July 2006 and is ongoing, but data recorded since 15th October 2009 are not analysed here, providing 39 months of data for analyses. As with the Utiku landslide, monitoring of the Taihape landslide comprises surface motion, subsurface motion, ground water pressure, rainfall

and earthquake-ground accelerations. The key difference between the equipment used at Taihape to that at Utiku is that Taihape surface motion is recorded using a robotic total survey station, which measures prisms installed on the landslide.

5.3.1 Survey-prism error analyses

The robotic total-survey station sequentially seeks and measures the angle and distance to survey reflectors (prisms) at hourly intervals. There are 35 prisms on the landslide. These were installed sequentially in three campaigns, starting in the landslide toe and working upslope towards the head scarp. An additional three prisms were installed on stable ground, around the edge of the landslide, to act as back sights. For each hourly measurement the conversion from polar to rectangular coordinates is done automatically. These are averaged over 24 hour periods to give a daily record (termed observation). Periods of data loss have occurred, mainly as a result of poor visibility e.g. low cloud, fog and snow, these are summarised in Table 5.20.

Table 5.20 Summary of prism data

Prism	Date installed	No, days installed (to 15/10/2009)	No. 24 hour (daily) readings	No. days with no data	Data coverage
1a	22/03/2007	938	881	57	93.9%
2a	22/03/2007	938	881	57	93.9%
3a	22/03/2007	938	881	57	93.9%
4	1/07/2006	1202	1141	61	94.9%
5	1/07/2006	1202	1141	61	94.9%
6	1/07/2006	1202	1141	61	94.9%
7	1/07/2006	1202	1142	60	95.0%
8	1/07/2006	1202	1140	62	94.8%
9	1/07/2006	1202	1138	64	94.7%
10	1/07/2006	1202	1136	66	94.5%
11	1/07/2006	1202	1080	122	89.8%
12	1/07/2006	1202	1063	139	88.4%
13	1/07/2006	1202	1124	78	93.5%
14	1/07/2006	1202	1141	61	94.9%
15	1/07/2006	1202	1140	62	94.8%
16	1/07/2006	1202	1121	81	93.3%
17	1/07/2006	1202	1141	61	94.9%
18	1/07/2006	1202	1140	62	94.8%
19	10/07/2006	1193	1132	61	94.9%
20	10/07/2006	1193	1068	125	89.5%
21	12/01/2007	1007	944	63	93.7%
22	12/01/2007	1007	950	57	94.3%
23	12/01/2007	1007	950	57	94.3%
24	12/01/2007	1007	950	57	94.3%
25	12/01/2007	1007	950	57	94.3%
26	12/01/2007	1007	943	64	93.6%
27	12/01/2007	1007	950	57	94.3%
28	12/01/2007	1007	911	96	90.5%
29	12/01/2007	1007	933	74	92.7%
30	12/01/2007	1007	950	57	94.3%
31	10/05/2007	889	833	56	93.7%
32	10/05/2007	889	832	57	93.6%
33	10/05/2007	889	832	57	93.6%
34	10/05/2007	889	832	57	93.6%
35	10/05/2007	889	833	56	93.7%

5.3.1.1 Horizontal displacements

Scatter plots for those prisms on the landslide showing the deviations from the mean horizontal East- and North- coordinate values (observations) centred on the mean value, are shown in Figure 5.36. Each record represents the mean daily coordinates of the prism, calculated from measurements made during a 24-hour (daily) epoch. These plots are useful as they show the spread of observations about the mean.

The precision of the daily readings has been estimated for each prism by calculating the uncertainty on each 24-hour reading as per the procedure in Section 4.4.1.3. It is assumed that the variables are independent from one day to the next and the calculated residuals are normally distributed. These uncertainties are shown on the scatter plots, for those prisms on the landslide, as error ellipses at the 95% confidence limit. These error ellipses give a visual indication of whether movement beyond expected survey error has occurred. That is, if all observations lie inside the error ellipse then no movement can be inferred. These data show that only thirteen of the prisms on the landslide have a number of observations outside the associated 95% confidence limit. The error ellipses are orientated relative to the total station line-of-sight, with the major axes representing the angular error, orientated perpendicular to the line-of-sight of the total station, and the minor axes representing the distance error. These results indicate that the distance measurements are more accurate than the angular measurements, which is a characteristic of total station measurements (e.g. Anderson and Mikhail, 1998). These errors are summarised in Table 5.21.

Out of the thirteen prisms showing movement, only eight relate to landslide motion. Motion of prisms 01, 19, 20, 21 and 28 are due to either vandalism, or localised effects such as construction.

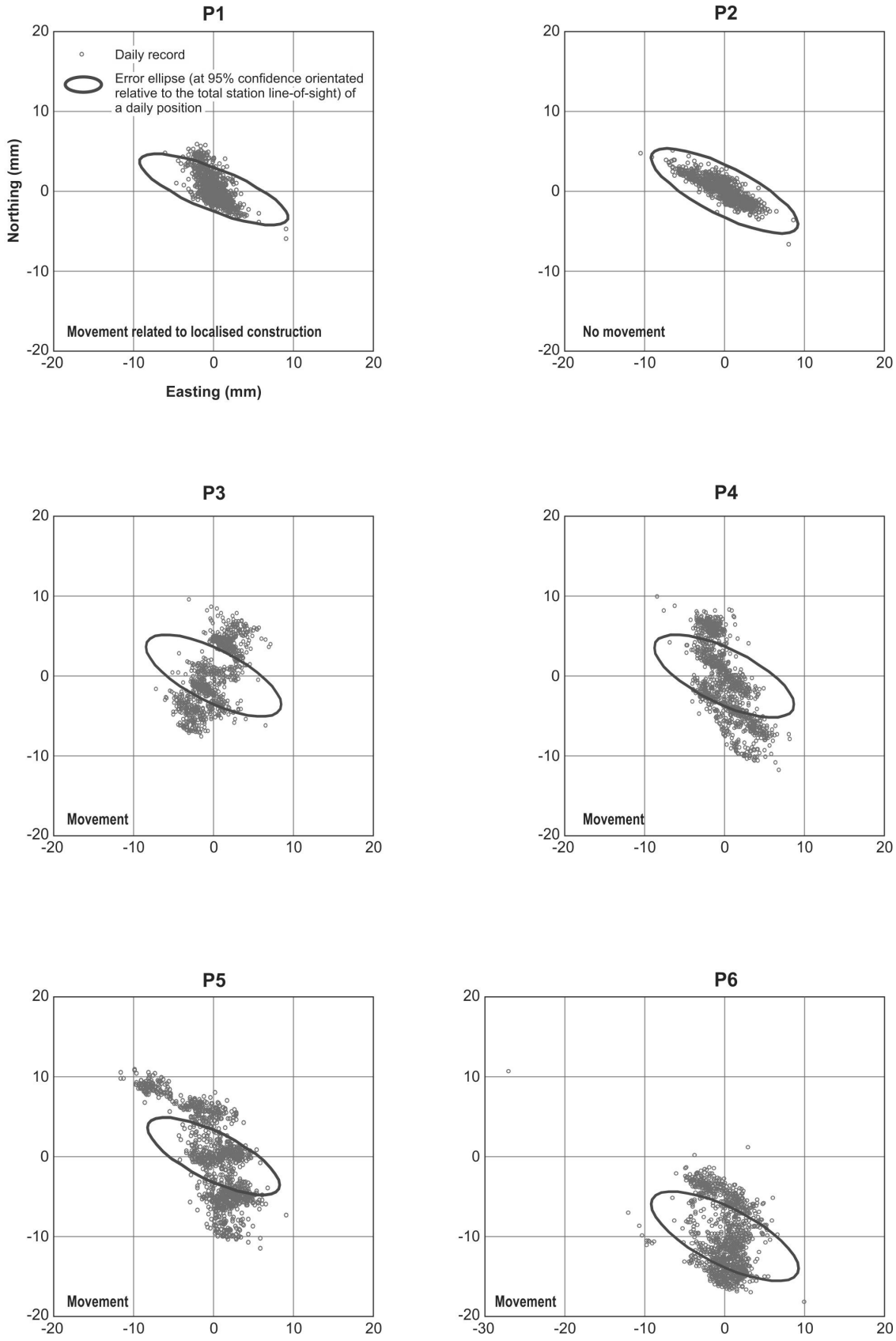

N.b. Scales vary between graphs to best represent the plotted data.

Figure 5.36a Scatter plots showing the deviations from the mean horizontal East- and North-coordinate values (observations), calculated for each 24-hour epoch, and associated errors, for all prisms on the Taihape landslide.

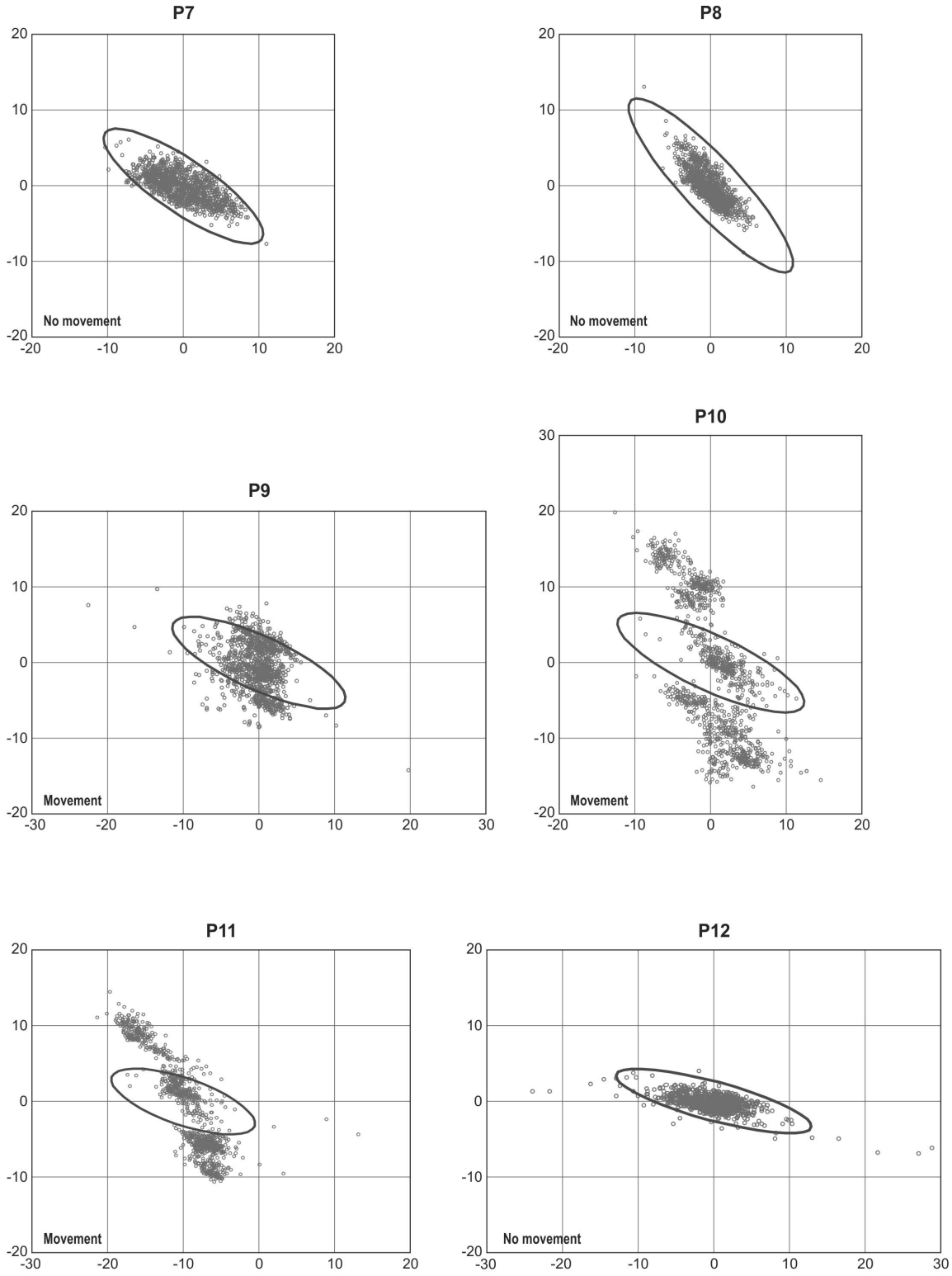

N.b. Scales vary between graphs to best represent the plotted data.

Figure 5.36b Scatter plots showing the deviations from the mean horizontal East- and North-coordinate values (observations), calculated for each 24-hour epoch, and associated errors, for all prisms on the Taihape landslide

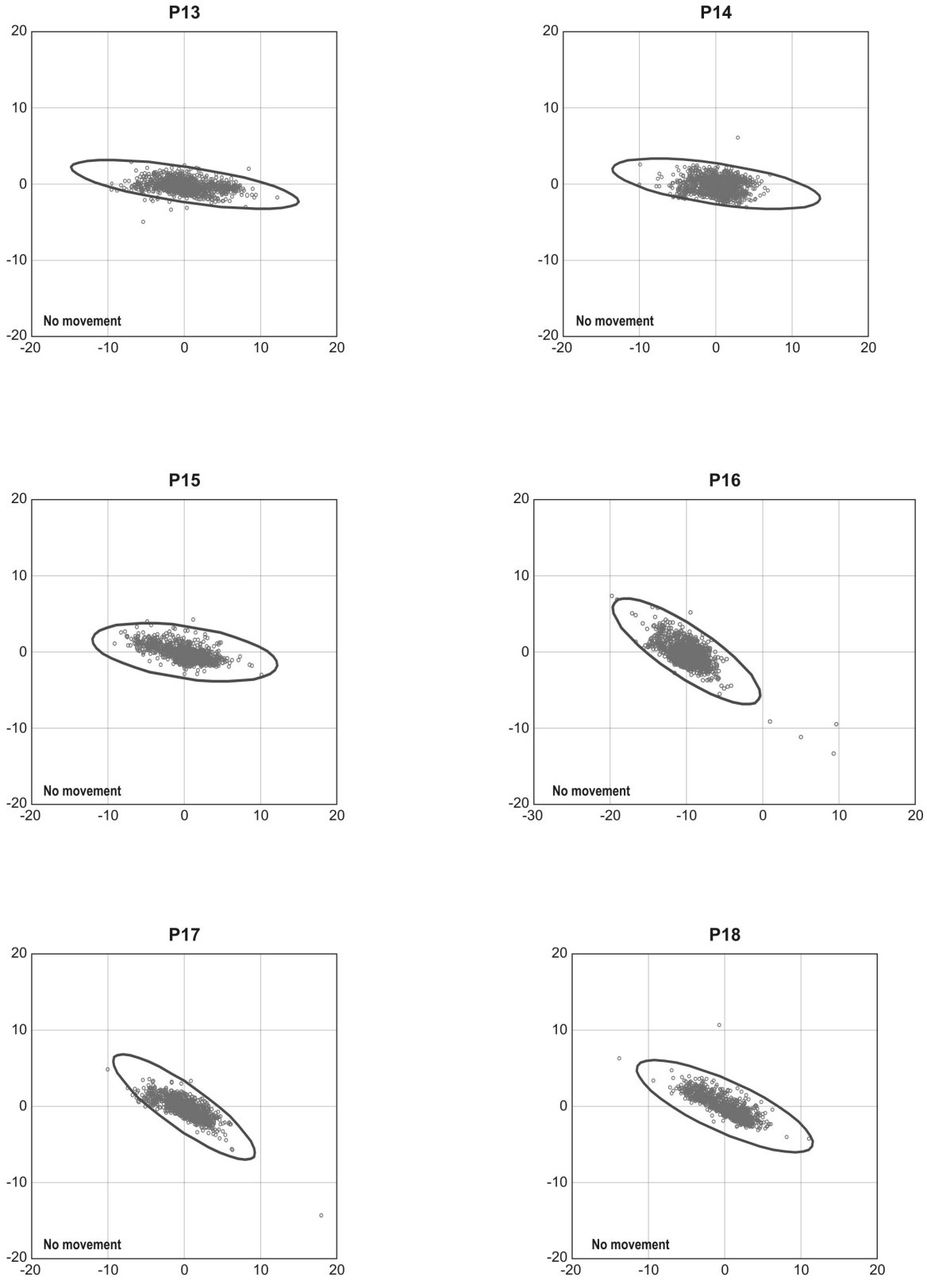

N.b. Scales vary between graphs to best represent the plotted data.

Figure 5.36c Scatter plots showing the deviations from the mean horizontal East- and North-coordinate values (observations), calculated for each 24-hour epoch, and associated errors, for all prisms on the Taihape landslide

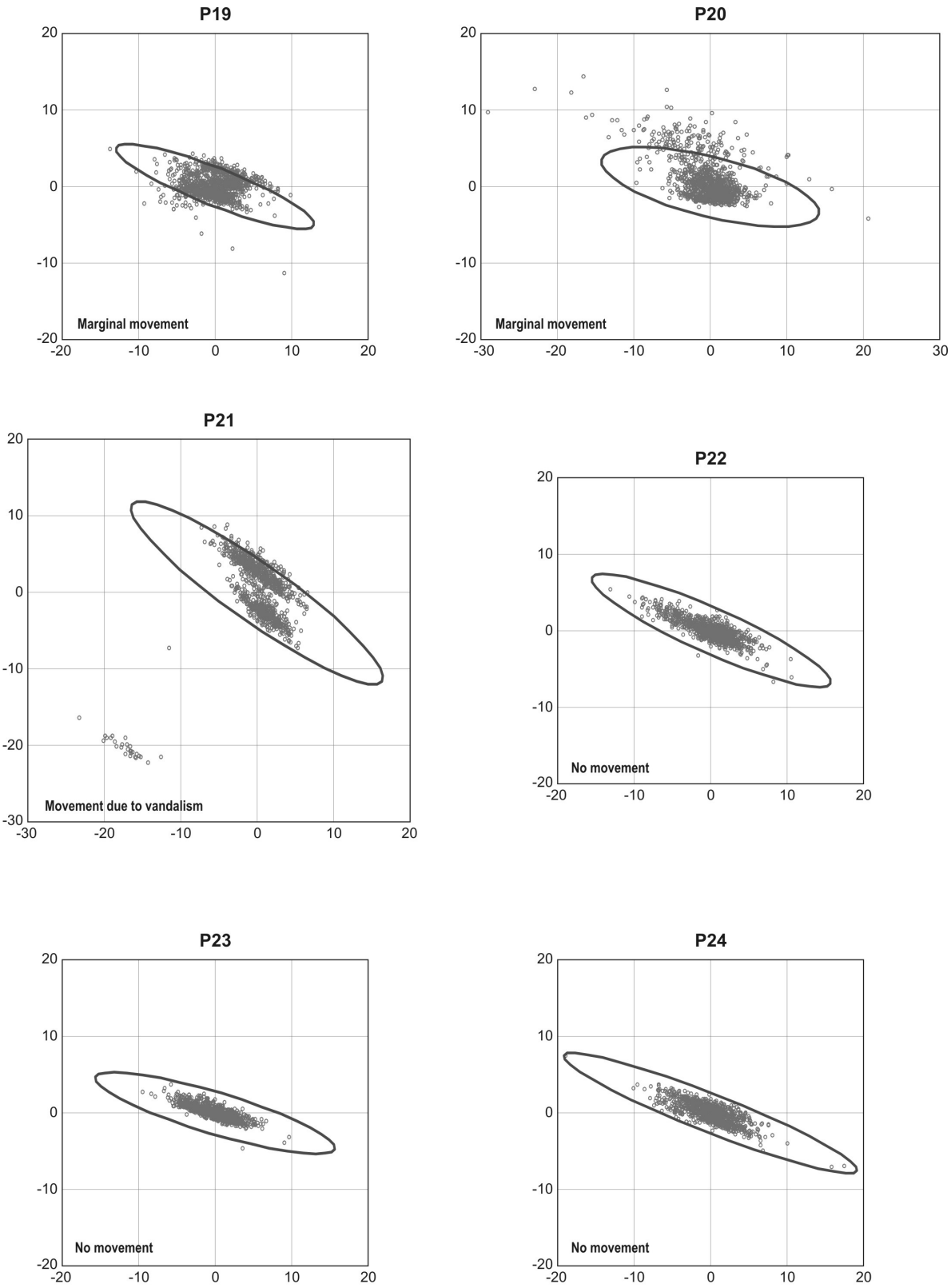

N.b. Scales vary between graphs to best represent the plotted data.

Figure 5.36d Scatter plots showing the deviations from the mean horizontal East- and North-coordinate values (observations), calculated for each 24-hour epoch, and associated errors, for all prisms on the Taihape landslide

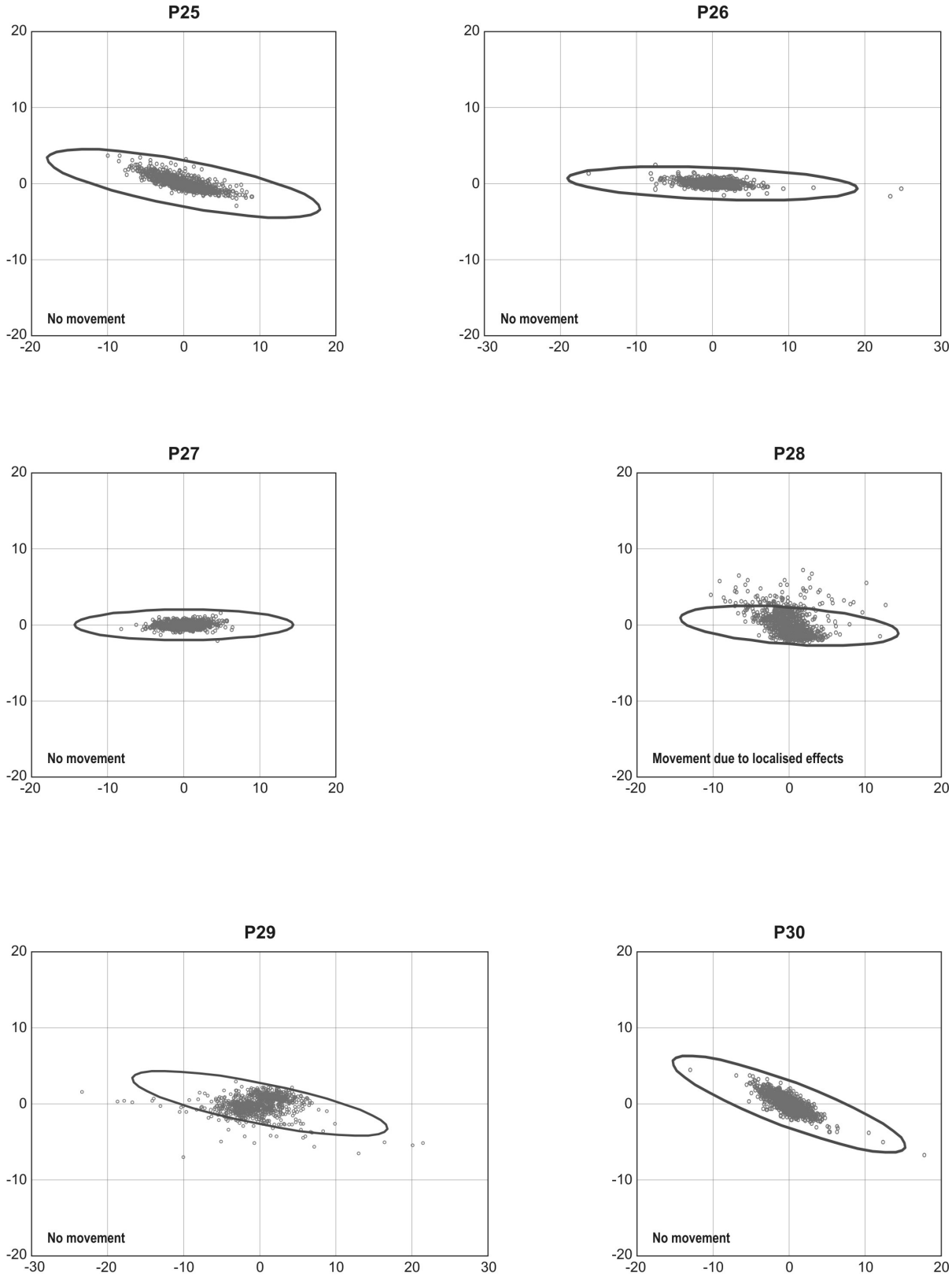

N.b. Scales vary between graphs to best represent the plotted data.

Figure 5.36e Scatter plots showing the deviations from the mean horizontal East- and North-coordinate values (observations), calculated for each 24-hour epoch, and associated errors, for all prisms on the Taihape landslide

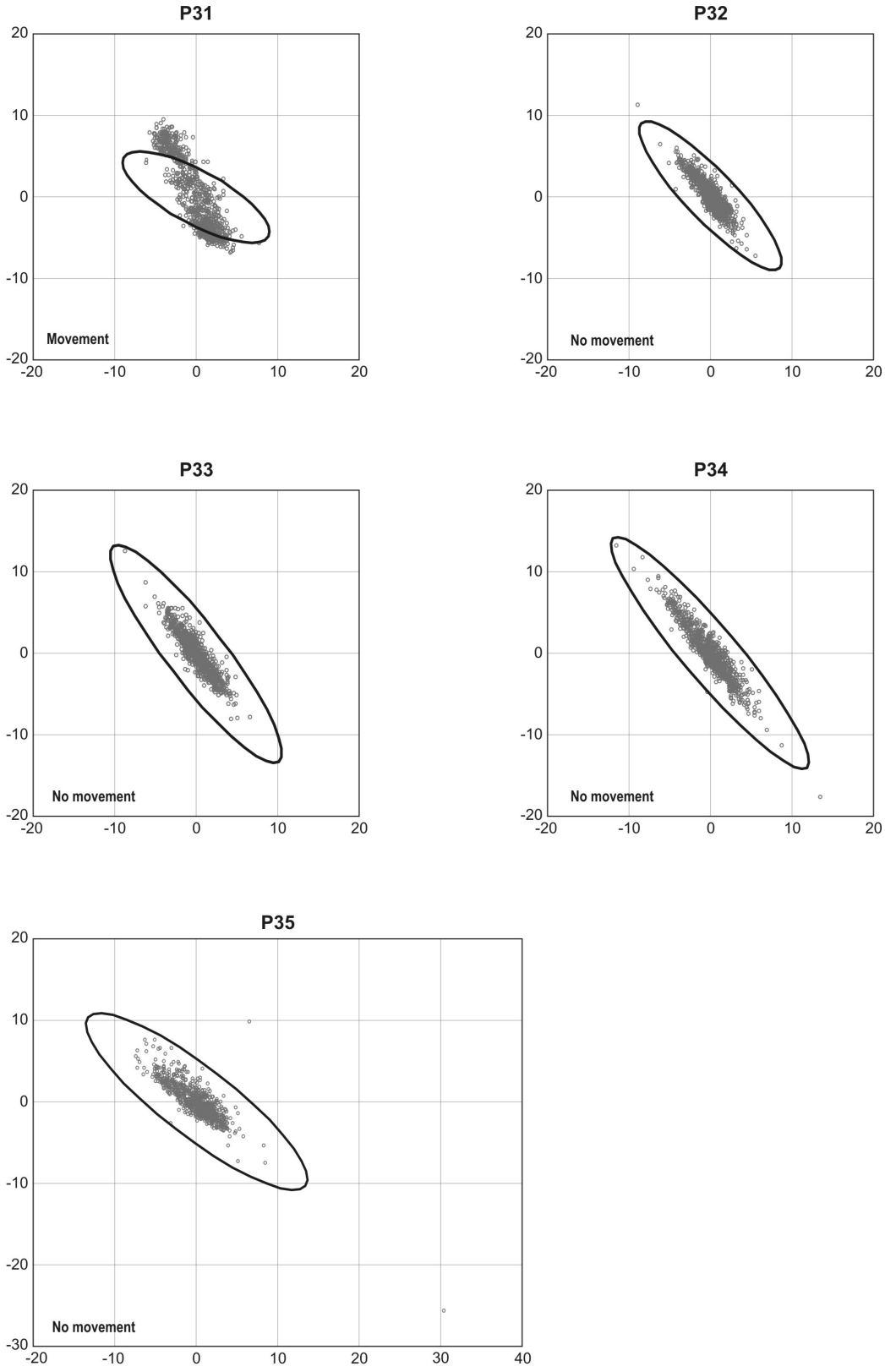

N.b. Scales vary between graphs to best represent the plotted data.

Figure 5.36f Scatter plots showing the deviations from the mean horizontal East- and North-coordinate values (observations), calculated for each 24-hour epoch, and associated errors, for all prisms on the Taihape landslide

Table 5.21 Prism measurement precision

Prism No.	Mean distance (from total station to prism)	Standard error (m)		Errors at the 95% confidence limit (m)		Movement outside 95% error
		σAngle	σDistance	σAngle	σDistance	
1a	505.3	0.004	0.001	0.010	0.003	Yes
2a	533.9	0.004	0.001	0.010	0.003	No
3a	590.4	0.004	0.001	0.009	0.003	Yes
4	578.8	0.004	0.001	0.010	0.003	Yes
5	613.3	0.004	0.001	0.009	0.003	Yes
6	688.3	0.004	0.001	0.010	0.004	Yes
7	697.0	0.005	0.001	0.013	0.004	No
8	793.1	0.006	0.002	0.015	0.004	No
9	700.9	0.005	0.001	0.012	0.004	Yes
10	679.4	0.006	0.002	0.014	0.004	Yes
11	621.5	0.004	0.001	0.010	0.003	Yes
12	777.9	0.005	0.001	0.013	0.003	No
13	809.1	0.006	0.001	0.015	0.002	No
14	747.1	0.006	0.001	0.014	0.003	No
15	698.5	0.005	0.001	0.012	0.003	No
16	678.8	0.005	0.001	0.011	0.003	No
17	668.3	0.005	0.001	0.011	0.003	No
18	760.4	0.005	0.001	0.013	0.003	No
19	828.6	0.006	0.001	0.014	0.002	Yes
20	791.5	0.006	0.002	0.015	0.004	Yes
21	941.2	0.008	0.002	0.020	0.004	Yes
22	958.5	0.007	0.001	0.017	0.003	No
23	959.7	0.007	0.001	0.016	0.003	No
24	1031.8	0.008	0.001	0.021	0.002	No
25	1035.5	0.007	0.001	0.018	0.003	No
26	1010.1	0.008	0.001	0.019	0.002	No
27	775.6	0.006	0.001	0.014	0.002	No
28	874.0	0.006	0.001	0.014	0.002	Yes
29	880.8	0.007	0.001	0.017	0.003	No
30	886.5	0.007	0.001	0.016	0.003	No
31	572.9	0.004	0.001	0.010	0.003	Yes
32	648.6	0.005	0.001	0.012	0.003	No
33	714.1	0.007	0.001	0.017	0.004	No
34	855.5	0.008	0.001	0.018	0.003	No
35	853.3	0.007	0.002	0.017	0.004	No

As with the UTK CGPS time series, a least-squares adjustment of the daily prism readings has been undertaken for the eight prisms with movement outside of error to determine horizontal motion vectors and associated errors. The results from the least-

squares adjustment are shown in Table 5.22 and as motion vectors on Figure 5.37. The time series plots have been colour-coded to reflect the timing of the records, with each colour code representing annual records. The time-series for all prisms show that positions have varied over the monitoring period. The largest changes in the time series plots for prisms 5, 10 and 11, where the plots show several clusters of data, which approximate to the different time periods. These data show that displacements are non-linear, as the clusters of data represent periods when the landslide was relatively static while the gaps between the clusters represent more-rapid motion. As for the Utiku landslide, these data suggest that displacements alternate between periods of acceleration and rest and that motion gradients are possibly non-linear, contrary to the assumption of the least-squares adjustment. However, over a longer time period, these variations may approximate to a constant rate.

Table 5.22 Taihape prism velocity and motion bearings from the least-squares analysis, for those prisms showing motion outside of error.

Prism No.	Least-squares adjustment	
	Bearing and error at the 95% confidence limit (°)	Velocity and errors at the 95% confidence limit (mm/year)
3a	205 ±(2)	6 ±(0.1)
4	169 ±(2)	5 ±(0.2)
5	156 ±(2)	6 ±(0.1)
6	310 ±(9)	2 ±(0.3)
9	200 ±(5)	2 ±(0.2)
10	170 ±(2)	8 ±(0.3)
11	152 ±(1)	7 ±(0.2)
31	337 ±(3)	5 ±(0.4)

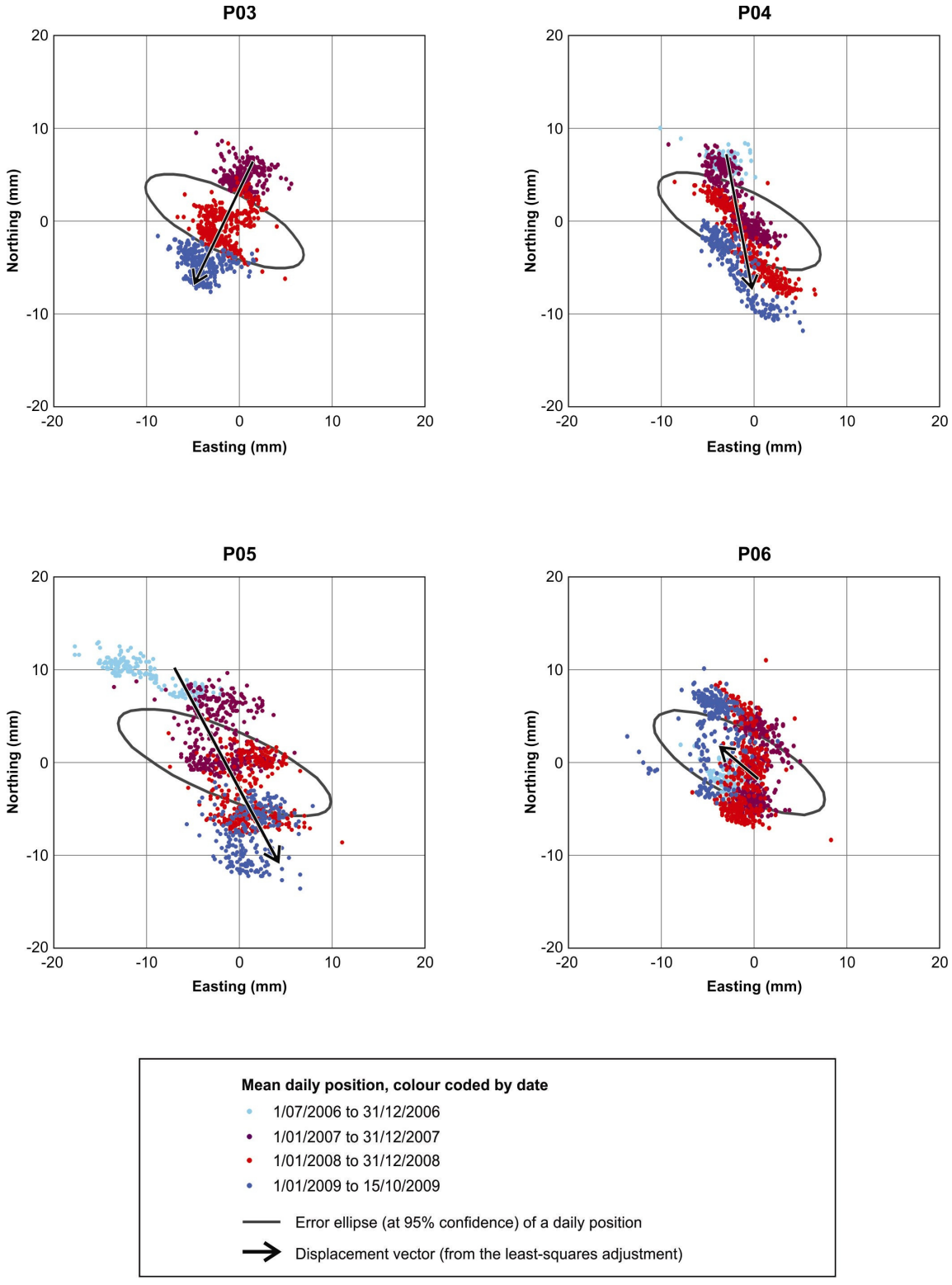

Figure 5.37a Scatter plots showing the deviations from the mean horizontal East- and North-coordinate values calculated for each 24-hour epoch, their associated errors and motion vectors, for prisms showing landslide movement.

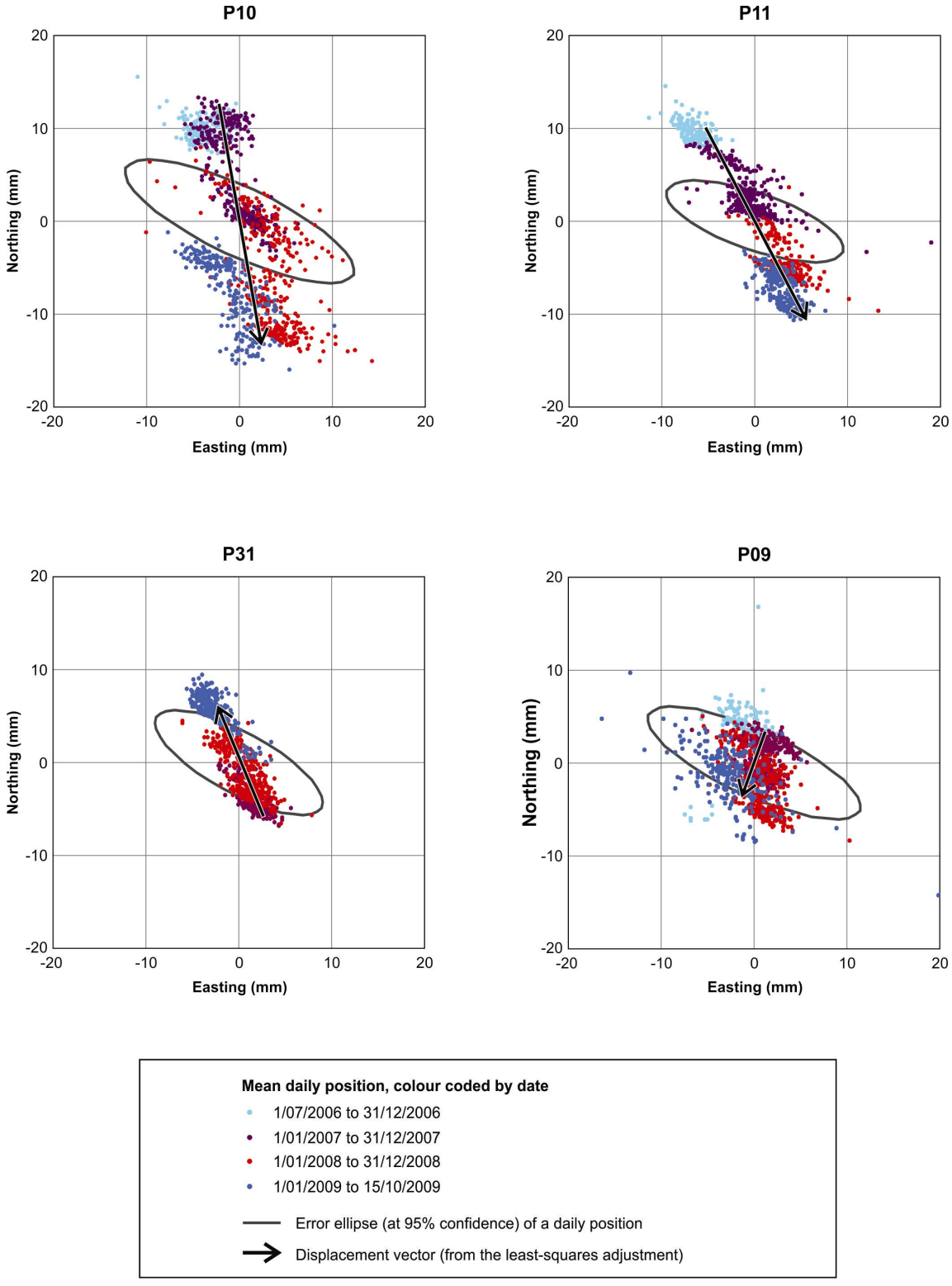

Figure 5.37b Scatter plots showing the deviations from the mean horizontal East- and North-coordinate values calculated for each 24-hour epoch, their associated errors and motion vectors, for prisms showing landslide movement

Only those prisms located on the toe of the landslide show movement outside of survey error. From the least-squares analyses, the main direction of landslide movement in the toe is between 152° and 205° (towards the South), which is in the direction of historical down slope displacements. Prisms 6 and 31, however, show movement in the opposite direction, upslope towards the North, which are inconsistent with the other prisms located in the area. The largest displacements were recorded at prism Nos. 10 and 11, which are located in a graben feature at the head of the toe slide-block (Chapter 4). These data indicate that, only about 11% of the landslide area has moved over the monitoring period, calculated using the geomorphological boundary that separates the toe-slide block, which contains prisms with movement outside error, from the surrounding inactive slide blocks.

5.3.1.2 Vertical displacements

To assess whether the vertical displacements are statistically significant, analyses using the least-squares method was carried out on the daily vertical time series from all of the prisms. Vertical motion is deemed to be statistically significant if the gradient on the vertical displacement time series is larger than the standard deviation of the gradient, at the 95% confidence limit. The vertical displacements of each of the eight prisms showing horizontal motion outside survey error are shown in Table 5.23.

Table 5.23 Vertical measurement precision and displacement magnitudes for the monitoring period.

Prism No.	Prism error[1] (mm)	Vertical motion gradient (mm/day)	Error on the vertical gradient at 95% (mm/day)	Difference between the gradient and 95% error (mm/day)	Total vertical displacement and errors at the 95% limit (mm)[2]
3a	6	-0.017	0.001	0.016	-16 ±(1)
4	6	0.001	0.001	0.000	1 ± (1)
5	7	0.004	0.001	0.003	5 ±(1)
6	8	0.007	0.001	0.006	9 ±(1)
9	8	0.003	0.001	0.002	4 ±(1)
10	7	0.003	0.001	0.002	3 ±(1)
11	6	0.007	0.001	0.006	8 ±(1)
31	7	-0.007	0.001	0.006	-7 ±(1)

[1] Estimate of the errors associated with the daily position of each prism by calculating the mean of the 24-hourly measurements (midnight to midnight UTC). Error expressed as the standard deviation of the mean at the 95% confidence limit.
[2] Errors calculated from the least-squares method assuming a linear relationship

Results indicate that vertical velocities are statistically significant for seven of the eight prisms. Prisms 31 and 3a show downward (-ve) movement, prisms 5, 6, 9, 10 and 11 all show minor upward movement and P4 shows no change. The largest downward motion

was recorded by prism 3a (-16 mm), on the toe of the landslide, a similar displacement was recorded at prism 31, about 25 m down slope (south) from prism 3a. Prisms 5, 6, 9, 10 and 11 all show significant minor positive vertical displacement (Figure 5.38), which is also the case for the majority of the other prisms outside the active toe area. These may be seasonal changes, as the time-series for these prisms suggest seasonal cycles, which approximate to winter (upward vertical motion) and summer (downward vertical motion) periods. These are shown more clearly by the smoothed trends of the daily time-series, derived using a Gaussian smoothing kernel following the procedure in Section 4.4.1.4. The monitoring period covers three summer and four winter periods, with each seasonal cycle representing a vertical change of 5 to 10 mm. It is probable that those prisms showing positive vertical displacements are being influenced by the additional winter cycle within the time-series. Also, for those prisms showing upward vertical motion, the displacement over the monitoring period (calculated from the least-squares adjustment), do not exceed the magnitude of the seasonal cycles.

To investigate this further, data representing two complete seasonal cycles was extracted for prisms 6 and 11 (those with the largest upward vertical displacements), and plotted as deviation from mean height. The data were then smoothed using a Gaussian smoothing kernel following the procedure in Section 4.4.1.4 to better show the seasonal fluctuations (Figure 5.39). The linear trend of the extracted time series was then calculated using the least-squares method, to assess the significance of the vertical motions. The analyses show that the vertical displacements, for both prisms, are statistically significant but downward. To assess whether any of the vertical displacement is related to landslide motion and not the seasonal cycles, it has been assumed that vertical prism velocities, from the least-squares method, must be greater than the mean seasonal variations. On this assumption, only prisms 3a and 31 show statistically significant vertical displacements, which are downward. For the other prisms it would take a further 3 to 4 years, at current movement rates, for displacements to accumulate to be outside of the recorded seasonal variations. Potential causes of the seasonal variations warrant further investigation but are beyond the scope of this study.

Although the least-squares method has shown that vertical displacements are statistically significant for prisms 3a and 31, they have been analysed assuming the velocity is constant. The time-series plots (Figure 5.39) show that this is not the case; in both plots there appear to be periods of short duration relatively rapid motion, represented by steps in the displacement plots, which occur over about 90-day periods and warrant further investigation.

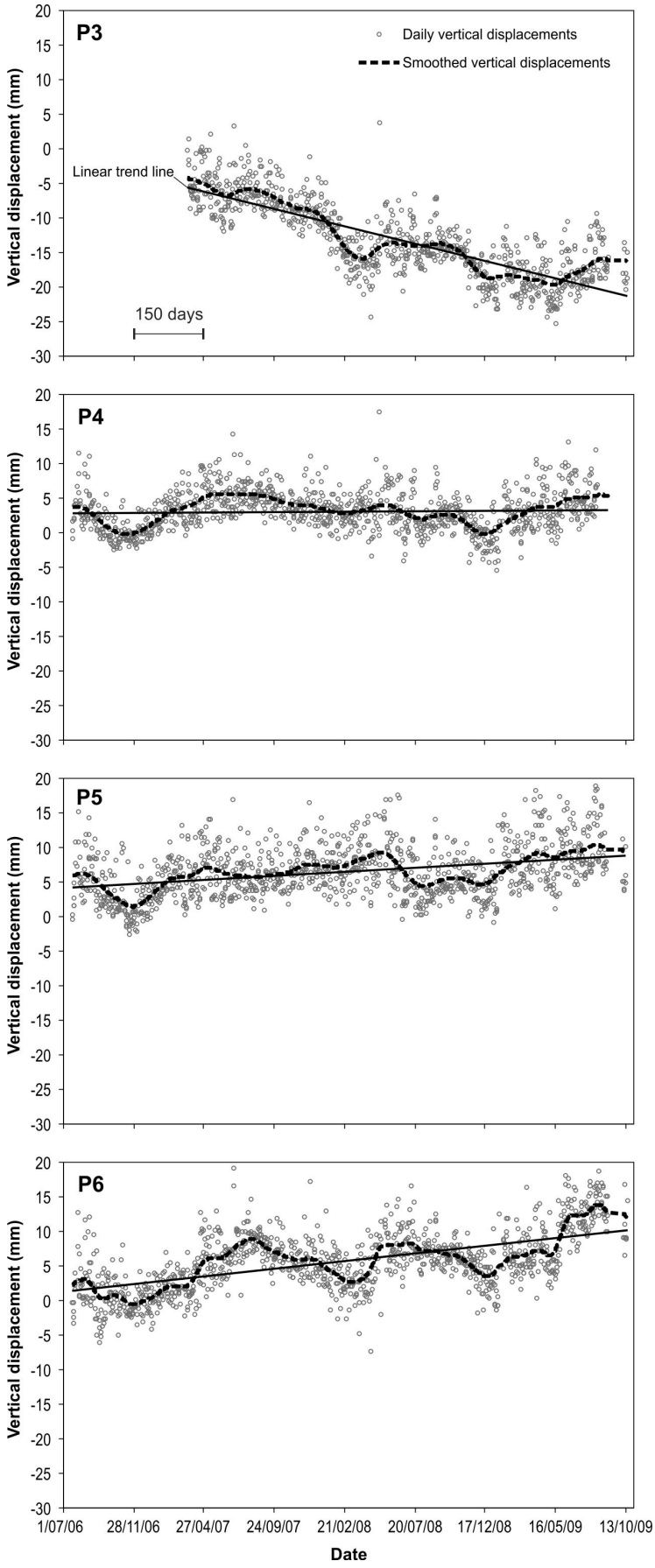

Figure 5.38a Cumulative vertical displacements against time for prisms on the active landslide. Daily and smoothed values are shown. Smoothed values are derived using a Gaussian smoothing kernel with a smoothing window where G_s = 5 mm.

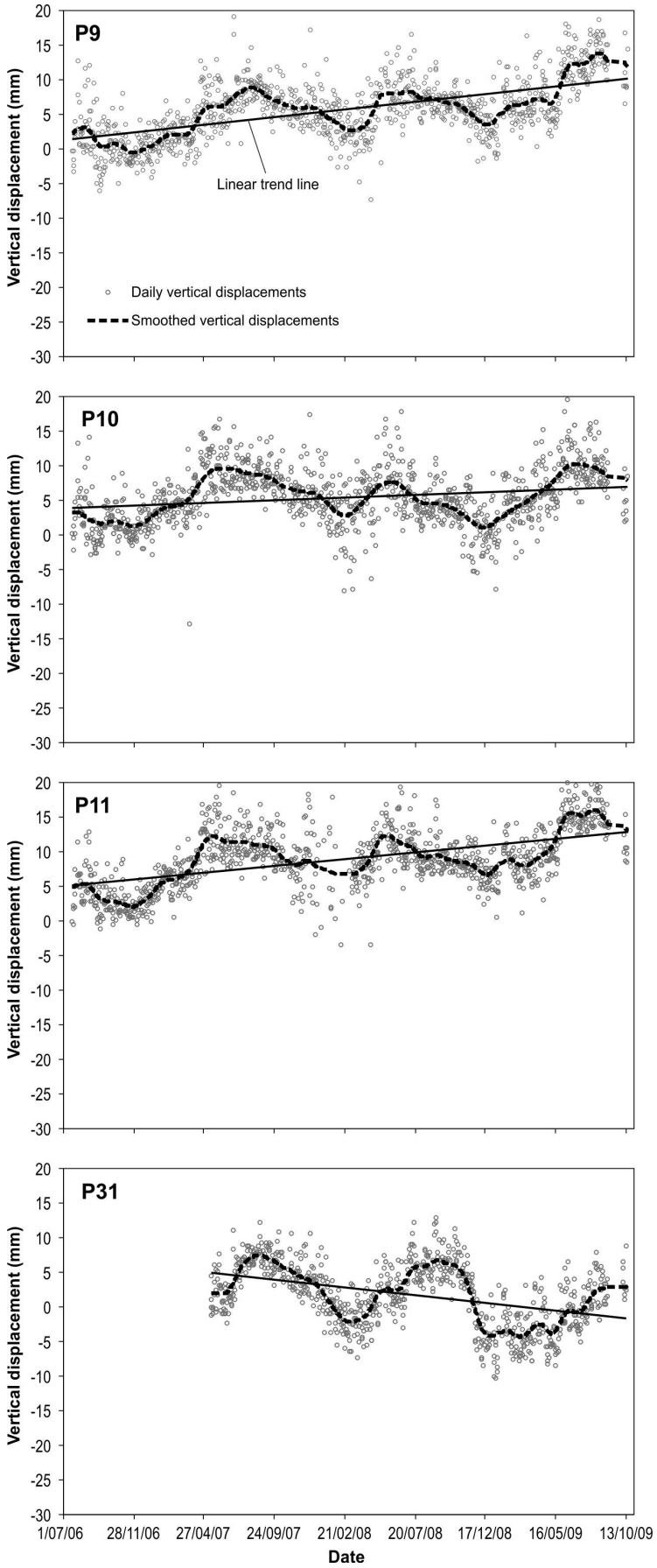

Figure 5.38b Cumulative vertical displacements against time for stations on the active landslide. Daily and smoothed values are shown. Smoothed values are derived using a Gaussian smoothing kernel where $G_s = 5$ mm.

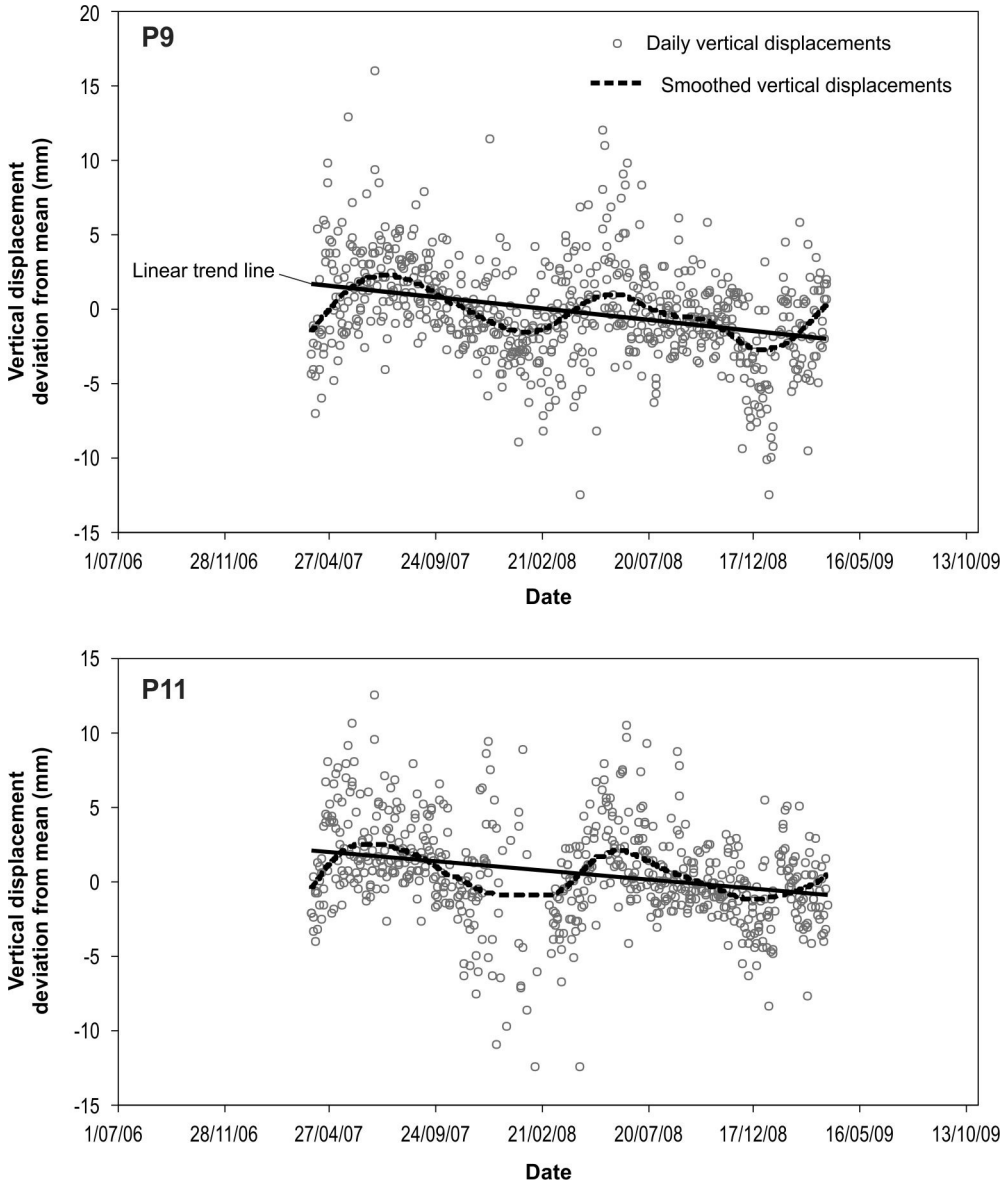

Figure 5.39 Two complete seasonal cycles extracted from the vertical time series from prisms 6 and 11. Daily and smoothed values are shown. Smoothed values are derived using a Gaussian smoothing kernel where G_s = 10 mm.

5.3.2 Landslide movement patterns

5.3.2.1 Cumulative displacements

To identify patterns in horizontal prism velocity, the daily time series from each of the eight prisms were plotted as cumulative horizontal displacements along their main movement bearings, which were derived from the least-squares adjustment (Table 5.24). Each time series was smoothed using a Gaussian smoothing kernel through the daily cumulative horizontal displacements, where G_s = 2 mm (Figure 5.40). The precision of the smoothing kernel was calculated as per the procedure described in Section 4.4.1.4; these estimates are shown in Table 5.24.

Table 5.24 Precision of smoothing kernel calculated as the difference between the daily and smoothed daily cumulative horizontal displacement measurements.

Prism	Horizontal movement Bearing (°)	Smoothing errors Standard deviation (mm)	Smoothing errors 95% confidence (mm)
3a	205	0.6	1.4
4	169	0.8	1.9
5	156	1.0	2.5
6	310	1.4	3.4
9	200	0.8	1.9
10	170	1.2	2.9
11	152	1.3	3.1
31	337	1.0	2.3

A summary of the displacements for each station over the monitoring period are listed in Table 5.25, and are plotted on Figure 5.41, along with the associated errors at the 95% confidence limit. For prisms 6 and 31 the movement bearings are upslope. The vertical displacements are also shown in Table 5.25. Prisms 3a and 31 are the only prisms showing vertical displacements greater than those due to the seasonal cycles.

Interpretation of the cumulative horizontal displacement plots (Figure 5.40), indicate two main types of motion: 1) short-duration, relatively rapid motions, in both upslope and downslope directions, which appear seasonal and are superimposed on; 2) longer-duration slower displacements over several years, which are only discernable from the long-term trends in the cumulative displacement plots. The short-duration relatively rapid motions have been termed “accelerated creep” and the longer-duration slower motions as “slow creep”.

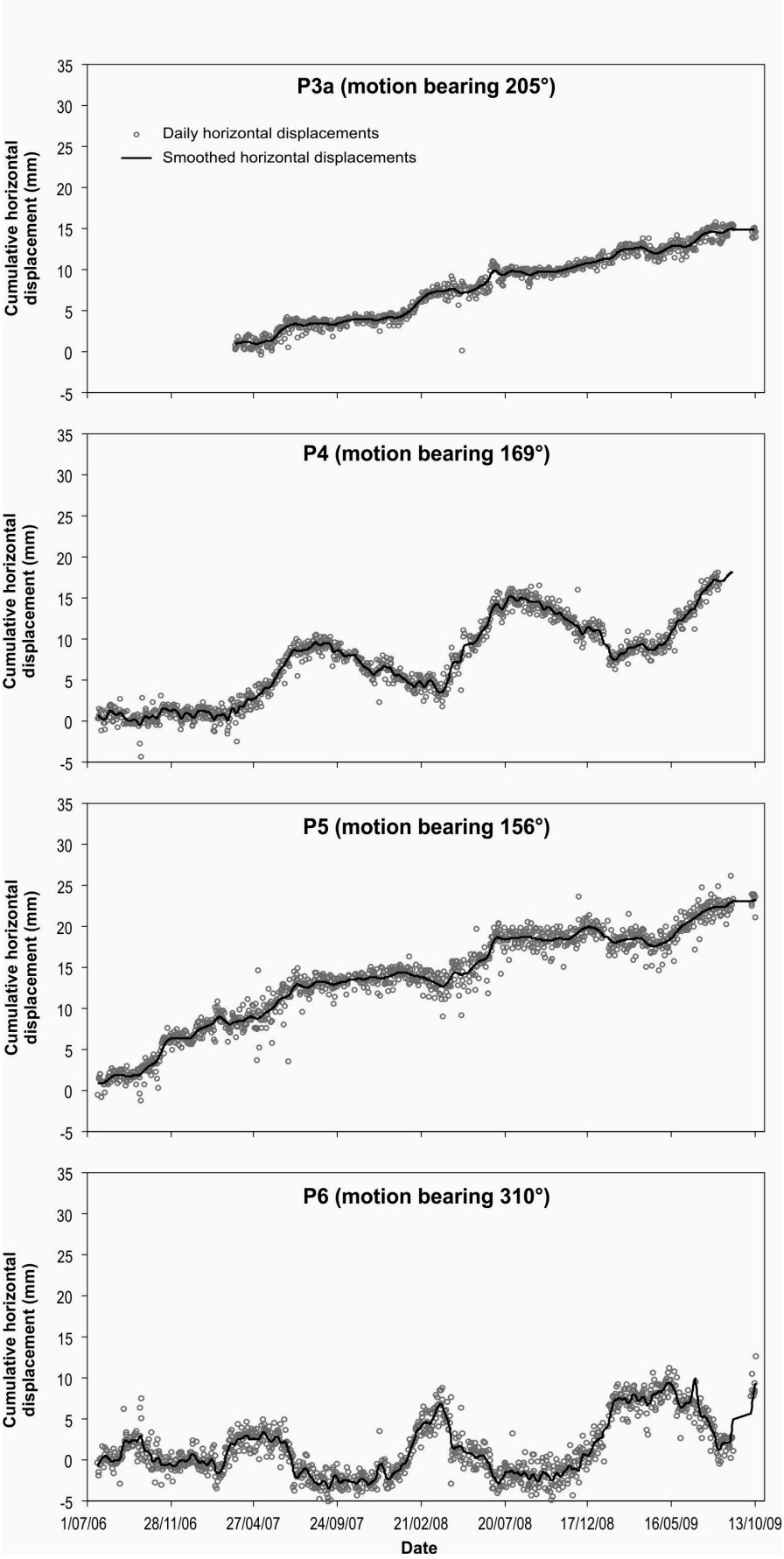

Figure 5.40a Cumulative horizontal displacements over time, calculated along their main movement bearings, for prisms on the active landslide. Daily and smoothed values are shown. Smoothed values are derived using a Gaussian smoothing kernel where G_s = 2 mm.

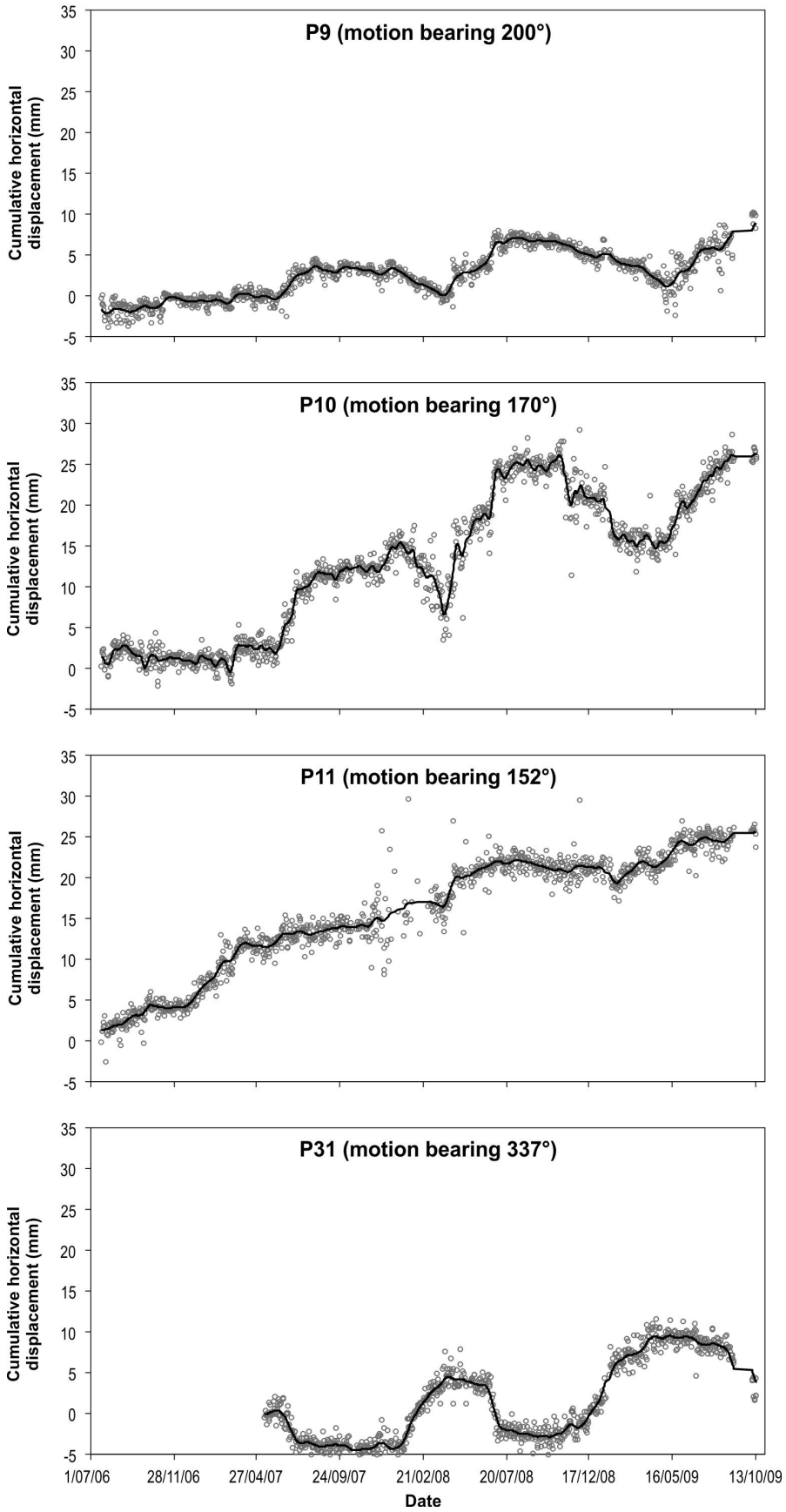

Figure 5.40b Cumulative horizontal displacements over time, calculated along their main movement bearings, for prisms on the active landslide. Daily and smoothed values are shown. Smoothed values are derived using a Gaussian smoothing kernel where G_s = 2 mm.

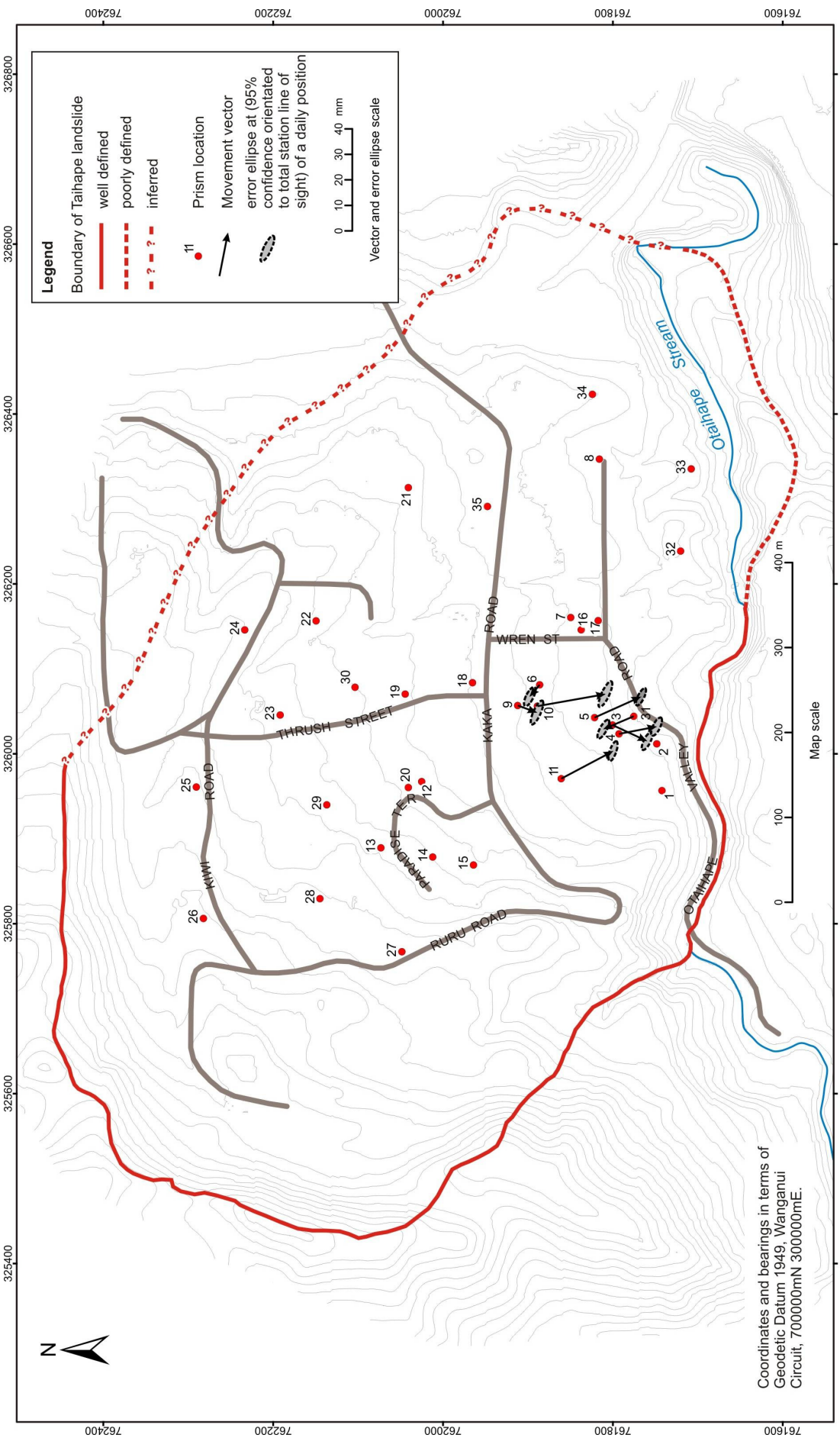

Figure 5.41 Map showing the magnitude and bearing of horizontal motions for prisms on the landslide, for those prisms where motion is greater then the 95% confidence limit.

Table 5.25 Summary of measured prism surface motion for the monitoring period, for those prisms where motion is greater then the 95% confidence limit.

Prism	Total horizontal motion in period and errors at 95%[1] (mm)	Mean cumulative horizontal motion and errors at 95%[1] (mm/year)	Motion bearing[1] (°)	Total height displacement and errors at 95%[1] (mm)
3a	14 ±(0.2)	6 ±(0.1)	205	-16 ±(1)
4	15 ±(0.6)	5 ±(0.2)	169	1 ±(1)
5	19 ±(0.4)	6 ±(0.1)	156	5 ±(1)
6	5 ±(0.8)	2 ±(0.3)	310	9 ±(1)
9	7 ±(0.5)	2 ±(0.2)	200	4 ±(1)
10	25 ±(1.0)	8 ±(0.3)	170	3 ±(1)
11	21 ±(0.6)	7 ±(0.2)	152	8 ±(1)
31	12 ±(1.0)	5 ±(0.4)	337	-7 ±(1)

[1]Calculated over the monitoring period from the least-squares method, errors at 95% confidence

5.3.2.2 Accelerated creep

The rationale used to help identify statistically significant accelerated creep from periods of rest or slow creep, is similar to that adopted for the Utiku data. It is assumed that motion is statistically significant if the cumulative horizontal displacements are larger than the standard deviation (at the 95% confidence limit), of any two daily cumulative displacements (Table 5.26).

To identify periods of accelerated creep which are outside survey error, the mean velocity of each station (mm/day along the main movement bearing), was calculated over a moving 60-day period. A 60-day period was used as this represents the approximate duration of each accelerated creep period, which is longer than the 14-day period adopted for the Utiku analyses. Statistically significant periods of accelerated creep are those where station velocities are greater than the standard deviation on the velocity at the 95% confidence limit, calculated from any two daily cumulative displacements over a 60-day period (Table 5.26). These periods are shown Figure 5.42.

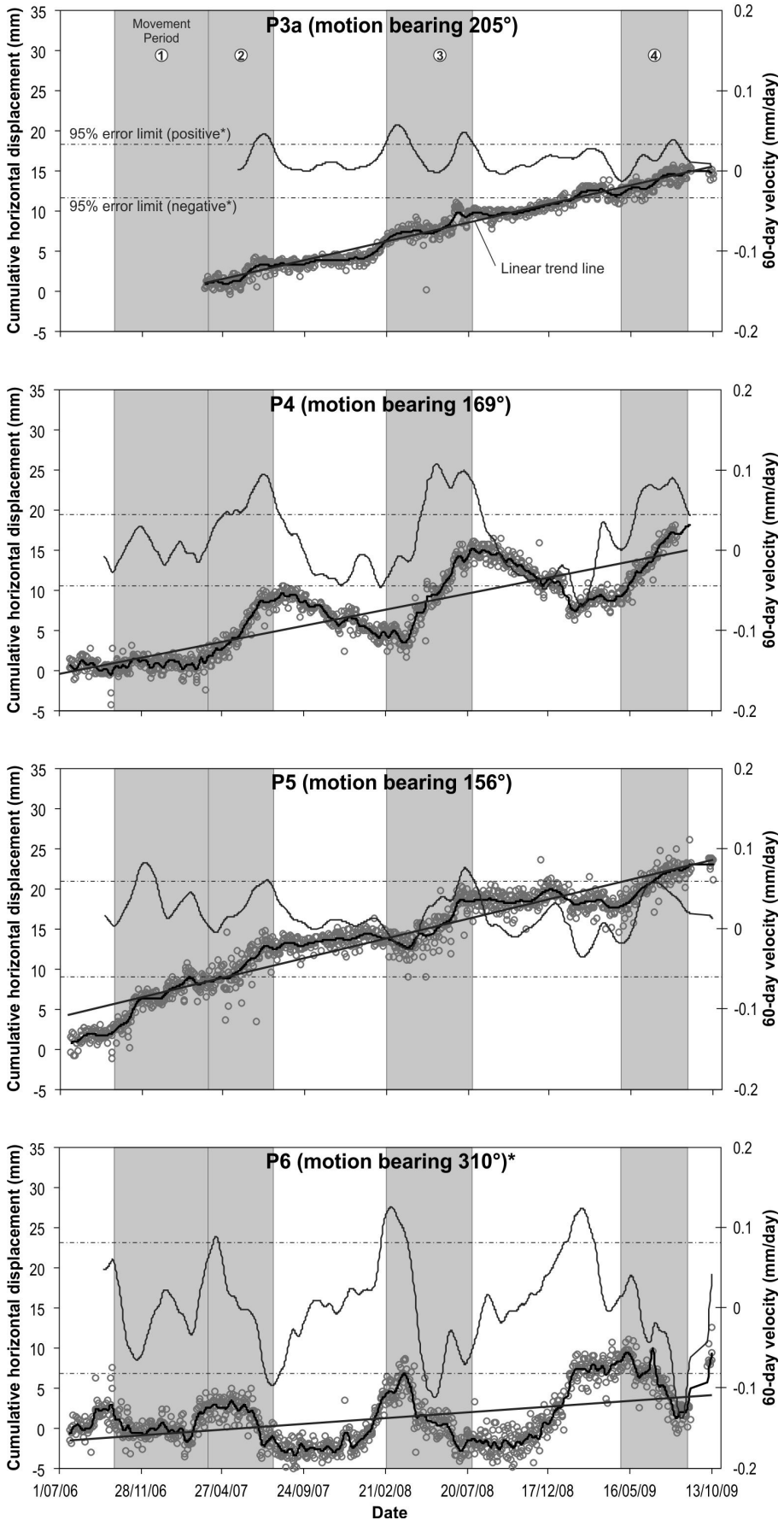

Figure 5.42a Daily and smoothed cumulative horizontal displacements of prisms on the active toe of the Taihape landslide. Prism velocity is calculated over a moving 60-day period with the 95% confidence limits shown. Smoothed displacements are calculated using a Gaussian smoothing kernel where G_s = 2 mm. Linear trends are fitted to the daily displacements.

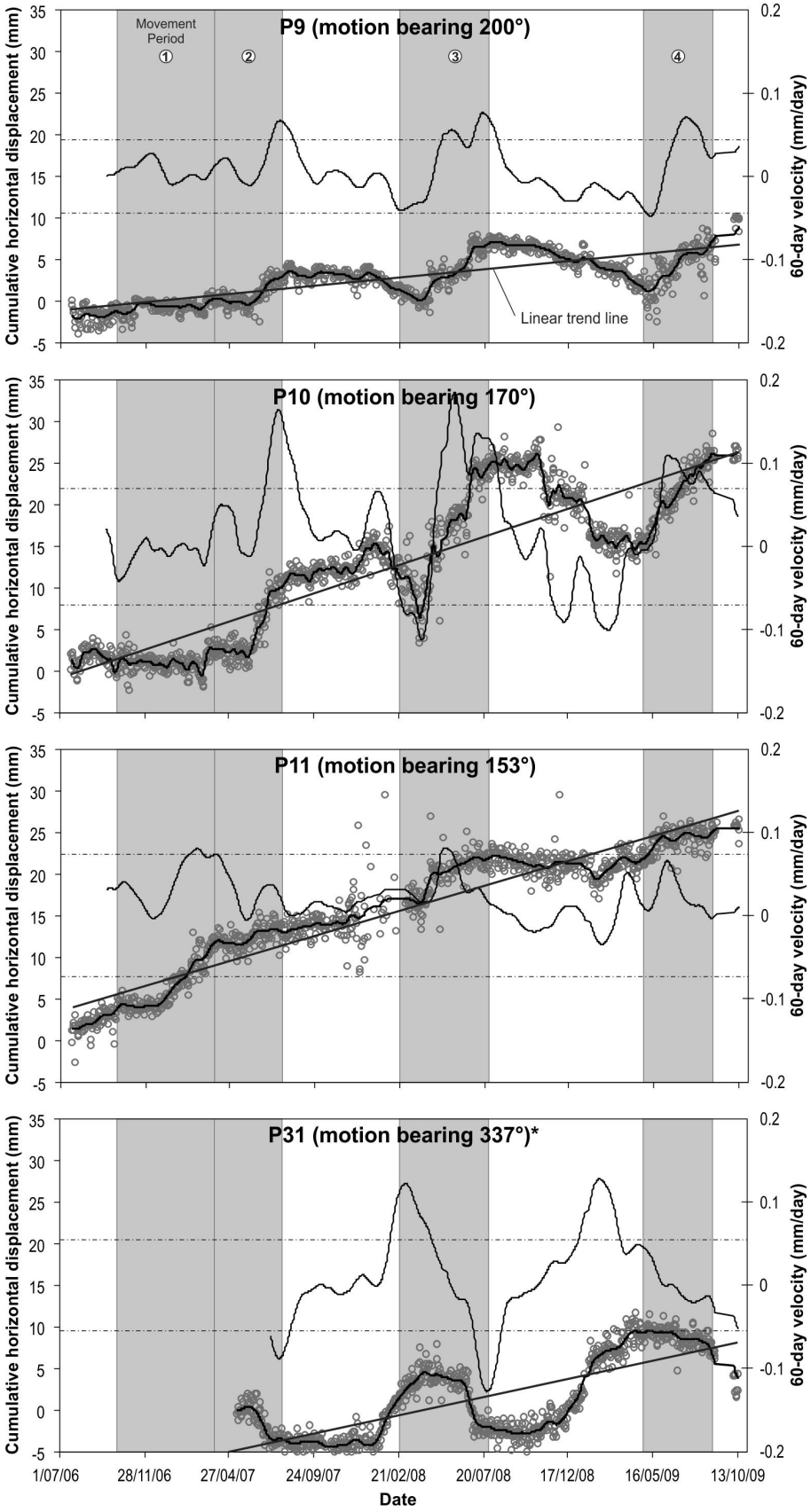

Figure 5.42b Daily and smoothed cumulative horizontal displacements of prisms on the active toe of the Taihape landslide. Prism velocity is calculated over a moving 60-day period with the 95% confidence limits shown. Smoothed displacements are calculated using a Gaussian smoothing kernel where G_s = 2 mm. Linear trends are fitted to the daily displacements.

Table 5.26 Cumulative horizontal displacement errors

Prism	Error of any two daily cumulative displacements[1]				Velocity[2] at the 95% confidence limit (mm/day)
	Standard deviation (mm)	90% confidence (mm)	95% confidence (mm)	99% confidence (mm)	
3a	0.8	1.8	2.0	2.5	0.03
4	1.1	2.4	2.7	3.4	0.05
5	1.5	3.1	3.6	4.4	0.06
6	2.0	4.3	4.9	6.0	0.08
9	1.1	2.3	2.6	3.3	0.04
10	1.7	3.6	4.1	5.1	0.07
11	1.8	3.9	4.4	5.5	0.07
31	1.3	2.9	3.3	4.1	0.05

[1] Calculated as the square root of two, times the standard deviation.
[2] Velocity (mm/day) is calculated at the 95% confidence limit calculated from any two daily cumulative displacements over a 60-day period.

Four main periods of statistically significant accelerated creep corresponding to downslope motion, were identified over the monitoring period. Periods 2, 3 and 4 were recorded by the majority of prisms on the landslide toe, while period 1 was recorded at prisms 5 and 11 only. Although four main periods of accelerated creep have been identified, the timing, duration and magnitude of the displacements between prisms, within these periods vary, therefore displacement of the prisms have been grouped temporally, with the groups approximating to periods when most prisms were moving.

Using the same methodology, statistically significant upslope accelerated creep motion has also been recorded. Prism displacements during these periods are similar in timing, duration and magnitude to the downslope displacements. These periods of upslope and downslope motion are also similar to those shown by the vertical time-series, in that they are cyclic, indicating a seasonality which approximates to the summer / winter cycles. This apparent seasonality has been investigated by using the time-series data for one of the back-sites (prism 1002), located on stable ground off the landslide (Figure 5.43). The same winter / summer seasonality can be observed in these plots, where the peak to trough differences represent fluctuations of about 2 mm in the east and north and about 5 mm in the vertical. However, the linear trends shown on these graphs indicate that over the monitoring period there has been no net change in the position of the prism.

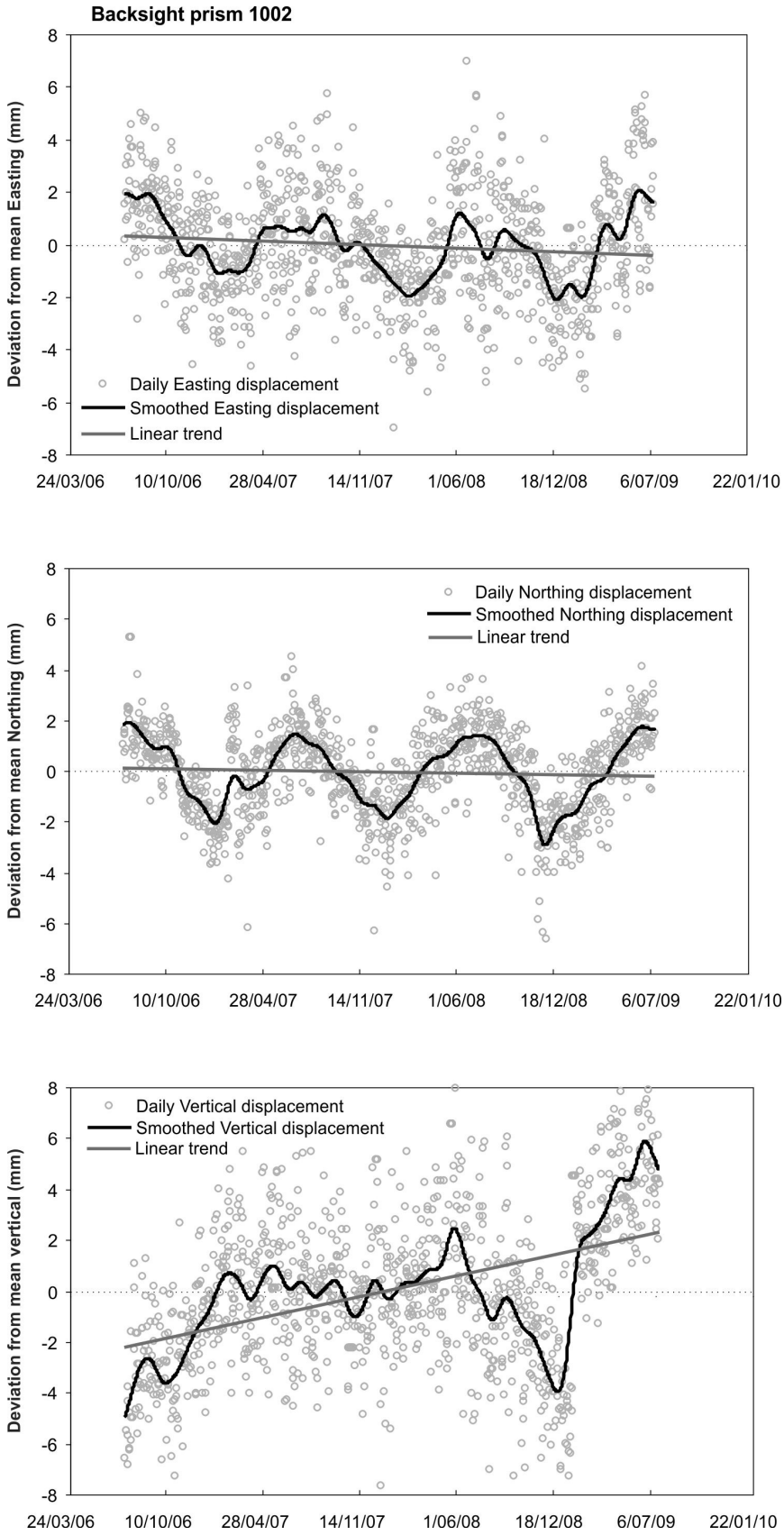

Figure 5.43 Time-series data for one of the back sites (prism 1002) located on stable ground off the landslide. Daily and smoothed values are shown. Smoothed values are derived using a Gaussian smoothing kernel where G_s = 2 mm. Linear trends are fitted to the daily displacements.

5.3.2.3 Seasonal accelerated- and slow-creep

The periods of up- and down-slope motion follow each other and repeat on about a yearly basis indicating seasonality, but with no net gain in down-slope displacement apparent. Those prisms in the active toe all display these similar cyclic trends, which are also present in the cumulative displacements of prisms outside the active area (Figure 5.44). In addition to the cyclic and relatively rapid motion, the prisms in the active toe also show a slow and steady down-slope motion trends (Figure 5.42), which are not present in the other prisms. This slow-creep motion appears to occur consistently through the monitoring period, with no change in rate apparent, but with the accelerated-creep motion superimposed on it.

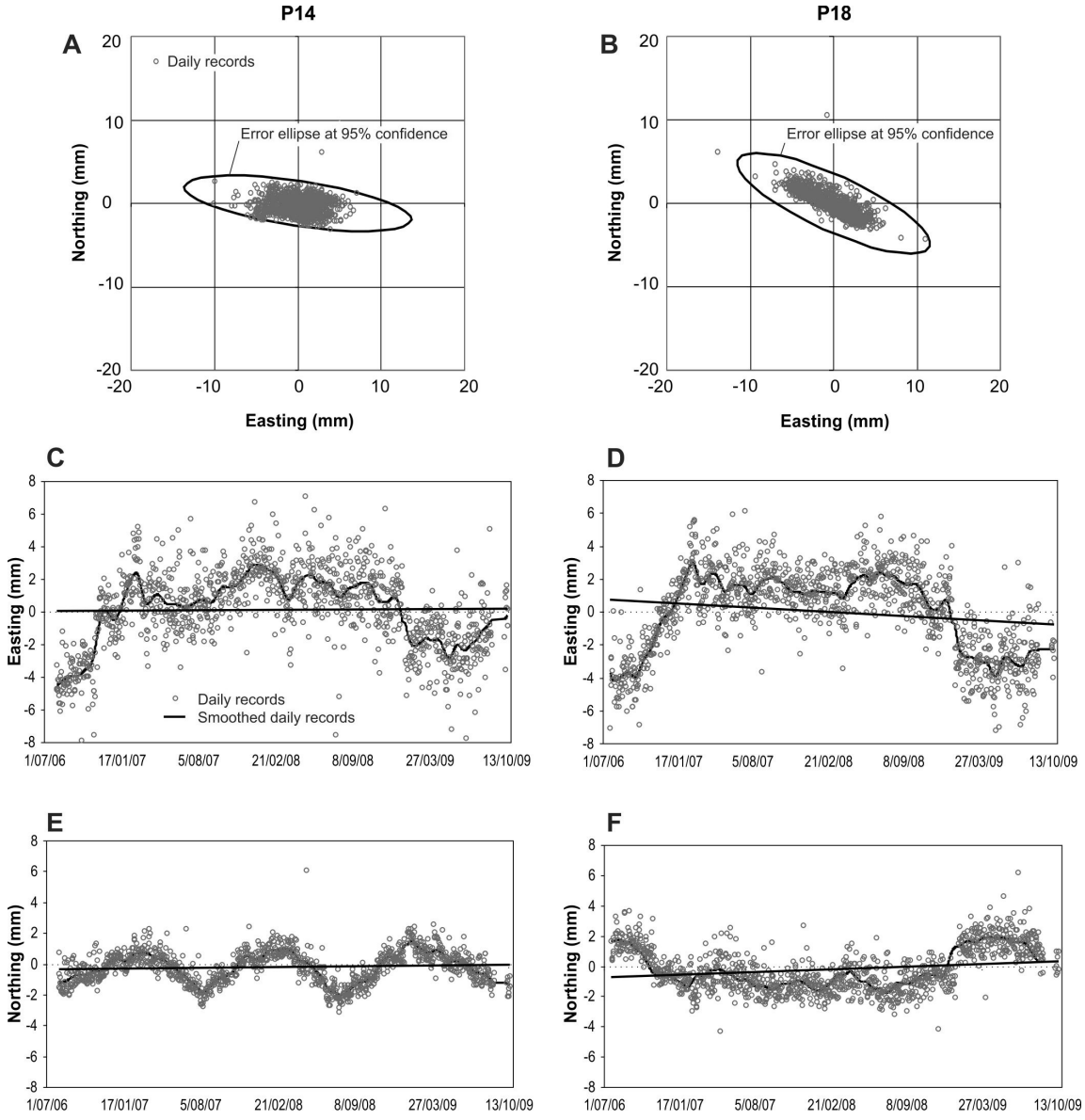

Figure 5.44 Time-series data for selected prisms outside the active landslide. A and B: Easting and northing scatter plots showing the daily positions of prisms P14 and P18. C, D, E and F: Cumulative Easting and Northing displacements of prisms 14 and 18. Daily and smoothed values are shown. Smoothed values are derived using a Gaussian smoothing kernel where G_s = 2 mm. Linear trends are based on the daily values.

To assess the patterns of the accelerated creep motion the cumulative horizontal displacements of the prisms in the active toe have been de-trended by subtracting the slow-creep motion gradients from the time series. These de-trended plots of prisms 4, 5 10 and 11 (Figure 5.45), show that the up- and down-slope motion is indeed cyclic and represents displacements of between ± 1.5 – 7.8 mm (with a mean of ± 4.4 mm) per cycle, which are about six-months long, and represent mean seasonal (yearly) variations of about 9 mm (Table 5.27). At prism 4 the annual cyclic motion has a magnitude of about 10 mm in the horizontal and the movement rate is about ±20 mm/yr, superimposed on a steady movement rate of about 5 mm/yr.

Table 5.27. Seasonal accelerated- and slow-creep motion for those prisms in the active toe of the Taihape landslide over the monitoring period.

Prism	Slow creep motion gradient (mm/day)[1]	Slow creep motion and errors at 95% (mm/year)[2]	Accelerated creep mean variation per cycle (about every 6-months) (mm)
3a	0.016	6 ±(0.1)	± 1.5
4	0.013	5 ±(0.2)	± 4.8
5	0.016	6 ±(0.1)	± 3.2
6	0.005	2 ±(0.3)	± 5.1
9	0.007	2 ±(0.2)	± 3.9
10	0.023	8 ±(0.3)	± 7.8
11	0.020	7 ±(0.2)	± 3.5
31	0.014	5 ±(0.4)	± 5.2

[1]Calculated from a least squares adjustment assuming a linear relationship
[2]Errors calculated using the least squares method at 95% confidence

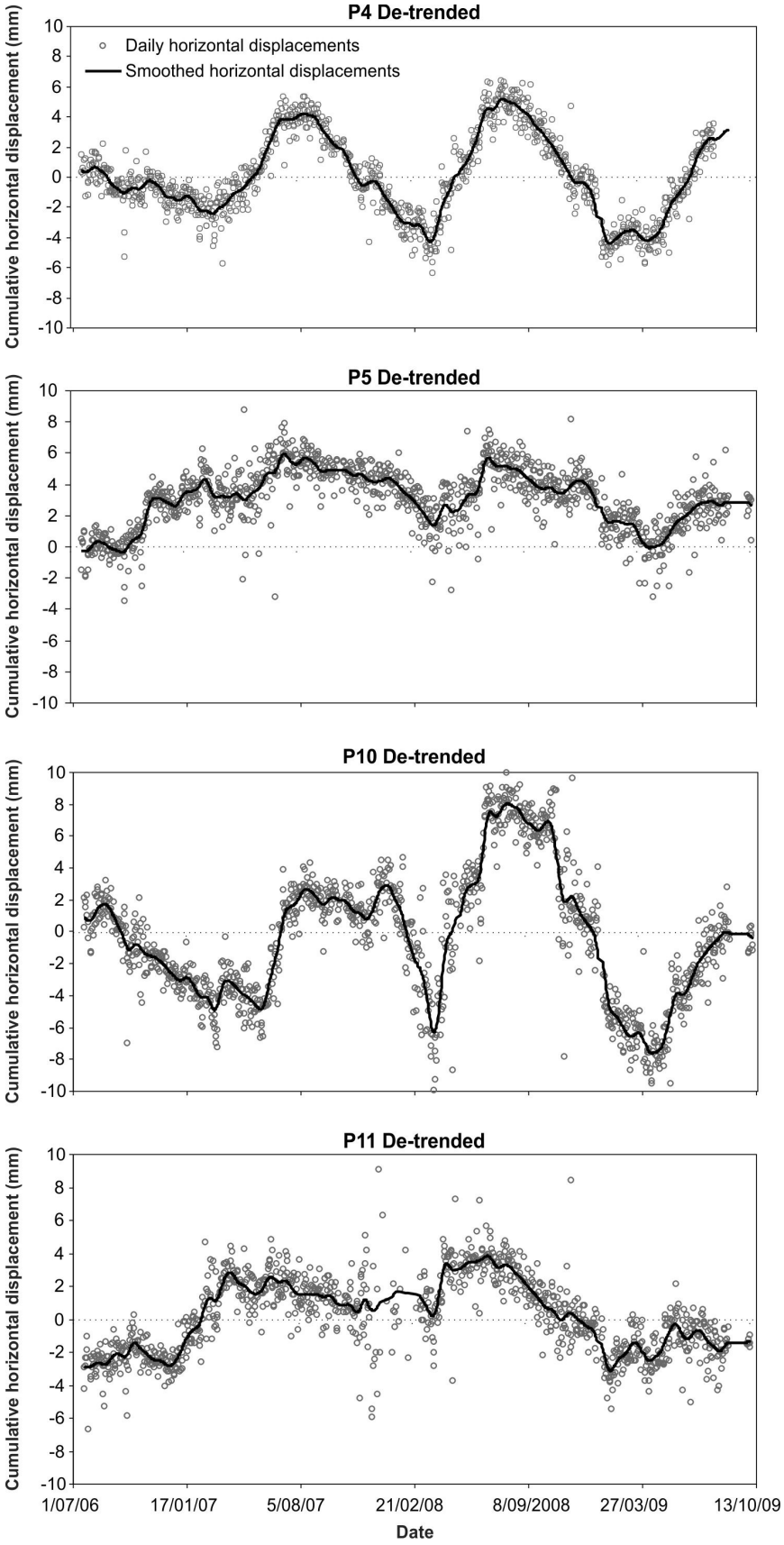

Figure 5.45 De-trended cumulative horizontal displacements of prisms 4, 5 10 and 11. De-trended by subtracting the slow-creep motion gradients from the time series. Daily and smoothed values are shown. Smoothed values are derived using a Gaussian smoothing kernel where G_s = 2 mm.

The four statistically significant periods of positive (down-slope) accelerated creep have been investigated further and are shown in Figures 5.46, 5.47, 5.48 and 5.49, for prisms 4, 5, 10 and 11, and are representative of the patterns shown by the other prisms in the active toe area. Prisms 4 and 5 are on the lower toe and prisms 10 and 11 are on the upper toe. The motions patterns of the prisms during the main accelerated creep movement periods fall into three main modes, these are: 1) static – no motion over the period of concern; 2) regular – mainly continuous motion over the period of concern; and 3) Irregular – discontinuous motion over the period of concern. Examples of these three different movement modes are shown on Figure 5.50. Regular motions are typically characterised by a constant motion gradient, while irregular motions comprise one or more small magnitude, short duration movement events.

Simple linear models have been used to calculate displacements and rates of displacement for the prisms, within each period of positive accelerated creep (Figure 5.51). Although linear models have been assumed, in reality the start and end of each motion event would involve a period of acceleration and deceleration, however, the resolution of the data does not allow these to be resolved. For both regular and irregular motion types peak velocities are achieved in less than one-day (bearing in mind the temporal resolution of the data is daily), indicating rapid acceleration to peak velocity, with the end of each motion period corresponding to an equally rapid deceleration to rest, or to slower, more regular movement rates. Each period of irregular motion on average lasts about 20 days, while regular motion events have a mean duration of about 80 days.

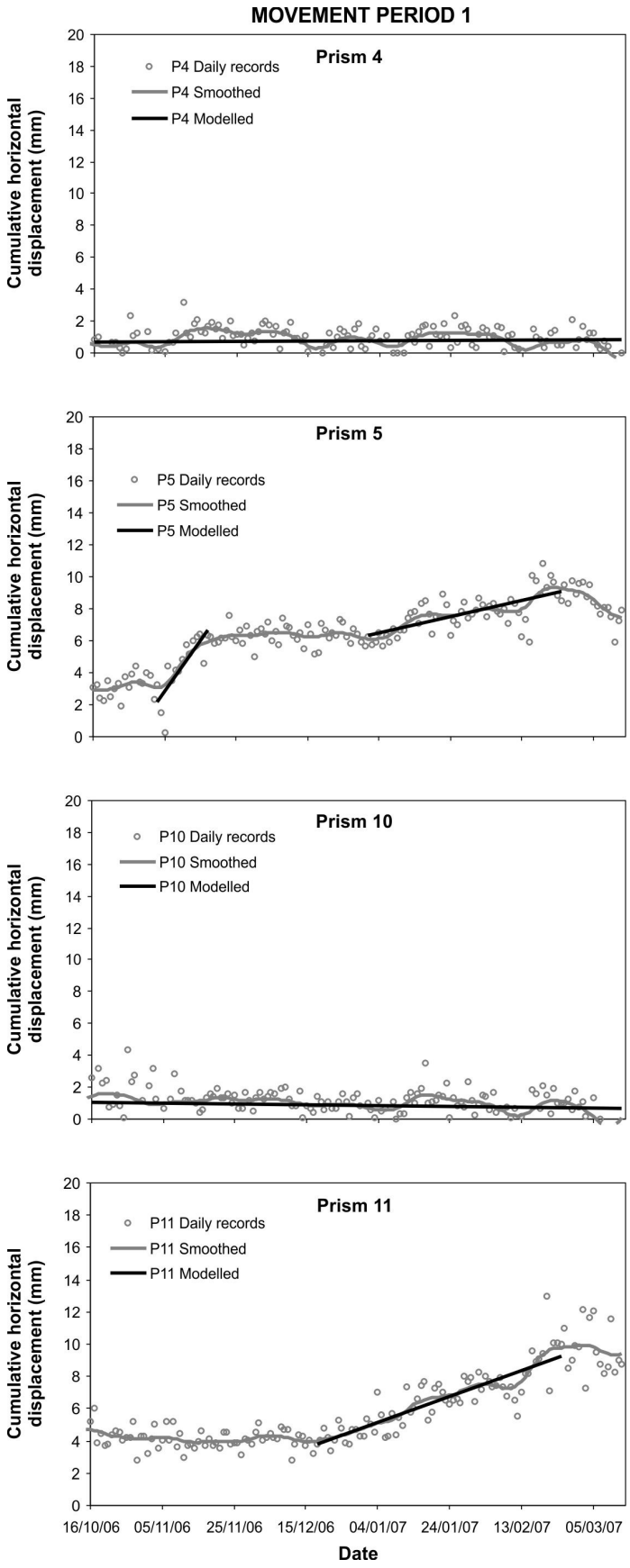

Figure 5.46 Cumulative horizontal displacements for accelerated creep period 1. Daily and smoothed values for prisms 4, 5, 10 and 11 are shown. Smoothed values are derived using a Gaussian smoothing kernel where G_s = 2 mm, and the linear trend is fitted to selected daily values.

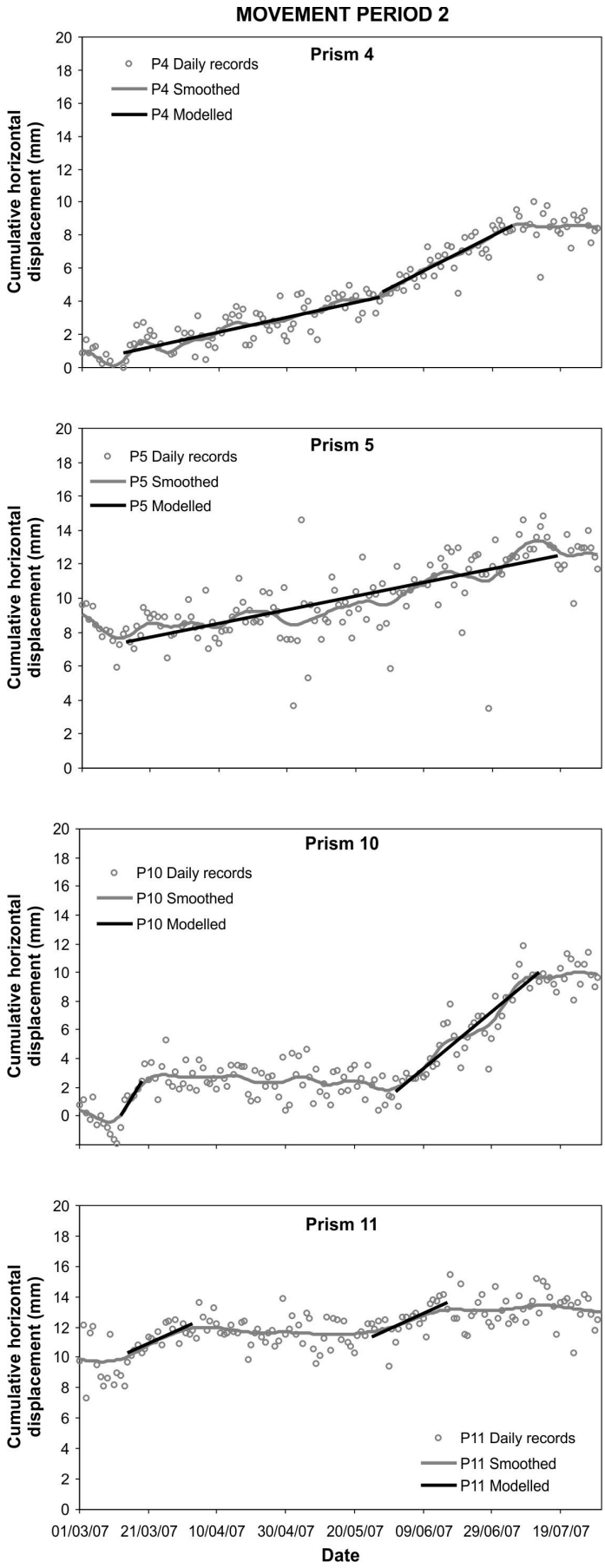

Figure 5.47 Cumulative horizontal displacements for accelerated creep period 2. Daily and smoothed values for prisms 4, 5, 10 and 11 are shown. Smoothed values are derived using a Gaussian smoothing kernel where G_s = 2 mm, and the linear trend is fitted to selected daily values.

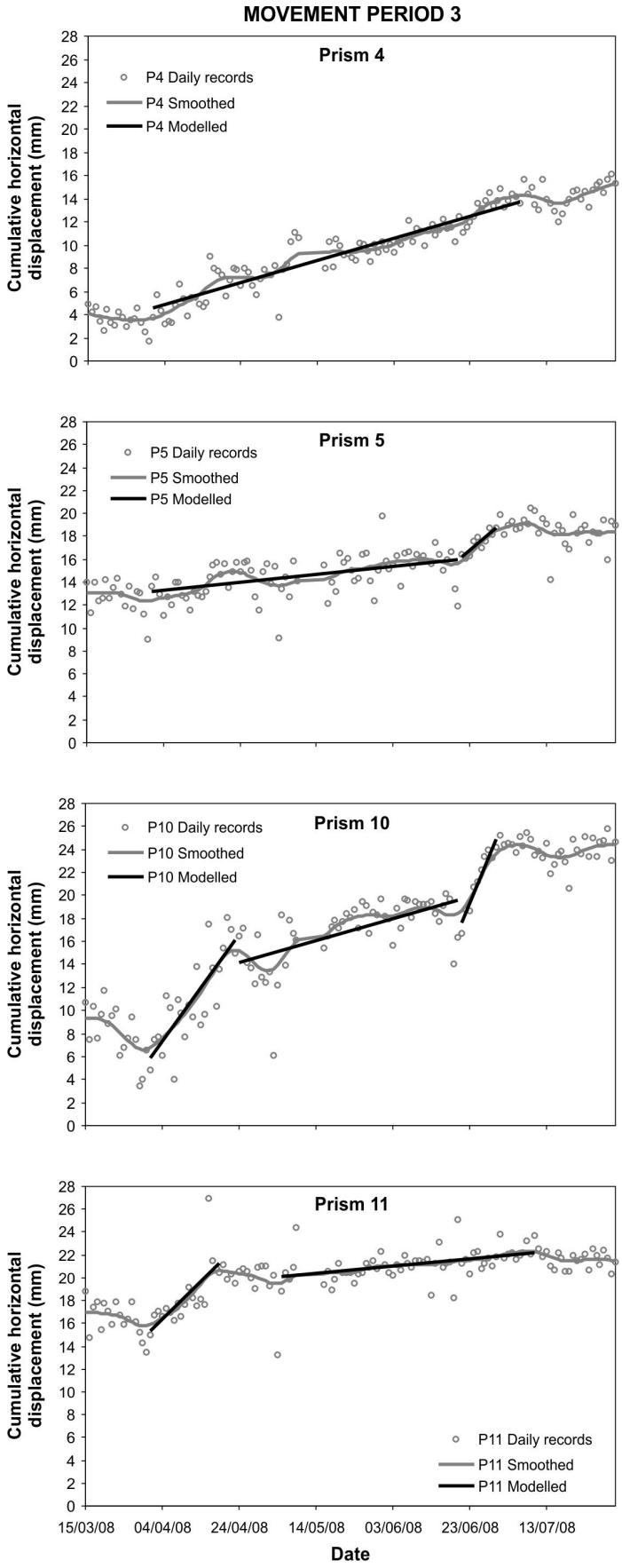

Figure 5.48 Cumulative horizontal displacements for accelerated creep period 3. Daily and smoothed values for prisms 4, 5, 10 and 11 are shown. Smoothed values are derived using a Gaussian smoothing kernel where G_s = 2 mm, and the linear trend is fitted to selected daily values.

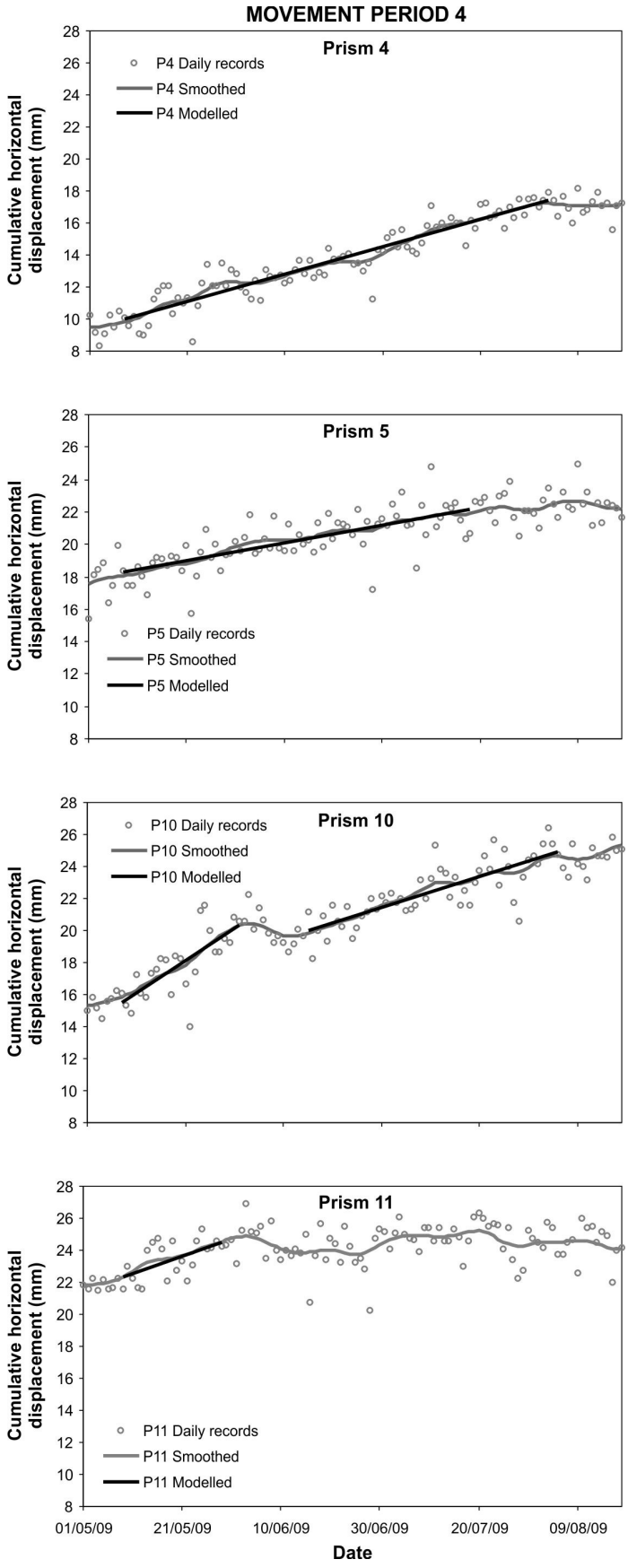

Figure 5.49 Cumulative horizontal displacements for accelerated creep period 4. Daily and smoothed values for prisms 4, 5, 10 and 11 are shown. Smoothed values are derived using a Gaussian smoothing kernel where G_s = 2 mm, and the linear trend is fitted to selected daily values.

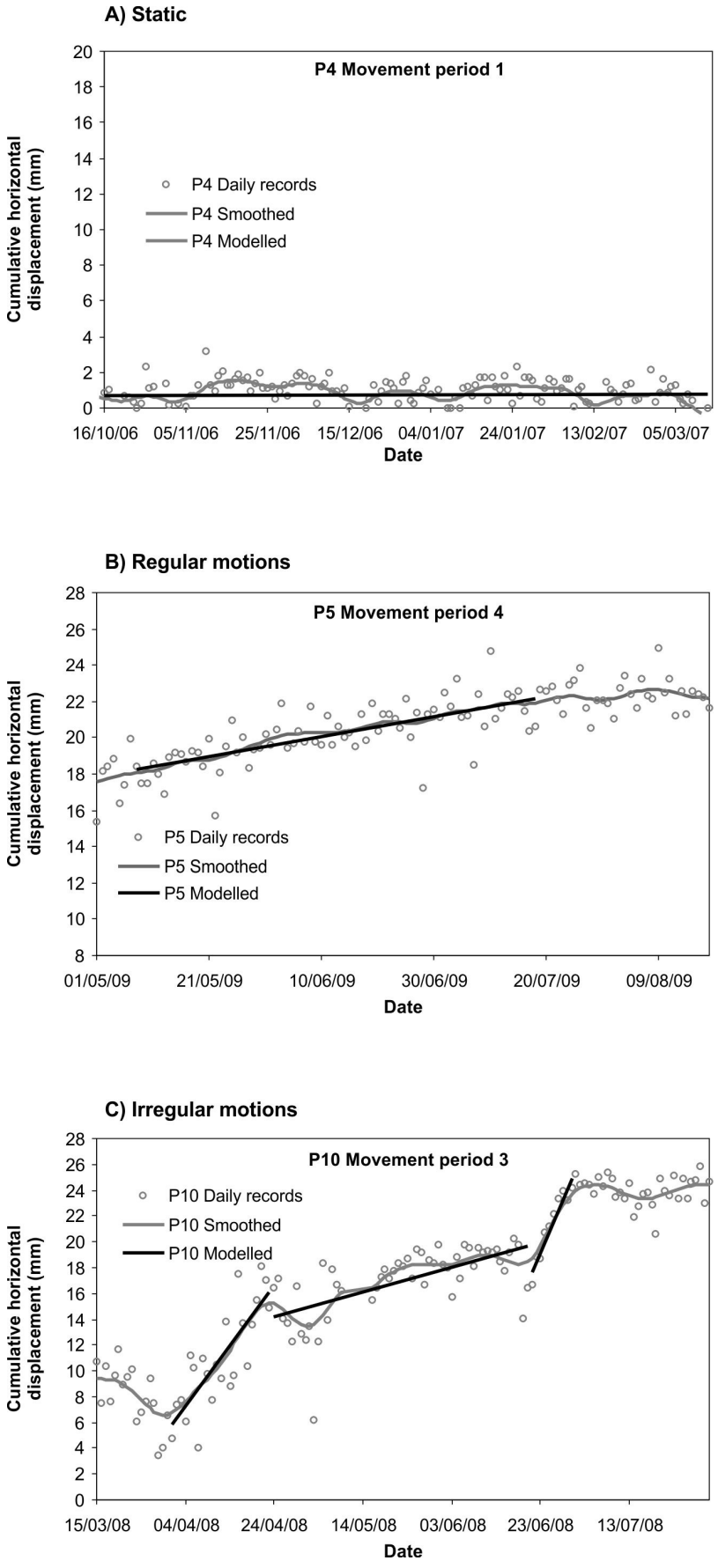

Figure 5.50 Examples of static, regular and irregular accelerated creep displacements shown by prisms 4, 5 and 10. Daily and smoothed values are shown. Smoothed values are derived using a Gaussian smoothing kernel where G_s = 2 mm, and the linear trend is fitted to selected daily values.

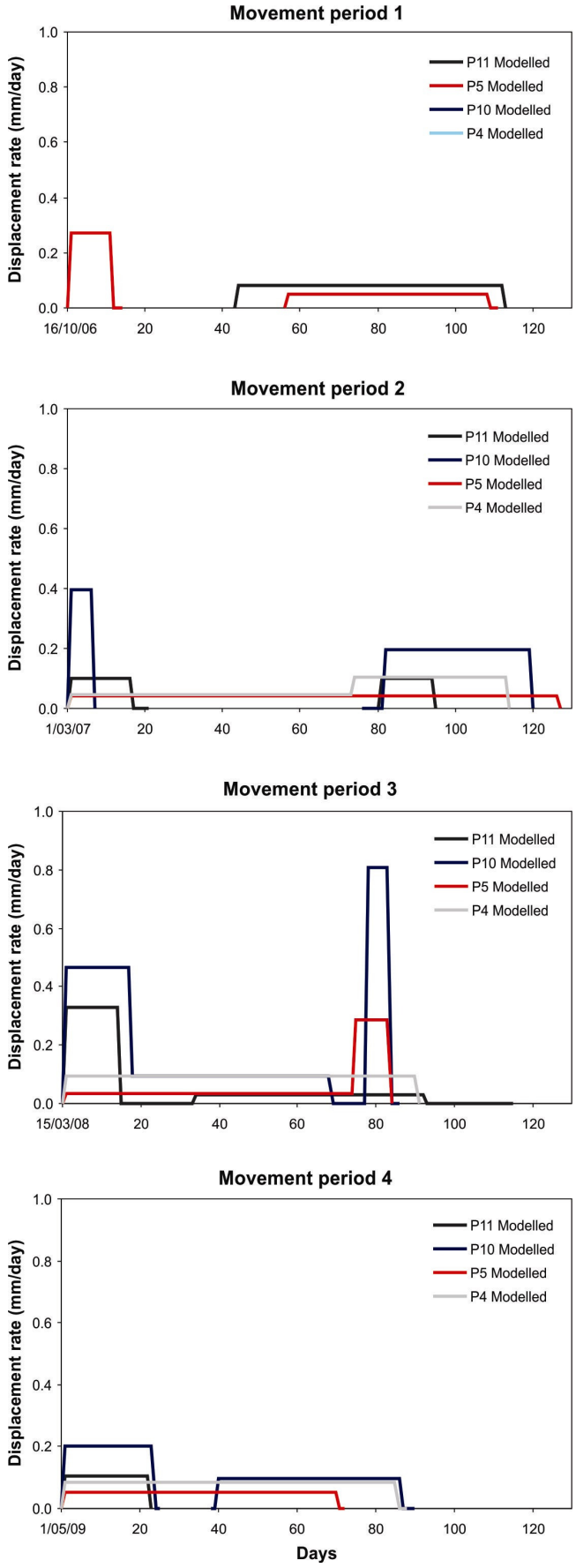

Figure 5.51 Displacement rates calculated for the four periods of accelerated creep. Rates are calculated by using simple linear models fitted to the daily cumulative displacements from prisms 4, 5, 10 and 11.

The duration and magnitude of each motion event during the four main periods have been plotted together, but partitioned into 'regular' and 'irregular' motion types. Both motion types do not show any statistically significant trends. Figure 5.52, shows that the rate of prisms 4 and 5 on the lower landslide toe are typically of the regular type (long-duration, small magnitude events), while prisms 10 and 11 on the upper landslide toe, are typically of the irregular type (short duration, small magnitude events). For accelerated creep periods 2, 3 and 4, motions of the lower toe and the upper toe prisms begin at the same time, however, the timing and duration of the motions, once triggered, can differ. Accelerated creep period 1 differs from the others, as motion starts in the lower toe, with the upper toe following about 30 days later. This movement period is not typical, as the other prisms do not show any motion. It therefore appears that these motions vary locally between the prisms. The complex motion patterns coupled with the seasonality would suggest that the recorded accelerated creep motions are unrelated to landsliding, but rather to other environmental factors, which require further investigation.

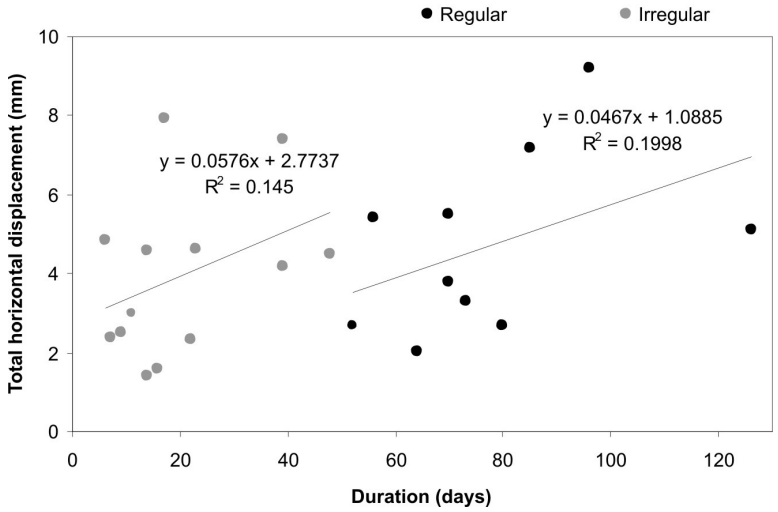

Figure 5.52 Duration and magnitude of all regular and irregular accelerated creep events.

5.3.2.4 Vertical creep

Two types of vertical creep motion have been identified: cyclic motion, where no net change occurs; and non-cyclic motion causing a net vertical change. Only two prisms (3a and 31), located on the lower toe, show any consistent lowering of the landslide surface, indicating a net-vertical change. All other prisms in the active toe show only cyclic motions, which is also true of those prisms outside the active toe (Figure 5.53). Although the prisms show a general up slope trend, this is not related to permanent upward motion of the landslide surface, but is rather caused by the extra winter cycle in the time series. The significance of the seasonal trends has been assessed for prisms 4, 5, 10 and 11 by de-trending the time series (Figure 5.54). This has been done by

subtracting the gradient of the time series, based on a linear trend of the daily records. For those in the active toe, the cyclic motions represent mean variations of about ± 5 mm, per cycle, which occur about every six months, and seasonal (yearly) variations of about 10 mm. For those outside the active toe (prisms 14 and 18), the mean variations are about ± 5 mm per cycle and are similar to the magnitudes of those in the active toe area. The back site prisms also show these seasonal cycles, but with smaller variations of about ± 2 mm per cycle, and are about 50% lower than those recorded on the landslide. These results suggest that the seasonal motions occur throughout the landslide, and to a lesser extent in the area outside the landslide.

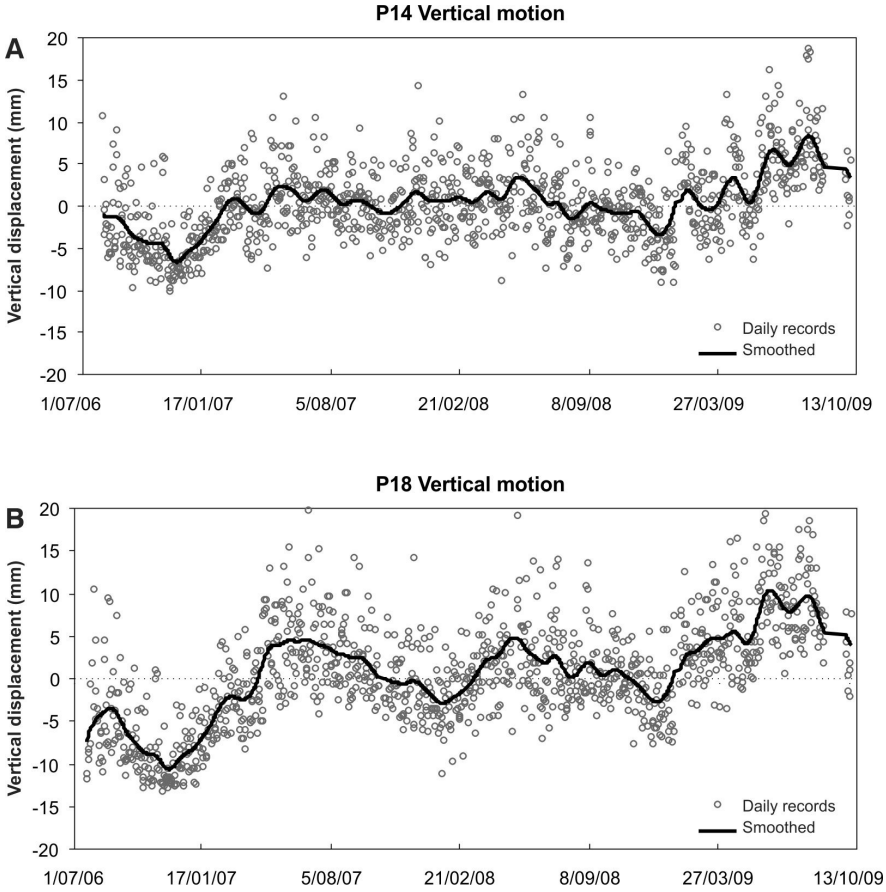

Figure 5.53 Seasonal vertical displacements of prisms 14 and 18, which are located on the landslide, but outside the active toe area. A: Prism 14. B: Prism 18. Daily and smoothed values are shown, with the smoothed values derived using a Gaussian smoothing kernel where G_s = 2 mm.

Table 5.28. Summary of vertical and horizontal motion during the monitoring period, for those prisms on the landslide toe.

Prism	Total slow creep motion over period and errors at 95%[1] (mm)	Total vertical motion over period and errors at 95%[1] (mm)	Long-sectional angle of translation (°)
31	13 ± (2)	- 7 ±(1)	28
3a	15 ±(1)	-16 ±(1)	47
4	15 ±(2)	No net change	Do not significantly differ from the angle of the slide surface
10	27 ±(3)	No net change	
11	23 ±(3)	No net change	

[1]Calculated over the monitoring period from the least-squares method, errors at 95% confidence

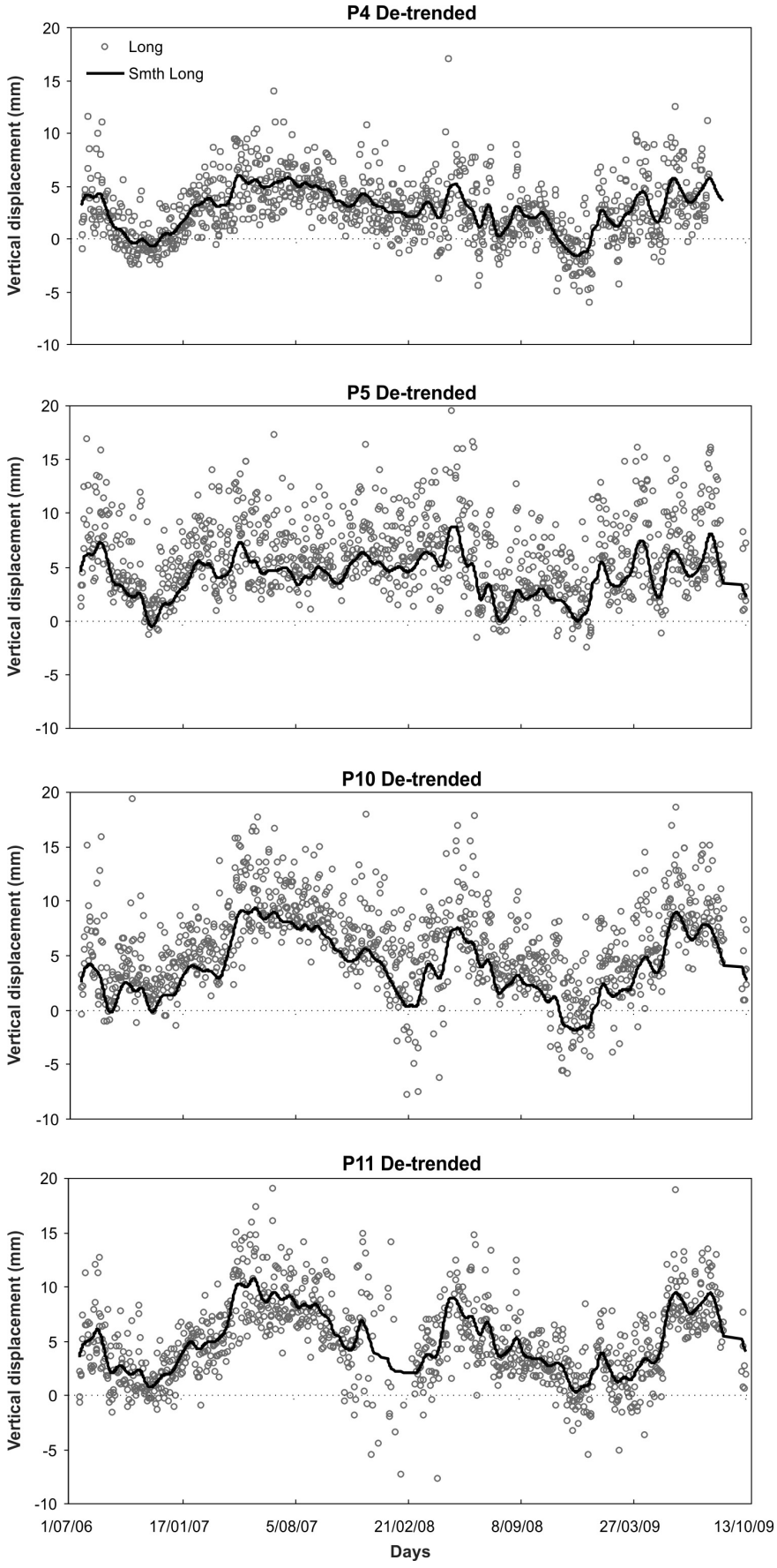

Figure 5.54 The cumulative vertical displacements of prisms 4, 5 10 and 11, which have been de-trended by removing the linear motion gradients. Daily and smoothed values are shown, with the smoothed values derived using a Gaussian smoothing kernel where G_s = 2 mm.

A longitudinal section through the landslide annotated with the slow- and vertical-creep motion vectors derived from the prisms closest to the section line is shown in Figure 5.55 and the details are summarised in Table 5.28. These data show that the angles of translation significantly differ from the angle of the slide surface, which is assumed to be about 7°. Figure 5.56 shows that vertical- and horizontal motion recorded by Prism 3a occurs at mostly discrete times, and follows a step-wise pattern where the periods of predominantly horizontal motion are followed by periods of horizontal and vertical motion. The periods of predominantly horizontal motion relate to the identified accelerated creep periods 2, 3 and 4, indicating that accelerated creep motion is predominantly horizontal. Slow- and vertical-creep motion, however occurs together but is interrupted by the accelerated creep motion events.

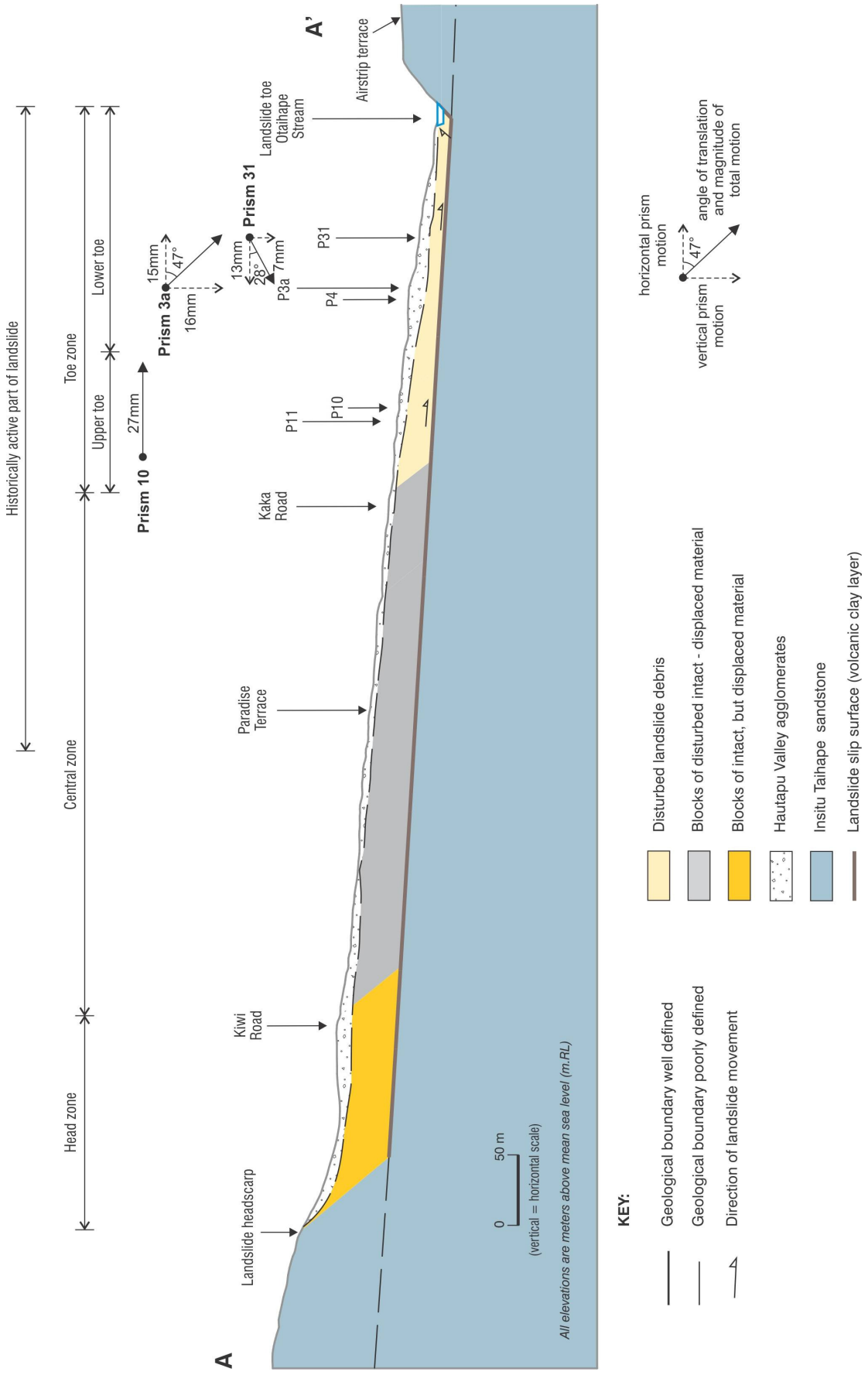

Figure 5.55 Longitudinal section through the landslide, which is annotated with the total vertical and horizontal displacements recorded at each prism along the section line, during the monitoring period. Section line A-A', Figure 3.16.

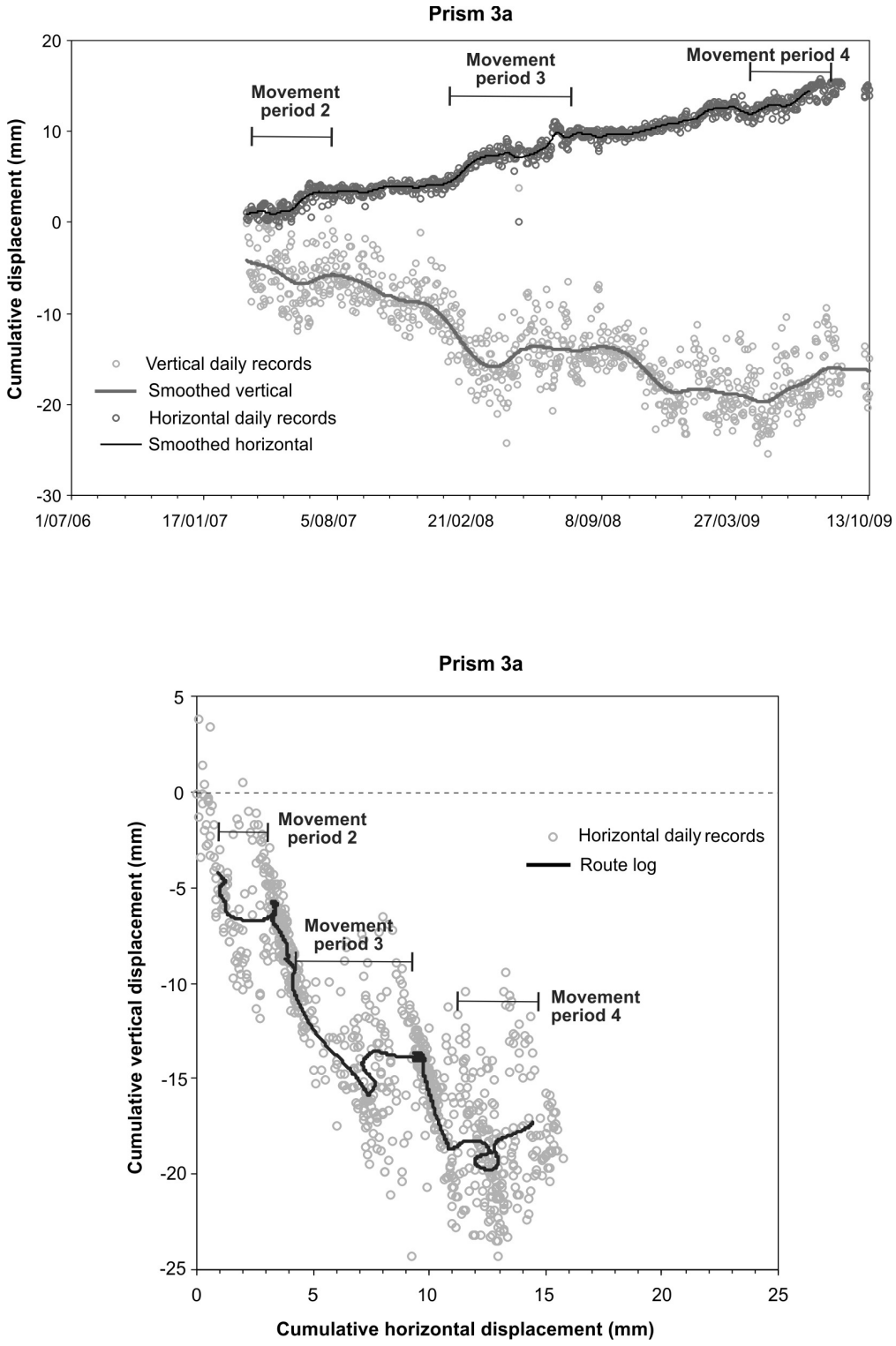

Figure 5.56 Cumulative horizontal and vertical displacements for prism 3a. A: Cumulative horizontal and vertical time-series data annotated with the main accelerated creep movement periods. Daily and smoothed values are shown, with the smoothed values derived using a Gaussian smoothing kernel where G_s = 2 mm horizontal, and 5 mm vertical. B: Corresponding daily cumulative horizontal and vertical displacements, daily values are smoothed using a Gaussian smoothing kernel where G_s = 10 mm.

The horizontal and vertical motion patterns of prism 31 have also been plotted (Figure 5.57), because they show a complex pattern containing several cycles of vertical and horizontal motion. The time series has been annotated with a route log, which

represents a projection, in the vertical plane, of the displacement vector over time. The route starts with horizontal motion in the downslope direction, accompanied by vertical positive (upward) motion, these are followed by predominantly vertical negative (downward) motion, which in turn is followed by upslope horizontal motion and then by vertical positive motion. The same cycles then repeat several times. However, the general trend of prism 31 indicates slow and steady rotation (back-tilting) and thinning of the landslide mass. The rotation can be seen in the mature gum trees planted around prism 31, which are also back tilting. The prism is located immediately downslope of a prominent landslide scarp, and may reflect motion along this scarp.

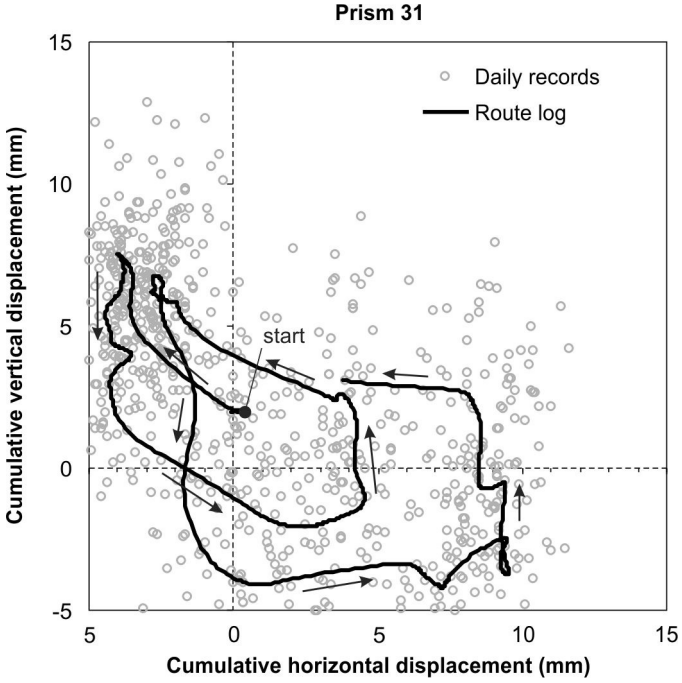

Figure 5.57 Cumulative horizontal and vertical displacements for prism 31. Corresponding daily cumulative horizontal and vertical displacements are shown. The route log is derived using a Gaussian smoothing kernel where G_s = 10 mm, the arrows indicate the chronological order of the data.

5.3.3 Subsurface motions

Subsurface displacements and their depth relative to the ground surface have been derived from five borehole inclinometers (BH1 to BH5). Over the monitoring period, only the inclinometers in BH1 and BH2, located in the toe of the landslide have shown shear displacements at depth (Table 5.29 and Figure 5.58). The inclinometer in BH3 has shown minor displacement at depth, however, the magnitude of this displacement is small. These results indicate the presence of one slip surface, at depths corresponding to those surfaces identified in the drillhole logs. All other inclinometers show no movement consistent with landslide displacement. These results are consistent with those shown by the prisms, where no surface motions, outside of the toe area, have been recorded.

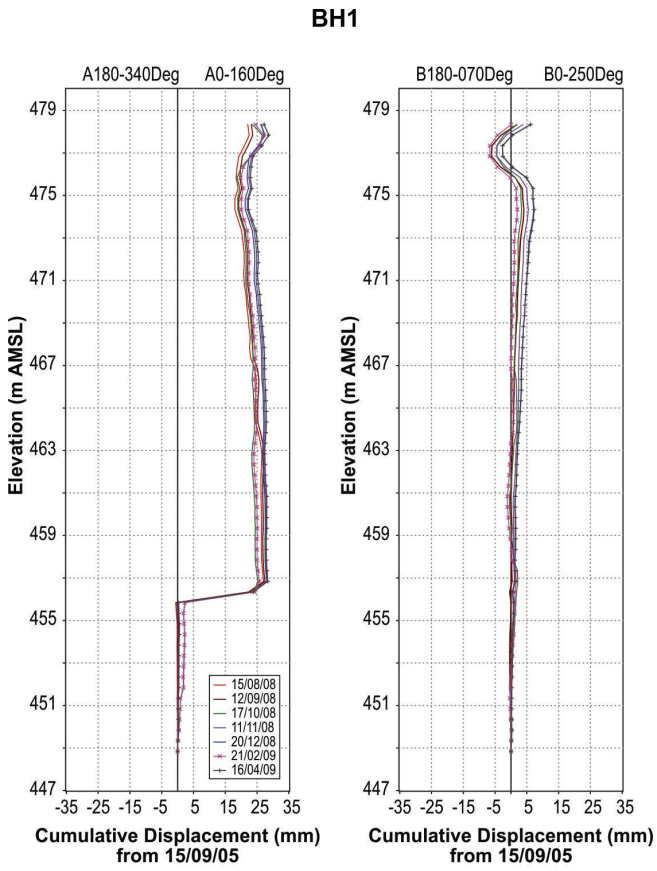

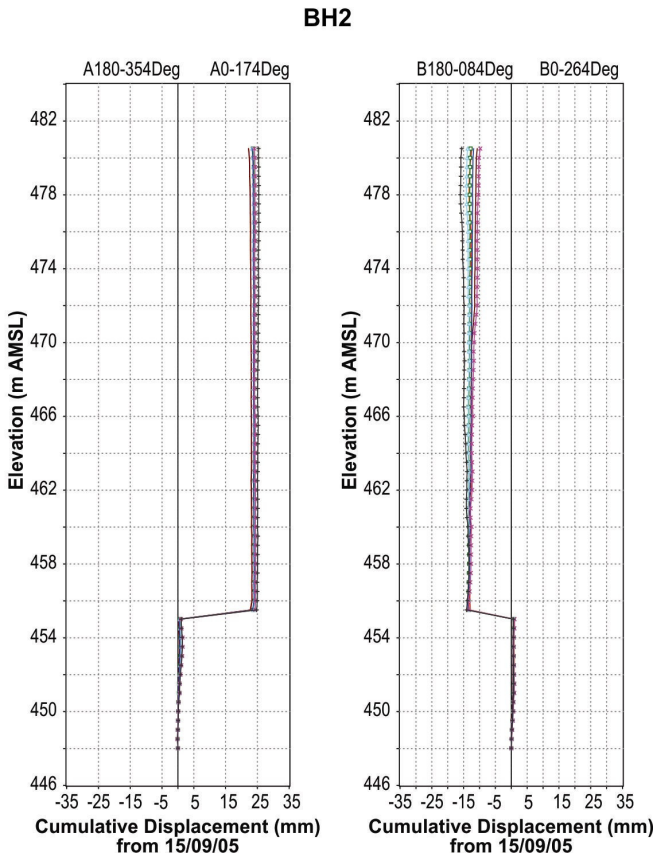

Figure 5.58a Cumulative inclinometer displacement records from inclinometers installed in BH1 and BH2, from 15/09/2005 to 16/04/2009.

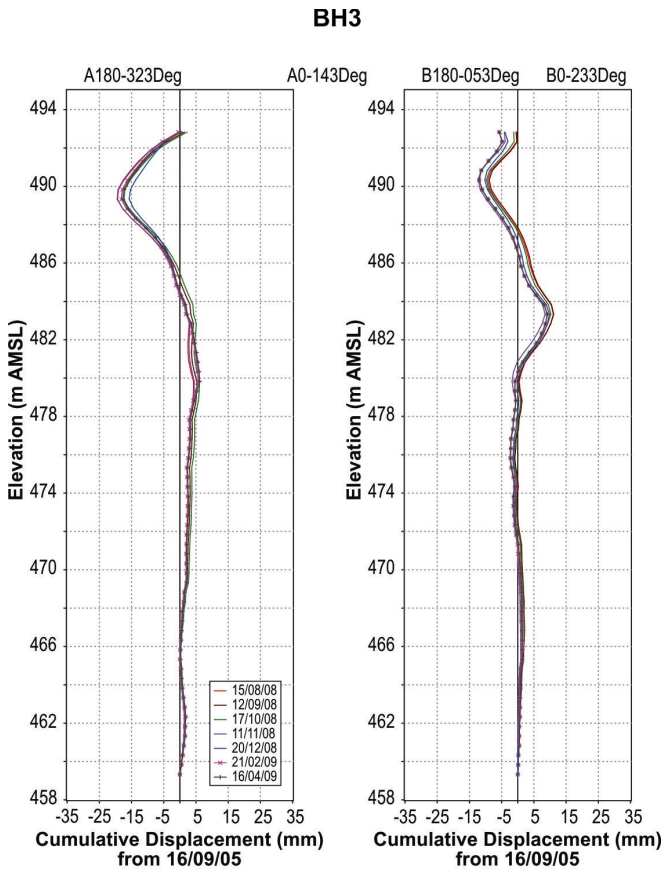

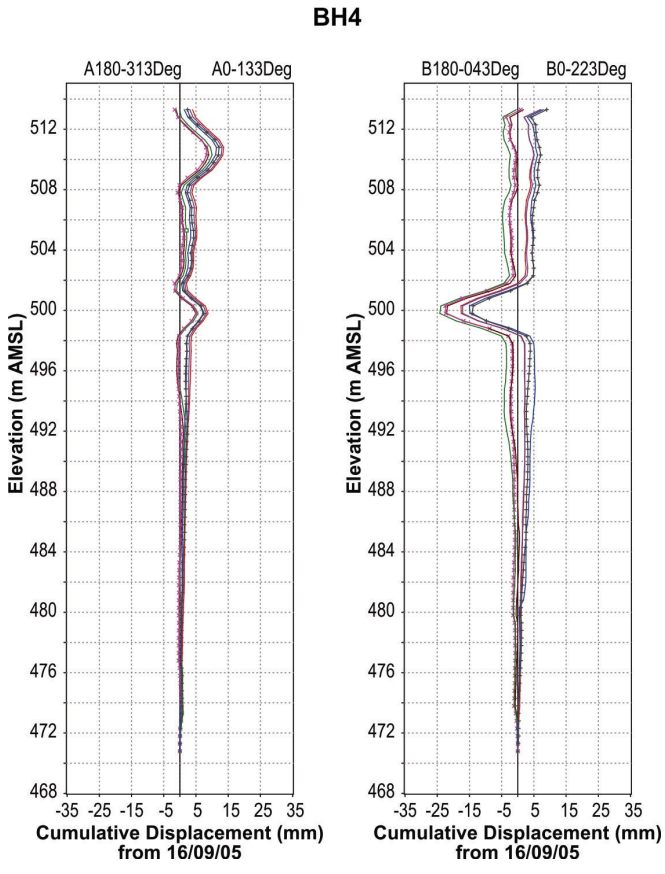

Figure 5.58b Cumulative inclinometer displacement records from inclinometers installed in BH3 and BH4, from 16/09/2005 to 16/04/2009.

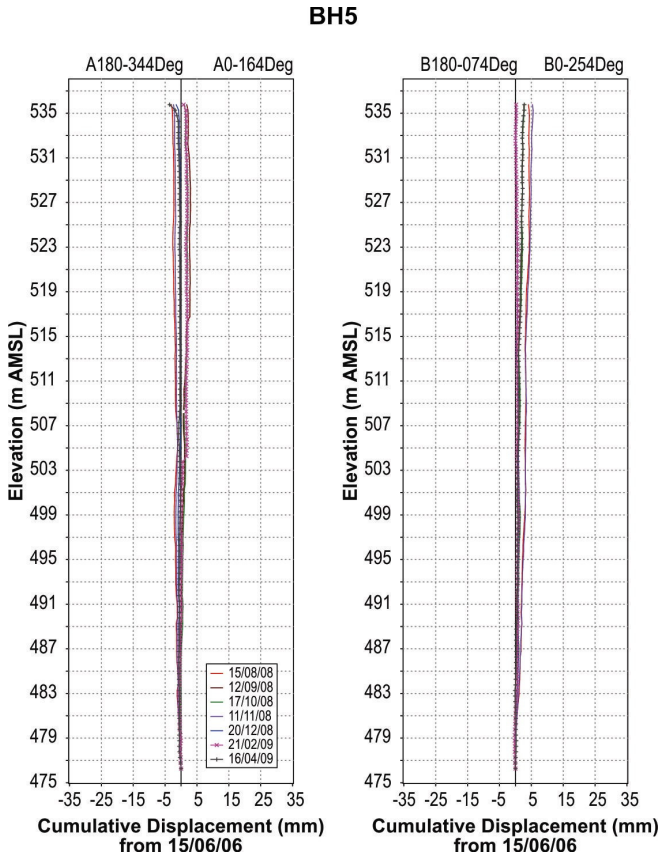

Figure 5.58c Cumulative inclinometer displacement records from inclinometers installed in BH5, from 15/06/2006 to 16/04/2009.

Table 5.29 Summary of inclinometer results (July 2008 to September 2009)

Inclinometer	Top of Inclo-Tube	Approx. Movement depth		Depth of logged slide surface[1]	Total movement in period[2] (mm)	Movement bearing[3] (°)
	m RL	m bgl	m RL	m RL		
BH1	450.8	22.3	428.5	428.1	24 (±3)	173 (±1°)
BH2	459.1	25.8	433.3	433.6	28 (±4)	142 (±1°)
BH3	465.4	N/A	N/A	441.3	N/A	N/A
BH4	485.5	N/A	N/A	452.3	N/A	N/A
BH5	508.4	N/A	N/A	465.3	N/A	N/A

[1]Depth of slide surface identified from logging of the drill holes
[2]Equipment precision calculated from the equipment specifications (Slope Indicator, 2005), and is based on measurements between two surveys, the reference survey and the most recent survey.
[3]Movement bearing errors calculated at 95% confidence limit.

Other motion, unrelated to shear displacement of the landslide can be observed in the inclinometer records. The records for BH3 and BH4 show sinusoidal-shaped deformation at depths of 11 and 13 m below ground level, respectively. These are thought to be due to the existence of voids between the inclinometer casing and the in-situ ground, which allowed the casing to deform into the voids (Stark and Choi, 2008). Borehole logs for these depths indicate core loss occurred at these intervals, which may be related to either voiding or particularly weak layers.

Subsurface motions derived from the inclinometers have a poor temporal resolution when compared to the prism data, but are adequate to assess the timing and rates of displacement along the slide surface. The magnitudes of horizontal displacement between the slide surface and the ground surface can only be assessed using the inclinometer installed at BH1 (lower toe), as the inclinometer at BH2 (upper toe) was sheared off about two months after installation of the prisms. The motion direction of inclinometer BH2 (142°) and prism 11 (152°), located about 5 m from inclinometer BH2, for this limited period of overlap are, however, comparable.

The motions recorded at BH1 have been compared to the slow creep motions recorded at the surface for prism 4, for the same time period (1/07/2006 to 15/10/2009), these are summarised in Table 5.30 and Figure 5.59. Prism 4 is located about 5 m east of BH1.

Table 5.30. Surface and subsurface comparison of motion

Location	Equipment type	Total displacement in period and errors at 95%[1] (mm)	Motion rate and errors at 95%[1] (mm/year)	Bearing[1] (°)
BH1	Inclinometer	8 ±(1.2)	3 ±(0.4)	173 ±(1)
Prism 4	Prism	16 ±(0.7)	5 ±(0.2)	169 ±(2)

[1]Errors calculated using the least squares method at 95% confidence, assuming a linear relationship

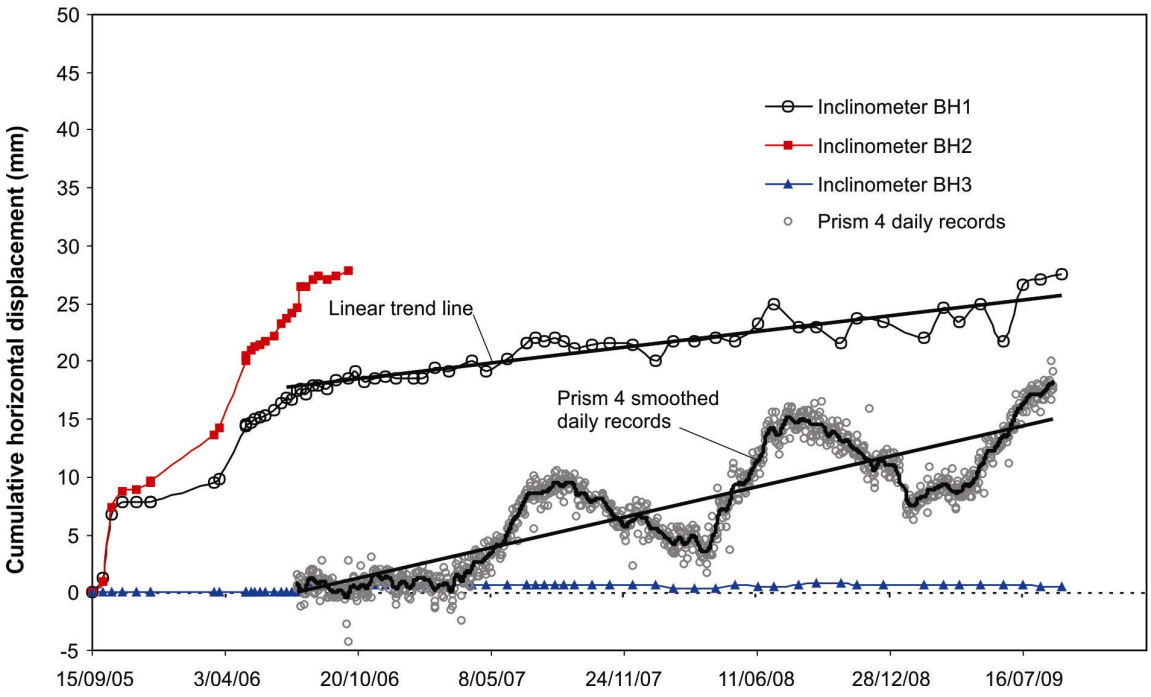

Figure 5.59 Cumulative displacements along the slide surface plotted with cumulative displacements at the surface.

These data show that the bearing of displacement for the same period is consistent between the slide surface and the ground surface. However, the motion rates do vary,

with those along the slide surface being about 50% less than those recorded at the surface. This anomaly may be related to the gradient of the cumulative horizontal displacement of prism 4, as this is dependent upon the number of seasonal cycles in the time series. What is interesting is that it is not possible to resolve any inclinometer displacements consistent with the timing of the cyclic accelerated creep motion recorded by the prism, which would imply that accelerated creep motion does not relate to displacement along the slide surface. The cumulative displacement of the slide surface does show several periods of accelerated creep motion at the very beginning of the monitoring, prior to installation of the prisms, however, unlike the surface seasonal accelerated creep, these displacements do not change direction. This initial period of motion resulted in the shearing off of inclinometer BH2 rendering it useless. Surface motion for this earlier period can only be assessed using the historical survey data, which has been compared to the inclinometer data. The comparison suggests that the inclinometers captured the tail end of the largest recorded accelerated creep event, which from the surface monitoring began in April 2004, and stopped, using the inclinometer records, in August 2006. Since August 2006 and up to October 2009, the inclinometer motions have been consistent with that of steady slow-creep.

5.3.4 Factors affecting prism movement

5.3.4.1 Rainfall

Rainfall recorded on the landslide at BH2 has been used for analyses purposes, and are the same records which were used for the Utiku analyses. Records from this rain gauge for the monitoring period are summarised in Table 5.31.

Table 5.31 Rainfall statistics for Taihape (1/07/2006 – 15/10/2009)

Total rainfall (over monitoring period)	3,202.8
Mean annual rainfall (mm)	962
Mean daily rainfall (mm)	2.6
Max. daily rainfall (mm)	49.8

Daily and cumulative rainfall totals for Taihape are shown in Figure 5.60. Cumulative rainfalls show alternating summer and winter trends, whereby summers (December to May), tend to be dryer (mean rainfalls ~2 mm/day) and winters (June to November) wetter (mean rainfalls ~3 mm/day). Cumulative deviation from mean daily rainfall calculated for the entire monitoring period show these seasonal trends more clearly (Figure 5.61). The rainwater input to the landslide during the monitoring period, using the annual rainfalls at Taihape, was 21 litres/sec for the landslide catchment, which is assumed to be 69.4 hectares. The Taihape landslide forms its own unique catchment,

however, surface runoff and evapotranspiration from the landslide catchment are not being measured. It is therefore not possible to estimate with any accuracy, the amount of surface water that would likely enter the groundwater system.

Daily rainfalls recorded during the monitoring period have been compared against the magnitude/frequency of daily rainfalls recorded during a longer record. These longer records, in this case between 1912 to present day, are from a gauge installed at Taihape (about 1 km from the landslide), which is operated by Rangitikei District Council. To date, the maximum daily rainfall recorded on the landslide during the monitoring period was 49.8 mm, which occurred on 18/12/2007, and has an annual exceedence probability of 42 % (once every 2.4 years, using the longer-term record), indicating that the rainfalls during the monitoring period were not exceptional and that the largest probable rainfall event for the monitoring period was achieved (Figure 5.62).

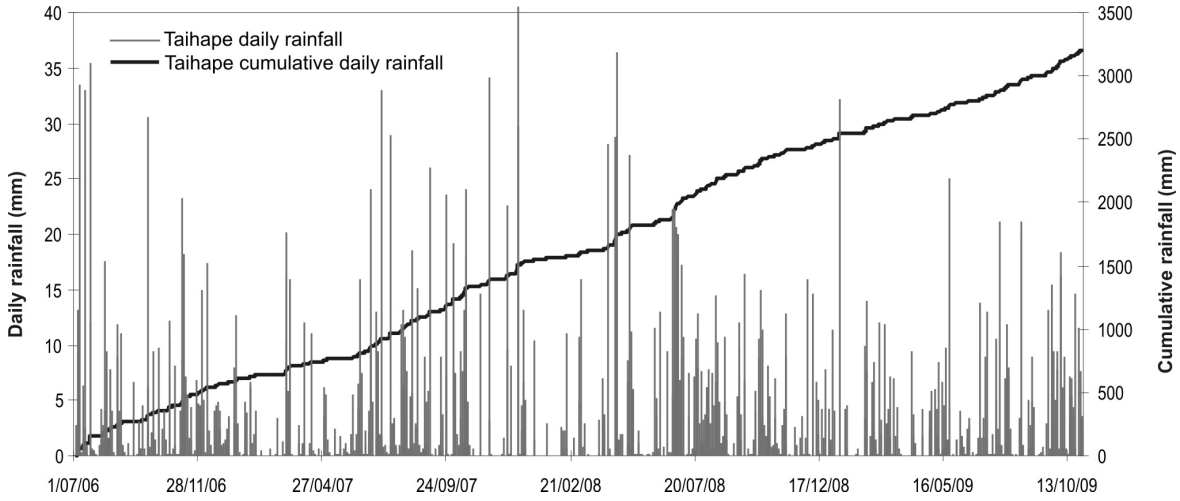

Figure 5.60 Taihape daily and cumulative rainfall

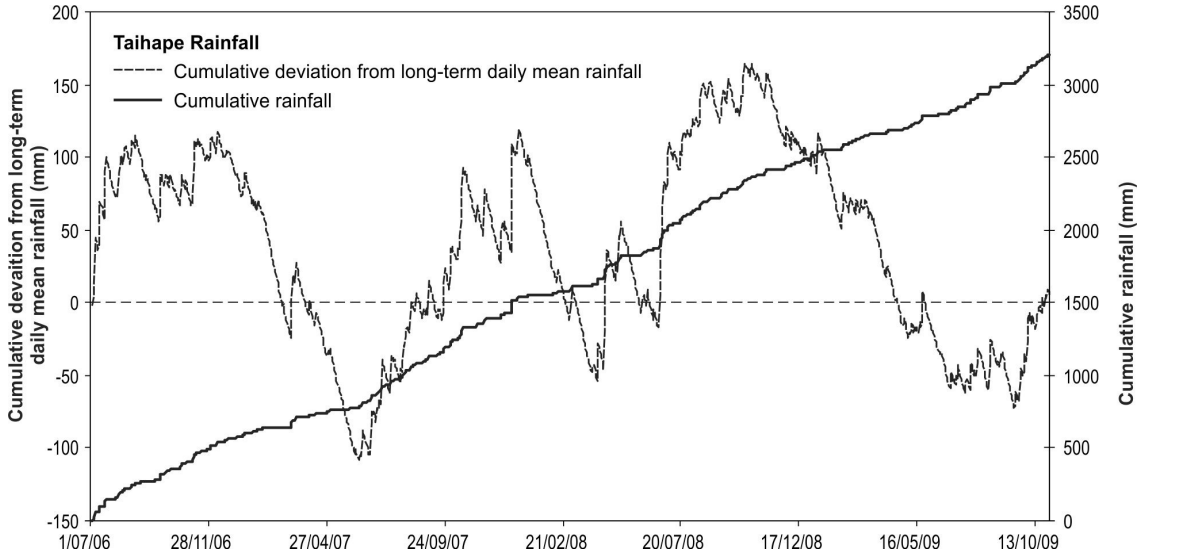

Figure 5.61 Cumulative deviations from daily mean rainfall (Taihape)

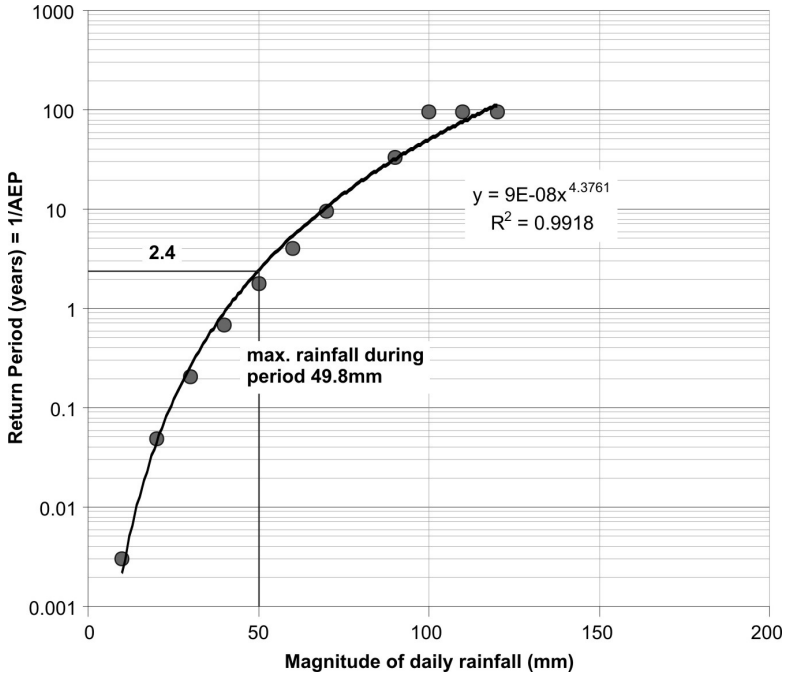

Figure 5.62 Rainfall magnitude and return period for the period 2/01/1912 to 31/10/2009. Data is from the Rangitikei District Council operated rain gauge at Taihape. The maximum rainfall recorded at the Taihape landslide rain gauge installed at BH2 during the period 1/07/2007 to 31/10/2009 is shown for comparison purposes.

5.3.4.2 Groundwater pressures

The vibrating-wire (VBW) instruments installed at Taihape are identical to those in the Utiku landslide. These instruments record pore pressures in Casagrande standpipe piezometer tubes which have sealed response zones above (but near to) the identified landslide slide surface (Chapter 4). All pore-pressure measurements used in these analyses are recorded at the sensor tip. No adjustments for the width of the Casagrande standpipe response zone, or depth of slip surface, have been applied.

The hourly gauge readings (in Hertz) from VBW piezometers BH1A, BH2A, BH3A and BH5A have been converted to pressures following the method discussed in Section 4. The hourly pressure measurements have then been averaged over each 24-hour period (UTC), to derive a daily average pore pressure for each instrument. Readings were then corrected for barometric effects (following the method detailed in Section 4), using data from the barometric-pressure sensor installed at Taihape. Statistics relating to this sensor are summarised in Table 5.15.

The stated precision of the VBW piezometers is ±0.1% of the operating pressure (Geokon, 2005), which for the Taihape piezometers is 700 kPa, giving an error of ± 0.7 kPa. This equates to about ±0.07 m of piezometric head.

A Gaussian smoothing kernel was used to smooth the corrected daily averaged pore

pressure time series for each piezometer to give an indication of the probable measurement precision. A G_s = 2 was used and the precision estimated as per the procedure in Section 4.4.1.4. The precision of the smoothing kernel for VBW piezometers BH1A, BH2A, BH3A and BH5A is about ±1.0 kPa (0.1 m H^2O), based on the standard deviation of the residual mean (Table 5.32). This is slightly larger than the equivalent value recorded for Utiku, indicating a more variable data set. The Taihape landslide is urban and subject to leakage from water and waste-water pipes and to domestic irrigation and so inputs from these sources may account for the larger variation shown in the Taihape pore-pressure time series.

Table 5.32 Precision of the smoothing kernel (G_s = 2 kPa) with respect to the corrected daily mean pore-pressure values.

Piezometer	Mean pore pressure (kPa)	Standard deviation from mean (kPa)	95% confidence limit (kPa)
BH1A	135.9	±1.0	±2.6
BH2A	179.1	±1.1	±2.7
BH3A	254.4	±1.0	±2.6
BH5A	320.4	±0.9	±2.4

The corrected pore-pressure time series for each VBW piezometers BH1A, BH2A, BH3A and BH5A, along with the smoothed time series are shown in Figure 5.63. In general the pore pressures at all piezometers follow the summer / winter rainfall cycle, whereby pressures decrease during the summer months and increase during the winter months. For piezometers BH1A and BH2A this seasonality is not evenly represented, as the pore-pressure recession limbs are less steep (typical gradients of -0.07 kPa/day), than the rising limbs (typical gradients of 0.22 kPa/day). These patterns are less pronounced in piezometers BH3A and BH5A, which show a more consistent and even trend in the gradients of the recession and rising limbs of pore-pressure response. Superimposed on the longer-term trends are multiple smaller magnitude short-duration changes in pore pressure, which give the time series plots a “saw-tooth” shape. Pore-pressure magnitudes decrease from the upper landslide to the lower landslide, which correspond to the decreasing depth of the landslide slide surface, from ground level, towards the toe. Piezometric head levels calculated from the pore pressures indicate levels are at, or above (artesian), ground level in the upper toe (BH2A) and central parts (BH3A) of the landslide.

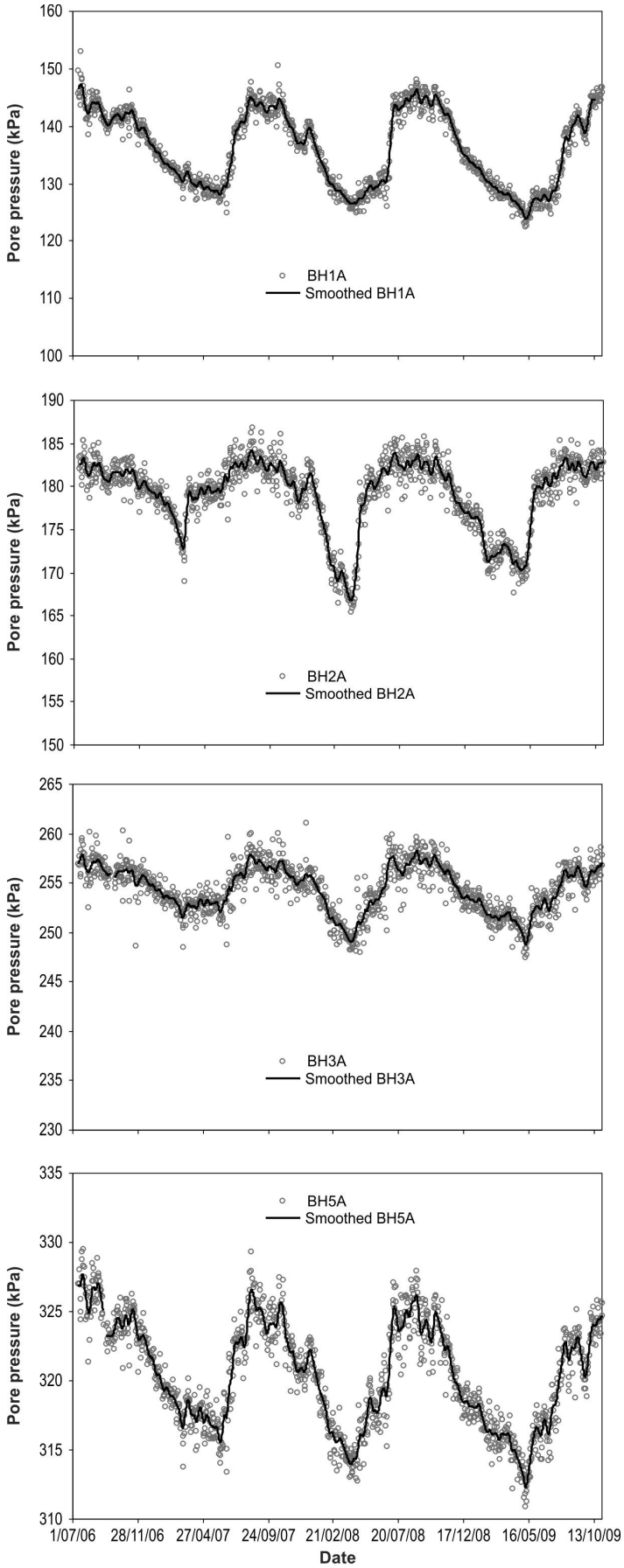

N.b. The scales vary between graphs

Figure 5.63 Pore pressures recorded at piezometers BH1A, BH2A, BH3A and BH5A over the monitoring period. Daily pore pressures and smoothed daily pore pressures are shown, with the smoothed values calculated from a Gaussian smoothing kernel where G_s = 2 kPa.

For comparison purposes the time series data from the piezometers have been plotted as deviation from mean pore pressures (Figure 5.64). Histograms of deviation from mean pore-pressure (corrected daily mean values), for BH1A, BH2A and BH5A are bimodal (Figure 5.65), which reflects the seasonal (winter/summer) variations in pore pressure shown by the time series. The histogram for BH2A, however, shows that pore pressures tend to be at higher than mean values for a longer proportion of time, than they are lower than mean. In contrast to the other piezometers, the histogram for BH3A is unimodal with pore pressures remaining about mean values throughout most of the monitoring period, indicating little seasonal variation. The largest deviations from mean pore pressures were recorded by piezometers BH1A and BH2A, which are located in the active part of the landslide. These show that maximum fluctuations in piezometric head levels are about 17.2 kPa (1.7 m) above and 13.6 kPa (1.4 m) below mean values, and represent seasonal fluctuations of between 4% and 13% from mean values (Table 5.33). Piezometers BH3A and BH5A, located in the central and upper part of the landslide, are similar with maximum fluctuations of about 9.1 kPa (0.9 m) above and 9.5 kPa (1.0 m) below mean values, representing seasonal fluctuations of 3% from mean values.

Table 5.33 Statistics relating to the corrected daily mean pore water pressures recorded at the VBW piezometers installed in BH1, BH2, BH3 and BH5, for the monitoring period.

Piezometer	No. of daily records	Mean value (kPa)	Deviations from mean (kPa)		Deviations from mean (m H^2O)		Standard deviation of the mean (kPa)
			Max.	Min.	Max.	Min.	
BH1A	1191	135.9	17.2	-13.4	1.8	-1.4	±6.6
BH2A	1191	179.1	7.8	-13.6	0.8	-1.4	±4.3
BH3A	1182	254.4	6.7	-6.9	0.7	-0.7	±2.5
BH5A	1185	320.4	9.1	-9.5	0.9	-1.0	±3.9

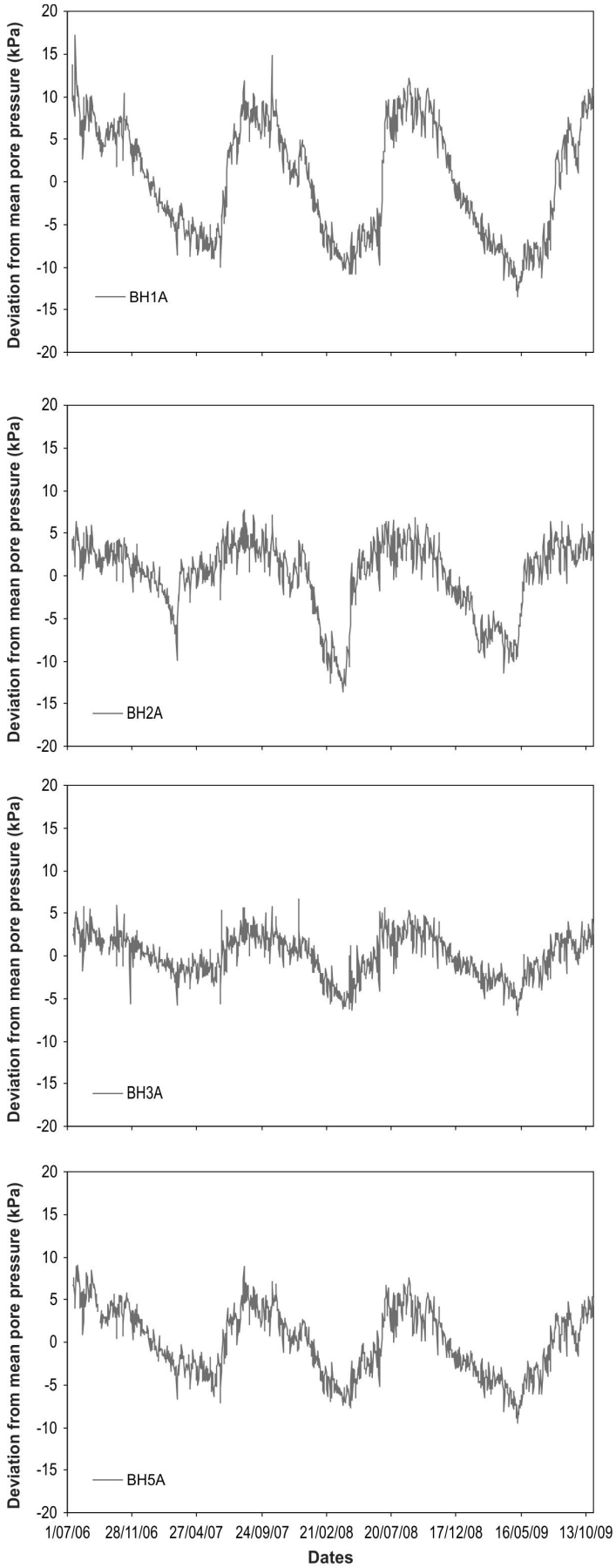

N.b. The scales vary between graphs

Figure 5.64 Deviation from daily mean pore pressures for piezometers BH1A, BH2A, BH3A and BH5A, showing daily pore pressure readings.

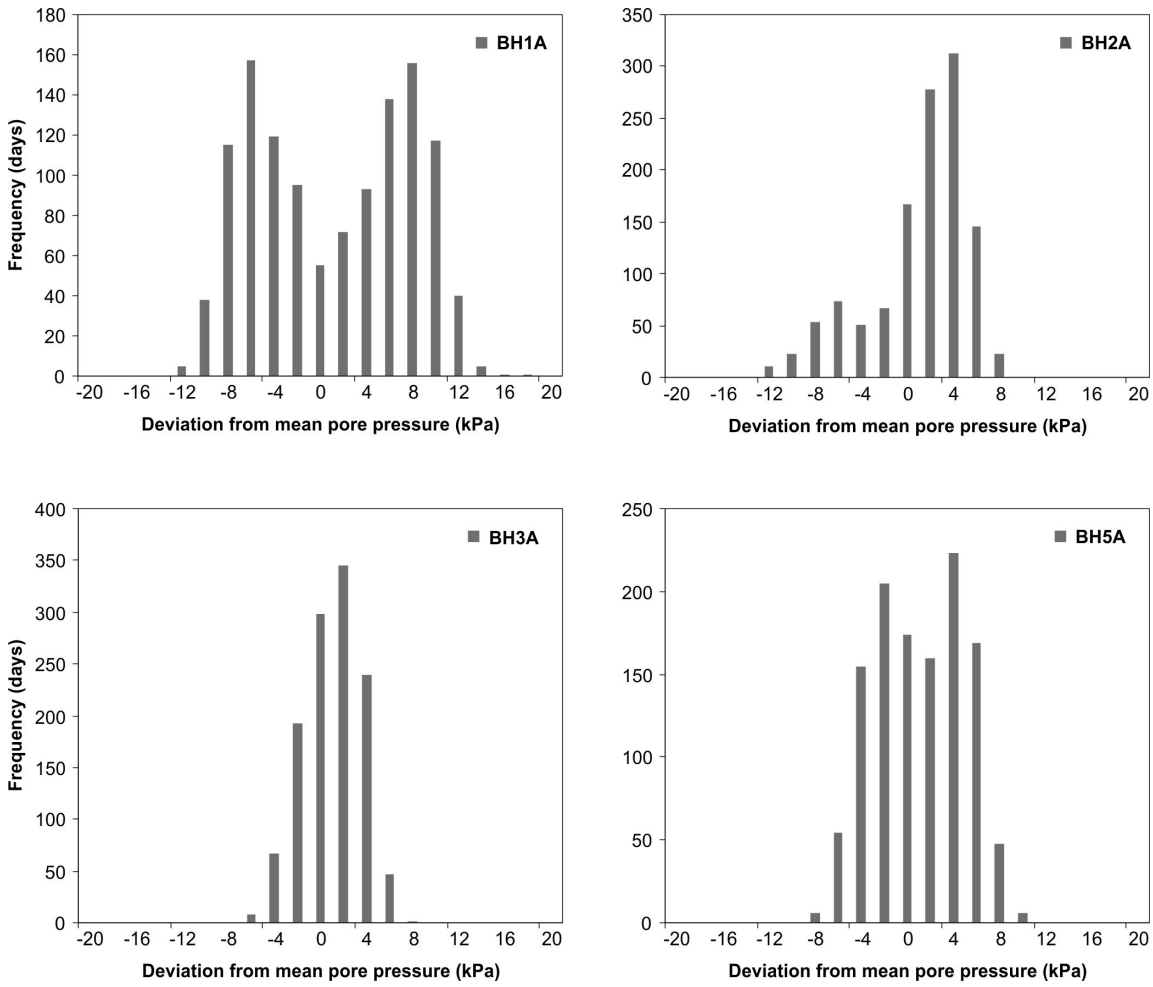

Figure 5.65 Histograms of deviations from daily mean pore-pressure, for piezometers BH1A, BH2A, BH3A and BH5A (daily pore-pressure readings).

Histograms of the daily (day-to-day) pore-pressure change for all piezometers are unimodal, and approximately normally distributed with standard deviations of about ± 1.3 kPa (Figure 5.66). These data suggest that the rate of pore-pressure change, for all piezometers, is slow, with larger pore-pressure changes taking several days to occur. The day-to-day changes in pore pressures recroded at Taihape are slightly larger than those recorded at Utiku, which are about ±1.0 kPa. The difference may be related to the potable, storm and waste water reticulation systems on the Taihape slide, but could also be related to other factors such as permeability of the ground and the stand pipe piezometer installation.

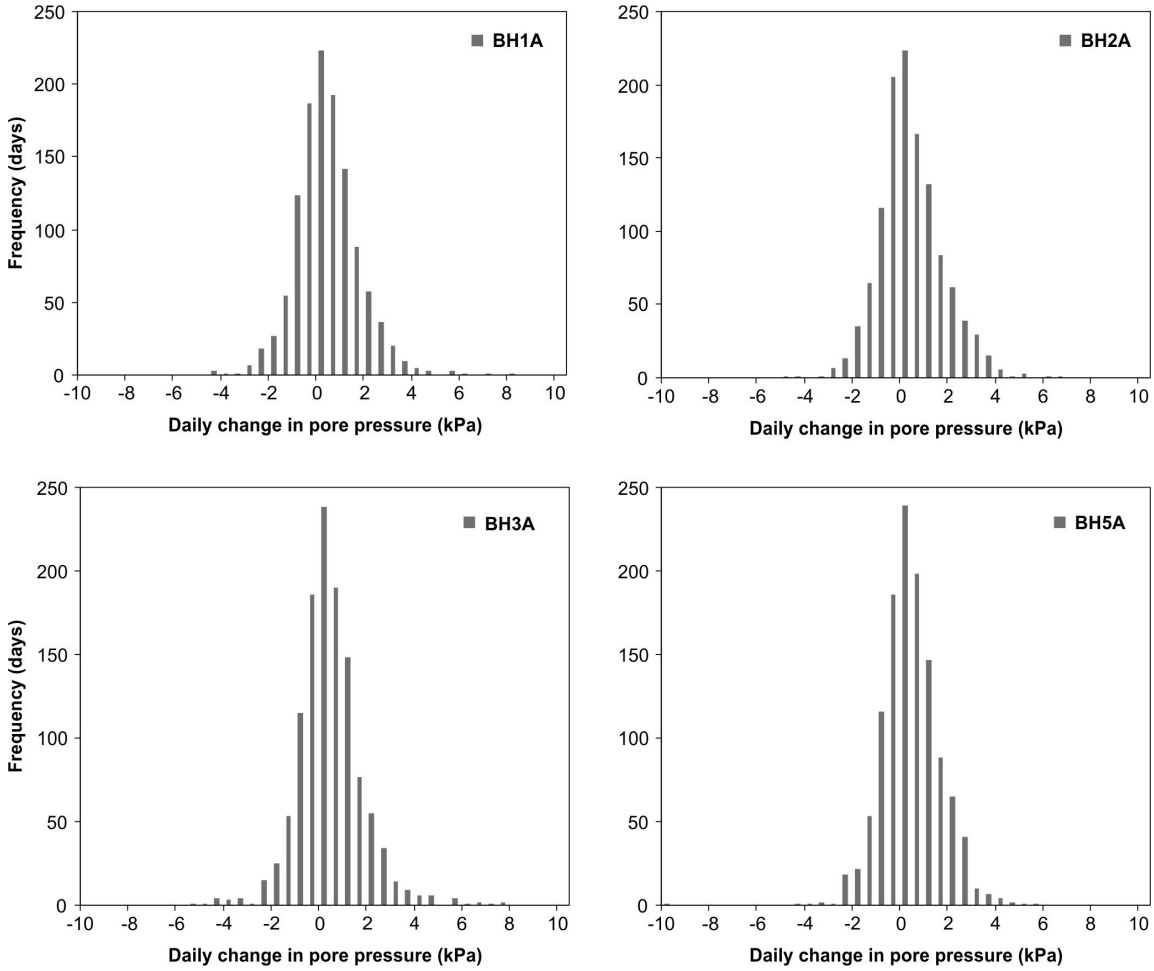

Figure 5.66 Histograms of the daily (day-to-day) change in pore pressure for piezometers BH1A, BH2A, BH3A and BH5A (daily pore-pressure readings).

5.3.4.3 Rainfall and groundwater pressures

The relationship between rainfall and pore pressure response has been assessed using the same methodology adopted for the Utiku analysis, whereby a correlation analysis was undertaken to determine relationships between pore pressure at each piezometer, and antecedent rainfall (as recorded on the landslide), in order to establish the time frame over which rainfall influences piezometer response. The results (Figure 5.67 and Table 5.34) show that the correlations for BH1A, BH3A and BH5A are highest for antecedent rainfalls accumulated over 12 to 19 weeks. The exception is BH2A where the correlation is highest for antecedent rainfalls accumulated over about 9 weeks, indicating that this piezometer responds more rapidly to rainfall than the others. This more rapid response could be related to the topographic position of the piezometer within a graben. All of these results imply that pore-pressures respond to long periods of wet weather rather than large magnitude, short-duration rainfalls.

Table 5.34 Results from the pore pressure rainfall correlation analysis.

Piezometer	Rainfall accumulation period (antecedent rainfall) (weeks)	Peak correlation
BH1A	16	0.82
BH2A	9	0.62
BH3A	12	0.74
BH5A	14	0.79

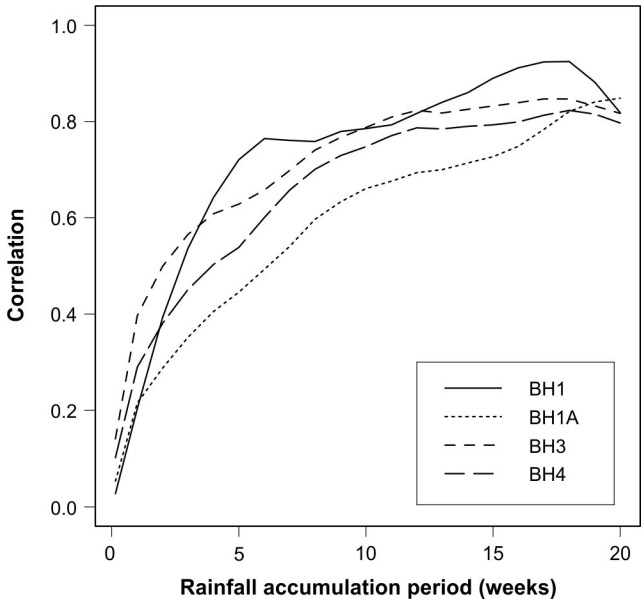

Figure 5.67 Results from the pore pressure and rainfall analysis. The pore pressure at a given time and the accumulated antecedent rainfall were assessed incrementally, using the daily rainfall and pore pressure values recorded on the landslide. The correlation analysis assumes a linear relationship between pore pressure and rainfall.

5.3.4.4 Landslide hydrogeology

Like Utiku, the hydrogeology of the Taihape landslide is complex. The linkages between surface water and groundwater are made more difficult due to the disturbed nature of the landslide mass and associated contrasting permeability of the materials, and the presence of preferential flow paths, e.g. grabens, sinkholes and tension cracks. It is made even more difficult as there are over 200 residential properties with associated potable, storm and waste water reticulation systems, on the landslide. These reticulation systems may account for the larger variation and more rapid day-to day changes shown in the Taihape pore-pressure time series when compared to the Utiku time series.

Borehole logs from Taihape indicate the landslide debris overlying the slide surface comprises a mixture of soil (remoulded Taihape Sandstone overlain in parts by Hautapu Valley Agglomerate and intact displaced rafts of Taihape Sandstone, which are highly

fractured (RQD ~ 20 to 50%) as a result of landslide motion. Below the slide surface the RQD of the intact sandstone is typically 100%. The abrupt change in material properties as well as the presence of the clay layer forming the slide surface would form a distinct hydrogeological boundary. It is therefore probable groundwater within the landslide mass is confined by this boundary.

Piezometric-head levels, calculated from the corrected daily mean pore-pressures from BH2A and BH3A, show that the piezometric surface is more or less coincident with the ground surface in the centre of the landslide, with artesian levels recorded during the wetter winter months. At BH1A and BH5A, which correspond to local high spots on the landslide, the levels are about 6 and 3 meters below the ground surface, respectively. Although no automated monitoring of the piezometer in BH4A was undertaken, the hand-dipped piezometric-head levels indicate artesian conditions predominated over much of the monitoring period. However, there is no evidence of ponded surface water around BH2A, BH3A and BH4A. There is, however, evidence of multiple springs and seepages in and around BH4A. The mean piezometric-head levels recorded during the monitoring period are shown on Figure 5.68. Piezometric-head contours have not been generated for Taihape as the piezometers are more-or-less in a straight line and so it is not possible to resolve the direction of groundwater flow across the landslide other than between the piezometers. However, groundwater flow appears to be sub-parallel to the dip of the slope based on a very limited assessment.

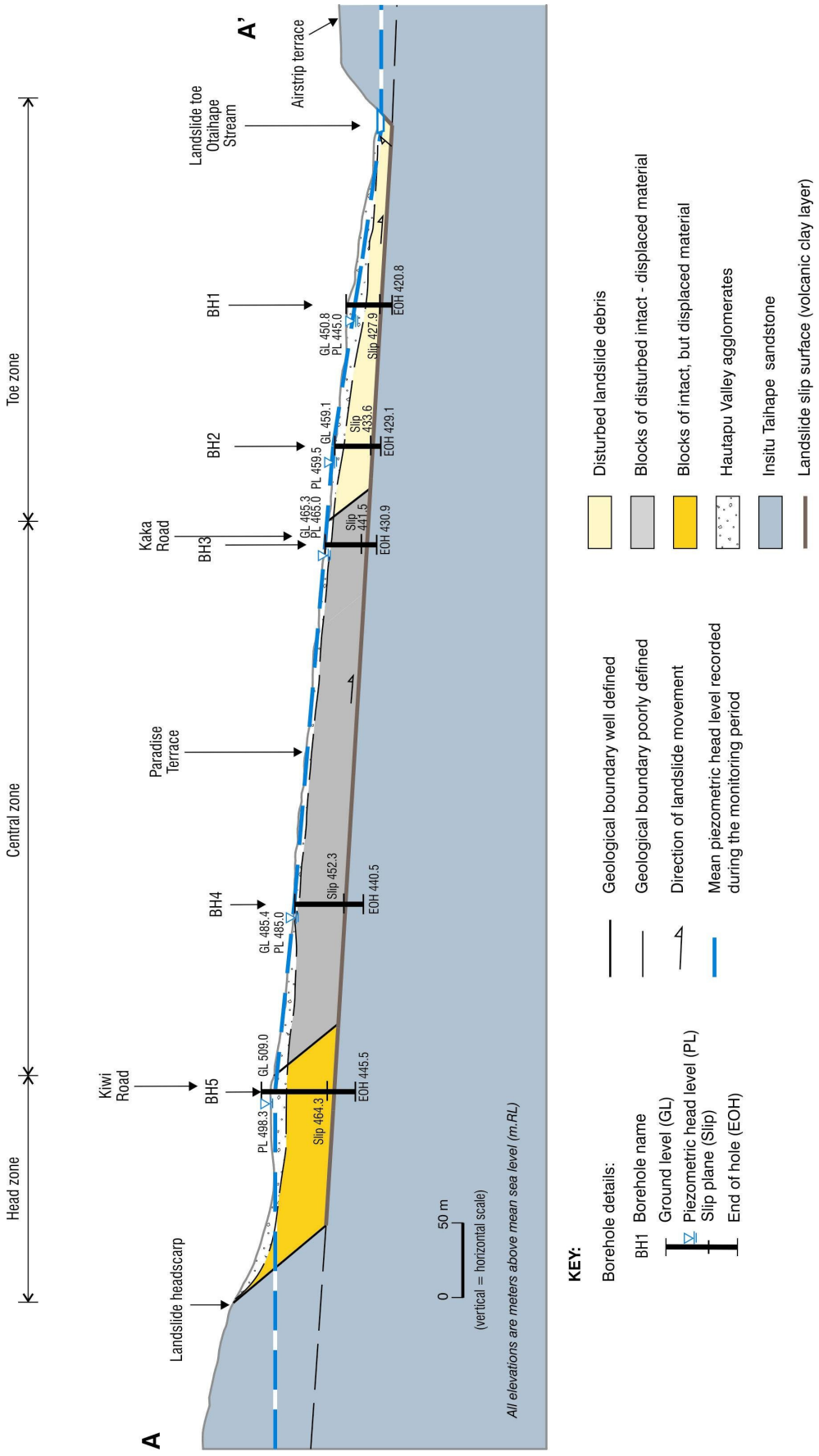

Figure 5.68 Longitudinal section through the landslide showing the mean piezometric head levels recorded during the monitoring period. Section line A-A', Figure 3.16.

These observations combined with the groundwater-monitoring data indicate that pore pressures recorded at depth by the vibrating-wire piezometers within the landslide are partially confined. This aquifer is thought to be bounded by the slide surface at its base, and by a combination of the Hautapu Valley Agglomerate and intact rafts of sandstone at its upper margin. The grabens, sinkholes, other soil pipes provide preferential flow paths for surface and shallower subsurface water into the deeper landslide mass.

The relative timing of pore-pressure responses between the piezometers on the landslide have been investigated for the different piezometers, starting at the landslide crest and moving toward the toe (these are shown in Figure 5.69). The relationship between BH5A and BH3A is linear, with a ratio of 0.6, indicating that the magnitudes of pore-pressure change between the piezometers differ. The gradient of the line suggests that the pore-pressure changes at BH5A are larger in magnitude than those at BH3A, although the timing of these changes between the two piezometers are similar, indicating no obvious hysteresis. The relationship between BH3A and BH2A is slightly hysteretic, and indicates a slight lag between the piezometers. Linear correlation suggests a ratio of about 1.5, with piezometer BH2A showing a larger magnitude of change. The nature of the hysteresis loop also indicates that pore pressures changes occur more rapidly at BH2A, on the rising limb, but are slower on the falling limb. This indicates that for BH2A the higher pore pressures are achieved more quickly and maintained longer than those at BH3A.

The relationship between piezometer BH2A and BH1A is strongly hysteretic, indicating an obvious lag between the piezometers. Linear correlation gives a ratio of about 1.1, indicating little difference in the magnitude of pore-pressure change between the piezometers. To better visualise the hysteretic nature of the relationship, each yearly period of data has been plotted separately (Figure 5.70). These graphs show that for the rising limb, pore pressures at BH2A initially respond more quickly than those at BH1A, however, the rate of change at BH1A eventually increases becoming more rapid than BH2A. These differences are not apparent for the descending (drainage) limb of the graphs, where the gradient between the piezometers are approximately constant. This would indicate that when pore pressures rise there is a lag between the upper toe (BH2A) and the lower toe (BH1A) of the landslide, with the pore pressures in the lower toe taking longer to rise than those on the upper (Figure 5.71). These anomalies maybe explained by the contrasting permeability's of the materials and the different topographic positions of the piezometers, where BH2A is located in a graben and BH1A at a local topographic high point.

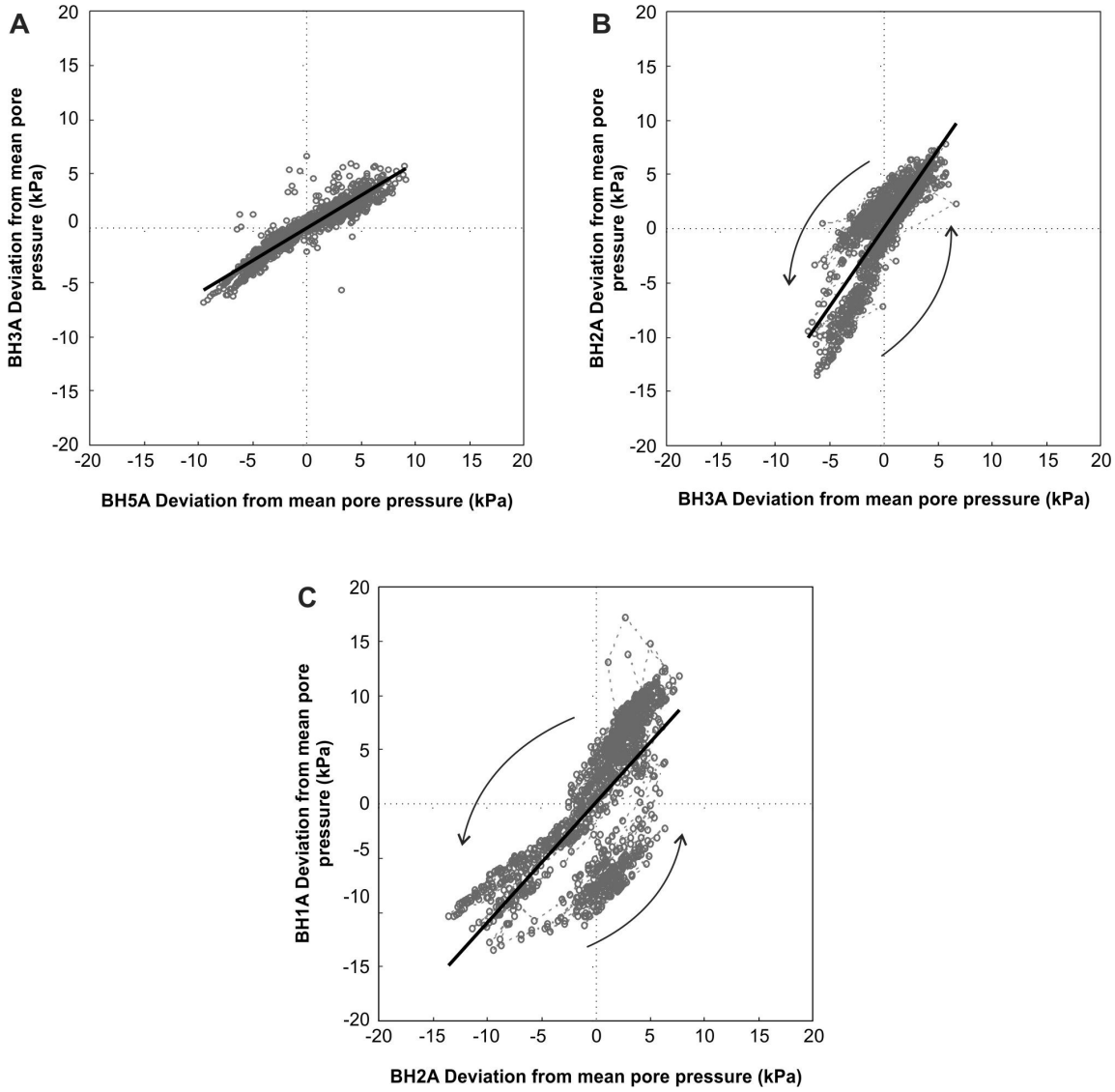

Figure 5.69 Simultaneous daily pore pressures for different piezometers plotted together. A: The landslide crest (piezometers BH3A and BH5A). B: the centre of the landslide (piezometers BH2A and BH3A). C: the landslide toe (piezometers BH1A and BH2A). Linear trend-lines are shown.

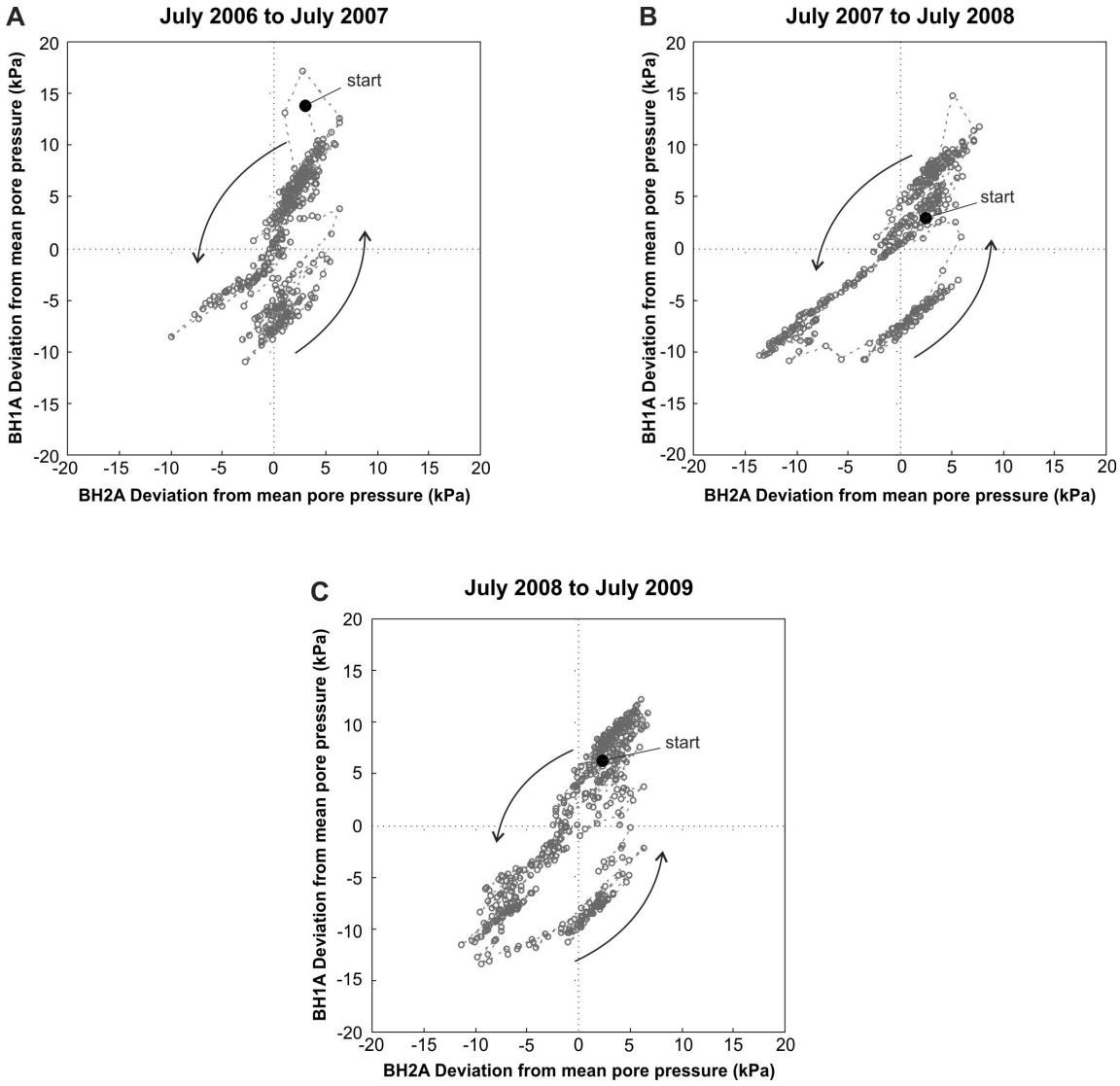

Figure 5.70 Simultaneous daily pore pressures for piezometers BH1A and BH2A plotted annually. A: July 2006 to July 2007. B: July 2007 to July 2008. C: July 2008 to July 2009. Linear trend0lines are shown.

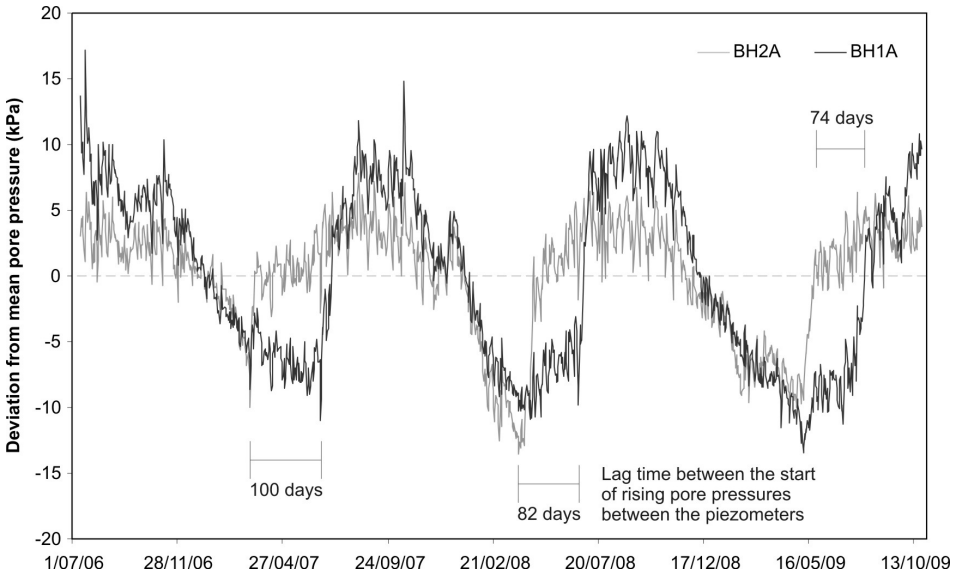

Figure 5.71 Relationship between pore pressures on the upper (BH2A) and lower (BH1A) landslide toe.

5.3.4.5 Earthquakes

During the monitoring period, none of the periods of prism motion (movement periods 1 to 4) can be related to earthquake ground accelerations, as no earthquakes occurred during these periods of movement. Several earthquakes have occurred during the longer-term monitoring period, and their associated ground accelerations, measured by the sensor located at Taihape Rural Hospital, are listed in Table 5.35.

The largest ground acceleration (PGA ~0.02 g) recorded on the landslide was in response to a M5.9 earthquake, which occurred on 25/08/2008 at 11:25:19 hours UTC (equivalent to a 1 in 3-year PGA, Stirling et al., 2000). This earthquake occurred when piezometric levels at all piezometers were greater than mean values. No prism displacements outside survey error were identified, indicating, like Utiku, that the landslide is not particularly sensitive to earthquake-induced ground accelerations.

Table 5.35 Earthquake ground accelerations recorded by the landslide instrumentation (Taihape).

Date UTC	Time (UTC)	Latitude	Longitude	Depth (km)	Magnitude (M_L)	Ground acceleration (Gal)
20/12/07	7:55:17	-38.87	178.49	44.24	6.87	0.69
4/02/07	7:14:27	-39.09	176.29	56.33	5.35	0.22
25/08/07	1:43:33	-40.45	174.86	51.4	5.13	0.29
5/10/07	1:22:12	-39.69	175.67	16.36	3.51	0.58
27/12/07	8:07:04	-38.95	175.67	117.48	5.45	0.79
28/12/07	6:03:38	-38.77	176.29	79.76	5.53	0.36
16/04/08	5:13:33	-39.78	175.79	11.08	3.46	0.87
25/08/08	11:25:19	-39.71	176.85	31.83	5.89	2.22
1/09/08	1:21:51	-39.1	175.89	85.09	5.83	1.75
1/09/08	1:21:51	-39.1	175.89	85.09	5.83	0.92
19/12/08	12:21:05	-38.24	176.13	186.88	5.82	0.27
15/10/09	8:59:48	-39.72	176.82	30.96	4.61	0.22
16/10/09	1:27:11	-39.62	176.00	47.82	4.73	0.82

5.3.4.6 Stream stage

Changes in the level of Otaihape Stream could influence landslide stability, through ongoing erosion removing toe support. The level of Otaihape Stream is monitored; however, no periods of landslide motion correlate with increased stream flows since monitoring of stream levels began in June 2008, although ongoing erosion by Otaihape stream is removing material from the toe of the landslide.

5.3.5 Summary of results – Taihape landslide

The robotic total station successfully recorded displacements (outside survey error), of several prisms installed on the landslide. Horizontal and vertical landslide velocities vary over time and are stepped, representing periods of acceleration and rest. All significant landslide displacements detected over the monitoring period are extremely slow (< 16 mm/year), Cruden and Varnes (1996). Interpretation of the cumulative horizontal displacement plots indicate two main types of motion: 1) short-duration, relatively rapid motions, in both upslope and downslope directions, which appear seasonal and are superimposed on; 2) longer-duration, slower displacements over several years, which are only discernable from the long-term trends in the cumulative displacement plots. Motion bearings are generally consistent with a downslope translational mechanism. The largest displacements were recorded in the area around prisms 10 and 11, which are located in a graben feature at the head of the toe slide block. These data indicate that, over the monitoring period, only the prisms in the toe area of the landslide have moved. The toe slide block comprises an area of approximately 11%, based its geomorphological boundary with the adjacent slide blocks.

The downslope slow-creep, recorded by the majority of prisms in the active toe area, is thought to be related to movement of the landslide, as displacements are consistent with the direction of historical motion. However, accelerated-creep may not relate to displacement of the landslide as these represent periods when some prisms were moving in an apparent upslope direction and to not correspond to displacements along the slide surface. These surface displacements appear cyclic and recur about every six-months, indicating a seasonality which approximates to summer / winter. The same seasonality has been identified in the records from the back sight prisms, located on stable ground as well as for other prisms on the stable part of the landslide. For prisms 6 and 31 the upslope motions are larger than the downslope ones and are thought to be, in part, related to landslide motion, although displacement of prism 6 is very small. Prisms 6 and 31 are located near geomorphological boundaries between slide blocks (Chapter 4). For prism 31 vertical motions have also been recorded, which when combined with the horizontal displacements indicate rotation.

Two of the five inclinometers installed on the landslide have recorded shear displacements at depths consistent with landslide movement. These two inclinometers (BH1 and BH2) are located in the toe area of the landslide and corroborate the results from the prism monitoring. These inclinometers indicate the presence of one slip surface, at depths corresponding to clay layers identified in the drillhole logs. However,

displacements along the slide surface are consistently less than those recorded at the surface.

Comparison of landslide displacements with earthquake ground accelerations and river-stage levels show no correlations, suggesting that landslide motion is primarily influenced by pore-pressure variations. Daily rainfalls and pore pressures (average of piezometer BH1A and BH2A), in the active area of the landslide have been compared to the cumulative displacement of selected prisms and are shown together on Figure 5.72. The comparisons indicate that the main periods of accelerated creep (both upslope and downslope) correspond to rising and falling pore pressure, with the upslope motions recorded by some of the prisms corresponding to periods when pore pressures were in recession. The rates of slow-creep motion do not appear to vary with pore pressure and are possibly unrelated to pore pressure variations.

Pore-pressure magnitudes decrease from the upper landslide to the lower landslide, which correspond to the decreasing depth, below ground level, of the landslide slide surface towards the toe. In general, the pore pressures at all piezometers follow a summer/winter cycle, whereby pore pressures decrease during the summer months and increase during the winter months. The largest deviations from mean pore pressures were recorded by piezometers BH1A and BH2A, which are located in the active part of the landslide. These show that maximum fluctuations are between 4% and 13% from mean values, representing a fluctuation of 31 kPa (about 3 m of head). Piezometers BH3A and BH5A, located in the central and upper part of the landslide, show maximum fluctuations of about 3% from mean values, representing a fluctuation of 19 kPa (about 2 m of head), which is less than that of the piezometers in the active landslide.

The pore pressure at a given time and the accumulated antecedent rainfall has been assessed incrementally by performing a correlation analysis assuming a linear relationship between pore pressure and rainfall. The results show that the correlation is highest for antecedent rainfalls accumulated over 12 to 16 weeks, indicating that pore pressures respond to long periods of antecedent rainfall. The daily change in pore-pressure magnitude for all piezometers on the landslide is slow, about $\pm$1.3 kPa at one standard deviation from mean values. These results indicate that pore pressures take time to reach peak values and are not quickly influenced by short duration, high magnitude rainfall.

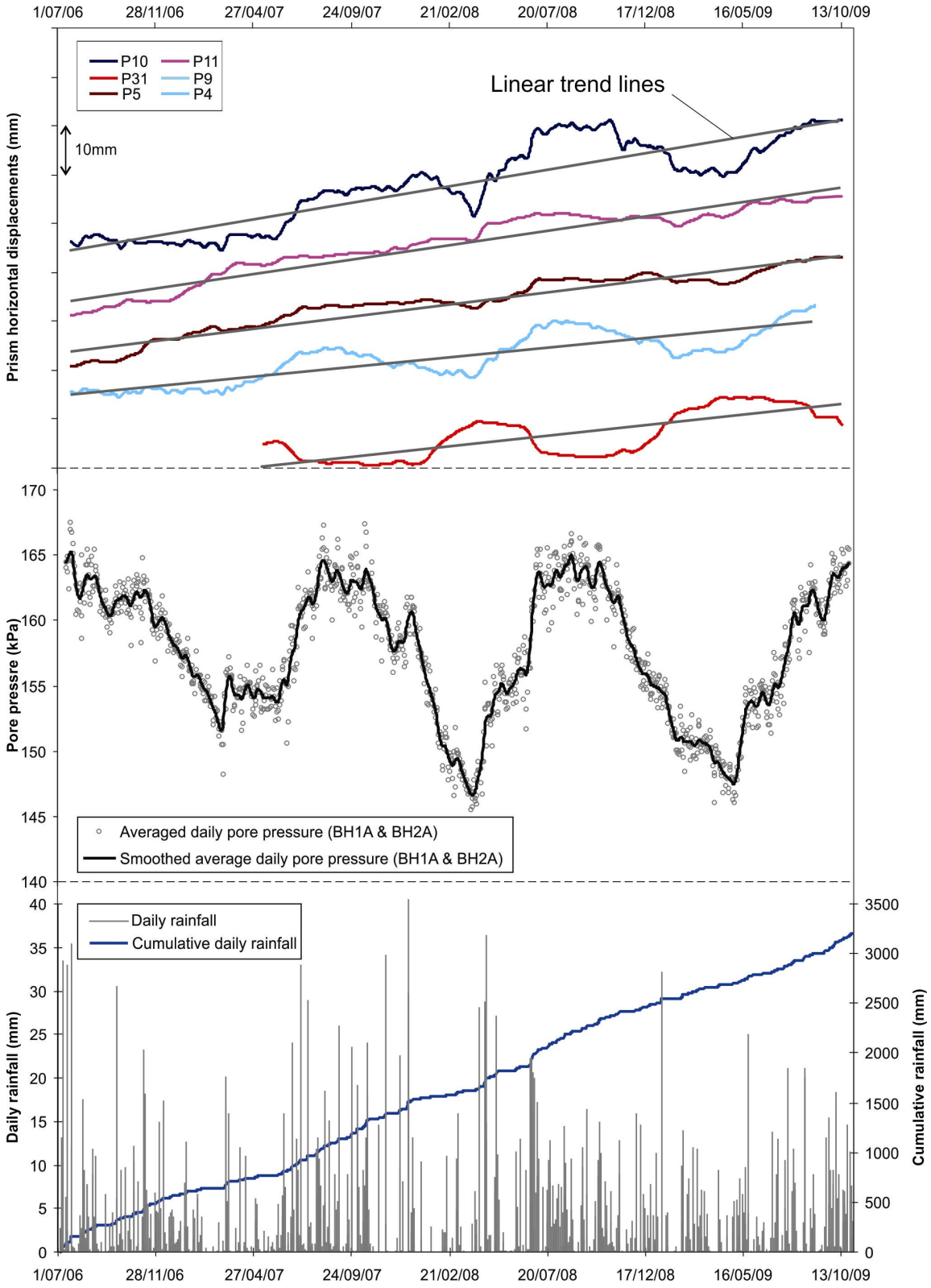

Figure 5.72 Relationship between cumulative horizontal displacements, pore pressures and rainfall for the Utiku landslide over the monitoring period. A: Smoothed cumulative displacements of prisms 4, 5, 9, 10, 11 and 31 along their main movement bearings (smoothed displacements calculated using G_s = 2 mm), with the linear trends of the daily cumulative displacements also shown. B: Daily pore pressures for piezometers BH1A and BH2A (smoothed using G_s = 2 mm). C: Daily and cumulative daily rainfall from the Taihape landslide gauge at BH2.

5.4 Historical motion

Historical movement data from the Utiku and Taihape landslides have been compiled to assess their long-term movement trends. These data can be compared with the more recently recorded data, allowing the recent motions to be put into a longer-term context.

5.4.1 Utiku landslide

5.4.1.1 Horizontal motion

Historically landside motion was recorded using a survey network established on the landslide in September 1965. This network initially comprised 22 survey pegs; the number changed over time as some pegs were lost and others were added. The horizontal motions of selected survey marks (those that were consistently monitored) have been plotted along their main motion bearings, derived from a least-squares adjustment (Figure 5.73). Historical motions can be classified as slow to extremely slow (Cruden and Varnes, 1996), and are consistent with a creeping landslide. However, the creep rates vary through time as well as location on the landslide. Cumulative horizontal displacement shows two main periods of landslide motion; 1) pre-1973 (September 1965 to December 1972), characterised by more rapid motions; and 2) post-1973 (January 1973 to July 2008), characterised by less rapid motions. The mean motions and bearings for these two periods are listed in Table 5.36.

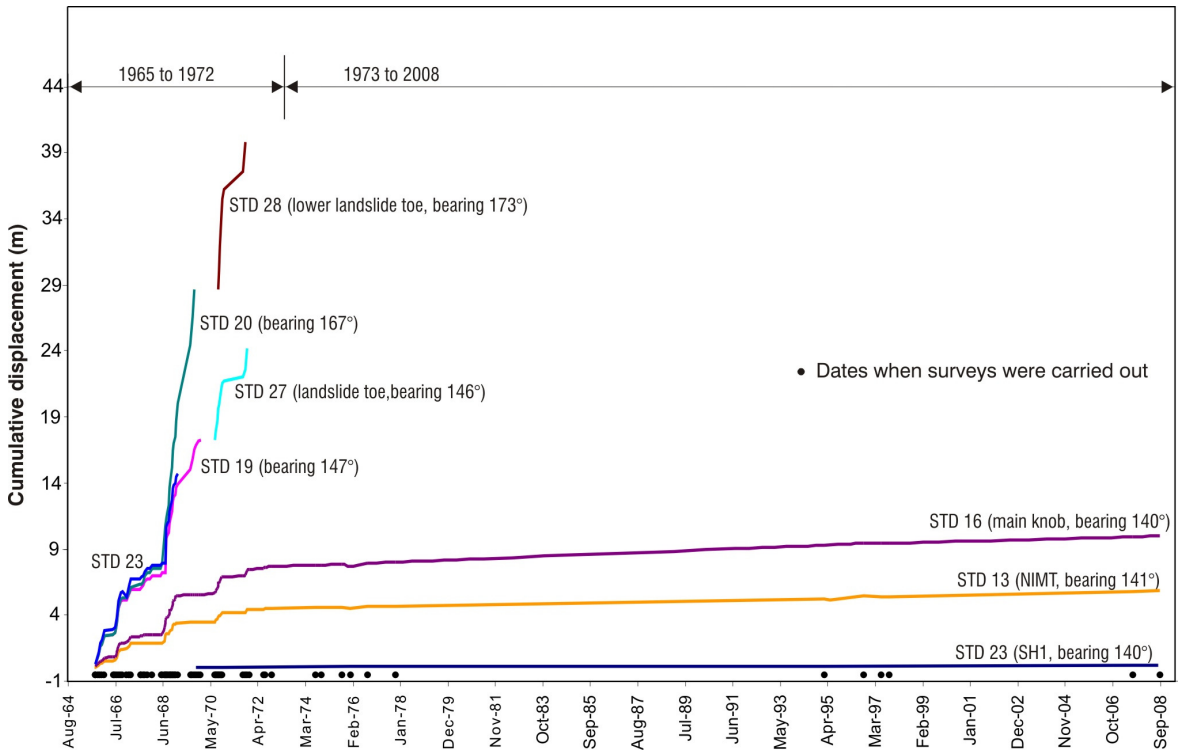

Figure 5.73 Historical cumulative horizontal displacements over time of selected survey marks plotted along their main motion bearings for the Utiku landslide. For survey peg locations refer to Figure 3.07.

Table 5.36 Summary of historical horizontal surface motion (Utiku)

Landslide location	Geomorphic position	Mean horizontal movement (m/year) and survey mark where recorded[1]		Mean movement bearing (°)
		Pre-1973	1973 to 2008	1965 to 2008
Lower landslide	Toe (Hautapu)	6.6 (20 & 28)	2.6 (95)	161
	Head	4.0 (19)	0.6 (PB13)	147
Upper landslide	Toe	1.1 (16)	0.1 (16)	143
	Head (NIMT)	0.6 (13)	0.05 (13)	134

[1] Survey mark locations shown on Figure 3.07.

The spatial extent of historical motions over the monitoring period has been modelled by calculating the average rate of displacement (m/year) for each of the consistently monitored survey pegs. The data have been subdivided into pre- and post-1973, with Figure 5.74 showing the 1965 to 1972 motions and Figure 5.75 the 1973 to 2008 motions. Generally, both figures show that landslide motions decrease in magnitude from the toe to the crest, although there appears to be a distinct change between the motion rates of the upper and lower landslide, with the boundary between the two coinciding with a distinct scarp. Motion bearings suggest that the landslide rotates about a vertical axis centred southwest of the landslide with the motion bearings of the upper landslide being about 130° to 140° and changing to about 150° to 160° in the middle and then 160° to 170° at the toe. The rotation is also corroborated by the lower magnitudes of displacement recorded along the south-western flank, compared to the larger ones recorded in the central and northern parts.

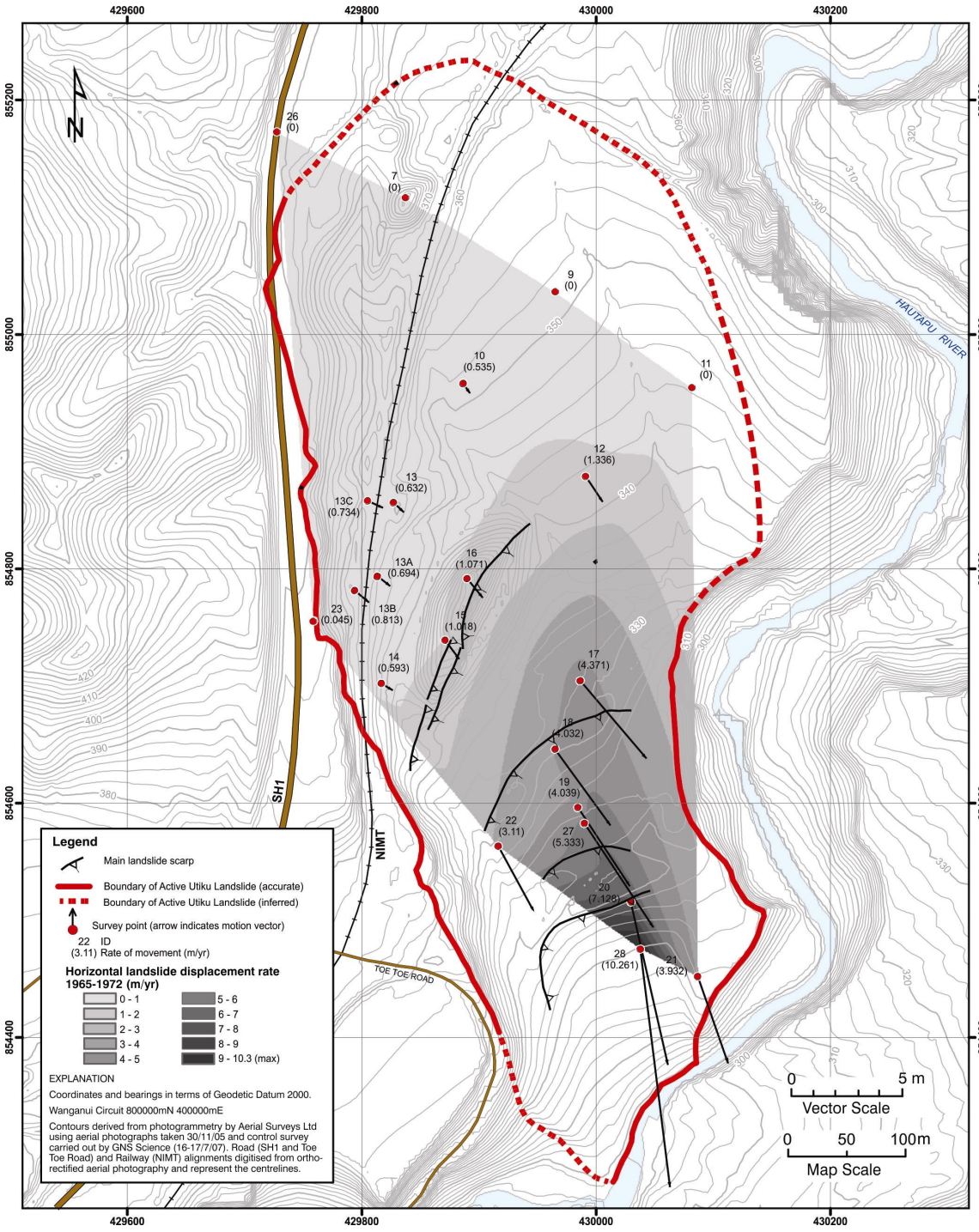

Figure 5.74 Pre 1972 displacements of the historical survey marks. Displacements calculated using the least squares method on the cumulative horizontal displacements.

Pre-1973 cumulative horizontal displacements, plotted along the main motion bearings are shown in more detail in Figure 5.76. These data show that for those marks on the lower landslide (survey marks 17, 19, 20 and 28), the motions are larger in magnitude and rate than those on the upper landslide (survey marks 13, 16 and 23). Although there are obvious differences in the magnitudes of displacement across the landslide, the timing of motions of the main periods of movement are synchronous (within the temporal resolution of the data) between the stations. Motions of the different stations, although different in magnitude, also show a similar form, characterised by steps in the

cumulative horizontal displacement over time (Figure 5.76). In detail, these steps typically have an open 'S'-shaped form representing initial rapid motion, followed by a period of constant or steady motion and then by an rapid decrease in motion, and are similar in form to the 'accelerated-creep' motions derived from the more recent monitoring of the landslide using CGPS, however, the recorded historical events are larger in magnitude. Each historical event typically lasts about 3 to 6 months (the temporal resolution of the historical monitoring was about 1 survey every 3 months). These more rapid periods of displacement are separated by longer duration slower motion, typically lasting 6 months or more, along with periods of rest.

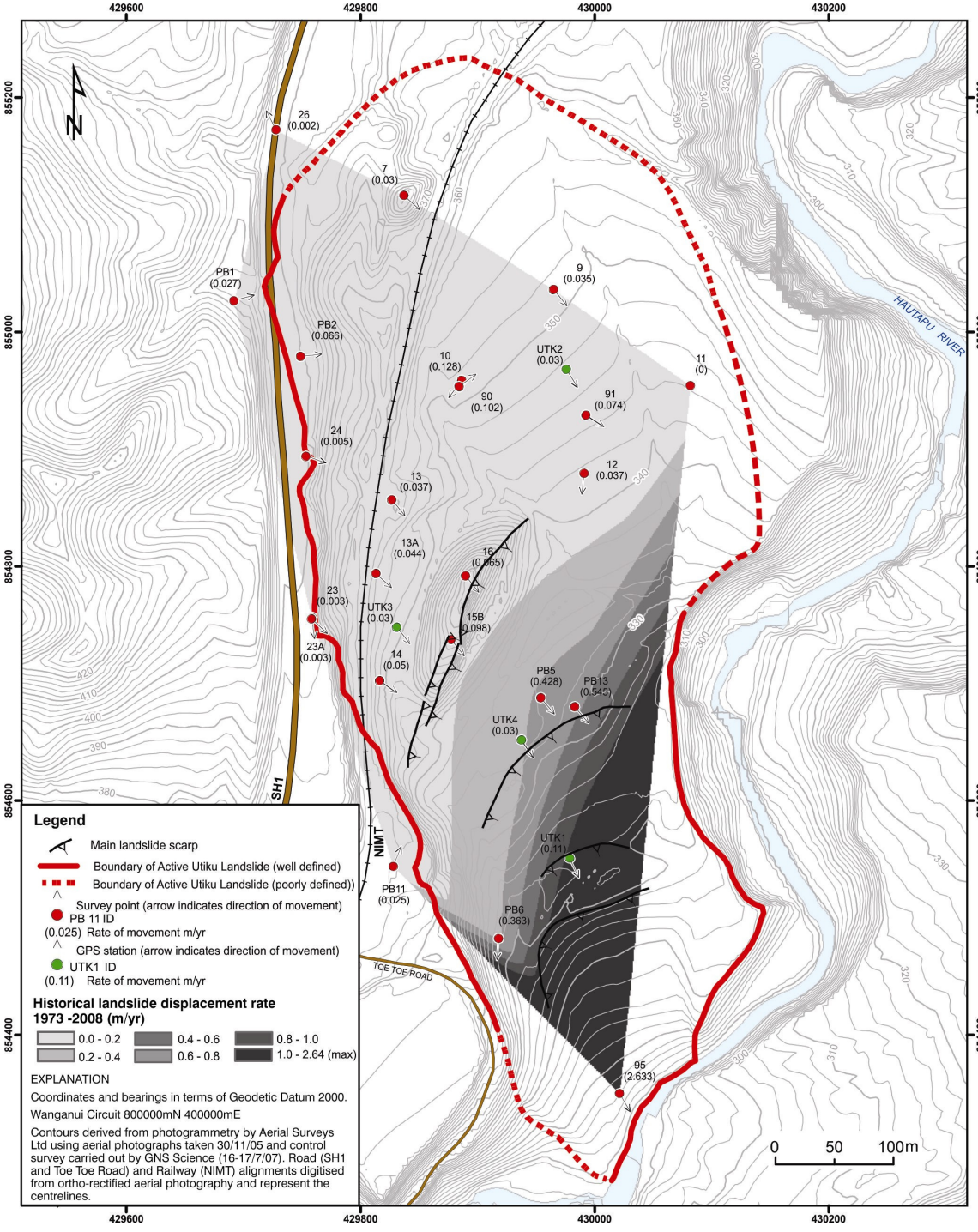

Figure 5.75 Post 1972 displacements of the historical survey marks. Displacements calculated using the least squares method on the cumulative horizontal displacements.

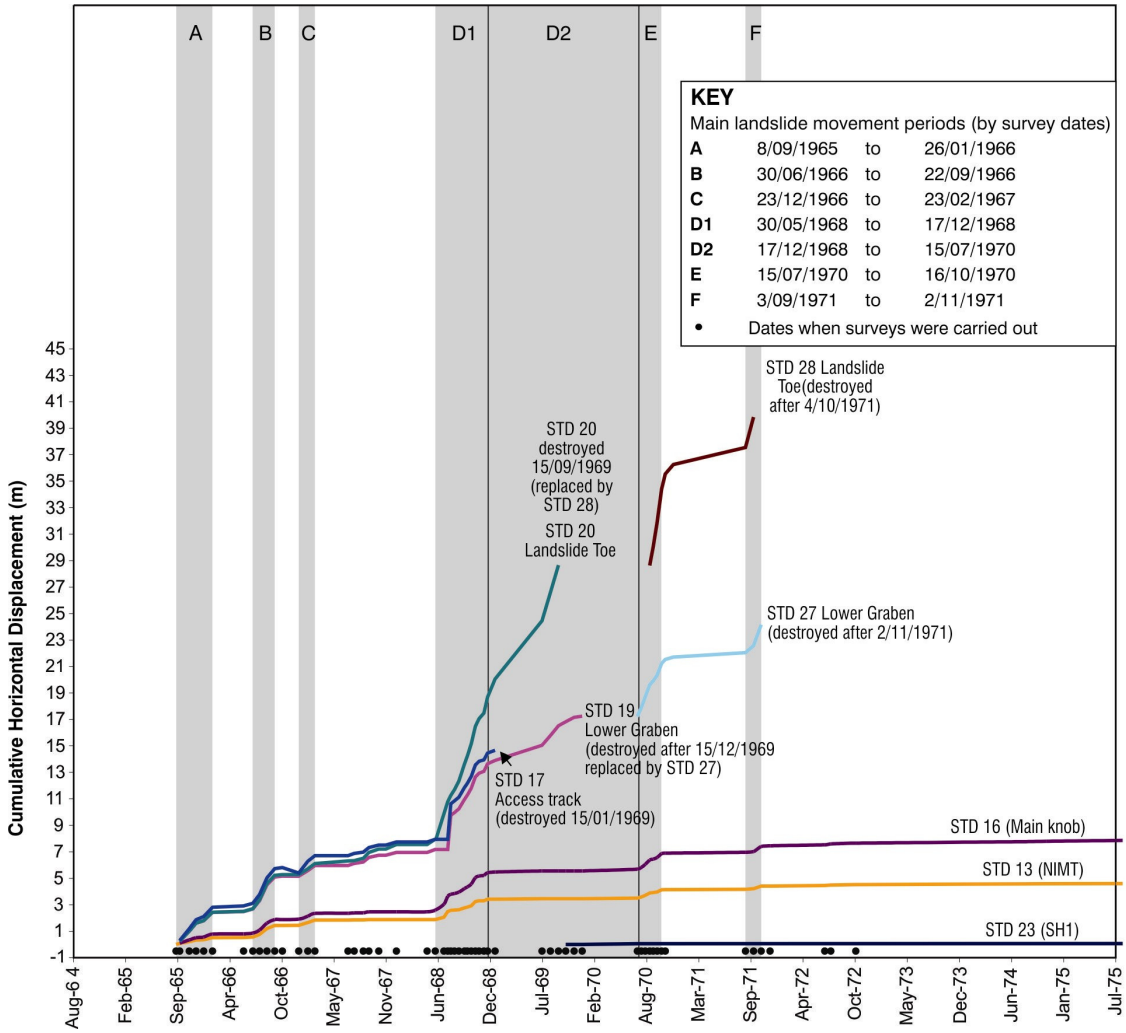

Figure 5.76 Pre 1972 horizontal cumulative displacements of selected survey marks plotted along their main motion bearings, derived from the least-squares analysis. Locations of the survey marks are shown on Figure 3.07.

From January 1973 to the start of the continuous monitoring (July 2008), motions appear to be that of long-duration slower motions, however, this interpretation is probably a function of the temporal resolution of the monitoring, as there was no monitoring between 1978 and 1995. It is possible that motion of the landslide during this period comprised multiple, short duration, larger magnitude movement events, similar in form, but of smaller magnitude and lower frequency to those recorded pre-1973.

The trigger for the 1965 to 1972 period of increased displacement is thought to have been rainfall. Rainfall data from the Taihape gauge has been plotted as the cumulative deviation from mean rainfall, and is shown against the historical horizontal displacements (Figure 5.77). This plot indicates that the large-magnitude accelerated-creep events correspond to a period when rainfalls were typically greater than mean. Conversely, since 1973 rainfalls have typically been less than mean values. The current positive trend of the rainfall-deviation plot suggests rainfalls are now typically greater

than mean values, but they are still not representative of the pre-1972 trends. Pore-pressure data from 1969, during the main period of historical accelerated creep, show that pore pressures during this period of increased rainfall were higher than those currently being recorded.

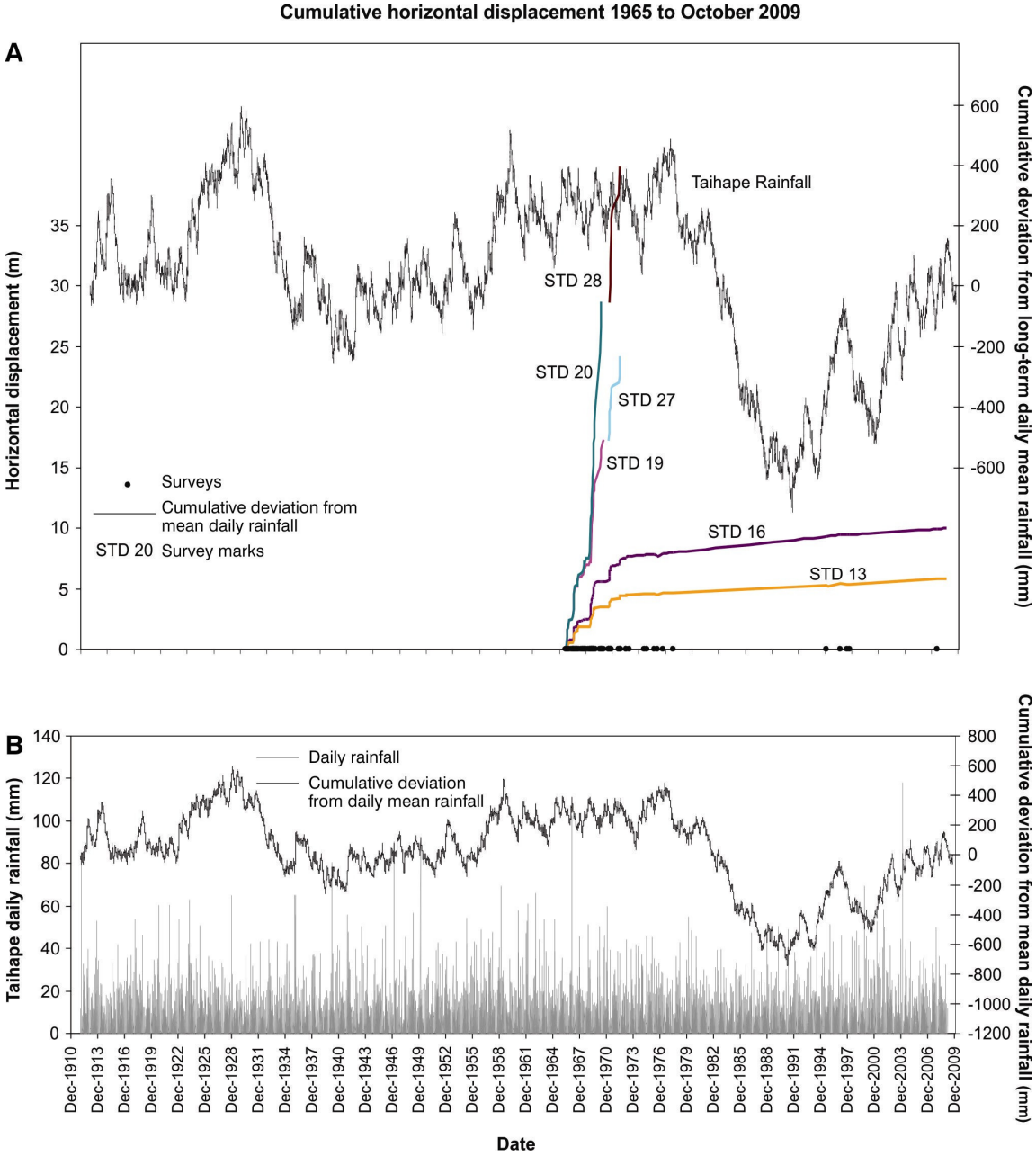

Figure 5.77 Historical displacements and rainfall. A: Cumulative horizontal displacements of selected survey marks plotted along their main motion bearing. B: Daily and cumulative deviation from the daily mean rainfall calculated from daily rainfalls recorded at the Rangitikei District Council gauge at Taihape.

Pre-historic landslide motion can be indirectly assessed using results from radiocarbon dating. The bottom and top of peat material sampled from BH3, located in the main graben in the upper landslide, behind (west) of the large knob of intact-displaced material were dated. The dates indicate a 1,879 ±35 yr age difference from the bottom (2,186 ±20 BP), to the top (307 ±30 BP), of the peat BP. If it's assumed that the graben

developed in response to the displacement of the knob from the current landslide head scarp, then the total displacement of the knob is about 130 m, calculated along a similar movement bearing to the historical one for this area. This suggests a mean displacement rate of about 0.07 m/year, which is similar to the post-1973 rates, but less than the 1965 to 1972 rates, which were about 0.6 m/year. Although care must be exercised when interpreting the rates derived from the radiocarbon dating, they would indicate that periods of rapid displacement, such as the one recorded between 1965 and 1972 either do not occur frequently, or are relatively short in duration.

5.4.1.2 Comparison of historical and recent horizontal motion

The motion magnitudes and bearings recorded by the CGPS stations are shown in Table 5.37 along with details of the historical motions from Table 5.36. The mean rates and directions of motion recorded between December 1973 and July 2008 are comparable to the mean rates recorded by the recent continuous monitoring, although the rates for the lower landslide are slightly higher. The changes in the motion rates with geomorphological position are also consistent, indicating motions increase from the upper to the lower landslide, accompanied by a rotation in motion bearing of about 30°.

Table 5.37 Comparison of historical and recent horizontal surface motion (Utiku)

Landslide location	Geomorphic position	Mean horizontal movement (m/year) and survey mark where recorded in brackets			Mean movement bearing (°)	
		Pre-1973	1973 to 2008	2008 to 2009	Pre-Jul 2008	Post-Jul 2008
Lower landslide	Toe (Hautapu)	6.57 (20 & 28)	2.63 (95)	0.87 (95)[1]	161	170
	Head	4.04 (19)	0.55 (PB13)	0.11 (UTK1)	147	155
Upper landslide	Toe	1.05 (16)	0.07 (16)	0.03 (UTK4)	143	146
	Head (NIMT)	0.62 (13)	0.04 (13)	0.03 (UTK3)	134	142

[1]Data calculated for historical survey mark 95, for the period September 2008 to September 2009.

Three main patterns of motion have been identified from the recent monitoring; accelerated-, slow- and vertical-creep. It has not been possible to resolve periods of vertical creep from the historical data as the temporal resolution of the data are poor. Accelerated creep motions, however, can be adequately resolved from the historical data, and like the recently recorded periods of accelerated creep are responsible for most of the recorded motion.

5.4.1.3 Vertical motion

There is only limited historical data available on vertical motion for some of the survey marks on the landside, these have been summarised in Table 5.38. The results show a similar trend to the horizontal motions, where motions increase towards the toe and

where recent motions are about similar to the post-1973 motions.

Table 5.38 Comparison of historical and recent vertical surface motion (Utiku)

Landslide location	Selected survey marks	Mean vertical surface movement (m/year), survey marks shown in brackets[1]		
		Pre-1973	1973 to 2008	2008 to 2009
Lower landslide	Toe	1.3 (28)	0.4 (95)	0.05 (95)[1]
	Crest	0.2 (18)	No data	0.03 (UTK1)
Upper landslide	Toe	No data	No data	0.01 (UTK4)
	Crest	0.07 (13)	0.01 (13)	0.02 (UTK2)

[1] Survey mark locations are shown on Figure 3.07.

5.4.2 Taihape landslide

5.4.2.1 Horizontal motion

Landslide motions historically were recorded using a survey network established on the landslide in February 1985. This survey network originally comprised 16 survey pegs, which changed over time as some pegs were lost and others were added. Thirteen surveys of this network were completed between 1985 and 2008 with an average of 1 survey every 2 years, although there are intervals of up to 5 years between some surveys. Only northing and easting coordinate values are available because no historical levelling data were collected.

The horizontal motions and bearings of the survey pegs, derived from least-squares adjustment, have been modelled (Figure 5.78). The model data show that the most active part of the landslide has been the toe area, south of Kaka Road, and that much of the landslide, outside of this area, has shown no movement outside of error. For those survey pegs on the active landslide, motion bearings are consistently in a down-slope south-southeast direction. For comparison purposes the motion vectors derived from the recent monitoring are also shown on Figure 5.78, which indicate that the recently active area is comparable to the historically active one.

The timing of the motions, for selected survey pegs are shown on Figure 5.79, where the cumulative horizontal displacements of several survey pegs have been plotted along their main motion bearing. The historical displacement over time plot for survey mark INC CS (Figure 3.16), which is the only consistently monitored survey peg located in the landslide toe, indicates two main periods of motion the first between April 1988 and August 1993 and the second between April 2004 and October 2005. The more recent event was also recorded by several other survey pegs, which were installed on the landslide toe in October 2000. These two periods represent about 100 mm of total horizontal displacement per event. A summary of motion from the historical monitoring

can be found in Table 5.39.

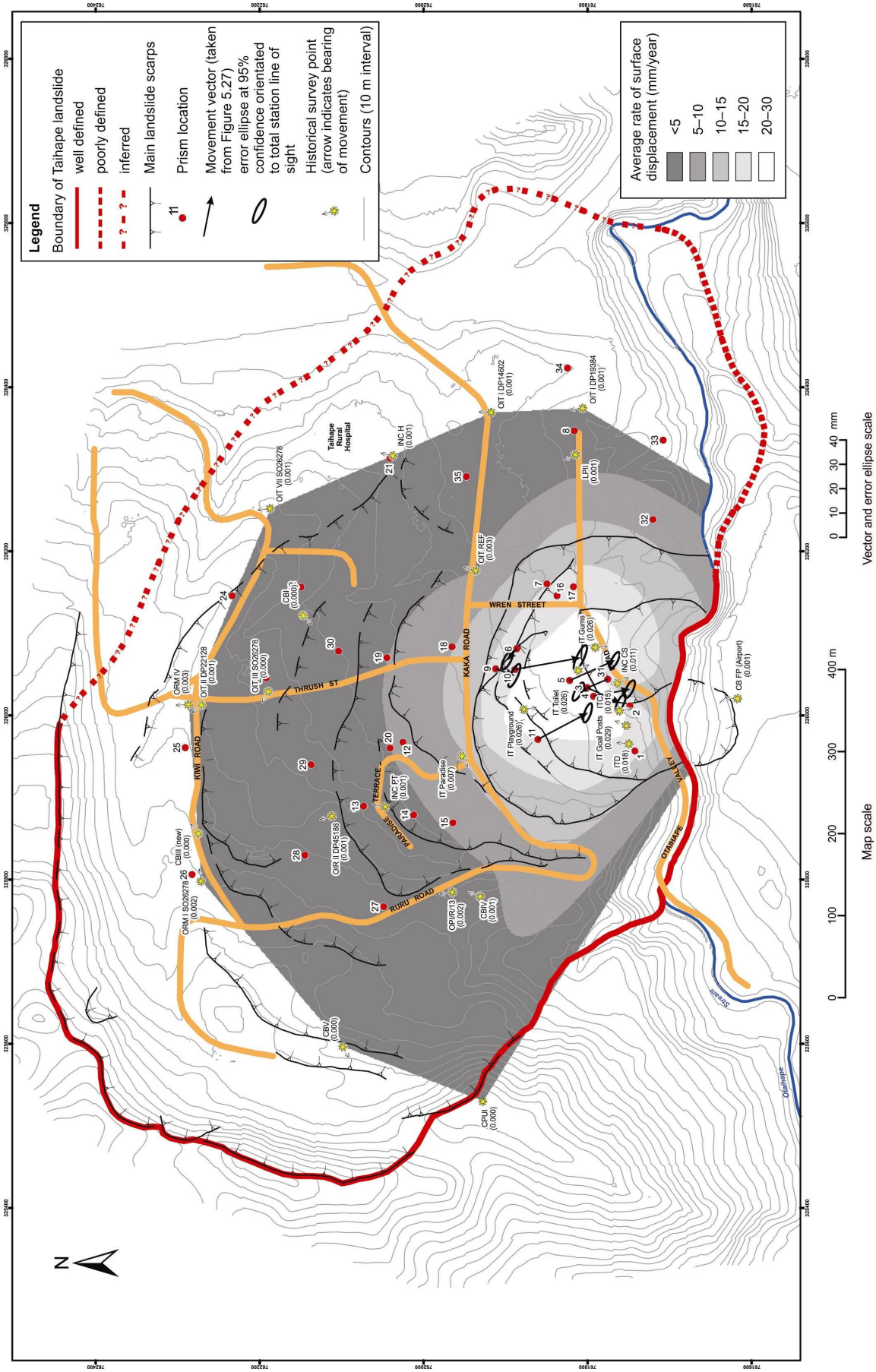

Figure 5.78 Historical horizontal displacements of selected survey pegs plotted along their main motion bearings for the Taihape landslide.

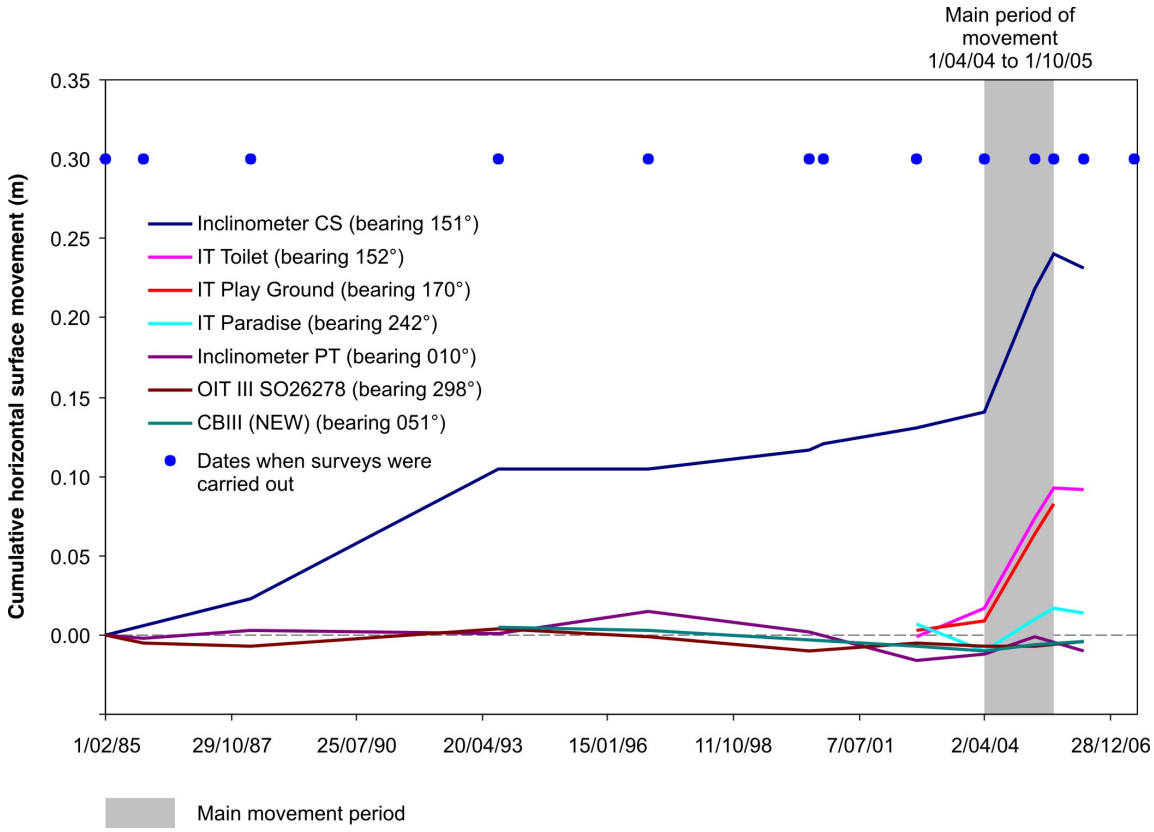

Figure 5.79 Historical cumulative horizontal displacements over time (1985 to 2006) of selected survey pegs on the Taihape landslide plotted along their main motion bearings.

Table 5.39. Summary of historical surface motion (Taihape)

Survey mark	Location	No. Days installed	Total surface movement (mm)	Average surface movement (mm/year)	Movement bearing (°)
INC CS	Lower Toe	8185	246	11	151
IT Toilet	Lower Toe	2464	172	26	152
IT Gums	Lower Toe	1826	128	26	177
IT Playground	Upper Toe	1826	128	26	170
IT Paradise	Central	2464	49	7	242
INC PT	Central	8185	33	1	10
OIT III	Central	8185	6	0	298
CBIII NEW	Upper	7030	7	0	51

Historical motion can be classed as very slow to extremely slow (Cruden and Varnes, 1996). However, the rates of creep vary through time as well as location on the landslide, indicating that the landslide is intermittently creeping. The largest monitored landslide motion occurred between April 2004 and October 2005, movement rates have since decreased. This movement event represents a step in the cumulative displacement time-series plot, however, the temporal resolution of the monitoring is poor and so the start and end dates for this event are a function of survey frequency

(Table 5.40).

Table 5.40. Summary of horizontal surface motion for the main movement period (April 2004 to October 2005) (Taihape)

Survey mark	INC CS	IT Toilet	IT Playground	IT Paradise	INC PT
Mean velocity (mm/day)	0.20	0.10	0.10	0.04	0.03
No. Days	791	791	791	791	791
Total displacement (mm)	160	80	80	30	20

Landslide movement prior to February 1985 is documented in a report by the Rangitikei-Wanganui Catchment Board and Regional Water Board (Johnston, 1983), however, no quantitative monitoring data are available. These older anecdotal accounts when combined with the more recent quantified data (from the historical survey network), indicate periods of increased landslide motion appear to recur about once every 30 years.

The timing of the main movement event has been compared with the record of rainfall at the Taihape rain gauge. Figure 5.80 is an extract from the daily rainfall and cumulative deviation from the mean daily rainfall shown in Figure 5.77, plotted with the cumulative horizontal displacements of selected survey marks on the Taihape landslide shown on Figure 5.79. The 2004-2005 movement event follows a major storm, locally referred to as the Manawatu storm, which occurred around 15th February 2004, and had an estimated, return period of 100 years (Horizons, 2004). In this storm 118 mm of rain was recorded at Taihape on 16/02/2004, which was the largest daily rainfall recorded at Taihape since formal records began in 1912. This daily rainfall has an annual exceedence probability of about 1% (once every 100 years), and occurred during a period when the annual rainfalls were greater than mean values, shown by a positive trend of the cumulative deviation from daily mean rainfall. It is interesting to note that the main period of displacement occurred about two months after the Manawatu storm, indicating a delayed landslide response to this event. However, this delay may be related to the gradual loss of toe support caused by increased stream erosion in response to the flooding relating to this event. This flooding washed away several sections of Otaihape Road, at the toe of the landslide (Figure 5.81).

Other wetter periods, when rainfalls were typically greater than mean, are apparent in the historical rainfall records. These occurred between 1920 and 1930 and 1965 and 1980, and approximately coincide with periods when damage to housing and infrastructure on the landslide were reported (Johnston, 1983).

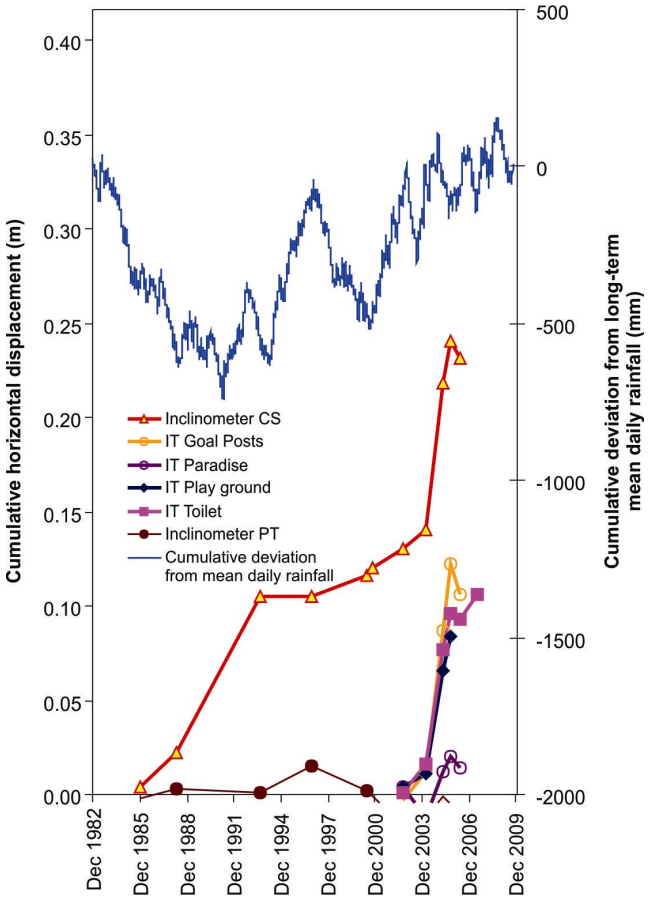

Figure 5.80 Historical displacements and rainfall, Taihape. Cumulative horizontal displacements of selected survey marks (locations shown on Figure 3.16) plotted along their main motion bearing with the cumulative deviation from the daily mean rainfall calculated from daily rainfalls recorded at the Rangitikei District Council gauge at Taihape.

Figure 5.81 Aerial photograph showing toe erosion at the Taihape landslide following the 2004 Manawatu storm (source: New Zealand Aerial Mapping).

5.4.2.2 Comparison of historical and recent horizontal motion

For comparison purposes, a summary of the motion magnitudes and bearings recorded by the prisms are shown in Table 5.41 along with a summary of the historical motions.

Table 5.41 Comparison of historical and recent horizontal surface motion (Taihape)

Landslide location	Mean horizontal movement (mm/year)		Mean movement bearing (°)	
	1985 to 2006	2006 to 2009	1985 to 2006	2006 to 2009
Lower Toe	26	6	167	169
Upper Toe	26	8	167	170
Central	7	0	242	0
Head	0	0	0	0

The historical mean movement rates were larger than those recently recorded by the prisms, but are dominated by the main monitored period of movement between April 2004 and October 2005. The bearings of motion are consistent between the historical

and recent motions, and the rates of motion indicate a general increase towards the toe. Historically, motions of the central part of the landslide have been recorded, but the recent monitoring shows no motion of this area. The recent high resolution monitoring has allowed three main patterns of motion to be resolved: accelerated-, slow- and vertical-creep.

5.5 Numerical modelling

Numerical modelling has been undertaken to check that the residual shear-strength of the clays forming the slip surfaces of the Utiku and Taihape landslides derived from the laboratory testing of slip surface material, and from the literature (Chapter 4), are correct and appropriate and that the monitored pore pressures and calculated stresses are representative. Modelling was carried out using both limit equilibrium (LE) and finite element (FE) software. For the LE modelling, the method of Morgenstern and Price (1965) was used to ensure that all equilibrium and boundary conditions were satisfied.

5.5.1 Utiku landslide

For Utiku two scenarios were back-analysed: 1) the mean maximum piezometric-head levels recorded prior to the onset of accelerated creep-movement periods 1, 2 and 3, assuming they represent the levels when the landslide was at its limit of equilibrium (factor of safety ~1), which are referred to as base levels; and 2) the mean maximum piezometric-head levels recorded during the accelerated-creep movement periods, this was done to make sure that the factor of safety dropped below 1.0, indicating instability. The FE models were calibrated using the mean surface displacements recorded from the CGPS equipment during accelerated creep periods 1 to 3. Although the landslide mechanism is that of a wedge and therefore truly a 3-D problem, two 2-D sections were analysed: section A-A' representing the upper landslide, and B-B' the lower landslide (Figure 3.08), which are both parallel to the main directions of landslide displacement in these areas and therefore account for the change in motion direction down the landslide. A fully specified slip surface function was used as the slide surface is well defined from drill holes and inclinometer monitoring. Additional pressure from water-filled tension cracks located at each major head scarp (boundary between the various slide blocks), were included in the analyses. It has been assumed that the piezometric levels equate to pore-pressures recorded along the slide surface.

The sensitivity of the landslide to changes in: a) cohesion (c') and friction (ϕ') of the landslide debris; and b) the residual friction angle (ϕ_r') of the slide-surface clay, were assessed using the parameters from laboratory testing as the initial inputs for the models (Table 3.04). For the landslide debris shear strength parameters were adopted

based on the consolidated undrained triaxial tests carried out on the intact displaced rafts of sandstone from the Taihape landslide (Table 3.07). These gave mean parameters of c' = 35 ±(5) kPa and ϕ' = 37° ±(8). Results using these mean parameters show that a change in ϕ' of 1° = 0.5% change in the factor of safety, and a change in c' of 1 kPa = 0.2% change in the factor of safety, indicating stability is not controlled by the strength of the debris overlying the slide surface.

For the slide-surface clay the mean parameters of ϕ_r' = 8.3° ±(1.0) and c' = 0 kPa, were used. A change in ϕ_r' = 1° causes a 15% change in the factor of safety, indicating the stability of the landslide is extremely sensitive to changes in ϕ_r' of the clay, which is expected given the low-angle slide surface. However, back-analysis using pore pressure conditions relating to scenario 2 indicate that to achieve a factor of safety < 1.0 a ϕ_r' = 8° for the slide-surface clay is required.

There are implications associated with using 2-D analysis techniques for the Utiku landslide, as the shear resistance which would be mobilised along the landslides western boundary cannot be taken into account. As a result the shear strength parameters adopted for the slide-surface clay in the 2-D analyses are likely to be over estimated. The influence of the western boundary on the shear resistance has been estimated using wedge-stability software SWEDGE™. The material strength parameters adopted for the western flank are the same as those for the remoulded debris in the toe of the landslide where c' = 0 kPa and ϕ_r' = 28° ±(5°), assuming the material is at residual strength. All other parameters are the same as those adopted for the 2-D LE analysis. Base level pore-pressure conditions were also adopted. Results show a reduction in the shear stress (increase in the factor of safety) of about 13% ±(4), which would have the effect of reducing the ϕ_r' of the slide surface clay from 8° to about 7°.

Analyses of the sensitivity of the landslide to changes in piezometric head levels above and below the base levels was carried out for Sections A-A' and B-B' assuming ϕ_r' = 8° for the slide-surface clay.

5.5.1.1 Upper landslide

The LE analysis shows that the landslide factor of safety, when the piezometric levels are at base level, is about 1.03, (Table 5.42). The analyses also indicate that the factor of safety of the different slide-blocks decreases upslope (north) from the toe (Figure 5.82), indicating the upper landslide is being driven from the crest by what must be near vertical displacement of the upper slide block (around the picnic area), which is pushing the other slide-blocks down slope.

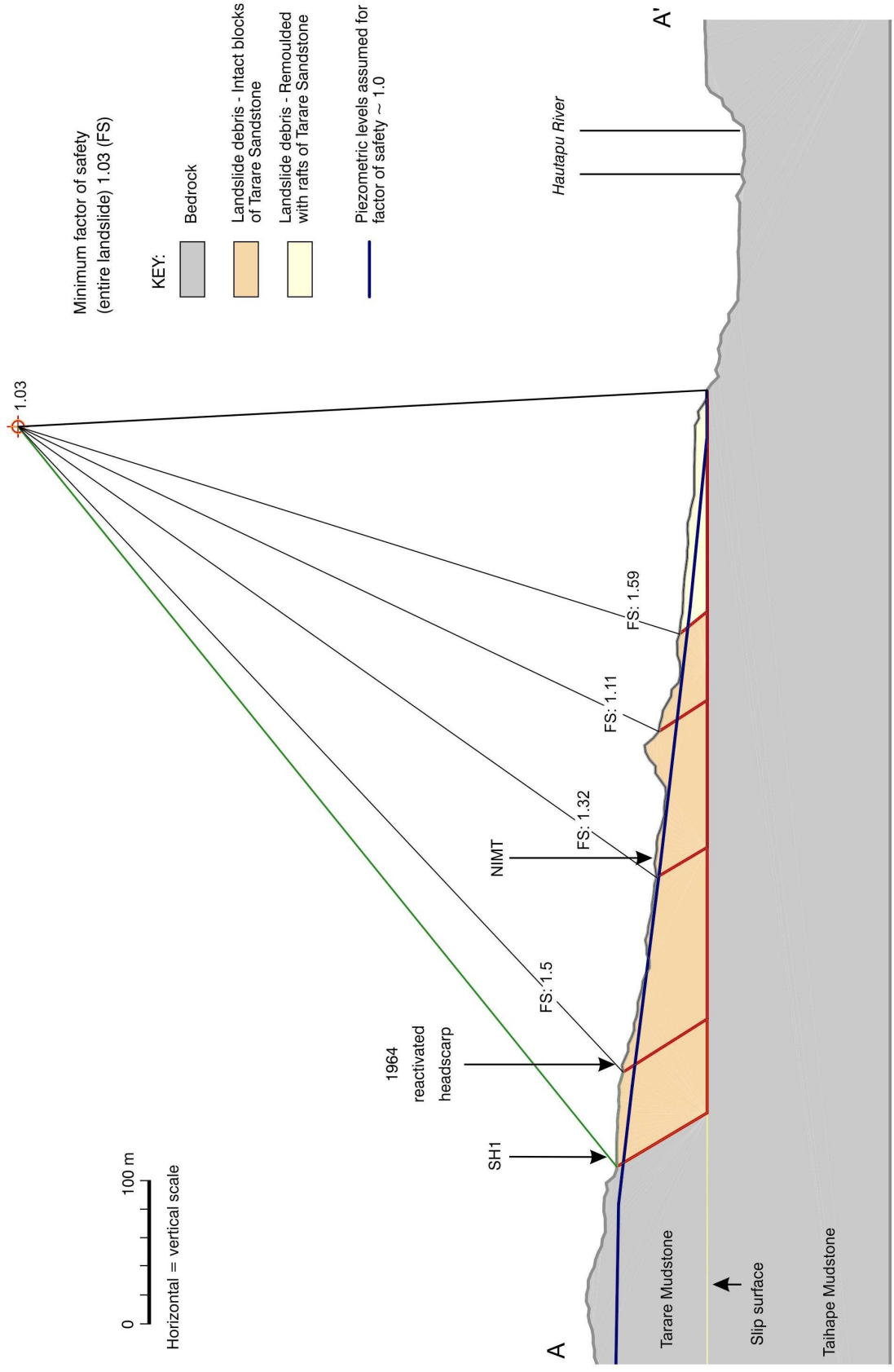

Figure 5.82 Limit equilibrium stability analyses for the upper Utiku landslide Section A-A', Figure 3.08.

Results from the sensitivity analyses indicate that the factor of safety decreases in response to increases in piezometric head levels and that for 1 m changes in piezometric levels, relative to base levels, the factor of safety changes by approximately 3% to 4%, confirming that the landslide is sensitive to relatively small changes in piezometric levels.

Table 5.42. Section A-A' results from the stability analysis

Piezometric levels (at locations of the monitoring points) (m AMSL)					Factor of safety SLIDE	Factor of safety PHASE
Level	BH1	UTK3	UTK4	UTK1[2]	GLE method	SSR
0.0 (base levels)	369.3	349.1	328.4	316.3	1.03	1.03
Max recorded during movement periods	370.8	350.2[1]	329.0	316.6	0.99	0.99
Sensitivity analyses with respect to base level conditions						
- 1.0	368.3	348.1	327.4		1.06	1.06
- 2.0	367.3	347.1	326.4	316.0	1.09	1.08
- 3.0	366.3	346.1	325.4		1.11	1.11
+ 1.0	370.3	350.1	329.4	317.3	0.99	0.99
+ 2.0	371.3	351.1	330.4	318.3	0.97	0.97
+ 3.0	372.3	352.1	331.4	319.3	0.94	0.94

[1]Piezometric levels for BH3 are for movement period 3 only
[2]Piezometric levels for UTK1 (PZA) used in the stability model take into account the offset and elevation difference between UTK1 and Section line A-A', with 316.0 m RL being the lowest piezometric level used, as this corresponds to the elevation of the landslide slip surface

5.5.1.2 Lower landslide

Section B-B' (Figure 3.08) represents the lower part of the landslide, including the toe at the Hautapu River, and is the most active and disturbed part. There is a lack of piezometric data in this area, as PZA is the only groundwater monitoring point in the lower landslide. Piezometric levels below UTK1 have been inferred from site observations and from the general piezometric trends. Limit equilibrium results (Table 5.43) show that the landslide factor of safety decreases towards the toe, which is related to the ability of the landslide mass to translate down dip along the clay layer rather than along its strike, as the upper landslide, but also reflects the modification of the landslide toe by the Hautapu River (Figure 5.83). The apparent dip of the landslide slip surface along the movement direction is approximately 3°, compared to the slip surface in the upper part of the landslide, which is about 1°. The sensitivity analyses indicate that the factor of safety decreases in response to increases in piezometric head levels, where 1 m changes in piezometric levels, relative to base levels, relate to about 4% change in the factor of safety (Table 5.43).

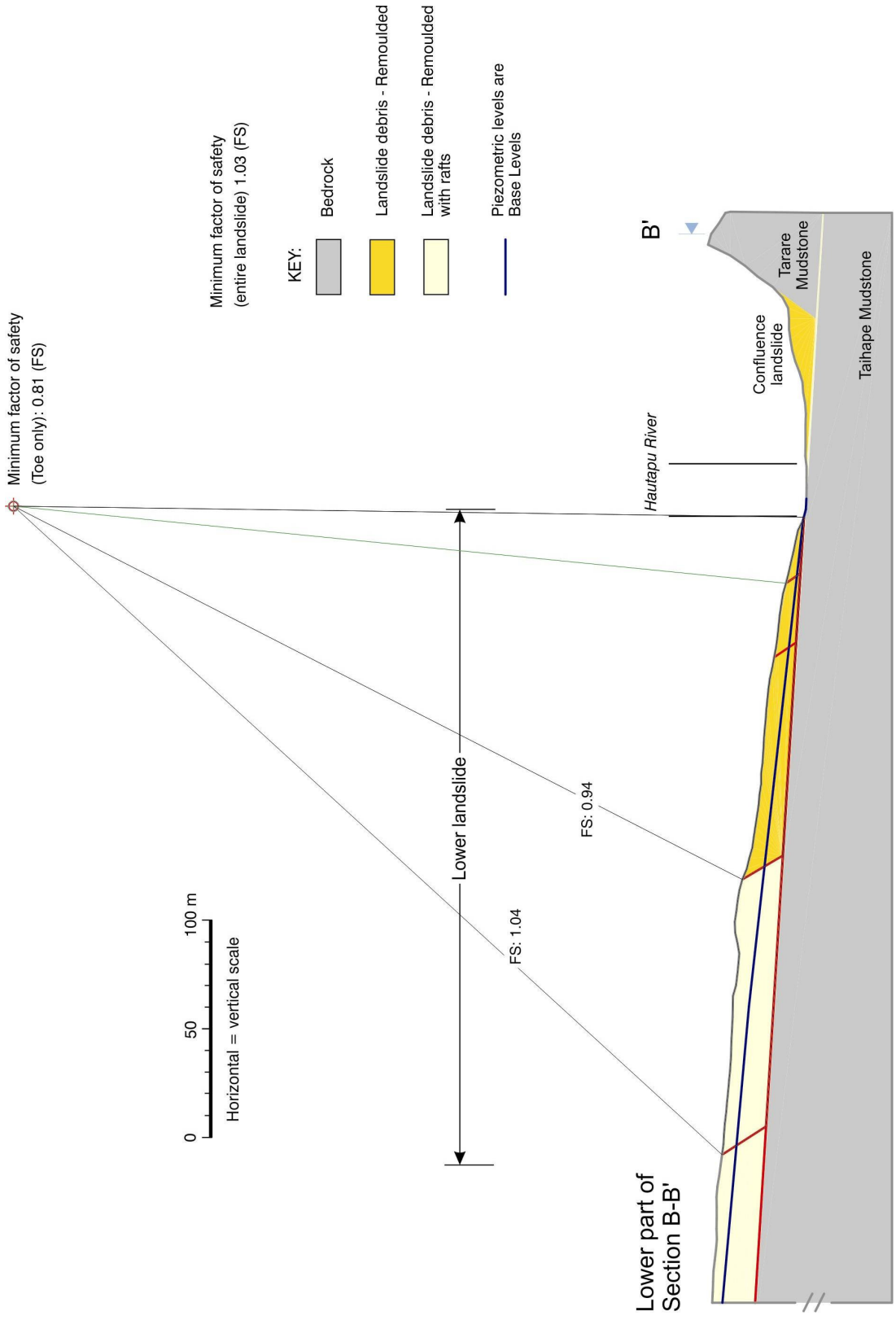

Figure 5.83 Limit equilibrium stability analyses for the lower Utiku landslide Section B-B', Figure 3.08.

Table 5.43. Section B-B' results from the stability analysis

Piezometric level (at locations of the monitoring points) (m AMSL)			Factor of safety lower landslide	Factor of safety toe area only (remoulded materials)
Level	UTK4	UTK1	SLIDE GLE method	
0.0 (base levels)	328.4	316.0	1.03	0.94
Max recorded during movement periods	329.0	316.5	0.99	0.91
Sensitivity analyses with respect to base level conditions				
- 1.0	327.4	315.0	1.07	0.97
- 2.0	326.4	314.0	1.11	1.00
- 3.0	325.4	313.0	1.14	1.02
+ 1.0	329.4	317.0	1.00	0.91
+ 2.0	330.4	318.0	0.96	0.88
+ 3.0	331.4	319.0	0.92	0.86

5.5.1.3 Modelled displacements

Finite element analyses for section A-A' (Figure 3.08) was carried out to back-analyse landslide displacements in response to changes in piezometric levels, using the mean displacements and levels recorded during movement periods 1 and 3 (from Table 5.44).

Table 5.44 Modelled and recorded landslide motion, Section A-A'

Piezometric levels	Modelled horizontal landslide displacements (mm) (at locations of monitoring points)			
	BH1A[1]	UTK3	UTK4	UTK1
0 (base level)	0.0	0.0	0.0	0.0
Mean maximum piezometric levels recorded at each piezometer during accelerated creep movement periods 1 and 3	5	10	10	10
	Recorded mean displacements (mm)			
	5	9	8	9

[1]Displacements calculated from the inclinometer installed in BH1A

Considering the inaccuracies in the models and techniques used, modelled total displacements at ground level are consistent with the mean motions recorded during movement periods 1 and 3, indicating that the adopted parameters, monitored pore pressures and calculated stresses are representative of the conditions within the landslide. The shear strains calculated by the FE model, show that during movement periods 1 and 3 the upper slide-block (around the picnic area), does indeed form an active wedge as the displacement vectors show this area subsiding, with the vectors further down slope being consistent with a translational mechanism, parallel to the slide surface (Figure 5.85). No CGPS monitoring of this upper slide-block has been undertaken to confirm this, although the patterns of cracking do indicate some parts of this area are subsiding, particularly State Highway 1. Therefore, in summary, the results from the LE and FE modelling show that displacements are being driven primarily by increases in pore pressure along the slide surface.

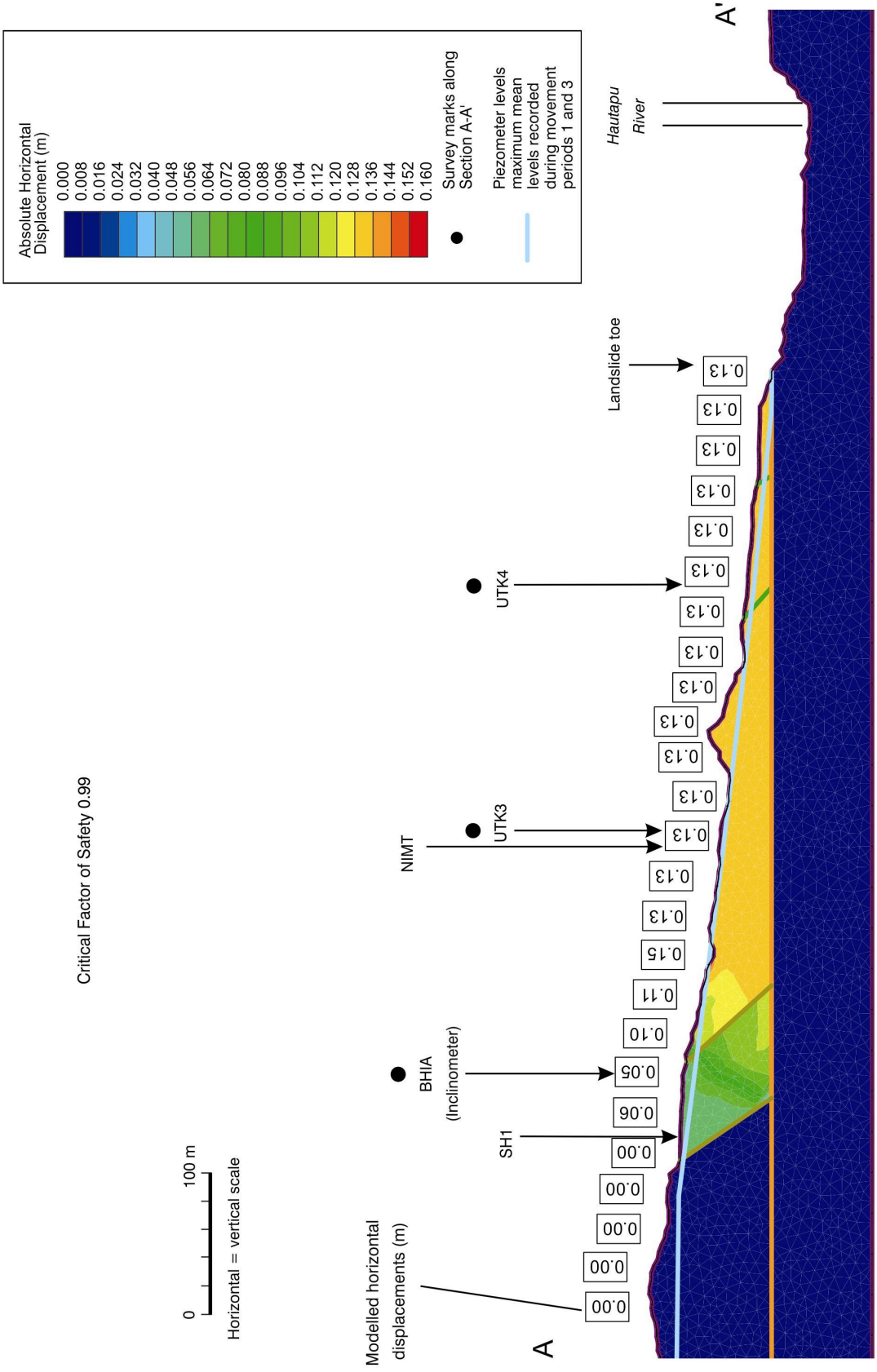
Absolute Horizontal Displacement (m)
0.000
0.008
0.016
0.024
0.032
0.040
0.048
0.056
0.064
0.072
0.080
0.088
0.096
0.104
0.112
0.120
0.128
0.136
0.144
0.152
0.160
Survey marks along Section A-A'
Piezometer levels maximum mean levels recorded during movement periods 1 and 3
Hautapu River
A'
Landslide toe
UTK4
NIMT
UTK3
BHIA
(Inclinometer)
SH1
A
Modelled horizontal displacements (m)
0.00
0.00
0.00
0.00
0.00
0.06
0.05
0.10
0.11
0.15
0.13
0.13
0.13

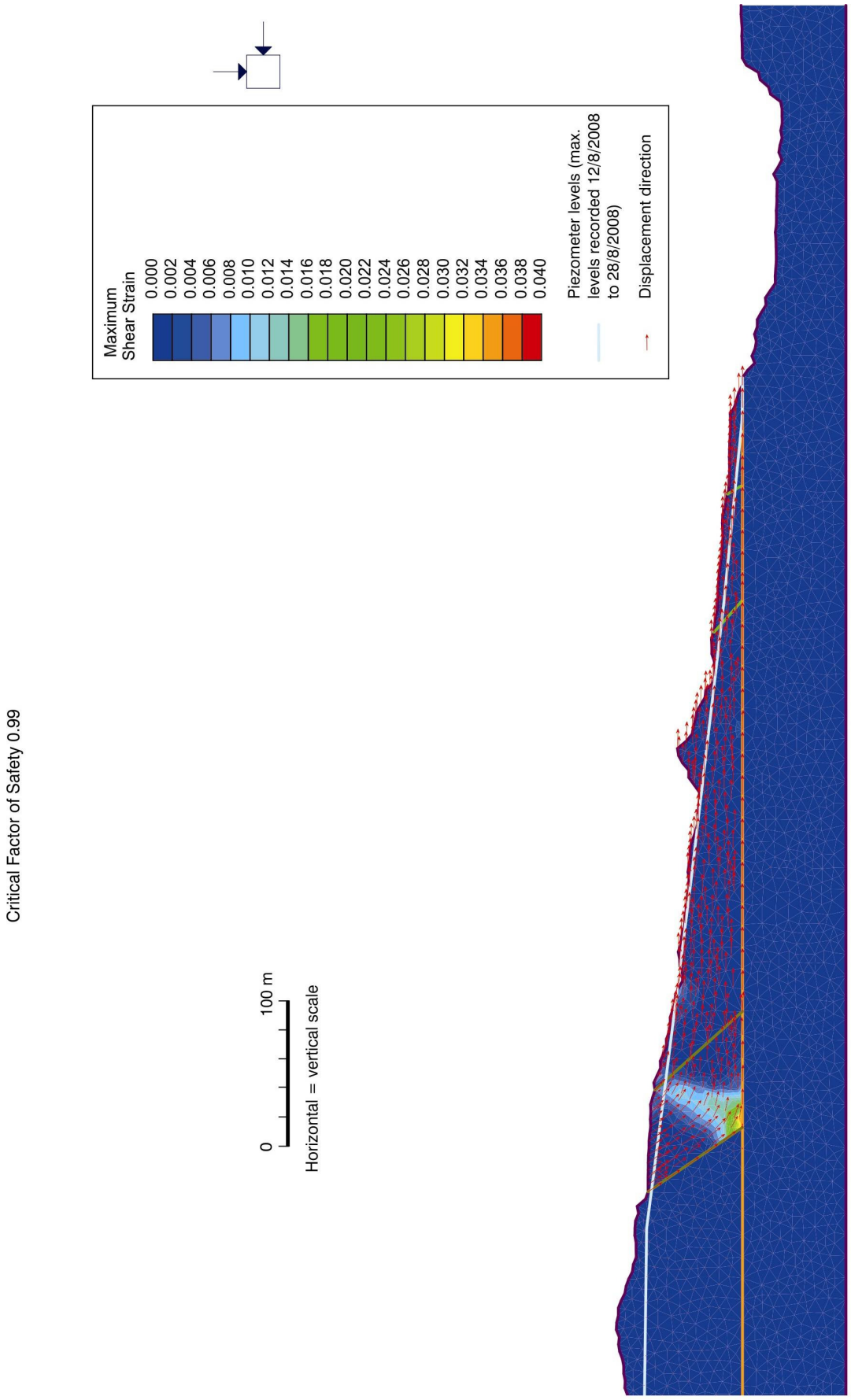

Figure 5.85 Finite element shear strains for the upper Utiku landslide, Section A-A', Figure 3.08.

5.5.2 Taihape landslide

At Taihape stability analyses were undertaken assuming that the landslide factor of safety was below 1.0, and has been below 1.0 for most of the monitoring period as motion recorded at the ground surface and at depth along the slide surface has been slow and steady. As the rate of motion has not varied in response to the recorded pore pressure changes, the mean piezometric levels recorded during the monitoring period were used for the analyses (Table 5.45) referred to as mean levels. Section line A-A' (Figure 3.16) was analysed, which passes through the active toe zone, and the bearing of the section line corresponds to the main direction of landslide movement.

The sensitivity of the landslide to changes in: the residual friction angle (ϕ_r') of the slide-surface clay; and toe unloading caused by drainage line incision were assessed. For the slide-surface clay the mean parameters of ϕ_r' = 8.3°±(1.0) and c' = 0 kPa were adopted as per the Utiku analyses. Results show that a change in ϕ_r' of 1° causes a 10% change in the factor of safety, indicating that like Utiku the stability of the Taihape landslide is extremely sensitive to changes in friction of the clay. However, back-analysis using the maximum and minimum piezometric head levels recorded during the monitoring, assuming the landslide factor of safety = 1.0 at the minimum recorded piezometric head levels, a ϕ_r' = 9° for the slide-surface clay is required.

Table 5.45 Results from the stability analyses (Taihape)

Piezometric head level (m AMSL)						Toe factor of safety SLIDE
Level	BH1A	BH2A	BH3A	BH4A[1]	BH5A[1]	GLE method
0.0 (mean)	444.1	458.9	464.7	485.0	498.3	0.94
- 1.0	443.1	457.9	463.7	485.0	498.3	0.97
+ 1.0	445.1	459.9	465.7	485.0	498.3	0.90
+ 2.0	446.1	460.9	466.7	485.0	498.3	0.87
+ 3.0	447.1	461.9	467.7	485.0	498.3	0.84

[1] Piezometric levels for BH4A and BH5A are assumed to be fixed at mean levels as they are outside the active toe area of the landslide.

The limit equilibrium analysis shows that the factor of safety for the landslide toe, when the piezometric levels are at mean level, is below 1 (Figure 5.86). The analyses also indicate that the factor of safety of the lower toe slide-block is higher than the upper toe-block, indicating the upper toe is buttressed by the lower toe. As expected the sensitivity analyses indicate that the factor of safety decreases in response to increases in piezometric head levels. For 1 m changes in piezometric levels, relative to mean levels, the factor of safety changes by approximately 4%.

It is normally assumed that once the factor of safety drops below 1.0, landslide velocity increases with increasing pore pressure, and this relationship has been found to be non-linear (e.g. Corominas et al., 2005). However, at Taihape landslide velocity has remained steady throughout the monitoring period, even though piezometric head levels have fluctuated in the active toe by about ±1 m from mean levels, which represents an 8% change in the factor of safety. The lack of any relationship suggests that the movement of the Taihape landslide is controlled by another factor, which given the confined nature of the landslide toe, is most likely to be fluvial erosion and loss of toe support. Sensitivity of the model to toe unloading was assessed by systematically lowering the bed of Otaihape Stream by 1.0 m increments (below the current level) while maintaining the current geometry of the stream cross section. The results show that for every 1.0 m of incision the factor of safety reduces by about 5%, confirming the landslide is particularly sensitive to loss of toe support.

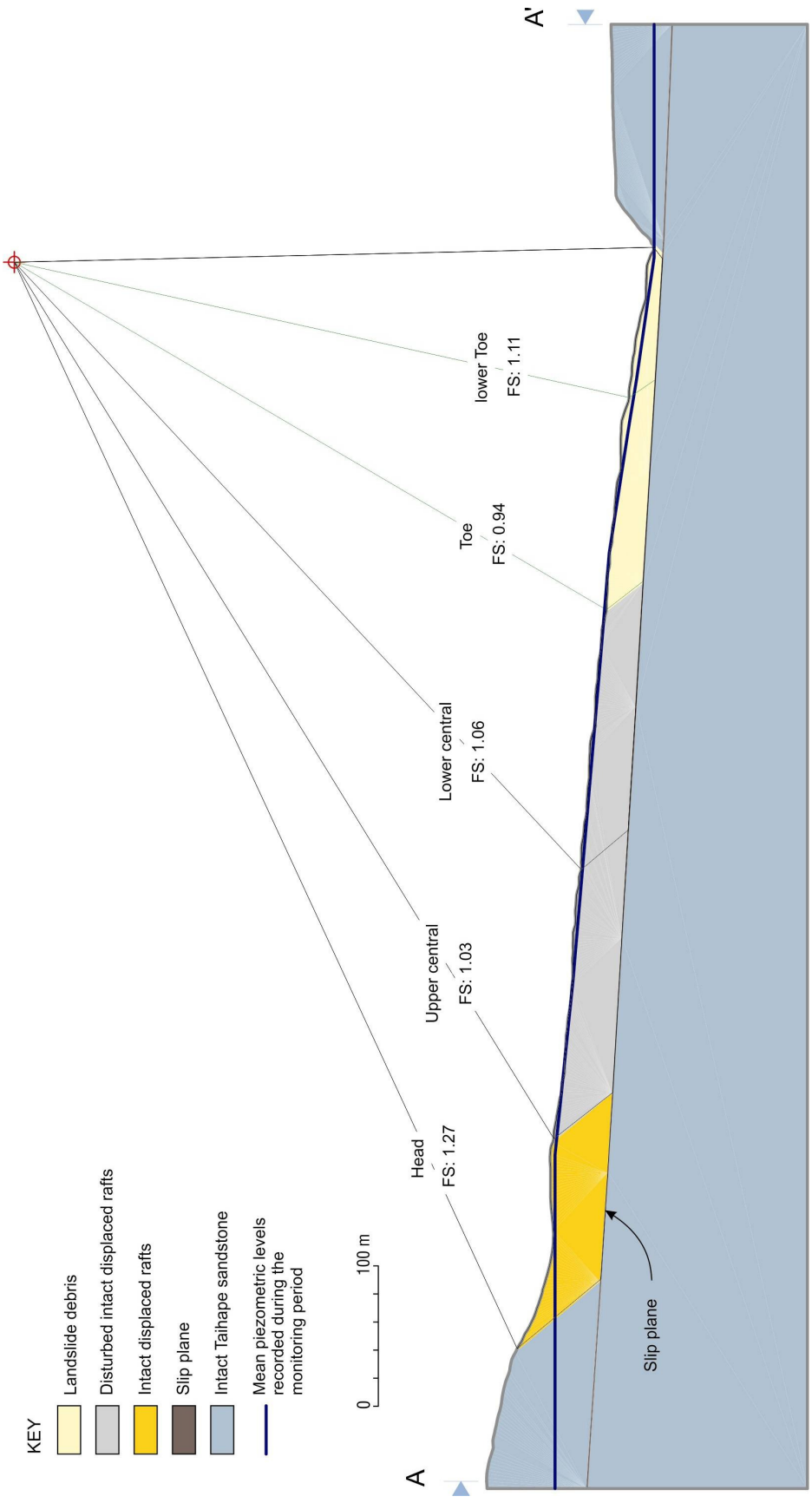

Figure 5.86 Limit equilibrium stability analyses for the Taihape landslide Section A-A', Figure 3.16.

5.6 Summary

The monitoring networks installed on the two landslides have recorded periods of significant landslide motion. The temporal and spatial resolution of the surface monitoring networks, combined with the precision of the equipment, was appropriate to characterise the extremely-slow to very-slow movements of both landslides. With respect to the surface movement, rainfall, pore pressure and earthquake monitoring equipment, the temporal and spatial resolution of this equipment has allowed the periods of surface motion to be related to potential triggering factor(s).

The surface movement patterns of both landslides are similar, with rates that can be classified as extremely slow to very slow (16 mm/yr < x < 1.67 m/yr, Cruden and Varnes, 1996). Horizontal and vertical velocities of the landslides vary over time and are stepped, typically representing periods of acceleration and rest. The cumulative horizontal displacements from both landslides indicate two main types of motion: 1) short-duration, relatively rapid displacement, which typically occur over weeks; and 2) longer-duration slower displacements, at constant gradients, typically lasting many months and years. The short-duration relatively rapid motions have been termed “accelerated creep” and the longer-duration slower motions have been termed “slow creep”. At Taihape, accelerated creep displacements are unrelated to landslide motion, as they relate to periods of upslope and downslope motion, which are cyclic and recur about six-months, and require further consideration. The temporal resolution of the surface monitoring networks indicate that certain parts of these landslides, defined as “slide blocks”, can move at different times and rates independent of one another, indicating that the landslides are translating as series of discrete blocks.

Vertical velocities at both landslides follow a similar pattern to that of the horizontal velocities, i.e. alternating periods of slow acceleration and rest. The longitudinal displacement vector, which represents in two-dimensions the movement angle from the horizontal, has been calculated from the vertical and horizontal motion data, for both landslides. This angle should, in theory, relate to the angle of the slide surface along which the various landslide slide blocks are translating. The angles of the slide surfaces shown in the long sections of the Utiku and Taihape landslides (Chapter 4), are inclined at about 0° to 7° from the horizontal and are much shallower than the long-sectional angles of displacement, and will be further investigated.

The recorded surface and subsurface motion can be correlated, but is made difficult due to the poor temporal resolution of the inclinometer monitoring. At both landslides the inclinometers have recorded shear displacements at depths corresponding to the sheared clay layers, which were identified from the logging of drillholes. The

magnitudes of total displacement are comparable to those recorded at the surface indicating each is translating along a unique slip surface, although surface displacements are consistently larger in magnitude. The surface and subsurface motion data from both landslides supports their geomorphological classification as complex reactivated translational rock slides (Cruden and Varnes, 1996), or block slides (Panet, 1969).

Comparison of landslide motion with earthquake peak ground accelerations (PGA) and river stage levels indicate no correlation for the landslides during the monitoring period. The statistically significant motions recorded during the monitoring period, are primarily influenced by other factors. Daily rainfalls and pore pressures from both landslides have been compared to surface displacement time series. The comparisons indicate that for the Utiku landslide, the main periods of accelerated-creep motion correspond to increases in pore pressure. At Taihape, accelerated-creep motion is seasonal with no net-change in prism position apparent. The upslope and downslope accelerated creep-motion correlates to increasing and falling pore pressure and is possibly unrelated to landside displacement as it is cyclic and will be investigated further. For both landslides, periods of slow creep do not appear to be related to pore-pressure or any other monitored factor.

For both landslides piezometric head levels, calculated from the pore pressures, follow a summer/winter cycle, whereby pore pressures decrease during the drier summer months and increase during the wetter winter months. This is especially true of the Taihape landslide, were the longer monitoring record allows these seasonal cycles to be better observed. Although the summer / winter pore pressure trends are obvious in the records, the changes are relatively small. For the Taihape landslide, the largest deviations from mean pore pressure represent seasonal fluctuations of between 3% and 13% from mean values (31 kPa), and for the Utiku landslide between 3% and 6% from mean values (29 kPa). These indicate that Piezometric head levels are close to ground level for many months of the year, but can exceed ground level (i.e. become artesian) during the wetter winter months.

The relationship between rainfall and pore pressure is an important factor to assess, as pore pressures in general are assumed to be driven by rainfall. The daily (day-to-day) changes in pore pressure at both landslides are not fast, between ±1 kPa (Utiku) and ±1.3 kPa (Taihape), based on the standard deviation of the mean pore pressures recorded by the piezometers, and the gradients of the rising pore pressure limbs are typically between 0.1 to 0.2 kPa/day for both landslides. Results from the correlation analysis show that for both landslides the correlation is highest for antecedent rainfalls

accumulated over 10 to 15 weeks, indicating that pore pressures respond to long periods of antecedent rainfall. These results imply that pore-pressure responses, including those that triggered the accelerated-creep motion (at Utiku), are a result of long periods of wet weather rather than large magnitude short-duration rainfalls. Further consideration of these relationships is needed.

The numerical modelling confirms that the assumed landslide geometries, material parameters, pore pressures and displacements derived from the monitoring are appropriate and representative of landslide conditions. The modelling also shows that for the Utiku landslide it is increases in pore pressure that are driving displacement of the landslide along the slide surface. For the Taihape landslide the modelling infers that drainage line incision is controlling displacement along the slide surface, as the upper toe slide block is less stable than the lower toe slide block, with the confined lower toe acting as a buttress.

CHAPTER 6 DISCUSSION

This chapter discusses the significance of slow, reactivated landslides and compares the monitoring systems installed at the Utiku and Taihape landslides with other comparable systems detailed in the scientific literature. This is followed by discussion of the motion patterns of such slow landslides, focusing on the relationship between rainfall and groundwater, and then the relationship between groundwater and landslide motion. Using the field data and analytical techniques, some mechanisms thought to govern their motion are then evaluated.

6.1 Contributions to knowledge – multi-interdisciplinary approaches

This research presents a high-resolution dataset on the movement of two landslides in North Island, New Zealand. The dynamics and controls upon these landslides have been investigated by combining multiple interdisciplinary approaches including geology, geomorphology, geotechnics and geomatics.

Conceptual engineering geological and geomorphological models were derived for both landslides based on existing historical monitoring results, results from ground investigations, interpretation of aerial photographs and field mapping. These conceptual models guided the selection and positioning of the installed monitoring equipment on each landslide, and were used to identify the geological materials where geotechnical laboratory testing was deemed necessary to derive material parameters for modelling. Geotechnical slope stability modelling techniques were used to bring together the conceptual models with the laboratory and monitoring data, in particular to check that the landslide geometries and material parameters were correct and appropriate and that the monitored pore pressures and surface and sub-surface displacements of the landslides and calculated stresses were representative.

Without such an approach the mechanisms governing the motion of these landslides could not have been adequately resolved. This approach, combined with the high temporal- and spatial-resolutions and measurement precisions of the installed monitoring equipment has significantly benefited this research.

6.2 Significance of large, slow, deep-seated translational landslides

Tertiary-age sedimentary rocks cover about 17% of the New Zealand surface area and are host to many large landslides. The Taihape and Utiku landslides are two of over 7,000 mapped landslides > 10,000 m^2 in plan area in these materials, the majority of

which are inferred to be slow-moving, relatively deep-seated, translational slides (Dellow et al., 2005). The most infamous of these is the Abbotsford landslide (Hancox et al., 1980; Hancox, 2007), which slowly accelerated from rest over months to fail rapidly on 8th August 1979, severely damaging infrastructure in particular residential housing. Some 2,920 mapped landslides are in Tertiary-age sedimentary rocks in the lower North Island of New Zealand. They vary in size from the smallest 10,000 m^2 (a function of air-photo resolution), to the largest 14M m^2. The magnitude-frequency distribution of these landslides is well modelled by a power-law (Figure 6.01). The size of the Utiku and Taihape landslides with respect to the magnitude-frequency distribution are unexceptional. In the lower North Island, an area of 50,000 km^2, Tertiary-age materials account for 20,000 km^2 of the total surface area, with 6% of this being classed as landslide. About 310 km of road, 7 km of railway and 1 km of gas pipeline pass across these landslides. Several of them, including the Taihape landslide are well populated.

The susceptibility of the Tertiary-age materials to landslides has been attributed to the 'soft' and poorly consolidated (extremely weak to weak, UCS = <1 to 20 kPa, NZGS, 2005) nature of the rocks; the deep incision of the rivers; folding and faulting; and in many cases the presence of bedding-plane defects (bedding-plane shears) and regionally persistent clay seams along which sliding may occur (Stout, 1977; Thompson, 1982; Mountjoy and Pettinga, 2006; Reyes, 2007). In most of the documented slides in Tertiary-age materials, slip occurs along thin planar horizons of clay, termed 'clay-seams' (Thompson, 1982), which are parallel or sub-parallel to bedding. Thompson (1982) recognised eight clay seams within the Utiku and Tarare Sandstone Groups, at different stratigraphic levels. The composition of such clays was studied by Stout (1977), Thompson (1982), and Reyes (2007), who summarises that many of the clay seams in the Taihape-Utiku area are smectites of the montmorillonite group. These clay seams are believed to originate from volcanic ash deposited in the Wanganui Basin during deposition of the Utiku and Tarare Sandstone Groups (Townsend et al., 2008). The ash is thought to be related to volcanism in the Coromandel area, about 300 km north of Taihape, comprising ignimbrites, rhyolites, rhyo-dacites, tuffs and volcaniclastic sediments of the Coromandel group. These volcanic materials erupted during the middle to late Miocene and early Pliocene, when sediments of the Utiku and Tarare Sandstone Groups were being deposited.

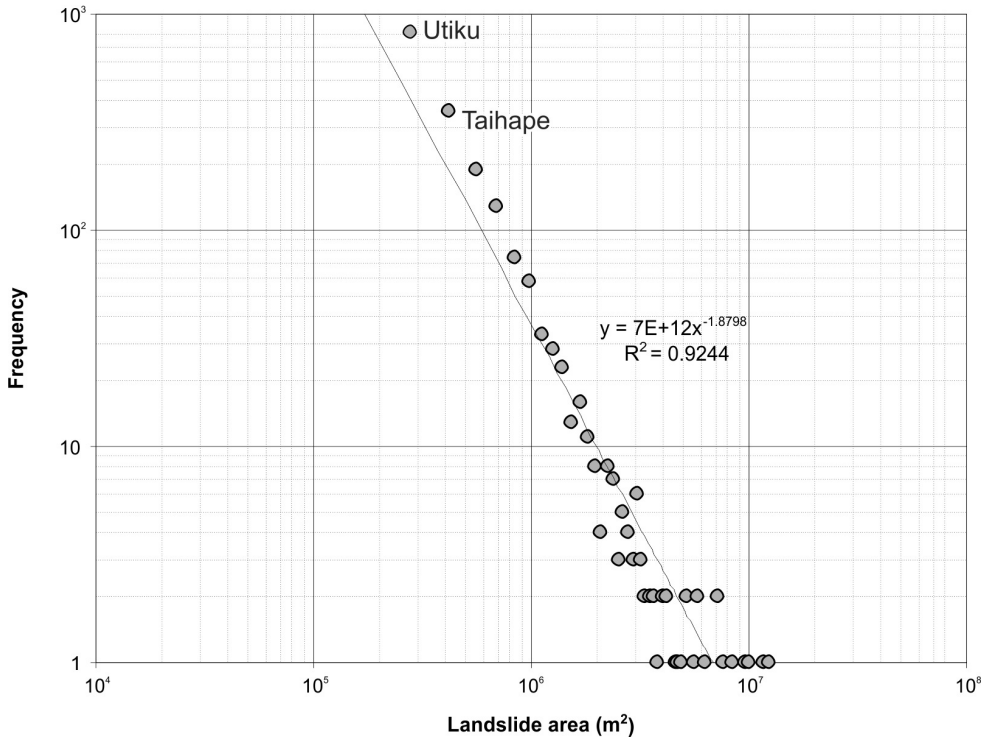

Figure 6.01 The magnitude-frequency distribution of translational landslide area in Tertiary-age sedimentary rocks of the lower North Island of New Zealand.

Clay seams are regionally persistent in the Utiku-Taihape area, and together with regional tectonic structures and down-cutting by streams and rivers, control the occurrence of large, deep-seated slides. The Poroa Slide complex, comprises about 20 landslides covering an area of 10 km^2 (Thompson, 1982) bounded to the south by the Rangitikei River and to the west by the Hautapu River. The Poroa complex is on the opposite side (east) of the Hautapu River to the Utiku slide. Much of the Poroa slide is believed to be translating along the same clay layer as the Utiku slide, but instead of moving along strike the Poroa slides are moving more down dip towards the south. Other slides recognised in the Poroa complex are translating along stratigraphically older clay layers, which due to their dip direction relative to the down-cutting of the Hautapu River, has allowed them to daylight, making movement kinematically feasible.

Shear-strength parameters of the slide surface materials from the Utiku and Taihape landslides have been compared to those from the slide surfaces of other landslides situated in similar materials elsewhere in New Zealand. These include the Abbotsford landslide (Salt et al., 1980; Hancox, et. al., 1980), the Waikorora Bluff landslide (Massey and Palmer, 2007) and the Confluence landslide (Kilsby, 2007). Data from laboratory ring- and direct-shear testing and numerical back analysis calculated using a) infinite slope (Morgenstern and Price) at various points on the landslides where the depth of movement and pore pressure conditions at failure were recorded, and b) limit equilibrium (adopting the method of Morgenstern and Price, 1965) of critical sections through the landslides using the conditions recorded at failure, have been compared

(Figure 17). Linear regression on back-analysed data (infinite slope method), gives a coefficient of variation (r^2) of 0.82, with a cohesion (y-intercept) of 3 ±(3) kPa, and gradient of 0.13 ±(0.01) for 13 degrees of freedom; and on laboratory data $r^2 = 0.93$, y = 4 ±(6) kPa and the gradient = 0.15 ±(0.02) on 21 degrees of freedom, indicating a strong correlation between shear stress and normal stress at failure. The data indicate residual-strength values: back analysis $\phi_r = 7.2° \pm(0.5)$; and lab test $\phi_r = 8.3° \pm(1.0)$. The liquid limits of the Utiku and Taihape tested clays are between 85 and 140, which give similar ϕ_r values to those tested by Mesri and Capeda-diaz (1986) and Stark et al., (2005) for clays within this range. The analyses indicate that the clays forming the slip surfaces of the Abbotsford, Waikorora Bluff, Confluence, Utiku and Taihape landslides, as well as being similar in composition, are geotechnically statistically identical.

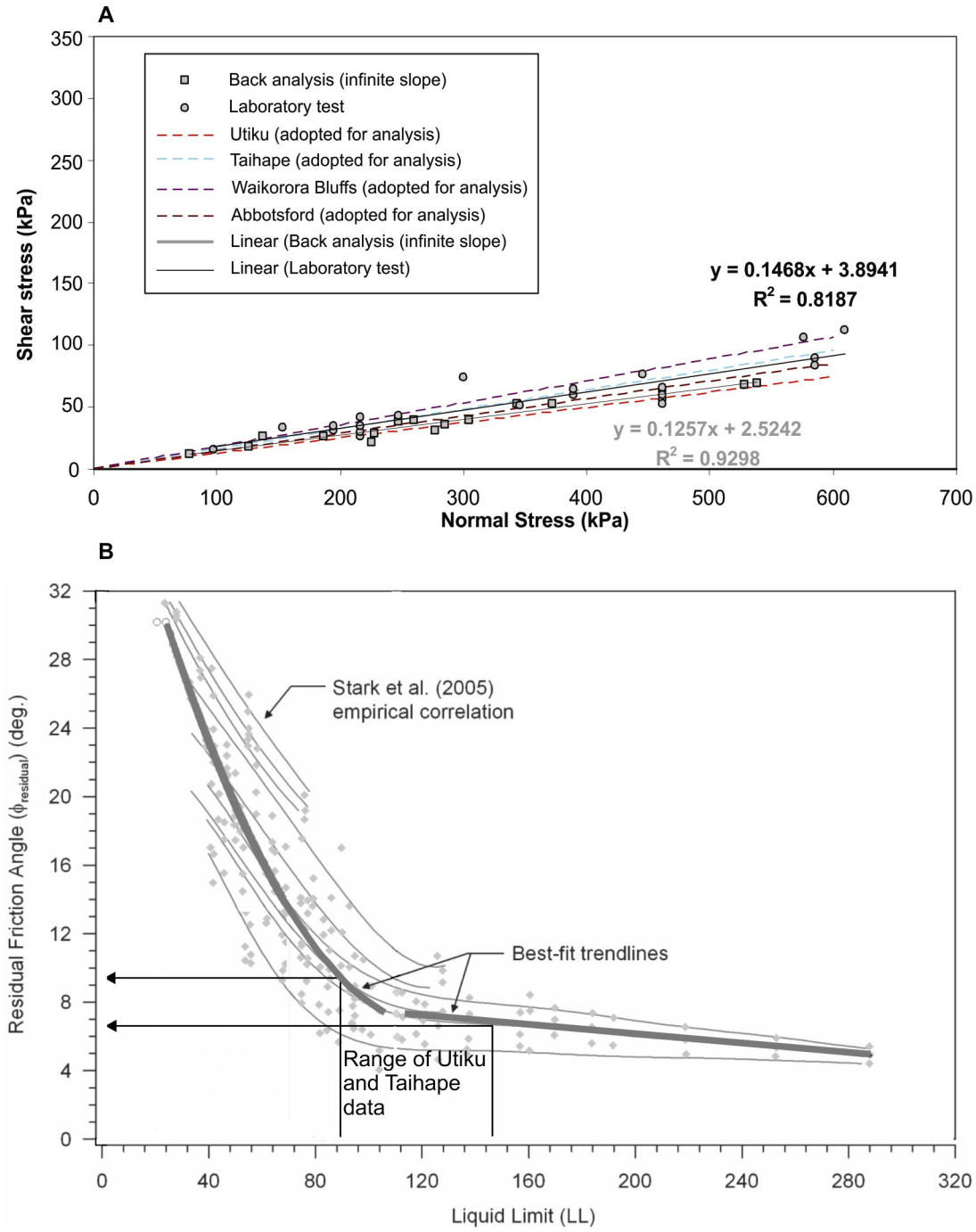

Figure 6.02 A: Residual shear-strength parameters of the slide-surface materials from the Utiku and Taihape landslides compared to those from the slide surfaces of other landslides in Tertiary sedimentary rocks elsewhere in New Zealand. These include the Abbotsford landslide (Salt et al., 1980; Hancox, et. al., 1980), the Waikorora Bluff landslide (Massey and Palmer, 2007) and the Confluence landslide (Kilsby, 2007). These data are from laboratory ring-shear testing and numerical back analysis calculated using a) infinite slope (Morgenstern and Price) at various points on the landslides where the depth of movement and pore pressure conditions at failure were recorded, and b) limit equilibrium analysis (using the method of Morgenstern and Price, 1965) of critical sections through the landslides using the conditions recorded at failure. B: Relationship between liquid limit (LL) and residual friction angle redrawn from Stark et al. (2005), and annotated with the range of LL from the Utiku and Taihape slide-surface clays.

As well as occurring in Tertiary-age materials slow-moving landslides also occur in other materials in New Zealand. Some examples are the Cromwell Gorge landslides which occur in Mesozoic-age quartz-feldspathic mica-schists (Gillon and Hancox, 1971;

McFarlane, 2009). These types of slow-moving landslide are found widely around the world, with many examples discussed in the literature, including the UK (Moore et al., 2007), Spain (Corominas et al., 2005, 2008; Gonzalez et al., 2008), Italy (Bertini, 1984; Picarelli, 2004), Japan (Nakamura 1984; Matsuura et al., 2008), and America, (Schulz et al, 2009a; 2009b; Zangerl et al., 2010). Mansour et al., (2010) reviewed 50 cases relating to the vulnerability of different kinds of facilities to extremely slow, very slow and slow slides from around the world, collating their statistics, including method of displacement, monitoring equipment used and motion rates. These 50 examples show that accumulation of slow movement over time can lead, in some cases, to total disruption of the serviceability of facilities located on them. In some cases loss of life could occur if the landslide accelerates, however there are very few examples where increased movement rates have caused loss of life. One non-fatal example was the Abbotsford landslide (Hancox, 2007). Mansour et al., (2010), show that buildings and residential houses may tolerate higher slide velocities than other facilities before serviceability is lost, with bridges and dams being identified as the least tolerant facilities.

The above discussion indicates that the Utiku and Taihape slides are not unique. Rather they are two of many similar slides occurring in a variety of geological material around the world. The understanding gained from analysis of the detailed motion patterns of these two slides may be widely applicable to many other similar landslides.

6.3 Success of the monitoring systems

The estimated precisions of the motion measurements from the two surface-movement monitoring systems are of similar magnitude, although error ellipses for the Taihape prisms in the horizontal plane are markedly elliptical when compared to those from GPS, which are almost circular (summarised in Table 6.01). These differences are due to the different survey techniques, Taihape being total station theodolite at a fixed point and Utiku being continuous GPS from moving satellites. These differences are well understood and documented in the surveying literature e.g. Anderson and Mikhail (1998). From a comparison of the precision of each system, it can be seen that the total station and prisms is more precise than GPS.

Table 6.01 Summary of surface movement errors from the monitoring

Landslide	Mean errors at one standard deviation			Data coverage
	mm	mm	mm	
Utiku	±6.0 Easting	±5.4 Northing	±22 Height	99.4 %
Taihape	±5.6 normal to line of sight	±1.1 Distance	±7 Height	93.7 %

The standard error between any two individual readings are about 8.5 mm (easting) and 7.7 mm (northing) for Utiku, and 8.1 mm (normal to line of sight), and 1.7 mm (distance) for Taihape. It takes about 10 days (Utiku) and 20 days (Taihape), based on the mean monitored movement rates of these two landslides, for motion outside error to be recognised. The precision limits on the smoothed cumulative horizontal motion data are about 2.3 mm for Utiku and 1.4 mm for Taihape (at one standard deviation). However, these are still high relative to the daily maximum motion rates observed on the landslides; with rates of about 3 mm/day at Utiku during the accelerated creep periods, and about 0.5 mm/day at Taihape during the seasonal creep periods. Because of this, monitoring at temporal resolutions more frequent than daily would be of little use. However, it would be worthwhile to compare the errors on the daily record with those records from 1-hour, 6-hour and 12-hour epochs, which may allow the accelerated-creep motion start and stop times to be resolved more closely. For the prism monitoring, it would be possible to increase the frequency from hourly to half-hourly measurement cycles, giving 48 records per-day instead of 24. However, increasing the frequency means increasing power consumption and on remotely powered sites this can be problematic, especially during winter. Considering the motion rates of the landslides, the daily temporal resolution used for this study is adequate.

Regarding the spatial resolutions in the surface-monitoring networks, the Utiku network is more limited than that at Taihape. The Utiku network comprises 4 points on the landslide and 1 reference point, while the Taihape network comprises 35 points on the landslide and 3 reference points. The Taihape prism network is also more adaptable, as prisms can be added and replaced relatively easily and at relatively little cost, especially when compared to the costs associated with installing additional CGPS sites.

Another issue to consider is “monument noise”, defined as the errors introduced by the way in which the surface-monitoring equipment is anchored to the ground, as discussed by Beavan (2005). At Utiku there appear to be no resolved motions unrelated to landsliding, possibly because the monuments comprise 6 m long I-Beams cemented 4.5 to 5 m into the ground. At Taihape many of the prisms show cyclic upslope and downslope motion which appear to be seasonal and unrelated to landsliding. The poles on which the prisms are mounted at Taihape are not as deep, or as sturdy as the I-beams at Utiku, and therefore seasonal changes in the upper part of the landslide may be amplified by tilt of these poles in response to near surface shrinkage and swelling of the ground caused by e.g. changing soil moisture. However, the poles were all installed approximately 1.5 m into the ground and cemented vertically, with recent measurements showing that they are still vertical. The back-site prisms show similar phenomena and these are located on purpose-built survey monuments tied into rock.

Prisms 4 and 5 are mounted on buildings with reinforced concrete raft foundations, which should limit any localised near-surface effects. Therefore, it is likely that monument errors are relatively minor at both sites and that the recorded motions do indeed relate to environmental as well as landslide factors.

The other monitoring equipment in use comprises vibrating-wire piezometers, rain gauges and strong-motion sensors, which are widely-used standard monitoring equipment for landslides. The results, particularly from the vibrating wire piezometers, are of adequate precision and comparable temporal resolution to the surface-monitoring networks, and so have allowed periods of motion to be compared with the potential triggering factors, mainly pore-pressure changes. The inclinometer data have the lowest temporal resolution as they were manually monitored; although in-situ inclinometers are available, their cost appeared to be prohibitive at the beginning of the project. It has not been possible to link all periods of surface motion with motions at depth along the slide surface for the Utiku landslide because inclinometer surveys were carried out on average every 2 months. However, the temporal resolution of the inclinometer monitoring at Taihape was bi-monthly, and so it has been possible to link surface and subsurface motions. The cost of doing this over a three year period has been substantial, raising a question whether the cost of in-situ inclinometers was as prohibitive as it first appeared. The inclinometer results were very useful for verifying the depth of motion, and at Taihape, due to the increased temporal resolution, have been used to assess the rates of motion along the slide surface.

6.3.1 System robustness

The CGPS monitoring network was generally more robust and required less maintenance than the robotic total station and prism network. On average the data coverage for the GPS system was about 99%, while the prism network was 94%, even though the prism network has been installed for nearly 4 years compared to the 2 years of GPS monitoring at Utiku. The robotic total station required annual servicing, and so it was removed from site for a 2-week period each year, but no replacement instrument was installed. In addition, as the total station needs to have a clear line-of-site to each prism, when this is obscured no measurement can be made. At Taihape, wood smoke and fog sometimes prevented prism measurement. At Utiku line-of-sight would have been obscured by mature pine trees, making prism monitoring impractical without tree removal. At Utiku there were no suitable vantage points to mount a total station, considering the range is about 2,000 m. For the GPS network, terrestrial line-of-sight is not an issue, but having clear sky-view is essential. As can be seen by a comparison of the errors from the back sites (about 4.5 mm easting and 3.5 mm northing) with those from the landslide (6 mm easting and 5.4 mm northing) where the differences are

typically 2 mm at one standard deviation. Even for the GPS on the landslide the errors at UTK2 where sky view is limited are worse than those at UTK4 where sky view is clear.

An integral part of these monitoring networks has been wireless communications and automated data transfer, processing and display systems. These were all be-spoke designs and were unique to each landslide and type of equipment used. None of the data losses can be attributed to problems with these systems. Considerable effort by the GNS Science GeoNet team went into the design and construction of these systems, including the installation of the equipment, communications power and programming.

6.3.2 Comparison of these systems with those from the literature

The monitoring systems installed at Utiku and Taihape have been compared to other systems installed on similar landslides. These are the Slumgullion landslide, which is a translational debris slide (Schulz et al., 2009a) in Colorado, USA; the Sechilienne landslide, which is a complex in-part translational rock slide (Helmstetter and Garambois, 2010) in the French Alps; and the Vallcebre landslide, which is a translational rock slide (Corominas et al., 2005) in the Eastern Pyrenees, Spain. Details of the monitoring systems installed on these are summarised in Table 6.02.

Many other examples of landslide monitoring systems exist in the literature, Reid et al. (2008) list 12 landslides that are being monitored by the USGS using a variety of sensors similar to those listed in Table 6.02. For slow moving slides the most difficult factor to monitor is the temporal resolution of the surface and subsurface displacement. Mansour et al. (2010) summarises that for forty five extremely slow to slow slides from around the world, movement monitoring comprised: Inclinometers 58%; surface surveying 31%; geomorphological mapping 13%; extensometers 9%; and remote sensing (including InSAR and TLS) 9%. These data suggest that borehole inclinometers are the preferred method of monitoring landslide movement, however, the tubes in which the inclinometers are placed are susceptible to shearing, making them costly to replace. The lack of continuous GPS (CGPS) for landslide monitoring in the literature suggests that it is either to expensive to install or that the data processing is too complicated. However, when compared to the cost of down-hole inclinometers (including the cost of the drillhole) CGPS are cost effective.

From the reviewed literature it is apparent that the monitoring systems installed at Utiku and Taihape have typically higher temporal- and spatial-resolutions and measurement precisions than those of other comparable systems. There is also a lack of information in the literature, with the exception of a few papers (e.g. Schulz et al., 2009a and

2009b), where the estimated precision of the measurements from the different instruments have been stated and data losses due to equipment malfunction quantified. The near-real time monitoring networks as Utiku and Taihape, and the way in which these allow the data to be transferred from site to office, processed and displayed, make it easier to ensure that the system works correctly and therefore limiting the loss of data. The systems at Utiku and Taihape appear to be more robust than many others in the literature.

Table 6.02 Details of other reported monitoring systems installed on landslides

Landslide	Installed instrumentation (temporal resolution)					
	Surface motion	Subsurface motion	Precipitation	Barometric	Groundwater	Seismic
Slumgullion	Manual RTK GPS surveys of 19 monitoring points (approx. 3.5 surveys/year) 2 extensometers in different locations (hourly)	None	Rain, snow fall and snow depth at one location (hourly)	Air temperature (hourly)	3 vibrating wire piezometers (VBW) sealed in one borehole (hourly) 1 un-vented shallow strain gauge piezometer in a standpipe (hourly)	None
Vallcebre	Manual RTK GPS surveying of 30 monitoring points (approx. 6.5 surveys/year) 5 extensometers (20 minutes)	5 borehole inclinometers	Rainfall (20 minutes but not on the landslide)	Not known	6 VBW (20 minutes)	None
Sechilienne	Manual surveying using RTK GPS and theodolites Remote sensing using InSAR (weekly to monthly) Extensometers (temporal resolutions unknown) Camera and video (as and when)	4 Borehole inclinometers	Rainfall (daily but not on the landslide)	Not known	VBW in boreholes (number unknown)	3 seismological stations
Utiku	Manual RTK GPS and theodolite surveys of 45 monitoring points (approx, 4 surveys/year) 5 continuous GPS receivers (30 second epochs resolved to 24 hourly periods)	2 borehole inclinometers (approx. 6 surveys/year)	2 rain gauges (as and when)	Barometric pressure and temperature	5 VBW installed in boreholes and river stage	1 strong motion accelerometer (triggered by ground accelerations over a threshold 6 temporary seismometers
Taihape	Manual RTK GPS and theodolite surveys of 20 monitoring points (approx, 0.5 surveys/year) Robotic total station and 35 prisms (hourly)	5 borehole inclinometers (approx. 24 surveys/year)	2 rain gauges (as and when)	Barometric pressure and temperature	5 VBW installed in boreholes and river stage	1 strong motion accelerometer (triggered by ground accelerations over a threshold

6.4 Landslide movement

6.4.1 Patterns of landslide movement

Movement patterns of the Utiku and Taihape landslides can be classified as stages three and four (reactivate occasionally and active) in the classification of Leroueil et al. (1996), as movement of each landslide is occurring along a fully developed slip surface, which is at residual strength (Skempton, 1985), with recorded motions being unsteady and nonuniform. Unlike Taihape, the head scarp of the Utiku landslide is actively retrogressing, but the debris is not fully incorporated into the landslide mass, in these areas the movement of the landslide may be classified as stages 1 and 2 (pre- and post-failure) (Leroueil et al., 1996).

Although the term 'creep' has been used to describe the deformation of slope materials under constant shear stress prior to failure, Terzaghi (1950) used the term 'creep' to describe slow post-failure motion. Creep in the context of this study refers to the post-failure velocity of the landslide mass with no reference to the mechanism of deformation. Surface motion patterns on the Utiku and Taihape slides are repetitive, with three types of motion predominating: accelerated creep, slow creep and vertical creep, punctuated by periods of rest. The displacements vary in both magnitude and duration resulting in unsteady non-uniform motion. These motion patterns are not unique and appear to be similar to other slow, very slow and extremely slow landslides (Cruden and Varnes 1996) sliding on thin layers of predominantly clay.

Long-term monitoring records from such landslides (e.g. Angeli et al., 1996; Leroueil et al., 1996; Moore et al., 2007; Schulz et al., 2009b; Zangerl et al., 2010) suggest that these patterns can continue for years and that the *status quo* is repeating periods of faster movement (accelerated creep) of varying magnitudes and rates, punctuated by periods of slow creep and inactivity (Figure 6.03).

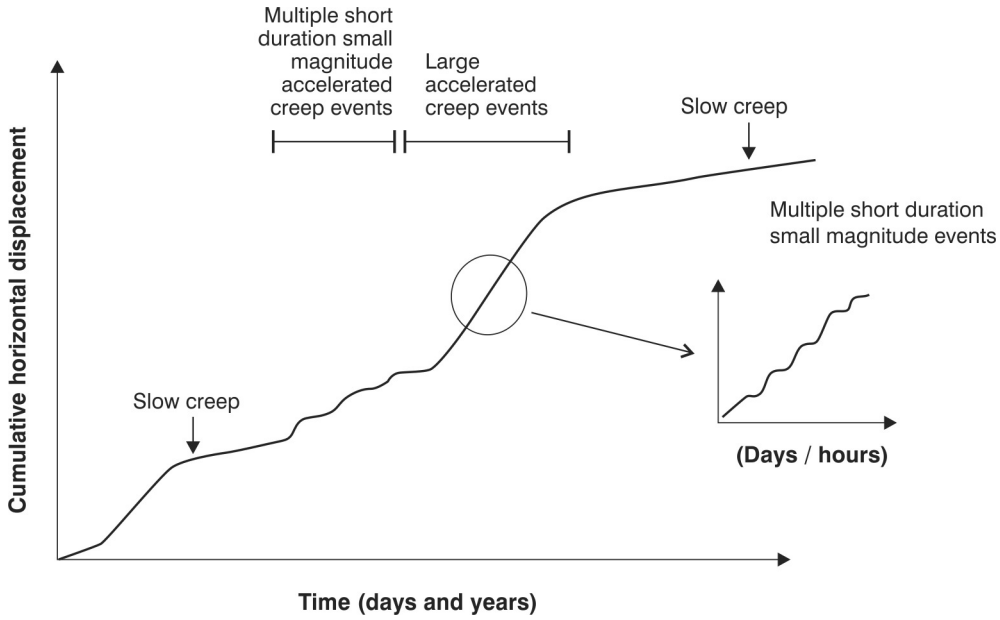

Figure 6.03 Schematic diagram showing the typical patterns of horizontal landslide surface displacements over time, derived from the movement patterns of similar slides documented in the literature.

The relationship between motion patterns and the morpho-dynamic setting as described by Petley et al., (2005) are also relevant for the Utiku and Taihape landslides. Surface displacement at Utiku generally increases transversely away from the western flank, and longitudinally towards the toe. The lower toe is influenced by the Hautapu River with erosion and loss of toe support evident in the field. Taihape differs, however, as the toe of the landslide is confined. At Taihape, the largest monitored surface displacements occurred on the upper toe rather than the lower toe, which implies longitudinal compression between the upper and lower toe and slowly increasing resistance from the constraint imposed by the lower toe. The lower toe is influenced by Otaihape Stream, where episodic fluvial erosion and reduction in toe support is evident in the field. Unlike the Hautapu River at Utiku, Otaihape stream is a low-order stream course. However, it is prone to severe flooding and erosion as shown during the Manawatu storm in February 2004 when the road beside the stream on the landslide toe was removed by scour.

A consistent spatial pattern in both landslides is that the slide material appears to become more disaggregated towards the toe. Petley et al., (2005), note a similar pattern for the Tessina landslide in Italy.

A similar relationship between motion patterns and the morpho-dynamic setting is shown in Allison and Brunsden (1990) in plots of transverse motion. These plan-view horizontal displacement plots have a near symmetrical form (Figure 6.04), where motions are highest in the centre and decrease towards the flanks, implying frictional

resistance at the flanks. This surface-velocity pattern, based on the monitored prism displacements, is found at Taihape where the motion distribution on the upper toe is symmetrical and 'plug'-shaped (Allison and Brunsden, 1990) in plan, indicating that uniform velocities occur transversely across the slide-block (Figure 6.05). This is also found on the lower toe. There, however, the maximum velocity is slower than in the upper toe. The Utiku landslide differs. The velocity distribution, based on the monitored historical survey displacements, is asymmetrical, increasing slowly towards the eastern boundary with distance from the prominent western scarp. This suggests that increased friction along the western flank may be reducing velocities there, but less so along the eastern flank. This is consistent with the western flank being the thicker side of the wedge. It leads to apparent rotation about a vertical axis shown by the monitoring data and geomorphology. These relationships suggest that landslide geometry is constraining motion.

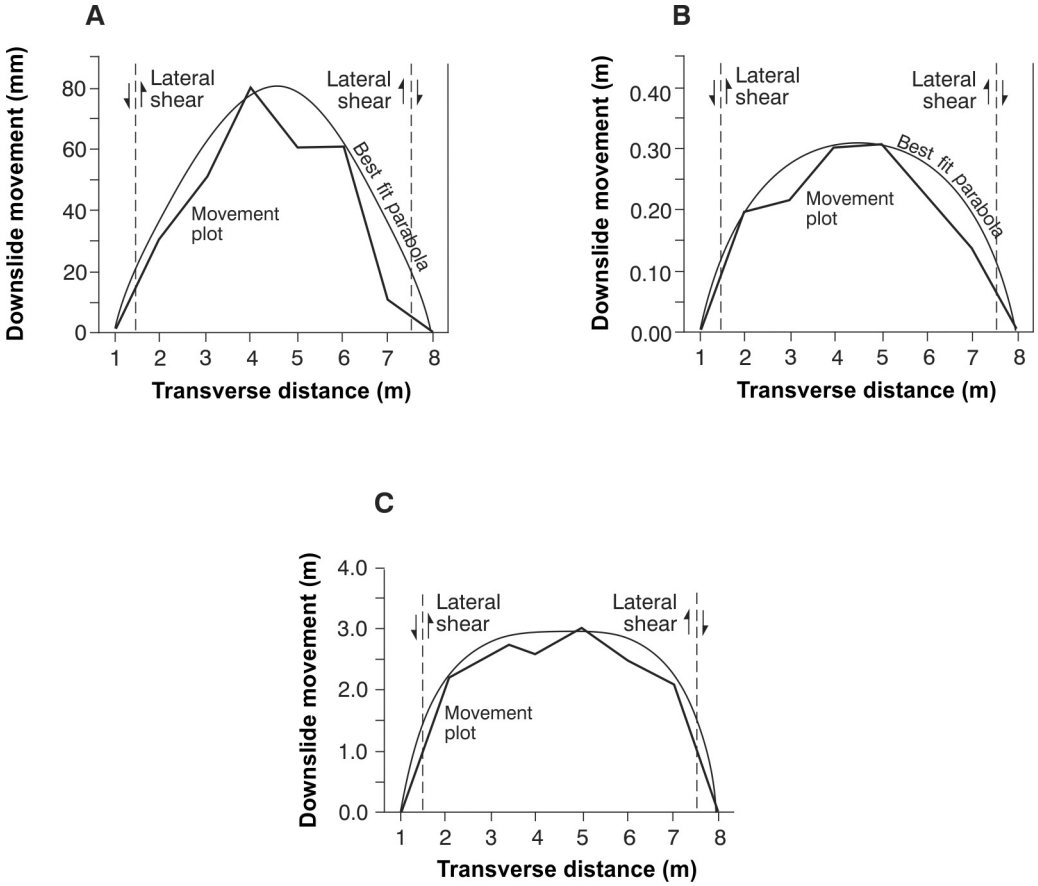

Figure 6.04 Plots of plan-view landslide horizontal displacement for different types of movement event. Redrawn from Allison and Brunsden (1990). A: Multiple movement event. B: Graded movement event. C: Surge movement event.

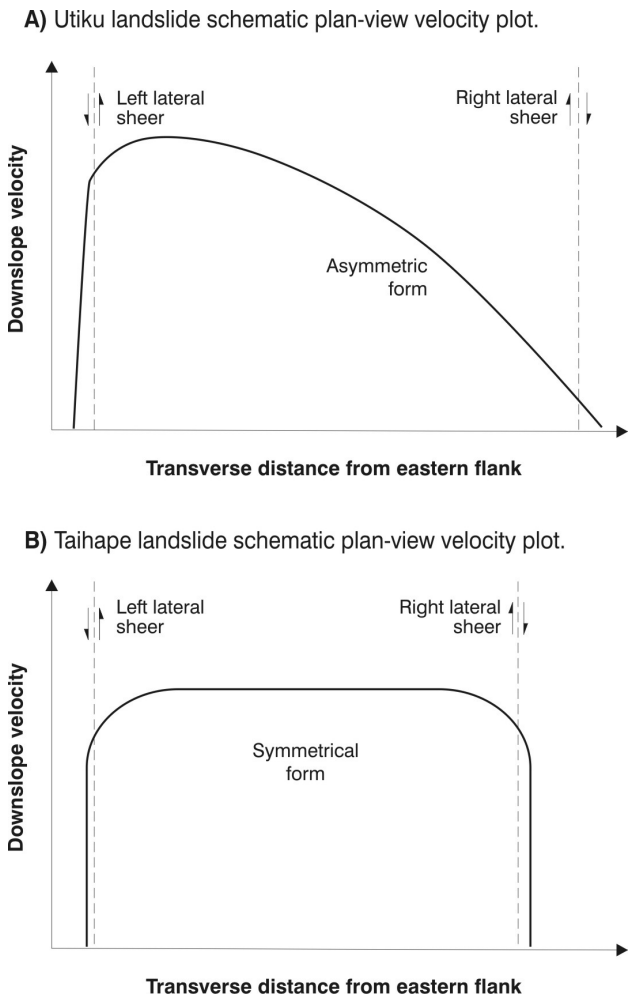

Figure 6.05 Schematic plan-view horizontal displacement plots for the Utiku and Taihape landslides. A: Utiku landslide. B: Taihape landslide.

6.4.2 Accelerated creep

Accelerated-creep motion is responsible for the largest landslide displacements, but has not been recorded at Taihape during this detailed surface-monitoring period. It was recorded only during the lower-resolution historical surface and sub-surface monitoring. This motion pattern is similar to that referred to by Allison and Brunsden (1990) as ‘multiple movement’ and ‘surge’ events. At Utiku, three periods of accelerated creep were recorded in high resolution, with many more recorded historically (1965 to 1972). The episodic accelerated–creep displacements differ in magnitude from millimetres to meters. The displacement versus time graphs have similar open ‘S’-shaped forms, indicating rapid acceleration, a period of steady faster creep motion, followed by rapid deceleration. Similar patterns are also seen in the inclinometer data from Taihape, but in the period before prism installation. The longest, most-closely monitored period of accelerated creep recorded at Utiku (movement period 2, UTK1 only) was shown to be several smaller magnitude, shorter duration events. It is possible that the historical, larger magnitude accelerated-creep-events (1965 to 1972) were also multiple, small

magnitude, short duration events that were not resolved at the temporal resolution of the monitoring data. Therefore, the movement patterns of the landslide appear to be similar over a range of scales (Figure 6.06).

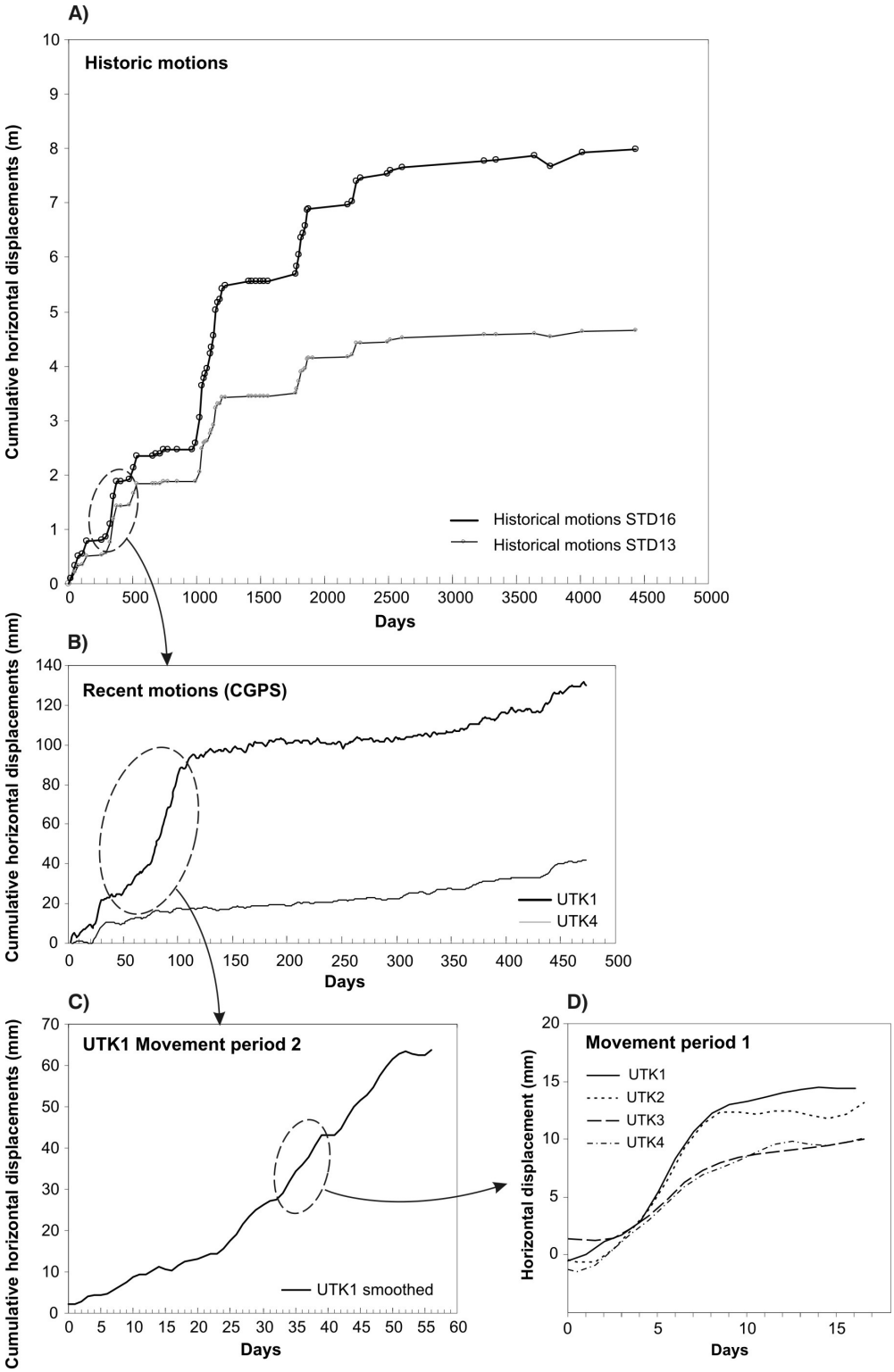

Figure 6.06 Cumulative horizontal displacements of the Utiku landslide over different scales. A: Historical cumulative horizontal displacements (pre 1972) of the survey marks. B: Cumulative horizontal displacement of GPS station UTK1 (from July 2008). C: Smoothed cumulative horizontal displacement of GPS station UTK1 for accelerated creep period 2. D: Smoothed cumulative horizontal displacement of GPS stations UTK1, UTK2 UTK3 and UTK4 for accelerated creep period 1.

At Utiku the periods of accelerated creep predominantly comprise horizontal displacement, with translational angles which do not significantly differ from the angle of the slide surface (i.e. near horizontal). Vertical displacements may also occur, but they are smaller than the precision of the vertical displacement measurements.

The relationship between pore pressure and surface movement for each period of statistically significant accelerated creep is shown in Figures 6.07, 6.08 and 6.09, where daily and smoothed daily pore pressures and cumulative horizontal motions have been plotted. These figures show that each accelerated-creep event coincides with an increase in pore pressure across the landslide. In most cases, the pore pressures shown in these figures are from piezometers located adjacent to the CGPS receivers, with the exception of movement period 1, where the records from piezometer BH2 were unusable, and mean pore pressures from BH3 and BH4 were substituted.

Pore pressures recorded before the onset of accelerated creep periods 1, 2 and 3 are shown in Table 6.03. The results show that the pore-pressures at initiation of movement vary from period to period. For movement period 1, the pore pressures in the upper landslide were higher than those during movement period 3, but pore pressures in the lower landslide during this latter period were higher than those recorded for movement period 1. This suggests that there is no consistent movement triggering pore-pressure threshold at each piezometer. Instead, it may be a combination of the changing pore pressures between the piezometers that triggers landslide movement.

Table 6.03 Maximum pore pressures recorded prior to the periods of accelerated creep (Utiku)

Piezometer (from landslide head scarp to toe)	Pore pressures recorded prior to onset of accelerate creep periods					
	Movement period 1		Movement period 2		Movement period 3	
	Pore Pressure (kPa)	Piezometric level (m AMSL)	Pore Pressure (kPa)	Piezometric level (m AMSL)	Pore Pressure (kPa)	Piezometric level (m AMSL)
BH1	537.3	369.8	N/A	N/A	526.8	368.7
BH3[1]	422.0	349.2	N/A	N/A	419.7	349.0
BH4	187.5	328.5	N/A	N/A	184.5	328.2
PZA	130.2	315.9	136.0	329.7	137.7	316.6

[1]The piezometer in BH3 was not operating at the time of movement period one, therefore the assumed pore pressures were inferred from the average of pore pressures from BH1 and BH4.

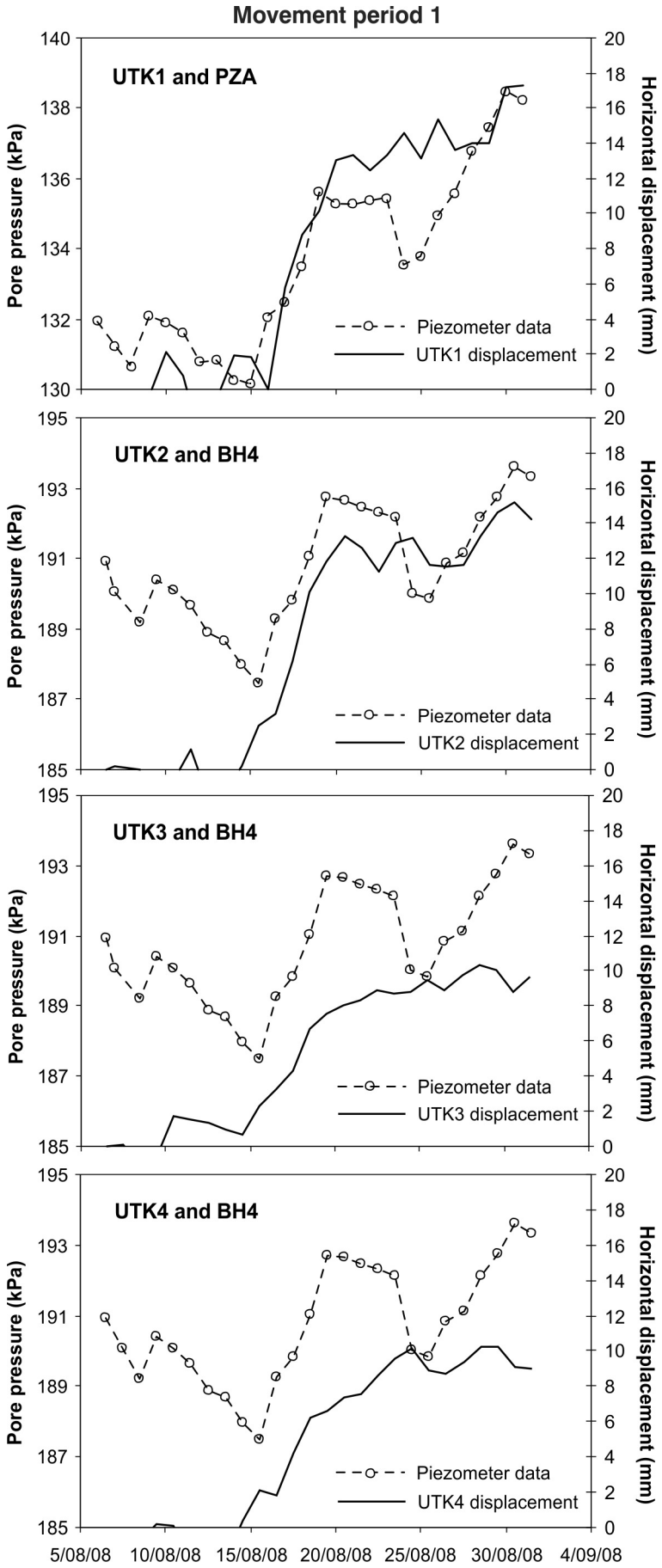

Figure 6.07 Relationship between pore pressure and displacement, Utiku landslide. Accelerated creep movement period 1. GPS stations UTK1, UTK2, UTK3 and UTK4, and pore pressures recorded by piezometers PZA and BH4. Pore pressures are daily mean values that have been corrected for barometric effects. Horizontal displacements are smoothed displacements calculated from the daily records using a Gaussian smoothing kernel, where G_s = 2 mm.

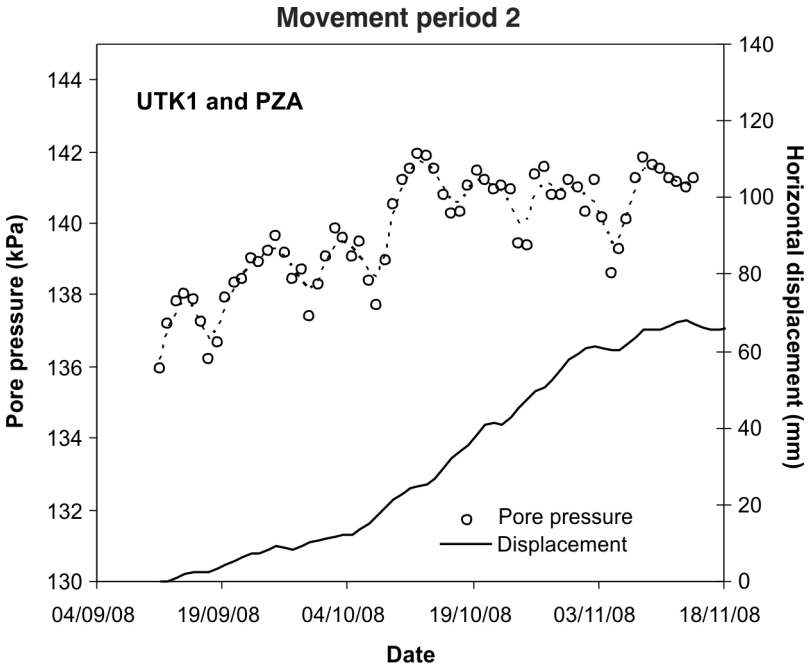

Figure 6.08 Relationship between pore pressure and displacement, Utiku landslide. Accelerated creep movement period 2. GPS station UTK1 and pore pressures recorded by piezometer PZA. Pore pressures are daily mean values that have been corrected for barometric effects. Horizontal displacements are smoothed displacements calculated from the daily records using a Gaussian smoothing kernel, where G_s = 2 mm.

The relationship between pore pressure and surface motion has been explored further by plotting together the daily horizontal displacement and corresponding daily mean pore pressure for each movement period (Figures 6.10, 6.11 and 6.12). These graphs confirm that for movement periods 1 and 3, all station motions initiate simultaneously within the daily resolution of the data, and that the onset of motion corresponds to an increase in pore pressure recorded at all piezometers on the landslide. Horizontal motion of the stations once initiated, accumulates at a constant rate as pore pressure increases. However, there comes a point, which varies between the different stations, when motion may stop despite the existence of high and sometimes increasingly higher pore pressures (Fig 6.10). Alternatively, motion can continue at a steady rate at a constant high pore pressure before stopping (Fig 6.11, Fig 6.12). For movement periods 1 and 3 all stations appear to cease horizontal motion simultaneously within the resolution of the daily data.

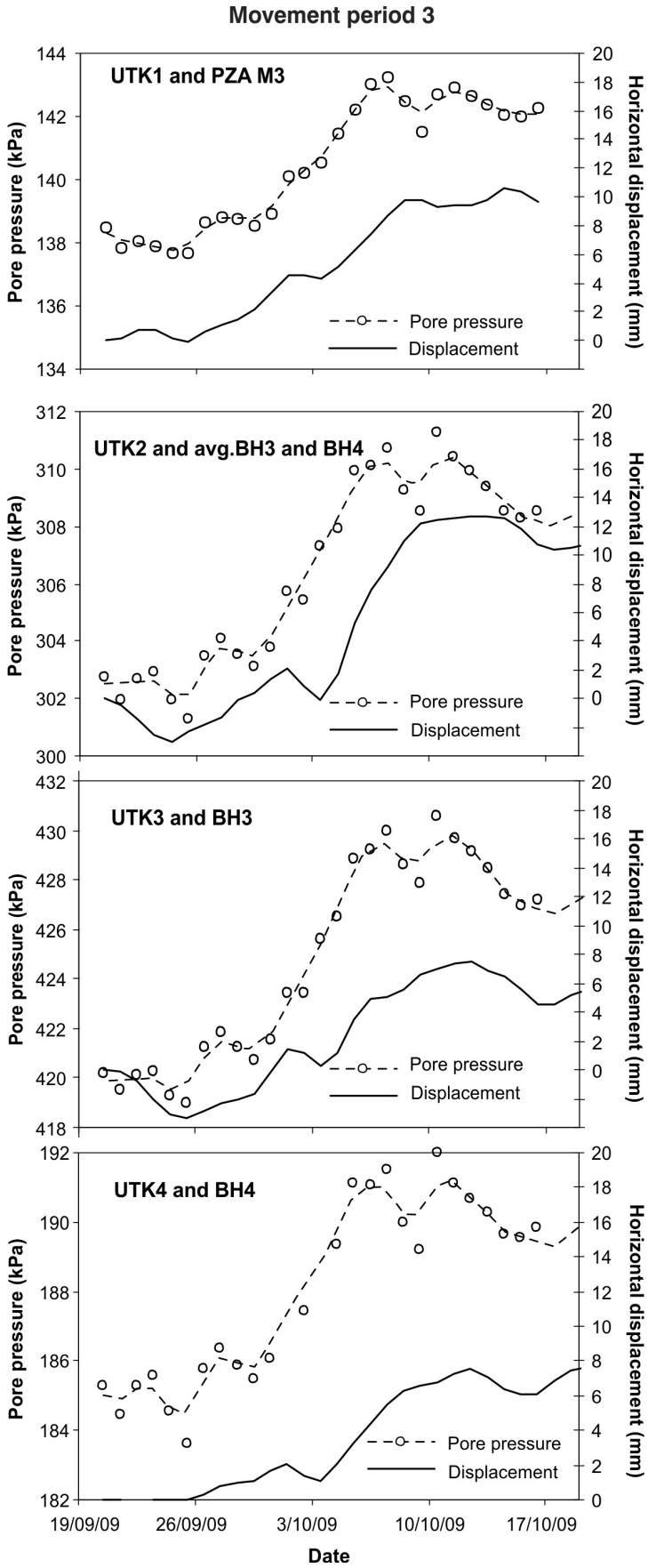

Figure 6.09 Relationship between pore pressure and displacement, Utiku landslide. Accelerated creep movement period 3. GPS stations UTK1, UTK2, UTK3 and UTK4 and pore pressures recorded by piezometers PZA, BH3 and BH4. Pore pressures are daily mean values that have been corrected for barometric effects. Horizontal displacements are smoothed displacements calculated from the daily records using a Gaussian smoothing kernel, where G_s = 2 mm.

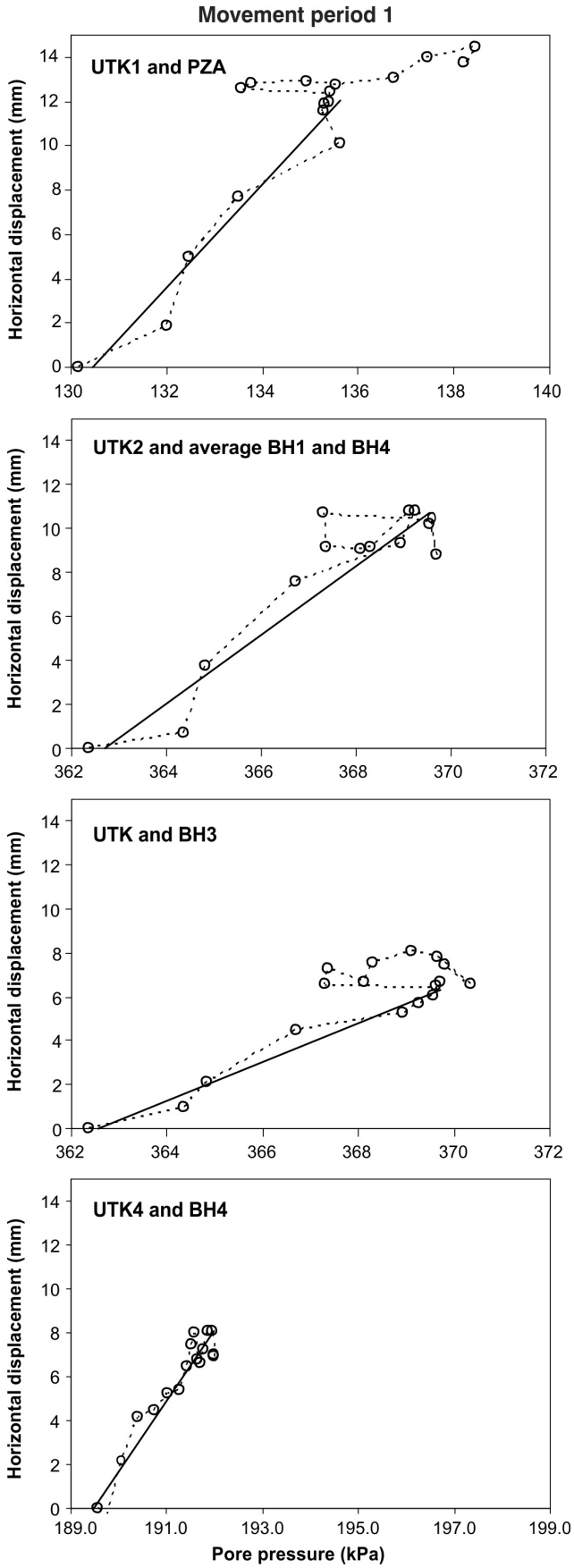

Figure 6.10 Utiku landslide pore pressures and horizontal displacements for accelerated creep period 1. Pore pressures recorded at piezometers PZA, BH1, BH3 and BH4 are daily mean values that have been corrected for barometric effects. Horizontal displacements are recorded at GPS stations UTK1, UTK2, UTK3 and UTK4 and are smoothed displacements calculated from the daily records using a Gaussian smoothing kernel, where G_s = 2 mm.

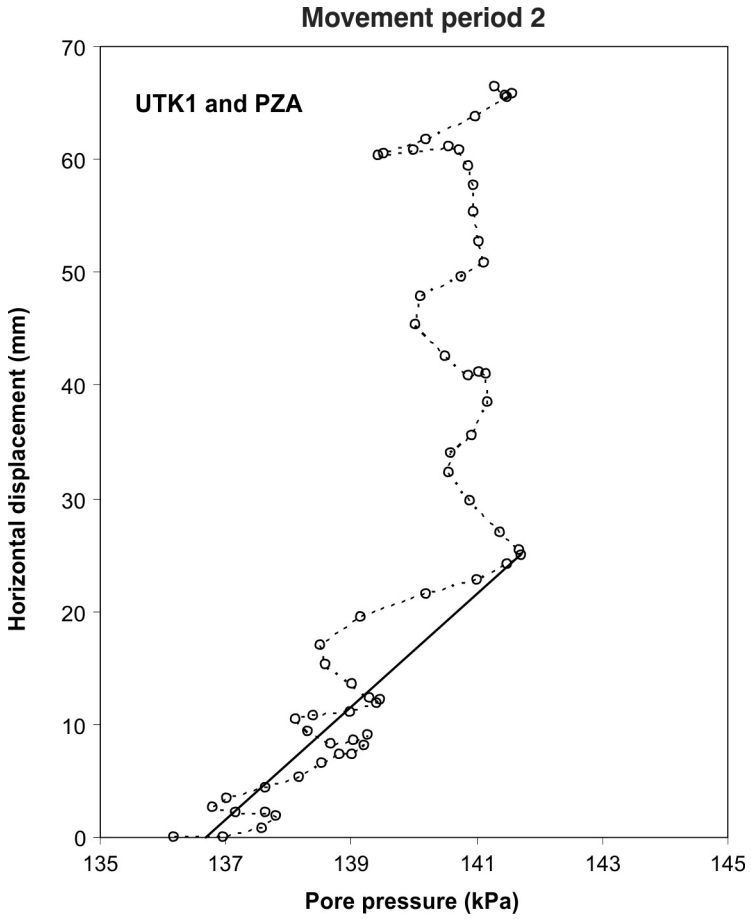

Figure 6.11 Utiku landslide pore pressures and horizontal displacements for accelerated creep period 2. Pore pressures recorded at piezometer PZA are daily mean values that have been corrected for barometric effects. Horizontal displacements are recorded at GPS station UTK1 and are smoothed displacements calculated from the daily records using a Gaussian smoothing kernel, where G_s = 2 mm.

Graphs of pore pressure and displacement rate for each CGPS station for movement periods 1 and 3 (Figures 6.13 and 6.14) show an initial rapid increase in displacement rate to peak values as pore pressures increase. However, as post-peak displacement rates decrease, pore pressures either remain constant, or actually increase. Movement period 3 actually appears to comprise two movement events that follow similar patterns, where the pore pressures at the end of each event are higher than those at the beginning. Patterns of pore pressure and displacement rate for movement period 2 are similar to periods 1 and 3, but this period comprises multiple movement events, which are shown as a series of spikes in the line representing the smoothed daily records. These represent rapid changes in landslide speed with changing pore pressures, although the main pore pressure trends show a general increase (Figure 6.15). As for movement periods 1 and 3, the cessation of motion does not coincide with a decrease in pore pressure. This means the landslide can be either stable or moving at the same value of pore pressure.

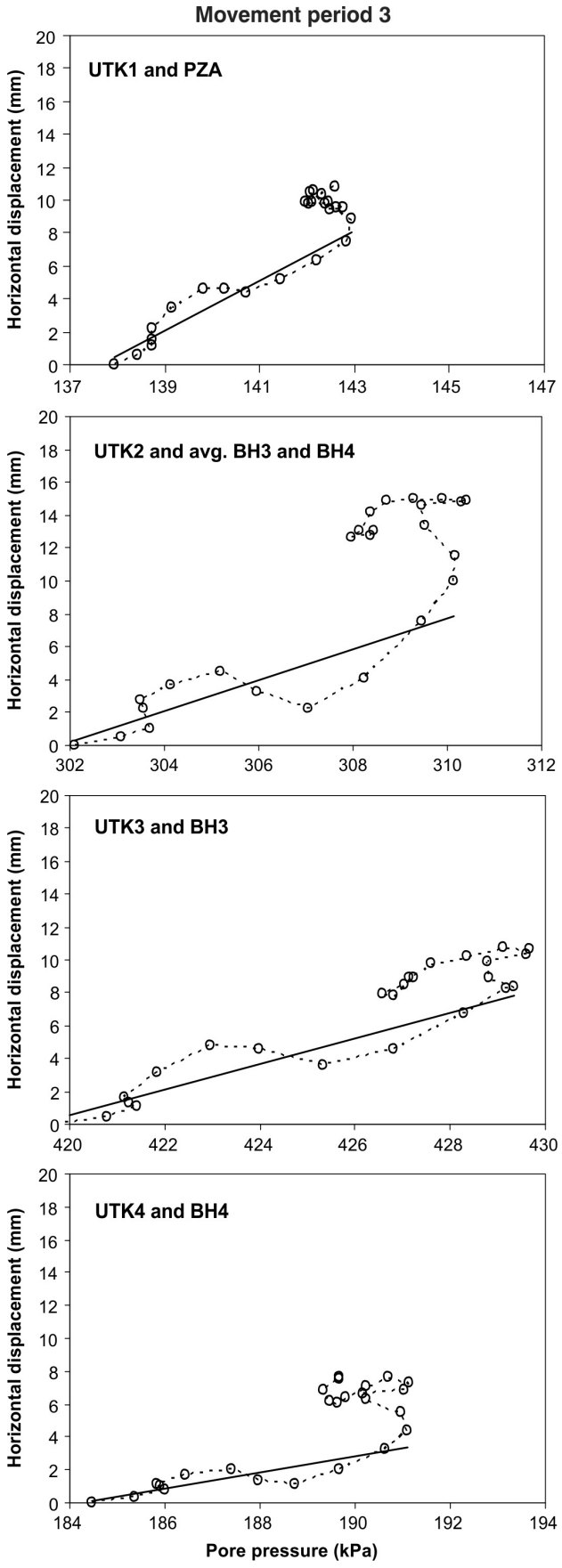

Figure 6.12 Utiku landslide pore pressures and horizontal displacements for accelerated creep period 1. Pore pressures recorded at piezometers PZA, BH3 and BH4 are daily mean values that have been corrected for barometric effects. Horizontal displacements are recorded at GPS stations UTK1, UTK2, UTK3 and UTK4 and are smoothed displacements calculated from the daily records using a Gaussian smoothing kernel, where G_s = 2 mm.

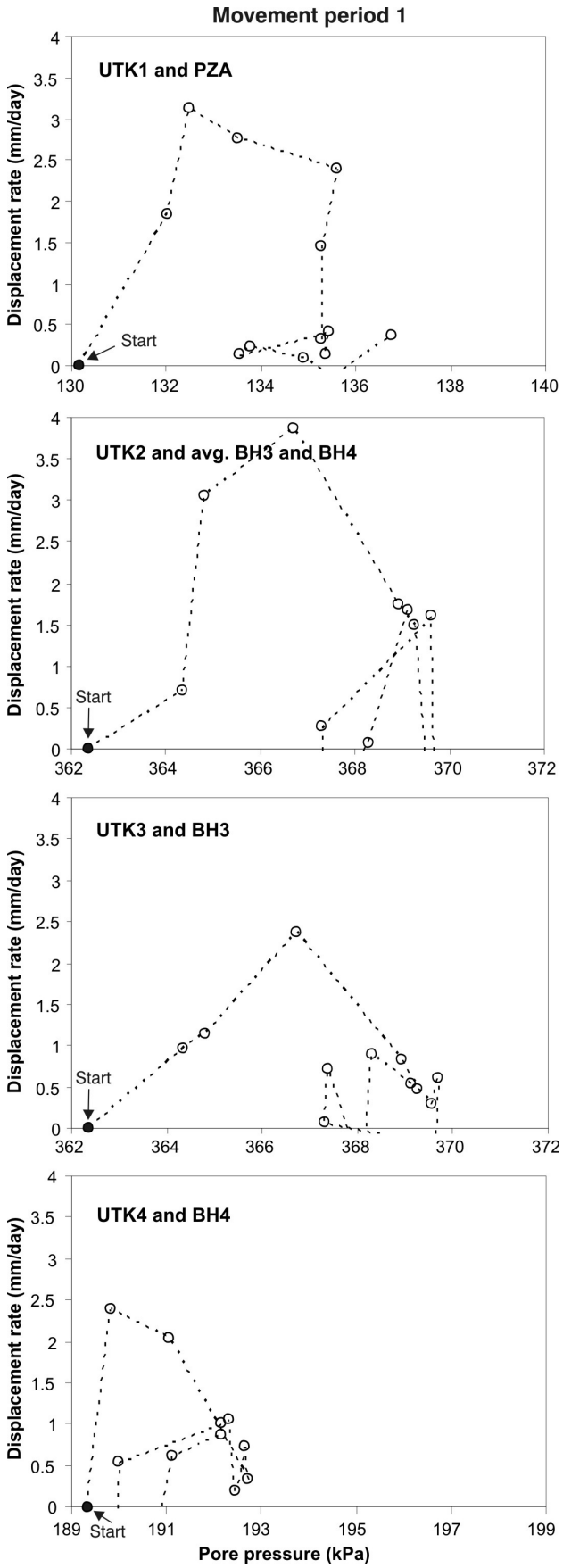

Figure 6.13 Utiku landslide pore pressures and displacement rates for accelerated creep period 1. Pore pressures recorded at piezometers PZA, BH3 and BH4 are daily mean values that have been corrected for barometric effects. Displacement rates are from GPS stations UTK1, UTK2, UTK3 and UTK4 and are calculated from the daily horizontal displacements which have been smoothed using a Gaussian smoothing kernel, where G_s = 2 mm.

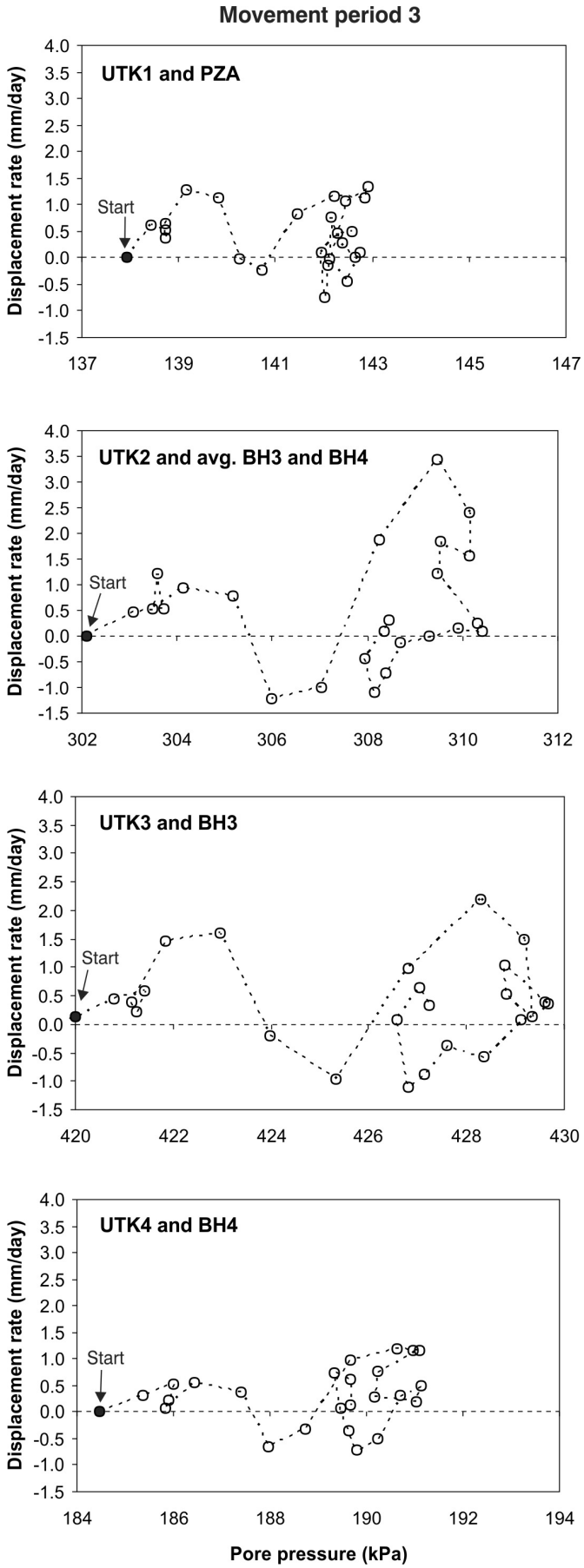

Figure 6.14 Utiku landslide pore pressures and displacement rates for accelerated creep period 3. Pore pressures recorded at piezometers PZA, BH3 and BH4 are daily mean values that have been corrected for barometric effects. Displacement rates are from GPS stations UTK1, UTK2, UTK3 and UTK4 and are calculated from the daily horizontal displacements which have been smoothed using a Gaussian smoothing kernel, where G_s = 2 mm.

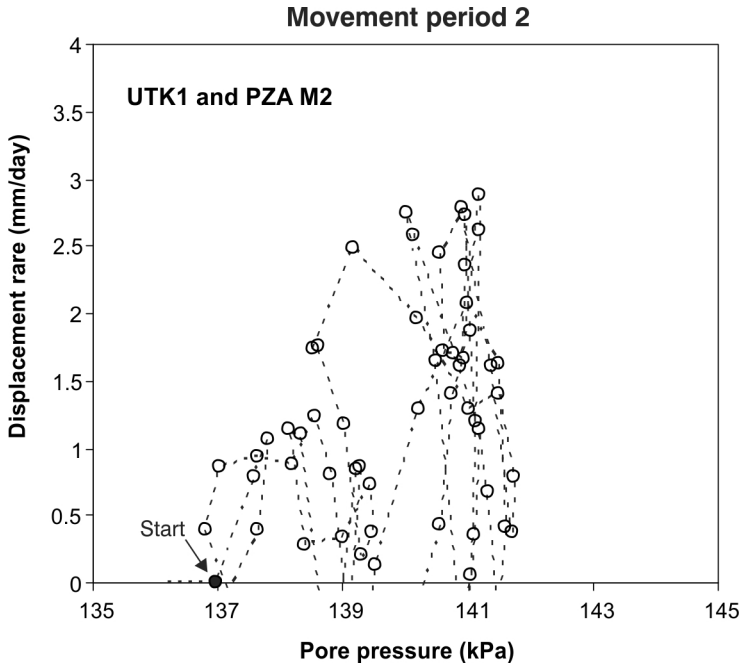

Figure 6.15 Utiku landslide pore pressures and displacement rates for accelerated creep period 1. Pore pressures recorded at piezometer PZA are daily mean values that have been corrected for barometric effects. Displacement rates are from GPS station UTK1 and are calculated from the daily horizontal displacements which have been smoothed using a Gaussian smoothing kernel, where G_s = 2 mm.

These relationships are similar to those reported by Nakamura 1984; Matsuura et al., 2008; Corominas et al., 2005 and Gonzalez et al., 2008, where different landslide velocities can occur at the same pore pressure value. Some authors have found that there is hysteresis in the movement in relation to observed groundwater fluctuations (van Asch et al., 2007). Nakamura (1984) found that for a particular landslide in Japan, the amount of landslide movement on the rising limb of groundwater level was larger than that observed over the lowering limb for the same ground water level. Similar hysteresis was also found by Gonzalez et al., (2008), Matsuura et al., (2008) and Bertini (1984). These findings suggest that landslide velocities vary between the rising and lowering limb of piezometric levels, but more importantly, that different velocities can occur at similar pore pressures (Figure 6.16).

The relationships between pore pressures, surface and subsurface displacement may also be more complicated. Although at Utiku, the onset of surface motion correlates with increased pore pressure, the motion recorded at the slide surface (inclinometer BH3A), may lag behind the surface motion by about four weeks. This interpretation, however, relies on a single measurement point and future measurement of similar lags is required to verify if such a lag might be real.

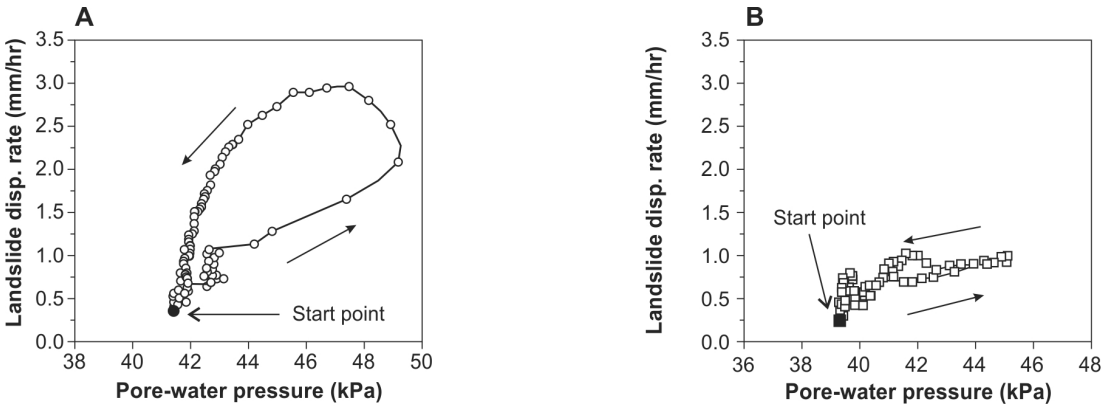

Hysteresis relationship between pore water pressure and landslide displacement for a landslide in the Tertiary materials of Japan (Matsuura *et al.,* 2008).

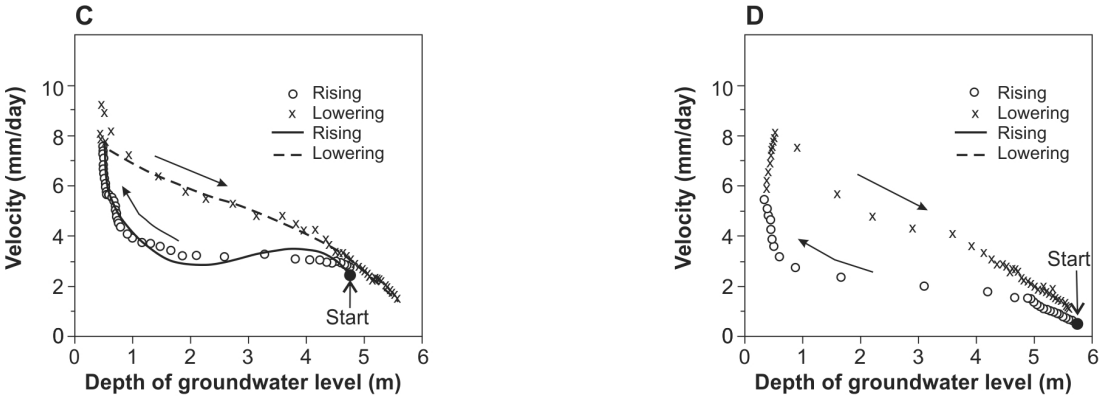

Velocities versus water table depths for January, February and March 1997.

Velocities versus water table depths for December 1997 and January 1998.

Hysteresis relationship between groundwater and landslide displacement for the Vallcebre landslide, Spain (Corominas *et al., ;* Gonzlaez *et al.,* 2008).

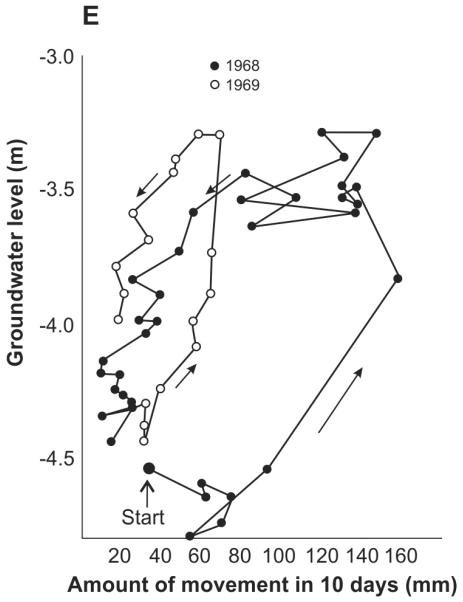

Groundwater and displacement of the Chausuyama landslide Japan (Nakamura, 1984).

Figure 6.16 Relationships between pore pressures and landslide displacement rates for monitored similar landslides in the literature. A and B: Landslides in Tertiary materials of Japan, (redrawn from Matsuura et al., 2008). C and D: Vallcebre landslide, Spain (redrawn from Corominas et al., 2005; Gonzalez et a;., 2008). E: Chausuyama landslide, Japan (redrawn from Nakamura, 1984).

6.4.3 Slow creep

Slow- and vertical-creep motion is steady over long periods of time at both landslides and is similar in form to the graded or gradual slip motion reported by Allison and Brunsden (1990). However, it does differ because slow creep motion occurs over months and years. At Taihape, steady, slow-creep motion appears to have occurred over the entire 3-year detailed-monitoring period. At Utiku, however, slow-creep motion has occurred over most of the monitoring record, but has been interrupted briefly by horizontal accelerated-creep events. Slow- and vertical-creep motions occur together but in reality, the intervals of accelerated creep are too brief for significant vertical motion to accumulate and so the amounts of vertical displacement during them cannot be resolved by the currently used survey methods. At Taihape, where vertical displacement is better resolved, the combined rate of motion from both slow- and vertical-creep at the surface is double the magnitude of displacement recorded on the slip surface. At Utiku, motion along the slide surface is also less than the displacement measured at the ground surface. The relative motion between the ground surface and the top of the slip surface indicate that the landslide mass, as well as sliding as a block, is also deforming plastically (i.e. engineering Type 2 and material science Type 3 creep, Table 2.01), with the translational angles of motion (relative motion vectors) being significantly steeper than the angle of the slide surface and therefore indicating the slide mass is thinning downslope.

For both landslides, horizontal slow-creep rates do not appear to vary with pore pressure as rates are near-constant during both the falling and rising limbs of the pore-pressure time series, indicating that slow-creep motion is unaffected by any apparent changes in pore pressure. For the Utiku landslide, the cumulative vertical displacement of station UTK1 has been plotted against pore pressure from piezometer PZA, and similarly for station UTK4 against piezometer BH4, representing the lower and upper parts of the landslide respectively (Figure 6.17). The general trend of the data indicates downward (negative) vertical displacement of about 34 mm/yr (lower toe) and 10 mm/yr (upper landslide). On the lower landslide, negative vertical displacement initially occurs with lowering pore pressure, but when pore pressure starts to rise there is no positive vertical motion. Similar behaviour is observed for the upper landslide, although the negative vertical motion is about half that of the lower landslide. The lack of consistent relationship suggests that vertical motion does not correlate with pore pressure.

For the Taihape landslide the cumulative vertical displacement of prism 3a has been plotted against pore pressure from piezometer BH1A (Figure 6.18).

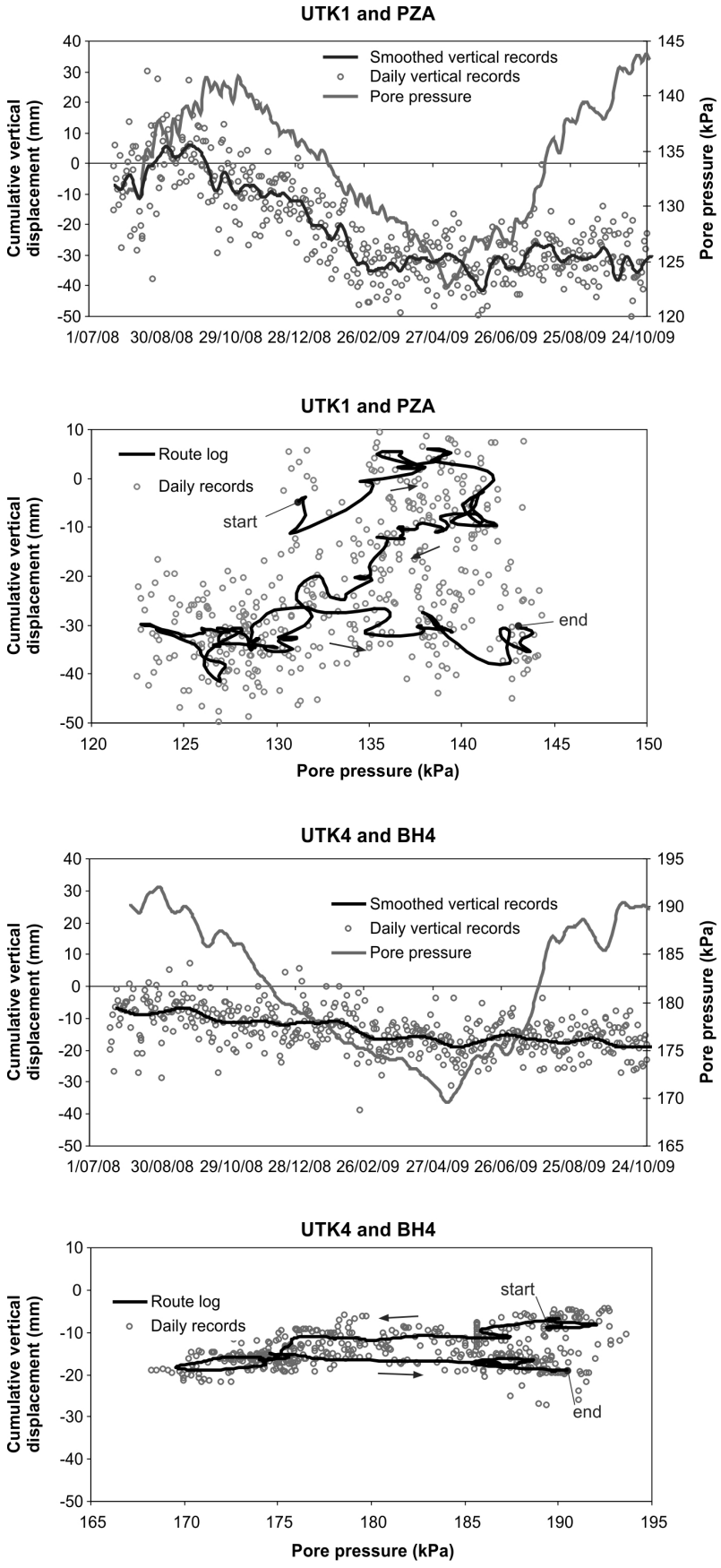

Figure 6.17 Pore pressures and cumulative vertical displacements for the Utiku landslide. Pore pressures represent daily corrected values and vertical displacements represent daily and smoothed daily values. Smoothing carried out using a Gaussian kernel where $G_s = 2$. Route logs are derived from a Gaussian smoothing kernel ($G_s = 5$) and the arrows indicate the chronological order of the data.

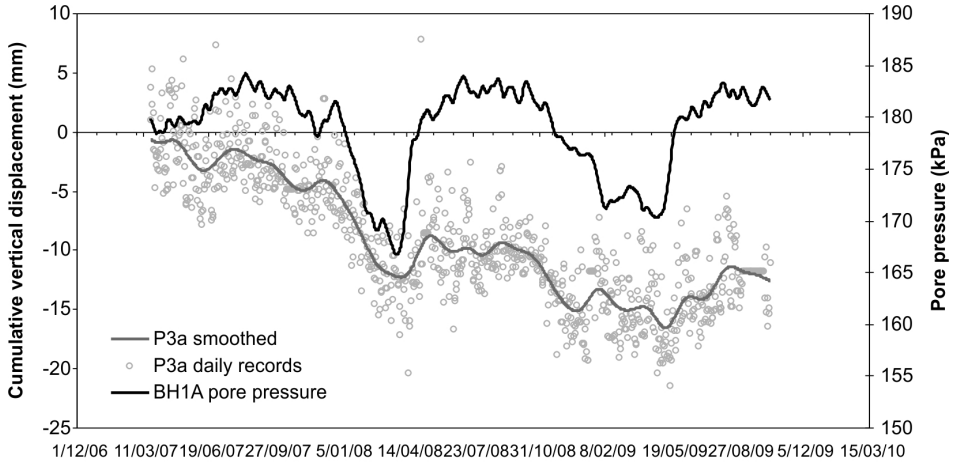

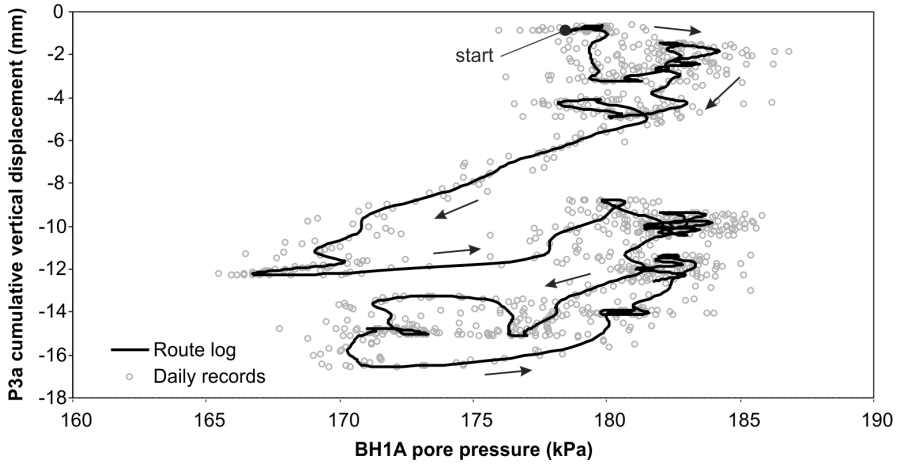

Figure 6.18 Pore pressures and cumulative vertical displacements for the Taihape landslide. Pore pressures represent daily corrected values and vertical displacements represent daily and smoothed daily values. Smoothing carried out using a Gaussian kernel where G_s = 2. Route logs are derived from a Gaussian smoothing kernel (G_s = 5) and the arrows indicate the chronological order of the data.

The general trend of the data indicates negative vertical motion at about 7 mm/yr and represents a steady thinning of the landslide mass, generally unrelated to pore pressure. Several relatively minor and rapid positive (vertically upward) motion periods also occur, which give the general negative motion trend a slightly stepped appearance. This upward (swelling) motion correlates to increases in pore pressure during the wetter winter months and is cyclic, which temporally in the interrupts low thinning of the landslide in this area. These patterns are also similar to those of prism 31.

6.4.4 Seasonal movements

At Taihape, the apparent accelerated-creep motion accounts for the largest displacements recorded during the monitoring period, but they occur in both the up-slope and the down-slope directions, appear somewhat cyclic and are longer in duration than those recorded at Utiku. The periods of up- and down-slope motion follow each

other and repeat on about a yearly basis indicating seasonality, but at some sites with no net gain in down-slope displacement apparent. The relationship between pore pressure and surface movement for a selected period of positive (downslope) accelerated creep (movement periods 3) is shown in Figure 6.19. The pore pressure records shown in this figure are from the piezometer located closest to the prism (prisms 4 and 5 and piezometer BH1A are located on the lower toe and prisms 10 and 11 and piezometer BH2A on the upper toe). Prism displacements are represented by a combination of the daily records, smoothed daily records and the modelled values, which are derived from fitting linear trends to the daily cumulative horizontal displacements.

The daily horizontal displacements recorded during movement period 3 have been plotted against the corresponding pore pressures (Figures 6.20). This shows that there is an obvious difference between the upper and lower toe of the landslide. The graphs representing the upper toe show that displacement initially increases with increasing pore pressure, but that the increases in displacement are steady with differing gradients between the prisms. However, those on the lower landslide show that displacements occur with no or little change in pore pressure. The graphs of pore pressure and displacement rate for prisms 4 and 10 (Figure 6.21), show an initial increase in displacement rate as pore pressure increases, but when displacement rates decrease, pore pressure either remains static, or increases. However, this relationship reverses for the prisms on the lower landslide, indicating a complex movement response to pore pressures that varies between the prisms. Although for some prisms these relationships are similar to those established for the periods of accelerated creep at Utiku, the displacements at Utiku, unlike Taihape, are not cyclic, do not change direction between upslope and downslope, and do correspond to motion recorded along the slide surface.

For comparison purposes, the motion of prism 14 located off the active landslide has been compared to the pore pressure from BH3A, about 20 m from the prism, also located off the active landslide. The cumulative displacement shows cyclic motion, with each annual cycle representing a magnitude of about 5 mm, with the periods of downslope (southward) motion being consistent with those on the active landslide. These cycles correlate well with pore pressure, indicating upslope (northward) motion during summer when pore pressures are low and down slope (southward) motion when pore pressures are seasonally high (Figure 6.22). However, no net change in prism position occurs. There is a lag between the peak pore pressure and peak motion cycle, with pore pressures peaking later than the prism motion, which may be caused by a lag between soil moisture and pore pressure. The soil moisture data in Figure 6.23, is taken from a NIWA operated site about 50 km north of Taihape, but is in the same climatic

region, and is assumed to be representative of regional soil-moisture conditions. The general long-term soil-moisture and pore-pressure trends are similar, in that they follow the same seasonal cycles, but soil moisture tends to increase and decrease more quickly than pore pressure, suggesting a lag does indeed exist. It is probable that the recorded cyclic motion is related to ground shrinkage and swelling in response to seasonal changes in soil moisture.

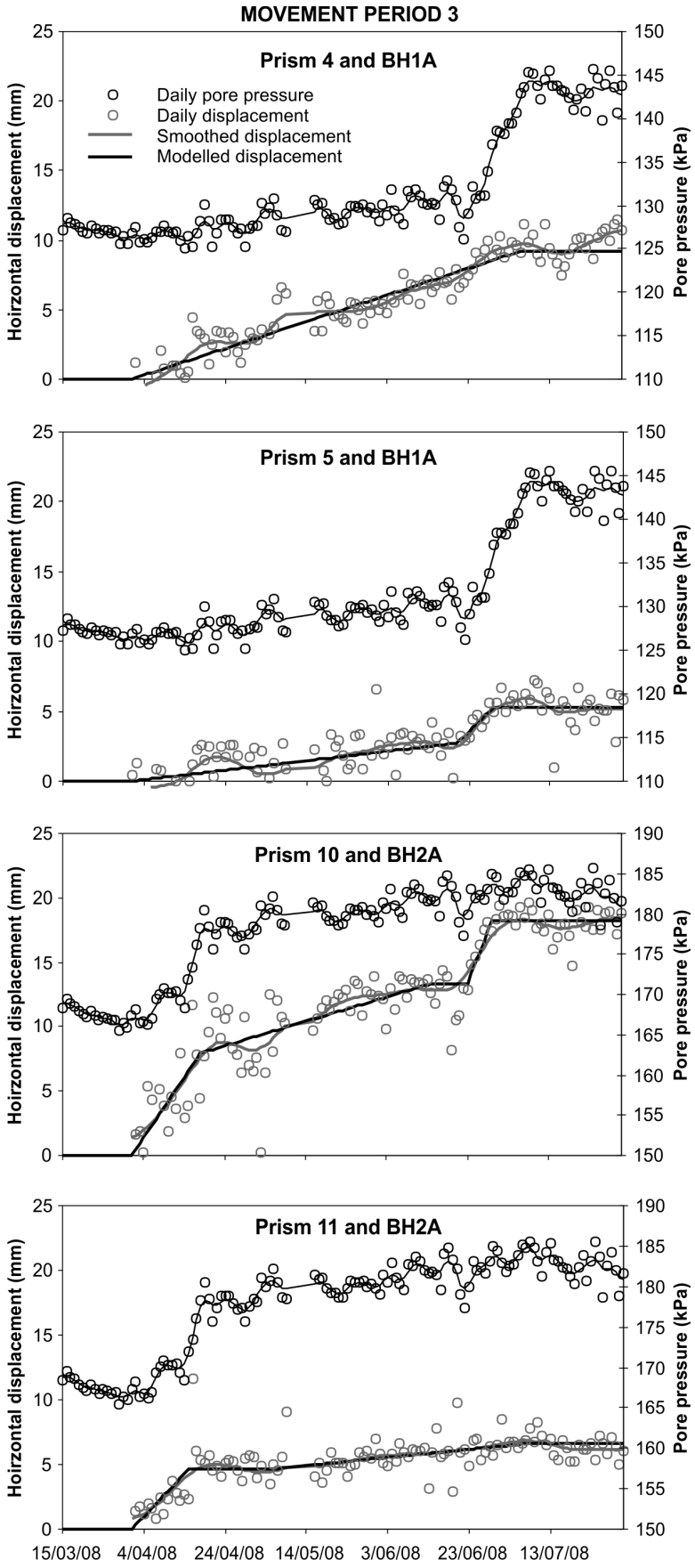

Figure 6.19 Seasonal accelerated creep recorded at the Taihape landslide for movement period 3. Records are from prisms 4, 5, 10 and 11, and piezometers BH1A and BH2A. Pore pressures represent daily corrected values and horizontal displacements represent daily, smoothed daily (using a Gaussian kernel where G_s = 2) and modelled values (using linear trends fitted to the daily values).

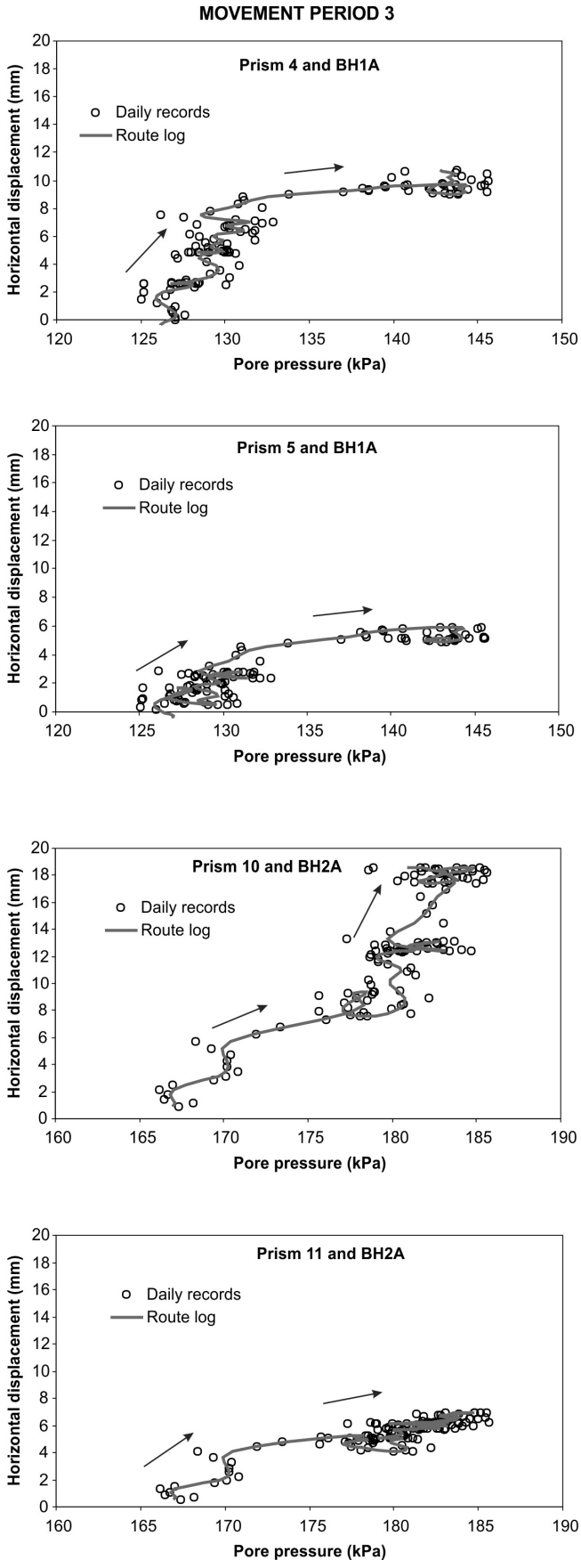

Figure 6.20 Pore pressures and displacements for seasonal accelerated creep movement period 3, Taihape landslide. Records are from prisms 4, 5, 10 and 11, and piezometers BH1A and BH2A. Pore pressures (corrected) and horizontal displacements represent daily values. Route logs are derived from a Gaussian smoothing kernel (G_s = 5) and the arrows indicate the chronological order of the data.

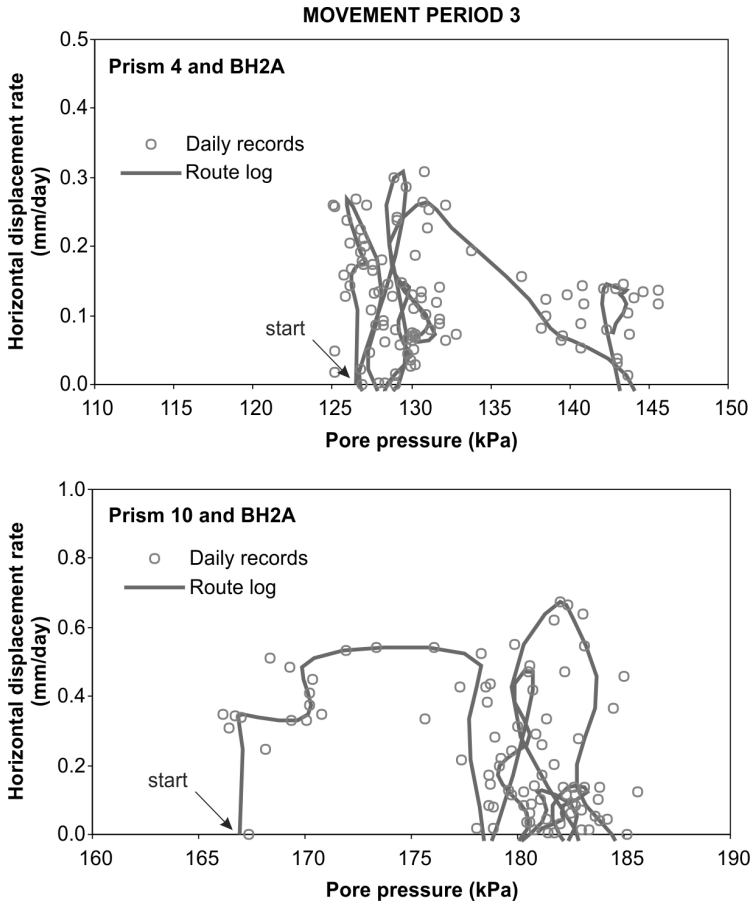

Figure 6.21 Pore pressures and displacement rates for seasonal accelerated creep movement period 3, Taihape landslide. Pore pressures recorded at piezometer BH2A and are corrected daily mean values. Displacement rates are from prisms 4 and 10 and are calculated from the daily horizontal displacements which have been smoothed using a Gaussian smoothing kernel, where G_s = 2 mm. Route logs are derived from a Gaussian smoothing kernel (G_s = 5) and the arrows indicate the chronological order of the data.

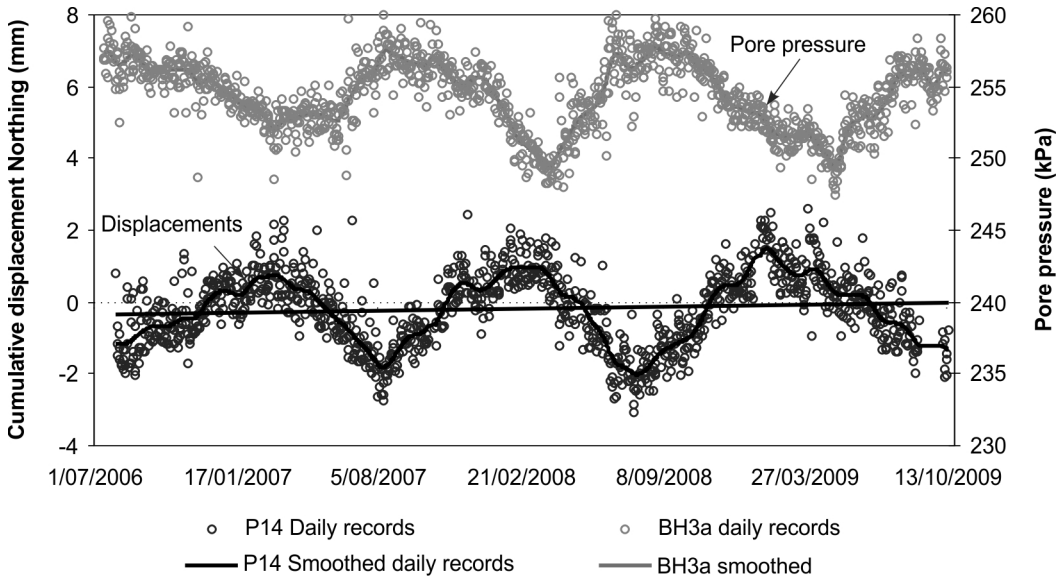

Figure 6.22 Seasonal variations in cumulative displacements plotted against corresponding pore pressures for a prism outside the active area of the Taihape landslide.

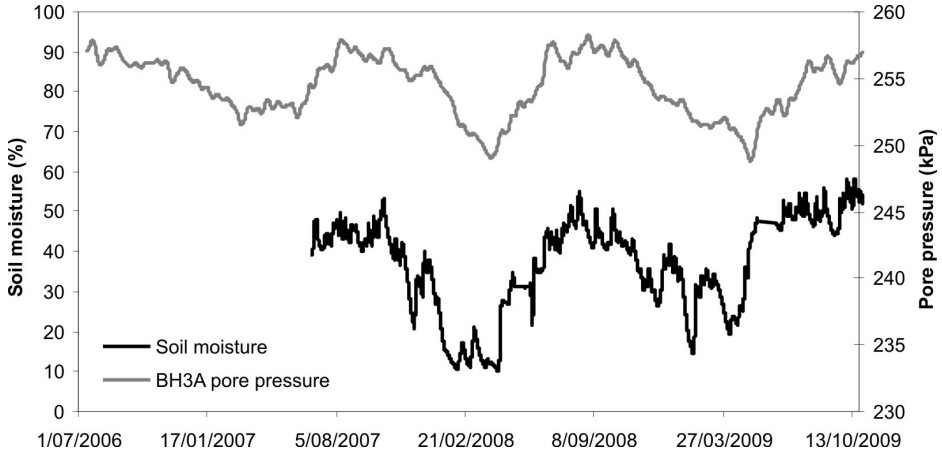

Figure 6.23 Comparison of soil moisture and pore pressures trends. Pore pressures are recorded at piezometer BH3A on the Taihape landslide and soil moisture is from a NIWA operated site about 50 km north of Taihape.

The apparent accelerated-creep motion recorded on the active landslide is thought to be related to seasonal variations in soil moisture which are correlated with pore pressure. At times the swelling adds to the slow creep motion to give apparently accelerated creep (downslope in the direction of landslide motion), and at times it subtracts to give an apparent cessation of surface motion or reversal of motion to upslope. At prism 4 the annual cyclic shrinkage and swelling has a magnitude of about 10 mm in the horizontal and the rate peaks at about ±20 mm/yr, this is superimposed on a steady slow creep of about 5 mm/yr. As the cyclic swelling and shrinkage is happening at about an order of magnitude faster rate than the steady creep, it is being resolved and is strongly influencing the observed data, while having very little to do with the landslide mechanism.

6.4.5 Pore pressure and movement patterns

The episodic, gradual and graded slip, and multiple or surge cumulative surface displacements described by Allison and Brunsden (1990) are comparable to the slow- and accelerated-creep cumulative surface displacements described for both Utiku and Taihape landslide, although slow creep motions are much longer in duration. These are also comparable to the surface movement patterns of other reactivated translational slides described in the literature e.g. Iverson, (1985); Allison and Brunsden (1990); Bracegirdle et al., (1991): Angeli et al., (1996); Petley et al., (2005); Moore et al., (2007);Matsuura et al., (2008); Ranalli et al., (2009); Schultz et al., (2009a; 2009b); Zangerl et al. (2010). Few of these studies discuss the patterns of landslide surface movement, although much effort has been made to link periods of movement with their triggering factor(s), of which pore pressure is the most frequently discussed trigger for landsliding.

Motion patterns on both landslides have limited correlation with pore pressure. Relationships between the accelerated- slow- and seasonal-creep motion patterns and pore pressures for the entire time series are shown in Figures 6.24, 6.25 and 6.26. These figures are annotated with the main periods of accelerated-, slow- and seasonal-creep, with arrows that indicate the data route log (chronological order, oldest to youngest). For Utiku, records from station UTK1 and piezometer PZA (lower landslide) show that the accelerated-creep periods 1 and 2 occur at the beginning of the time series and present a near-linear relationship, whereby horizontal motion increases in direct proportion to increasing pore pressures, this simple relationship then vanishes as motion continues but with pore pressures remaining relatively stable. Motion then changes from accelerated creep to slow creep, as pore pressure declines in response to the dryer summer months. The slow-creep motion continues at similar rates even as pore pressure begins to rise in response to the wetter winter months. Motion then accelerates (movement period 3), as pore pressures continue to rise to similar levels as occurred during periods 1 and 2.

Similarly for Taihape, cumulative displacements and pore pressures for prism 4 and piezometers BH1A have been used to illustrate the relationship between pore pressure and surface displacement on the lower toe of the landslide (Figure 6.25), and prism 10 and piezometer BH2A for the upper toe (Figure 6.26). These surface displacement records are dominated by relatively rapid seasonally cyclic motions which superficially appear similar to the accelerated creep motion at Utiku, at some prisms, however, these alternate between upslope and downslope directions but result in no cumulative displacement and unlike those at Utiku, are not represented by similar trends in motion at the slide base. The relationship between surface movement and pore pressure for both the lower and upper toe are slightly hysteretic. The hysteresis, represented by the positive and negative apparent accelerated creep motion, is interesting as it suggests a kind of steady-state to the system, where one system alternately follows another, in this case seasonally rising and falling pore pressures causing up-slope and down slope motion. The cycles of apparent accelerated creep are progressively, but slowly, moving down slope as there is a general increase in the cumulative horizontal displacement. This suggests that the apparent accelerated creep is seasonal and superimposed on steady slow-creep motion, which is unaffected by any change in pore pressure. These cyclic variations in motion probably relate to seasonal changes in soil moisture which in turn correlate with pore pressure. Similar magnitude seasonal fluctuations in soil moisture and associated motion could be present on the Utiku landslide, but the precision of the measurements at Utiku does not allow them to be resolved. It may also be that they are not being measured at Utiku because the monuments being used are deeply seated and may be anchored below the seasonally affected zone.

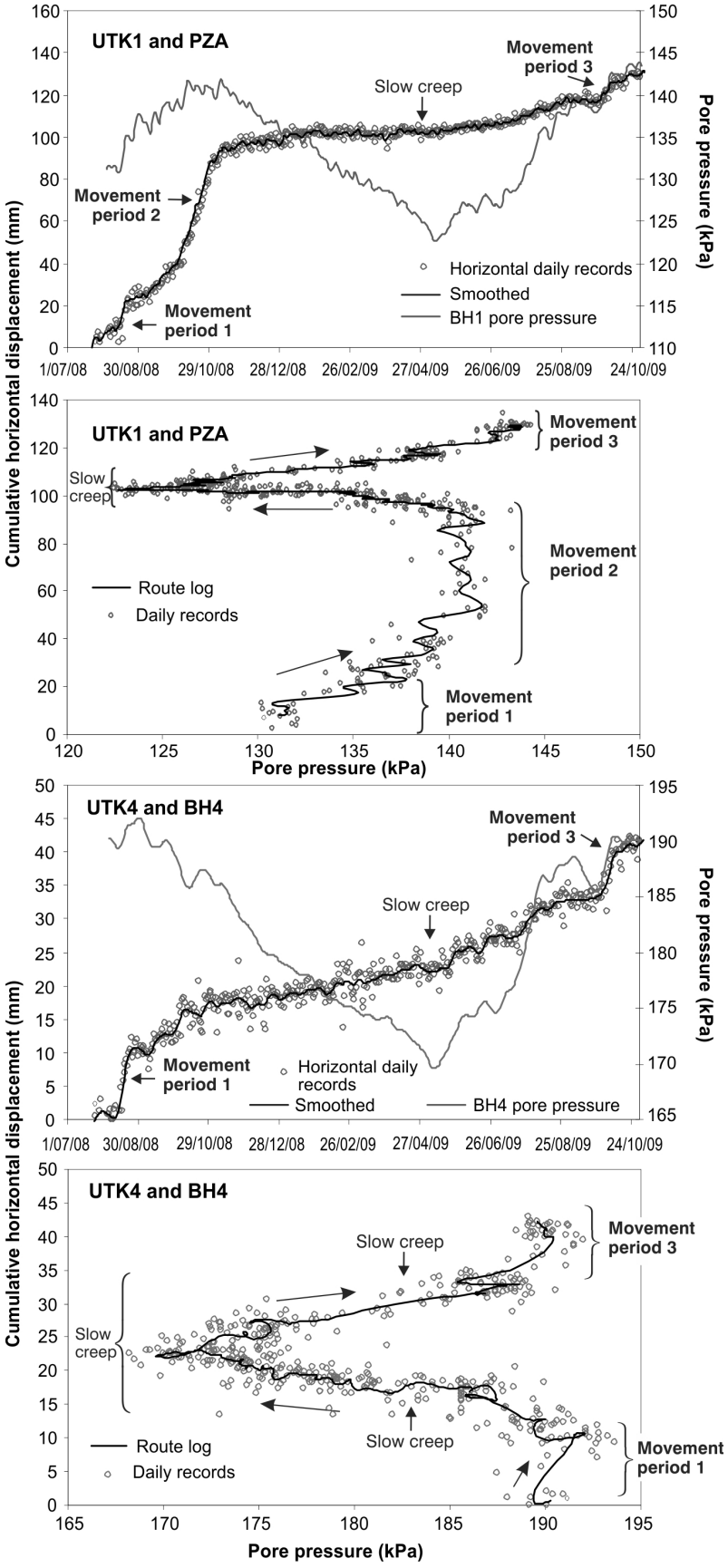

Figure 6.24 Pore pressures and cumulative horizontal displacement of the Utiku landslide. Records are from GPS stations UTK1 and UTK4, and piezometers PZA and BH4. Pore pressures represent daily corrected values and horizontal displacements represent daily and smoothed daily values (smoothed using a Gaussian kernel where G_s = 2). Route logs are derived from a Gaussian smoothing kernel (G_s = 5) and the arrows indicate the chronological order of the data.

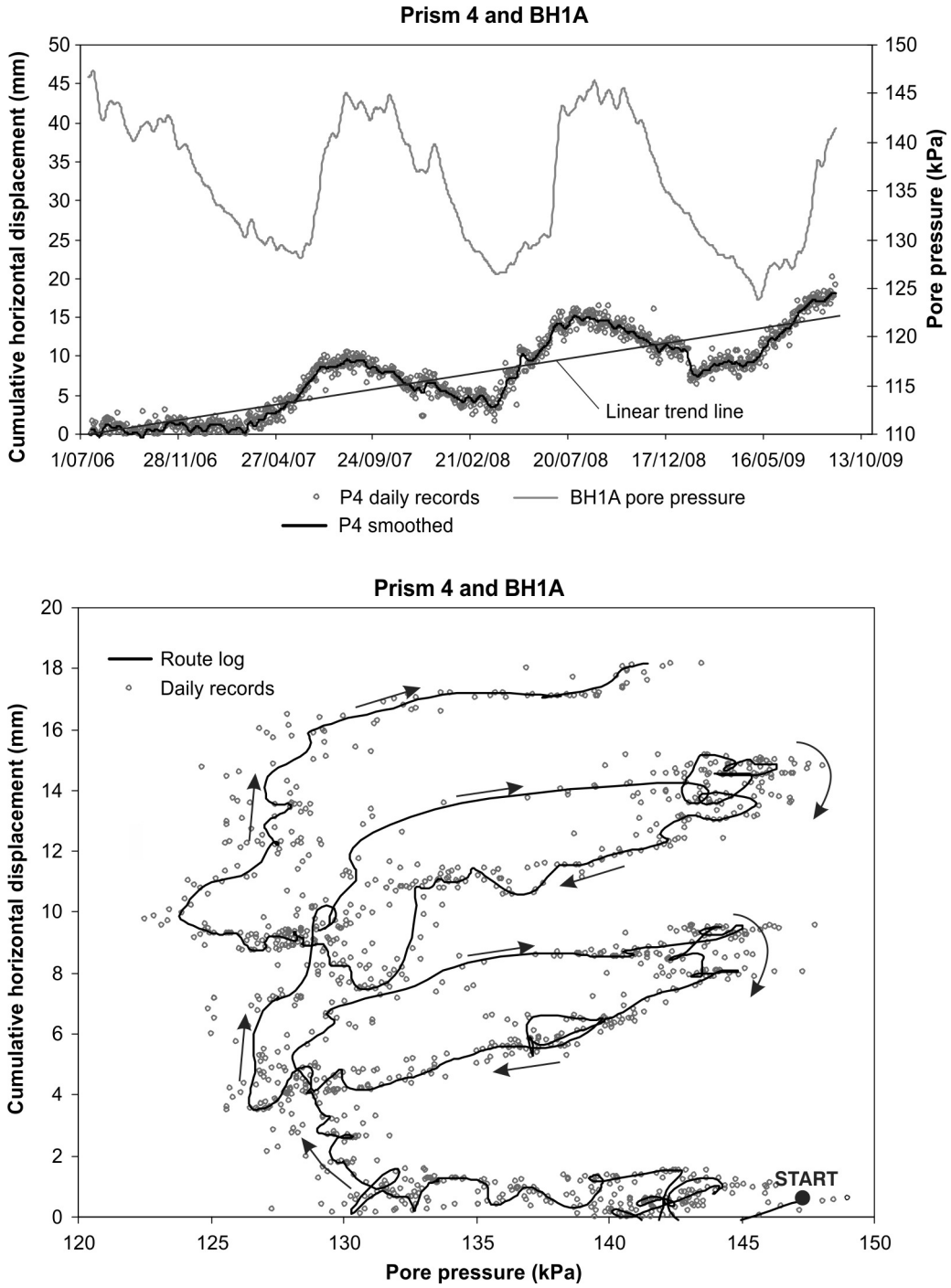

Figure 6.25 Pore pressure and cumulative horizontal displacement of the Taihape landslide, prism 4 and piezometer BH1A. Pore pressures represent daily corrected values and horizontal displacements represent daily and smoothed daily values (smoothed using a Gaussian kernel where G_s = 2). Route logs are derived from a Gaussian smoothing kernel (G_s = 5) and the arrows indicate the chronological order of the data.

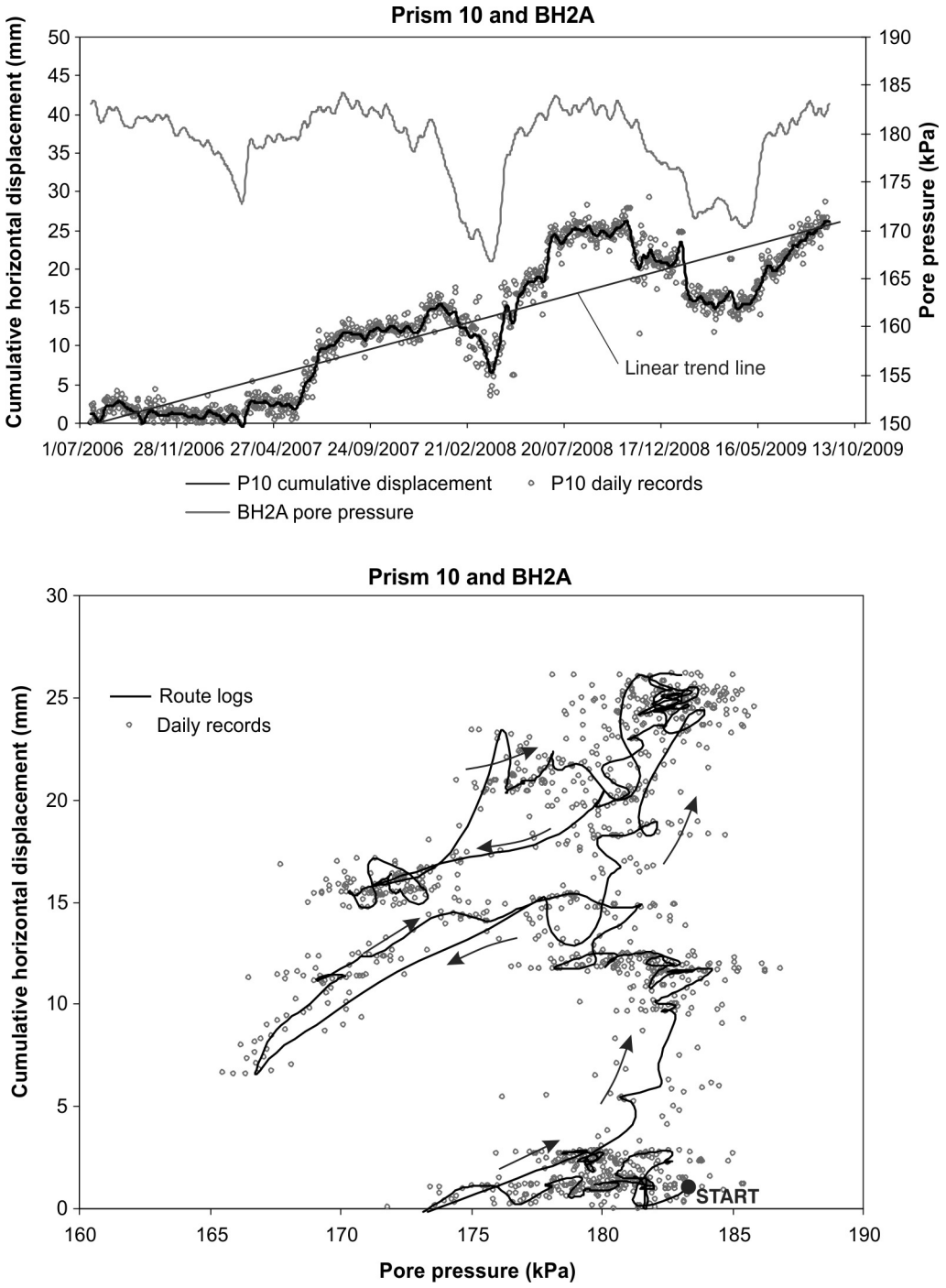

Figure 6.26 Pore pressure and cumulative horizontal displacement of the Taihape landslide, prism 10 and piezometer BH2A. Pore pressures represent daily corrected values and horizontal displacements represent daily and smoothed daily values (smoothed using a Gaussian kernel where G_s = 2). Route logs are derived from a Gaussian smoothing kernel (G_s = 5) and the arrows indicate the chronological order of the data.

At Utiku, each period of accelerated creep initiates with a period of positive acceleration coincident with a period of increasing pore pressure. However, following the initial acceleration, the landslide can either move at constant velocity or slow while pore pressures remain similarly high, indicating that pore pressures, although possibly triggering movement, do not control the arresting process.

For both landslides there appears to be no relationship between horizontal slow-creep

and pore pressure, as rates of motion remain constant through both rising and falling segments of the pore-pressure cycles. Vertical creep at both landslides can be detected during the long periods of slow creep because they are long enough for significant displacement to accumulate and these correlate with general lowering of pore pressure. Minor swelling is detected at Taihape when pore pressure rises, however, the plastic deformation and thinning of the landslide debris is generally faster than the swelling rate, and the seasonal swelling never returns the surface to the same elevation. For both landslides the slow-creep displacement vectors show motion is converging on their bases at angles that are significantly steeper than the dip of their respective slide surfaces.

The pore-pressure records, against which landslide motions have been assessed, are from the partially or wholly confined aquifers at or immediately above the sliding landslide base and may not be representative of pore pressures or soil-moisture conditions elsewhere in the body of the landslides, where neither are being monitored.

6.5 Observed versus traditional pore pressure and movement relationships

The dynamics of the Utiku and Taihape landslides, like all other landslides, are generally governed by the difference between driving forces (shear stresses), which depend on weight and slope, and are largely constant, and resisting forces (shear resistance) (Corominas et al., 2005). The movements of the Utiku and Taihape landslides are localised and partly comprise sliding of blocks over rigid bases, with slip occurring within a thin band of clay; a dynamic situation which is similar to many other slow-moving, reactivated landslides (Leroueil et al., 1996). In addition to basal siding, plastic deformation (Types 2 and 3 creep, Table 2.01) of the slide blocks above the clay slide-surface has been detected at both landslides, indicating that the blocks are not rigid, and that their plasticity can play a role in the dynamics of the landsliding.

The movement of glaciers has, for a long time, been known to comprise two components, basal sliding and internal plastic deformation (e.g. Embleton and King, 1968). These two components are similar to those identified for the Utiku and Taihape slides, with basal sliding detected mainly during periods of accelerated creep, and plastic deformation detected mainly during long periods of slow creep.

6.5.1 Basal sliding

The residual shear strength (τ_r) of the clay forming the slip surfaces can be estimated from the Mohr-Coulomb failure criterion (Leroueil et al., 1996). This relationship holds that the residual shear strength of the clay depends upon the effective stress and the

residual friction angle of the material (Equation 2.1). If an invariant friction angle is assumed for the material, then the residual shear strength becomes only a function of pore-pressure-induced changes in effective stress, where the difference between the driving and resisting forces can be estimated using e.g. the infinite slope method (Morgenstern and Price, 1965, Equation 2.2a).

The difference between the driving and resisting forces gives rise to an acceleration of the landslide mass, which can be estimated using Newton's law of motion that force is equal to the time derivative (rate of change) of linear momentum: hence if mass is not changing force is mass multiplied by acceleration (f=ma), for a point where infinite-slope conditions apply and where resisting forces are estimated using the Mohr-Coulomb criterion (Corominas et al, 2005).

$$m.a = \tau - \left(c' + \sigma'_n . \tan \phi'_r\right), \text{ or } m.a = \tau - \tau_r \qquad \text{Equation 6.1}$$

Forces can be calculated over a unit area of slide plane, where τ is the shear stress calculated using the infinite-slope method, cohesion (c) is 0 kPa as the material is at residual strength. In using this equation, it is assumed that landslide velocity is a function of the ratio of shear stress to shear resistance, and will therefore vary with pore pressure, if this is the only temporal variable, and that the slide surface is planar and the slope extends over a relatively long distance. Several authors find that values calculated using this equation tend to be very high and not comparable to measured values (Angeli et al., 1996), indicating the relationship does not explain all of the observed motion patterns.

Examples from monitored similar landslides in the literature show that there is a general relationship between pore pressure and landslide velocity. For example, detailed observations of slopes sliding on pre-existing slip surfaces at San Martino Italy (Bertini, 1984) and at Salledes France (Cartier and Pouget, 1988) show that movement and displacement rate follow variations in the pore-water-pressure regime, where the rate of movement depends on the applied shear stress (Leroueil et al., 1996). Many researchers have found that the pore pressure displacement rate plots show hysteresis, indicating different landslide velocities can occur at the same pore pressure (Nakamura, 1984; van Asch et al., 2007; Gonzalez et al., 2008; Matsuura et al., 2008; Bertini, 1984).

The hysteresis in the movement in relation to observed groundwater fluctuations is because pore pressure affects the resistance to flow, and hence affects the acceleration. It is always possible to have different velocities and the same acceleration, and the same velocities and different accelerations. The expectation, assuming Mohr-

Coulomb slip, is that if pore pressure is high enough for the landslide to accelerate, it ought to keep accelerating at the same pore pressure and it should accelerate faster as pore pressure keeps rising. The acceleration has to drop below zero before the landslide will appear to slow as momentum is lost. If it is still above zero then the landslide will continue to speed up, but possibly at a slower rate. In many of these documented slides, including at Utiku and Taihape, the surveyed positions of the landslide are not precise enough to closely monitor changes in the acceleration.

A similar, but more complex relationship has been found at the Utiku landslide, where the onset of accelerated-creep motion detected at the surface corresponds to an increase in pore pressure at the landslide base. The initial relationship between increasing pore pressure and increasing surface velocity is linear, and similar to the published relationships (e.g. Nakamura, 1984, van Asch et al., 2007; Gonzalez et al., 2008). However, there comes a point when surface velocity becomes independent of pore pressure and decreasing velocity can occur before decreasing pore pressure. Based on the infinite-slope method, and assuming pore pressure is the only variable, landslide velocity should increase with pore pressure induced decreases in the factor of safety and vice versa as observed by Bertini et al. (1984) and Cartier and Pouget (1998) (Figure 6.27). However, at Utiku, velocity tends not to slow when pore pressure reduces even though the latter should induce increased shear resistance. Indeed, motions tend to slow and arrest even when the calculated shear resistance, using the infinite slope method, along the slide surface is lower than at the initiation of motion (Figure 6.28). This implies that the landslide can be moving or stationary for the same apparent value of shear resistance. Figure 6.29 is a schematic diagram showing the relationship between pore pressure and surface velocities found in the literature compared to the observed relationship for the Utiku landslide. Although accelerated-creep motion has been recorded at Taihape by the inclinometers, only limited pore-pressure data are available for that period and so it has not been possible to examine this relationship.

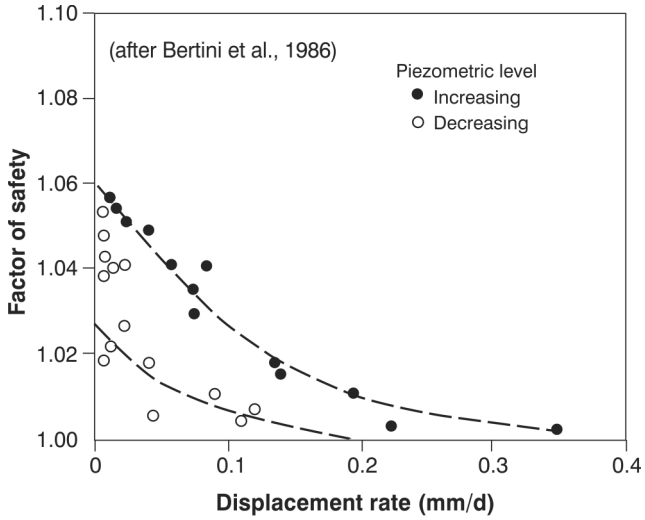

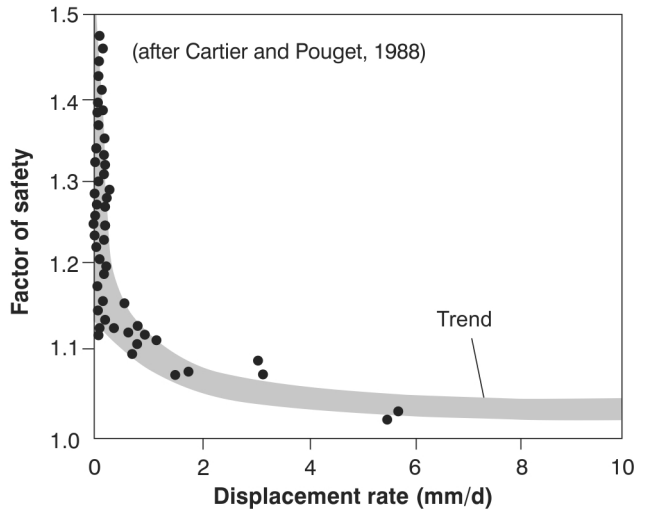

Figure 6.27 Relationships between the factor of safety and landslide displacement rates for two similar landslides discussed in the literature, where the factor of safety is controlled primarily by pore-pressure induced changes in the effective stress. A: redrawn from Bertini et al., 1986). B: redrawn from Cartier and Pouget, 1988.

The results from Utiku suggest that once slip occurs, the relationship between pore-pressure-induced changes in the residual shear strength of the slide surface and landslide velocity are either non-existent or highly non-linear and that the apparent shear strength is probably dependent upon other factors. Many authors have used viscosity functions to better describe and in some cases predict the motion patterns of these types of landslide assuming that once motion is triggered the landslides move as visco-plastic flows, rather than rigid-plastic frictional slip, e.g. Iverson (1985), Angeli et al., (1996); Corominas et al., (2005); van Asch et al., (2008); Ranalli et al., (2009).

Results from SEM analysis of the Utiku and Taihape slide-surface clays showed that the clays contain many discrete shear surfaces (slickensides), and so theoretically, displacement of the landslide could occur along any number of shear surfaces within

this material, and not all of the shear surfaces need to be utilised. Instead, the width of the shear band mobilised during a particular displacement period can change. The benefit of adopting visco-plastic flow models is that the width of the shear band can be taken into account, whilst still assuming Mohr-Coulomb slip. Due to the viscous nature of clay materials, the rate of movement should progressively increase as the factor of safety decreases, and conversely the rate of movement should decrease in response to a widening shear band (Cartier and Pouget, 1988; Bracegirdle et al., 1991; Leroueil, 1998).

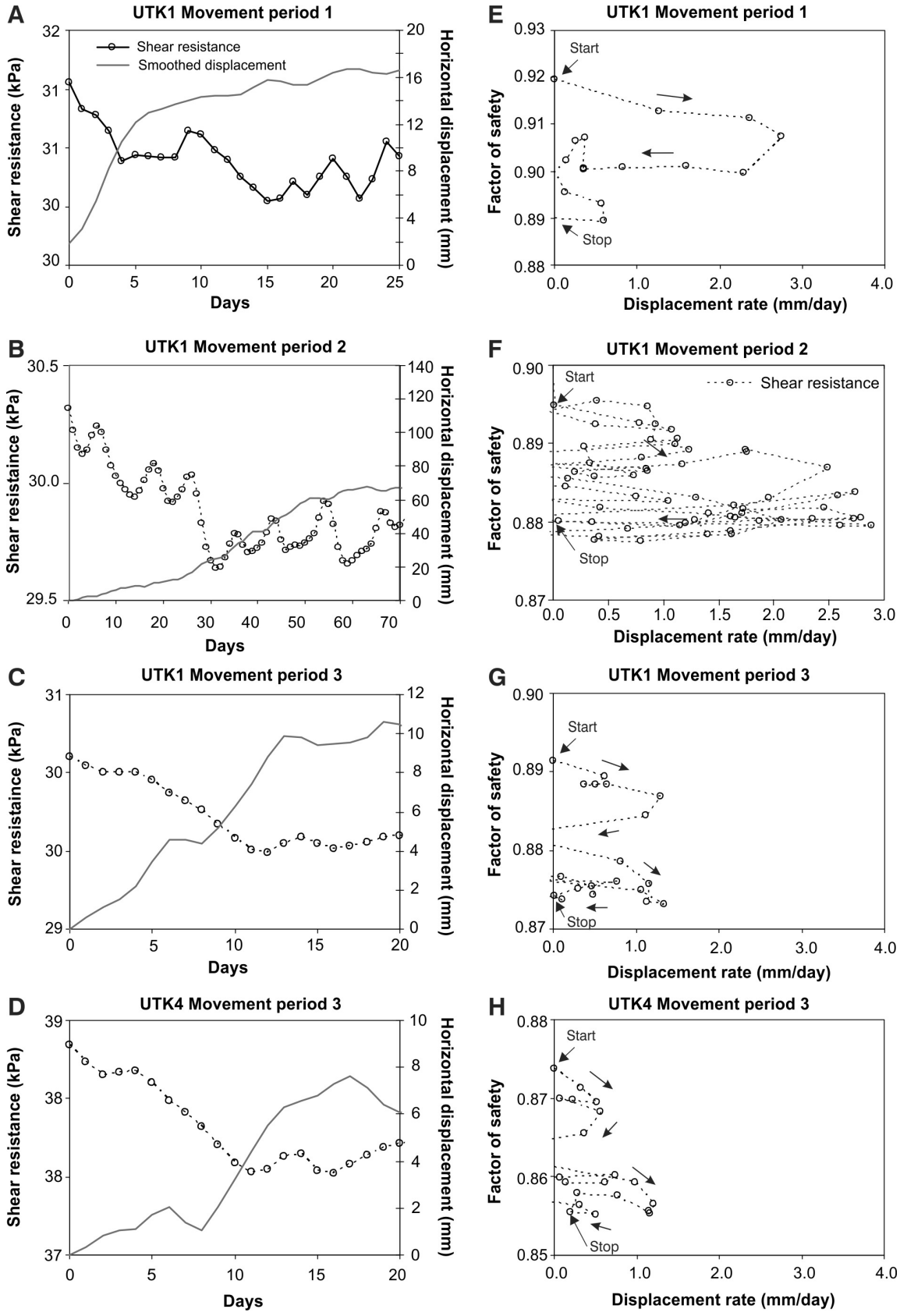

Figure 6.28 Relationship between shear resistance, factor of safety and displacement rate for the Utiku landslide during accelerated creep periods 1, 2 and 3. A to D: Shear resistance calculated at the slide surface at GPS stations UTK1 and UTK4, using the Mohr-Coulomb failure criterion and daily pore pressures from piezometers PZA and BH4, assuming $\phi_r' = 8°$ for the slide-surface clay. Horizontal displacements are smoothed daily displacements, smoothed using a Gaussian kernel where $G_s = 2$. E to H: Factor of safety calculated from the infinite slope method, and displacement rates are calculated from the daily cumulative horizontal displacements. Arrows indicate the chronological order of the data.

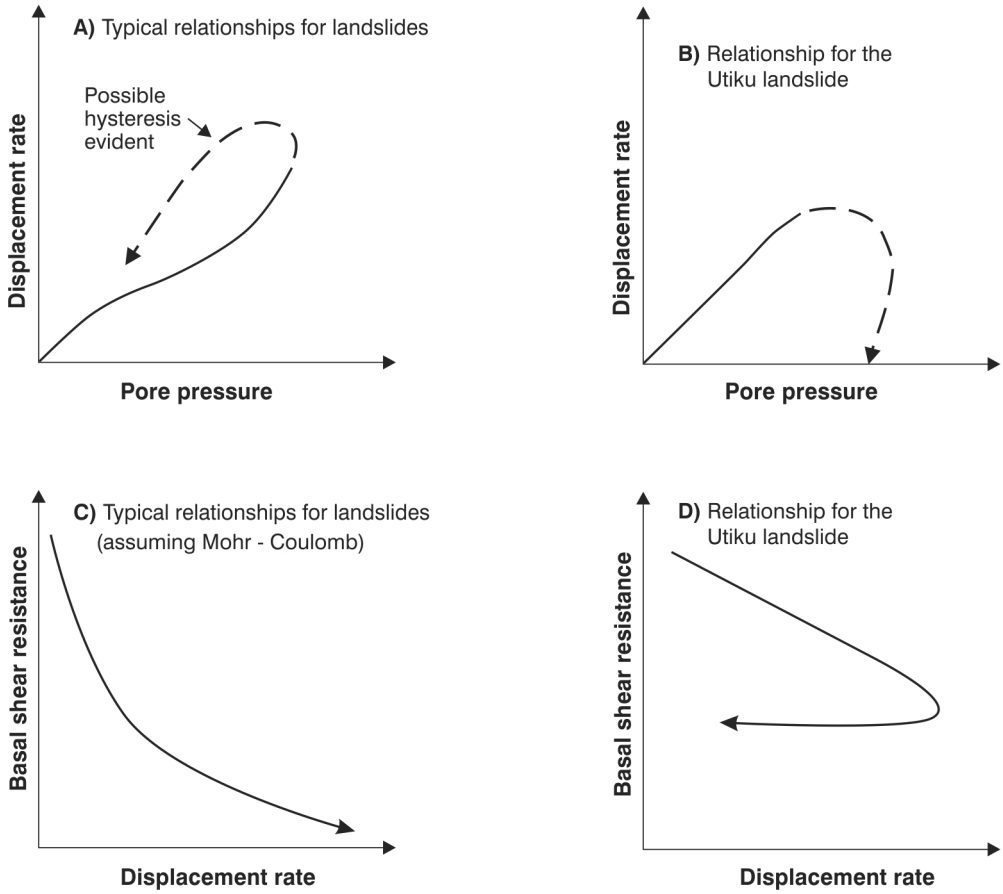

Figure 6.29 Schematic diagrams comparing the relationships between pore pressures and displacement rates for monitored similar landslides in the literature and the Utiku landslide. A and B: Displacement rate and pore pressure. C and D: shear resistance at the landslide base (slip surface) and displacement rate.

To further explore the relationship between landslide displacement rate and pore pressure at the Utiku landslide, a modified Mohr-Coulomb failure criterion has been suggested that includes a viscous-resistance component, assuming that the clay forming the slip surface is a visco-plastic rather than purely plastic material. Bingham's viscosity model has been used (Equation 2.5), which is described in Angeli et al. (1996), as the shear surface is thin (< 5 cm), a linear velocity profile i.e. Newtonian viscosity has been assumed (van Asch et al., 2007). The apparent viscosity of the slip-surface clay can be calculated using equation 2.4 (Section 2.3.2), where the depth of movement and piezometric levels are known, and where the thickness of the shear surface has been measured, assuming that the entire band is mobilised during an event. The viscosity has been calculated by back analysis of the individual periods of accelerated-creep motion recorded at Utiku. It was not possible, however, to derive from back-analysis, the apparent viscosity of the landslide shear band, because the factor of safety, calculated using the infinite-slope method, does not drop below 1 for any of the positions on the landslide where the slip-plane depth and pore pressures are known. This method cannot take into account the additional driving forces applied from the

upper part of the landslide, as shown by the finite element and limit equilibrium modelling. In an attempt to explore the relationship between viscosity and motion of the Utiku landslide, the modelled inclination of the shear band was increased and the viscosity for different motion rates calculated.

Results for station UTK1, show that the apparent viscosity decreases asymptotically as displacement rate increases (Figure 6.30) (plotted as 1/viscosity the relationship is linear). The error line shown on the figures refers to the 95% error on the velocity. This suggests that the apparent viscosity of the clay is about 10 to 20 GPa s (based on the calculated 14-day moving mean velocity of the GPS station), and that apparent viscosity is low at the onset of movement and decreases with increasing displacement rate, and as velocity decreases, apparent viscosity increases until movement stops.

Calculations show that apparent viscosity varies in response to displacement rate and possibly time. Gonzalez et al. (2008) found that a constant viscosity gives a linear relationship between pore pressure and displacement rate, however, the relationship between pore pressures and velocity is non-linear, which is also the case for those landslides showing hysteresis e.g. Bertini et al. (1984); Gonzalez et al. (2008); Matsuura et al., (2008), (Figure 6.31), suggesting that the apparent viscosity and therefore apparent shear resistance are controlled by other factor(s).

These other factors may, for example, include: rate-induced changes in shear strength of the slip-surface clay i.e. a dynamic rather than static ϕ_r, caused by either rearranging the clay-particle bonds during shearing; and/or consolidation of the clay during motion. However, increasing resistance forces are also likely to occur as a result of landslide geometry e.g. increases in shear resistance along the landslide flanks as the landslides are three-dimensional, although most analyses are made using two-dimensional models. The interaction between the various slide-blocks forming the landslide mass, e.g. buttressing and mass transfer are factors that Morgenstern (1995) and Ferrari et al., (2010), identified as the main controls on slow-moving landslides.

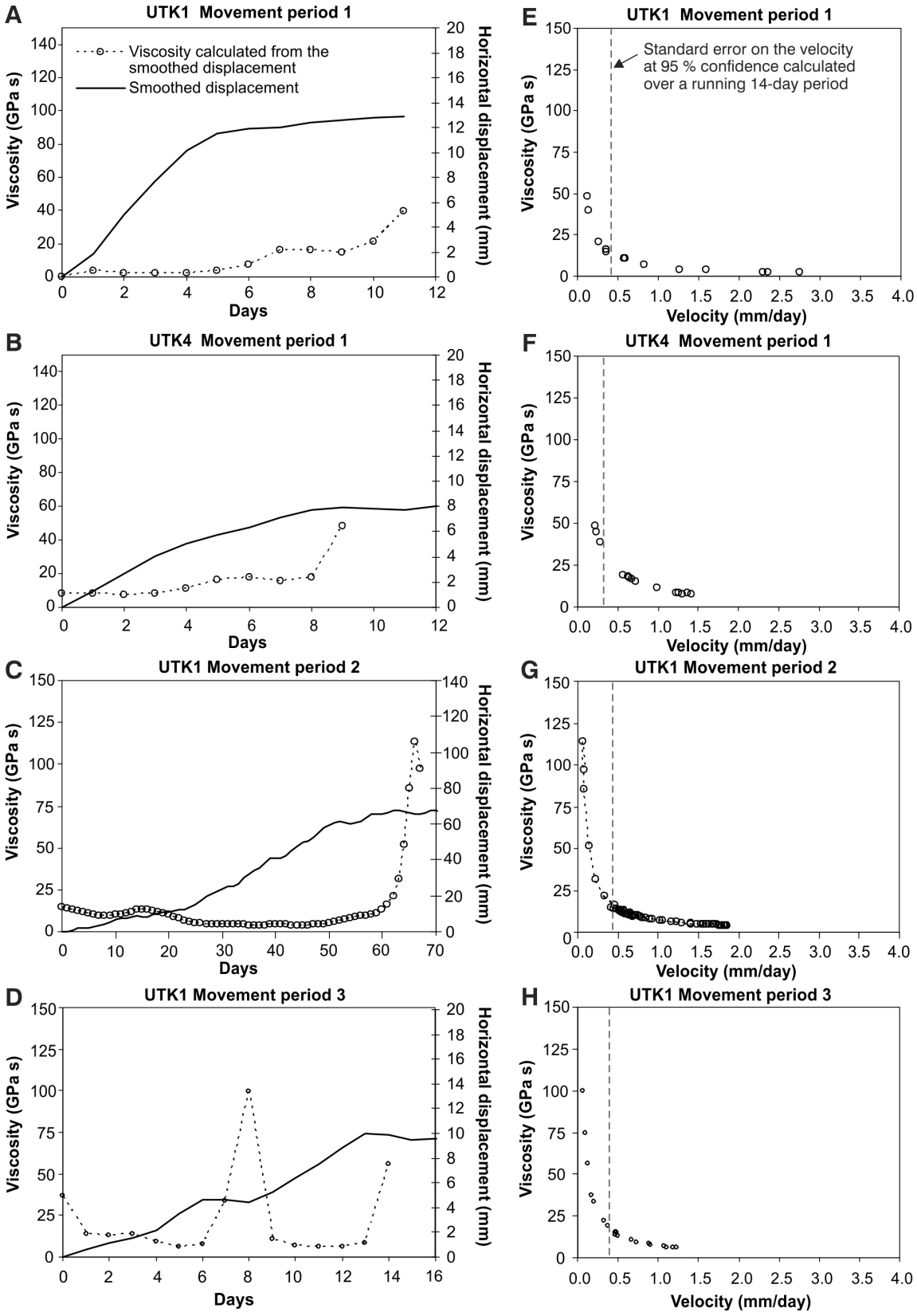

Figure 6.30 Relationship between the apparent viscosity of the slide surface material and landslide displacement rate for accelerated creep movement periods 1 to 3, Utiku landslide. A to D: Viscosity calculated at the slide surface at GPS stations UTK1 and UTK4, using Equations 2.3 and 2.4, and daily pore pressures from piezometers PZA and BH4, assuming $\phi_r' = 8°$ for the slip-surface clay. Horizontal displacements used to calculate viscosity and shown on the figure are smoothed daily displacements, smoothed using a Gaussian kernel where $G_s = 2$. E to H: Horizontal velocity calculated from smoothed daily displacements.

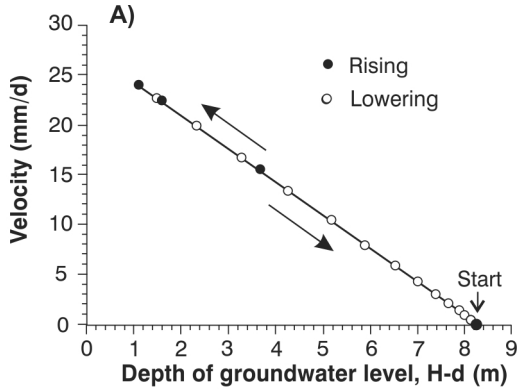

Results from the model velocities, u versus water table depths, H-d, including a viscous component.

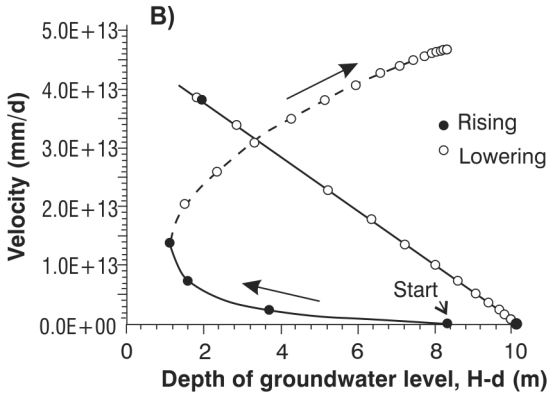

Results from the model velocities, u versus water table depths, H-d, without a viscous component.

Figure 6.31 Conceptual models of landslide displacement and pore pressure, considering static viscosity and variable viscosity (redrawn from Gonzalez et al., 2008).

6.5.1.1 Accelerated-creep and rate-dependent material properties

If it is assumed that landslide motion can be arrested by increases in the shear resistance of the clay forming the slide surface, then the increase must be caused by one or more of the following processes: the amount of displacement (strain); the rate of motion (strain rate), or the duration of motion. Leroueil (1998) showed that strain and strain rate are essentially equivalent. The smectite clay forming the slip-surface materials at Taihape and Utiku comprise layers of clay-mineral particles (arranged in 2:1, tetrahedral to octahedral layers linked by ionic/covalent bonds), linked by Van der Waals bonds (Bennett and Hulbert, 1986). The shear strength of the clay is therefore a function of the product of the number of contacts or bonds between the clay-particles, the displacement of each bond in the direction of the shear stress and the frequency of rupture of a single bond, which is assumed to reform in successive new positions in the course of strain (Pusch, 1976), assuming that the clay particles themselves are not disrupted. Mohr-Coulomb slip can occur by either or both of plastic deformation within clay particles and true Coulomb slip between particles. Strain working, strain rate, and simply time at appropriate pore pressures can change the water-layer thickness within

the clay particles, and change the internal bond strengths and hence plasticity (Bennett and Hulbert, 1986).

Petley (1966) reported shear-box tests on samples of London Clay and Edale Shale at velocities varying from between 0.05 and 140 mm/day, and found that the residual strength of these materials increased by up to 1% to 2% with the logarithm of the shear rate (Bracegirdle, 1991). Similar results were obtained by Lupini (1980) and Lemos (1986) on ring-shear tests on kaolin. Skempton (1985), using the work of Petley (1966) and Lupini (1980), summarised that at slow velocities (5 cm/year to 50 cm/day), the strength variations of London Clay and kaolin were about -3% and +5%, assuming 7 mm/day as mean, and that much larger increases in shear resistance occurred at velocities exceeding 100 mm/minute. These results suggest that at slow strain rates similar to those recorded at Utiku and Taihape landslide, the residual friction angle of the clay material should not change. However, it is noted that these results are for London Clay and kaolin that have liquid limits (LL) of about 80, which is markedly different to the smectite clays forming the slide surfaces at Utiku and Taihape that have LL of about 140. Bracegirdle (1991), based on the relationships identified by Petley (1966), Lupini (1980) and Lemos (1986), proposed an empirical relationship between shear resistance of the clay and rate of shearing (Figure 6.32).

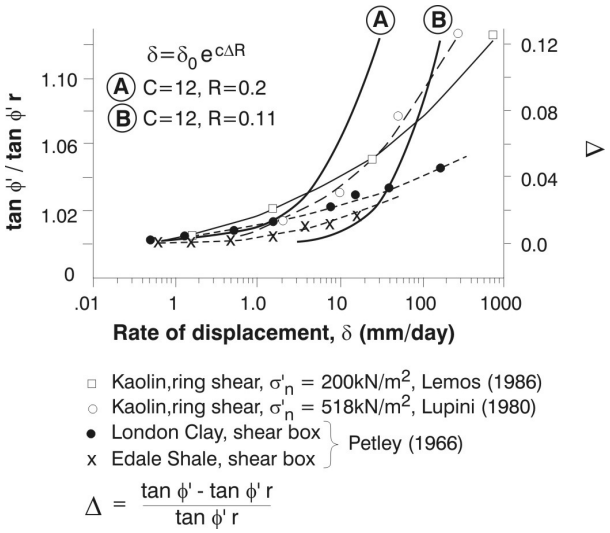

Figure 6.32 Empirical relationships showing the influence of rate of shearing on residual shear strength (redrawn from Bracegirdle et al., 1991).

Based on the limit-equilibrium analyses, an increase in friction angle (ϕ_r) of about 0.2° would be required to arrest the motions of the Utiku landslide during the recorded accelerated-creep motion. Using the relationship proposed by Bracegirdle (1991), including the mean constants (C = 12 and R = 0.2 and 0.11) and assuming a shear velocity of 0.01 mm/day (i.e. pseudo static conditions), a mean velocity of >15 mm/day would be required to achieve the necessary increase in shear resistance. The maximum

recorded rates of motion at Utiku are about 3 mm/day, based on the daily resolution of the data. Using this relationship it appears unlikely that restructuring of the clay-particle bonds leading to increased shear strength would occur at these low rates of motion. However, peak speeds have been shown to occur within a day of being triggered, but the detection of these rates is a function of the temporal and spatial monitoring resolution, where daily motions are calculated. It could, therefore, be possible that peak speeds are higher than those being detected.

Increased shear resistance caused by increasing the number of bonds between clay particles may occur as a result of consolidation of the clay band. Strength regain caused by consolidation of the shear band as pore water is expelled, is a mechanism which has been discussed by Angeli et al., (1996, 2004), but in the context of strength regain during periods of rest rather than during periods of motion. However, consolidation can only occur if there is a change in mean stress. At Utiku and Taihape it is unlikely that the slide-surface clay is consolidating during periods of rest, as it is already very thin and the changes in mean stress are minor.

6.5.1.2 Morphology and movement – buttressing

For both landslides, pore-pressure patterns appear to be a function of the morpho-dynamic setting. The long-term pore-pressure trends over many months indicate that peak pore pressures are achieved at different times and at different locations on the landslides. The lag between the peak piezometer responses may allow different parts of each landslide to unlock and lock at different times. The stability analyses have shown that different slide-blocks have different factors of safety and therefore different movement-triggering pore-pressure thresholds.

The interaction between the slide blocks forming the Vallcebre landslide, Spain, was analysed by Ferrari et al., 2010 using a model based on two interacting rigid blocks, where the translating mass keeps its basic shape. Ferrari et al., 2010 show that during periods of displacement there is a transfer of mass from the upper slide block to the lower toe-slide block, and that the stability of the Vallcebre landslide is controlled by the geometry and mass of the toe-slide block, which acts as “shear key” and which is being eroded by fluvial incision. This mechanism has perhaps been recorded at Taihape where the upper-toe block is moving faster than the down-slope lower-toe block, and therefore is increasing stress on the lower-toe block at the same time as some of the shear resistance on the upper-toe block is caused by the lower toe, i.e. a transfer of mass. It is possible that the largest magnitude motion event that occurred following flooding in response to the 2004 Manawatu rain storm, could have been caused by fluvial erosion of the landslide toe. Hence the accelerated creep motions at Taihape

may be caused by loss of toe support rather than by an increase in pore pressure. A loss of toe support was observed following the Manawatu event but a pore-pressure increase is only inferred. This is confirmed by the numerical modelling, which showed that for every 1.0 m of incision the factor of safety reduces by about 5%. Similarly at Utiku, the landslide is being driven by near vertical displacement of the upper slide block, which is pushing the other slide-blocks down slope.

6.5.1.3 Morphology and movement – landslide geometry

The Utiku and Taihape landslides both involve multiple semi-rigid blocks sliding over rigid bases, but they are geometrically different, with Utiku involving sliding on two essentially perpendicular planes invoking a wedge mechanism, while Taihape is essentially planar. At the Utiku landslide, there is apparent downslope rotation about a vertical axis towards the western flank shown by the decrease in motion magnitudes towards the western flank, and the geomorphology of the graben features, which widen eastwards. These suggest that shear resistance along the western flank is significant. In the absence of constraint in that direction, the landslide would translate directly down dip on the clay layer. The western scarp, however, constrains it from doing this, so that when shear resistance on the basal surface decreases, it is likely that normal stresses along the western flank increase as a result of loading by the active landslide mass. The increased normal stress (normal to the dip direction of the western flank), should cause an increase in shear resistance (assuming Mohr-Coulomb friction), which may cause landslide motion to slow. The increase in shear resistance was estimated using wedge-stability software SWEDGE™ (Section 5.5.1). Results showed that the western flank reduces the shear stress (increases the factor of safety) by about 13% ±(4), which would have the effect of reducing the ϕ_r' of the slide-surface clay from 8° to about 7° or the effect of reducing pore pressures by about 2 to 3 m. The western flank is therefore an important control on the stability of the Utiku landslide.

The above hypothesis is somewhat similar to the mechanism proposed by Schulz et al. (2009b) where decreased pore pressures along the landslide margins are thought to cause increased shear resistance along the boundaries of the landslide, which arrest motion. However, unlike the Slumgullion landslide, it is not the lowering of pore pressures along the flanks that lead to increased shear resistance, but rather the increased shear resistance caused by an increase in the normal stress as the western flank is loaded during an accelerated creep event caused by rising pore pressure at the base.

6.5.2 Plastic deformation

The slow- and vertical-creep motion at Utiku and Taihape landslides appears to be constant without any rate dependency. Although pore pressures are high enough to reduce shear resistance to allow frictional slip along the base, the steady motion is not regulated by pore pressure because the landslides do not speed up or slow down in response to changing pore pressures. This behaviour differs from other landslides. For example, in southwest Colorado, the Slumgullion slide appears to be almost constantly active, but daily cyclic changes in shear resistance have been shown to cause the landslide motion to be cyclic and modulated by the daily atmospheric tide (Schulz et al., 2009b). In addition to landslide motion along the slide surface, the disparity at both Utiku and Taihape landslides between ground-surface and slide-surface motion magnitudes and vectors suggest that the landslide masses are also undergoing plastic deformation resulting in down-slope thinning. Plastic deformation appears to be unrelated to pore-pressure changes, although the latter are measured only at the landslide base, their correlation with soil moisture suggest that they should be representative of pore-pressure trends at other levels.

At Taihape, only about half of the slow- and vertical-creep motion can be attributed to displacement along the slide surface, and similar motion may occur at Utiku. At Taihape, the difference accounts for horizontal motion of about 8 mm (over the monitoring period), which is occurring distributed through the slide mass between the ground surface and the slip surface. At Utiku, the slow- and vertical-creep motion accounts for about 60 mm/year displacement at an angle of about 56° from horizontal (Station UTK1). At Taihape, it accounts for about 11 mm/year at an angle of about 47° from horizontal (Prism 3a), and cannot be attributed to motion along the slide surface. These motion patterns represent distributed plastic shear deformation and thinning of the slide masses, down-slope towards the toe, and may in-part be driving the sliding displacement at the slide surfaces. This may also be the case in many other similar landslides. One example is the Ventnor landslide in the Isle of White, UK, where Moore et al. (2007) report that between 1995 and 2005 rates of motion recorded at the Lowtherville graben were 6 mm/year horizontal motion and 33 mm/year vertical motion, giving a translational angle of displacement of about 80°. These displacements represent a period of predominantly slow-creep motion, which was punctuated by a period of accelerated creep between November 2000 and February 2001 (Figure 6.33). These patterns are similar to those recorded at Utiku and Taihape landslides, where the displacement vectors from Ventnor during the 1995 to 2005 period represent a general thinning of the slide mass, possibly related to plastic deformation.

The plastic deformation of the landslide mass, overlying the slide-surface clay, shown by the slow- and vertical-creep motion is effectively caused by deformation under constant shear stress. Using the terminology proposed by Hutchinson (1988), this deformation behaviour relates to “pre-failure creep” (Type 2 and 3, Table 2.01).

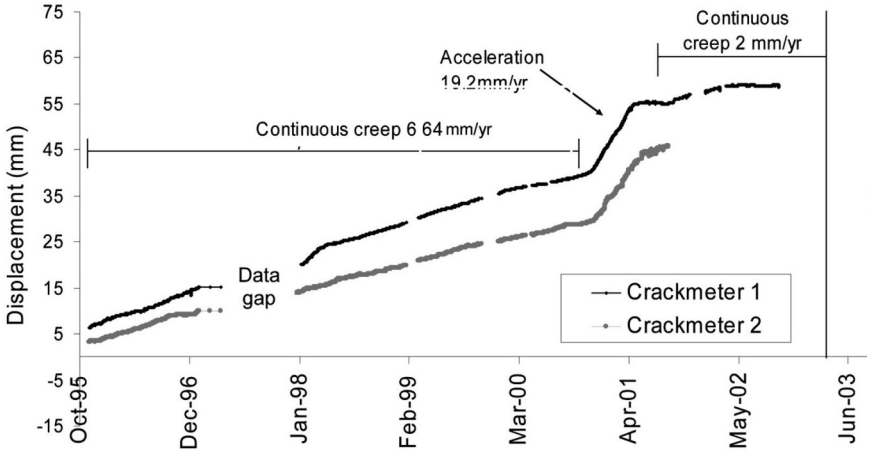

Figure 6.33 Cumulative displacement over time recorded at the Lowtherville graben on the Ventnor landslide, Isle of White, UK (redrawn from Moore et al., 2007).

6.5.2.1 Pore pressure and movement, some considerations

The slow- and vertical-creep motion recorded at both landslides show no correlation with pore pressure. Slow- and vertical-creep motion has occurred over most of the monitoring period, with no detected change in rate even though, at both landslides, the recorded fluctuations in pore pressures should have caused about an 8% change in their factor of safety. The slow creep motion recorded at the Ventnor landslide between October 1995 and November 2000 (Figure 6.33) also does not vary with changes in pore pressure (Figure 6.34).

One possibility to explain this behaviour at Utiku and Taihape is that the recorded pore-pressure fluctuations come from just above the slide surface, and are not representative of pore pressure at the slide surfaces; this would be possible if the clay forming the shear zone were highly impermeable. Another is that the measured confined aquifers may only be responding to changing load on them. If an increase in normal stress on the top of an aquifer decreases the aquifer pore space, and the pore fluid cannot escape fast enough, undrained loading will occur (Hutchinson and Bhandari, 1971). If the structure of the material is unchanged, however, the pore pressure will only increase in response to increasing elastic strain in particles in the aquifer, and the decrease in effective stress will be balanced by the increase in normal stress transmitted through the grains, hence the shear resistance along the slide surface may remain unaltered. At Taihape, the correlation between soil-moisture trends and pore-pressure trends suggests that the increase in normal stress could be caused solely by

the increasing weight of the wetted near-surface materials by infiltrating rainfall. At Utiku, however, increases in pore pressures above a threshold value appear to trigger accelerated creep, suggesting that there, some infiltration is eventually reaching the aquifer and increasing the water volume in it. This also may have happened at Taihape in 2004, but if it did, it had drained away before detailed monitoring began. However, it is more likely that increased shear resistance along the landslide flanks and between the slide-blocks (mass transfer and buttressing) is the primary constraint on landslide motion.

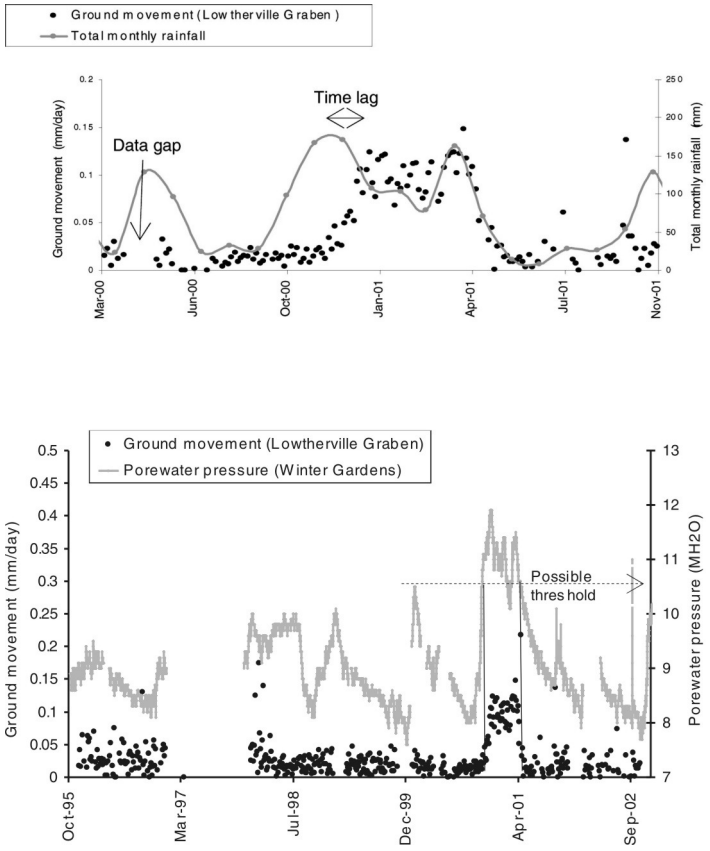

Figure 6.34 Pore pressure and rainfall over time recorded for the Ventnor landslide (redrawn from Moore et al., 2007).

6.6 Rainfall and pore-pressure relationship

The velocity response to the rise and fall of the water table for many low-angle landslides appears to depend on the initial hydrological conditions of the ground and on the magnitude and duration of the rainfall (Gonzalez et al., 2008). At Utiku, only the onset of recorded accelerated-creep motion can be attributed to increasing pore pressure, which historically have accounted for the largest displacement magnitude events.

In the Taihape-Utiku area, groundwater is being recharged through both rainfall and much less importantly snow melt. For the Utiku and Taihape landslides, however, the

relationship between rainfall and pore pressure indicates pore pressures do not respond quickly to rainfall and that that the pore-pressure responses, which triggered the accelerated creep motion (at Utiku), are a result of long periods of wet weather rather than large magnitude, short-duration rainfalls. This may be because the hydrogeology of such large landslides is complex, due to the small-scale anisotropies of the materials (and therefore contrasting porosity and permeability), and the larger-scale heterogeneities of the landslide mass (van Asch et al., 2007), e.g. grabens, sinkholes and tension cracks. These larger-scale features provide preferential flow paths for surface water to enter the landslide mass. However, due to ongoing deformation, it is likely that these types of creeping landslide "re-plumb" themselves during periods of movement, suggesting that their detailed hydrogeology may be constantly changing. Additionally, or alternatively, the measured aquifers are confined and may be somewhat isolated from rainwater. The apparent 2-month delayed response of the Taihape landslide following the 2004 Manawatu storm (equating to the 1-in-100 year daily rainfall), may suggest that it takes time for surface water to enter the landslide groundwater system. These findings are similar to those of Matsuura et al., (2008), who found that constant and prolonged water inputs caused larger changes in pore pressure than shorter, more intense inputs. Many authors believe that the poor response of landslide motion to rainfall is due to the size and depth of the landslides studied and their complex hydrogeology (e.g. Gerald and Olivier, 1993; Corominas and Moya, 1999; Van Asch et al., 1999).

Both Utiku and Taihape landslides are large and have complex hydrogeology. The slow response of pore pressures to rainfall and the long-term (about 4 months) antecedent rainfalls needed to raise pore pressures creates difficulties in establishing movement-triggering rainfall thresholds for these landslides (e.g. Glade et al., 2000; Guzzetti et al., 2007). Linking recorded rainfalls with movement-triggering pore-pressure thresholds would perhaps be more useful. Moore et al., (2007) identified a close association between the recorded pattern of landsliding on the Isle of White at Undercliff, UK and prolonged periods of heavy rainfall; that is the occurrence of 'wet years' and the resulting high groundwater levels (Lee, 2010). In upper Ventnor, Isle of White, UK, ground movement of the landslide has been associated with 4-month antecedent effective rainfall (4AER) totals that have occurred, on average, every 50 years or more (Lee, 2010). However, it is not known whether the 4AER is dominated by multiple days of smaller magnitude rainfall or fewer, shorter duration, higher magnitude events. Peak pore pressures recorded on the Ventnor landslide are reported to lag peak monthly rainfalls by about one month (Moore et al., 2007) indicating a similar complex response of groundwater to rainfall (Figure 6.34). Although there appears to be a good correlation the 4AER have been steadily increasing, indicating that rainfall is not stable (Lee,

2010), suggesting rainfall in the past cannot be a proxy for landslide movement in the future. Lee (2010) benefited from having rainfall records extending back to 1839, however, many studies, do not have this extent of data available.

With many studies the lack of pore-pressure data from depth within the landslide mass means that rainfall is often used as a proxy for pore pressure. In some cases this may be correct, however, in the case of Utiku and Taihape, rainfall is only a very crude proxy for pore pressure conditions.

Studies of other translational slides, moving on clayey materials show similar results. Corominas et al. (2005) found that at the Vallcebre landslide in the eastern Pyrenees of Spain, piezometers showed an initial rapid response to rainfall, but peak water levels were attained at different times at different piezometers, and were dependent on the permeability of the adjacent materials and the position of the piezometer in the landslide (Figure 6.35). Piezometers located in tension zones (piezometer S5, Figure 6.35), showed smaller variations in groundwater level and faster drainage, which was thought to be a function of open cracks forming preferential drainage pathways in the tension zones and causing apparently higher permeability (Corominas et al., 2005). This may apply also to other large, deep-seated translational slides, especially where pore-water distributions vary from place to place within the same landslide (Bertini et al., 1984; Angeli, 1996; van Asch et al., 2007; and Matsuura et al., 2008). Schulz et al., (2009a) show that at the Slumgullion landslide, pore pressures vary between the landslide body and its margins, where during periods of landslide acceleration, pore pressures away from the margins in the landslide body rise, while those on the margins fall. Schulz et al., (2009a) suggest that the decreased pore pressures along the landslide margins lead to increased shear resistance along the boundaries of the landslide, which subsequently arrest motion.

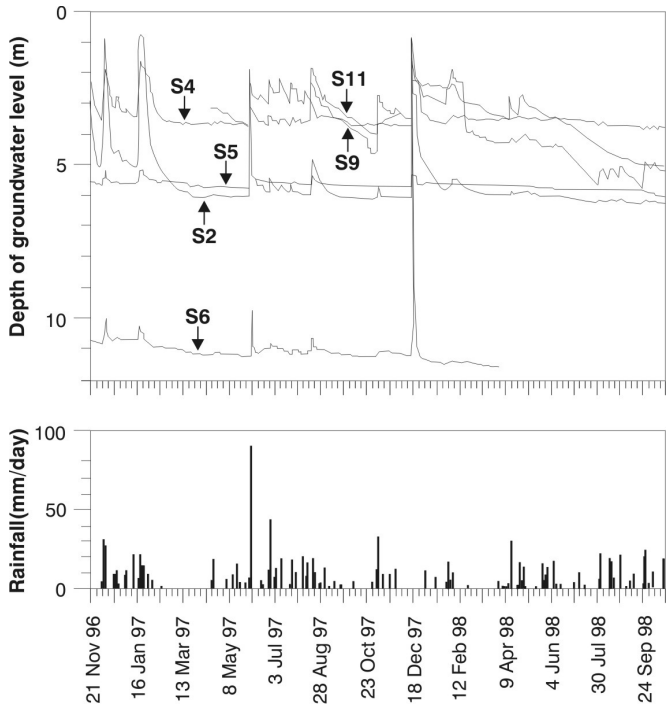

Figure 6.35 Rainfall and groundwater data from the Vallcebre landslide in Spain (redrawn from Corominas et al., 2005).

Lags between pressure responses at different piezometers in the Utiku and Taihape landslides suggest that pore pressures are somewhat dependent on the morpho-dynamic setting of the piezometer in the landslide. At Taihape, piezometer BH2A is in a tensional zone (graben) and responds quickly to rainfall, reaching peak pore pressures before the piezometer BH1A that is located in a compressional zone. At Utiku, the piezometer BH3 is in a graben and piezometer BH4 is in the central part of the landslide, but there are no significant lags between the pressure measurements at piezometers BH3 and BH4 indicating they are statistically similar although located in different morpho-dynamic settings.

Pore pressures from Utiku piezometers (PZA and BH4) have been compared with those from Taihape (BH1A and BH2A) to assess similarities in behaviour (Figure 6.36). The plots show hysteresis (shown clearly in plots A and C and less so in plots B and D), which indicates a repeating consistent lag between the landslides. The plots of pore pressure indicate that in general Taihape BH1A and Utiku PZA and BH4 always follow similar trends, however, Taihape BH2A behaves differently; it reaches peak pressures more quickly and is the only piezometer located in an extensional graben zone. Despite the hysteresis, simple linear regression of the data in plots B and D have coefficients of variation (r^2) of 0.95 and 0.77 on 453 and 451 degrees of freedom respectively. This suggests that pore-pressure trends at other landslides in the area would closely follow the trends shown at Utiku and Taihape. Hence, if motions between the two landslides

correlated then the pore pressures at both Utiku and Taihape could be used to indicate the likelihood of motion at nearby similar landslides. However, no such correlation in motion can be found between Utiku and Taihape landslides, possibly because the length of the monitoring overlap between the two is very short, but also because pore-water pressures are only one factor controlling the stability of these landslides.

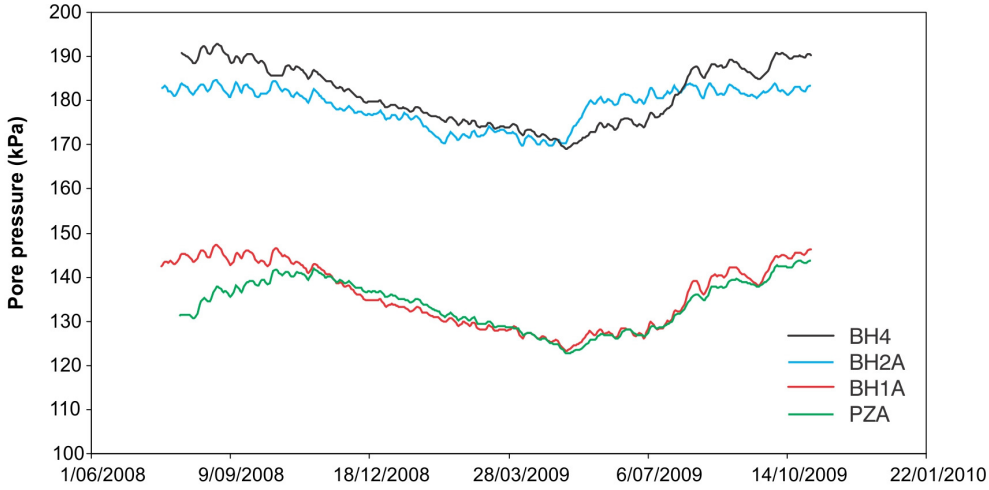

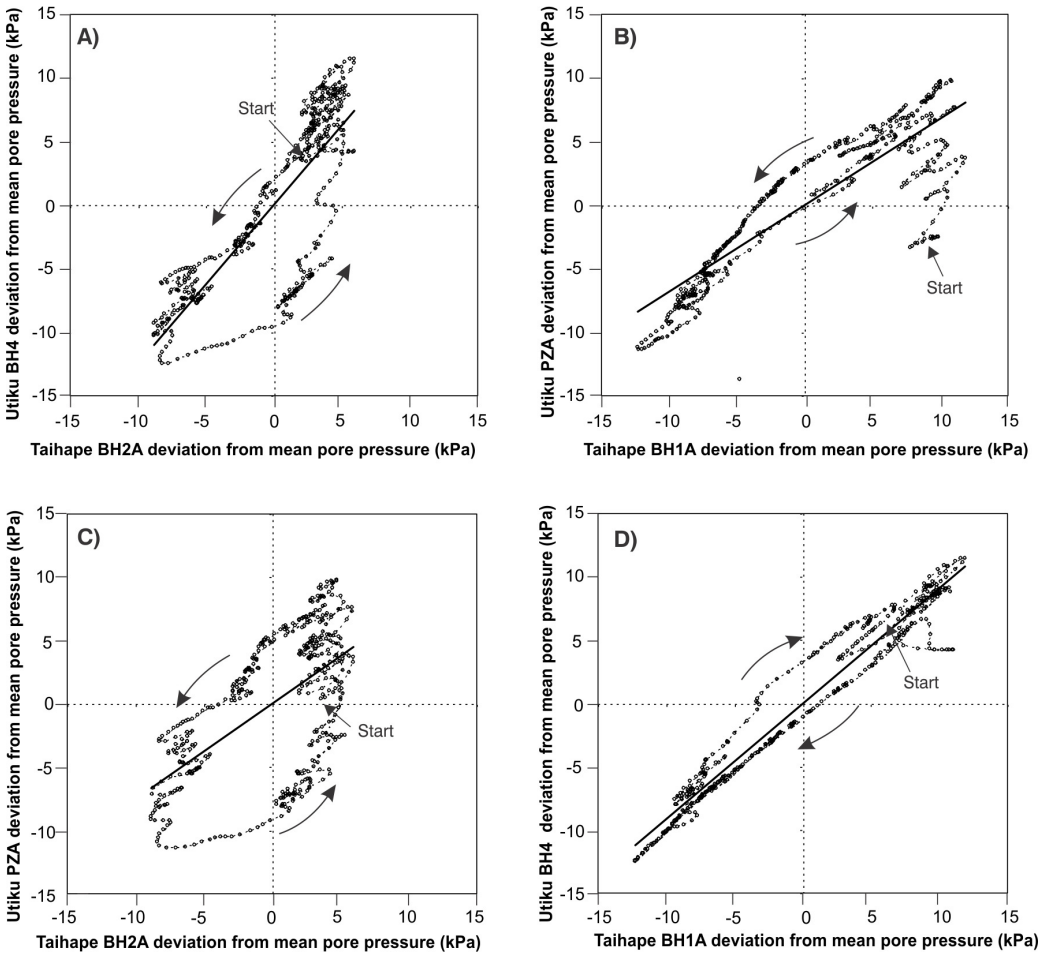

Figure 6.36 Comparison of the daily pore pressure records from the Utiku and Taihape landslides. A: Taihape BH2A and Utiku BH4. B: Taihape BH1A and Utiku PZA. C: Taihape BH2A and Utiku PZA. D: Taihape BH1A and Utiku BH4.

6.7 Earthquakes

The seismic hazard factor for the Utiku and Taihape area is 0.33g equivalent to the 1/500-year peak ground acceleration (PGA) for rock (New Zealand Standard NZS 1170.5, 2004), which is approximately equivalent to a shaking of intensity MM 8 based on the mean and mean plus one standard deviation correlation of Murphy and O'Brien (1977). A PGA hazard curve for Utiku and Taihape was generated using the New Zealand probabilistic seismic model (Stirling et al., 2000; 2002), to determine 10-year, 100-year and 1000-year PGA values (Figure 6.37 and Table 6.04).

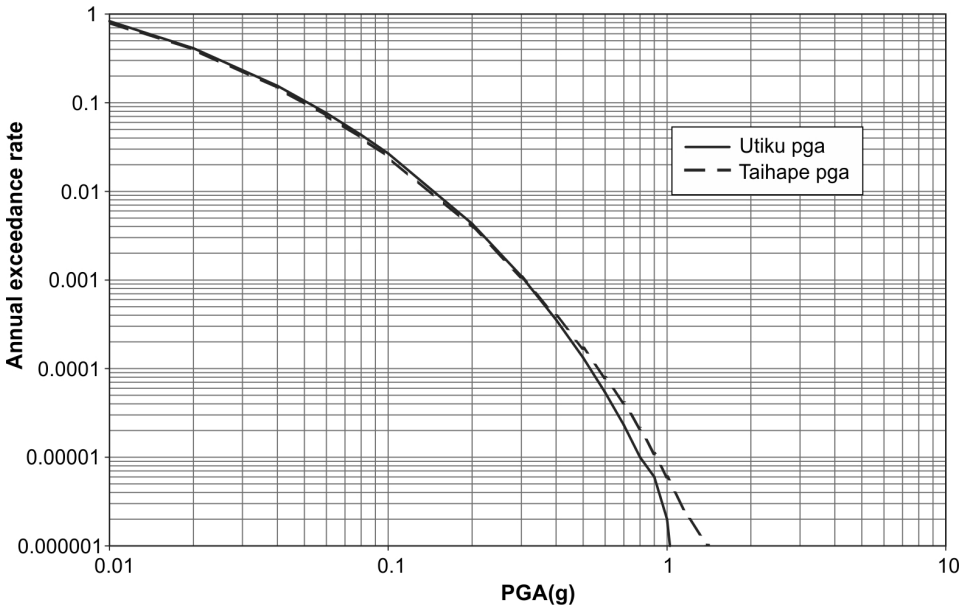

Figure 6.37 PGA hazard curve for Utiku and Taihape area generated using the New Zealand probabilistic seismic model (Stirling et al., 2000; 2002).

Table 6.04 Peak ground accelerations for given return periods for the Utiku and Taihape areas

Return period(yr)	PGA (g)
10	0.05
100	0.14
1000	0.40

During the monitoring, none of the periods of landslide acceleration for either Utiku or Taihape landslides can be attributed to earthquake ground motions, even though peak ground accelerations associated with several earthquakes were recorded on the landslides during the study period (Chapter 5).

Historical-precedent evidence suggests that no displacements from earthquakes have ever been recorded at Utiku (1965 to present). A ground motion equivalent to the 10-year PGA (Table 6.04) was recorded at Mangaweka about 8 km SSW of Utiku, on 10/06/1975 at 10:11:20 UTC, in response to the Dannevirke earthquake (M_w 5.6, depth

33km, epicentre located about 66 km SSE from Utiku). Surface-movement monitoring was carried out pre- and post-10/06/1975 Dannevirke earthquake and no landslide movement was detected, even though the stability of the landslide should have been low as the earthquake occurred in winter, when pore pressures should have been seasonally high.

The lack of any landslide response to recorded earthquake ground accelerations is corroborated by recent empirical work (Hancox et al., 2002), which also shows that it is unlikely that reactivation or acceleration of these landslides would occur at MM < 7, however, accelerated creep at MM > 7 cannot be ruled out. A recent example is the Harper Hills landslide complex, parts of which were reactivated during the M_w 7.1 Darfield, New Zealand, earthquake on 4th September 2010 (Massey et al., 2010). These landslides comprise large and relatively deep-seated dip slope failures, involving translation of material along smectite-rich clay seams, with maximum down slope displacements of about 1.0 m recorded. The nearest strong motion sensor to these landslides (about 7 km to the east) recorded a PGA of 62 %g (6.2 m/s/s) equivalent to a shaking intensity of MM 9, using the correlation of Murphy and O'Brien (1977).

6.8 Synthesis

Three systems have been identified, which together account for the observed unsteady and non-uniform surface motions: 1) basal-sliding; 2) plastic deformation and basal sliding; and 3) seasonal shrinkage and swelling. Only the long-term cumulative net surface displacement meets the definition of landsliding.

Frictional basal sliding is represented by simultaneous periods of accelerated creep at the ground surface and along the slip surface. This motion accounts for the largest displacements recorded at both landslides, both historically and more recently. At Utiku, displacement vectors, or longitudinal angles of translation are predominantly horizontal, and are sub-parallel to the apparent-dip angle of the slide surface. Once triggered by pore-pressure increase, accelerated-creep motion does not tend to arrest with pore-pressure induced increases in shear resistance. Sliding velocity appears to be regulated, in order of importance, by: 1) buttressing and mass transfer between the slide-blocks forming the landslide mass, this is particularly important at Taihape, where the landslide toe is confined; 2) friction developed along the sides of the slide-blocks, considering the landslides as true 3-D features, especially considering the wedge-shaped geometry of the Utiku landslide; and possibly 3) rate-induced changes in shear resistance of the material forming the landslide slide-surface, although at the rates of motion recorded at Utiku it is unlikely that motions are being arrested by rate-induced increases in the shear resistance of the clay at the slide surface.

At both landslides, the slow- and vertical-creep cannot only be attributed to motion along the slide surface; it must also be attributed to plastic deformation within the slide mass. At Taihape, only about 50% of the slow- and vertical-creep motion can be attributed to displacement along the slide surface, which may also be the case at Utiku where such low motion is not resolved. At Utiku, the slow and vertical creep accounts for about 60 mm/year displacement at an angle of about 56° from horizontal (Station UTK1), and at Taihape, about 11 mm/year at an angle of about 47° from horizontal (Prism 3a). This component of surface motion appears to be unrelated to pore-pressure fluctuations, as landslide velocity does not vary with fluctuating pore pressures. This motion component represents plastic thinning of the slide masses, as they progress down slope towards the toe.

Superimposed on the steady slow-creep are other motions that are unrelated to landsliding. At Taihape these account for surface displacements of about 20 mm/year (10 mm per half year in alternating directions) and therefore they dominate the horizontal motion records and are similar in form to the periods of accelerated creep recorded at Utiku. Although the inclinometers recorded several accelerated creep events prior to prism installation, these other 'apparent' accelerated creep motions relate to seasonal shrinkage and swelling of the landslide mass in response to changing soil moisture, which is correlated to pore pressure. These changes result in periods of cyclic vertical and horizontal motions, which cause no net cumulative displacement from year to year, and are unrelated to sliding of the landslide along the slide surface. These seasonal motions have been resolved at Taihape, where the vertical surveying precision of the total station is better than that of the GPS at Utiku. Although it has not been possible to resolve such motion at Utiku, it is expected that these seasonal changes also occur there, as possibly shown by the time series from station UTK3. However, the inability to detect this motion in the records may also be because the GPS podiums extend to, and may be anchored at depths below those affected by the seasonal changes. The depths to which the seasonal variations extend are unknown and they may only be a near-surface phenomenon. The surface-movement-monitoring results from Taihape suggest that it is not possible to resolve temporal variations in real landslide motion that are smaller than the extraneous motions. At Taihape, the extraneous surface motion has a seasonal cycle and is about an order of magnitude larger than actual landslide surface motion, rendering it impossible to detect variations in real landslide surface motion within periods of less than about 9 months.

The lack of any detected motion in response to earthquake ground shaking is conspicuous and suggests that these types of landslide may not be susceptible to

reactivation by earthquakes with associated ground shaking intensity < MM 7. Seismic slope-stability models such as Newmark (1965) and Ambraseys and Menu (1988), suggest that currently moving landslides, such as Taihape and Utiku, should be extremely sensitive to dynamic earthquake loading, but no such sensitivity has been detected.

Figures 6.38 and 6.39 are conceptual models illustrating the relationship between recorded motion patterns, pore pressures, material strength, landslide geometry and geomorphological position for the Utiku and Taihape landslides. These models could also be used to describe the movement mechanisms of other similar reactivated landslides documented in the literature, where cumulative-displacement trends comprise accelerated creep, slow creep and rest, which recur frequently through the record at varying magnitudes and durations, and are the status quo.

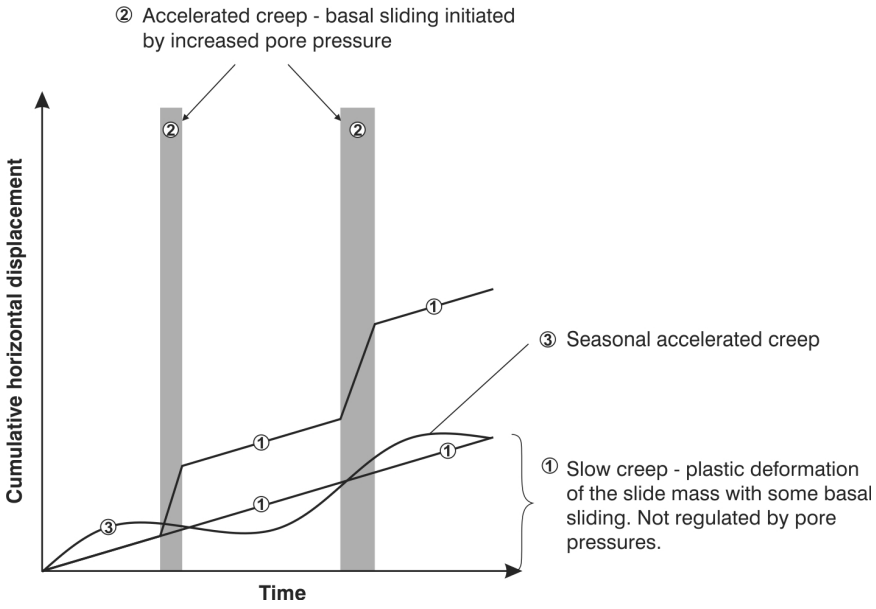

Figure 6.38 Conceptual model illustrating the relationship between pore pressures and movement patterns of deep-seated translational slides as represented by the Utiku and Taihape landslides.

Figure 6.39 shows that as a given block moves down slope the displacement rate transitions through the four movement patterns as described by Petley et al., (2005). The accelerated-, slow- and vertical-creep motion recorded at Utiku and Taihape relate to Type III and IV motion, where disintegration and deformation of the slide mass increase towards the toe and are accompanied by decreasing material strength. At Utiku, there is a transition to Type IV motion as the slide mass becomes completely disintegrated and transformed into an earth flow, which could be explained by the effects of loss of shear strength, perhaps through increased pore pressures, or the ability of the landslide mass to move more down-dip along the basal clay layer (leading to increased shear stress). At Taihape, Type III motion continues into the landslide toe with no apparent change in process identified. The disintegration and loss of strength

are accompanied by basal sliding of the slide mass, which increases in rate with distance below the crest. Plastic deformation of the slide mass also increases towards the toe as the debris becomes disaggregated and is remoulded (post failure Type 4 creep, Table 2.01) and less constrained by the landslide geometry.

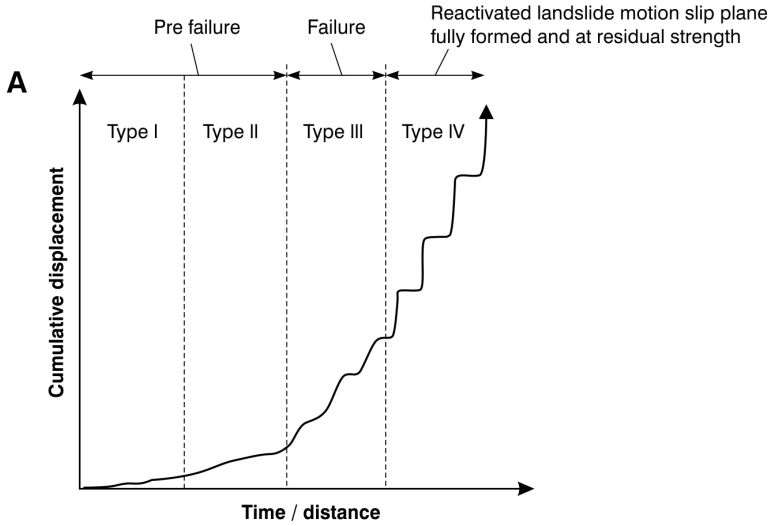

Schematic motion patterns of the Tessina landslide
(Petley *et al.*, 2005)

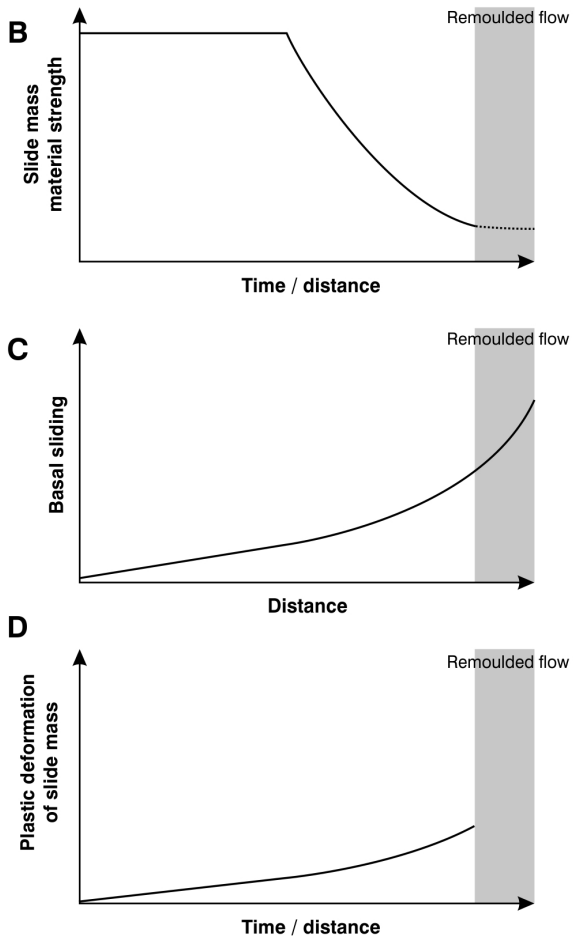

Figure 6.39 Conceptual model illustrating the relationships between motion patterns, material strength, landslide geometry and geomorphological position for deep-seated translational slides as represented by the Utiku and Taihape landslides. A: Cumulative displacement patterns, redrawn from Petley et al., (2005). B: Slide mass material strength. C: Basal sliding. D: Plastic deformation of the slide mass.

For these types of slow- to extremely slow-moving landslides, the shear stresses and shear resistances operating within the landslide are finely balanced and therefore rapid changes in motion may result from relatively small changes in stress. This was shown by the increased rates in motion recorded at Utiku between 1965 and 1972, and at Taihape between April and October 2005. These periods of increased motion are thought to have been triggered by rainfall-induced changes in pore pressures at Utiku and/or rainfall-induced scour, with loss of toe support at Taihape. However, the rates of pore pressure change have been shown to be slow, with peak pore pressures responding to about 4 months of antecedent rainfall, which reflects the complex hydrogeology of these types of landslide, which is true of other similar landslides e.g. Corominas et al., (2005); and Matsuura et al., (2008). For many of these landslides, long-term rainfall, pore pressure and movement data is unavailable, in such cases movement-triggering rainfall thresholds like those proposed by Moore et al., (2007), should be correlated with direct pore pressure measurements.

CHAPTER 7 CONCLUSIONS

The primary aim of this research was to study the relationship between landslide motion and its causes, with reference to large, slow moving reactivated translational rock slides, utilising data collected from high temporal- and spatial-resolution monitoring.

7.1 Principal findings

Two deep-seated, reactivated translational slides were selected to represent over 7,000 mapped landslides of this type in Tertiary-age sedimentary rocks of New Zealand. Each was closely monitored with an automated network of instruments to detect and measure the effects of rainfall, pore pressure, earthquakes and river stage on changing surface and subsurface movement patterns, with sufficient resolution to link periods of movement to their triggering factors. From the reviewed literature it is apparent that the monitoring systems installed at Utiku and Taihape have typically higher temporal- and spatial-resolutions and precisions than those of other comparable systems. The dynamics and controls upon these landslides have been investigated by combining multiple interdisciplinary approaches including geology, geomorphology, geotechnics and geomatics. Without such an approach the mechanisms governing the motion of these landslides could not have been adequately resolved.

The deformation behaviour at the two slides during the period of observation would best be described as episodic post-failure creep (Hutchinson 1988). Patterns of creep typically comprise periods of accelerated-, slow- and vertical-creep, punctuated by periods of rest, which may occur with varying frequency and at different times within the seasonal record. Periods of displacement may vary in duration and displacement rates may vary, resulting in a net cumulative displacement trend which is unsteady and non-uniform. However, the prehistoric motion records derived from radiocarbon and relative dating techniques suggest the prehistorical motion rates are similar to those rates recorded more recently, indicating that motion patterns over longer periods of time are essentially constant.

Three systems were identified, which together accounted for the recorded unsteady and non-uniform motions: 1) basal-sliding; 2) plastic deformation and basal sliding; and 3) seasonal (summer/winter) shrinkage and swelling. Basal sliding, caused by frictional slip along this clay seams was represented by simultaneous periods of accelerated creep at the ground surface and along the slip surface. This motion accounted for the largest horizontal displacements recorded at both landslides, both historically and more recently. Once triggered by pore-pressure increase, accelerated-creep motion did not

tend to be arrested by decrease in basal pore pressure. Instead, sliding velocity was constrained by, in order of importance: 1) buttressing and mass transfer between the slide-blocks forming the landslide mass, this is particularly important at Taihape, where the landslide toe is confined; 2) friction developed along the sides of the slide-blocks, considering the landslides as true 3-D features, especially considering the wedge-shaped geometry of the Utiku landslide. Although rate-induced changes in shear resistance of the material forming the landslide slide-surface have been considered, the rates of motion recorded at Utiku make it unlikely that motions are being arrested by rate-induced increases in the shear resistance of the clay at the slide surface.

Historical periods of accelerated creep (at Utiku and Taihape slides) were also thought to have been triggered primarily by rainfall-induced changes in pore pressure and/or rainfall-induced flooding and loss of toe support. For these types of slow- to extremely slow-moving landslides, the shear stresses and shear resistances operating within the landslide are finely balanced and therefore rapid changes in motion may result from relatively small changes in stress. This was shown by the increased rates in motion recorded at Utiku between 1965 and 1972, and at Taihape between April and October 2005. These periods of increased motion are thought to have been triggered by rainfall-induced changes in pore pressures at Utiku and/or rainfall-induced fluvial erosion, with loss of toe support at Taihape. However, the rates of pore pressure change have been shown to be slow, with peak pore pressures responding to about 4 months of antecedent rainfall and not to high magnitude short-duration rainfall events, indicating that these types of landslide are hydrogeologically complex.

At both landslides, the slow horizontal- and vertical-creep motion could be attributed both to slip along the slide surface and to plastic deformation of the slide mass, as not all the recorded surface motion could be attributed to displacement along the slide surface. As a result plastic deformation is causing the slide mass to thin downslope towards the toe. These components of landslide motion were unrelated to basal pore-pressure fluctuations, as landslide velocity did not vary with fluctuating basal pore pressure. The poor relationship between varying pore pressure and the slow horizontal- and vertical-creep is because this motion is also being regulated, in part by the geometry of the landslides.

Superimposed on the steady, slow creep were other motions that were found to be unrelated to landsliding. At Taihape, these accounted for surface displacements of about 20 mm/year (10 mm per half year in alternating directions) and therefore they dominated the horizontal motion records and were similar in form to the periods of accelerated creep recorded at Utiku. The surface-movement monitoring results from

Taihape showed that it was only possible to resolve variations in real landslide motion that were larger than the extraneous motion. At Taihape, the extraneous surface motion had an annual cycle and was about an order of magnitude larger than the motion due to landsliding, rendering it impossible to recognise variations in real landslide surface motion within periods of less than about nine months, based on the rates recorded during the monitoring period. This impacts on any conclusions made from monitoring records covering shorter time periods. Indeed, the precision on the mean daily horizontal positions of the GPS stations and prisms, about 2.3 mm and 1.4 mm at one standard deviation, respectively, are still high relative to the daily maximum motion rates observed on the landslides. Considering the motion rates of the landslides, the daily temporal resolution used for this study was adequate. Higher temporal resolution (using more frequent monitoring) would be of little use, considering the increased errors associated with, for example, GPS positions derived from 1-hour monitoring epochs. When designing such a system for hazard warning, the temporal resolution of the monitoring must be considered with respect to the anticipated speeds of the landslide, with care taken when interpreting data covering only short periods of time.

During the monitoring, none of the periods of landslide acceleration for either Utiku or Taihape landslides could be attributed to earthquake ground motions, even though peak ground accelerations associated with several earthquakes were recorded on the landslides during the study period. Historical-precedent evidence suggests that no displacements from earthquakes have ever been recorded at Utiku or Taihape. The lack of any landslide response to recorded earthquake ground accelerations is corroborated by recent empirical work (Hancox et al., 2002), which also shows that it is unlikely that reactivation or acceleration of these landslides would occur at ground shaking intensities < MM 7, however, accelerated creep at intensities > MM 7 cannot be ruled out.

A conceptual model, modified from Petley et al., (2005), illustrating the relationships between recorded landslide-motion patterns, material strengths, landslide geometry, movement mechanisms and morpho-dynamic setting has been proposed. In summary, as a given block moves downslope, the displacement transitions through the four movement patterns as described by Petley et al., (2005). The accelerated-, slow- and vertical-creep motion relate to Type III and IV motion, where disintegration and deformation of the slide mass increases towards the toe, which is usually accompanied by decreasing material strength, and in some cases, a transition to Type IV motion as the slide mass completely disintegrates and is incorporated into an earthflow. The disintegration and loss of strength is accompanied by basal sliding of the slide mass, which increases in rate with distance from the landslide crest. Plastic deformation of the

slide mass generally increases towards the toe as the landslide mass thins and becomes disaggregated and remoulded and less constrained by the landslide geometry.

Although the monitored deformation patterns at the two landslides have been episodic post-failure creep, at rates varying from extremely slow to slow, movement rates of these types of landslide can increase. The Abbotsford landslide (Hancox 1980), slowly accelerated from rest over months to fail rapidly on 8th August 1979, confirming that in such landslides, the shear stresses and shear resistances operating become finely balanced and therefore rapid changes in motion may result from relatively small changes to the system.

7.2 Recommendations for further research

Based on this research, recommendations are made for future research to advance the knowledge on the processes and mechanisms which both trigger and arrest the motion of slow-moving reactivated translational slides. The main questions raised by this research are:

- Do basal sliding and plastic deformation processes, which account for the observed movement patterns of the Utiku and Taihape landslides, account for the movement patterns of other slow-moving translational slides in different materials, and are their motions being constrained by their geometry? Can quantitative monitoring of other similar landslides in different materials confirm this?
- Considering the landslides in three dimensions, can lateral friction and internal buttressing (mass transfer) be quantified using three dimensional slope stability modelling software?
- Can higher temporal resolutions of slip-surface displacement better constrain the process?
- During the monitoring, none of the periods of landslide acceleration for either Utiku or Taihape landslides could be attributed to earthquake ground motions, even though measurable ground accelerations associated with several earthquakes were recorded on the landslides during the study period. Does this suggest these types of landslide are not susceptible to earthquake ground accelerations, or at what point are they susceptible?

The Taihape and Utiku landslides are two of over 7,000 mapped landslides > 10,000 m^2 in plan area in Tertiary-age sedimentary rocks of New Zealand. Many similar landslides also occur in other geological materials both in New Zealand and overseas, e.g. the Clyde Reservoir landslides, New Zealand, which typically comprise deep-seated

translational slides in mica schist (Gillon and Hancox, 1992; McFarlane, 2009). The quantitative monitoring applied to the Utiku and Taihape landslides could be applied to other similar landslide in different materials to assess similarities and differences in the mechanisms governing their motion.

Both landslides have been modelled using conventional two-dimensional approaches, but clearly these can only approximate what clearly are three-dimensional problems. To better understand the roles of buttressing and landslide geometry as controls on displacement requires three-dimensional modelling, using appropriate software such as FLAC3D. By back-analysing the recorded displacements and pore-pressure conditions using the material parameters derived from laboratory analyses, it should be possible, for example, to quantify the likely increases in shear resistance along the western flank of the Utiku landslide and therefore determine whether increased frictional resistance along this flank is a significant factor in arresting motion.

Higher temporal resolution monitoring of slip-surface displacements are required to investigate how plastic deformation of the slide mass may relate to displacement along the slide surface. There are two techniques which could be used, 1) in-situ inclinometers; and 2) time-domain reflectometry (TDR). The benefit of TDR over in-situ inclinometers is that shear displacements over the entire length of the borehole could be recorded, therefore allowing zones of plastic deformation to be located. However, compression (thinning) of the slide mass cannot easily be monitored using either technique.

REFERENCES

Abramson, L. W., Lee, T. S., Sharma, S., and Boyce, G. M. 2002. *Slope stability and stabilisation methods. Second edition*. Pub. John Wiley & Sons, INC.

Allison. R.J., Brunsden, D. 1990. Some mudslide movement patterns. In: Earth Surface Processes and Landforms 15 (4) pp. 297 - 311.

Ambraseys, N.N., Menu, J.M. 1988. Earthquake-induced ground displacements. Earthquake engineering and structural dynamics, Vol. 16, pp. 985 – 1006.

Anderson, J. M., Mikhail, E. M. 1998. Surveying theory and practice. Seventh edition. Pub. WCB McGraw-Hill. pp. 50-71.

Angeli, M. G., Gasparetto, P. Menotti, R. M., Pasuto, H., Silvano, S. 1996. A visco-plastic model for slope analysis applied to a mud slide in Cortina d'Ampezzo, Italy. Quarterly Journal of Engineering Geology. Vol. 29. pp. 233 – 240.

Angeli, M. G., Gasparetto, P., Bromhead, E. 2004. Strength-regain mechanisms in intermittently moving landslides. In: Proceedings of the 9th International Symposium on Landslides. Rio de Janeiro. Vol. 1. Taylor and Francis, London (pub). pp. 689 – 696.

ASTM D6230:05. 2005. Standard test method for monitoring ground movement using probe-type inclinometers. 10.1520/D6230-98R05.

Atkinson, B. K., Meredith, P. G. 1987. The theory of subcritical crack growth with applications to minerals and rocks. In: *Fracture mechanics of rock – Academic*

Beavan, J. 2005. Noise properties of continuous GPS data from concrete pillar geodetic monuments in New Zealand and comparison with data from U.S. deep drilled braced monuments. In: *Journal of Geophysical Research.* Vol. 110, B08410, doi:10.1029/2005JB003642, 2005.

Beavan, J. 2010. Notes about processing and the creation of GPS time series. http://www.geonet.org.nz/resources/gps/gps-processing-notes.html. GNS Science. GeoNet project.

Belz, D. T. G., 1967. Investigation of subsidence at Utiku. In: *Soil and Water*, 1967, 19-22.

Bennett, R. H., Hulber, M. H. 1986. Clay microstructure. International Human Resources Development Corporation, Boston. pp 88-115.

Bertini, T., Cugusi, F., D'Elia, B., Rossi-Doria, M. 1984. Climatic conditions and slow movements of colluvial covers in Central Italy. In: *Proceedings of the IV International Symposium on landslides, Toronto 1984*. Vol 1. pp 367 – 376.

Bhandari, R.K., 1988. Special lecture: some practical lessons in the investigation and field monitoring of landslides. Proceedings of the 5th International Symposium on Landslides. Balkema, pp. 1435-1457.

Bracegirdle, A., Vaughn, P. R., Hight, D. W., 1991. Displacement prediction using rate effects on residual strength. In: *Landslides, proceedings from the VI International symposium on Landslides*. Christchurch, New Zealand. Bell (ed). pp 343 – 347.

Carson, M. and Kirkby, M., 1972. Hillslope Form and Process. University Press, Cambridge, 475 pp.

Cartier, G., Pouget, P. 1988. Etude du compartement d'un remblai construit sur un versant instable. Le remblai de Salledes (Puy de Dome). Report No. 153. Laboratoire Central de Ponts et Chaussee Paris. France.

Cooper, M. R., Bormhead, E. N., Petley, D. J., Grant, D. I. 1998. The Selborne cutting stability experiment. In: *Geotechnique.* Vol. 48. pp. 83 – 101.

Cornforth, D. H., Vessely, D. A. 1991. Factors of safety during landslide movements. In: *Landslides, proceedings from the VI International symposium on Landslides*. Christchurch, New Zealand. Bell (ed). pp 367 – 374.

Corominas, J., Moya, J., Ledesma, A., Lloret, A., Gili, J. A. 1999. Monitoring of the Vallcebre landslide, Eastern Pyrenees, Spain. In: *Proceedings of the International symposium on Slope Stability Engineering.* IS-Shikoku' 99. Matsuyama. Japan. pp 1239 - 1244.

Corominas, J. 2000. Landslide and climate. In: *The VIII International Symposium on Landslides*. Cardiff, UK. Bromhead. E. N. (ed). Keynote lectures. CD Rom.

Corominas, J., Moya, J., Ledesma, A., Lloret, A., Gili, J. A. 2005. Prediction of ground displacements and velocities from groundwater level changes at the Vallcebre landslide (Eastern Pyrenees, Spain). In: Landslides. Vol. 2. pp. 83-96.

Cotton, C.A. 1944. Volcanoes as landscape forms. Whitcombe and Tombs, Christchurch. Pp 415.

Craig, R.F., 1997. Soil Mechanics. Spon Press, London. pp. 485.

Crosta, G. B., Agliardi, F. 2002. Failure forecast for large rock slides by surface displacement measurements. In: *Canadian Geotechnical Journal*. Vol. 40. pp. 176 – 191.

Cruden, D. M. & Varnes, D. J. 1996. Landslide types and processes. In: *Landslide: investigation and mitigation.* Turner, K. A. & Schuster, R. L. editors. Special report, Transportation Research Board, National Research Council, 247. Chapter 3, 36-75.

Dawson, E.M., Roth, W.H., Drescher, A. 1999. Slope stability analysis by strength reduction. In. Geotechnique. Vol. 49. No. 6. pp. 835-840.

Dellow, G.D., McSaveney, M.J., Stirling, M.W., Berryman, K.R. 2005. A probabilistic landslide hazard model for New Zealand. p. 24 In: Pettinga, J.R.; Wandres, A.M. (eds) *Geological Society of New Zealand 50th annual conference, 28 November to 1 December 2005, Kaikoura : programme & abstracts.* Geological Society of New Zealand. Geological Society of New Zealand miscellaneous publication 119A.

Embleton, C., King, C. A. M. 1968. Glacial and periglacial geomorphology. St Martin's Press, New York. pp. 92-111.

Feldmeyer, A.E., Jones, B.C., Firth, C.W., Knight, J. 1943. Geology of the Palmerston – Wanganui Basin "West-Side", North Island, New Zealand. In*: Superior Oil Company of New Zealand,* unpublished report.

Ferrari, A., Ledesma, A., Gonzalez, D. A., and Corominas, J. 2010Effects of the foot evolution on the behaviour of slow-moving landslides. In: *Engineering Geology*. DOI: 10.1016/j.enggeo.2010.11.001.

Fell, R., Hungr, O., Leroueil, S. and Riemer, W., 2000. Keynote lecture - geotechnical engineering of the stability of natural slopes, and cuts and fills. *N: Proceedings of the Geoengineeing Conference*, Melbourne, pp. 21-120.

Geokon. 2005. Model 4500 vibrating wire piezometer. Data sheet. http://www.geokon.com/products/datasheets/4500.pdf

Geokon. 2008. Model 4500 vibrating wire piezometer. Instruction manual.

Gerald, G., Olivier, J. 1993. Predicting landslides from rainfall in a humid, sub-tropical region. In. Geomorphology. Vol. 8. pp. 165-173.

Gillon, M.D., Hancox, G.T., 1992. Cromwell Gorge landslides: a general overview. In: Bell, D. (Ed.), Proc. 6th Int. Symp. Landslides, Christchurch, vol. 2, Balkema, Rotterdam, pp. 83–102.

Glade, T., Crozier, M., Smith, P. 2000. Applying probability determination to refine landslide-triggering rainfall threshold using an empirical antecedent daily rainfall model. In. Pure and applied Geophysics. Vol. 157. pp 1059-1079.

Gonzalez, D. A., Ledesma, A., Corominas, J. 2008. The viscous component in slow moving landslides: A practical case. In: *Landslides and engineering slopes*. Chen et al. (eds). pp 237 – 242.

Green, G. E., Mikkelsen, P. E. 1988. Deformation measurements with inclinometers. Transportation Research Record. 1169. Transportation Research Board, Washington. pp. 1-5.

Guzzetti, F., Peruccacci, S., Rossi, M., Stark, C. P. (2007). Rainfall thresholds for the initiation of landslides in central and southern Europe. Meterol. Atmos. Phys. Vol. 98. pp 239-267.

Hancox, G.T., Bishop, D.G., McKellar, I.C., Suggate, R.P., Northey, R.D. 1980. 1979 East Abbotsford Landslide. Engineering geological data and factors related to the cause of the slide. NZ Geological Survey. Report EG 332, 3 March 1980.

Hancox, G.T., Perrin, N.D., and Dellow, G.D. 2002. Recent studies of historical earthquake-induced landsliding, ground damage and MM intensity in New Zealand. Bulletin of the New Zealand Society for Earthquake Engineering, Vol. 35 No. 2, 2 June 2002. pp 59-95.

Hancox, G. T. H. 2007. The 1979 Abbotsford Landslide, Dunedin, New Zealand: A retrospective look at its nature and causes. In: *Landslides*.

Helmstetter, A., Sornette, D., Grasso, J.R., Andersen, J.V., Gluzman, S. and Pisarenko, V., 2004. Slider block friction model for landslides: Application to Vaiont and La Clapiere landslides. *Journal of Geophysical Research-Solid Earth*, 109(B2), 15pp.

Helmstetter, and A. Garambois, S. 2010. Seismic monitoring of the Sechilienne Rockslide (French Alps): analysis of seismic signals and their correlation with rainfall. *Journal of Geophysical Research*. In Press.

Hendron, A. J., and Patten, F. D. 1985. The Vaiont Slide. In: *US Corps of Engineers Technical Report.* GL-85-8.

Horizons Regional Council. 2004. Storm, civil emergency – *Storm and flood report, February 2004*. Report No. 2004/EXT/591

Hungr, O. 1995. A model for the runout analysis of rapid flow slides, debris flows, and avalanches. *In: Canadian Geotechnical Journal.* 32. pp. 610-623.

Hutchinson, J.N. Bhandari, R. K. 1971. Undrained loading, a fundamental mechanism of mudflows and other mass movements. Geotechnique. Vol. 21. No. 4. pp. 353-358.

Hutchinson, J.N., 1988. General report: morphological and geotechnical parameters of landslides in relation to geology and hydrogeology. *Proceedings of the 5th International Symposium of Landslides*. Balkema, pp. 3-35.

Iverson, R.M., 1985. Dynamics of slow landslides: a theory of time dependent behaviour. In: Abrahams, A. D. (Ed), Hillslope processes. Binghampton Symposium in Geomorphology No. 16. pp. 297 – 317

Iverson, R.M., 2005. Regulation of landslide motion by dilatancy and pore pressure feedback. Journal of Geophysical Research-Earth Surface, 110(F2): Article no.-F02015.

Journeaux, T. D., Kamp, P. J. J., Naish, T. 1996. Middle Pliocene cyclothems, Mangaweka region, Wanganui Basin, NZ: a lithostratigraphic framework. In: *NZ Journal of Geology and Geophysics*, 39: 135-149.

Johnston, R.M.S. 1983. Taihape land stability survey report. Rangitikei-Wanganui Catchment Board and Regional Water Board, December 1983.

Ker, D. S. 1972. Renewed movement on a slump at Utiku, N.Z. Journal of Geology and Geophysics, 13, 996-1017.

Kilsby, C. An engineering geological appraisal of the Utiku Landslide, North Island, New Zealand. University of Portsmouth, M.Sc. Thesis.

Kerr, J., Nathan, S., Van Dissen, R., Webb, P., Brunsdon, D., King, A., 2003. Planning for Development of Land on or Close to Active Faults: A guideline to assist resource management planners in New Zealand GNS Client Report 2002.124, prepared for the Ministry for the Environment (ME Report 453).

Kilburn, C. J., Petley, D. N. 2003. Forecasting giant, catastrophic slope collapses: Lessons from Vajont, Northern Italy. In: *Geomorphology.* Vol. 54 (1-2). pp. 21 – 32.

Lee, E. M. 2009. Landslide risk assessment: the challenge of estimating the probability of landsliding. In. Quarterly Journal of Engineering Geology and Hydrogeology. Vol. 42. pp. 445-458.

Lee, J.M., Bland, K.J., Townsend, D.B., Kamp, P.J.J. (comp). In prep: Geology of the Hawke's Bay area. Institute of Geological and Nuclear Sciences 1:250 000 geological map 8. Lower Hutt. Institute of Geological and Nuclear Sciences Limited.

Leica. 2010. Leica TCA1800, TCA2003 and TC2003. Fact sheet: http://www.leica-geosystems.com/downloads123/zz/tps/tps2000/brochures/TPS2000_brochure_en.pdf.

Lemos, L. J. L. 1986. The effect of rate of shear on residual shear strength of soil. PhD Thesis. University of London.

Leroueil, S., Locat, J., Vaunat, J., Picarelli, L. and Faure, R. 1996. Geotechnical characterisation of slope movements. In. Proceedings of the Seventh International Symposium on Landslides, (Ed. K. Senneset) Trondheim, Norway, Balkema, Rotterdam. Vol 1, pp.53-74.

Leroueil, S. (1998) Elements of time-dependent mechanical behaviour of overconsolidated clays. Proc. 51st Canadian Geotechnical Conf., Edmonton, Vol.2: pp.671-677.

Lerouiel, S. 2001. Natural slopes and cuts: movement and failure mechanisms. In: *Geotechnique.* Vol. 51. 3. pp. 197 – 243.

Litchfield, N. 2003. Maps, stratigraphic logs and age control data for river terraces in the eastern North Island. In: *Institute of Geological and Nuclear Sciences Report*. SR2003/31.

Litchfield, N., Ellis, S., Berrymen, K., Nicol, A. 2007. Insights into subduction-related uplift along the Hikurangi Margin, New Zealand, using numerical modelling. In. Journal of Geophysical Research. Vol. 112.

Lupini, J. F. 1980. The residual strength of soils. PhD Thesis. University of London, UK.

Lupini, J. F., Skinner, A. E., Vaughn, P. R. 1981. The drained residual strength of cohesive soils. In: *Geotechnique*. Vol. 31. No. 2. pp. 181 – 213.

Malet, J. P., Van Asch, Th. W. J., Van Beek, R., Maquaire, O. 2005. Forecasting the behaviour of complex landslides with a spatially distributed hydrological model. In: *Natural Hazards and Earth System Sciences.*

Mansour, M. F., Morgenstern, N. R., Martin, D. Expected damage from displacement of slow-moving slides. In: *Landslides Journal*. DOI 10.1007/s10346-010-0227-7.

Massey, C. I., Palmer, N. 2007. Monitoring landslide movement and triggering factors in near real-time, examples from translational landslides in New Zealand. In. Slope Stability 2007 – Y Potvin (ed), Perth, Australia. pp. 439 to 447.

Massey, C. I., Nelis, S. 2008. Landslide monitoring data and its application to risk management, an example from New Zealand. In: *Proceedings of the First World Landslide Forum*. 18 – 21 November 2008. United Nations University, Tokyo, Japan. pp 409 – 411.

Massey, C.I, McSaveney, M.J., McColl, S. 2009. Waikorora landslide review of slope stability hazards. In: *GNS Science client report for Vector Ltd.* In press.

Massey, C.I.; Manville, V.R.; Hancox, G.T.; Keys, H.J.; Lawrence, C.; McSaveney, M.J. 2010. Out-burst flood (lahar) triggered by retrogressive landsliding, 18 March 2007 at Mt Ruapehu, New Zealand: a successful early warning. Landslides. DOI: 10.1007/s10346-009-0180-5.

Massey, C. I., Petely, D. N., and Rosser, N. 2010. Harper Hills Landslides, Canterbury, New Zealand. *GeoNet Landslide Response Report.* http://www.geonet.org.nz/docs/landslide/reports/Harper_Hills.pdf.

Matsuura, S., Asano, S., Okamoto, T. 2008. Relationship between rain and/or meltwater, pore-water pressure and displacement of a reactivated landslide. In: *Engineering Geology*. Vol. 101. pp. 49 – 59.

McFarlane, D. F. Observations and predictions of the behaviour of large, slow-movng landslides in Schist, Clyde Dam reservoir, New Zealand. In: *Engineering Geology*. DOI: 10.1016/j.enggeo.2009.02.005.

McSaveney, M. J., and Griffiths, G. A. 1987. Drought, rain, and movement of a recurrent earthflow complex in New Zealand. In: *Geology.* Vol. 15. pp. 643 – 646.

McSaveney, M. J., and Massey, C. I. 2010. A micro-mechanics approach to earthquake-triggering of landslides. p. 3341-3347 (paper 400) In: *Williams, A.L.; Pinches, G.M.; Chin, C.Y.; McMorran, T.J.; Massey, C.I. (eds) Geologically active : delegate papers 11th Congress of the International Association for Engineering Geology and the Environment, Auckland, Aotearoa, 5-10 September 2010*. Boca Raton, Fla: CRC Press

Mesri, G., Cepeda-Diaz A. F. 1986. Residual strength of clays and shales. In. Geotechnique. Vol. 36. No. 2. pp. 269–274.

Milne, J.D.G. 1973a. Upper Quaternary geology of the Rangitikei Basin, North Island, New Zealand. In: *PhD thesis.* Massey University.

Milne, J.D.G. 1973b. Map and sections of river terraces in the Rangitikei Basin, North Island, New Zealand. In: *New Zealand Soil Survey Report 4*.

Moore, R., Carey, J., McInnes, R.G. & Houghton, J. 2007. Climate change , so what? Implications for ground movement and landslide frequency in Ventnor Undercliff, Isle of White. In: *McInnes, R.G., Jakeways, J., Fairbank, H. & Mathie, E. (eds) Landslides and Climate Change: Challenges and Solutions*. Balkema, Rotterdam, 335–344.

Morgenstern, N.R. 1995. Keynote paper: The role of analysis in the evaluation of slope stability. *Landslides,* Bell (ed). Balkema, Rotterdam,.

Morgenstern, N. R., and Price, V. E. 1965. The analysis of the stability of general slip surfaces. In: *Geotechnique.* Vol. 15. No. 1. pp. 79 – 93.

Mountjoy, J., and Pettinga, J. R. 2006. Controls on large deep-seated landslide in soft rock terrain. Rock mass defects and seismic triggering. In: *Earthquakes and Urban Developments.* Proceedings of the New Zealand Geotechnical Society, 2006 Symposium, Nelson, New Zealand.

Murphy, J.R., O'Brien, J.L. 1977. The correlation of peak ground acceleration amplitude with seismic intensity and other physical parameters. In: *Bulletin of the Seismological Society of America,* 67 (3); pp 877-915.

Naish, T., Kamp, P. J. J. 1995. Pliocene-Pleistocene cyclothems, Wanganui Basin, New Zealand; a lithostratigraphic framework. *New Zealand Journal of Geology and Geophysics*. 1995. Vol. 38. pp. 223-243.

Nakamura, H. 1984. Landslides in silts and sands mainly in Japan. In: *Proceedings of the IV International Symposium on landslides, Toronto 1984*. Vol 1. pp 155 – 185.

Newmark, N. 1965. Effects of earthquakes on dams and embankments. *N: Geotechnique*, Vol. 15, No. 2, pp. 139 – 160.

New Zealand Geotechnical Society. 2005. Description of soil and rock. In: *Guidelines for the field classification and description of soil and rock for engineering purposes.*

New Zealand Standard. 2004. NZS 1170.5 Structural design actions Part 5: Earthquake actions New Zealand. Dec 22, 2004.

Ng. K. Y. 2007. Mechanisms of shallow rainfall-induced landslides in residual soils in humid tropical environments. University of Durham, UK. PhD Thesis.

Nieuwenhuis, J. D. 1991. Variations in the stability and displacements of a shallow seasonal landslide in varved clays.

Olson, J. E. 2001. Predicting facture swarms – the influence of subcritical crack growth and the crack –tip process zone on joint spacing in rock. In: *The initiation, propagation and arrest of joints and other factures*. Cosgrove, J. W., Engelder, T. (eds). Geological Society Special publication 231. pp. 73 – 88.

Panet, M. 1969. Discussion of K.W. John's Paper (ASCE Proc. Paper 5865, March 1968). Journal of the Soil Mechanics and Foundation Division, ASCE, Vol. 95, No. SM2, pp 685-686.

Pasuto, M. Soldati, A. 1990. Some cases of deep-seated gravitational deformations in the area of Cortina d'Ampezzo (Dolomites)', The Proceedings of the European Short Course on Applied Geomorphology, 2, 91-104.

Petley, D. J. 1966. The shear strength of soils at large strains. In: *PhD thesis, University of London*.

Petley, D. N., Allison, R. J. 1997. The mechanics of deep-seated landslides. In: *Earth Surface Processes and Landforms.* Vol. 22. pp. 747 – 758.

Petley, D. N., Bulmer, M. H. K., Murphy, W. 2002. Patterns of movement in rotational and translational slides. In: *Geology*. Vol. 30. (8). pp. 719 – 722.

Petley, D.N., Mantovani, F., Bulmer, M.N., Zannoni, A. (2005). The use of surface monitoring data for the interpretation of landslide movement patterns. Geomorphology. 66 (1-4) pp. 133-147.

Phoon, K. K., Kulhawy, F. H. Characterization of geotechnical variability. In. Canadian Geotechnical Journal. Vol 36. No. 4. pp. 612-624.

Picarelli, L., Urciuoli, G., Russo, C. 2004. Effect of groundwater regime on the behaviour of clayey slopes. In: *Canadian Geotechnical Journal*. Vol 41. pp 467 – 484.

Picarelli, L. 2007. Considerations about the mechanics of slow active landslides in clay. *In: Progress in landslide science*. Sassa, K., Fukuoka, H. Wang, F., Wang, G. editors. Chapter 3. pp. 27-57.

Price, M. 2009. Barometric water-level fluctuations and their measurement using vented and non-vented pressure transducers. In. Quarterly journal of engineering geology and hydrogeology. Vol. 42. Part 2. pp. 245-250.

Pusch, R. 1976. Shear deformation of clay microstructure. In. Proceedings of the VII International Congress on Rheology. Gothenburg, Sweden, August 23 to August 27, 1976.

Ranalli, M., Gottardi, G., Medina-Cetina, Z., Nadim, F. 2009. Uncertainty quantification in the calibration of a dynamic viscoplastic model of slow slope movements. In. Landslides. Online first. DOI 10.1007/s10346-009-0185-0.

Read, S.A.L., Miller, P.J. 1990. Characterisation and classification of New Zealand Tertiary age sedimentary soft rocks. In. Bridge design and research seminar, 1990. Volume 4: Road engineering in soft rock materials. RRU Bulletin 84. pp. 1 to 25.

Reid, M. E., Baum, R. L., LaHusen, R. G., Ellis, W. L. 2008. Capturing landslide dynamics and hydrological triggers using near-real-time monitoring. In. Landslides and engineered slopes. Chen et al., (eds). pp. 179-191.

Reyes, A.G. 2007. Petrological study of selected Taihape landslide rock samples. In: *The Institute of Geological and Nuclear Science. Science Report,* 2007/32.

Saito, M. 1965. Forecasting the time of occurrence of a slope failure. In: *Proceedings of the 6th International Conference on Soil Mechanics and Foundation Engineering*. Vol. 2. pp 537 – 539.

Saito, M. 1969. Forecasting time of slope failure by Tertiary creep. In: *Proceedings of the 7th International Conference on Soil Mechanics and Foundation Engineering*. Vol. 2. pp 677 – 683.

Sarma, S. K. 1973. Stability analysis of embankments and slopes. In: *Geotechnique*. Vol. 14. No. 2. pp. 75 – 101.

Sassa, K.; Fukuoka, H.; Wang, G.; Ishikawa, N. 2004. Undrained dynamic-loading ring-shear apparatus and its application to landslide dynamics. In. Landslides. Vol. 1. pp. 7-19.

Savitzky, A., Golay, M.J.E. (1964). Smoothing and Differentiation of Data by Simplified Least Squares Procedures. In: Analytical Chemistry. Vol. 36 (8). pp.1627–1639. doi:10.1021/ac60214a047.

Schulz, W. H., McKenna, J. P., Kibler, J. D., Biavati, G. 2009a. Relations between hydrology and velocity of a continuously moving landslide – evidence of pore=pressure feedback regulating landslide motion? In. Landslides. Vol. 6. pp 181-190.

Schulz, W. H., Kean, J. W., Wang, G. 2009b. Landslide movement in southwest Colorado triggered by atmospheric tides. In. Nature Geoscience. Vol. 2. pp. 863-866.

Schuster, R, L., Krizek, R. J. 1978. Landslides analysis and control. In: *Special report 176. Transport Research Board*. Commission on Sociotechnical Systems, National Research Council. National Academy of Sciences, Washington D. C.

Schuster, R, L., Highland. L. M. 2007. The Third Hans Cloos Lecture. Urban landslides: socioeconomic impacts and overview of mitigative strategies. In: *Bulletin of the Engineering Geology and the Environment.* Volume 66. Number 1, March 2007.

Sharpe, C.F.S. 1938. Landslides and the Related Phenomena: A Study of Mass Movements of Soil and Rock. Pageant, New Jersey, 137pp.

Shroder, J.F., Cverckova, L. and Mulhern, K.L., 2005. Slope-failure analysis and classification: review of a century of effort. Physical Geography, 26(3): 216-247.

Slope Indicator. 2005. Digitilt inclinometer probe. Data sheet. Durham Geo Slope Indicator. http://www.slopeindicator.com/pdf/digitilt-vertical-inclinometer-probe-datasheet.pdf

Skempton, A. W. 1966. Bedding-plane slip, residual strength and the Vaiont landslide. In: Geotechnique. Vol. 16. pp. 82-84.

Skempton, A.W. and Hutchinson, J.N., 1969. Stability of natural slopes and embankment foundations, state-of-the-art report. Proceedings of the 7th International Conference on Soil Mechanics and Foundation Engineering, Mexico, 4, pp. 291-340.

Skempton, A. W. 1985. Residual strength of clays in landslide, folded strata and the laboratory. In: *Geotechnique*. Vol. 35. No. 1. pp. 3 – 18.

Sornette, D., Helmstetter, A., Andersen, J.V., Gluzman, S., Grasso, J.R. and Pisarenko, V., 2004. Towards landslide predictions: two case studies. Physica A-Statistical Mechanics and Its Applications, 338(3-4): 605-632.

Stark, T. D., Choi, H., and McCone, S. Drained shear strength parameters for analysis of landslides. *Journal of geotechnical and geoenvironmental engineering*. pp. 575 – 588. DOI: 10.1061/(ASCE)1090-0241(2005)131:5(575)

Stark, T. D., Choi, H. 2008. Slope inclinometers for landslides. In. Landslides. Vol. 5. Number 3. August 2008. pp. 339-350.

Stirling, M.; McVerry, G.; Berryman, K.; McGinty, P.; Villamor, P.; Van Dissen, R.; Dowrick, D.; Cousins, J.; Sutherland, R. 2000: Probabilistic seismic hazard assessment of New Zealand: New active fault data, seismicity data, attenuation relationships and methods. Lower Hutt, Institute of Geological and Nuclear Sciences.

Stirling, M.W., McVerry, G.H., Berryman, K.R., 2002. A new seismic hazard model for New Zealand. Bulletin of the Seismological Society of America 92:1878-1903

Stout. M. L. 1977. The Utiku landslide, North Island, New Zealand. In: *Geological Society of America, Reviews in Engineering Geology.* Volume III. pp 171 to 184.

Te Punga, M.T. 1952. The geology of Rangitikei Valley. New Zealand Geological Survey. Memo No. 8.

Terlien, M.T.J., 1998. The determination of statistical and deterministic hydrological landslide-triggering thresholds. Environmental Geology, 35(2-3): 124-130.

Terzaghi, K., 1936. The shearing resistance of saturated soils. Proceedings of the 1st International Conference on Soil Mechanics, Cambridge, MA, 1, 54-56.

Terzaghi. K., Peck, R. B. 1948. Soil mechanics in engineering practice. Second edition 1967. John Wiley and Sons Inc. Chapter 2. pp 112-127.

Terzaghi, K. 1950. Mechanism of landslides. In: *Geological Society of America.* (ed.), Application of geology to engineering practice: Berkley Volume. Geological Society of America, New York. Pp 83 – 123.

Thompson, R.C. 1982. Relationship of geology to slope failures in soft rocks of the Taihape-Mangweka area, Central North Island, New Zealand. University of Auckland PhD Thesis.

Tomlinson, M. J. 1995. Foundation design and construction. Sixth edition. Longman Scientific and Technical, (pub). pp 196-197.

Trimble. 2010. Trimble NetRS GPS reference station. Fact sheet: http://facility.unavco.org/project_support/polar/whatnew/NetRS.pdf.

Urciuoli, G., Picarelli, L, Leroueil, S. 2007. Local slope failure before general slope failure. In: *Geotech. Geol. Eng. Vol.* 25 (1). Pp 103 – 123.

Van Asch, Th. W. J., Van Genuchten, P. M. B. 1990. A comparison between theoretical and measured creep profiles of landslides. In: *Geomorphology*. Vol. 3. pp 45 – 55.

Van Asch, Th. W. J., Van Beek, L. P. H., Bogaard. 2007. Problems in predicting the mobility of slow-moving landslides. In: *Engineering Geology*. Vol 91. pp 46 – 55.

Van Genuchten, P. M. B., De Rijke, H. 1988. On pore pressure variations causing slide velocities and accelerations in seasonally active landslide. In: *Earth Surface Processes and Landforms.* Vol. 14. Issue 6. pp 577-586.

Varnes, D. J. 1978. Slope movement types and processes. In: *Special report 176: Landslides Analysis and Control.* Schuster, R. L., Krizek, R. J. (eds). Transport Research Board. Commission on Sociotechnical Systems, National Research Council. National Academy of Sciences, Washington D. C.

Varnes, D.J., 1983. Time-deformation relations in creep to failure of earth materials. Proceedings of the 7th Southeast Asian Geotechnical Conference, 22-26 November 1982, Hong Kong, pp. 107-1302.

Voight, B. 1989. A relation to describe rate-dependent material failure. Science (Washington D. C.). Vol. 243. pp. 200 – 203.

Wallace, L. M., Beavan, J. 2004. Subduction zone coupling and tectonic block rotations in the North Island, New Zealand. In. Journal of Geophysical Research. Vol. 109. DOI: 10.1029/2004JB003241.

Wieczorek, G. F. 1996. Landslide triggering mechanisms. In: *Landslide: investigation and mitigation.* Turner, K. A. & Schuster, R. L. editors. Special report, Transportation Research Board, National Research Council, 247. Chapter 4, 76-90.

Williams, K., Sinclair, T. 2010. Living with landslides on the move. In. Geohazards at the leading edge. International Association of Engineering Geologists, 2010 Congress. Auckland New Zealand. Balkema. In Press.

Yen, B. C. 1969. Stability of slopes undergoing creep deformation. In: *Journal of soil Mechanics and Foundation Engineering*. Vol. 4. pp. 1075 – 1096.

Zangerl, C. Eberhardt, E. Perzlmaier, S. 2010. Kinematic behaviour and velocity characteristics of a complex deep-seated crystalline rockslide system in relation to its interaction with a dam reservoir. In. *Engineering Geology.* Vol. 112. pp. 53-67.

Zaruba, Q. Mencl, V. Landslides and their control. In. *Developments in Geotechnical Engineering Vol. 31*. 2nd Edition. 1969. pp. 99-132. Elsevier.